

Unclassified

AD 734236

Security Classification

DOCUMENT CONTROL DATA - R & D

(Security classification of title, body of abstract and indexing annotation must be entered when the overall report is classified)

1. ORIGINATING ACTIVITY (Corporate author)	2a. REPORT SECURITY CLASSIFICATION
Vertol Division The Boeing Company P. O. Box 16858, Philadelphia, PA 19142	Unclassified
3. REPORT TITLE	2b. GROUP
Four Prop Tilt Wing with Cyclic Pitch Propellers: Results of Full Span Wind Tunnel Test/Phase II	N/A

4. DESCRIPTIVE NOTES (Type of report and inclusive dates)

Contractor Test Report (December 1970)

5. AUTHOR(S) (First name, middle initial, last name)

Kolesar, Charles

6. REPORT DATE	7a. TOTAL NO. OF PAGES	7b. NO. OF REFS
June 1971	294	2
8a. CONTRACT OR GRANT NO.	9a. ORIGINATOR'S REPORT NUMBER(S)	
F33615-70-C-1000	Boeing Vertol Document	
b. PROJECT NO.	D170-10039-1	
c. Task Area Number:	9b. OTHER REPORT NO(S) (Any other numbers that may be assigned this report)	
d. Work Unit Number:	AFFDL TR 71-91, Reference 4	
10. DISTRIBUTION STATEMENT		
Approved for public release; distribution unlimited.		
11. SUPPLEMENTARY NOTES	12. SPONSORING MILITARY ACTIVITY	
	Air Force Flight Dynamics Laboratory Wright-Patterson AFB, Ohio 45433	

13. ABSTRACT

This report presents the results of wind tunnel test BWWT 067, the Phase II test of a two phase test program, performed in the Boeing-Vertol V/STOL wind tunnel on a powered four prop tilt wing full scale model equipped with cyclic pitch propellers for longitudinal control. Items evaluated through transitional flight, include cyclic pitch effectiveness, descent performance with cyclic pitch inputs, the effect of cyclic on longitudinal and lateral/directional stability plus the influence of cyclic action on the effectiveness of the aircraft surface controls (stabilizer for longitudinal trim and differentially deflected flaps/spoiler for roll/yaw control).

An in-ground effect investigation with a moving ground plane was also conducted to establish the influence of the ground on cyclic pitch effectiveness and on stability characteristics with cyclic pitch inputs.

Unclassified
Security Classification

14 KEY WORDS	LINK A		LINK B		LINK C	
	ROLE	WT	ROLE	WT	ROLE	WT
Cyclic Pitch Propellers						
Descent Capability						
Double Slotted Flaps						
Hover						
In-Ground Effect						
Lateral/Directional Stability and Control						
Longitudinal Stability and Control						
Propeller Hub Pitching Moment						
Propeller Normal Force						
Slats						
Tilt Wing Aircraft						
Transitional Flight						

REV LTR

THE **BOEING** COMPANY

VERTOL DIVISION • PHILADELPHIA, PENNSYLVANIA

CODE IDENT. NO. 77272

NUMBER D170-10039-1

TITLE FOUR PROP TILT WING WITH CYCLIC PITCH

PROPELLERS: RESULTS OF FULL SPAN

WIND TUNNEL TEST/PHASE II

ORIGINAL RELEASE DATE JUNE 1971. FOR THE RELEASE DATE OF
SUBSEQUENT REVISIONS, SEE THE REVISION SHEET. FOR LIMITATIONS
IMPOSED ON THE DISTRIBUTION AND USE OF INFORMATION CONTAINED
IN THIS DOCUMENT, SEE THE LIMITATIONS SHEET.

MODEL _____ CONTRACT F33615-70-C-1000

ISSUE NO. _____ ISSUED TO: _____

PREPARED BY Charles E. Kolesar DATE 6/17/71
APPROVED BY Charles E. Kolesar DATE 6/17/71
C. E. Kolesar
APPROVED BY K. B. Gilmore DATE 6/30/71
K. B. Gilmore, Mgr., V/STOL Technology
APPROVED BY W. L. Lapinski DATE 6/30/71
W. L. Lapinski, Program Manager

DISTRIBUTION STATEMENT A	
Approved for public release; Distribution Unlimited	

FORM 48280 (6/68)

SHEET i

III

D D C
RECORDED
DEC 28 1971
REGULATORY
C

LIMITATIONS

This document is controlled by Aerodynamics, Org. 7400

All revisions to this document shall be approved by the
above noted organization prior to release.

ACTIVE SHEET RECORD

SHEET NUMBER	REV LTR	ADDED SHEETS				SHEET NUMBER	REV LTR	ADDED SHEETS			
		SHEET NUMBER	REV LTR	SHEET NUMBER	REV LTR			SHEET NUMBER	REV LTR	SHEET NUMBER	REV LTR
i						39					
ii						40					
iii						41					
iv						42					
v						43					
vi						44					
vii						45					
1						46					
2						47					
3						48					
4						49					
5						50					
6						51					
7						52					
8						53					
9						54					
10						55					
11						56					
12						57					
13						58					
14						59					
15						60					
16						61					
17						62					
18						63					
19						64					
20						65					
21						66					
22						67					
23						68					
24						69					
25						70					
26						71					
27						72					
28						73					
29						74					
30						75					
31						76					
32						77					
33						78					
34						79					
35						80					
36						81					
37						82					
38						83					

ACTIVE SHEET RECORD

SHEET NUMBER	REV LTR	ADDED SHEETS			SHEET NUMBER	REV LTR	ADDED SHEETS			REV LTR
		SHEET NUMBER	REV LTR	SHEET NUMBER			SHEET NUMBER	REV LTR	SHEET NUMBER	
84					129					
85					130					
86					131					
87					132					
88					133					
89					134					
90					135					
91					136					
92					137					
93					138					
94					139					
95					140					
96					141					
97					142					
98					143					
99					144					
100					145					
101					146					
102					147					
'03					148					
-04					149					
105					150					
106					151					
107					152					
108					153					
109					154					
110					155					
111					156					
112					157					
113					158					
114					159					
115					160					
116					161					
117					162					
118					163					
119					164					
120					165					
121					166					
122					167					
123					168					
124					169					
125					170					
126					171					
127					172					
128					173					

ACTIVE SHEET RECORD

SHEET NUMBER	REV LTR	ADDED SHEETS				SHEET NUMBER	REV LTR	ADDED SHEETS			
		SHEET NUMBER	REV LTR	SHEET NUMBER	REV LTR			SHEET NUMBER	REV LTR	SHEET NUMBER	REV LTR
174						218					
175						219					
176						220					
177						221					
178						222					
179						223					
180						224					
181						225					
182						226					
183						227					
184						228					
185						229					
186						230					
187						231					
188						232					
189						233					
190						234					
191						235					
192						236					
193						237					
194						238					
195						239					
196						240					
197						241					
198						242					
199						243					
200						244					
201						245					
202						246					
203						247					
204						248					
205						249					
206						250					
207						251					
208						252					
209						253					
210						254					
211						255					
212						256					
213						257					
214						258					
215						259					
216						260					
217						261					

ACTIVE SHEET RECORD

SHEET NUMBER	REV LTR	ADDED SHEETS				SHEET NUMBER	REV LTR	ADDED SHEETS			
		SHEET NUMBER	REV LTR	SHEET NUMBER	REV LTR			SHEET NUMBER	REV LTR	SHEET NUMBER	REV LTR
262											
263											
264											
265											
266											
267											
268											
269											
270											
271											
272											
273											
274											
275											
276											
277											
278											
279											
280											
281											
282											
283											
284											
285											
286											
287											

REVISIONS			
LTR	DESCRIPTION	DATE	APPROVAL

FORM 46282 (12/65)

IX

SHEET vii

ABSTRACT

This report presents the results of wind tunnel test BVWT 067, the Phase II test of a two phase test program, performed in the Boeing-Vertol V/STOL wind tunnel on a powered four prop tilt wing full span model equipped with cyclic pitch propellers for longitudinal control. Items evaluated through transitional flight, include cyclic pitch effectiveness, descent performance with cyclic pitch inputs, the effect of cyclic on longitudinal and lateral/directional stability plus the influence of cyclic action on the effectiveness of the aircraft surface controls (stabilizer for longitudinal trim and differentially deflected flaps/spoiler for roll/yaw control).

An in-ground effect investigation with a moving ground plane was also conducted to establish the influence of the ground on cyclic pitch effectiveness and on stability characteristics with cyclic pitch inputs.

KEY WORDS

Cyclic Pitch Propellers

Descent Capability

Double Slotted Flaps

Hover

In-Ground Effect

Lateral/Directional Stability and Control

Longitudinal Stability and Control

Propeller Hub Pitching Moment

Propeller Normal Force

Slats

Tilt Wing Aircraft

Transitional Flight

NOMENCLATURE

The following nomenclature was used for Model VRO68Q in BVWT 067. Additional nomenclature is included in the Data Reduction section of this report.

Symbol

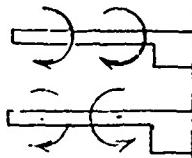
A_p	Propeller disc area	ft. ²
α_F	Fuselage angle of attack relative to freestream	degrees
$\alpha_{W_{EFF}}$	Effective wing angle of attack	degrees
B_1	Fuselage	
b	Wing span	ft.
c	Mean aerodynamic wing chord	ft.
γ	Cyclic angle (positive ~ nose down pitching moment)	degrees
D	Propeller diameter	ft.
δ_F	Flap angle	degrees
F_1	Wing fence configuration	
f_1	Basic double slotted flaps	
0.75	Propeller blade pitch angle at .75R	degrees
H_1	Horizontal tail	
h	Height of outboard propeller plane to ground plane in hover	inches
i_w	Wing incidence angle	degrees
J	Propeller advance ratio, $\frac{V}{nD}$	
L	Aircraft lift	lbs.
M	Aircraft pitching moment (positive ~ nose up)	ft.lbs.

N_1	Nacelle configuration	D170-10039-1
n	Propeller rotational speed	rps
P_1	Collective hubs	
P_2	Cyclic hubs	
Q	Shaft torque	ft-lbs
Q_1	Basic slat configuration	
q	Freestream dynamic pressure	lbs/ft ²
q_s	Slipstream dynamic pressure, $q+T/A_p$	lbs/ft ²
R	Propeller blade radius	ft.
r	Radial station along blade	ft.
ρ	Density	slugs/ft ³
S	Wing area	ft. ²
λ	Horizontal stabilizer incidence relative to waterline	degrees
T	Propeller thrust	lbs.
T_j	Jet thrust from air motor	lbs.
V	Velocity	ft/sec.
V_F	Full scale aircraft velocity	knots
V_1	Vertical tail	
W_1	Wing	
X	Aircraft longitudinal force, positive forward	lbs.
x	Longitudinal distance	ft.
z	Vertical distance	ft.

Superscripts - (Superscripts are in sequence, left wing tip to fuselage centerline)

f^{60} Flap at 60°

$p^{1,1}$ Both propellers turning down inboard



$p^{1,2}$ Both propellers turning down between nacelles

Q^{10} Slat setting, see notes

Q^* Slat setting, see notes.

NOTES: 1) According to the notation used, slat setting $Q^{10,10,10,*}$ indicated that all slat segments inboard of the wing tip were set at Q^{10} position with the exception of the segment inboard of the inboard nacelle which was set at Q^* position.

TABLE OF CONTENTS

SECTION	PAGE
1.0 INTRODUCTION	7
2.0 MODEL DESCRIPTION AND INSTALLATION	10
2.1 Wing Geometry	10
2.2 Propeller, Hub Geometry	22
2.3 Nacelle Description	26
2.4 Fuselage Geometry	29
2.5 Horizontal Tail Position and Geometry	29
2.6 Vertical Tail Location and Geometry	30
2.7 Model Installation	34
2.8 Test Facility	38
3.0 INSTRUMENTATION AND EQUIPMENT	40
3.1 Model Instrumentation	40
3.2 Data Acquisition System	41
4.0 DATA REDUCTION	43
5.0 TEST PROCEDURE AND TEST CONDITIONS	48
5.1 Test Procedure	48
5.2 Test Conditions	55
6.0 TEST RESULTS AND DISCUSSION	66
6.1 Yaw Control in Hover	67
6.1.1 Hover Yaw Control Power	68
6.1.2 Hover Download due to Yaw Control	69
6.1.3 Effect of Cyclic Pitch on Hover Yaw Control	71
6.2 Cyclic Pitch Control in Hover	77
6.2.1 Effect of Horizontal Tail on Cyclic Pitch Control	77
6.3 Low Speed Descent Performance	79
6.3.1 Effect of Cyclic Pitch on Descent Capability	79

TABLE OF CONTENTS

<u>SECTION</u>	<u>PAGE</u>
6.4 Longitudinal Stability and Control in Transition	91
6.4.1 Cyclic Pitch Control Effectiveness .	94
6.4.2 Effect of Cyclic Pitch on Longitudinal Stability	100
6.4.3 Horizontal Tail Effectiveness with Cyclic Pitch Inputs	136
6.5 Lateral/Directional Stability in Transition	154
6.5.1 Empennage Off Lateral/Directional Stability	155
6.5.2 Empennage On Lateral/Directional Stability	156
6.5.3 Vertical Tail Effectiveness	157
6.5.4 Effect of Horizontal Tail on Vertical Tail Effectiveness	193
6.5.5 Effect of Cyclic Pitch on Lateral/Directional Stability	198
6.6 Cross-Coupling of Cyclic Pitch with Roll/Yaw Surface Controls	210
6.7 Longitudinal Characteristics in Ground Effect	218
6.7.1 Influence of Ground on Out-of- Ground Effect Longitudinal Characteristics	218
6.7.2 Cyclic Pitch Control Effectiveness in Ground Effect	236
6.8 Lateral/Directional Stability in Ground Effect Including Cyclic Pitch Effects . .	257
7.0 CONCLUSIONS.	284
REFERENCES.	287

1.0 INTRODUCTION

Wind tunnel test BVWT 067 was conducted in the 20ft. x 20ft. test section of the Boeing-Vertol V/STOL wind tunnel on a full span (9.04ft.) model of the Model 170 four propeller tilt wing aircraft that utilizes cyclic pitch propellers for low speed longitudinal control. This test, which covered the month of December 1970, was the Phase II test of a two phase test program performed on sting mounted VR068Q model. Results of the Phase I test, conducted in July/August 1970, are reported in Reference 1.

This air motor powered model with 2.14ft. diameter propellers, incorporated an internal six component strain gage fuselage balance and a six component strain gage balance mounted in each nacelle between the cyclic pitch propeller hub assembly and the air motor. A similar propeller/cyclic pitch hub/nacelle balance/air motor assembly was tested as an isolated propeller during May 1970 as a part of the contract (Reference 2).

The primary objectives of this Phase II test were:

a. Yaw Control in Hover

Complete the hover yaw control testing with an investigation of the yaw control capability of a combined flap/spoiler configuration, down flap deflection on one wing and spoiler deflection on the opposite wing, plus a configuration with differential flaps and spoilers.

b. Low Speed Descent Performance

Complete the investigation started in the Phase I test evaluating the effect of cyclic pitch on descent capability.

c. Cyclic Pitch Effectiveness in Transition

Determine the longitudinal control capability of the cyclic propellers at points through transition with selected combinations of wing tilt angle and flap angle.

d. Longitudinal Stability with Cyclic Pitch Inputs

Establish the influence of cyclic pitch on both the horizontal tail-off and tail-on longitudinal stability characteristics in the transition regime.

e. Basic Lateral/Directional Stability in Transition

Determine the vertical tail effectiveness and tail-on lateral/directional stability characteristics at selected combinations of wing incidence, flap angle and slipstream thrust coefficient.

f. Lateral/Directional Stability with Cyclic Pitch Inputs

Establish the effect of cyclic pitch on the tail-on lateral/directional stability characteristics at points through transition.

g. Aircraft Surface Control Power Coupled with Cyclic Pitch

Determine whether cyclic pitch inputs exert an influence on the stabilizer control effectiveness in transitional flight and on the flaps and spoilers used for roll/yaw control in transition (depending upon the wing tilt) and for yaw control in hover.

h. Effect of Ground Proximity on Longitudinal Characteristics and Cyclic Pitch Control

Determine the resultant changes in transitional longitudinal characteristics due to an in-ground effect condition and its influence on the cyclic pitch effectiveness.

i. Effect of Ground Proximity on Lateral/Directional Stability with and without Cyclic Pitch Inputs

Establish whether ground effect influences the basic lateral/directional characteristics of the aircraft as determined for transition and evaluate the changes resulting from cyclic pitch application. Investigate for ground recirculation.

Four prop Model VRO68Q utilizes a 9.23 aspect ratio tapered wing with a straight leading edge, propellers overlapped 7% in diameter, full span slats and full span large chord double slotted flaps that incorporate a movable fore flap which "nests" when the flap is retracted. Longitudinal and vertical location of the propeller hub centerlines with respect to the wing leading edge were chosen to maximize descent capability, using as a basis the data acquired in mid-1969 during a Boeing-Vertol wind tunnel test of a semispan four prop tilt wing model, the primary objective of which was to investigate the effect of propeller hub location on descent performance with overlapped propellers. The slat and double slotted flap configurations

used on Model VRO68Q were also established from data acquired during the 1969 Boeing-Vertol four prop tilt wing wind tunnel test program, that included investigations of single vs double slotted flaps and full span slats vs Kruger leading edge flaps for the purpose of maximizing descent performance. Two wing fences per wing, one at the fuselage side and the other, $18\frac{1}{2}$ of a propeller diameter outboard, were used to contain the stall occurring on the wing center section. The swept vertical tail incorporated a tail volume of .083 and the horizontal tail mounted high on the vertical had a tail volume coefficient of 1.33.

2.0 MODEL DESCRIPTION AND INSTALLATION

The general arrangement and geometry of full span Model VRO68Q and wind tunnel installation details are presented in this section. Figure 1 is a photograph of this model as installed in the Boeing Vertol V/F TOL wind tunnel for the subject test.

2.1 WING GEOMETRY (See Figure 2)

The model utilizes a tapered wing with the following geometry:

Span	9.036 ft.
Root chord	1.263 ft.
Tip chord	0.696 ft.
Mean Aerodynamic Chord (MAC)	1.007 ft.
Taper ratio	0.551
Area	8.850 ft. ²
Aspect ratio	9.225
Wing 1/4c sweep	1.6° fwd.
Dihedral	0°
Wing pivot position	
X-Axis	42.56% MAC aft of wing L.E.
Z-Axis	11.67% MAC below w.c.p.

Basic Wing Sections

Root	NACA 64 ₄ 221
Tip (actually 1.047 b/2)	NACA 64 ₂ 215
Inboard Nacelle Wing Chord/Prop Diameter	0.492
Outboard Nacelle Wing Chord/Prop Diameter	0.376
Slats (from wing tip to body centerline)	15% basic wing chord

Double Slotted Flaps

39% basic wing chord (when retracted)
23.5% chord Fowler action

Slats

The Model VR068Q tapered wing incorporated a 15% chord full span leading edge slat of the design illustrated in Figure 3. Figures 4 and 5 show the slat positioned at tip and root sections, respectively. The slat, which extended spanwise across the fuselage to the body centerline (wing root), was attached to the basic wing leading edge with preset brackets, and were arranged in nine spanwise segments (wing tip to wing tip). One segment per wing extended from the wing tip to the outboard nacelle; the slat between the nacelles was divided into two equal span segments; one segment extended from the side of the inboard nacelle to the fuselage; and finally, one segment covered the entire width of the fuselage. This arrangement enabled the slats to be set differentially according to the direction of rotation of the propeller blades in front of each slat segment.

The slat angle, gap and trailing edge location used for this test were based on previous Boeing-Vertol tilt wing testing that was conducted for the purpose of maximizing descent capability. In general, the Q¹⁰ slat setting shown in Figures 3 and 4 was used behind a "down-going" propeller blade and the Q* setting was used behind an "up-going" propeller blade.

Flaps

The large chord double slotted flaps used in test BVWT 061 are shown in Figures 6 and 7, which present the arrangement of the flaps for the 40°, 50°, and 60° deflections. Figures 6 and 7 depict tip and root sections, respectively. Nacelle length precluded extending the flaps behind the nacelles, thus splitting the flaps into three spanwise segments: outboard, mid-span, and inboard. The lengths of these segments were as follows:

<u>Flap Segment</u>	<u>Length</u>
Outboard	STA 54.215" (tip) to STA 45.789"
Midspan	STA 41.789" to STA 21.875"
Inboard	STA 17.875" to STA 7.145" (side of body)

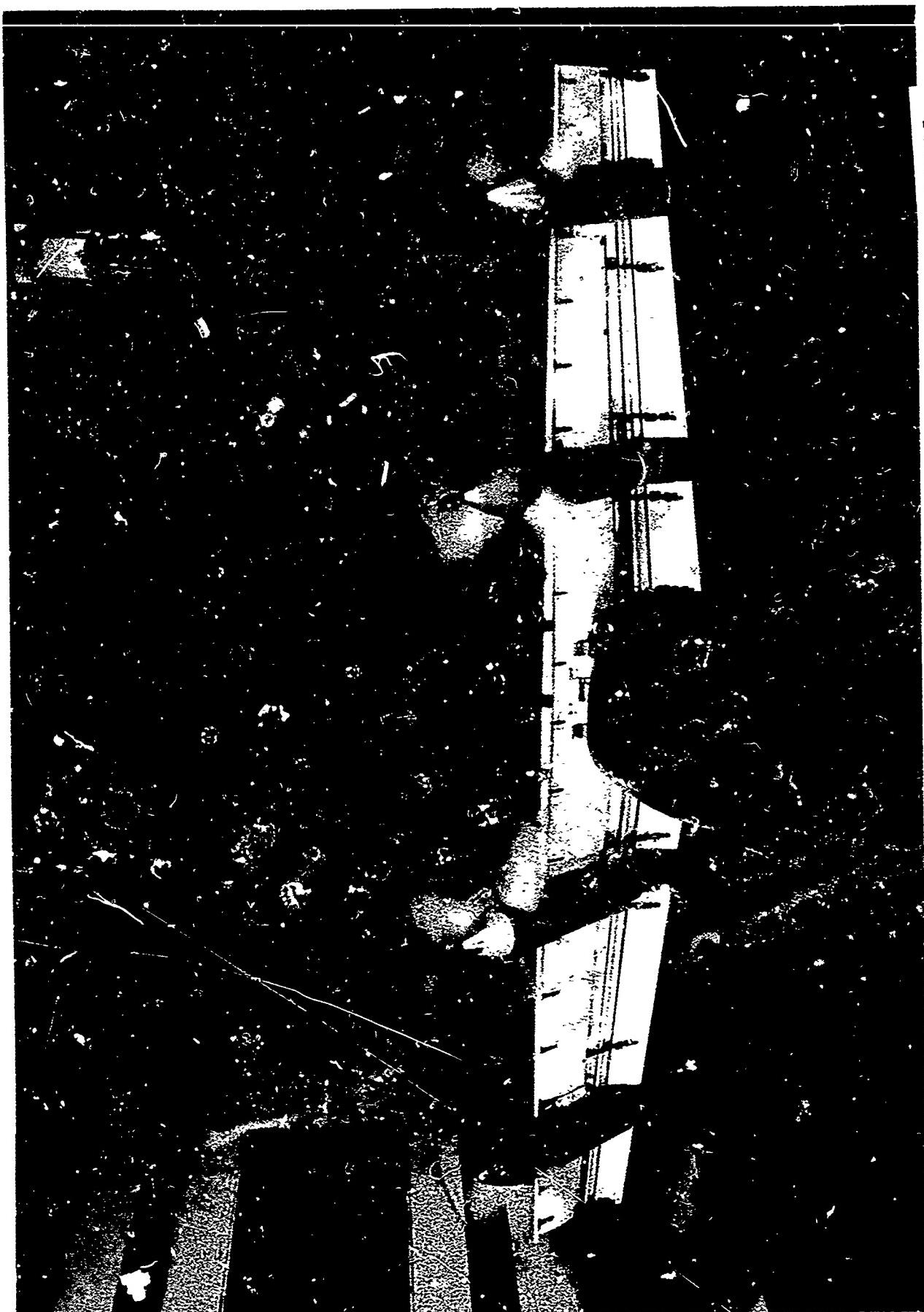
The flaps were 39% chord in the retracted position. In this position, the fore flap "nests" against the main flap as shown in Figure 8. During the initial portion of the flap extension,

the "nested" fore flap/main flap assembly is moved aft 23.5% of the basic wing chord. This value represents the Fowler action. For the first 20° of flap deflection, the fore flap remains "nested" as shown in Figure 9. As the flap is deflected to a higher angle, the main flap moves away from the fore flap, resulting in an extended flap chord of 49% at the 40° flap angle. The geometric relationship between the fore flap and main flap was held constant between 40° and 60° flap angle (the maximum angle tested). Gaps and locations used for the double slotted flaps were determined from previous test data.

Yaw control in hover is provided by flap down-travel on one wing, plus spoiler and flap up-travel on the opposite wing. The arrangement of the flap in the up-travel position for hover is illustrated in Figure 9.

D170-10039-1

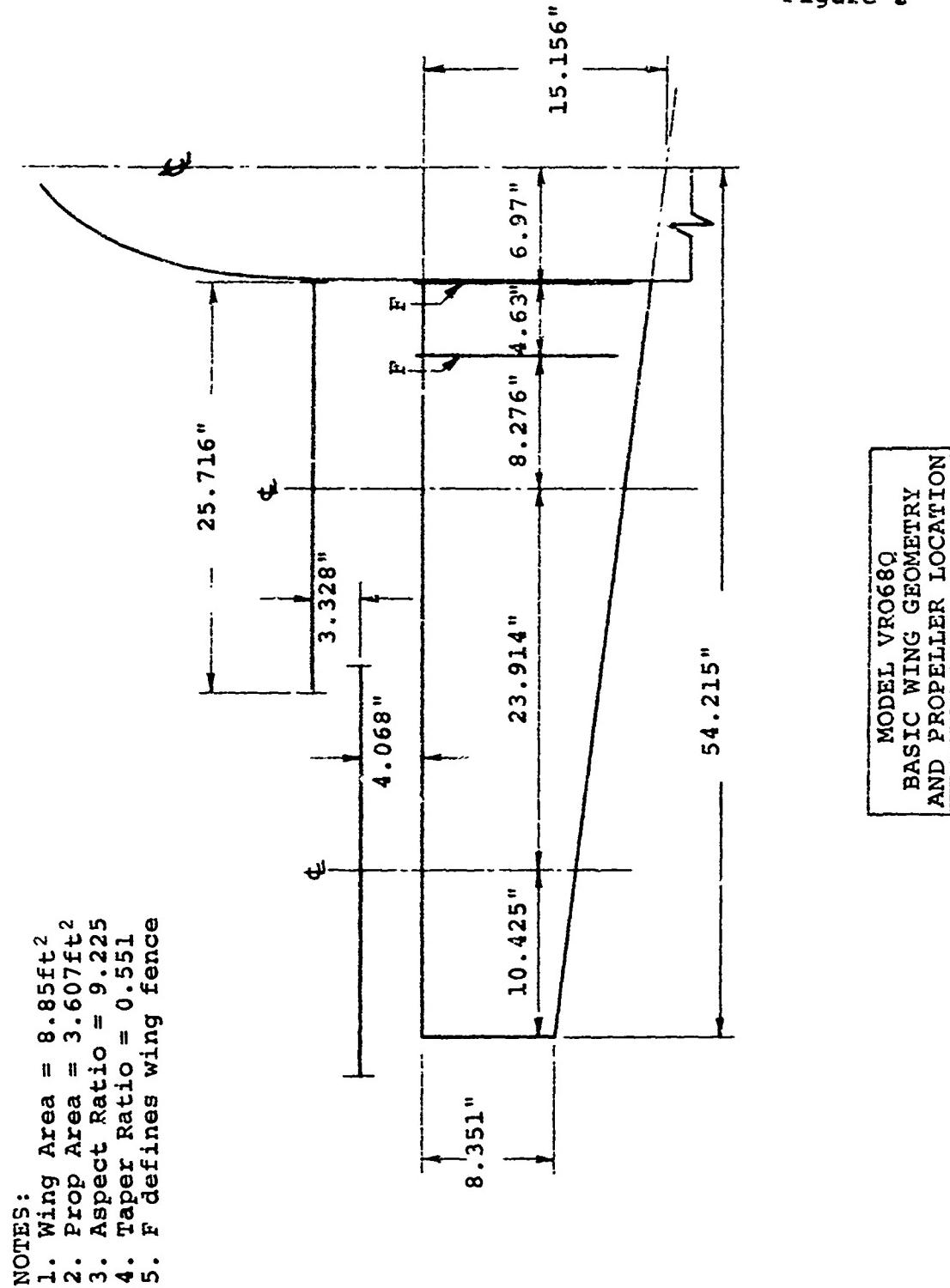
Figure 1



NOT REPRODUCIBLE

FULL SPAN MODEL VRO68Q
INSTALLATION IN BOEING-VERTOL
V/STOL WIND TUNNEL WITH MOVING GROUND BELT

Figure 2



D170-10039-1

Figure 3

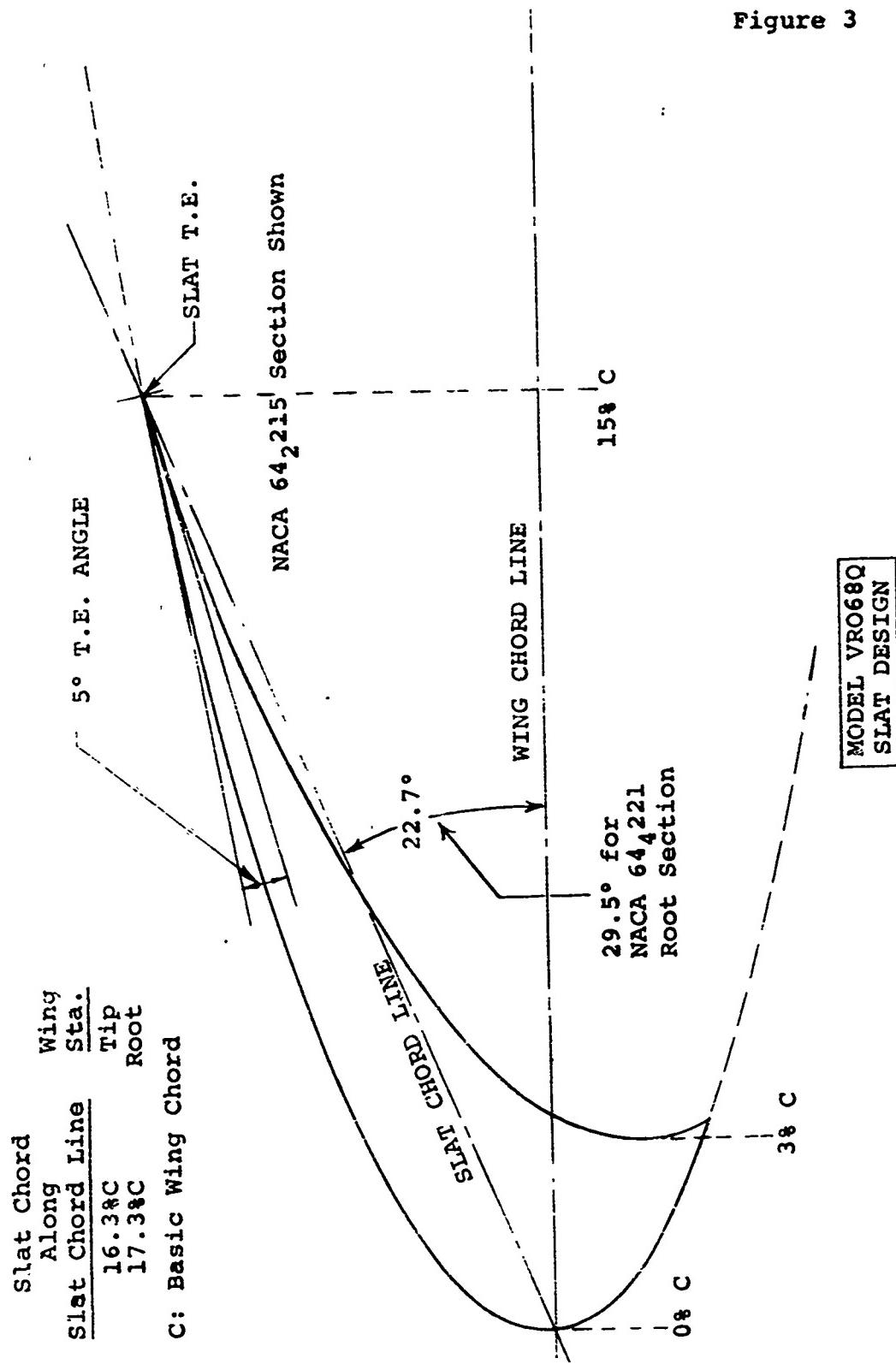
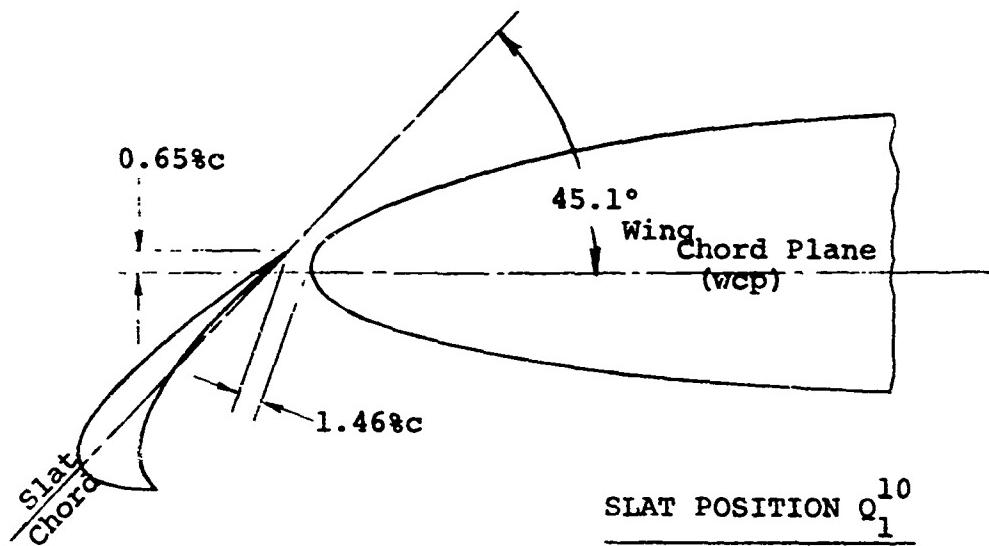
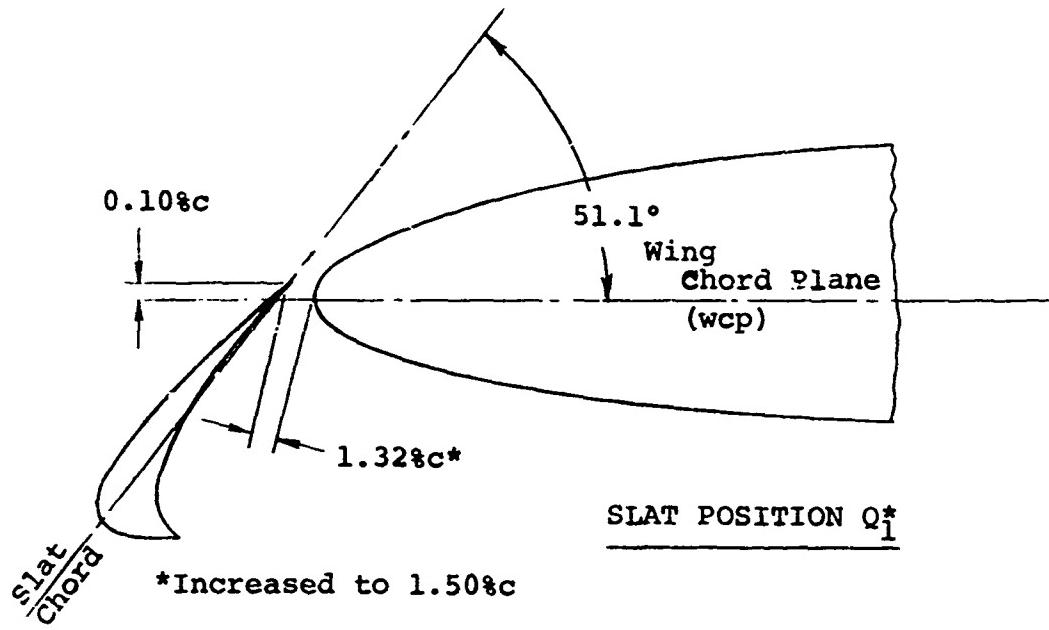


Figure 4



MODEL VRO68Q
SLAT POSITIONS
TIP SECTION

Figure 5

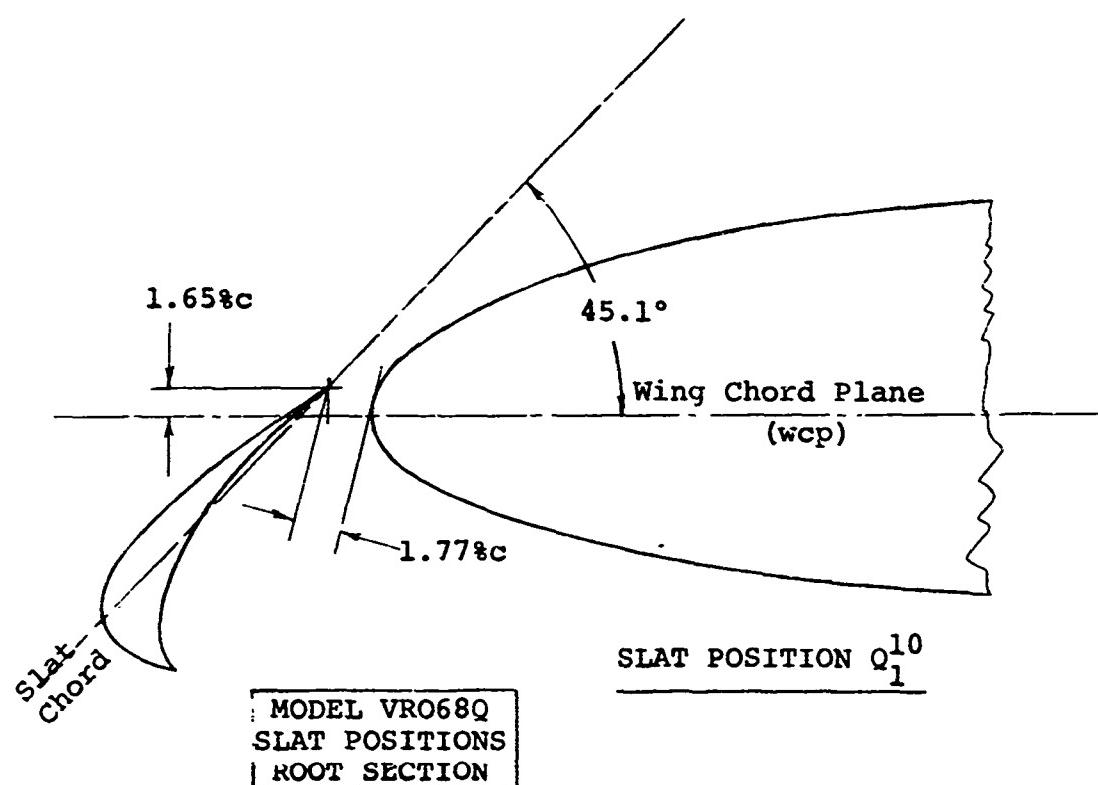
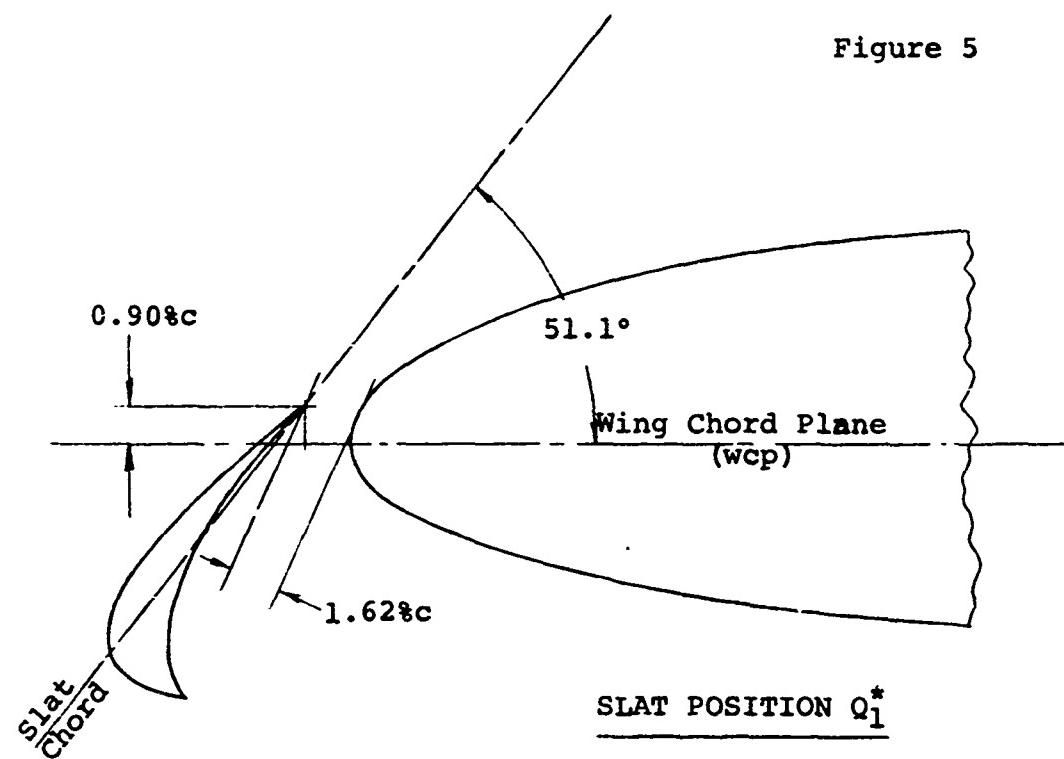


Figure 6

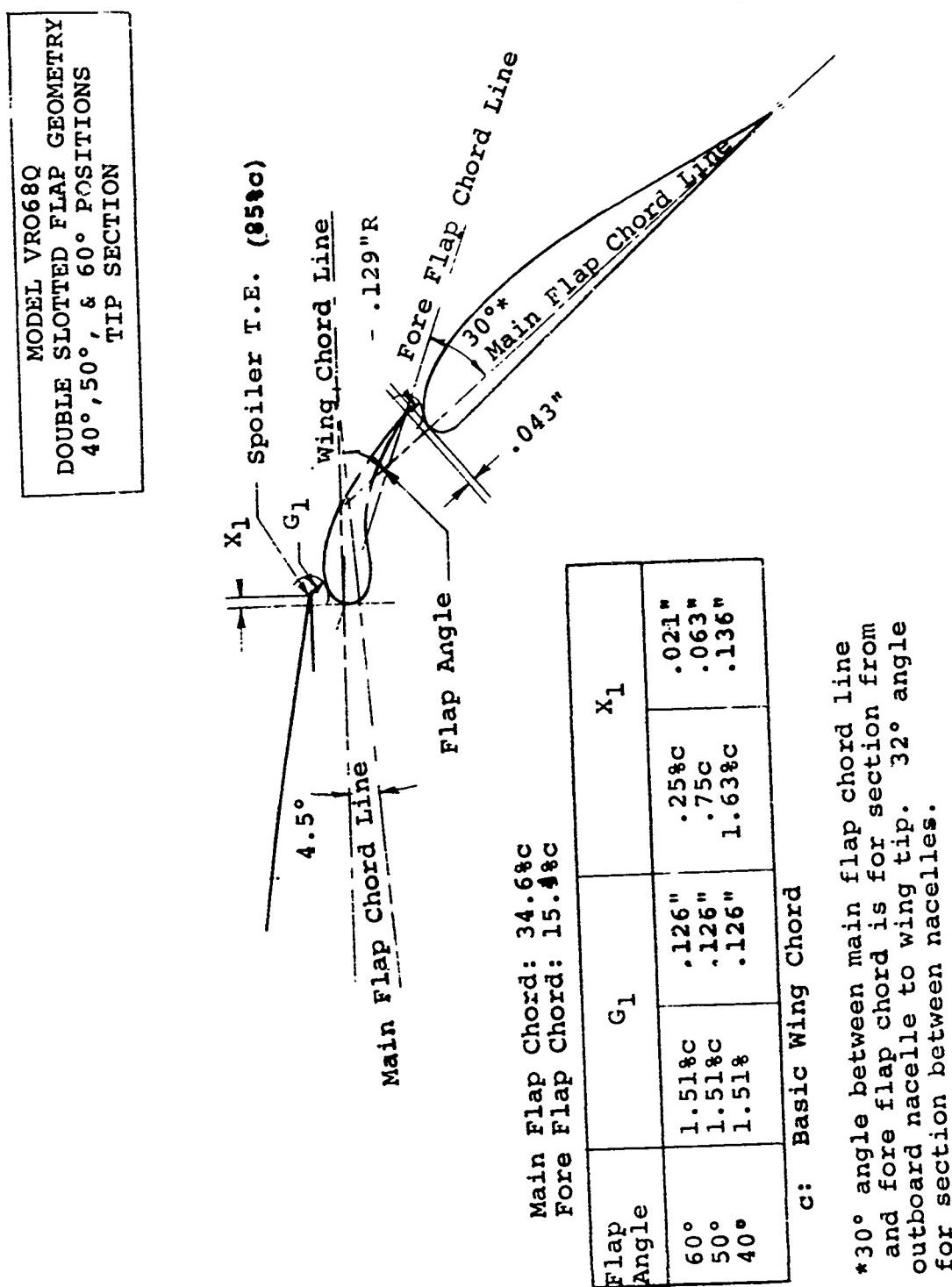
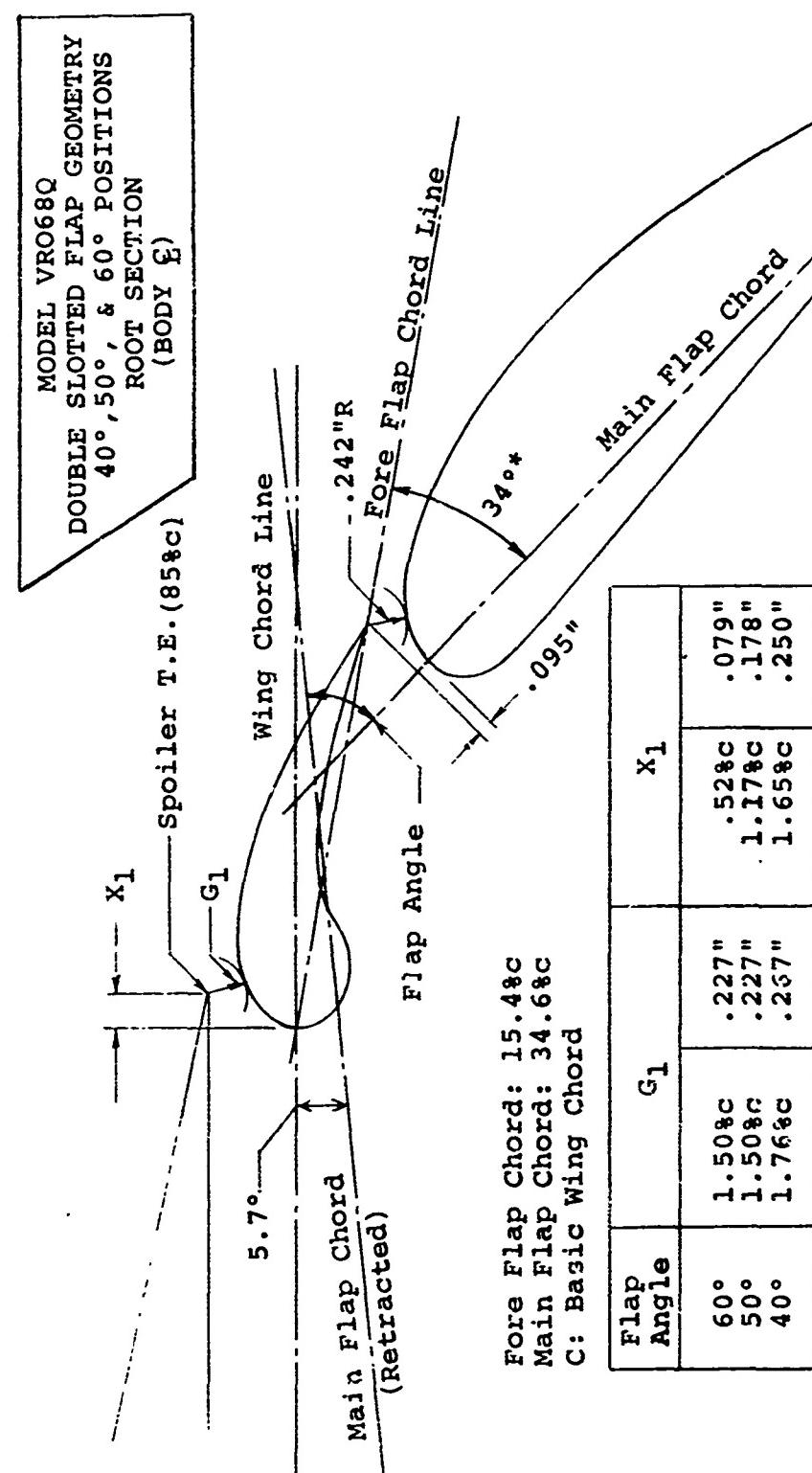
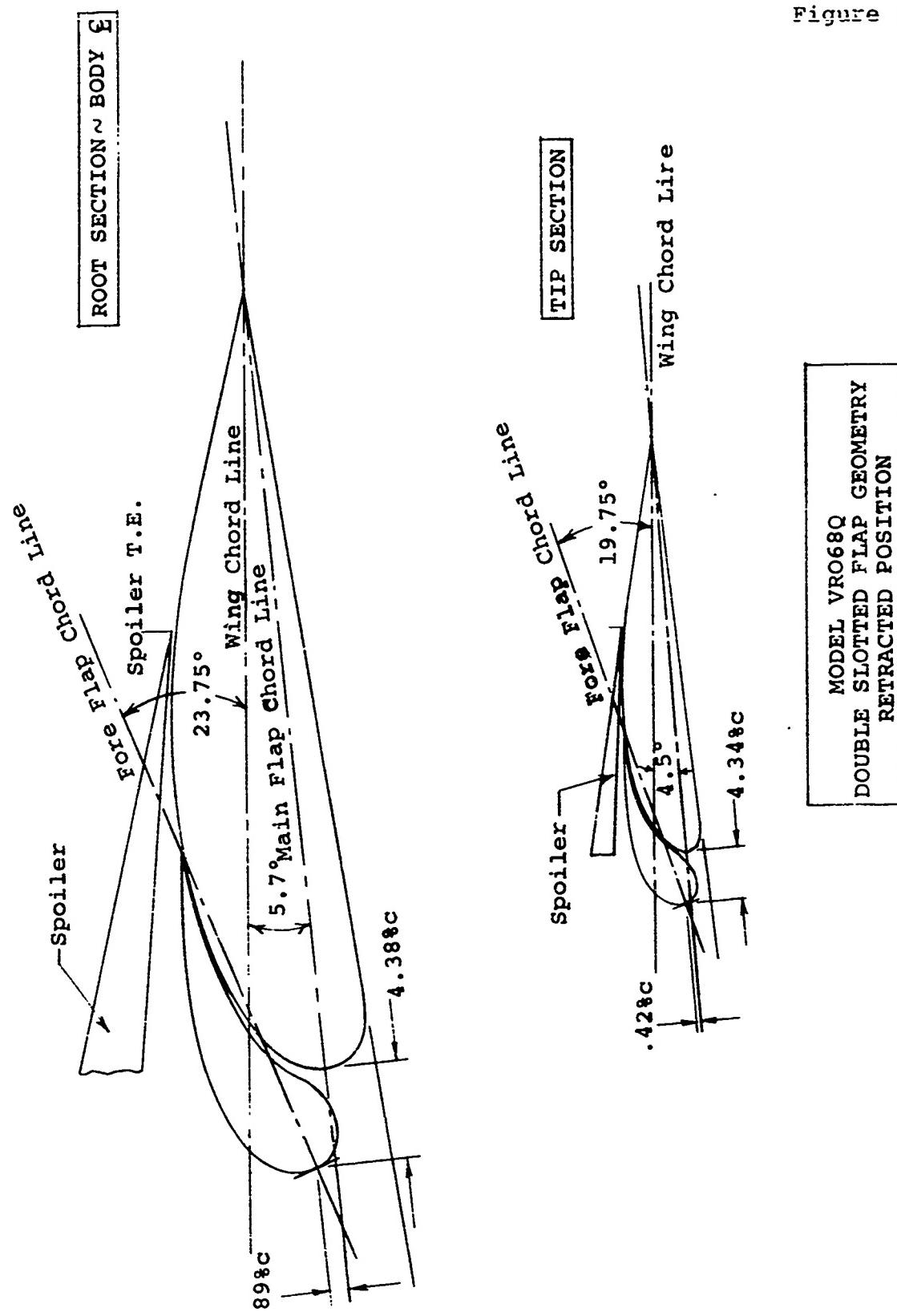


Figure 7



*34° angle between main flap chord line and fore flap chord line is for section from root to inboard nacelle. 32° angle for section between nacelles.

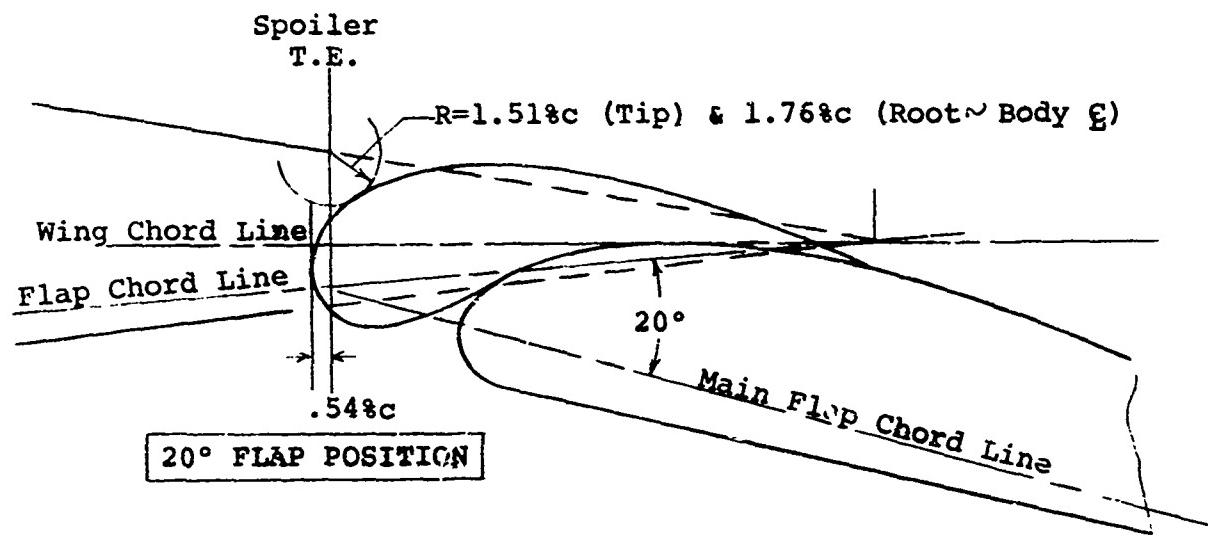
Figure 8



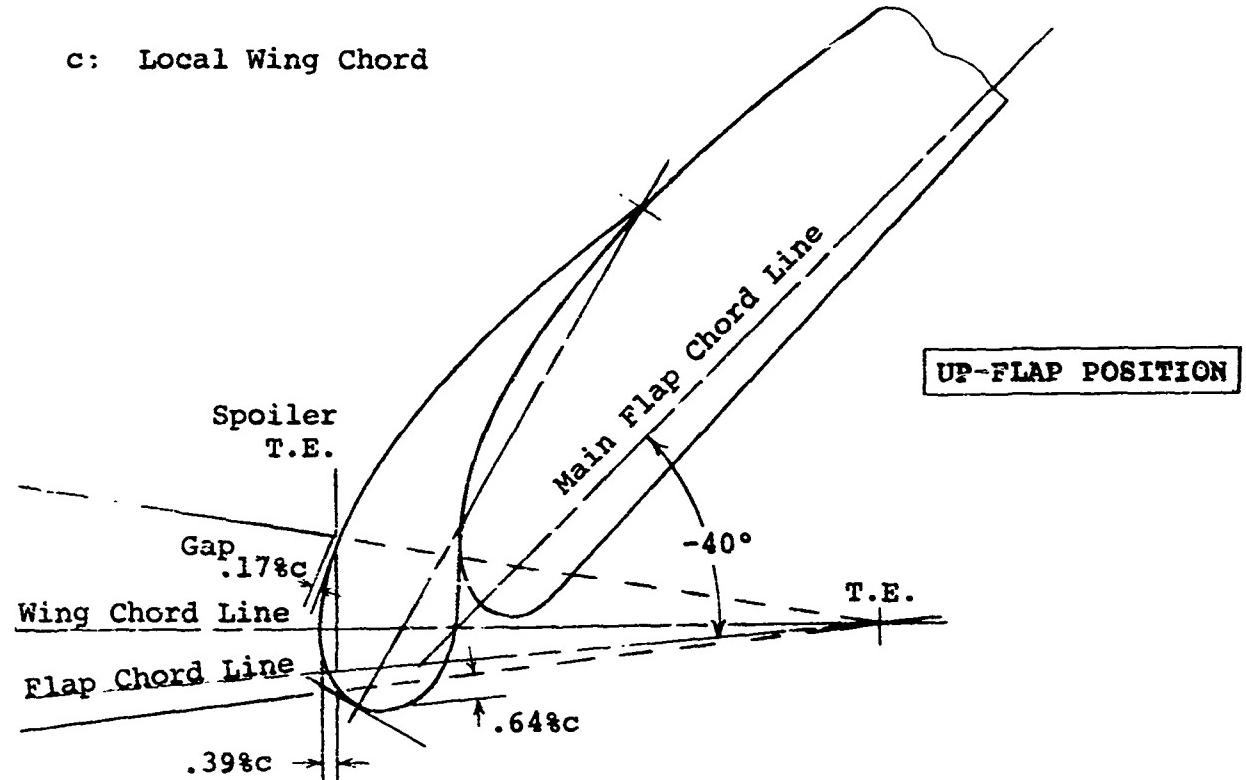
DL70-10039-1

Figure 9

MODEL VRO68Q
DOUBLE SLOTTED FLAP GEOMETRY
20° AND UP-FLAP POSITIONS



c: Local Wing Chord



Geometric characteristics of the propeller blade used in this test are shown in Figure 10. The variation with radial station, of blade chord, design lift coefficient, thickness ratio and blade twist are presented in this plot. Figure 11 depicts the blade planform. Note that the blade pivots for manual collective settings about the 35% chord line.

Three-way collective hubs were used during the non-cyclic portion of the test. These were replaced with three-way cyclic hubs, using identical propeller blades, when cyclic pitch was required. Both propeller collective and cyclic angles were manually adjusted.

Figure 12 is a photograph of the 4.80 in. diameter cyclic hub. This hub employed a swashplate mounted on a cyclic stack fixed to the front of the six component nacelle balance. The outer annulus of the swashplate was driven by scissors mounted on the rear face of the hub. Cyclic pitch was applied to the blades through a set of pitch links. Elastomeric (Lamiflex) bearings were used in the hub for blade retention and blade angle motion.

Principal dimensional information and airfoil designations for the propellers are listed below:

Diameter	2.143 ft
Disc area	3.61 ft ²
Root chord (at .2r/R)	3.20 in.
Tip chord	2.32 in.
Root section	NACA 64A030
Tip section	NACA 64A306
Activity Factor	160 per blade
Overall Blade Twist	33.5°

For the Phase II test, the radial elastomeric bearings used in the cyclic hubs for previous testing were replaced with needle roller bearings to improve the hub life. This modification necessitated moving each blade in the hub, 0.125 in. outboard to allow for the greater depth of this type of bearing. Each propeller tip was clipped 0.125 in. to retain the original propeller diameter of 2.143 ft. The 1% reduction in blade area was considered negligible.

EUGENE DIETZGEN CO.
MADE IN U.S.A.

1000 MAP DRAFTING PAPER
MILLIMETER

MODEL VRO68Q
PROPELLER
GEOMETRIC CHARACTERISTICS

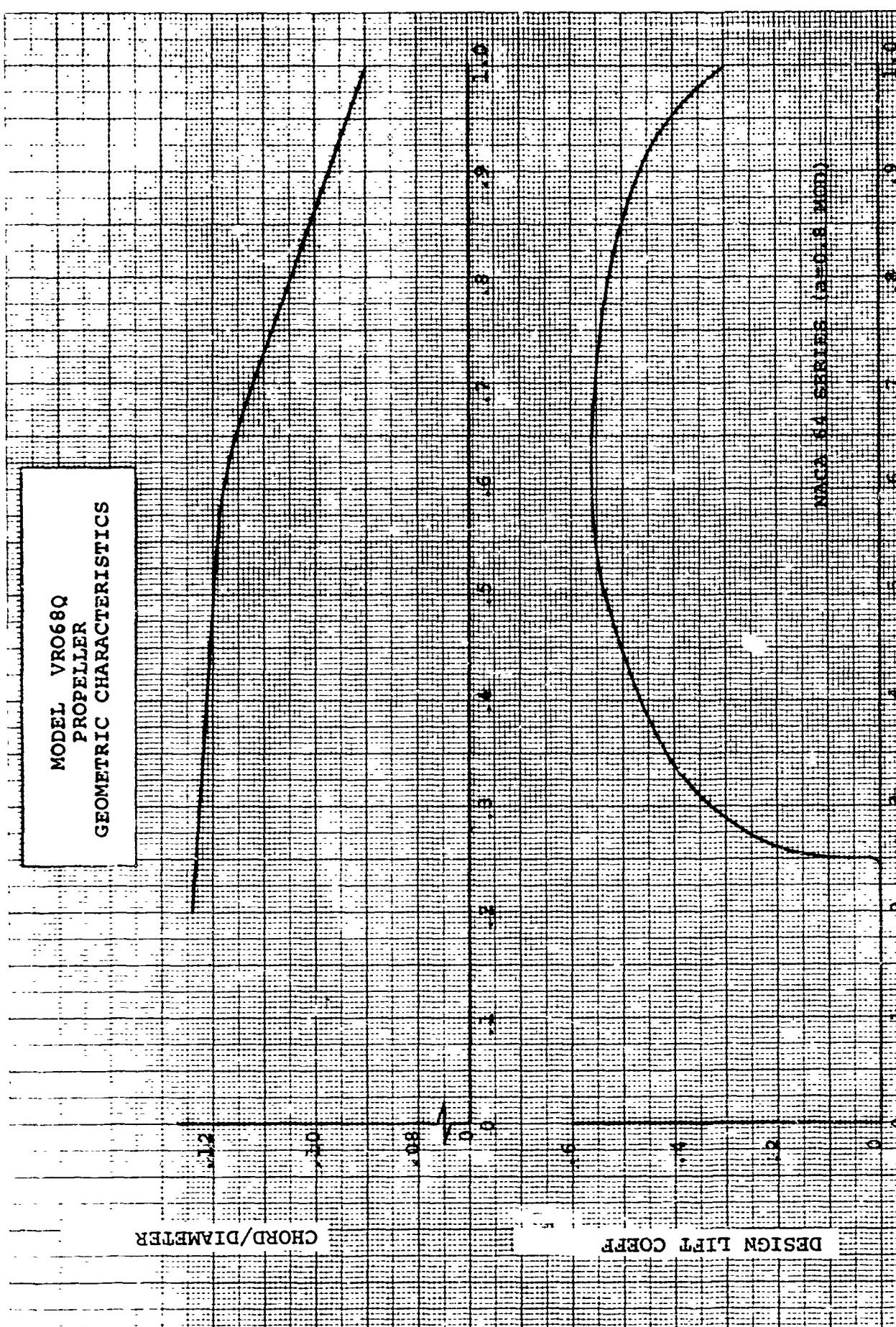
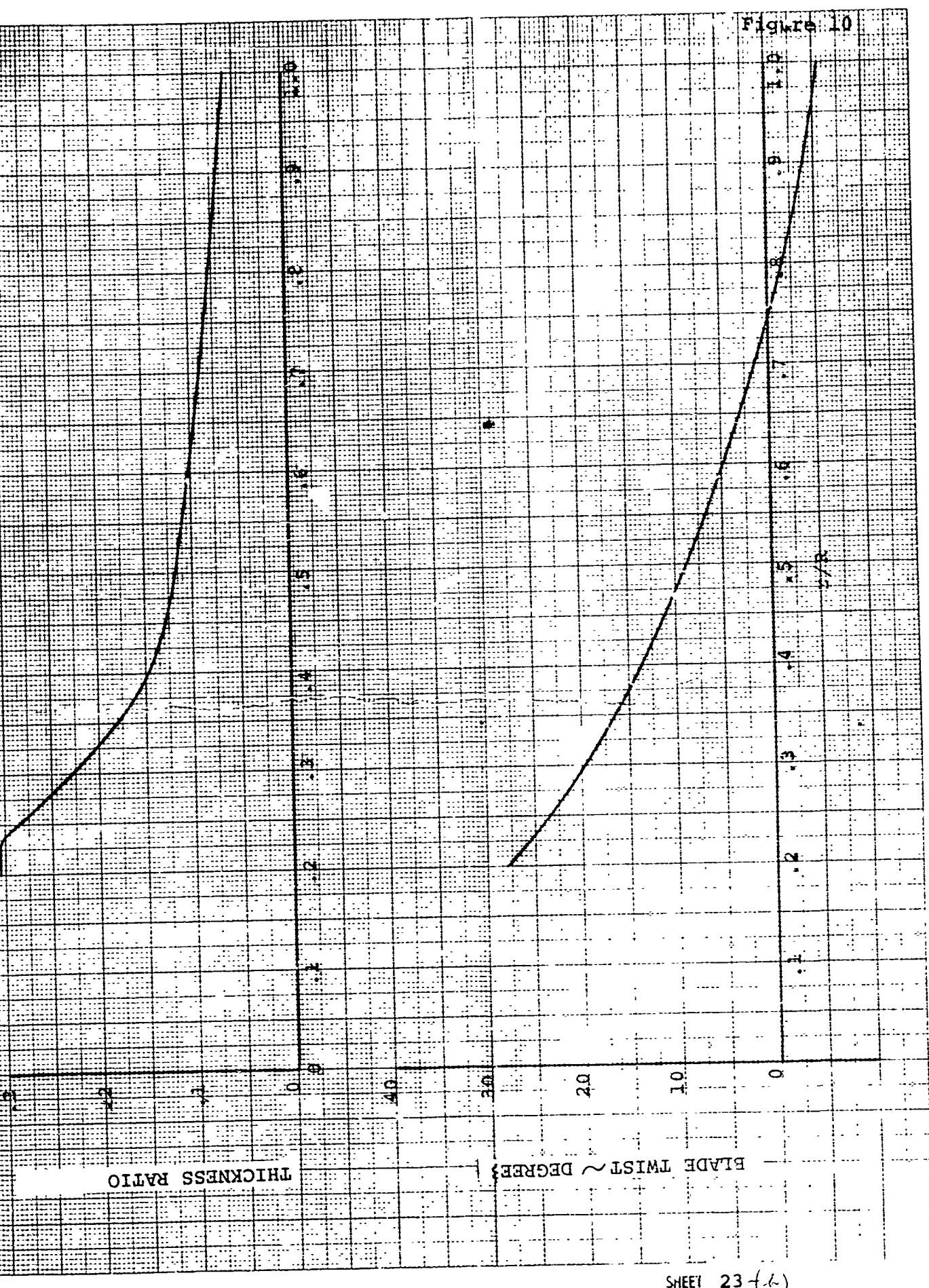


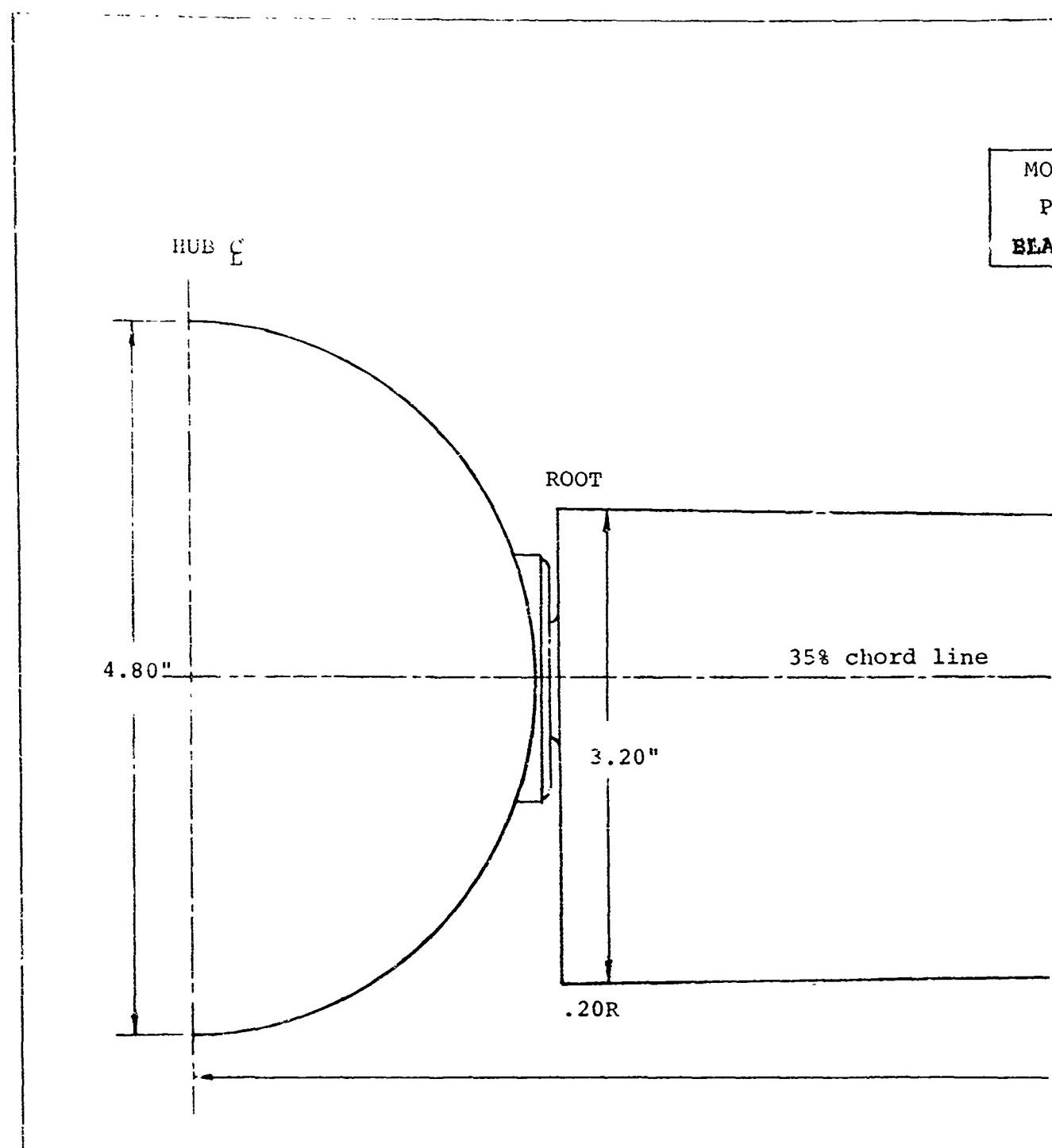
Figure 10



MOI

PJ

BLA



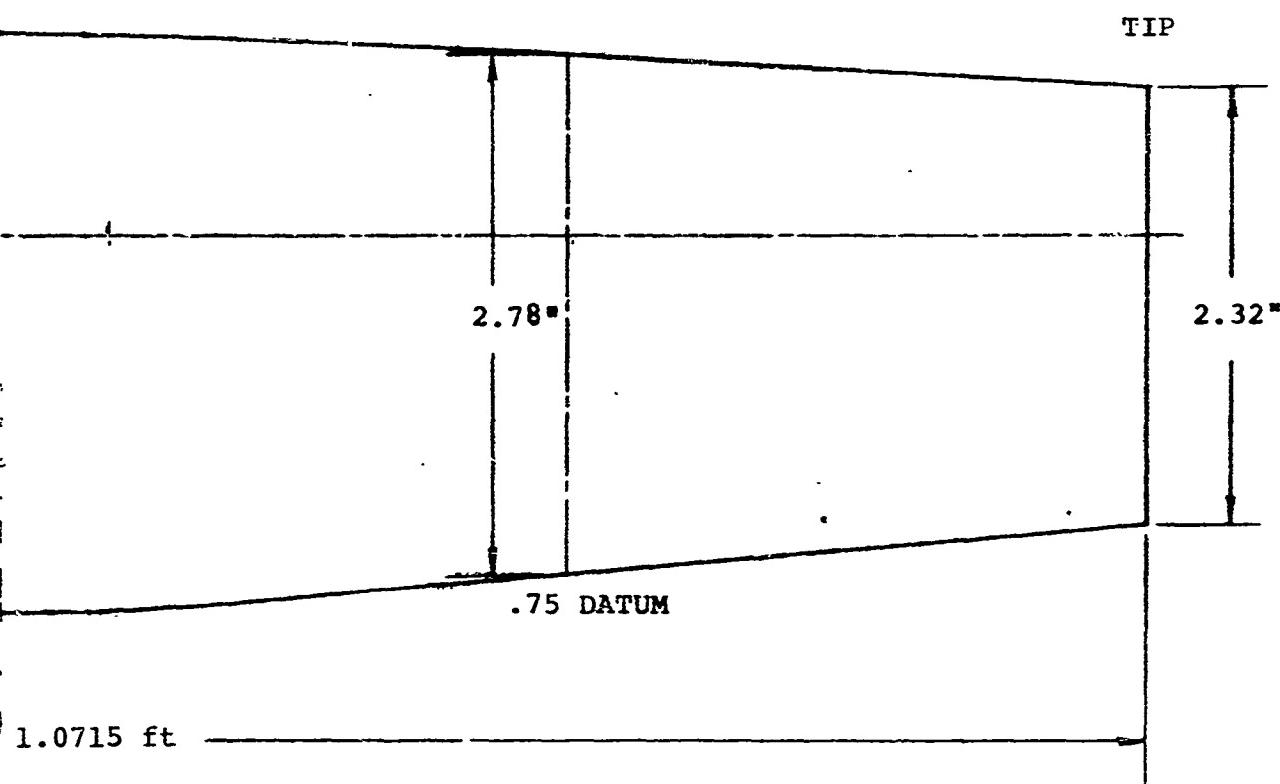
SCALE: FULL

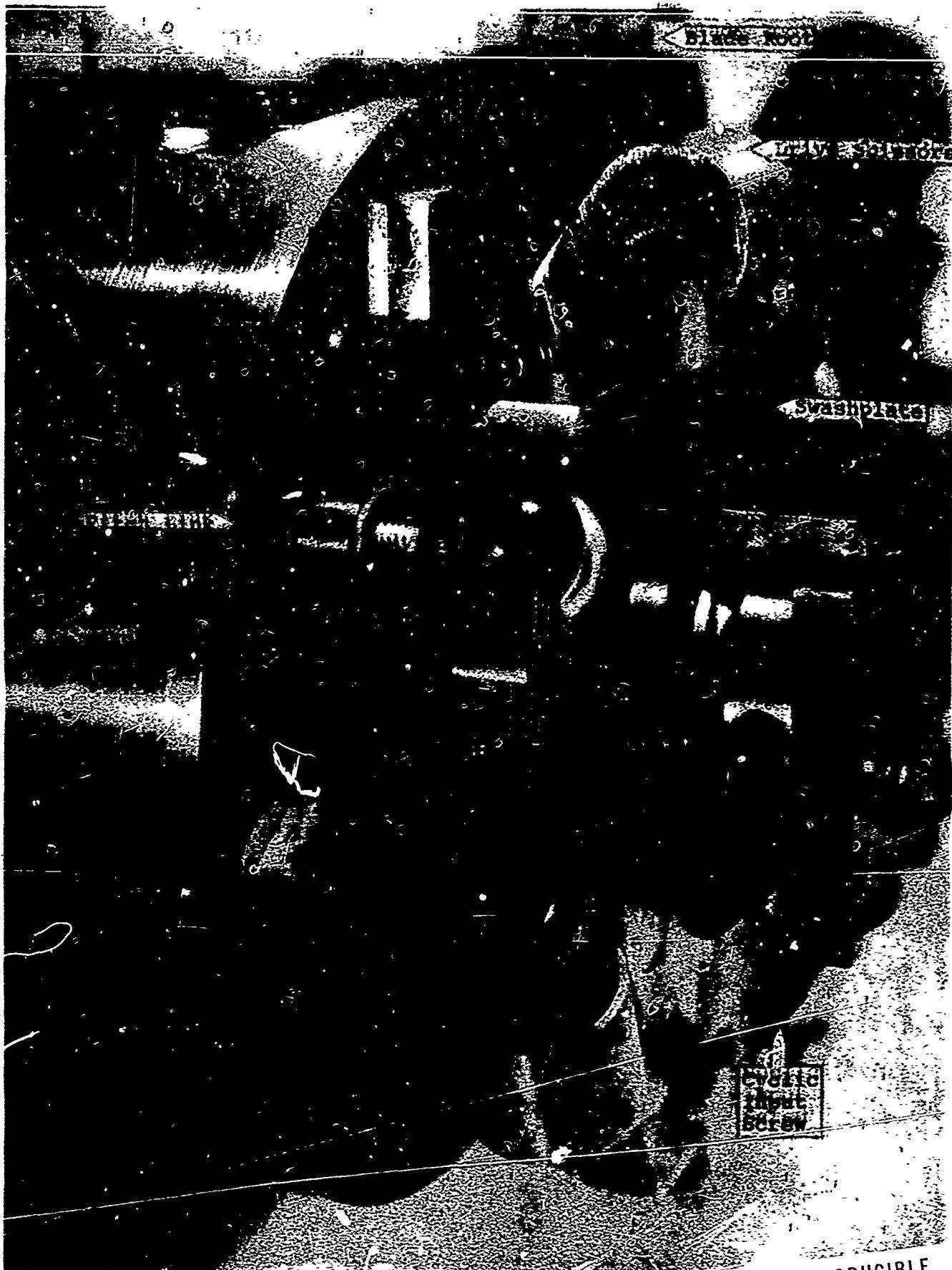
SIZE: Actual Dimensions (Untwisted)

NUMBER D17C-10039-1
REV LTR

Figure 11

EL VRO68Q
S PELLER
PLANFORM





Details of Cyclic Hub Mechanism

NOT REPRODUCIBLE

2.3 NACELLE DESCRIPTION

D170-10039-1

A schematic drawing showing the arrangement of the propeller hub, swashplate, slip ring, strain gage internal balance, and air motor in the inboard nacelle along with the geometric relationship of the wing with the nacelle and hub center is presented in Figure 13. Similar information is depicted for the outboard nacelle in Figure 14. Not shown in the two sketches is the flexible bellows coupling that joined the propeller shaft to the air motor drive shaft. This coupling, located 1.875 in. aft of the nacelle balance center, isolated propeller forces and moments.

The air motor power source, which utilizes a four stage turbine, is designed to deliver 90 shaft horsepower at 9000 RPM. At this design point, approximately 2 lb/sec of air flow is required. Compressed air was individually ducted out to the inboard and outboard air motors from the wing root thru parallel 1.125 inch diameter air passages located internally in the basic wing structure. A 90° bend was used to introduce the air into the top of the inboard motor plenum in front of the first stage turbine. The lack of sufficient wing spar material at the outboard nacelle as a result of the relatively high thrust line (See Figure 14) necessitated stopping the internal wing air passage short of the outboard nacelle and angling the air into the outboard motor plenum (45° from vertical) via a short air passage drilled into a wedge shaped piece of material which was bolted to the lower surface of the wing inboard of the outboard nacelle.

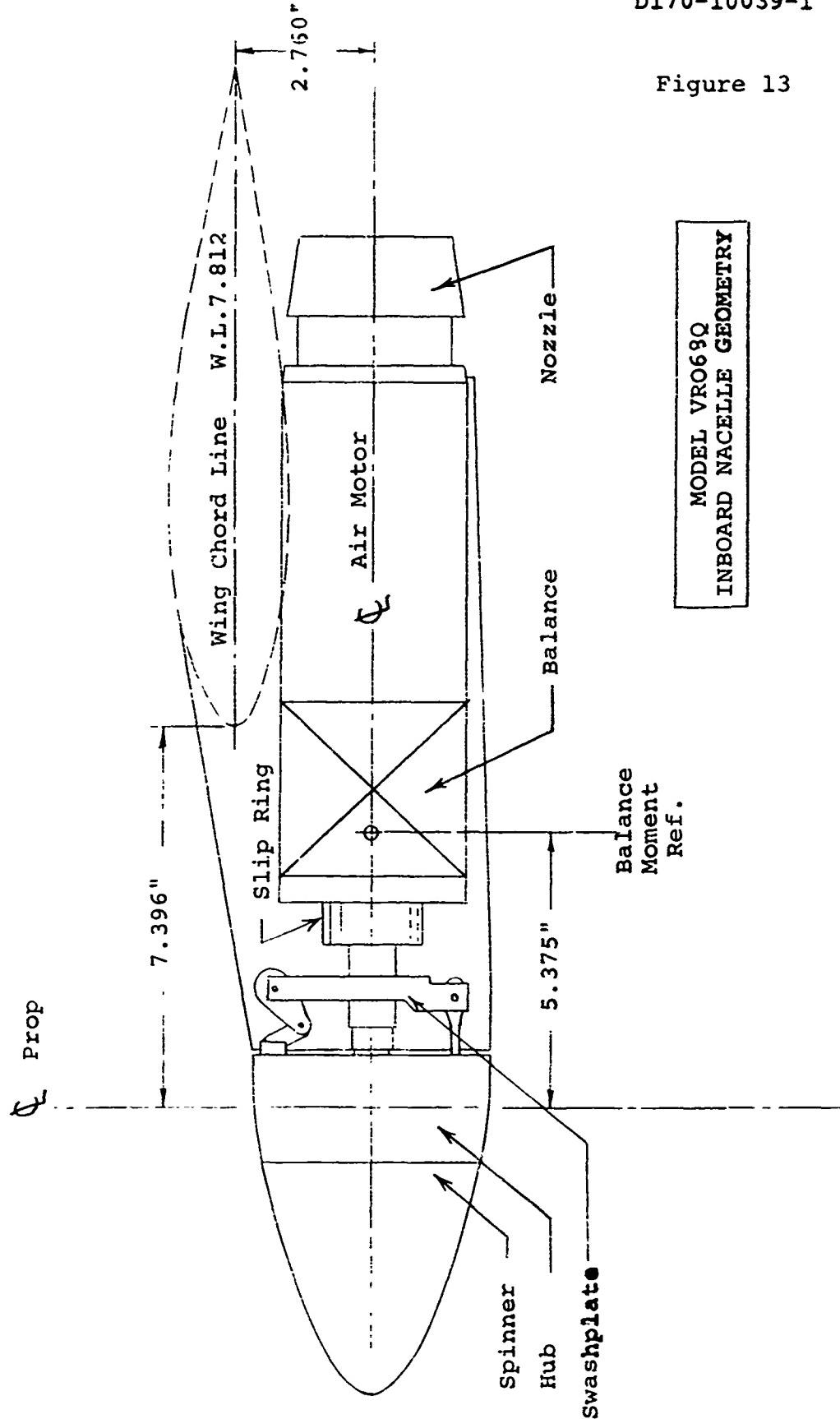
A diverging nozzle with eight straightening vanes for eliminating exhaust swirl was attached to the rear end of each motor.

The location of the propeller thrust line with respect to the wing chord plane, and the prop plane location with respect to the wing leading edge in terms of percentage of local wing chord, can be determined from the information presented in Figures 13 and 14. These values are listed below.

<u>Prop Hub #</u>	<u>Distance below wing chord plane</u>	<u>Distance ahead wing leading edge</u>
Inboard	.218 z/c	.584 x/c
Outboard	.181 z/c	.421 x/c

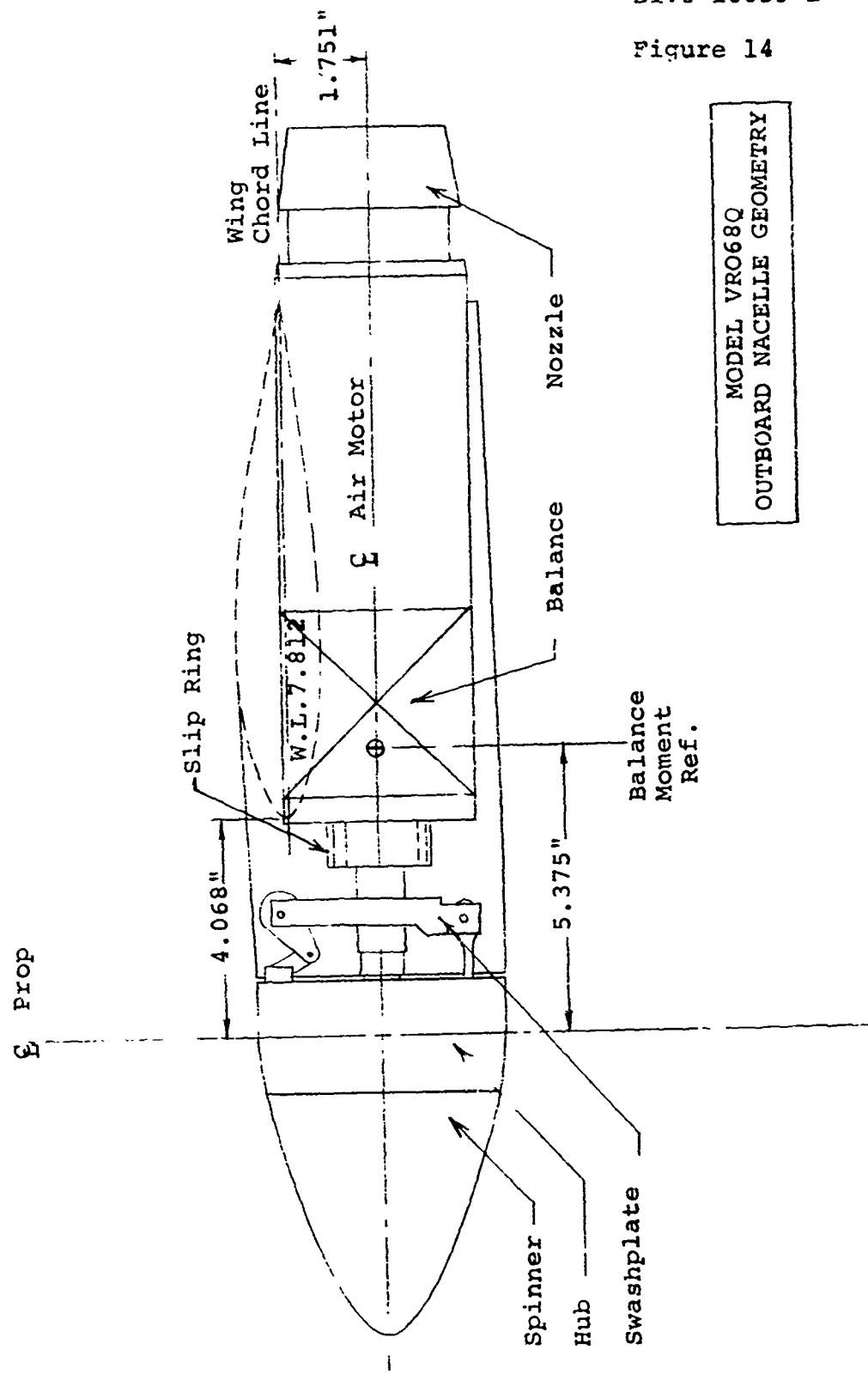
The above ratios were established using data obtained during a 1969 Boeing-Vertol semispan wind tunnel test of a four prop tilt wing model. In this test, various prop hub centerline locations with respect to the wing were evaluated to determine the effect on descent capability.

Figure 13



D170-10039-1

Figure 14



2.4 FUSELAGE GEOMETRY

The fuselage used on Model VR068Q, as shown in Figure 15, had a shape generally representative of a four propeller tilt wing transport-type aircraft designed for rear ramp loading. Body cross section was generally oval with flattened top, bottom, and sides in the vicinity of the wing. Principal dimensions of the fuselage are as follows:

Length	79.88 in.
Maximum width	13.94 in.
Maximum depth	14.85 in.

Locations of the wing and empennage are also illustrated in Figure 15. The wing was essentially buried in the down position, protruding only slightly above the fuselage crown line. At the rear of the wing center section over the fuselage, a spring loaded fairing was located. This fairing, hinged at its aft end to the top of the fuselage, was designed to slide along the top surface of the wing as the wing was tilted.

With the wing down, zero wing tilt, the fuselage/wing junctures were smoothly contoured. A fuselage cut-out was provided at the leading edge of the wing to enable the slat to extend over the wing center section as the wing was tilted.

Figure 15 shows the vertical and longitudinal locations of the fuselage balance with reference to the fuselage and wing. Note that the balance was located directly below the wing pivot.

2.5 HORIZONTAL TAIL POSITION AND GEOMETRY

The horizontal tail was positioned high on the fin as illustrated in Figure 15. An additional horizontal tail position, mid-fin, was available, however, this tail height was not utilized during Phase I test BVWT061.

Figure 16 depicts the geometry of the horizontal tail. This tail pivoted for stabilizer angular motion about a line perpendicular to the aircraft axis of symmetry and passing through the quarter chord point of its mean aerodynamic chord is shown in Figures 15 and 16. Stabilizer angles from +45° to -15° were available in 5° increments. Note in Figure 15, that with the maximum stabilizer angle of +45°, the leading edge of the root "unported" slightly.

Primary geometry characteristics of the horizontal tail are listed below.

Tail area, S_H

2.764 ft.²

Taper ratio	0.609
Aspect ratio	4.646
Tail arm, ℓ_H	4.288 ft.
Tail volume coefficient, $V_H = \frac{S_H \ell_H}{S_C}$	1.330
Dihedral	0°

2.6 VERTICAL TAIL LOCATION AND GEOMETRY

The location and geometry of the vertical tail used on Model VR068Q is shown in Figure 17. This fin, which utilized a NACA 0012 airfoil section, was positioned on the aft fuselage as illustrated in the noted figure and was swept back 40.4° (c/4 line) for the purpose of maximizing the tail arm of the horizontal tail mounted in a high position on the fin. Geometrical characteristics of interest follow.

Tail area, S_V	1.885 ft ²
Taper ratio	.518
Aspect ratio	1.271
Tail arm, ℓ_V	3.528 ft
Tail volume coefficient, $V_V = \frac{S_V \ell_V}{S_b}$.0832

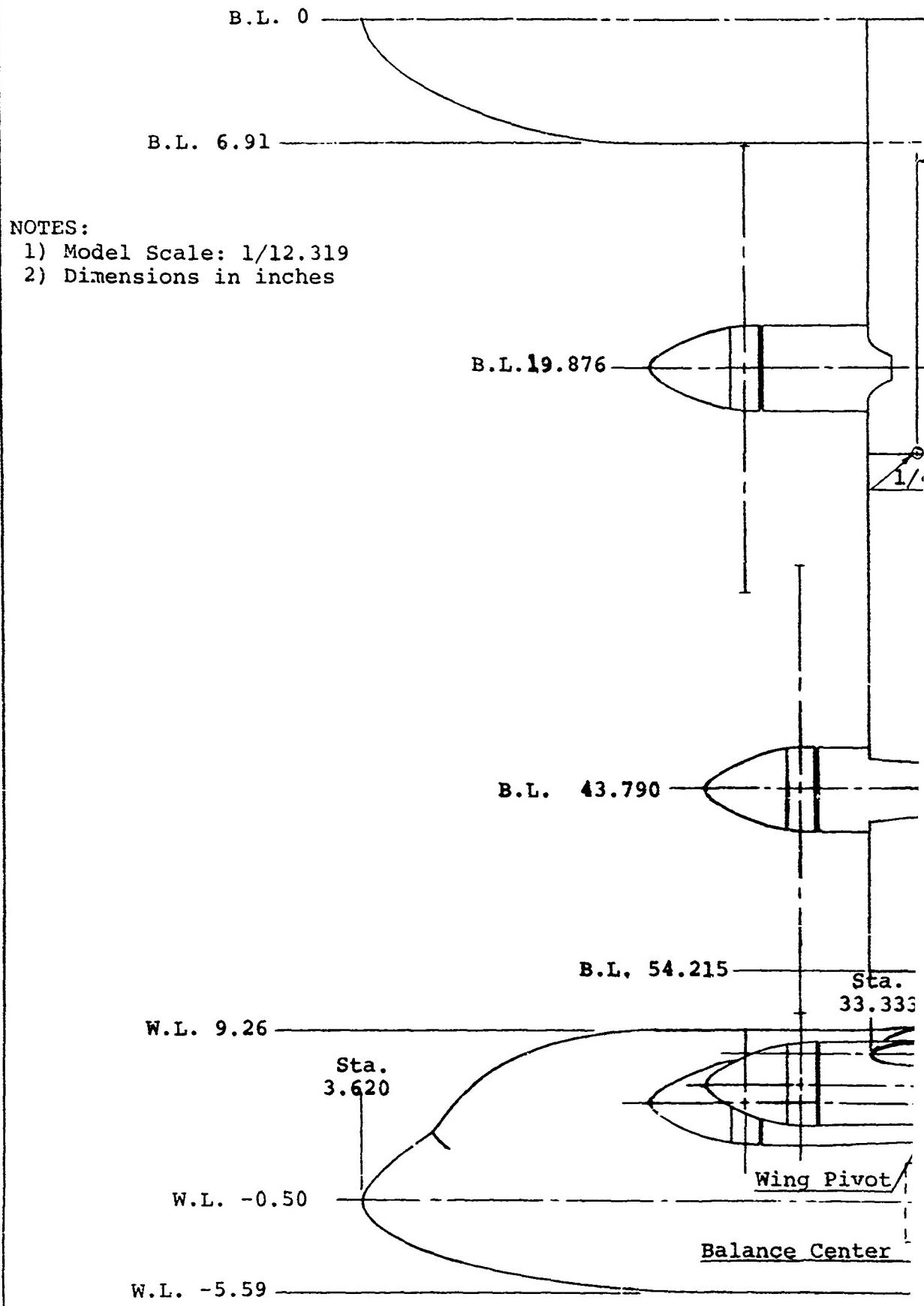


Figure 15

51.458"

MAC

1/4c

Hinge Line

B.L. 21.50

MAC

GENERAL ARRANGEMENT OF
FULL SPAN MODEL VR068Q

Sta. 38.476

W.L. 7.812
W.L. 6.402

Sta. 66.708

Sta. 78.687

MAC
1/4c

W.L. 25.490

15°

W.L. 23.035

45°

W.L. 6.91
W.L. 5.30

Sta. 83.50

W.L. -0.50

Model Sting Extension

Figure 16

MODEL VRO69Q
HORIZONTAL TAIL GEOMETRY

NOTES:

- 1) No anhedral or dihedral

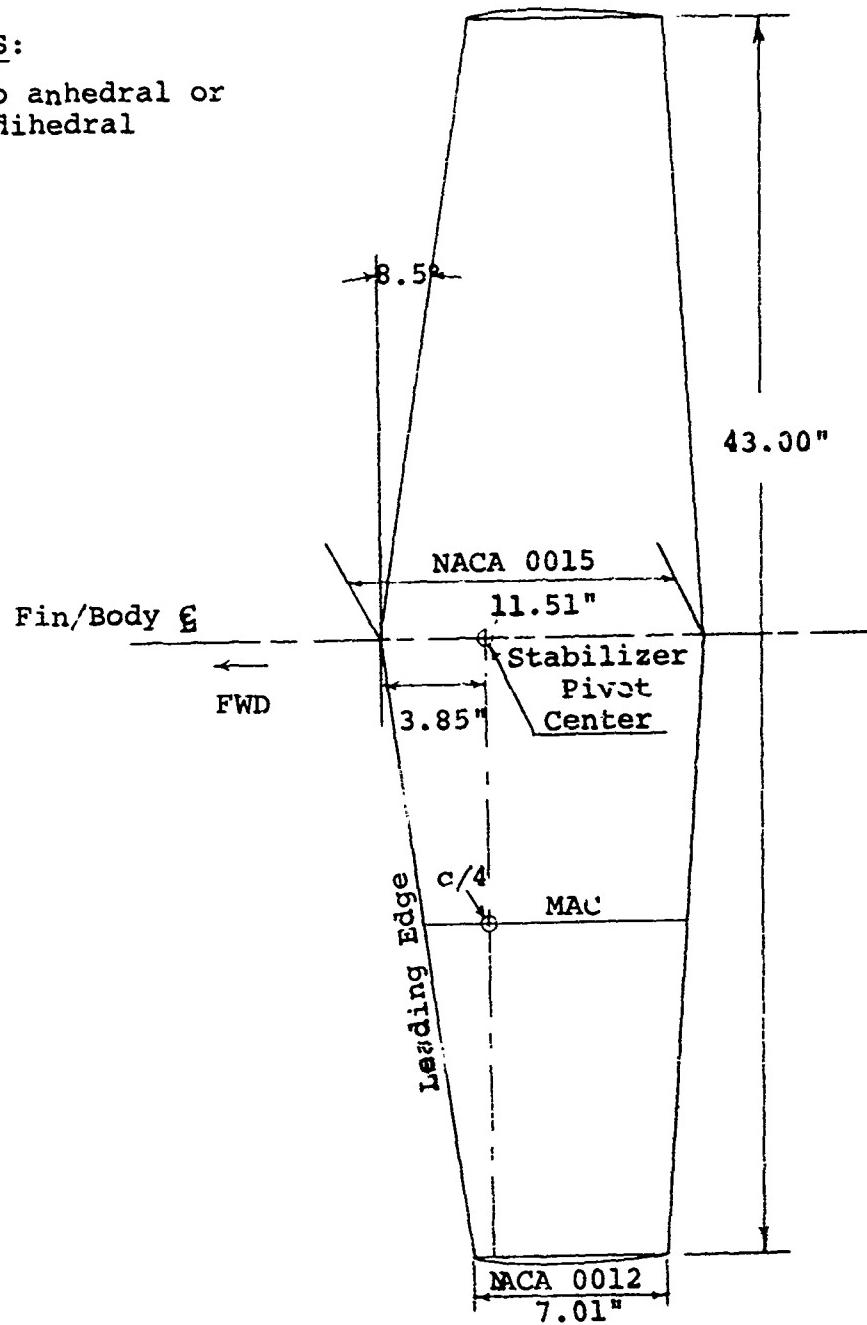
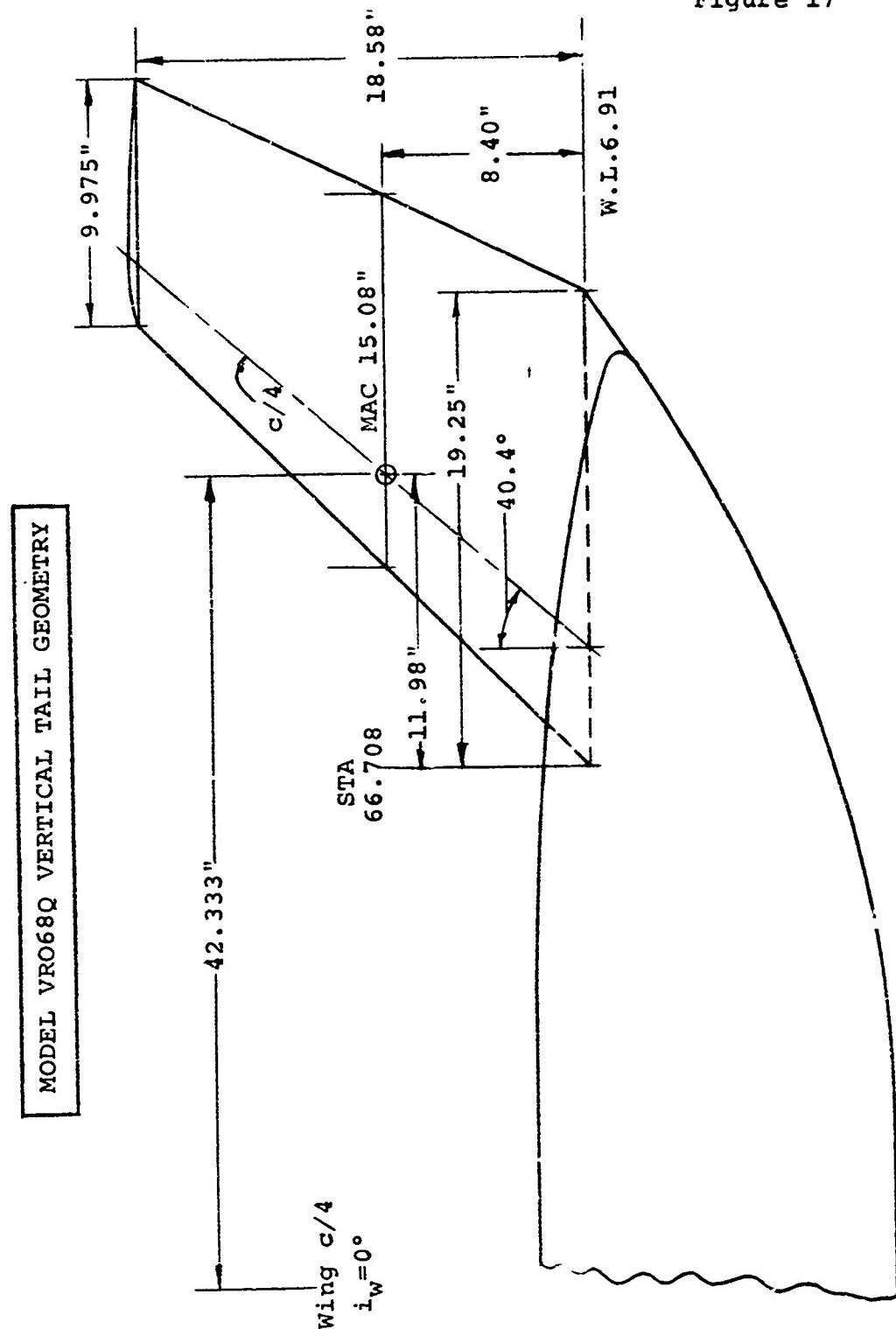


Figure 17



2.7 MODEL INSTALLATION

A schematic drawing of the model air supply system for powering the four pneumatic motors of Model VRO68Q is shown in Figure 18. High pressure air enters the model through the hollow sting extension. Interactions of the model air supply system on the fuselage balance measurements were minimized by ducting the air symmetrically past the balance from the forward section of the sting via dual ducts (one per fuselage side) and thence into a plenum chamber located forward of the balance in the frontal portion of the fuselage. A set of internal flexible bellows were used to connect the dual ducts to the plenum chamber structure.

Air for each air motor was individually ducted forward from the front wall of the plenum chamber, through separate motor control valves, and then aft over the top of the plenum chamber via four pipes which were connected to a hollow segmented air pivot joint. Four internal wing spanwise air ducts (one per motor) were used to direct the air outboard from the wing pivot joint into the forward portion of the air motors bolted directly to the wing.

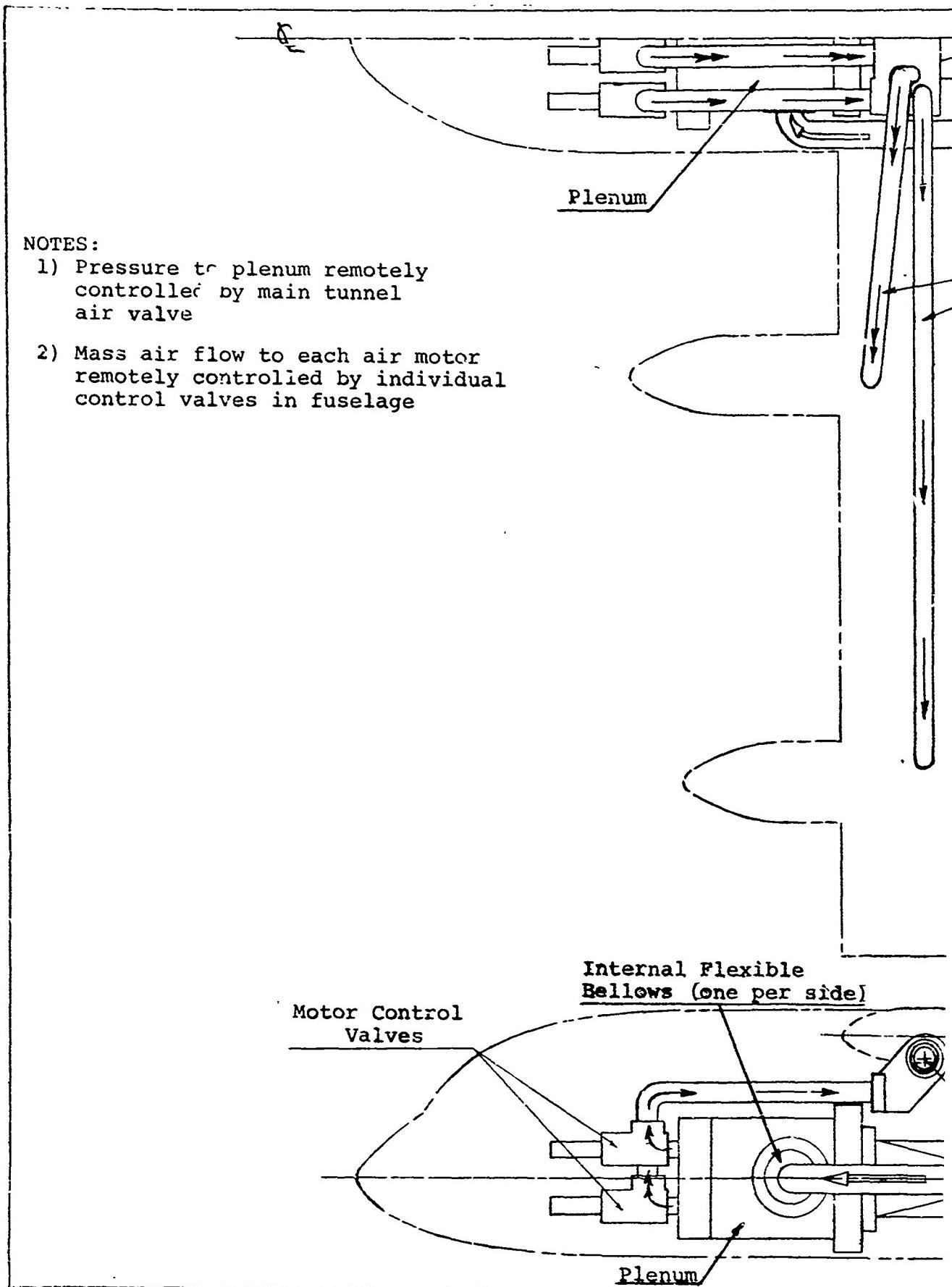
Mass flow into each motor was remotely controlled by the four individual motor control valves used in conjunction with the main tunnel compressor system controls which established the plenum chamber pressure.

Model VRO68Q utilized the main tunnel hydraulically driven sting support system. The 16 ft. long sting pivots, for model angle of attack motion, about its attachment point on a vertical moving strut, which enables the model to be retained near the center of the test section as the model is pitched. A "yaw adapter" that provides pure yawing motion for selected angles of attack, was attached to the forward end of the main sting. This "yaw adapter" also incorporates a horizontal pivot and pin arrangement for manually setting the desired "pre-bend" angle between the fuselage centerline of the model and the centerline of the main sting.

The desired wing angle of attack range for a prescribed combination of wing tilt angle and thrust coefficient was achieved by selecting the proper "pre-bend" angle. With zero "pre-bend", the available fuselage angle of attack range is -20° to +12°. The -20° angle is the limit imposed by the maximum up-travel of the vertical strut (contact with the tunnel ceiling). The maximum positive angle of the sting with respect to the tunnel centerline (+12°) results from the limit imposed by the minimum bend radius of the 3 inch diameter (I.D.) braided steel model air hose passing up the vertical strut, through the main sting and "yaw adapter", and into the tilt wing model sting extension which is bolted to the forward end of the yaw adapter.

Selection of a positive 10° "pre-bend" angle provides a fuselage angle of attack range of -10° to +22°, for example.

Figure 19 illustrates the installation of Model VR068Q on the main sting/strut assembly in the Boeing-Vertol V/STOL wind tunnel. Noted on the sketch are the locations of the pitch rotational center on the vertically moving strut and the yaw rotational center on the yaw adapter.



1 B

NUMBER D170-10039-1
REV LTR

Internal Wing
Air Ducts

MODEL R0680
SCHEMATIC DRAWING OF
MODEL AIR SUPPLY SYSTEM

Figure 18

Hollow Wing
Pivot

Balance

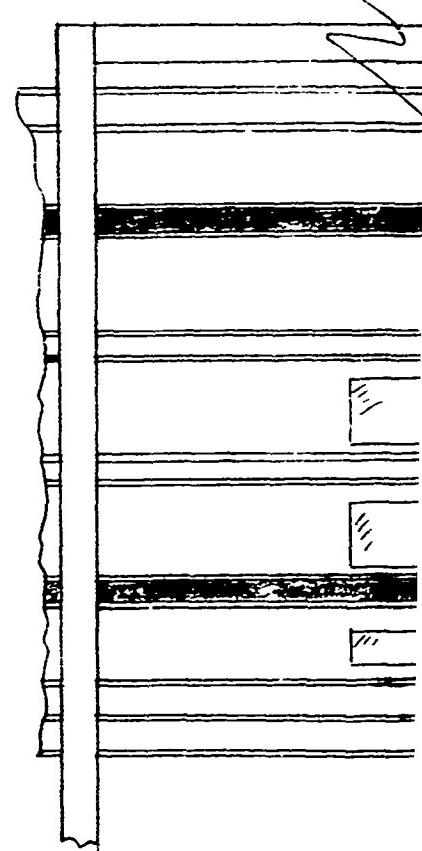
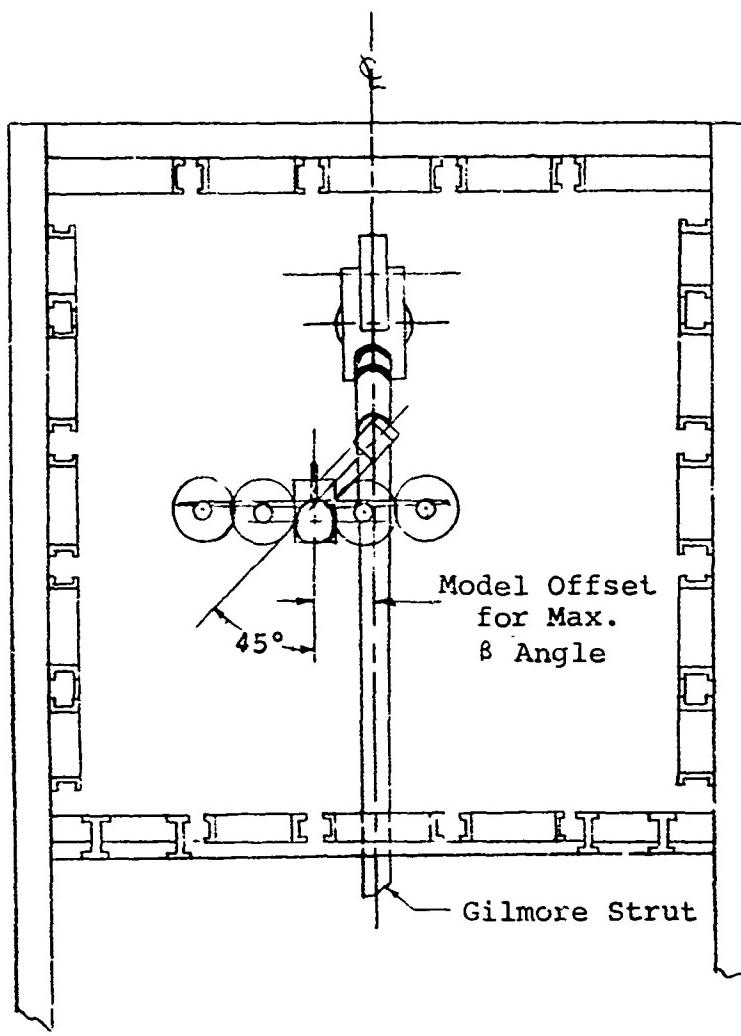
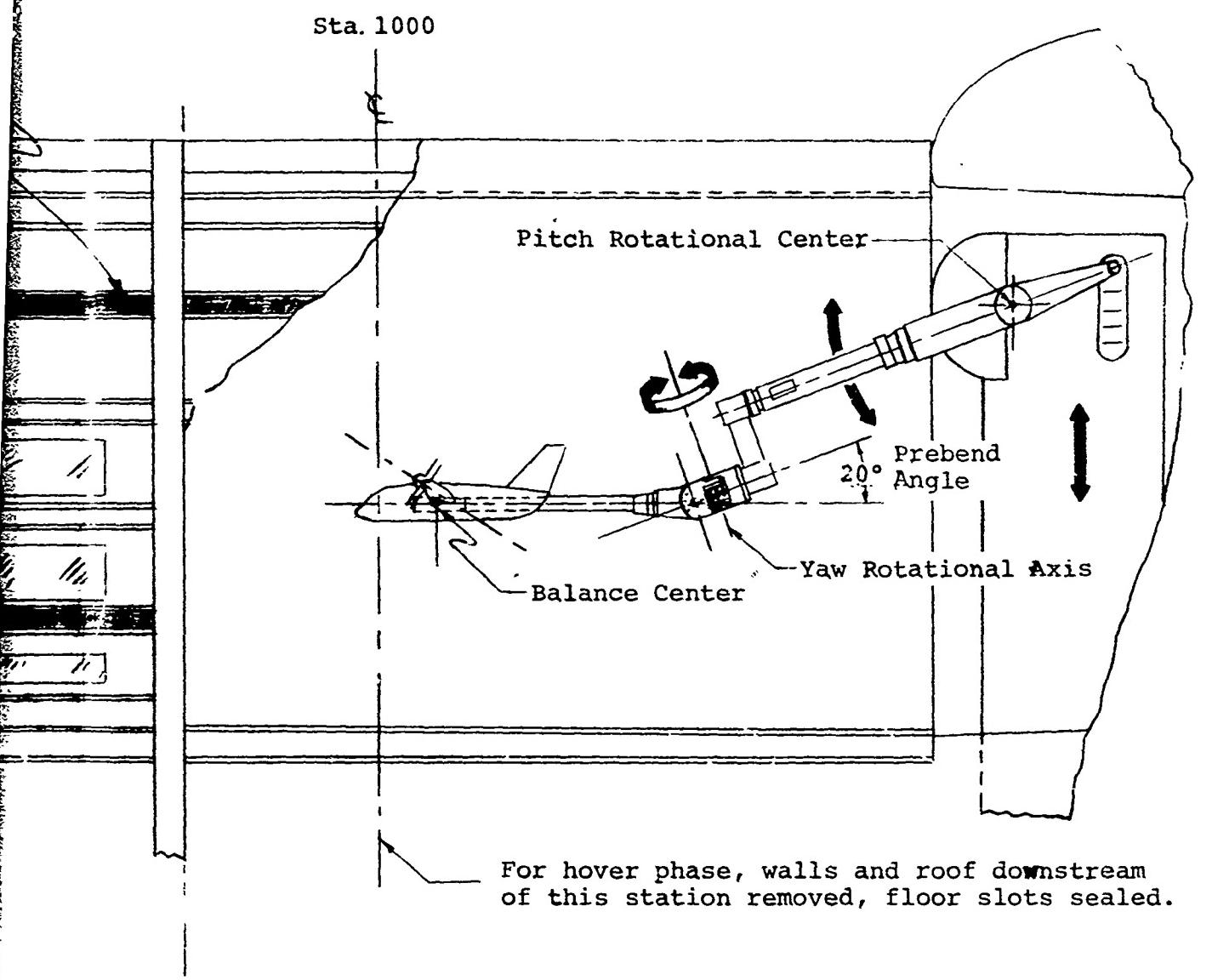


Figure 19



INSTALLATION OF MODEL VRC68Q
IN BOEING-VERTOL V/STOL WIND TUNNEL

2.8 TEST FACILITY

As mentioned previously, the test was conducted in a 20 ft high x 20 ft wide x 29 ft long test section of the Boeing-Vertol V/STOL wind tunnel. A schematic view of the facility is presented in Figure 20.

The slotted throat test section configuration was used for the transition or forward flight portion of the test. This tunnel configuration is obtained by removing covers from slots built into the test section walls, floor and ceiling. The slotted floor was replaced with the moving belt ground plane assembly for the in ground effect testing.

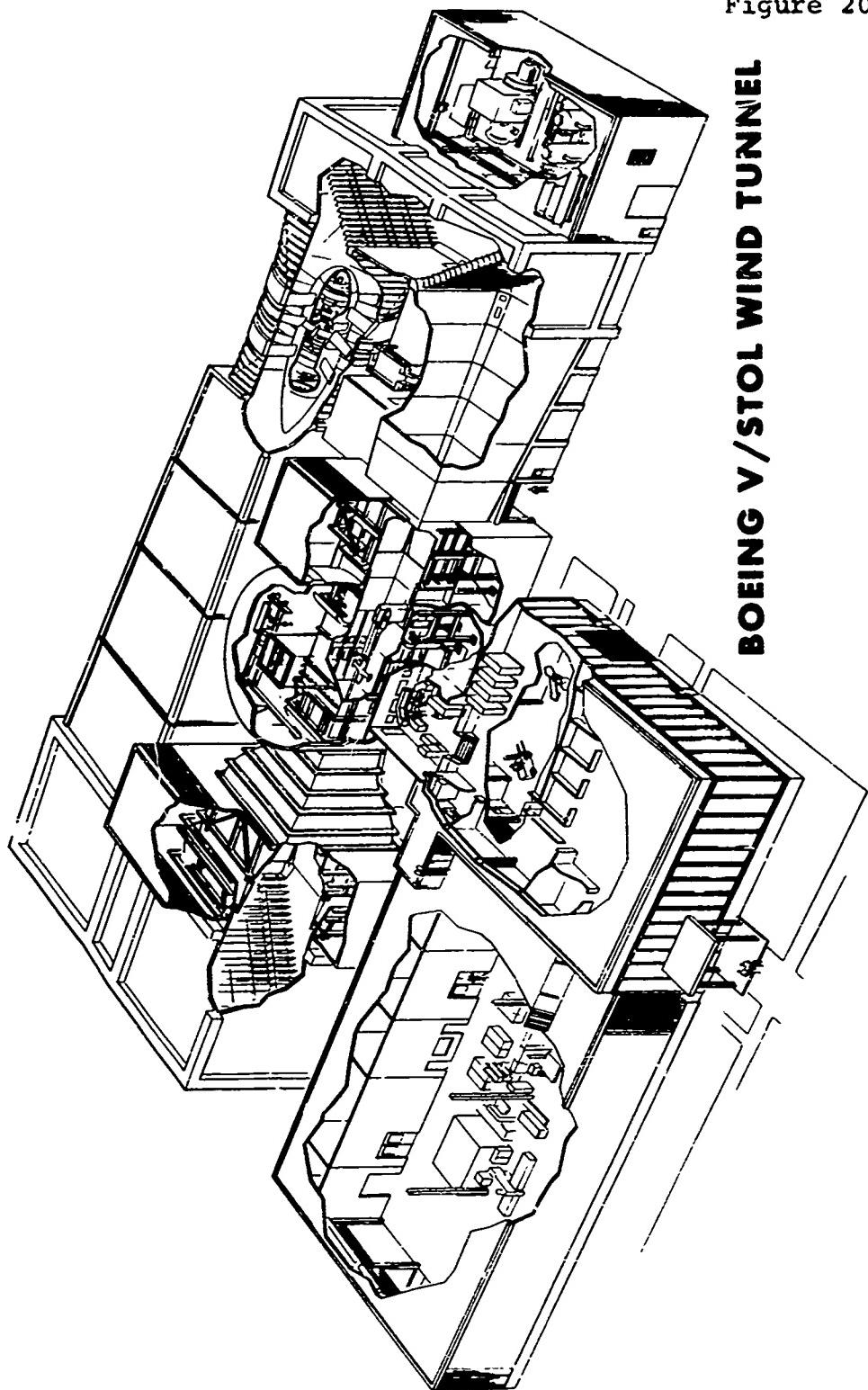
During the hover phase of the test, the 29 ft long x 20 ft high test section walls were removed and lowered into pits. The raising of the test section ceiling to the top of the 67 ft diameter plenum chamber that surrounds the test section provided a hover test area with a height, as measured from the solid test section floor used as a ground plane, of approximately 50 ft.

The auxiliary air for powering the four nacelle pneumatic motors was supplied by a 20 pound per second, 1000 psi compressor system.

D170-10039-1

Figure 20

BOEING V/STOL WIND TUNNEL



3.0 INSTRUMENTATION AND EQUIPMENT

D170-10039-1

3.1 MODEL INSTRUMENTATION

Model instrumentation consisted of the following items:

a) Six Component Strain Gage Fuselage Balance

Total aircraft normal force, axial force, pitching moment, yawing moment, rolling moment, and side force were measured by this balance, that was located with its longitudinal axis parallel to the body centerline and with the balance center directly below the wing pivot as shown in Figure 15.

b) Six Component Strain Gage Balance in Each Nacelle

Identical balances were used in the outboard and inboard nacelles and were similarly located as shown in Figures 13 and 14. Each balance measured propeller thrust, pitching moment, normal force, yawing moment, side force, and rolling moment. The rolling moment in this case was the friction torque produced by the bearings and cyclic pitch mechanism. In addition to measuring steady values, normal force, pitching moment, and propeller thrust from selected nacelles were displayed on oscilloscopes so that dynamic loads in the balance flexures could be monitored to prevent exceeding the fatigue allowables.

c) Strain Gaged Propeller Drive Shafts

Each nacelle assembly incorporated a high speed slip ring assembly for the purpose of transmitting electrical signals from the strain gage bridges measuring torque.

d) Tachometers

The rotational speed of each propeller was measured by a tachometer, installed internally behind the front bearing of the air motor. This type of tachometer worked on the pulse generator principle (thirty pulses per cycle). Four digital voltmeters were used for direct readouts following amplification of the signals.

e) Wing Tilt Angle Potentiometer

Wing tilt angle was measured using a precision potentiometer. A gearing arrangement was used to prevent potentiometer slippage due to model motions.

f) Bearing Temperature Thermocouples

Each propeller shaft thrust bearing, located in the nacelle

stack, was instrumented. The four bearing temperatures were displayed on the control panel for model condition monitoring purposes.

g) Air Passage Metering Valve Position Indication

Mass flow into each air motor was individually controlled by a metering valve. The position of these four valves was displayed on the overhead control panel as an aid in setting up the four air motors for a constant RPM operation.

h) Nacelle Balance Rolling Moment (Friction Torque)

The rolling moment signal from each of the nacelle balances was displayed in the overhead panel on one of the safety meters used for monitoring dynamic data. Any increase above the characteristically low friction torque in a cyclic hub/air motor assembly would be immediately recorded by the nacelle roll balance, permitting a rapid shut down if necessary.

3.2 DATA ACQUISITION SYSTEM

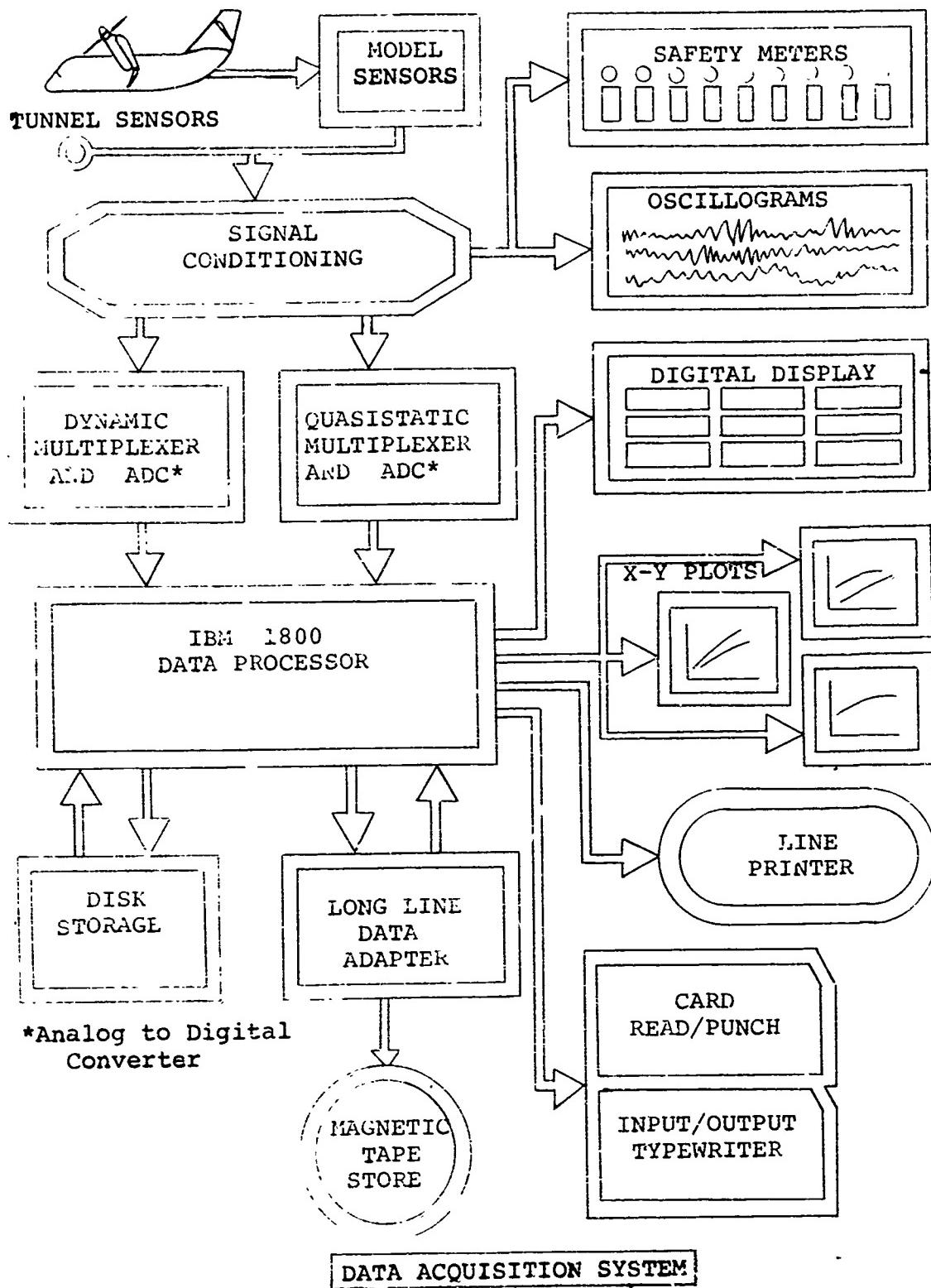
The flow diagram of the wind tunnel data system used in this test is shown in Figure 21. This data system can accept up to 120 channels from the model and the tunnel itself. These signals are routed as illustrated to an IBM 1800 computer for processing and data reduction. The computed results are tabulated by a line printer and selected quantities are plotted by the X-Y plotters. Final data is stored on magnetic tape.

A digital display of any nine channels is also available during testing for monitoring purposes. Dynamic data of six quantities can be continuously displayed on oscilloscopes. This provides assistance in preventing balance or structural limits from being exceeded.

A choice of sampling rates in terms of samples per channel/sec. and in sampling time periods is available. The sampling process is accomplished with channel switching devices called multiplexers.

D170-10039-1

Figure 21



4.0 DATA REDUCTION

At each test point, measurements were taken for computing and printing out on-line the quantities listed below.

Air supply line pressure	psi
Density, ρ	slugs/ft ³
Freestream dynamic pressure, q	lb/ft ²
Fuselage angle of attack, α_F (correction applied for sting deflection)	degrees
Sideslip angle, β	degrees
Model height, h	inches
Propeller speed (each propeller)	RPM
Shaft torque (each propeller)	ft.lbs.
Tunnel velocity, V	ft/sec
Wing tilt angle, i_w	degrees

The following aircraft forces and moments were measured by the fuselage balance.

Normal force (positive: up)	lbs.
Axial force (positive: forward)	lbs.
Pitching moment (positive: nose up)	ft.lbs.
Yawing moment (positive: nose right)	ft.lbs.
Rolling moment (positive: right wing down)	ft.lbs.
Side force (positive: to the right)	lbs.

Balance interaction corrections to these measured forces and moments were calculated and applied on-line using the balance interaction matrix incorporated into the data program. Static pressure tares, resulting from the high pressure mod... ir supply lines extending forward from the model sting extension into the plenum chamber located in the frontal portion of the fuselage, were also applied on-line. The static pressure tare curves inserted into the data program were linear and of the following magnitude at 220 psi, a typical operating line pressure in hover.

Normal force: -2.2 lbs.

D170-10039-1

Axial force: -4.5 lbs.

Pitching moment: 0 ft.lbs.

Yawning moment: +1.2 ft.lbs.

Rolling moment: 1.6 ft.lbs.

Side force: -1.4 lbs.

at each test point, the value

air motor was established by entering the jet thrust correction "look-up" tables incorporated into the computer program as a function of shaft torque. The components of jet thrust inherent in the measured values of aircraft normal force, axial force, and pitching moment were extracted on-line, as a function of wing tilt angle.

Finally, model weight tare values for a particular wing tilt/fuselage angle combination and model configuration were determined and applied on-line using the appropriate weight tare equations inserted into the data program.

Aircraft normal force and axial force from the fuselage balance were resolved on-line into the wind axis system in order to compute

Aircraft pitching moment measured by the fuselage balance was transferred on-line to the wing pivot for runs wherein wing tilt angle was varied (fuselage angle was held constant) and to an aircraft c.g. position representative of the wing tilt angle for runs wherein fuselage angle was varied (wing tilt angle held constant) or yaw angle was varied.

Aircraft forces and moments were reduced on-line to the following coefficient form based on slipstream dynamic pressure.

$$\text{Lift coefficient, } C_{L_s} = \frac{L}{q_s S}$$

Longitudinal force coefficient, $C_{X_s} = \frac{X}{q_s S}$

$$\text{Pitching moment coefficient, } C_{M_s} = \frac{M}{q_s CS}$$

(where c =MAC of tapered wing)

$$\text{Side force coefficient, } C_{y_s} = \frac{\text{Side force}}{q_s S}$$

$$\text{Yawing moment coefficient, } C_{n_s} = \frac{\text{Yawing moment}}{q_s S_b}$$

$$\text{Rolling moment coefficient, } C_{\lambda_s} = \frac{\text{Rolling moment}}{q_s S_b}$$

Aircraft lift, longitudinal force and pitching moment were also reduced on-line into the following non-dimensional form.

$$\frac{L}{qb^2}, \quad \frac{D}{qb^2} \quad (\text{positive aft for drag}), \quad \frac{M}{qb^2 c}$$

Each of the four internal nacelle balances measured the following forces and moments.

Thrust, T (positive:forward)	lbs.
Prop normal force (positive:up)	lbs.
Prop pitching moment (positive:nose up)	ft.lbs.
Prop side force (positive:to the right)	lbs.
Prop yawing moment (positive: nose right)	ft.lbs.
Prop rolling moment (same as friction torque)	ft.lbs.

A balance interaction matrix for each nacelle balance, as developed from the static calibration, was incorporated into the on-line computer program. Interaction corrections to the measured propeller forces and moments were calculated and applied using the appropriate nacelle interaction matrix. Weight tares due to the weight of the propeller/hub assembly were then calculated and corrections applied on-line.

Pitching moment and yawing moment that were measured about the balance center were transferred to the hub so that hub moment coefficients could be calculated at the plane of the propeller. The following propeller-type coefficients were computed and printed out on-line for each of the four propellers.

$$\text{Advance ratio, } J = \frac{V}{nD}$$

$$\text{Thrust coefficient, } C_T = \frac{T}{\rho n^2 D^4}$$

Prop pitching moment coefficient,

$$C_{M_p} = \frac{\text{Prop pitching moment}}{\rho n^2 D^5}$$

D170-10039-1

$$\begin{aligned}\text{Prop shaft power coefficient, } C_p &= \frac{\text{Shaft power}}{\rho n^3 D^5} \\ &= \frac{2\pi(\text{Shaft torque})}{\rho n^2 D^5}\end{aligned}$$

$$\text{Prop normal force coefficient, } C_{NF_p} = \frac{\text{Prop normal force}}{\rho n^2 D^4}$$

$$\text{Prop side force coefficient, } C_{SF_p} = \frac{\text{Prop side force}}{\rho n^2 D^4}$$

$$\text{Prop yawing moment coefficient, } C_{YM_p} = \frac{\text{Prop yawing moment}}{\rho n^2 D^5}$$

Friction power coefficient,

$$C_{P_F} = \frac{2\pi(\text{Balance rolling moment})}{\rho n^2 D^5}$$

Coefficients of prop thrust, prop pitching moment, and prop normal force in slipstream notation were also calculated and printed out on-line for each propeller per the following listing.

$$\text{Thrust coefficient, } C_{T_s} = \frac{T}{q_s A_p}$$

$$\text{Prop pitching moment coefficient, } C_{MP_s} = \frac{\text{Prop pitching moment}}{q_s S c}$$

Prop normal force coefficient,

$$C_{NF_s} = \frac{\text{Prop normal force}}{q_s S}$$

where $q_s = q + T/A_p$

Full scale aircraft rate of descent in ft/min and velocity in knots were computed on-line at each test point by the following equations inserted in the data program.

$$R/D = 60 \left(\frac{D}{qb^2} \right) \cdot \sqrt{\frac{2W}{\rho b^2}} \cdot \sqrt{\frac{1}{\left[\left(\frac{L}{qb^2} \right)^2 + \left(\frac{D}{qb^2} \right)^2 \right]^{3/2}}}$$

$$V_F = .592 \sqrt{\frac{2W}{\rho b^2}} \left(\frac{qb^2}{L} \right)$$

The weight term used in the above equations was commensurate with a typical full scale tilt wing aircraft operating at its maximum gross weight in the "V" mode which corresponded to a wing loading (W/S) of 66 lb/ft². This value was increased to 73.5 lb/ft² to account for the difference between the average tunnel density used in the above equations ($\rho = .00228$ slugs/ft³) and the typical atmospheric design conditions of 3000 ft/90°F ($\rho = .00204$ slugs/ft³) for a full scale tilt wing.

The following equation was used in the data program to compute propeller induced velocity, w , in ft/sec.

$$w^4 + w^3 \cdot 2V \cos i_w + w^2 V^2 = \left(\frac{T}{2\rho A_p} \right)^2$$

The above parameter was used to determine the effective wing angle of attack, α_w^{EFF} , at buffet onset. This angle is defined as the angle between the wing chord and the resultant velocity at the wing. The resultant velocity was obtained by adding vectorially, the tunnel velocity and the induced velocity at the leading edge of the wing, assuming full contraction of the propeller wake at the wing leading edge.

Three wind tunnel X-Y plotters were used to produce on-line plots of the following during pitch sweeps.

Force polars in terms of C_{L_s} vs C_{X_s}
or L/qb^2 vs D/qb^2

Lift curves in terms of C_{L_s} vs α_f
or L/qb^2 vs i_w

Pitching moment curves in terms of $M/qb^2 c$ vs i_w
or C_{M_s} vs α_f

During yaw sweeps these plotters were used to develop the following on-line plots.

Yawing moment curves in terms of C_{n_s} vs β
Rolling moment curves in terms of C_{l_s} vs β
Side force curves in terms of C_{y_s} vs β

No tunnel wall corrections were applied to the data.

5.0 TEST PROCEDURE AND TEST CONDITIONS

5.1 TEST PROCEDURE

The fuselage and four nacelle strain gage balances were checked statically with the model built-up and installed in the test section (i.e., plumbing was installed and the nacelles were assembled) by applying known forces and moments on each balance. These applied forces and moments were compared to those calculated and printed out on-line, via the computer, using the prime balance sensitivities developed during the previous Phase I test of the same model. The resultant calibration checks confirmed the established balance calibrations and showed that sensitivity adjustments were required in only a couple channels of the four nacelle balances. Balance interaction matrices utilized in the on-line computer program were those developed for the Phase I test and included in the case of the fuselage balance interaction matrix, the constraining effect of the plumbing for the air motors.

The installed model was then statically pressurized in increments to determine the effect on the measured forces and moments from the fuselage balance, of the high pressure air lines extending forward from the sting, across the fuselage balance, and into the plenum chamber located in the nose of the fuselage. Static pressure tares developed from this calibration were incorporated into a look-up routine in the data program so that corrections could be applied on-line to forces and moments sensed by the fuselage balance.

Sting deflections due to the net vertical force (lift minus model weight) acting on the model were established by hanging known weights on the model and measuring the true fuselage angle of attack with an inclinometer. The resultant correction curve, showing incremental fuselage angle of attack as a function of net vertical force, was inserted into the computer program so that the indicated fuselage and wing angle of attack could be adjusted on-line to true values.

Due to the different resultant stiffnesses of the inboard and outboard nacelle when mounted on the model, it was necessary to dynamically balance each of the propeller/hub assemblies in place on the wing. The balancing target in each case was $\pm 10\%$ of the allowable fatigue load for nacelle balance pitching moment and normal force, which were monitored via oscilloscope displays during the test.

The jet thrust produced by each air motor was determined by individually running each motor in place on the model with a cylindrical cross section "propeller" installed and zero

tunnel q. This tubular "propeller" was utilized so that the air motor torque could be absorbed without the simultaneous production of propeller thrust. The calibration curves as obtained from resolving fuselage balance yawing moment are presented in Figure 22, as a function of shaft torque. These curves, which are in agreement with the corresponding calibration curves developed during the Phase I test (see Figure 20 of Reference 1 test report), were incorporated into the computer program so that the jet thrust produced by each motor could be extracted on-line as a function of wing tilt angle from the forces and moments measured by the fuselage balance.

Of interest is the variation of shaft torque with RPM^1 during the jet thrust calibration runs, the data for which is shown in Figure 23. Since the cylindrical tube prop operates in the static condition at basically a constant torque coefficient (Reynolds number effects on drag coefficient excluded), the variation of shaft torque should be approximately linear with RPM^2 . In addition, as a result of utilizing the same tubular prop for the various calibration runs, the same shaft torque should have been recorded at a particular RPM on each of the calibrations runs. The data shown on Figure 23 is in general agreement with these comments, however, a comparison of this figure with the similar Figure 169 presented in Appendix B of the Phase I test report will show that at 5000 RPM, a typical propeller operating speed, the shaft torque measured for the the Phase II test was 8.5% greater. Of this 8.5% value, 5% is accounted for by the higher air density prevailing during the Phase II air motor calibration runs and the remaining 3.5% is accounted for by the higher calibration sensitivities obtained during the Phase II test when the instrumented shafts were calibrated in place on the assembled model with the aid of a special calibration fixture used to lock the air motor.

Two separate sets of propeller hub assemblies (collective hubs and cyclic pitch hubs that were designed for the 4500-5000 RPM operating regime) are available for Model VRO68Q, both of these being used during the Phase I test program. Since the majority of the data runs planned for the Phase II test program were directly involved with investigating cyclic pitch inputs, the primary exception being the testing devoted to establishing the lateral/directional stability characteristics in transition, a decision was made to conduct the entire Phase II test with the cyclic pitch hub assemblies. A decision otherwise would have necessitated the dynamic balancing plus thrust balancing of two separate hub assemblies and interchanging the hub systems several times during the program to match the different modes of testing.

Prior to performing the actual data runs with the propeller hub assemblies installed, it was necessary to balance the thrusts from the four propellers. This procedure was straightforward in the initial hover portion of the test, wherein the collective blade angle of each propeller was manually adjusted until the maximum thrust difference between propellers was within 1% of the total thrust from the four propellers. A total propeller thrust of 241 lbs. was developed with 5000 RPM and an average blade angle of 12.5° for the out of ground effect hover condition. This thrust level compares to a Phase I test value of 230 lbs. for the same condition. During the forward flight portion of the test, it was necessary to examine the thrust balance at the tunnel dynamic pressures and representative wing tilt angles for which data was to be acquired and adjust the collective settings accordingly.

Weight tares were taken for each significant model configuration. Subsequent to the incorporation of the weight tare data into the on-line data program, wind-off data points were acquired at a couple of model angles to ensure that the weight tare routine was accurately functioning.

As mentioned previously, test BVWT 067 was performed using three different tunnel test section configurations: (1) walls/ceiling removed and solid floor for the hover portion, (2) slotted walls/ceiling/floor for the forward flight transition portion, and (3) slotted walls and ceiling/moving belt ground plane for the in ground effect testing.

In the hover runs, ground height was varied, with the wing tilt angle being held constant at 90° and fuselage angle at zero degrees. Five values of model height above the tunnel floor were preselected, with the height measured vertically from the plane of the outboard propeller. These heights corresponded to 4.0, 2.0, 1.5, 1.25, and 1.0 propeller diameters.

A dynamic problem has been experienced on sting mounted Model VRO68Q operating in the hover mode with the wing tilted at 90°, that resulted in a scatter of the yawing and pitching moment data. The distance from the center of the fuselage balance to the tunnel sting pivot on the vertical strut was over 25 ft. This problem, which manifested itself in a long period random-type model oscillation (approximately 10 second period), was largely circumvented by increasing the time period for data sampling to 10 seconds and averaging the moments from a minimum of three data points at the most dynamically critical test conditions.

Three separate test procedures were used during the forward flight transition portion of the test: (1) wing tilt angle

pitch sweeps with the fuselage level for the descent performance runs, (2) fuselage angle pitch sweeps with a fixed wing tilt angle for the longitudinal stability and control runs, and (3) yaw angle sweeps with wing tilt angle and fuselage angle fixed for the lateral/directional stability and control runs. The model was offset laterally in the test section with respect to the tunnel centerline by turning the "dogleg" sting adapter 45° (See Figure 19). This offset enabled large sideslip angles to be attained when the model was yawed to the left. Transition runs, both longitudinal and lateral/directional runs, were conducted with a constant tunnel q and propeller RPM (except the zero thrust coefficient, C_{T_s} , runs, wherein propeller RPM was reduced as the model was pitched to maintain zero propeller thrust).

For the in-ground effect testing, the slotted test section floor was lowered, then stowed, and the moving ground belt floor was installed in its place. The electrically driven belt was adjusted in velocity via the belt speed control mounted in the console. Belt speed was matched to the tunnel speed displayed in fps on the overhead test monitor panel (data is transmitted into the test monitor from on-line data computations and then is transcribed into digital form). Actual belt velocity in fps was also digitally displayed on a direct readout counter. The electrical pulses into this counter were generated by a magnetic pickup (320 tooth gear) mounted on the belt follower.

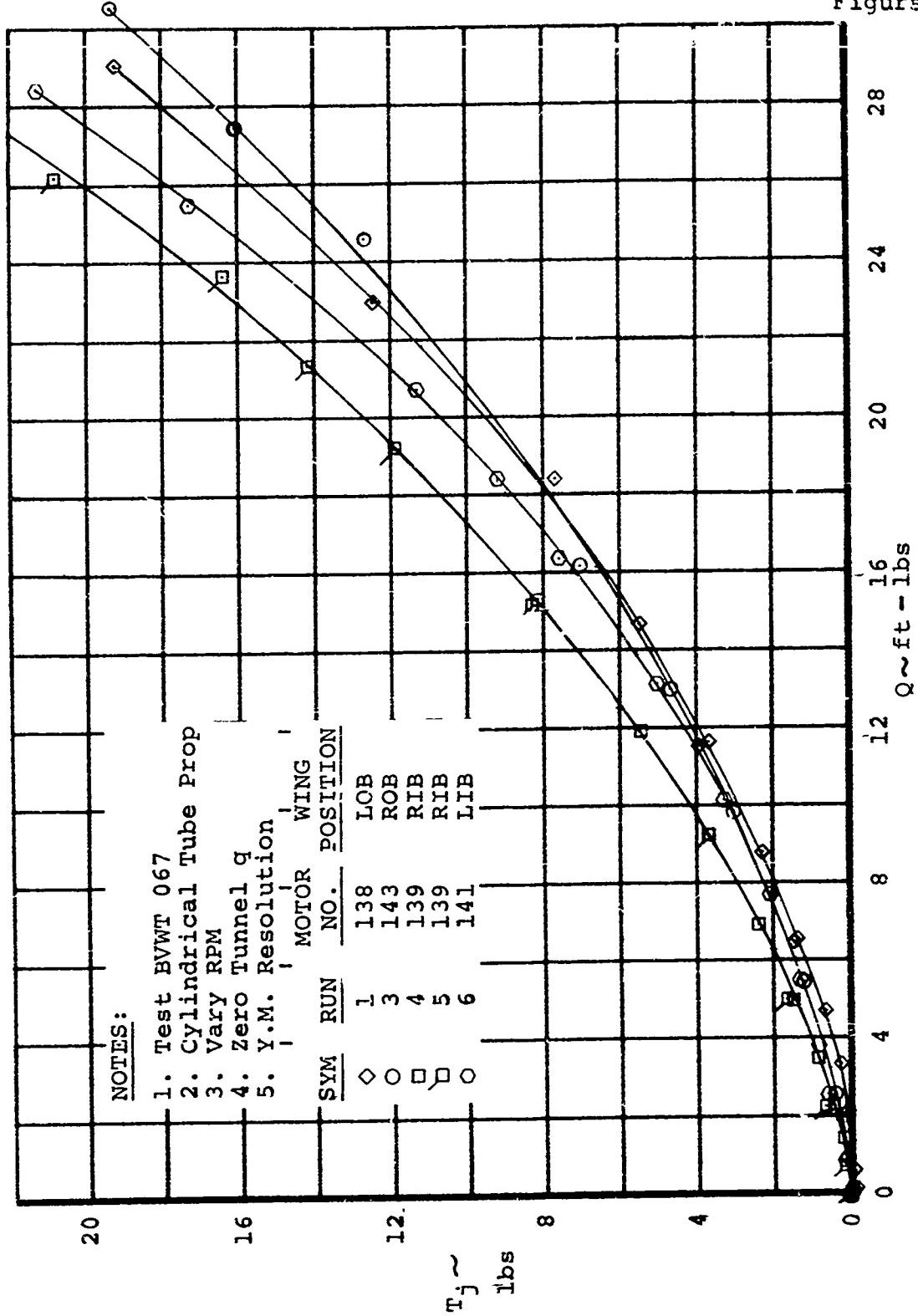
In-ground effect testing was performed with a level fuselage at a fixed ground height representative of a flight condition with the wheels 3 ft. off the ground. Since model pitching (fuselage angle pitching) is limited with a sting mounted model operating in proximity to the moving ground belt and since longitudinal characteristics were desired over a large wing angle range, pitch data was obtained using wing tilt angle sweeps. Lateral/directional testing was conducted using yaw sweeps and zero prebend angle to preclude rolling the model as the model was yawed (this would occur as a result of the yawing axis on the sting being located aft of the prebend rotational center - see Figure 19).

Maximum tunnel dynamic pressure utilized during test BVWT 067 occurred during the zero thrust runs. The lowest tunnel q used ($1.0q_1$) was that that could be achieved with reasonable accuracy. This q value established the maximum test value of C_{T_s} . Tunnel dynamic pressures between these two extremes were selected to achieve the desired spread of C_{T_s} values.

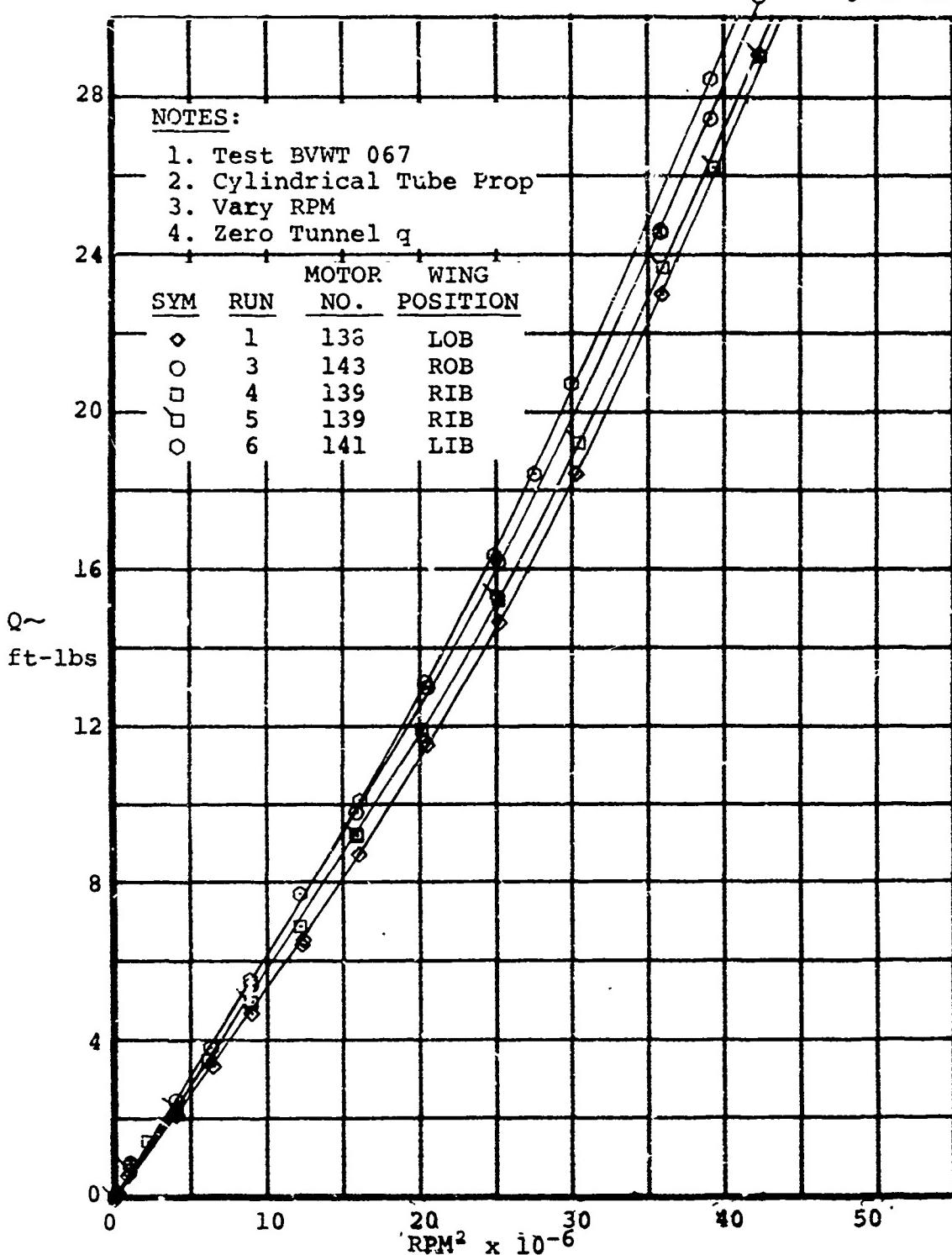
Throughout the test, dynamic loads as measured by the nacelle

D170-10039-1

balances (pitching moment and normal force from the four propellers and thrust of two of the propellers) were continuously monitored via oscilloscope presentations to ensure that fatigue loads inside the four nacelles were not exceeded. The drive shaft bearing temperatures in each of the nacelles and nacelle rolling moment (friction torque) were also continuously monitored to prevent running with overheated or damaged bearings.



AIR MOTOR JET THRUST CALIBRATIONS



VARIATION OF SHAFT TORQUE
DURING JET THRUST CALIBRATIONS

5.2 TEST CONDITIONS

Tabulations on the following pages summarize the data runs performed during the subject test (BVWT 067) in terms of key test variables. The runs have been arranged in sets according to test objectives. Air motor jet thrust calibrations runs and thrust balancing runs required for "setting-up" the model, have been deleted from the listings. All data runs were performed with the P1,2 prop rotation (props turning down between the nacelles).

The range of slipstream thrust coefficient evaluated during the forward flight longitudinal stability and control testing with cyclic pitch varied from 0.27 C_{Ts} to a maximum C_{Ts} of 0.93. This testing was phased so that the longitudinal stability and trim with the smaller wing tilt angles (15°) was examined at the low end of the C_{Ts} spectrum and large wing tilt angles (up to 55°) were examined at the high end. Cyclic pitch inputs were similarly phased with the largest cyclic angles being investigated at the highest C_{Ts} values where cyclic control requirements are a maximum. Lateral/directional stability testing was conducted in a similar manner.

D170-10039-1

BVWT 067
 RUN SUMMARY
 HOVER

RUNS	CYCLIC ANGLE	FLAP ANGLE LEFT/RT WING/WING	SPOILER ANGLE LEFT/RT WING/WING	OBJECTIVE
10/11	0	0/60°	0/0	Yaw Control
12		✓	60°/0	
13	↓	-40°/60°	↓	
14/15	+6°	0/60°	↓	Effect of Cyclic on Yaw Control
16	-6°	✓	↓	✓
17	+6°	0/0	0/0	Effect of Tail on Cyclic Control

NOTES:

1. Wing tilt angle: 90°
2. Ground height varied for each run
3. Average collective setting with cyclic hubs: 12.5°
4. Slats retracted
5. Propeller speed: 5000 RPM

BVWT 067
LONGITUDINAL RUN SUMMARY
FORWARD FLIGHT (TRANSITION)

RUN	i_w	FLAP ANGLE	STAB ANGLE	CYCLIC ANGLE	RPM	NOM C _{Ts}	OBJECTIVE
21	Vary	60°	---	+4°	5000	.85	Low Speed
22			---			.75	Descent
23			---			.58	Capability
24			---			.37	
25			---	+6°	5000	.85	
26			---			.75	
27			---			.58	
173			---		4500	.58	

NOTES:

1. Wing tilt angle sweeps
2. Full span slat setting: Q*, 10, 10, *
3. Average collective setting with cyclic hubs: 12.8°
4. Zero fuselage angle
5. Horizontal tail off

D170-10039-1

BVWT 067
 LONGITUDINAL RUN SUMMARY
 FORWARD FLIGHT (TRANSITION)

RUNS	i_w	FLAP ANGLE	STAB ANGLE	CYCLIC ANGLE	RPM	NOM C_{T_s}	OBJECTIVE
31 33 39	15° ↓	60° ↓	5° ↓	0 +4° -4°	5000 ↓	.30 ↓	Cyclic Pitch Control/Tail On
30 32 38	15° ↓		5° ↓	0 +4° -4°		.45 ↓	
50 35/61 37/70	30° ↓		15° ↓	0 +4° -4°		.55 ↓	
51 34/60 36/69	30° ↓		15° ↓	0 +4° -4°		.70 ↓	
52 54 171 65 169A	45° ↓		35° ↓	0 +4° +6° -4° -6°	4500 5000 4500	.81 ↓	
53 55 170 66 169	55° ↓		35° ↓	0 +4° +6° -4° -6°	5000 4500 5000 4500	.93 ↓	

NOTES:

1. Fuselage angle sweeps
2. Average collective setting with cyclic hubs: 12°

D170-10039-1

BVWT 067
LONGITUDINAL RUN SUMMARY
FORWARD FLIGHT (TRANSITION)

RUNS	α_w	FLAP ANGLE	STAB ANGLE	CYCLIC ANGLE	RPM	NOM C_{T_s}	OBJECTIVE
47	15°	60°	---	0	5000	.30	Cyclic Pitch Control/Tail Off
43			---	+4°			
42			---	-4°			
48	30		---	0		.55	
58			---	+4°			
67			---	-4°			
49	45°		---	0		.81	
59			---	+4°			
71			---	+6°			
68			---	-4°			
40	15°	60°	0°	-4°	5000	.30	Stabilizer Control with Cyclic
39			+5°				
41			+10°				
42			---				
45			0°	+4°			
111			+5°		4500		
46			+10°		5000		
43			---				
64	30°		+5°	-4°		.55	
63			+10°				
37/70			+15°				
67			---				
57			+5°				
56			+10°				
35/61			+15°				
58			---				

NOTES:

1. Fuselage angle sweeps
2. Average collective setting with cyclic hubs: 12°

D170-10033-1

BVWT 067
LATERAL/DIRECTIONAL RUN SUMMARY
FORWARD FLIGHT (TRANSITION)

RUN	i_w	FLAP ANGLE	STAB ANGLE	CYCLIC ANGLE	RPM	NOM C_{T_s}	OBJECTIVE
94 95	0 ↓	0 ↓	---	0	5000	0 .20	Stability. Empennage Off
96 97	0 ↓	40° ↓				0 .20	
98 99 100	15° ↓	60° ↓				.25 .50 .70	
101 102 103	30° ↓	60° ↓				.55 .70 .81	
104 105	45° ↓	60° ↓	↓	↓	↓	.81 .92	↓

NOTES:

1. Yaw angle sweeps
2. Zero fuselage angle
3. Vertical/horizontal tails off
4. Average collective setting with cyclic hubs: 12°

D17C-10039-1

BVWT 067

LATERAL/DIRECTIONAL RUN SUMMARY
FORWARD FLIGHT (TRANSITION)

RUN	i_w	FLAP ANGLE	STAB ANGLE	CYCLIC ANGLE	RPM	NOM C _{Ts}	OBJECTIVE
92	0 ↓	0 ↓	0 ↓	0	5000	0	Stability/ Empennage On
93						.20	
85	0 ↓	40° ↓	0 ↓			0	
86						.20	
76	15° ↓	60° ↓	+10° ↓			.25	
77						.50	
78						.70	
87	30° ↓	40° ↓	+15° ↓			.55	
88						.70	
89						.81	
79	30° ↓	60° ↓	+15° ↓			.55	
80						.70	
81						.81	
82	45° ↓	60° ↓	+25° ↓			.81	
83						.92	
84	55° ↓	60° ↓	+35° ↓			.93	
90	0 ↓	40° ↓	---	↓		0	Stability/"T"
91			---			.20	Horizontal Tail Off

NOTES:

1. Yaw angle sweeps
2. Zero fuselage angle
3. Vertical tail on
4. Average collective setting with cyclic hubs: 12°

BVWT 067
LATERAL/DIRECTIONAL RUN SUMMARY
FORWARD FLIGHT (TRANSITION)

RUN	i_w	FLAP ANGLE	STAB ANGLE	CYCLIC ANGLE	RPM	NOM C_{T_S}	OBJECTIVE
106 107 117 118	15° ↓	60° ↓	+10° ↓	+4° ↓ -4° ↓	4500 ↓	.25 .50 .25 .50	Stability/ with Cyclic Pitch
108 109 119 120	30° ↓	60° ↓	+15° ↓	+4° ↓ -4° ↓		.55 .70 .55 .70	
110 116 172 167	45° ↓	60° ↓	+25° ↓ +35° ↓ +25°	+4° ↓ -4° ↓ +6° ↓ -6° ↓		.81	

NOTES:

1. Yaw angle sweeps
2. Zero fuselage angle
3. Empennage on
4. Average collective setting with cyclic hubs: 12°

D170-10039-1

BVWT 067
 RUN SUMMARY/CROSS COUPLING
 OF ROLL CONTROLS AND CYCLIC PITCH CONTROL
 FORWARD FLIGHT (TRANSITION)

RUN	i_w	FLAP ANGLE	SPOILER ANGLE	CYCLIC ANGLE	RPM	NOM C_{T_s}
		LEFT / RT WING / WING	LEFT / RT WING / WING			
125	15	40° / 60°	40° / 0	0	4500	.25
123 126 121	30 ↓	40° / 60° ↓	40° / 0 ↓	+4° 0 -4°		.55 ↓
124 127 122	45 ↓	40° / 60° ↓	40° / 0 ↓	+4° 0 -4°		.81 ↓

NOTES:

1. Fuselage angle sweeps
2. Stabilizer angle: +20°
3. Average collective setting with cyclic hubs: 12°

BVWT 067
 LONGITUDINAL RUN SUMMARY
 FORWARD FLIGHT IN GROUND EFFECT
 $h/D = 1.25$

RUN	i_w	FLAP ANGLE	STAB ANGLE	CYCLIC ANGLE	RPM	NOM C_{T_s}	OBJECTIVE
140	VARY	40°	---	0	4500	.81	Effect of Ground Proximity on Longitudinal Characteristics
141			↓			.70	
142			↓			.55	
143			↓			.25	
128		60°	---			.81	
129			↓			.70	
130			↓			.55	
131			↓			.25	
149		40°	---	+4°		.81	Cyclic Pitch Control/I.G.E.
150			↓			.70	
151			↓			.55	
152			↓			.25	
153		40°	---	-4°		.81	
154			↓			.70	
155			↓			.55	
156			↓			.25	
147		40°	+10°	0		.55	Horizontal Tail Effectiveness/ I.G.E.
144			+ 5°				
148			0				
146			-10°				

NOTES:

1. Wing tilt angle sweeps
2. Zero fuselage angle
3. Moving ground plane
4. Average collective setting with cyclic hubs: 12°

D170-10039-1

BVWT 067
 LATERAL/DIRECTIONAL RUN SUMMARY
 FORWARD FLIGHT IN GROUND EFFECT
 h/D=1.25

RUN	i_w	FLAP ANGLE	STAB ANGLE	CYCLIC ANGLE	RPM	NOM CT _S	OBJECTIVE
132	15° ↓	60° ↓	10° ↓	0 ↓	4500	.70	Basic Lat./Dir. Stability I.G.E.
133						.50	
134						.25	
135	30° ↓	60° ↓	15° ↓	0 ↓		.81	
136						.70	
137						.55	
138	45° ↓	60° ↓	25° ↓	0 ↓		.81	
139						.92	↓
158	15° ↓	60° ↓	10° ↓	-4° +4°		.50 ↓	Effect of Cyclic on Lat/Dir. Stability I.G.E.
163							
159	30° ↓	60° ↓	15° ↓	-4° -4°		.81	
160						.70	
161				+4° +4°		.81	
162						.70	
164	45° ↓	60° ↓	25° ↓	+4° +6° -6° -4°		.92 ↓	
165							
166							
157							↓

NOTES:

1. Yaw angle sweeps
2. Zero fuselage angle
3. Empennage on
4. Moving ground plane
5. Average collective setting with cyclic hubs: 12°

6.0 TEST RESULTS AND DISCUSSION

The primary objectives of the second test (Phase II) of the full span four prop tilt wing Model VR068Q, which was equipped with cyclic pitch propellers for low speed longitudinal control, were outlined in the Introduction and consisted of the following major topics.

- a. Yaw Control in Hover
- b. Low Speed Descent Performance with Cyclic Pitch
- c. Longitudinal Stability and Control in Transition with Cyclic Pitch
- d. Lateral/Directional Stability in Transition Including Effect of Cyclic Pitch
- e. Cross-Coupling of Cyclic Pitch with Aircraft Surface Controls
- f. Longitudinal Characteristics in Ground Effect Including Cyclic Pitch Effectiveness
- g. Lateral/Directional Stability in Ground Effect Including Effect of Cyclic Pitch

Data from the subject test can be used in conjunction with the data acquired during the Phase I test of the same model (Reference 1). Also, data obtained during the isolated prop test of a similar prop/hub/nacelle assembly (Reference 2) can be used to determine the effect of the wing/flap system on cyclic pitch control effectiveness.

6.1 YAW CONTROL IN HOVER

Yaw control in hover is achieved by differential wing surface deflections, that is, the double slotted flaps are deflected down on one wing, and the spoilers plus the flaps (if required) are deflected up on the opposite wing. The flap arrangement for downward flap deflections on the right wing is depicted in Figures 6 and 7. Figure 9 shows the spoiler location and up-flap configuration used on the left wing.

The hover mode yaw control testing accomplished during Phase I testing (BVWT 061) and Phase II testing (BVWT 067) was conducted with the leading edge slats retracted, a wing tilt angle of 90°, horizontal tail removed, and the P_1, P_2 prop rotation (both props turning down between the nacelles). Data was acquired at five preselected ground heights which varied from an h/D of 4.0 to an h/D of 1.0. The parameter h/D, has been defined as the ratio of the distance between the outboard propeller plane and ground plane to the propeller diameter. Results of the hover yaw control testing are presented in terms of the non-dimensional yawing moment parameter $Y.M./lT$, wherein

Y.M., aircraft yawing moment	ft.lbs.
l , average distance from inboard and outboard propeller ξ 's to fuselage ξ (2.653 ft. on the model)	ft.
T, propeller thrust (total)	lbs.

The hover yaw control power available with the following configurations was measured during the Phase I test.

- a. Double slotted flaps deflected down on the right wing, clean left wing.
- b. Up-flap deflection on the left wing, clean right wing.
- c. Differential flap deflection, flaps down on the right wing and up on the left wing.
- d. Spoilers deflected up on the left wing, clean right wing.

During Phase II, yaw control in hover was evaluated with flaps deflected down on the right wing in combination with spoilers on the left wing and also spoilers plus flaps deflected up on the left wing. In addition, the effect of cyclic pitch control inputs on yaw control power was examined.

6.1.1 Hover Yaw Control Power

Figure 24 presents the hover yaw control available with flaps deflected down on the right wing plus spoilers deflected up on the opposite wing, along with a comparison of the control power that would have been available if the individual contributions of flaps and spoilers were directly additive. The comparison curve was developed from the flaps alone and spoilers alone data shown in Figure 24 which was obtained during the Phase I test (BVWT 061).

Also shown in Figure 24 is the data from a check run made in BVWT 067 with the double slotted flaps deflected 60° on the right wing/clean left wing. This data, which is directly comparable with the data from Run 42 of BVWT 061, reflects an incremental decrease in hover yaw control power over that previously measured with the same configuration. An explanation for this decrease involves disc loading. Yaw control power testing was conducted in BVWT 061 with the collective hubs rotating at 6800 RPM. This operating format resulted in an average out-of-ground effect hover disc loading of 33.4 lbs/ft^2 when a collective blade angle setting of 14° was used. In contrast, the cyclic hubs used during BVWT 067 allowed a maximum propeller operating speed of 5000 RPM. This model configuration provided an equivalent disc loading of 16.7 lbs/ft^2 with 12.5° of collective. It is reasonable to assume that the decrease in Reynolds number associated with the reduction in disc loading resulted in lower flap turning effectiveness and consequently a lower yawing moment capability.

Further, it would be anticipated that Reynolds number would not influence spoiler turning effectiveness to the degree that it effected flap turning effectiveness. Thus it appears that some loss in yaw control power occurred when down flaps/right wing were tested along with up spoiler/left wing over that that can be attributed to Reynolds number effects, ie, in Figure 24 compare the average increment of h/D 's of 4.0 and 2.0 between the two differential control surface lines and the increment between the two 60° flaps alone lines, the increment being considerably larger for the former case. This noted loss is discussed later.

Figure 25 illustrates the change in yawing moment capability when up flaps were used in combination with spoilers on the left wing. The incremental improvement obtained out-of-ground effect diminished to zero in-ground effect. As a consequence, an up-moving flap does not appear to have sufficient effectiveness to warrant its use as a yaw control device in hover when a spoiler is already being considered.

The Phase I test report (Reference 1) discussed the apparent anomaly wherein the measured yawing moment capability decreased between ground height values (h/D) of 2.0 and 4.0. In actuality an out-of-ground effect condition exists at h/D 's greater than 2.0, and it would be expected that the measured yawing moment would not change between values of h/D of 2.0 and 4.0. Wires with long wool tufts attached were strung across the test section in front of the model to investigate the possibility of flow recirculation in the test area. No noticeable tuft movement could be discerned during the vertical traverses of the model. Even though this check was negative, some amount of flow recirculation could be present, however, it would be necessary to employ the use of an accurate anemometer and take measurements at several locations around the model and at a couple of model heights to completely investigate the possibility.

Model dynamics was noted in the Phase I test report as a possible source of anomaly. In the hover testing, it was observed via oscilloscope presentations that model dynamics, which manifested itself in the oscillatory nature of the data, was most severe at a model height of 2.0 h/D .

As pointed out on Page 80 of the Phase I test report (Reference 1), the necessary value of the non-dimensional parameter $Y.M./\delta T$ is 0.293 for a representative tilt wing transport-type aircraft hovering at its design "V" gross weight of 86,930 lbs and meeting a 0.5 radian/sec² yaw angular acceleration level.

6.1.2 Hover Download due to Yaw Control

Figure 26 presents the loss in vertical lifting capability associated with the use of wing control surfaces for hover yaw control. The download shown in this figure was calculated as a percentage of the total propeller thrust as measured at each data point.

$$\text{Hover Download, } \delta T = \left(1 - \frac{\text{Normal Force}}{T} \right) 100$$

Figure 26 shows the download as a function of ground height for the following configurations tested during BVWT 067: down flaps on one wing alone, down flaps (right wing) plus up spoilers (left wing), and down flaps (right wing) plus up spoilers and flaps (left wing). Comparative data presented in Figure 26 with dashed lines faired through the points was obtained in BVWT 061. The hover download data from BVWT 061 is comprised of the clean wing, up spoilers on one wing alone and down flaps on one wing alone configurations. In each case tested, the download varies from a maximum for the out-of-ground effect condition to a net upload at the lowest model

height evaluated ($h/D=1.0$). This upload is probably a result of the positive pressures being generated on the bottom of the fuselage.

One item of interest that is apparent from an examination of Figure 26 is that the incremental download due to the spoilers deflected up on one wing plus the incremental download due to the flap deflected down on the opposite wing is less than that measured for the combined yaw control configuration. It was previously observed that the yaw control capability with the combined control was less than that measured for the individual parts. An explanation for this situation is that transverse flow from one side of the aircraft to the opposite side occurred with the differential control configuration. The transverse flow reduced the yawing moment capability and at the same time increased the download as a result of higher negative pressures on the bottom of the fuselage.

The overall measured download of 14.2% for the 60° spoiler/left wing plus 60° flap/right wing configuration (Run 12) is high with respect to the 11.7% download previously measured for the 40° up flap/left wing plus 60° flap/right wing configuration and presented in Figure 45 of the Reference 1 test report. Hover download measurement is extremely sensitive to the accuracy of the data. A check was made of the balance calibrations used for the reduction of the BVWT 067 Phase II data and these prime sensitivities were compared to those used for reducing the BVWT 061 Phase I data. This exercise showed the propeller thrust data from the Phase II test to be 2.5% higher in magnitude than the corresponding data recorded from the Phase I test as a result of calibration differences. Calculations established that the downloads registered during Phase II were 2.2% larger than comparative download data from Phase I. A download adjustment of 2.2% to the Run 12 data would bring the download for this run (12%) instead of 14.2%) in line with Phase I data, however, a download adjustment of this magnitude is probably on the high side; i.e., compare in Figure 26 the 60° flap deflection/right wing alone run from BVWT 067 to similar data from BVWT 061. The download from Phase II (5000 RPM) should have been somewhat lower than the download from Phase I (6800 RPM) to be consistent with the corresponding yawing moment data comparison presented in Figure 24, but not excessively less.

The above investigation also indicates that the non-dimensional yawing moment ($Y.M./iT$) measured during Phase II was 2.5% relatively lower in magnitude than the values recorded from the Phase I test.

During the analysis of the download data from BVWT 067, it was noticed that the propeller thrusts at an h/D of 4.0 were

1.2% to 2% higher than those measured at an h/D of 2.0 during Runs 12 and 13. This difference which does not appear to be reasonable, increased the download accordingly at an h/D of 4.0.

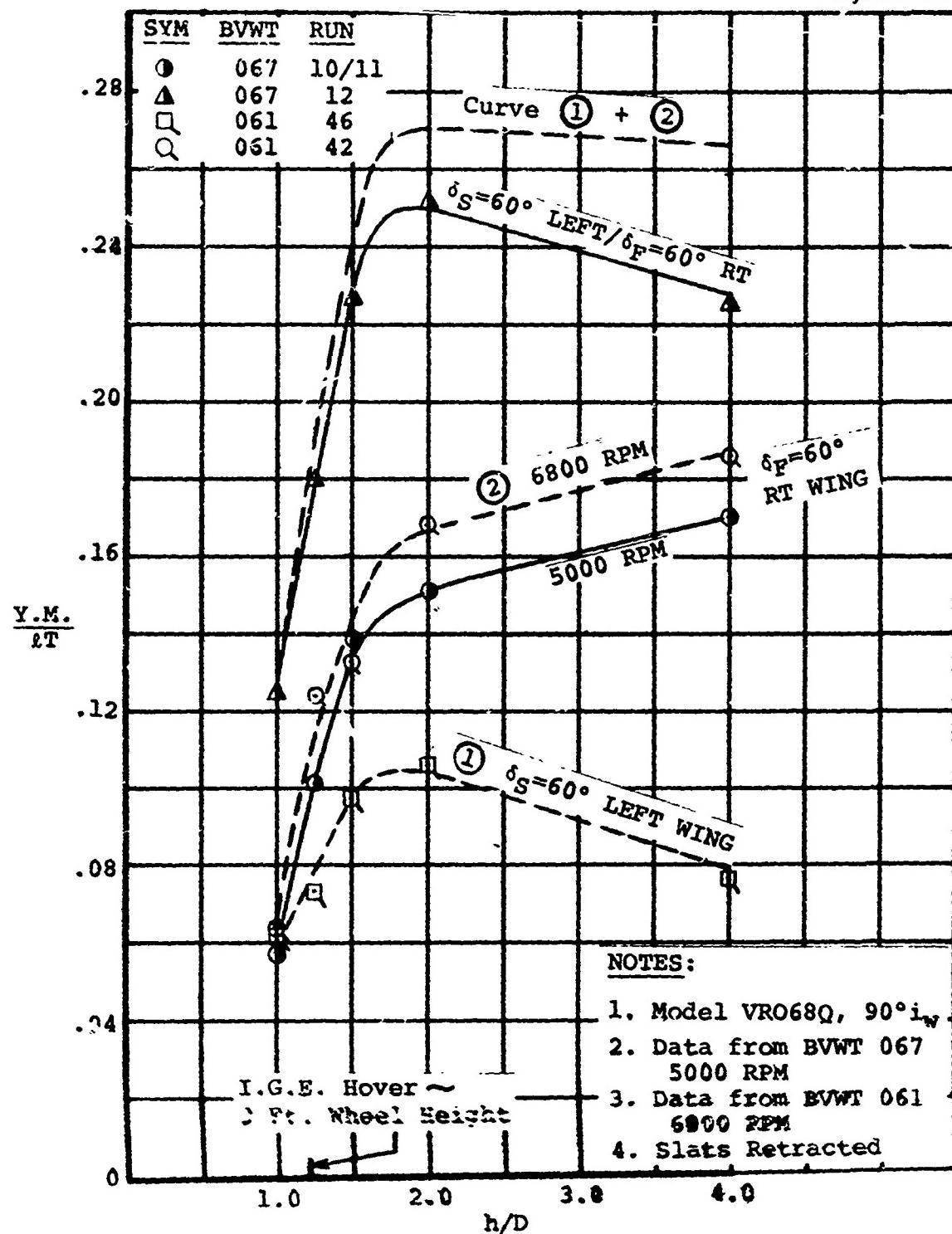
6.1.3 Effect of Cyclic Pitch on Hover Yaw Control

Two runs were performed during BVWT 067 to evaluate the effect of cyclic pitch inputs on hover yaw control capability. In this investigation, a yaw control configuration of spoilers deflected 60° on the left wing plus flaps deflected 60° on the right wing was selected for the evaluation. Cyclic pitch inputs of +6° were used. The results from the testing are presented in Figure 27.

It can be seen that positive cyclic (nose down pitching moment) increases the yaw control power while negative cyclic (nose up moment) produces an opposite effect. This variation is a result of the location of the propeller centerlines (both inboard and outboard) below the wing chord plane in combination with the shift in the center of pressure cutting across the propeller disc due to cyclic pitch action. Positive cyclic shifts the center of pressure closer to the wing chord plane thus increasing the dynamic pressure acting over the wing. Negative cyclic has an opposite effect - a shift in the center of pressure further away from the wing.

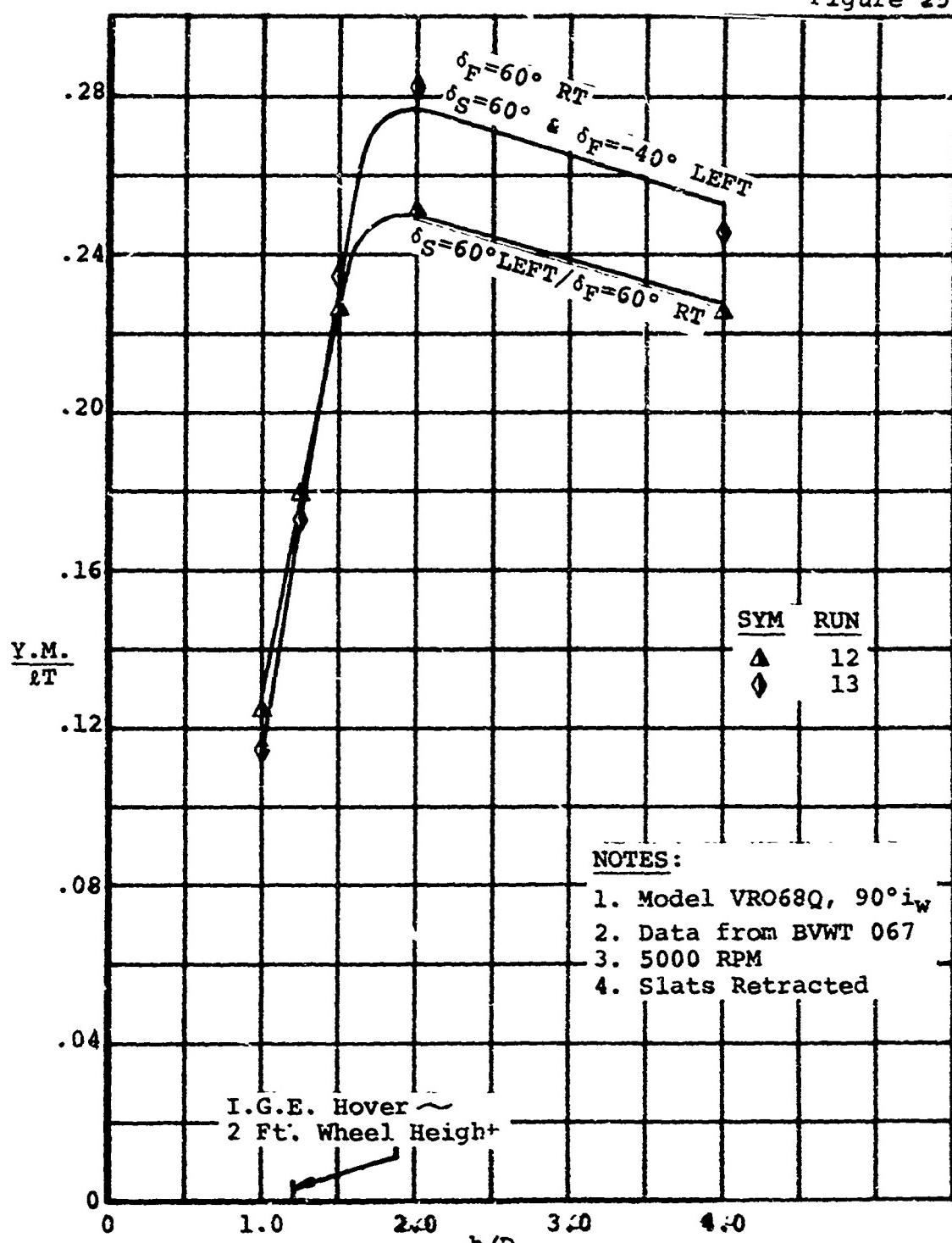
The hover download data presented in Figure 28, a companion plot to Figure 27, corroborates this explanation. The increase in hover download with positive cyclic pitch is consistent with the improvement in yaw control capability with positive cyclic.

Figure 24



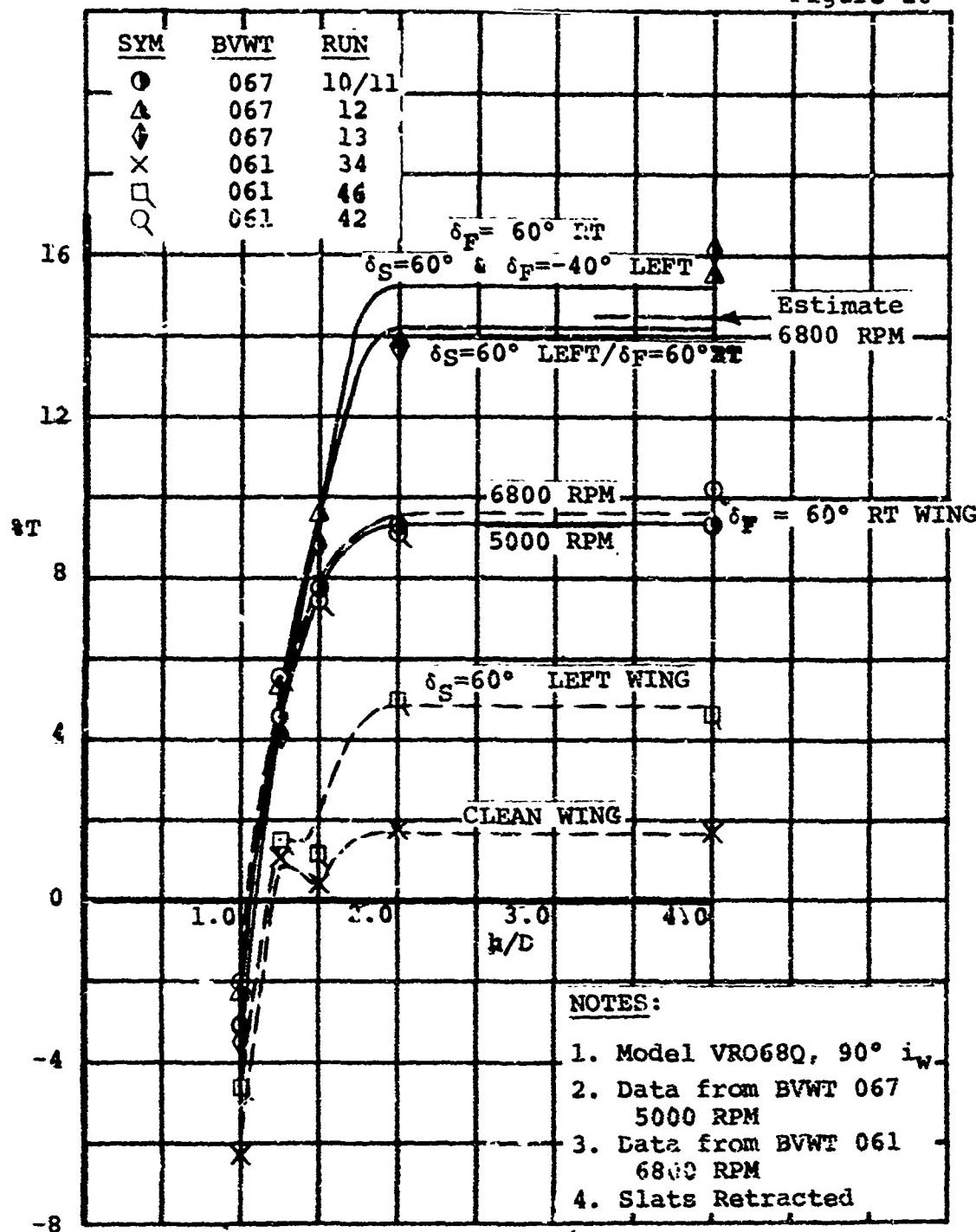
HOVER YAW CONTROL BUILDUP WITH
FLAPS (RT WING) AND SPOILERS (LEFT WING)

Figure 25



HOVER YAW CONTROL
 DOWN FLAPS ~ RIGHT WING
 UP FLAPS AND/OR SPOILERS ~ LEFT WING

Figure 26



HOVER DOWNLOAD DUE TO
FLAP AND SPOILER DEFLECTIONS

Figure 27

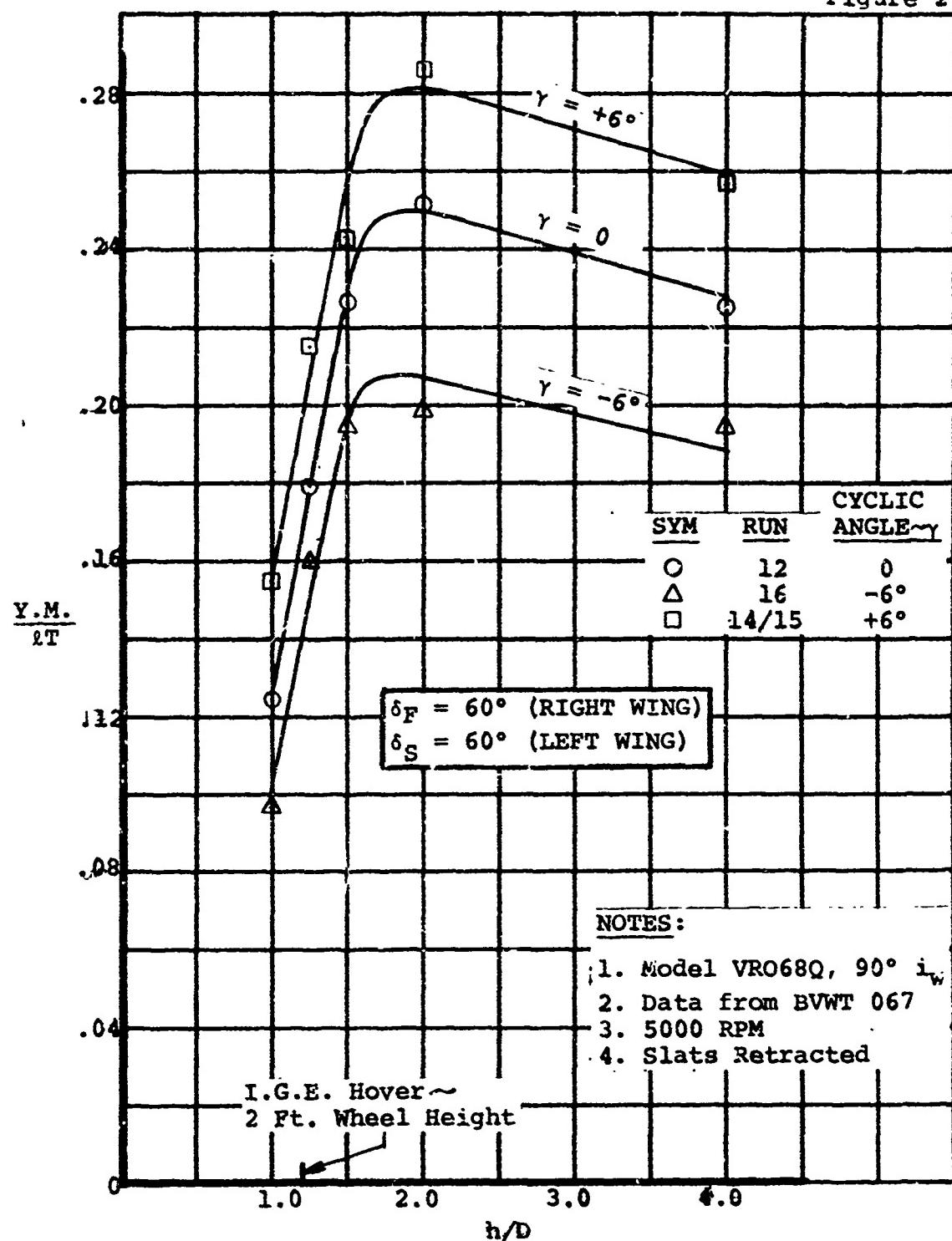
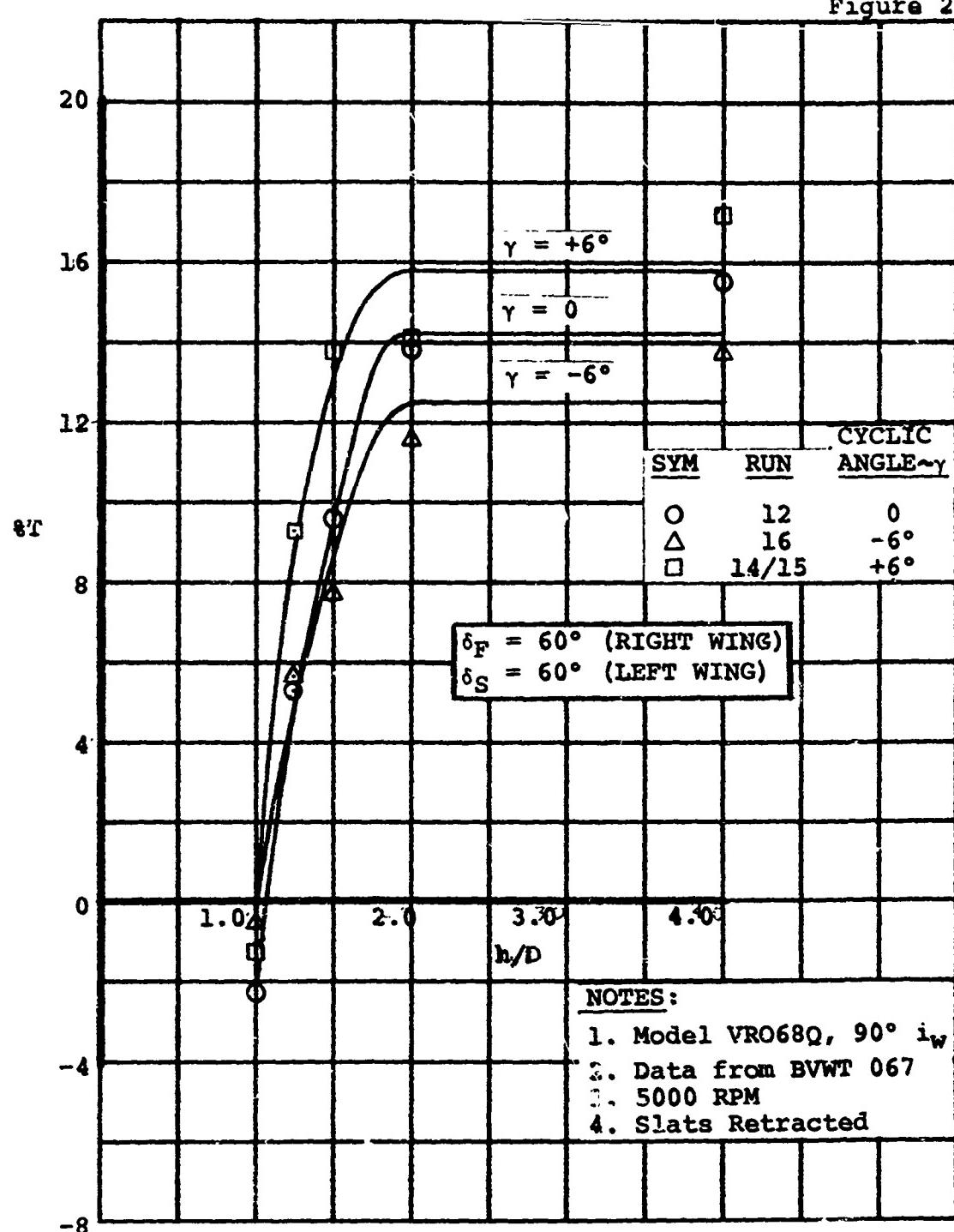
EFFECT OF CYCLIC PITCH
ON HOVER YAW CONTROL

Figure 28



EFFECT OF CYCLIC PITCH ON
HOVER DOWNLOAD DUE TO YAW CONTROL

6.2 CYCLIC PITCH CONTROL IN HOVER

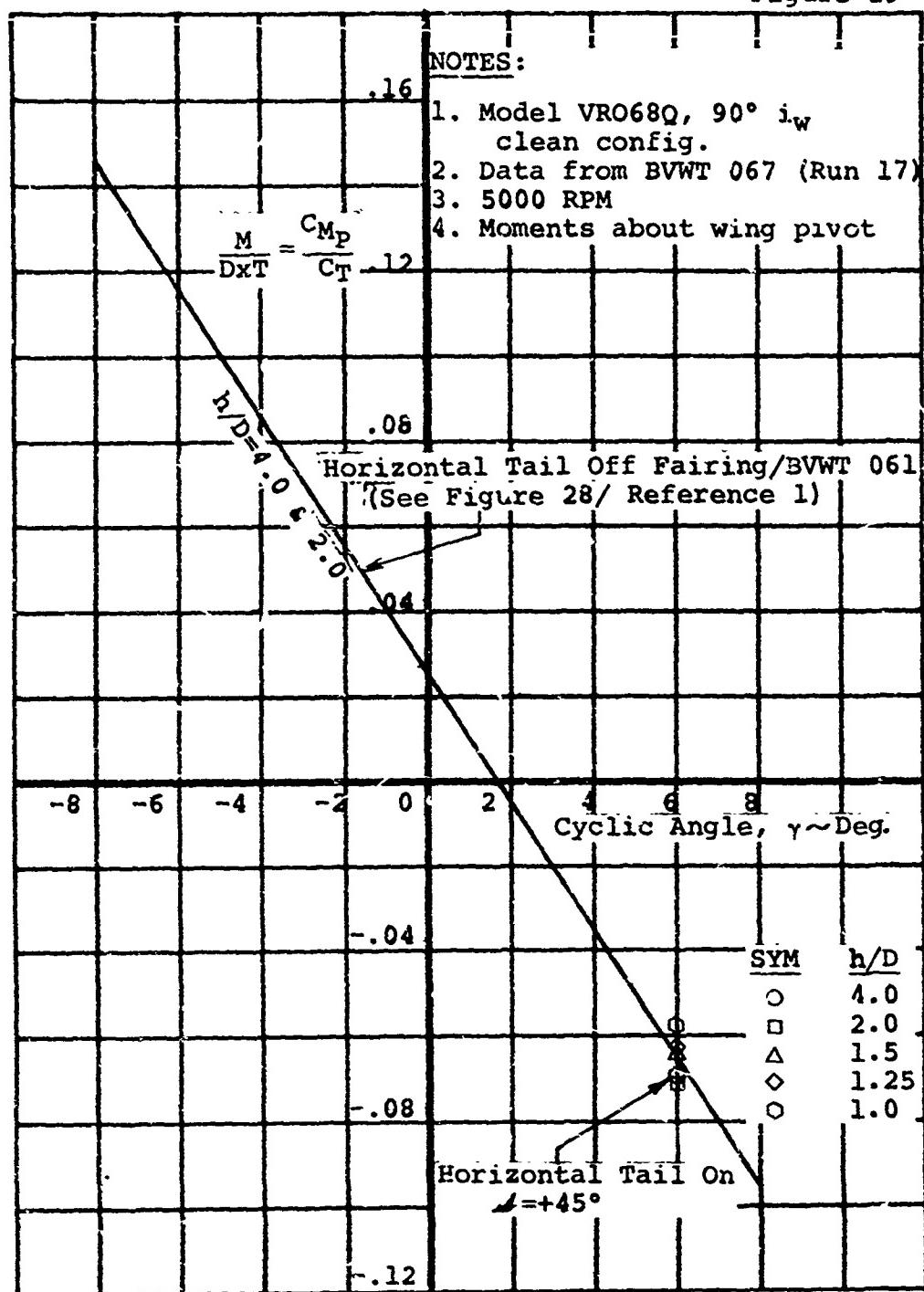
6.2.1 Effect of Horizontal Tail on Cyclic Pitch Control

The effectiveness of the propellers in producing aircraft pitching moment when cyclic pitch is applied was investigated in the hover mode during Phase I test BVWT 061. Since this testing was conducted with the horizontal tail removed, a run was made during BVWT 067, (varying ground height in hover) with the horizontal tail on in order to investigate possible pitching moment interference effects between the propellers and the tail.

A cyclic pitch angle of $+6^\circ$ was selected for the run as this case would maximize the downwash in the regime of the horizontal tail thus maximizing potential interference effects on aircraft pitching moment. The horizontal tail was set at a typical stabilizer angle for hover ($+45^\circ$).

Figure 29 presents the results of this investigation. Depicted on the chart is the fairing for cyclic pitch control effectiveness derived from BVWT 061 (Reference 1) with the horizontal tail off. This line is applicable to an out-of-ground effect hover condition (h/D 's of 4.0 and 2.0). It can be noted that the horizontal tail on data measured during BVWT 067 with a cyclic angle of $+6^\circ$ agrees well with the previously derived "tail off" fairing and the data exhibits only a small variation with ground height, leading to the conclusion that the horizontal tail has not appreciable effect on aircraft pitching moment in the hover mode.

Figure 29



EFFECT OF HORIZONTAL TAIL ON PITCHING MOMENT DUE TO CYCLIC
VARYING GROUND HEIGHT IN HOVER

6.3 LOW SPEED DESCENT PERFORMANCE

One of the critical design items for a tilt wing aircraft is the low speed descent capability. (Boeing-Vertol has been using as a design goal, a minimum descent rate of 800 fpm up to a flight speed of 42.5 kt and a descent angle of 12° at higher speeds.)

The leading edge slat and double slotted flap configurations utilized on Model VR068Q, were developed during the 1969 Boeing-Vertol wind tunnel test program of a four prop tilt wing aircraft as a means of meeting the descent rate goal. In the same test program, the placement of the propeller hub ξ 's with respect to the wing leading edge, was investigated with regard to maximizing descent performance. Test results were incorporated into the design of Model VR068Q. The P1,2 prop rotation direction (props turning down between the nacelles) used during the two phase test program on Model VR068Q was also selected on the basis of previous wind tunnel tests to maximize descent capability.

The low speed descent capability testing concerned with cyclic pitch effects was commenced during the Phase I test (BVWT 061) with a wing configuration consisting of double slotted flaps deflected 60° and full span slats positioned to the Q^{*10,10,*} setting. In this setting, each slat segment located behind an up-turning propeller is deflected to a higher angle. During these test runs investigating the reduction in descent capability with positive cyclic angles, damage occurred to the cyclic hubs, necessitating a delay in the completion of this investigation to the Phase II test.

6.3.1 Effect of Cyclic Pitch on Descent Capability

The results of the testing during BVWT 061 and BVWT 067, that investigated the effect of cyclic pitch on descent performance are presented in Figure 30. Descent rate at buffet onset is shown as a function of full scale aircraft velocity, V_F. As discussed in the Data Reduction section, V_F and R/D were calculated using a wing loading of 73.5 psf and test section atmospheric conditions. It was necessary for data consistency between the two tests, to adjust the Phase II data for the difference between the test section air density occurring in the Phase II test and that prevailing during the Phase I test ($\rho = .00228$ slugs/ft³).

Descent capability at buffet onset was determined by establishing the wing incidence angle at which initial stall or separation occurred on the wing outboard of the inboard set of fences, i.e. outboard of the region between fences shown in

Figure 2. Inboard areas where stall was tolerated comprise the wing center section over the fuselage, the area behind the gap between the propeller tip and fuselage side, and the region between the fences - sections over which the low freestream q or less than full slipstream q prevail and roll disturbances are minimal.

In selecting the buffet onset angle, tuft photographs and observer written comments were studied in conjunction with corresponding force polars presented in terms of L/qb^2 vs X/qb^2 rather than the slipstream notation C_{L_s} vs C_{X_s} . With polars in the L/qb^2 vs X/qb^2 format, initial stall coincides with a definite break in the curve at thrust coefficients up to $0.65 C_{T_s}$ or speeds greater than 55 knots. At lower speeds, the stall buildup is gradual and at a wing angle 10° beyond that selected for buffet onset, the flow remains attached on 75% of the wing.

Another curve that has been found useful in determining the descent performance is the variation with C_{T_s} of the effective wing angle of attack, $\alpha_{W_{EFF}}$, at buffet onset. (The latter parameter is described in the Data Reduction section.) This curve and the companion plot of wing incidence angle at buffet onset vs C_{T_s} should be reasonably smooth and consistent as can be noted in Figure 31.

Previous Boeing-Vertol tilt wing testing has shown that positive cyclic angles (nose down pitching moment) reduces descent capability and negative cyclic improves it. In line with these results only positive cyclic angles were evaluated in the subject test program. Figure 30 shows that the loss in descent rate due to positive cyclic averages 100 fpm per degree of cyclic at 62 knots with a reduction in the average to 50 fpm per degree of cyclic at a flight speed of 38 knots. This reduction in the loss rate at low speeds is consistent with the hover yaw control testing (discussed previously) that shows positive cyclic to be beneficial and negative cyclic to have the reverse role.

A large portion of the loss in descent performance with positive cyclic has been associated with a reduction in the slipstream turning effectiveness. Evidence of this is inclusive in Figure 31 which presents the buffet onset angles corresponding to the descent data plotted in Figure 30. Buffet onset angles are shown as wing angles of attack at initial stall and as the calculated effective wing angles of attack defined as the angle between the wing chord and the resultant velocity vector at the wing. At $0.77 C_{T_s}$ (49 knots) the 4° decrease in wing buffet onset angle resulting from the application of 6° of

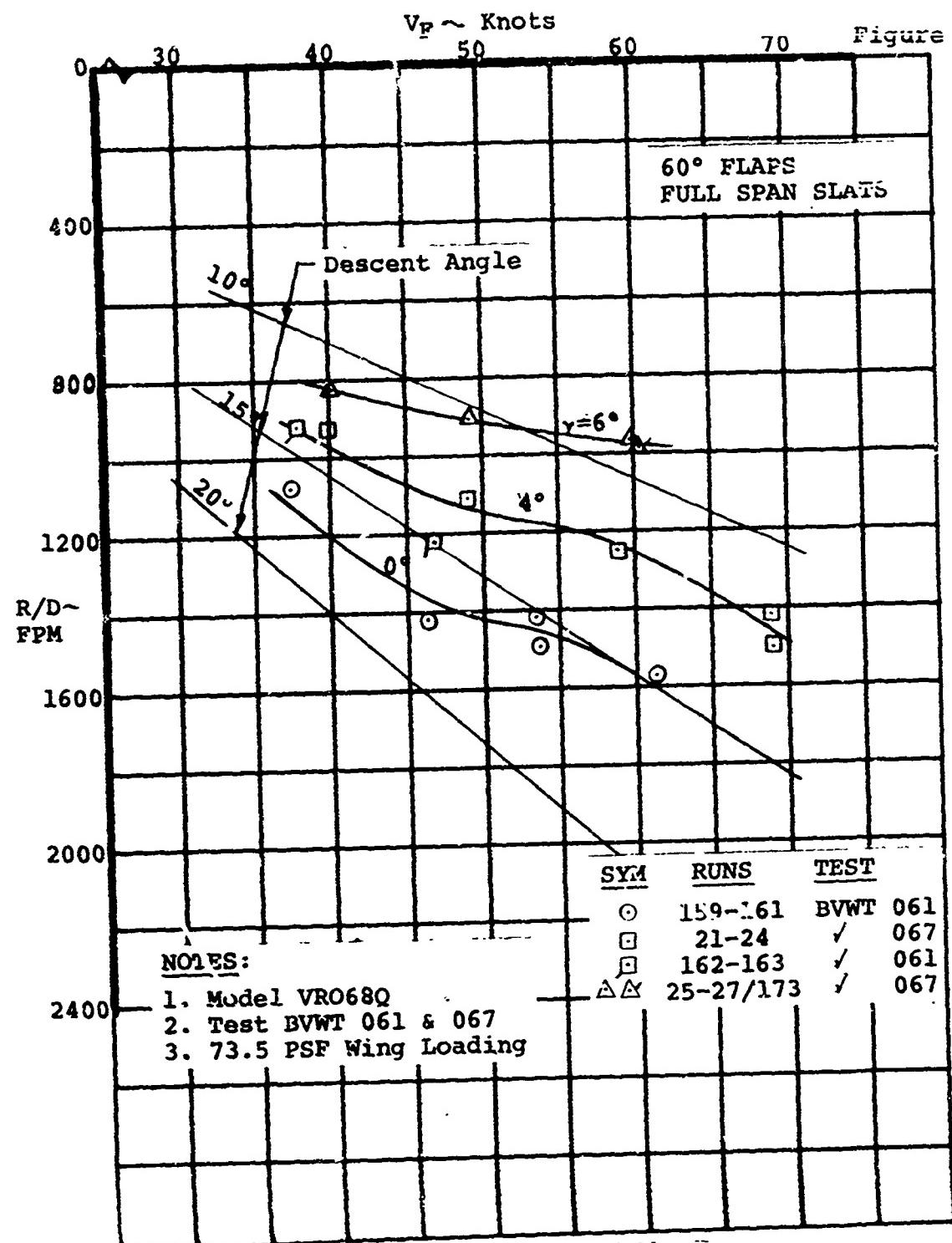
D170-10039-1

positive cyclic represents only 175 fpm out of the total 500 fpm loss in descent performance. The remainder of the loss, 325 fpm, reflects the reduction in turning effectiveness.

Note that Figure 31, which presents data from wing sweep runs with the fuselage set at 0° , expresses buffet onset angles in terms of wing incidence angle plus fuselage angle ($i_w + \alpha_f$). This was necessary in order to account for the incremental wing angle of attack being produced by the upward deflection of the model on the sting due to the high lift forces generated. The increment in angle of attack from sting deflection is accounted for by a calculation routine in the data reduction program.

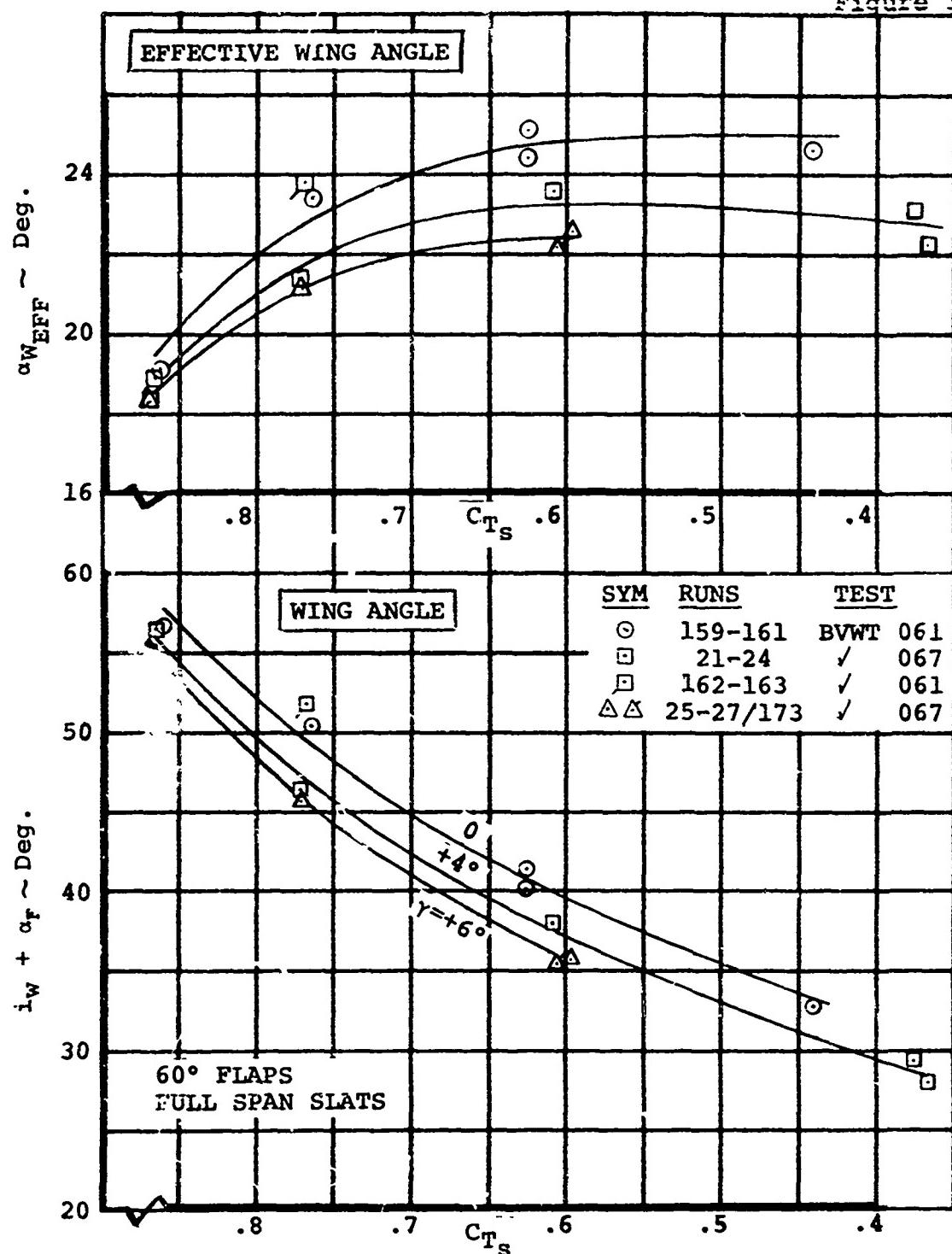
Figures 32 through 37 present the basic data from the runs that were conducted for the purpose of determining the low speed descent capability. The data is presented as plots of L/qb^2 vs X/qb^2 (force polars), L/qb^2 vs i_w (lift curves), and M/qb^2c vs i_w (moment curves). Marked off on each force polar plot are the selected buffet onset points and a .3g deceleration line (corresponds to 16.7° descent angle) for reference purposes. Figure 38 depicts the variation of slipstream thrust coefficient prevailing during the $\pm 4^\circ$ cyclic runs with 5000 RPM and an average collective setting of 12.8° .

Figure 30



EFFECT OF CYCLIC PITCH ON
LOW SPEED DESCENT CAPABILITY

Figure 31

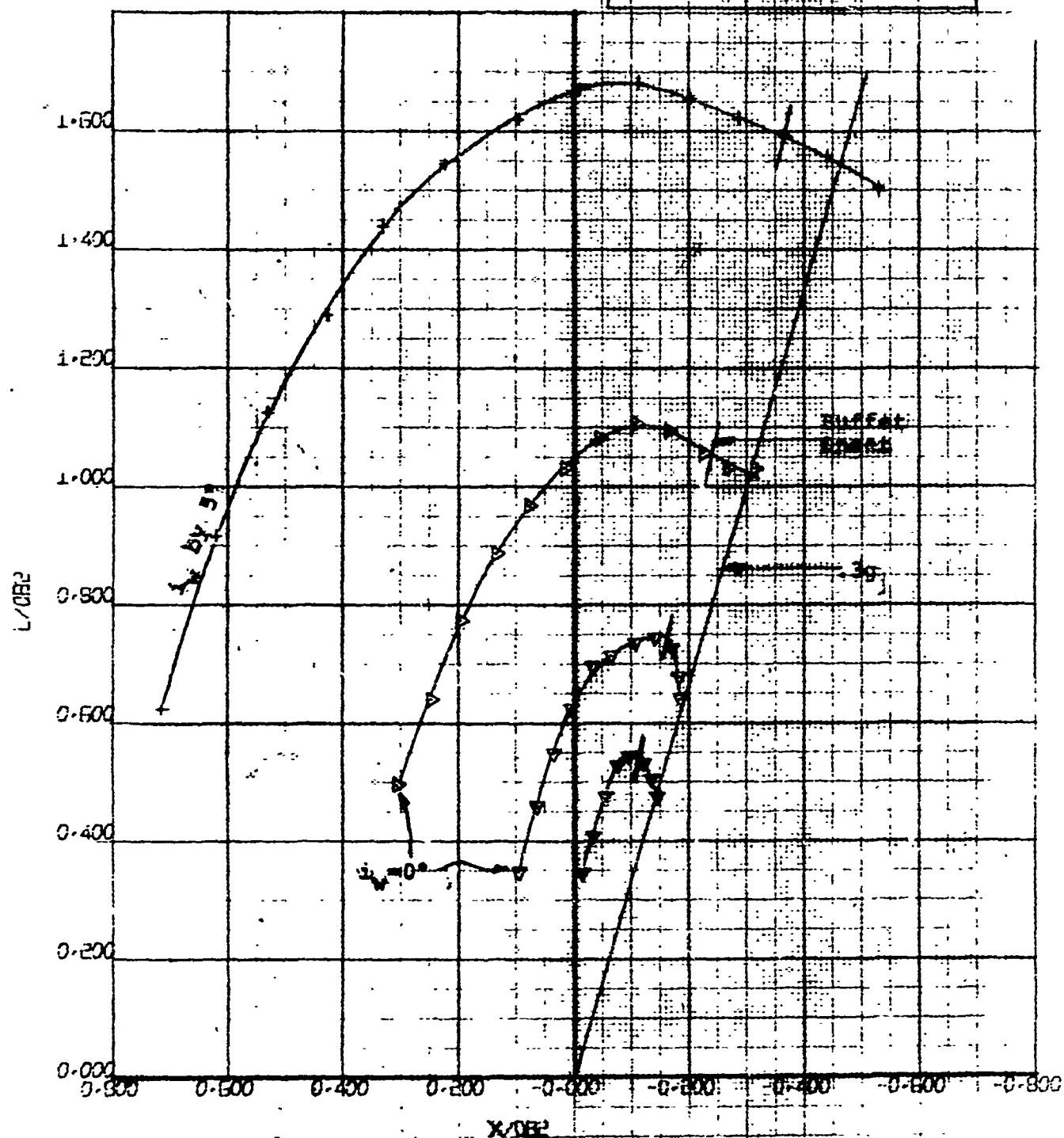
EFFECT OF CYCLIC PITCH ON
BUFFET ONSET ANGLE

RUN	SYM	α
21	+	2.76
22	▷	4.70
23	▽	8.49
24	▼	14.0

NUMBER D170-30039-1
REV. LTR.

Figure 82

DESCENT CAPABILITY CURVE
 $\delta_y = 60^\circ$, FULL SPAN SLATS
NO AILERONS



FOUR-PROP 111 WING MODEL VARIOUS (FULL SPAN) LOADS VS. X/D_{DP}	BWWT 67 1/ 4/71
---	-----------------------

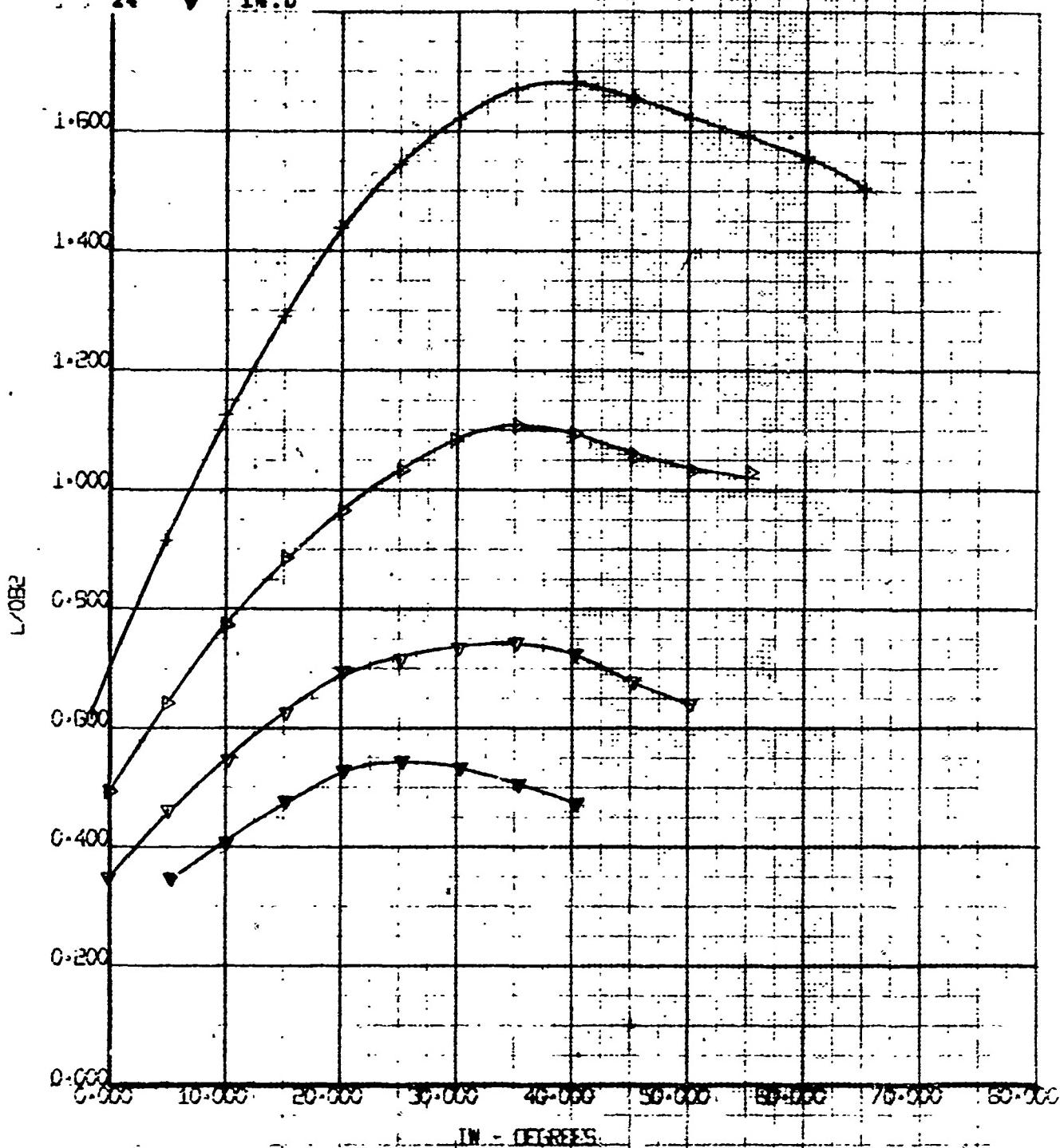
NUMBER D170-10039-1

REV. LTR.

Fig 20-33

RUN	SYM	α
21	+	2.75
22	>	4.70
23	▽	5.45
24	▼	14.0

PERCENT CAPABILITY DIAGR.
 $\delta_T = 60^\circ$ FULL SPAN SLATS
 14.0 DEG TILT



FOUR-PROP TILT WING
 MODEL WROSCH (11' SPAN)

BWWT
 67

1/4/71

NOT REPRODUCIBLE

SHEET 85

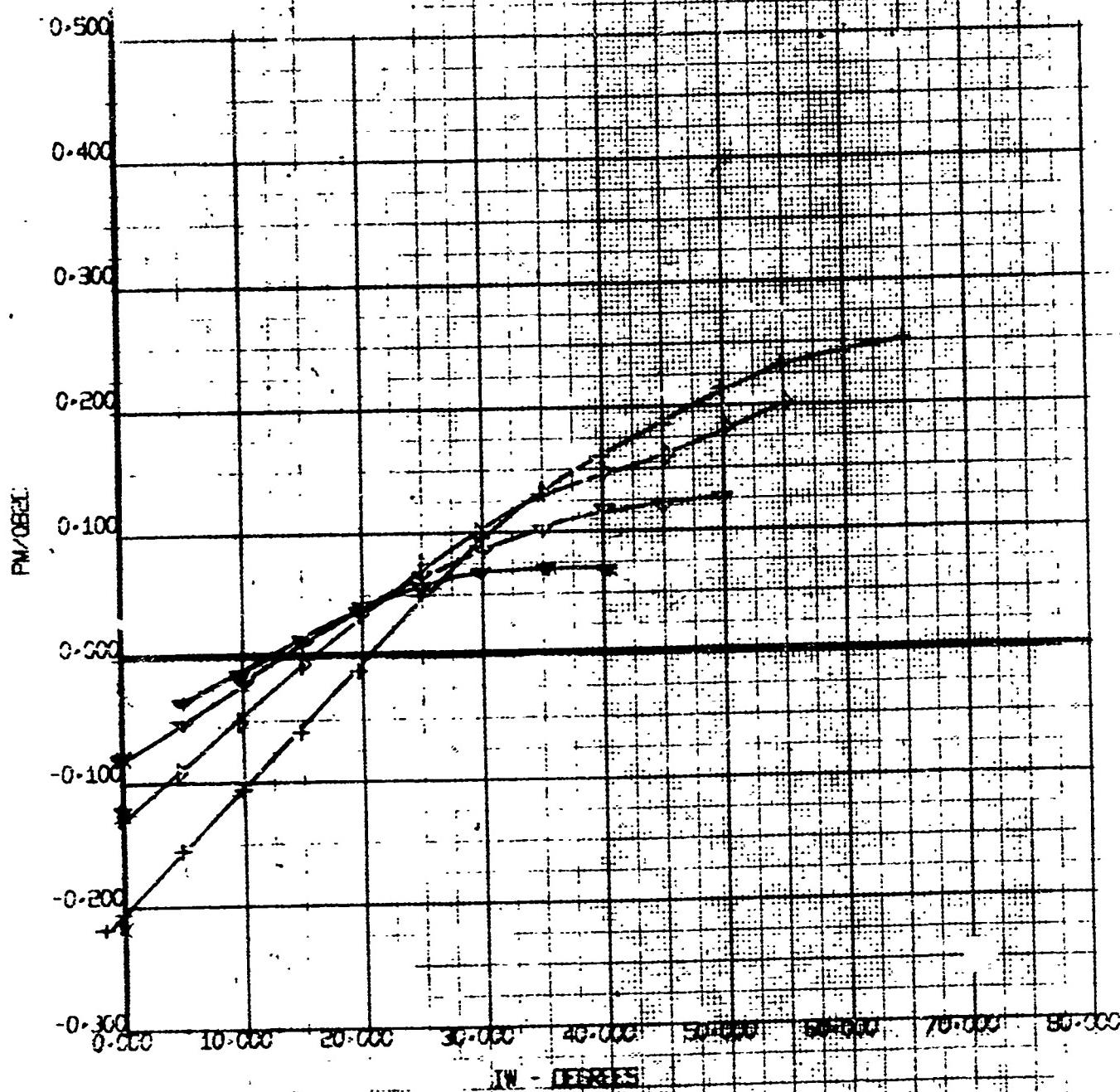
NUMBER B170-16039-1

REV. E TDP.

Figure 38

RUN	SYM	q
21	+	2.76
22	△	4.70
23	▽	8.49
24	▼	14.0

DISCRETE INTEGRALITY RUNS
 $\delta_p = 5.0^\circ$, WITH SPAN SLATE
 LIFT COEFFICIENT



FILER-PROP TILT WING
 MODEL VRCB6(FULL SPAN)
 PM(OBET) VS. TW

BWWT
67

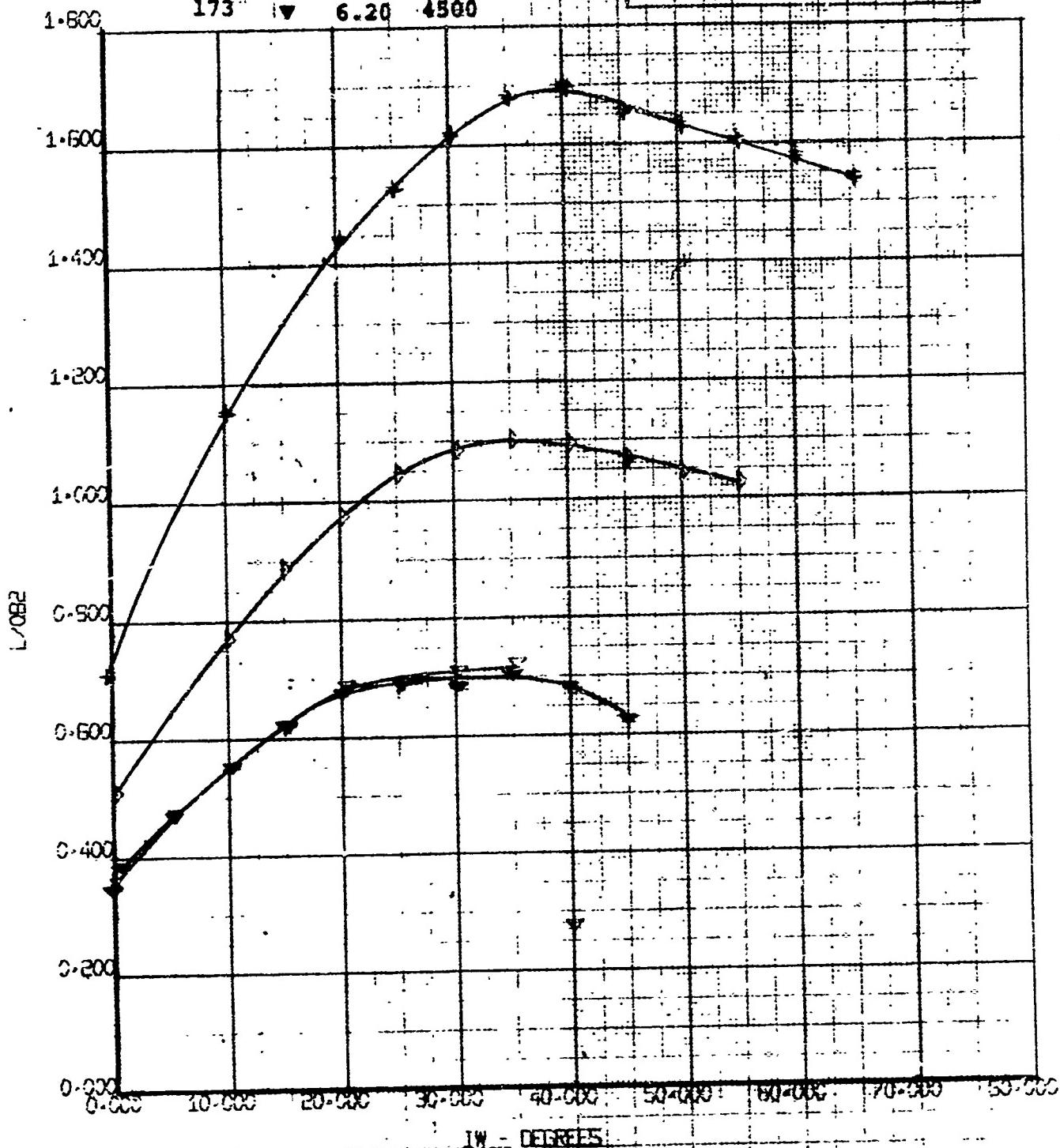
12/7/70

NUMBER D170-10039-1

REV. LTR. Figure 35

RUN	SYM	q	RPM
25	+	2.76	5000
26	>	4.70	/
27	▽	8.49	/
173	▼	6.20	4500

DESCRIBE CAPABILITY RUNS
AIRCRAFT: VROGGS (FULL SPAN)
TEST: CYCLIC



NOT REPRODUCIBLE

FOUR-PROP. TILT WING
MODEL VROGGS (FULL SPAN)
L/0.082 VS. IW

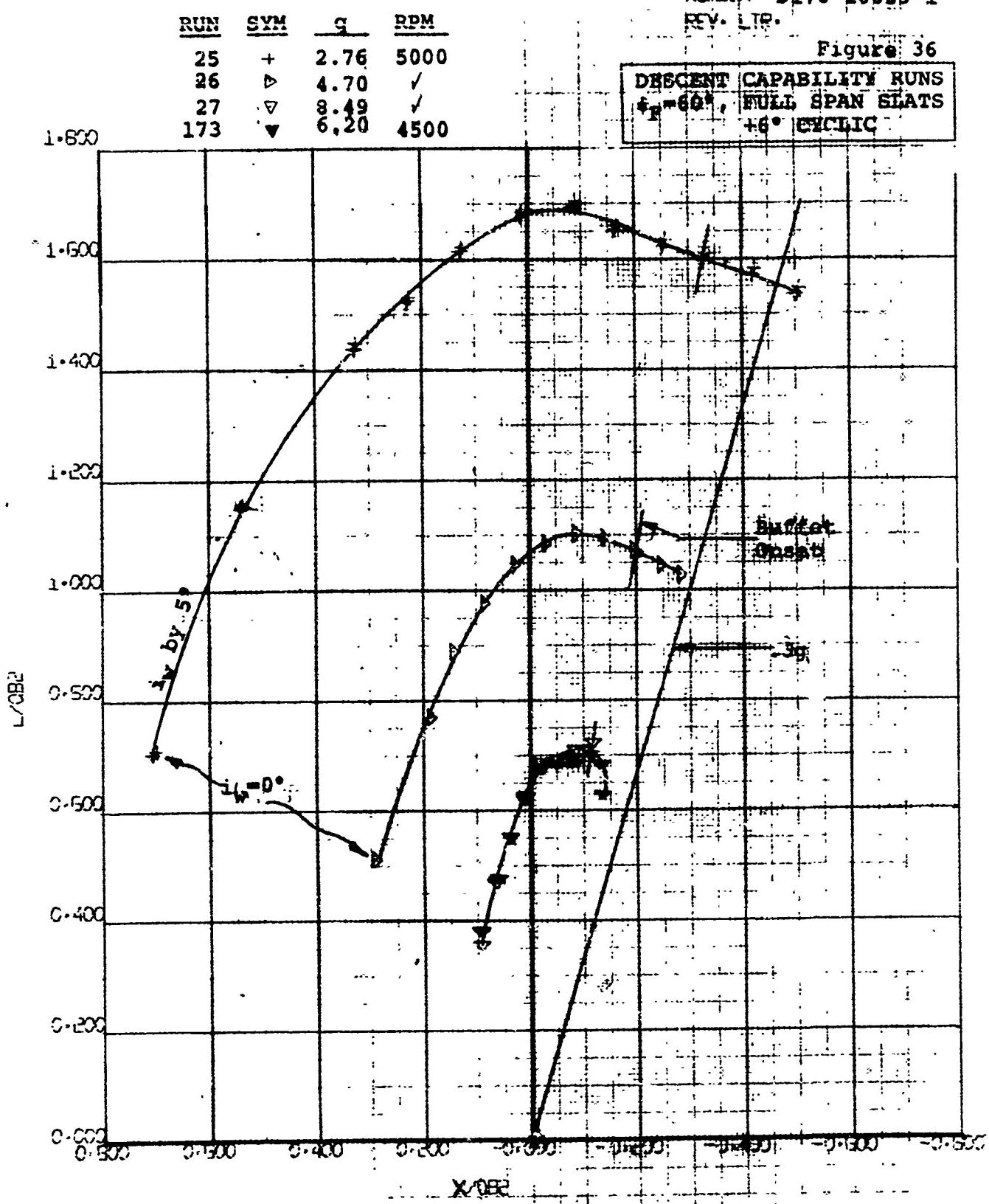
BVWT
67

12/7/70

NUMBER D170-10039-1
REV. LTP.

Figure 36

DESCENT CAPABILITY RUNS
 $\delta_F = 60^\circ$, FULL SPAN SLATS
 $+6^\circ$ CYCLIC



FOUR-PROP TILT WING
MODEL VROB6 (FULL SPAN)
L/D_{BP} VS. D/L_{BP}

BWNT
67

12/7/70

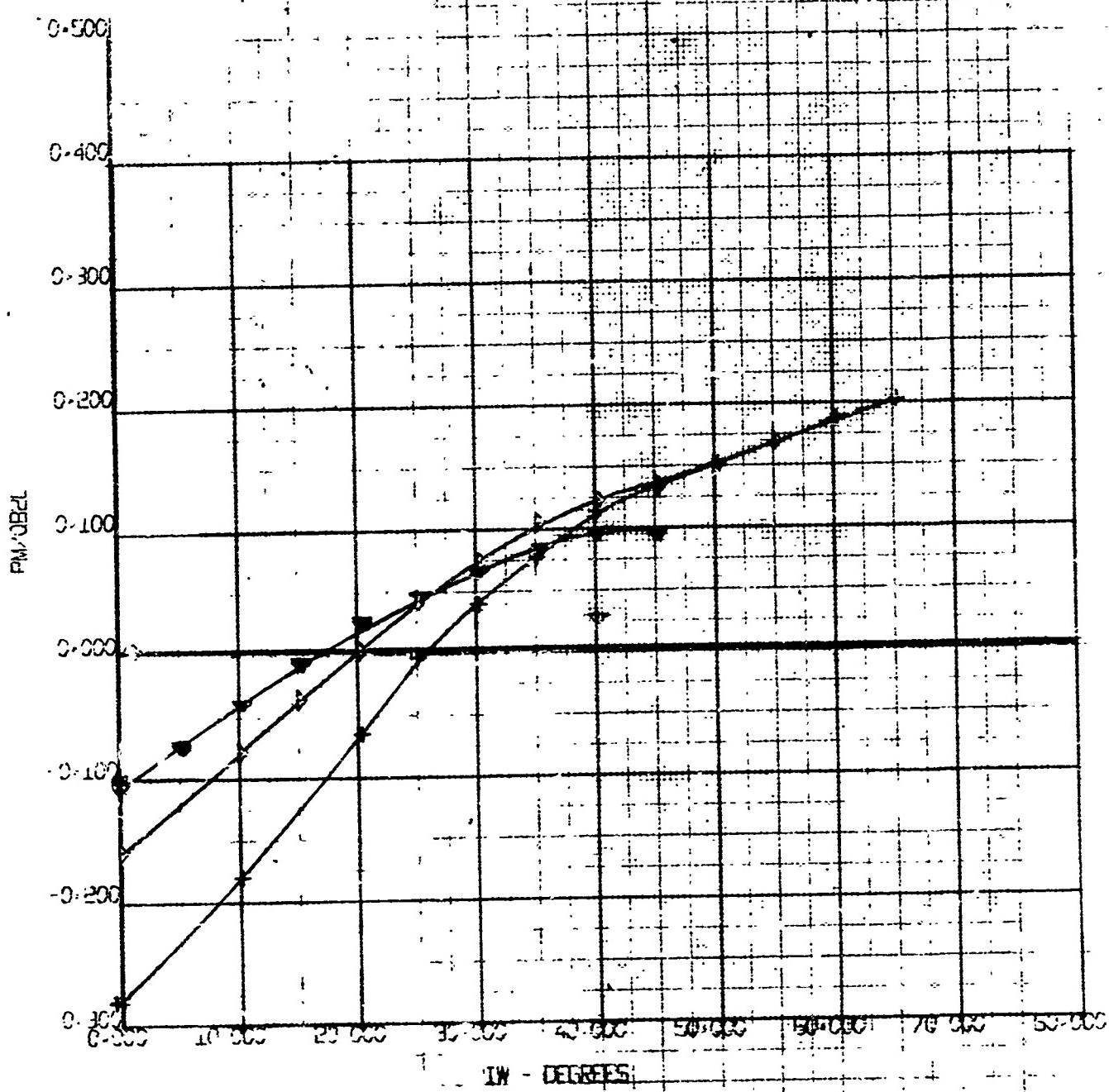
NUMBER DJ70-10039-1

REV. LTR.

Figure 37

RUN	SYM	q	RPM
25	+	2.76	5000
26	>	4.70	
27	▽	8.49	
173	▼	6.20	4500

DISCRETE CANTILEVER WINGS
 $\delta_p = 60^\circ$, FULL SPAN SLATS
 $+ 6^\circ$ CYCLIC



FOUR-PROP TILT WING	EVWT 6°
MODEL V20BB (FULL SPAN)	
PM/DBL VS. TW	12/7/70

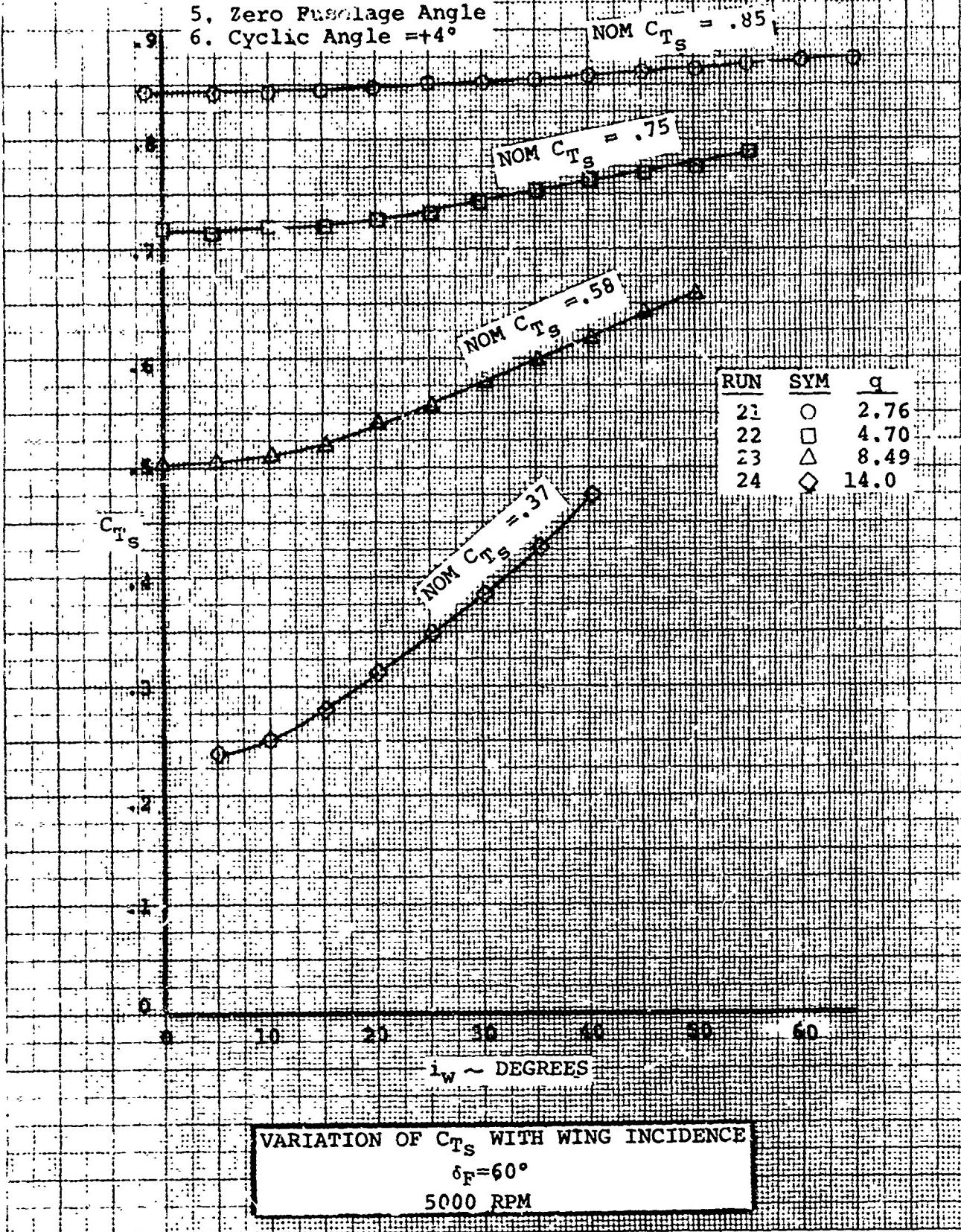
NOT REPRODUCIBLE

SHEET 89

NOTES:

1. Model VR068Q
2. Data from BVWT 067
3. Full Span Slats
4. Horizontal Tail Off
5. Zero Fuselage Angle
6. Cyclic Angle $= +4^\circ$

Figure 38



6.4 LONGITUDINAL STABILITY AND CONTROL IN TRANSITION

Longitudinal control with cyclic pitch and its effect on the basic aircraft longitudinal characteristics were investigated through the transition flight regime with and without the horizontal tail depicted in Figure 16. High positioning of this tail on the vertical fin as illustrated in Figure 15 resulted in a horizontal tail volume coefficient of 1.33. The potential influence of cyclic pitch inputs on the horizontal tail effectiveness was also evaluated.

Fuselage pitch runs were performed at constant RPM for selected combinations of wing tilt angle and flap angle that were representative of typical combinations required in transition. Data was taken at wing incidence settings ranging from 15° to 55° with 60° of flap angle. The slipstream thrust coefficient (C_{T_S}) for these runs varied from 0.3 for the 15° wing tilt angle case to 0.93 for the 55° wing tilt angle case. Runs were made with a sufficient number of cyclic pitch angular settings and stabilizer settings to meet the test objectives.

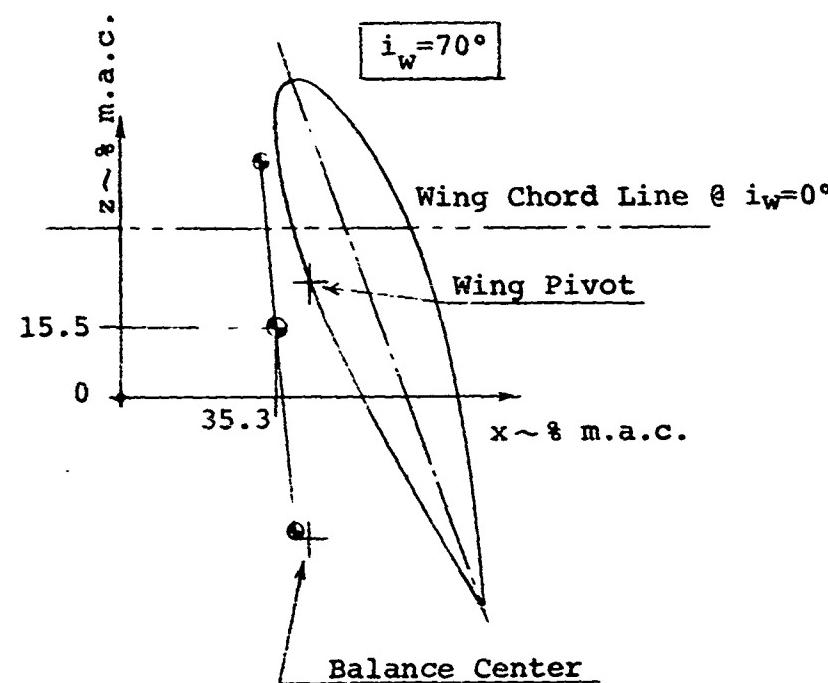
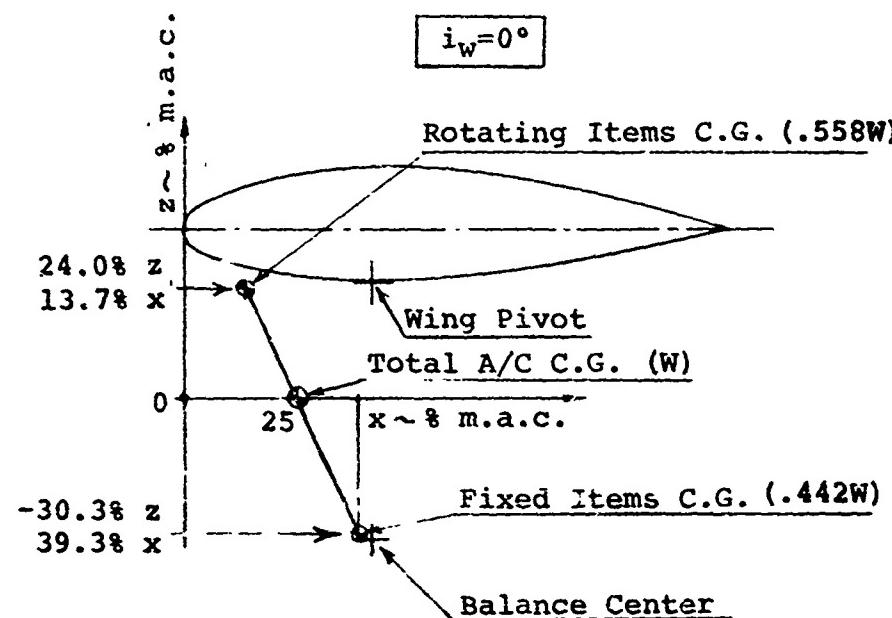
As mentioned in Section 2.7 of this report, the wing angle of attack range for evaluation with a prescribed combination of wing tilt angle and thrust coefficient was adjustable per the sting "pre-bend" angle selection. These "pre-bend" angles were chosen prior to each set of runs so that the data could be acquired at or near representative flight conditions.

All moments obtained during the longitudinal stability runs were transferred to a representative mid-center of gravity. This center of gravity moves up and back as the wing tilt angle increases. Positions of the c.g. for the various wing tilt angles used, were calculated by utilizing the scaled wing-down longitudinal and vertical locations for the fixed mass c.g. and rotating mass c.g. (with respect to the wing chord line) of a representative transport-type four prop tilt wing aircraft with a V-mode gross weight of 86,930 lb. (and no dihedral), plus the wing pivot location of the model. Model scale with respect to this aircraft was 1/12.3.

Figure 39 shows the relative locations of the rotating mass c.g., fixed mass c.g., and resultant aircraft c.g. to the wing pivot for the wing down case and 70° wing tilt case. The movement of the aircraft c.g. with wing tilt angle that was used in the data reduction program is illustrated in Figure 40. As can be seen, the movement of the c.g. for a wing angle change from zero to 70° is 10.3% MAC aft and 15.5% MAC up.

D170-10039-1

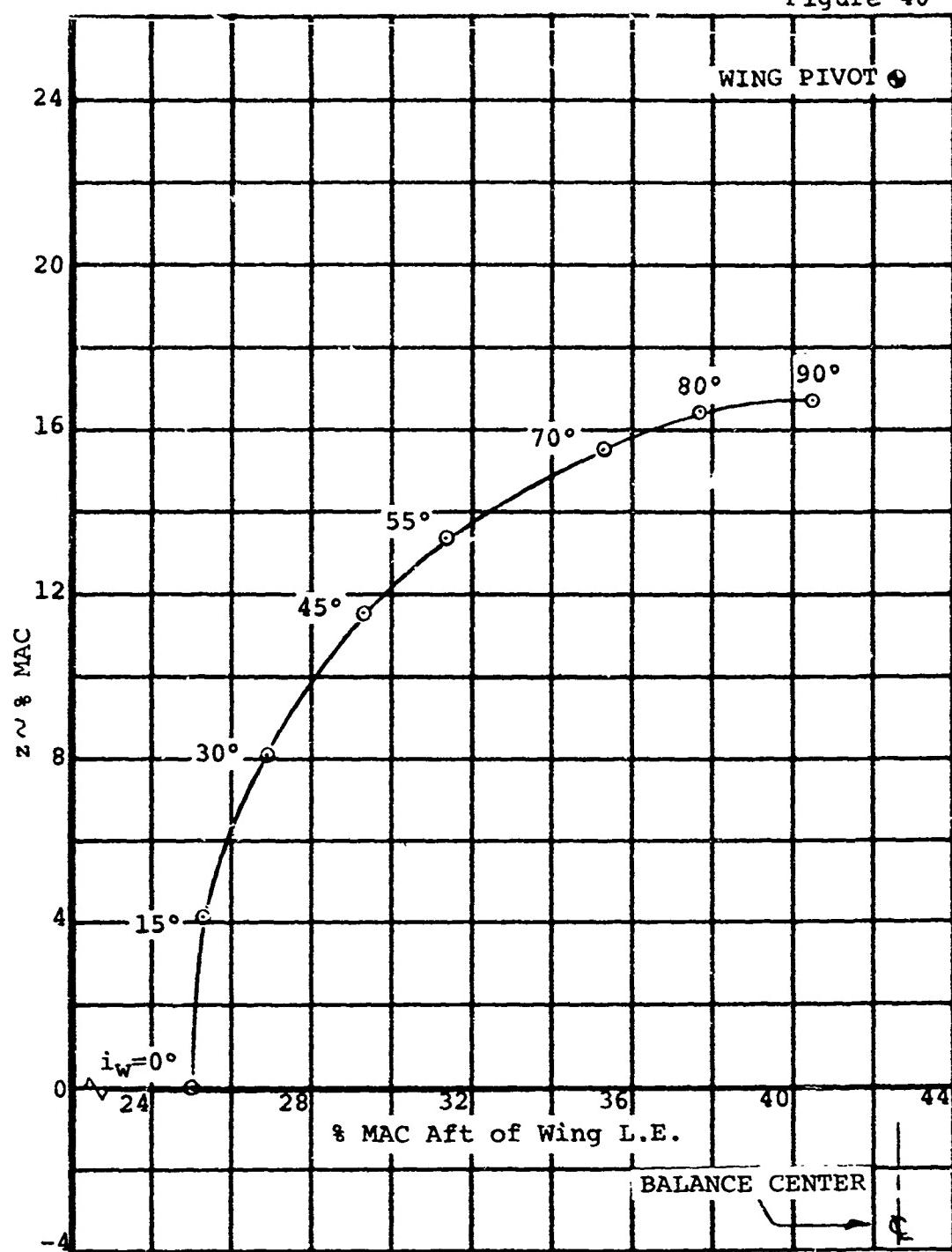
Figure 39



SCHEMATIC RELATIONSHIP BETWEEN
FIXED AND ROTATING PORTIONS OF A/C WEIGHT

D170-10039-1

Figure 40



MOVEMENT OF A/C CENTER OF GRAVITY
WITH WING TILT

6.4.1 Cyclic Pitch Control Effectiveness

Of concern in the investigation of the control capability of installed cyclic propellers was the large increase in basic hub pitching moment produced at high propeller shaft angles or wing tilt angles with the high lift system extended, a condition experienced in descent. Figure 147 of Reference 1 shows that the initial rate of build-up of hub pitching moment on the installed propeller is about three times that of the isolated propeller for the various advance ratios (J) tested with the full span slats extended and flaps deflected to 60°. However, the curves, especially for the outboard props appear to be bending over or "peaking" at much lower angles of attack than the isolated prop. The cyclic pitch control testing performed on the full span model was directed towards determining the possible wing/flap effects on cyclic pitching moment characteristics.

Figure 41 presents a comparison in slipstream coefficients of the pitching moment capability per degree of cyclic obtained on the full span model with those measured on the 1/12th scale isolated propeller model at directly comparable conditions of 5000 RPM and 12° of blade angle. The data presented, is for shaft angles corresponding to essentially constant descent angles over the thrust coefficient range. As indicated, higher shaft angles, which are within 5° of the respective wing tilt angles in this presentation, are required at the larger thrust coefficients or lower forward speeds. The descent case was selected for this presentation, since the combination of shaft angle and wing configuration, full span slats deployed and 60° of flap deflection, would potentially have the largest adverse effect on cyclic pitch effectiveness, due to the increased basic hub pitching moment and possible flow distortion.

Except for the lowest thrust coefficient condition tested (.32 C_T _s), the cyclic pitch effectiveness measured about a mid c.g. of the full span model was larger than that recorded at the hub of the isolated prop model. It is not apparent, even though the data indicates otherwise, that the wing and flaps have a favorable influence on the effectiveness in the C_T _s regime where the cyclic requirements are largest (higher C_T _s values), since it is not apparent that the increase in effectiveness recorded on the full span model is not merely reflecting the favorable change in prop normal force with cyclic previously noted in the hover mode and discussed on Page 62 in Reference 1.

The data slopes shown in Figure 41 for both horizontal tail-on and tail-off configurations were obtained from the curves of

slipstream pitching moment vs cyclic angle presented in Figure 42 and 43, respectively. These figures illustrate the uniformity of the data over the conditions evaluated and the linearity of the control through the range of cyclic angles tested.

The variation of pitching moment per degree of cyclic with fuselage angle for a typical set of test runs, performed with 45° of wing tilt and at a nominal C_{T_s} of 0.81, is presented in Figure 44 for both tail-on and tail-off cases. As indicated for this example, and which is typical for the other conditions tested, the effectiveness decreased at a moderate rate of about 15% from the lowest to the highest shaft angle tested, the important point being that no noticeable decrease occurred as a result of wing stall. This decrease with shaft angle, previously noted when analyzing the isolated prop data and shown in Figure 41, is largely a ramification of the slipstream notation system. All 1/12th scale test runs were performed with a constant propeller RPM and tunnel speed or q , the result being that propeller thrust and slipstream q (q_s) increased with the propeller shaft angle, α_p . Therefore, a hub pitching moment that was found to be virtually independent of shaft angle in propeller notation will appear to decrease when transcribed to the slipstream notation. Part of the decrease can be identified with the small percentage change in lift accompanying cyclic pitch inputs.

Both Figures 41 and 42 show some difference between the cyclic pitch effectiveness measured with the tail on and off. The data in Figure 41, for the descent case, indicates that the tail exerts some favorable influence at thrust coefficient values greater than 0.40.

Figure 41

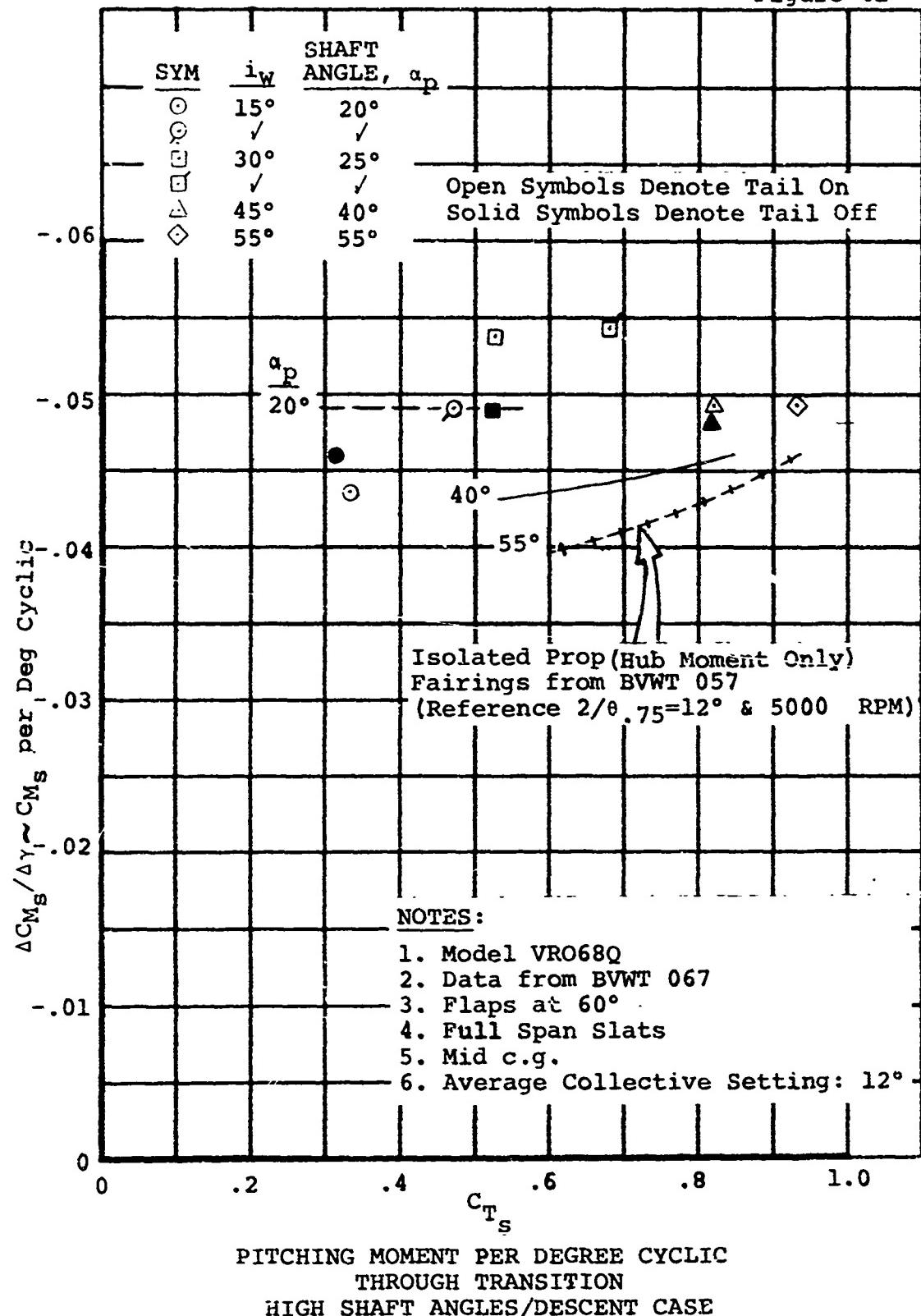


FIGURE 42

NOTES:

1. Model VRO58Q
2. Data from BVWT 067
3. Flaps at 60°
4. Full Span Slats
5. Mid c.g.

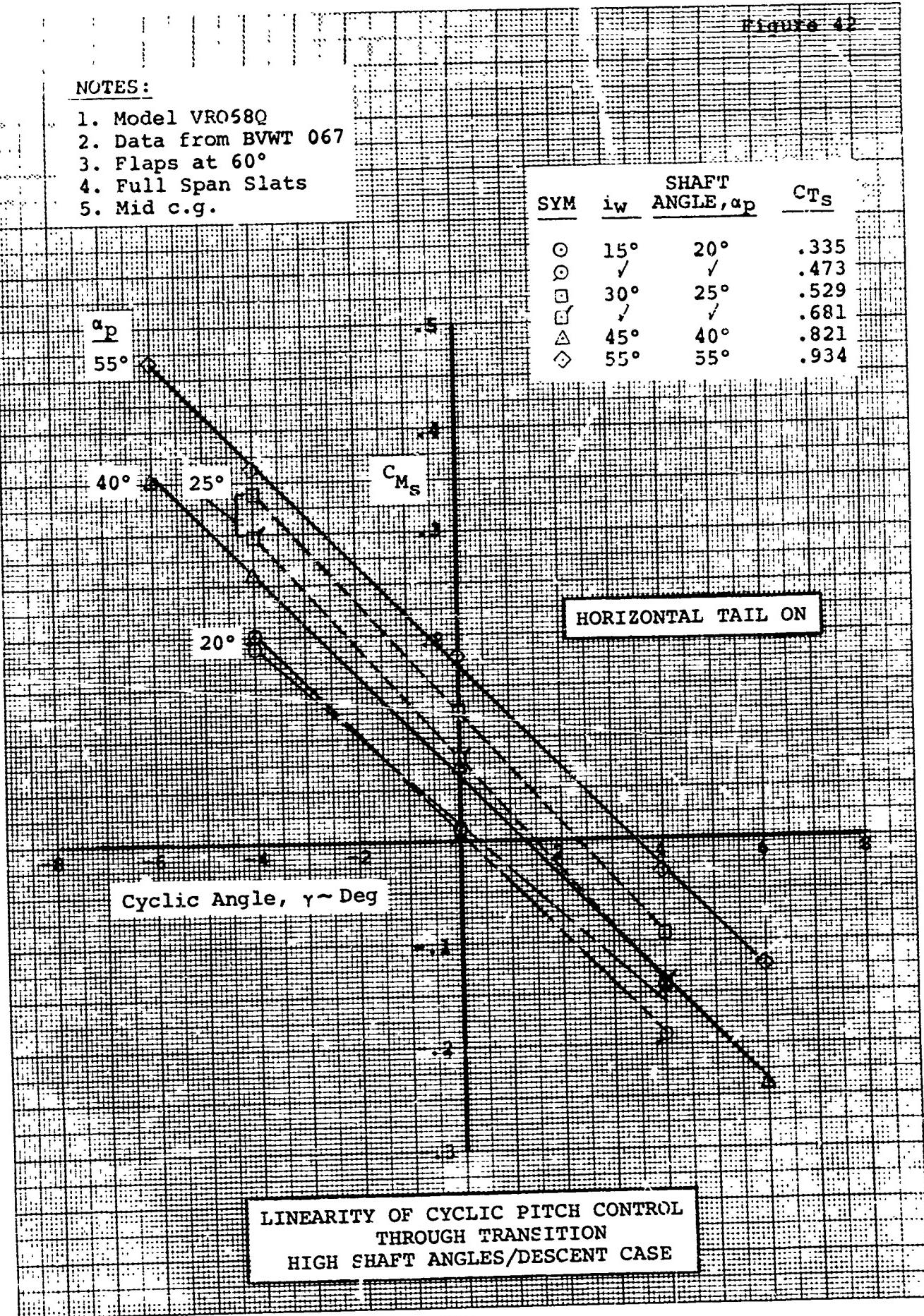


Figure 43

SYM	i_w	SHAFT ANGLE, α_p	C_{Ts}
O	15°	20°	.318
□	30°	25°	.524
△	45°	40°	.819

NOTES:

1. Model VRO68Q
2. Data from BVWT 067
3. Flaps at 60°
4. Full Span Slats
5. Mid c.g.

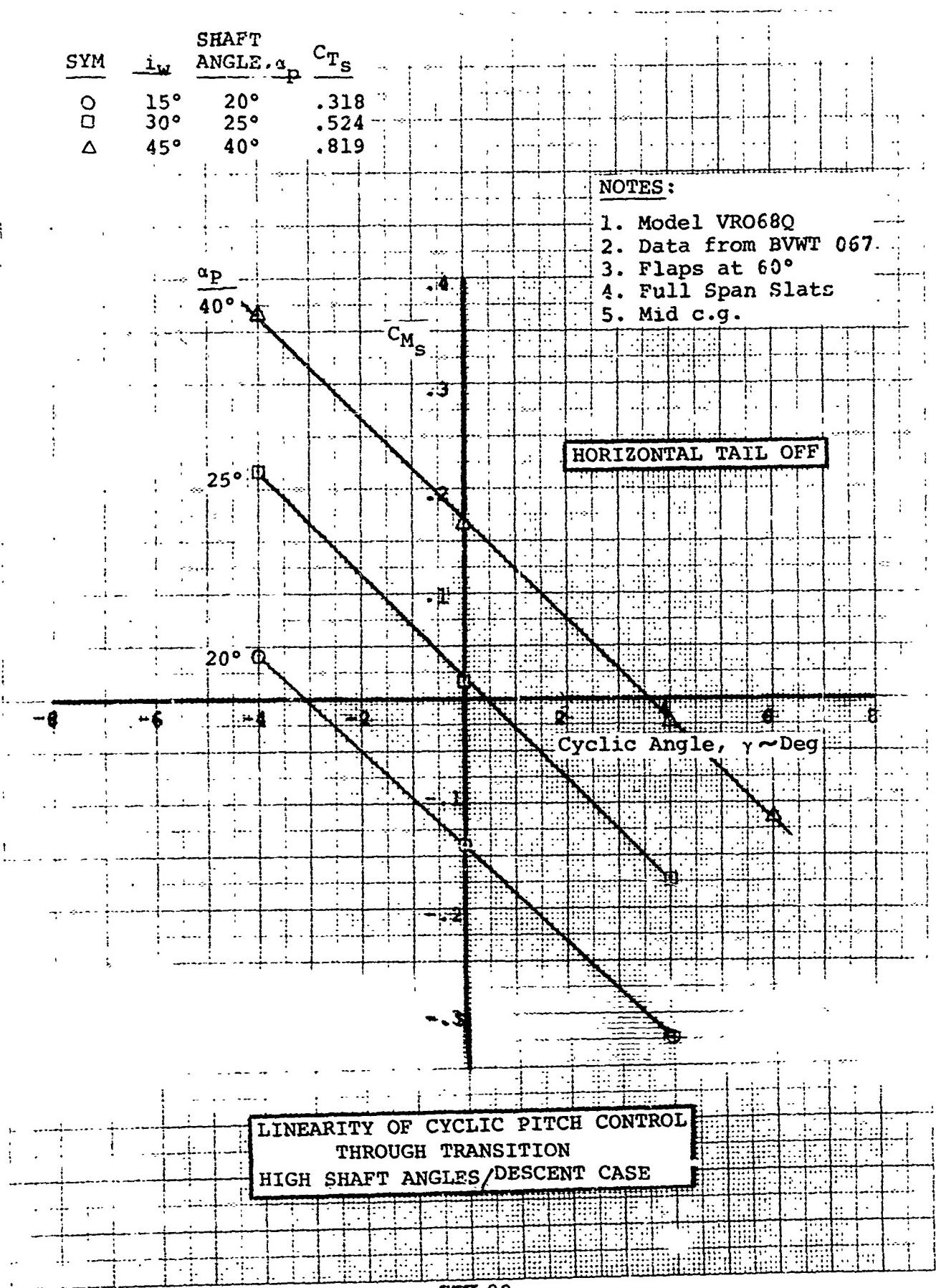
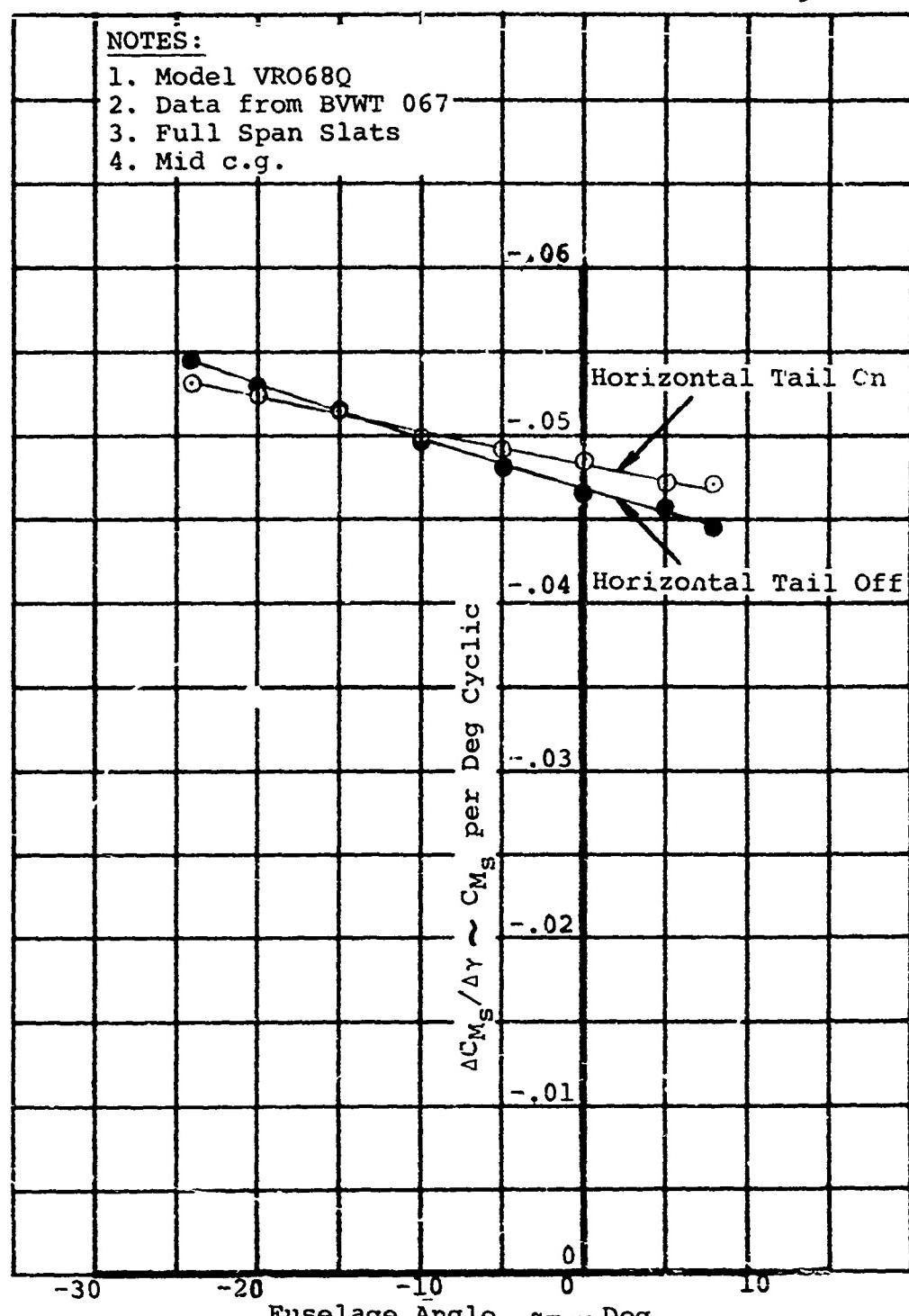


Figure 44



VARIATION OF CYCLIC PITCH EFFECTIVENESS

WITH FUSELAGE ANGLE

$$i_w = 45^\circ, \delta_F = 60^\circ, \text{ NOM } C_{T_S} = .81$$

4.4.2 Effect of Cyclic Pitch on Longitudinal Stability

The effect of cyclic pitch on longitudinal stability is inherent in the test runs performed both horizontal tail on and off for the purpose of establishing the cyclic pitch effectiveness. Figure 45 presents the measured tail-off and tail-on stability in the slipstream derivative form $C_{M_{S_a}}$. The data

shown for selected combinations of wing tilt angle and slipstream thrust coefficient through transition with 60° of flap, is applicable to the mid c.g. position described in Figure 40 which moves up and aft as the wing is tilted about the pivot located 42.6% of the mean aerodynamic chord (MAC) aft of the wing leading edge and 11.7% MAC below the wing chord plane.

Slopes shown in Figure 45 were measured from the pitching moment plots (C_{M_s} vs α_F) presented later in this report section and were extracted from the linear portion of the curves. The C_{T_s} value designated for each data point is the average value for the angle of attack range considered in choosing a slope.

Figure 45 presents two sets of data for the zero cyclic case. The data denoted by solid lines was obtained with a propeller RPM of 6800 during the Phase I test and the plotted points were acquired at the cyclic hub operating speed of 5000 RPM. The object of the dual set of data was to ascertain the quality of the information acquired at a Reynolds number lower than 1.2 (10^6) achieved with a RPM of 6800. The effect of stability can be noted to be small.

Figure 45 indicates that the application of cyclic pitch does not have a marked effect on longitudinal stability with the effect diminishing with increasing thrust coefficients or decreasing flight speeds. Positive cyclic angles can be seen to increase the tail-off instability and negative cyclic decrease the instability. Since the same incremental effects were recorded both tail-on and tail-off, the changes in stability probably reflect the combined influence of cyclic pitch on (1) propeller hub moment and normal force when interpreted in the slipstream notation and on (2) aircraft lift curve slope that increases with negative cyclic and decreases with positive cyclic.

Of concern during the testing was whether the thrustline offset occurring with cyclic pitch application would modify the downwash gradient and thus produce substantial changes to tail-on stability, especially at the lower range of thrust coefficients where the horizontal tail is particularly effective for stability and control. The change in q at the tail plane as a result of effectively raising or lowering the thrustline

with cyclic pitch would act in the opposite direction and tend to provide for example, increased tail-on stability with positive cyclic angles. Apparently the high tail positioning reduces any influence of cyclic pitch on the downwash gradient and q at the tail to a minimum with the only noticeable influence occurring at the lowest thrust coefficient tested and 15° of wing tilt. At this condition of $0.28 C_{T_s}$, the incremental change from tail-off to tail-on stability increased with positive cyclic and decreased with negative cyclic, thus indicating the q change at the tail to be the predominate effect.

Figures 46 through 77 include the basic data from which the cyclic pitch control capability and its effect on longitudinal stability were established. Figures 46 through 66 and Figures 67 through 77 present horizontal tail-on and horizontal tail-off data, respectively. The data, in slipstream notation, is presented in sets of three plots, C_{M_s} vs. α_f (pitching moment curves), C_{L_s} vs. C_{X_s} (force polars), and C_{L_s} vs. α_f (lift curves), in the order of increasing wing tilt angle and slipstream thrust coefficient, C_{T_s} . In these plots, CMCS, CLCS, and CXCS, which represent wind axis data, should be read as C_{M_s} , C_{L_s} and C_{X_s} , respectively. ALPHA signifies fuselage angle.

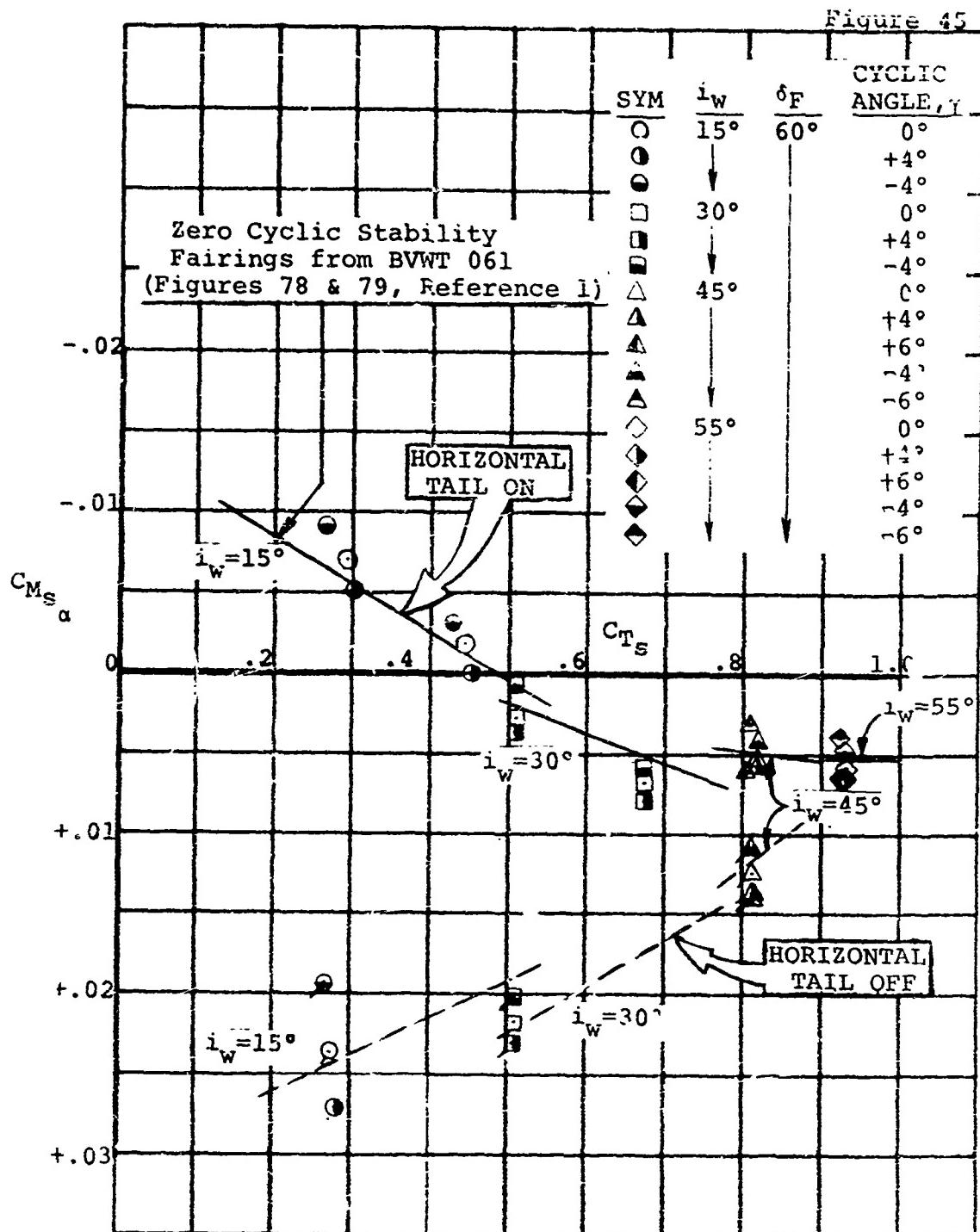
The following graphs contain series of runs with different cyclic pitch settings, all conducted at a constant propeller RPM or nominal C_{T_s} and a selected wing tilt/flap configuration. Noted on each force polar presentation are lines corresponding to 10° descent and 10° climb conditions. Interspersed between the sets of data are plots of the variation of slipstream thrust coefficient that occurred during the test runs.

Figure 63 presents typical full span model cyclic pitch control data, in this case, data acquired with 55° of wing tilt at C_{T_s} of 0.93 which represents a forward flight pat speed of approximately 30 knots. The linearity of the change in pitching moment with cyclic angle and the small variation in effectiveness with angle of attack is characteristic of the other cyclic pitch control data that was obtained.

An examination of the individual pitching moment plots, for example Figure 46 (15° wing tilt/ 60° flaps/.3 C_{T_s}), will reveal that the pitching moment varies linearly with fuselage angle of attack over the initial portion of the angle of attack range tested. At a particular angle of attack for a given test condition, the tail-on stability ($C_{M_{S_a}}$) appears to increase.

This characteristic was identified in Section 6.4.4 of Reference 1 as being concurrent with flow separation on top of the fuselage that in turn decreased the downwash gradient prevailing at the horizontal tail. Reference 1 also discussed the change in character of the flow aft of the tilted wing and lack of separation at combinations of high wing tilt angles (45° and above) and high thrust coefficients ($.92 C_{T_s}$) and the resulting linearity of the pitching moment curves over the angle of attack range evaluated. See Figure 64.

As stated previously, a comparison of the pitching moment data obtained during this test (BVWT 067) with a propeller speed of 5000 RPM and the data acquired during the Phase I test (BVWT 061) with a propeller speed of 6800 RPM showed little change in the measured aircraft stability. This comparison also showed a positive shift in pitching moment between the Phase II data and the Phase I data that amounted to $0.06 \Delta C_M$ at $0.3 C_{T_s}$ and 15° of wing tilt and a similar value at $0.81 C_{T_s}$ and 45° of wing tilt. The reason for this shift has not been firmly established at this time, but a source of a portion of the shift could have arisen as a result of a lower flap effectiveness ensuing from the lower Reynolds number of the Phase II test.



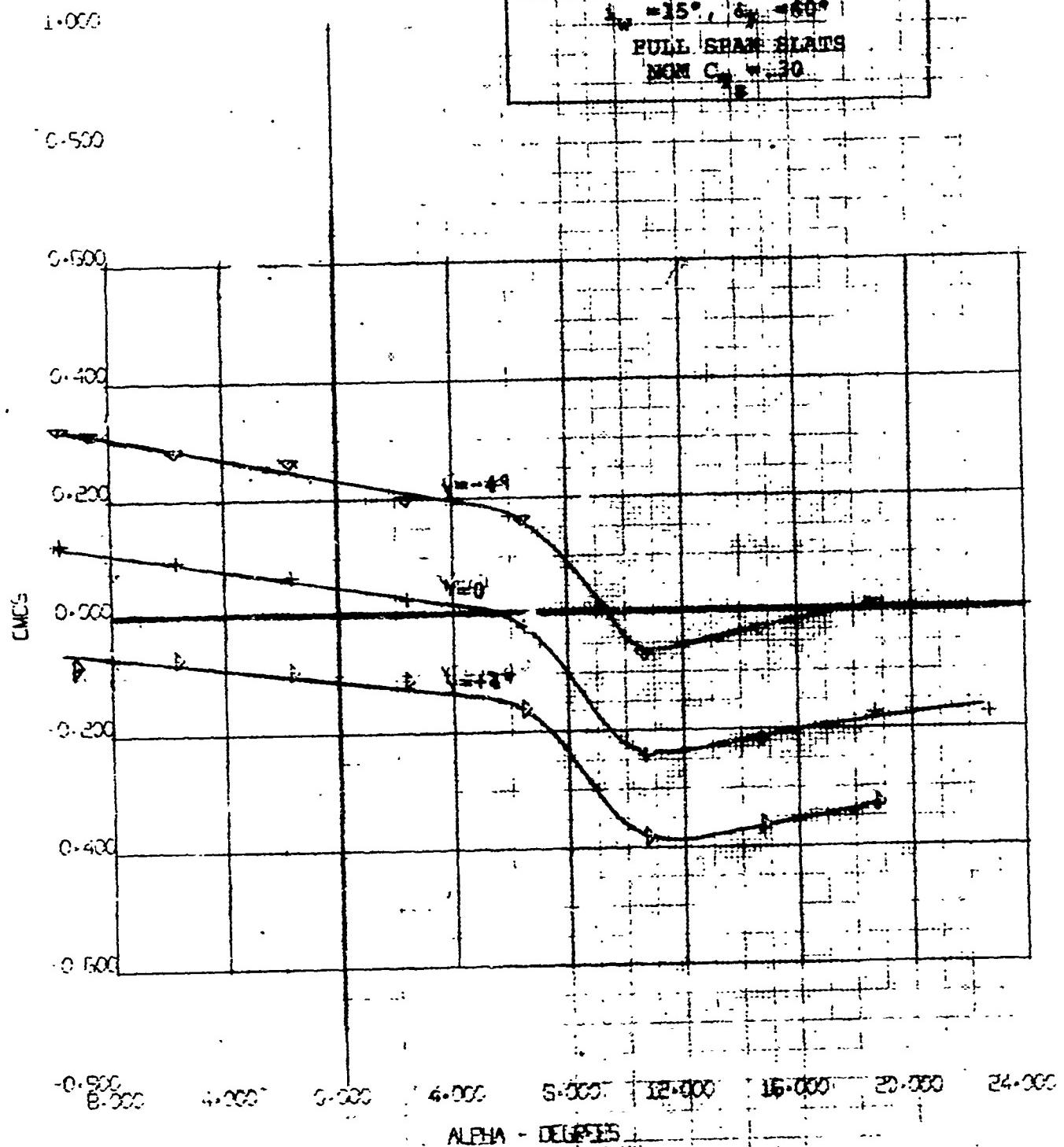
EFFECT OF CYCLIC PITCH ON LONGITUDINAL STABILITY

RUN SYM α γ
 31 + $+5^\circ$ 12.1 0
 33 △ $+4^\circ$
 39 ▽ -4°

NUMBER 5170-10039-1
 REV. LTR.

Figure 46

CYCLOIC PITCH COEFFICIENT, CM
 $\alpha_w = 15^\circ, \delta_w = 60^\circ$
 FULL SPAN SLATS
 NOM C_w = .30

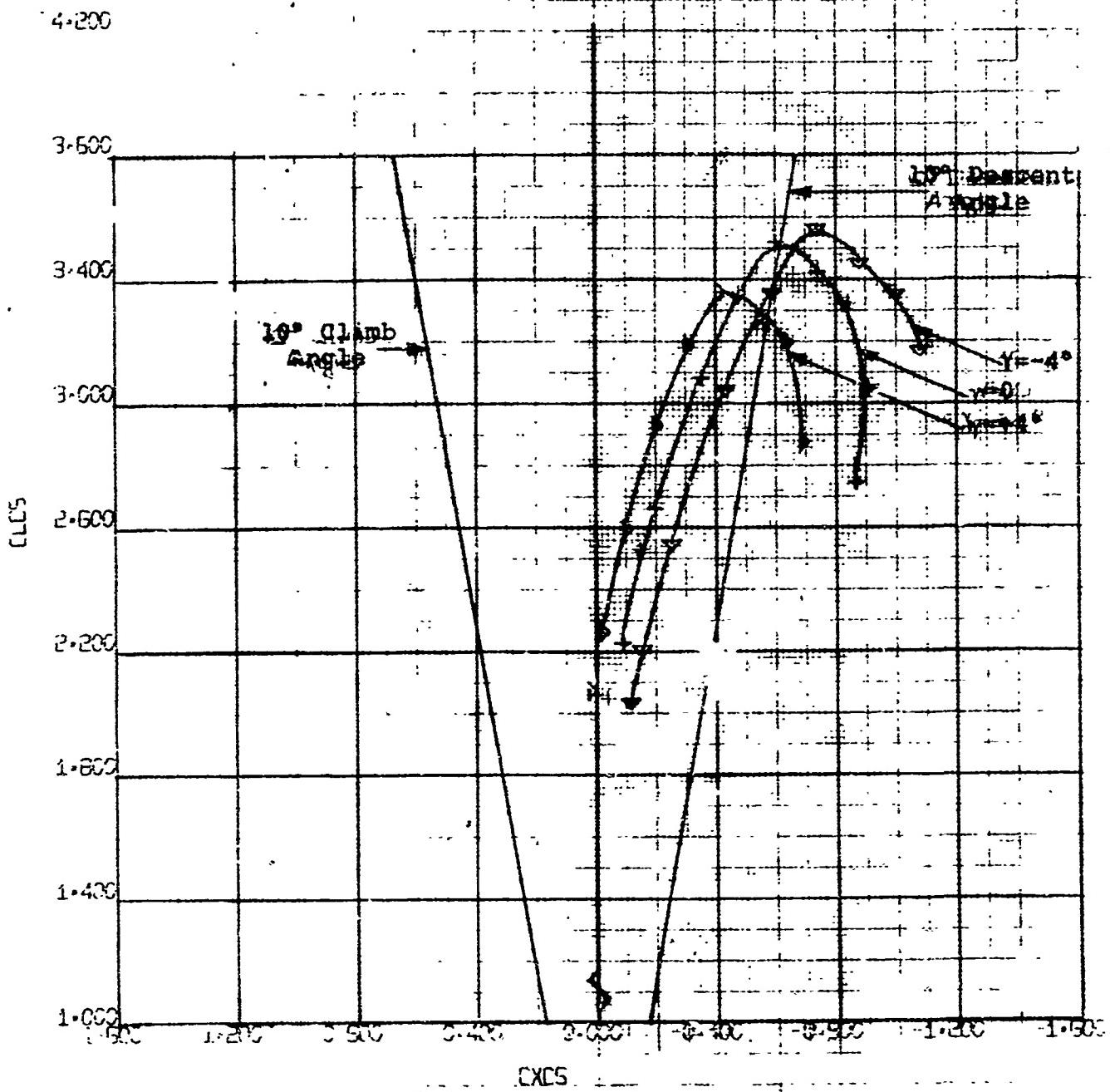


FOUR-PROP TILT WING MODEL W/ROTOR (FULL SPAN) CWS VS. ALPHA	BENT 6°
	12/6/70

Figure 57

RUN	SYM	α	q	γ
31	+	+5°	12.1	0
33	▷			+4°
39	▽			-4°

CYCLOC PITCH CONTROL/TAIL ON
 $i_w = 15^\circ$, $\delta_F = 50^\circ$
 FULL SPAN STAB
 NOM $C_T = .30$



FOUR-PROF TILT WING	BWWT
MODEL VROS8G (FULL SPAN)	67
CL _S VS. CL _{EX}	12/870

NOT REPRODUCIBLE

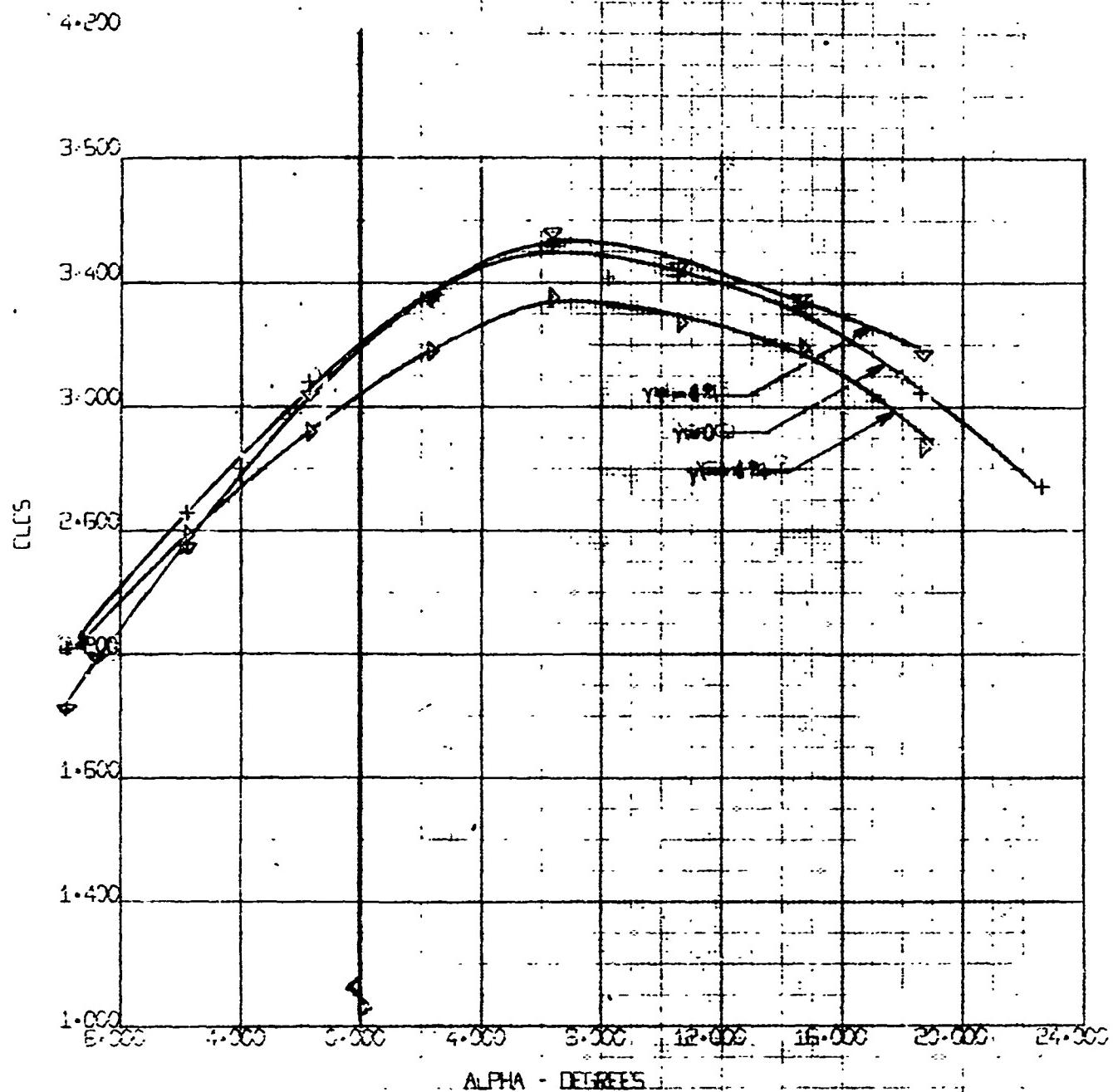
SHEET 105

NUMBER D170-10039-1
REV. LTR.

Figure 48

RUN SYM $\frac{q}{12.1}$ $\frac{\gamma}{0}$
 31 + +5°
 33 ▽ +4°
 39 △ -1°

CYCLOP PITCH CONTROL/TAIL ON
 $i_w = 15^\circ$, $\delta_p = 60^\circ$
 FULL SPAN SLATS
 NOM $C_m = .30$



FOUR-PROP TILT WING MODEL VROBG (FULL SPAN) CLS VS. ALPHA	BWWT 67 12/ 6.70
---	------------------------

NUMBER D17D-10039-1

REV. LTR.

FIGURE 49

RUN SYM $\frac{q}{g}$ $\frac{\gamma}{g}$

30 + +5° 9.1

32 ▷ +4°

38 ▷ -4°

1.000

0.800

0.600

0.400

0.200

0.000

-0.200

-0.400

-0.600

-0.500

B.000

4.000

0.000

4.000

8.000

12.000

16.000

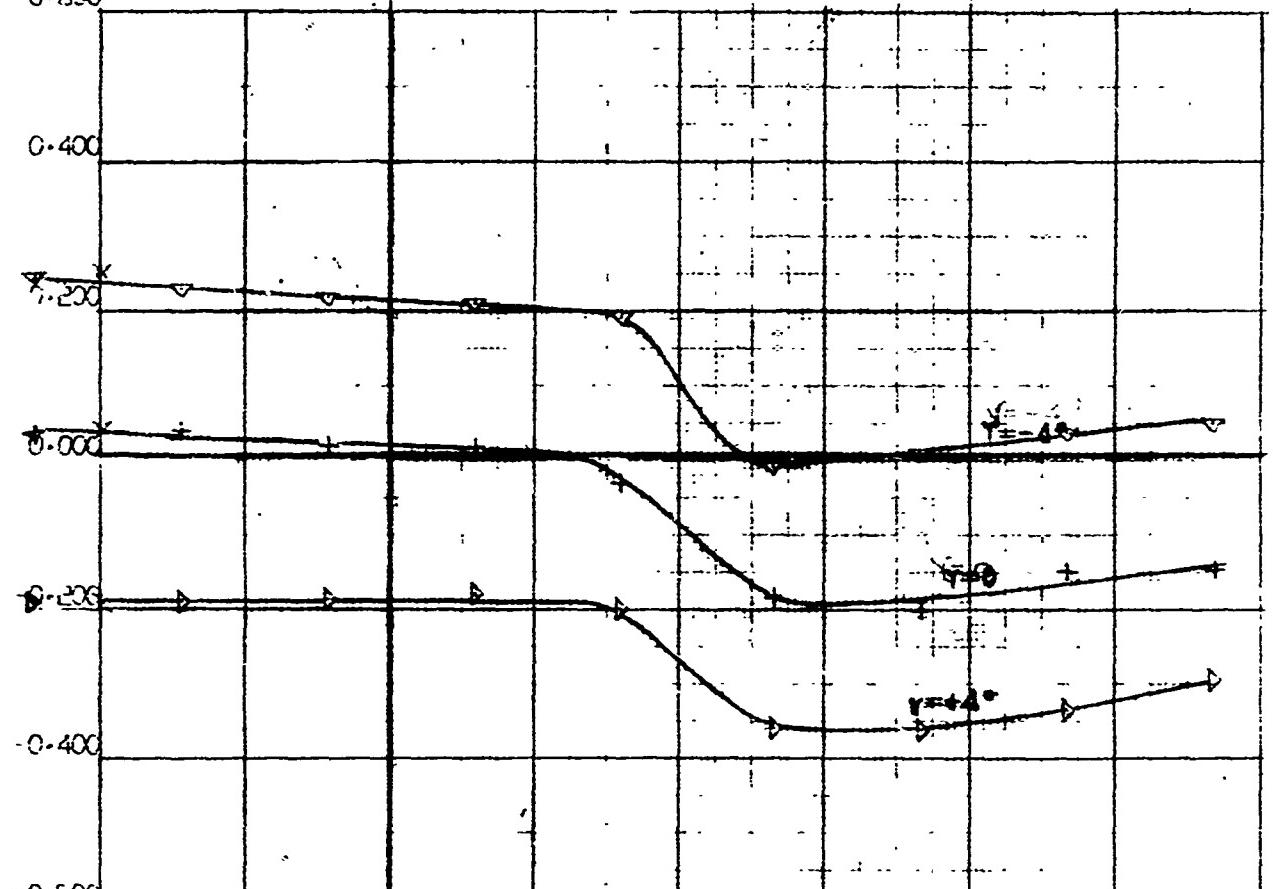
20.000

24.000

ALPHA - DEGREES

CYCLIC PITCH CONTROL/TAIL ON
 $i_w = 15^\circ$ $\delta_p = 60^\circ$
 FULL SPAN SLATS
 NOM. C_L = .45
 +8%

CMCS



-0.500 B.000 4.000 0.000 4.000 8.000 12.000 16.000 20.000 24.000

ALPHA - DEGREES

FOUR-PROP TILT WING MODEL VROBB (FULL SPAN)	BWNT 6/
CMCS VS. ALPHA	12/ 8/70

+

NOT REPRODUCIBLE

SHEET 107

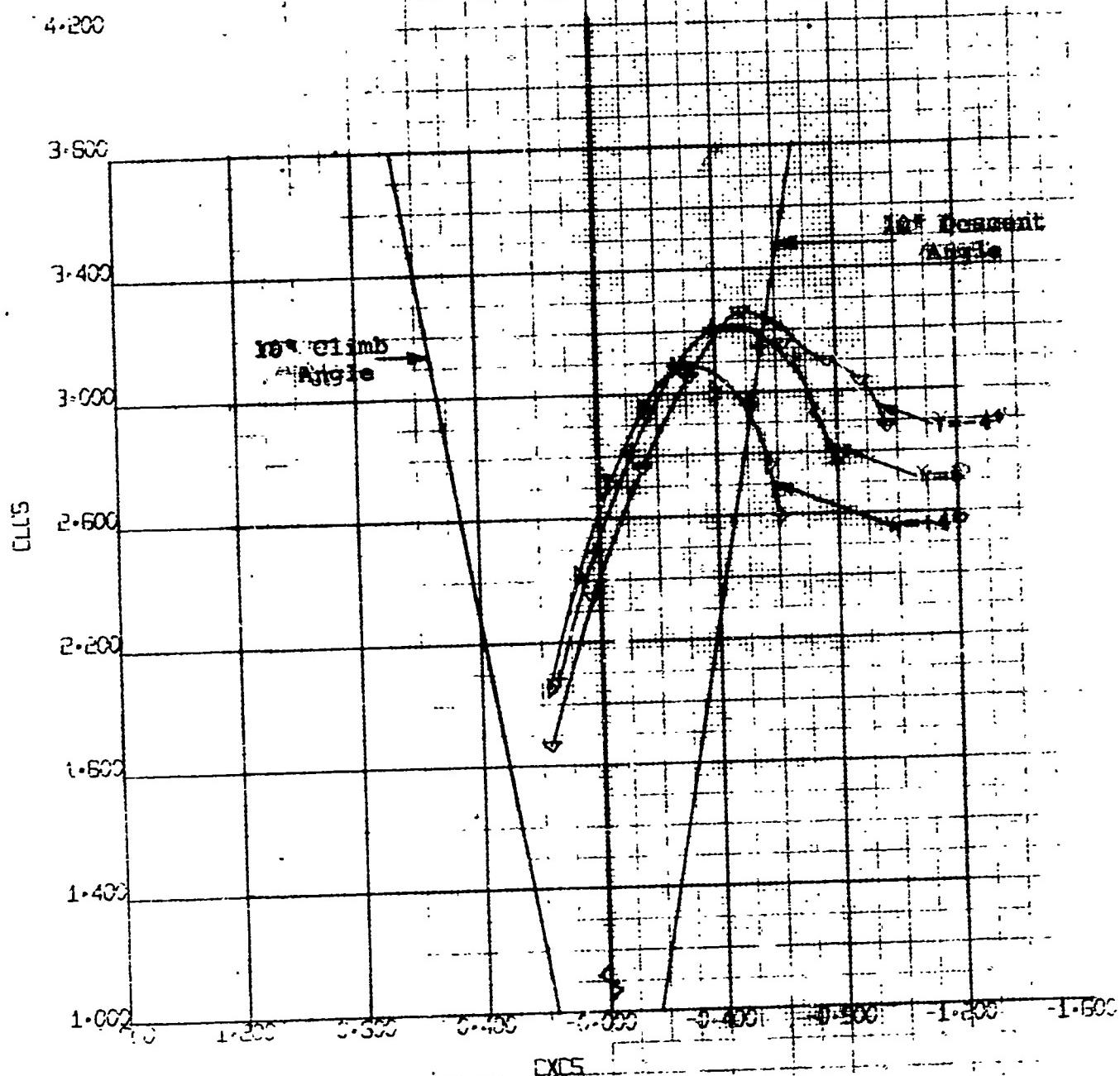
NUMBER D170-10039-1

REV. LTR.

Figure 50

RUN	SYM	$\frac{d}{G}$	G	γ
30	+	+5°	9.1	0
32	▷			+4°
38	▽			-4°

CYCLIC PITCH CONTROL TAIL ON
 $i_w = 15^\circ$, $i_t = -60^\circ$
 FULL SPAN SEATS
 NOM. $C_{T_B} = .45$



FOUR-PROP TILT WING	EWWT
MODEL YR280 (FULL SPAN)	67
CLCS VS. CLDS	12/6/70

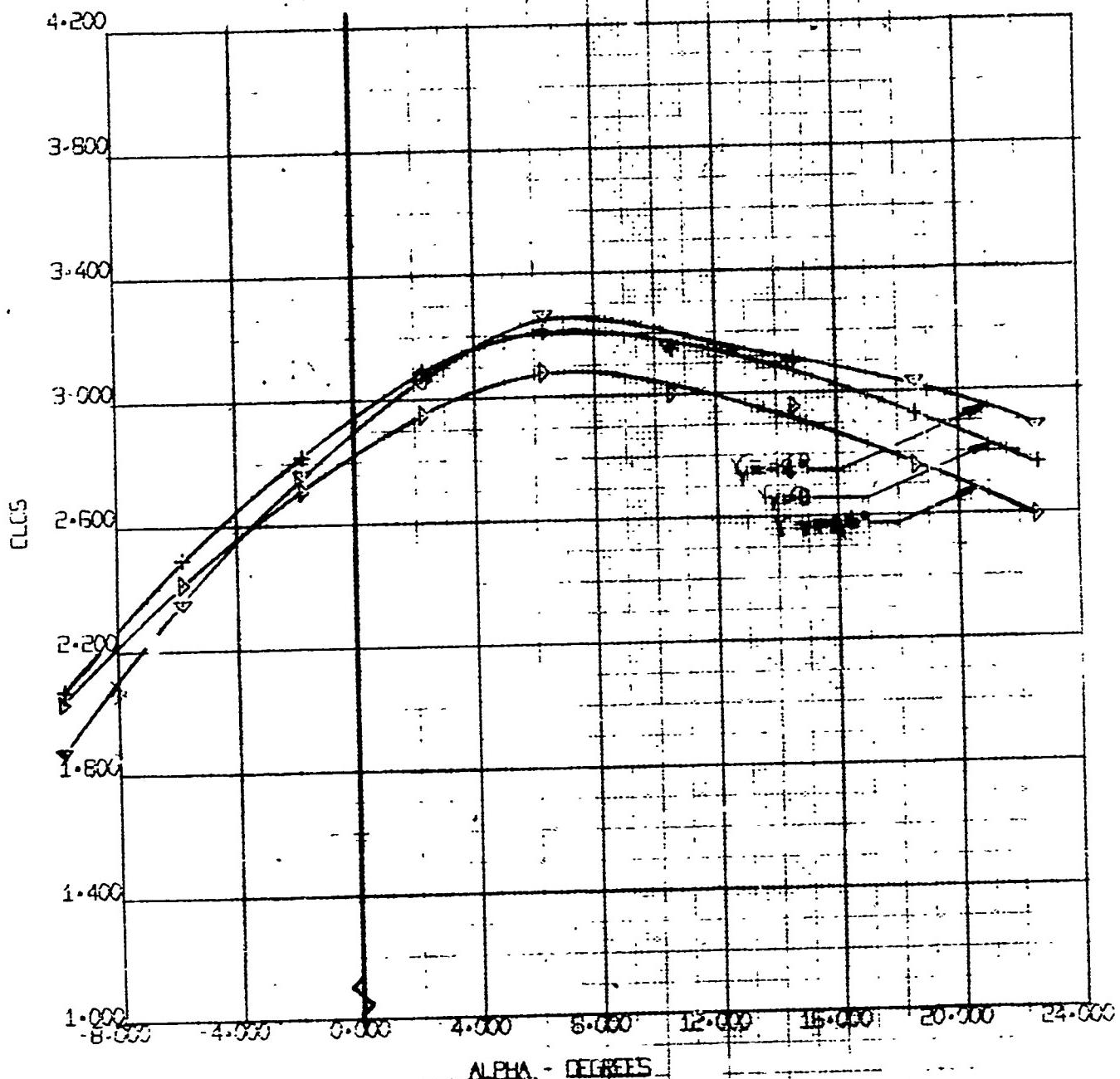
NUMBER D170-10039-1

REV. LTR.

Figure 51

RUN SYM $\frac{4}{6}$ $+5^\circ$ $\frac{9}{1}$ $\frac{Y}{6}$
 30 + ↓ ↓
 32 ▷ ↓ ↓
 38 ▷ ↓ ↓

CYCLOIC PITCH CONTROL/TAIL ON
 $i = 15^\circ$, $\beta = 50^\circ$
 FULL SPAN SLATS
 NOM $C_T = .45$



FOUR-PROP TILT WING	BWWT
MEET VRG69(FULL SPAN)	67
CLs VS. ALPHA	12/8/70

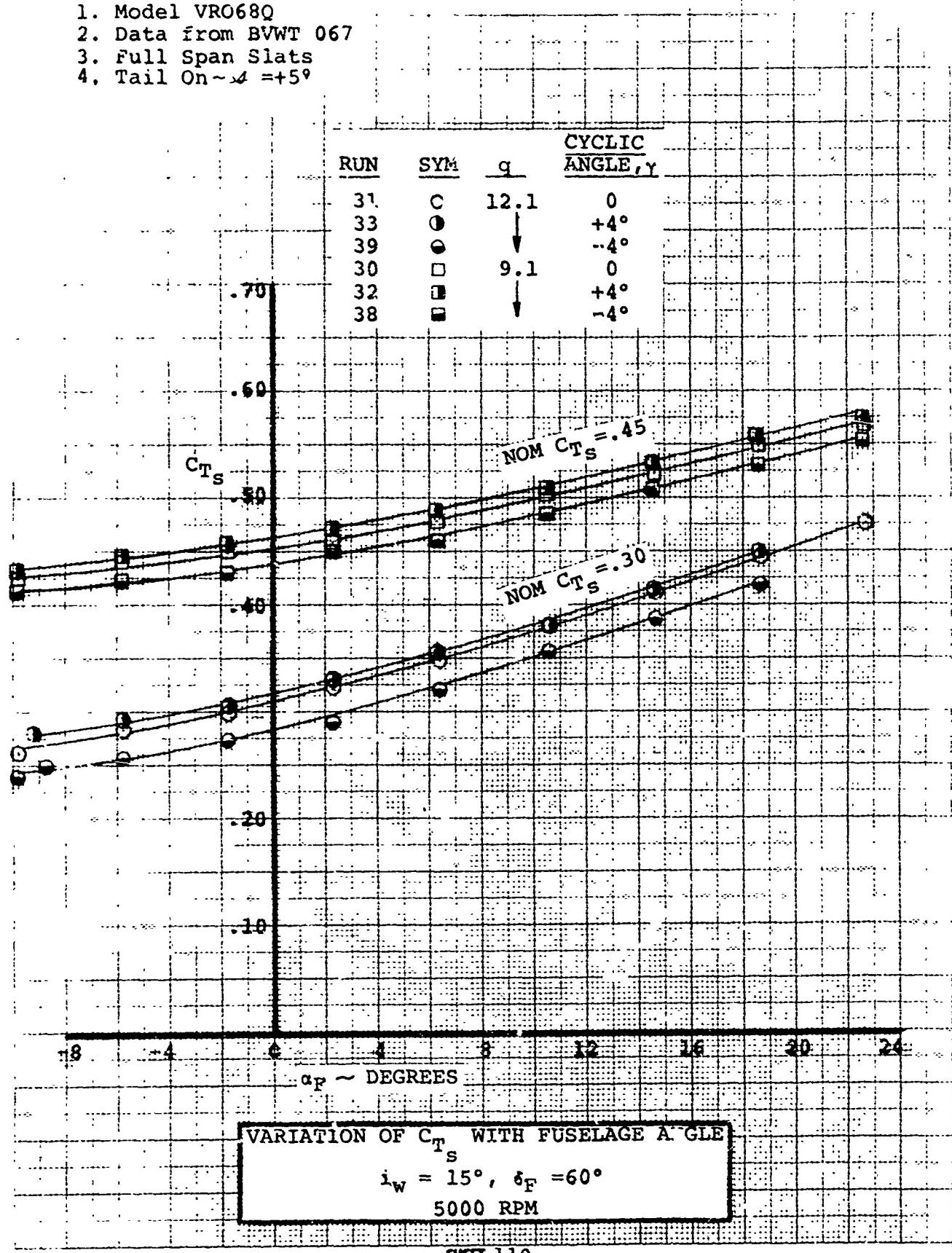
SHEET 109

NOT REPRODUCIBLE

Figure 52

NOTES:

1. Model VR068Q
2. Data from BVWT 067
3. Full Span Slats
4. Tail On ~ $\alpha = +5^\circ$



NUMBER D170-10039-1

REV. LTR.

Figure 53

RUN	SYM	α	q	γ
50	+	+15°	8.2	0°
35&61	▷ & R			+4°
37&70	▽ & R			-4°

1.000

CYCLOPITCH CONTROL/TAIL ON
 $\alpha_w = 30^\circ$, $\delta_w = 60^\circ$
 FULL SPAN FLAPS
 NOM. CT_s = .55

0.500

0.000

-0.500

-1.000

-1.500

-2.000

-2.500

-3.000

-3.500

-4.000

-4.500

-5.000

-5.500

-6.000

-6.500

-7.000

-7.500

-8.000

-8.500

-9.000

-9.500

-10.000

-10.500

-11.000

-11.500

-12.000

-12.500

-13.000

-13.500

-14.000

-14.500

-15.000

-15.500

-16.000

-16.500

-17.000

-17.500

-18.000

-18.500

-19.000

-19.500

-20.000

-20.500

-21.000

-21.500

-22.000

-22.500

-23.000

-23.500

-24.000

-24.500

-25.000

-25.500

-26.000

-26.500

-27.000

-27.500

-28.000

-28.500

-29.000

-29.500

-30.000

-30.500

-31.000

-31.500

-32.000

-32.500

-33.000

-33.500

-34.000

-34.500

-35.000

-35.500

-36.000

-36.500

-37.000

-37.500

-38.000

-38.500

-39.000

-39.500

-40.000

-40.500

-41.000

-41.500

-42.000

-42.500

-43.000

-43.500

-44.000

-44.500

-45.000

-45.500

-46.000

-46.500

-47.000

-47.500

-48.000

-48.500

-49.000

-49.500

-50.000

-50.500

-51.000

-51.500

-52.000

-52.500

-53.000

-53.500

-54.000

-54.500

-55.000

-55.500

-56.000

-56.500

-57.000

-57.500

-58.000

-58.500

-59.000

-59.500

-60.000

-60.500

-61.000

-61.500

-62.000

-62.500

-63.000

-63.500

-64.000

-64.500

-65.000

-65.500

-66.000

-66.500

-67.000

-67.500

-68.000

-68.500

-69.000

-69.500

-70.000

-70.500

-71.000

-71.500

-72.000

-72.500

-73.000

-73.500

-74.000

-74.500

-75.000

-75.500

-76.000

-76.500

-77.000

-77.500

-78.000

-78.500

-79.000

-79.500

-80.000

-80.500

-81.000

-81.500

-82.000

-82.500

-83.000

-83.500

-84.000

-84.500

-85.000

-85.500

-86.000

-86.500

-87.000

-87.500

-88.000

-88.500

-89.000

-89.500

-90.000

-90.500

-91.000

-91.500

-92.000

-92.500

-93.000

-93.500

-94.000

-94.500

-95.000

-95.500

-96.000

-96.500

-97.000

-97.500

-98.000

-98.500

-99.000

-99.500

-100.000

-100.500

-101.000

-101.500

-102.000

-102.500

-103.000

-103.500

-104.000

-104.500

-105.000

-105.500

-106.000

-106.500

-107.000

-107.500

-108.000

-108.500

-109.000

-109.500

-110.000

-110.500

-111.000

-111.500

-112.000

-112.500

-113.000

-113.500

-114.000

-114.500

-115.000

-115.500

-116.000

-116.500

-117.000

-117.500

-118.000

-118.500

-119.000

-119.500

-120.000

-120.500

-121.000

-121.500

-122.000

-122.500

-123.000

-123.500

-124.000

-124.500

-125.000

-125.500

-126.000

-126.500

-127.000

-127.500

-128.000

-128.500

-129.000

-129.500

-130.000

-130.500

-131.000

-131.500

-132.000

-132.500

-133.000

-133.500

-134.000

-134.500

-135.000

-135.500

-136.000

-136.500

-137.000

-137.500

-138.000

-138.500

-139.000

-139.500

-140.000

-140.500

-141.000

-141.500

-142.000

-142.500

-143.000

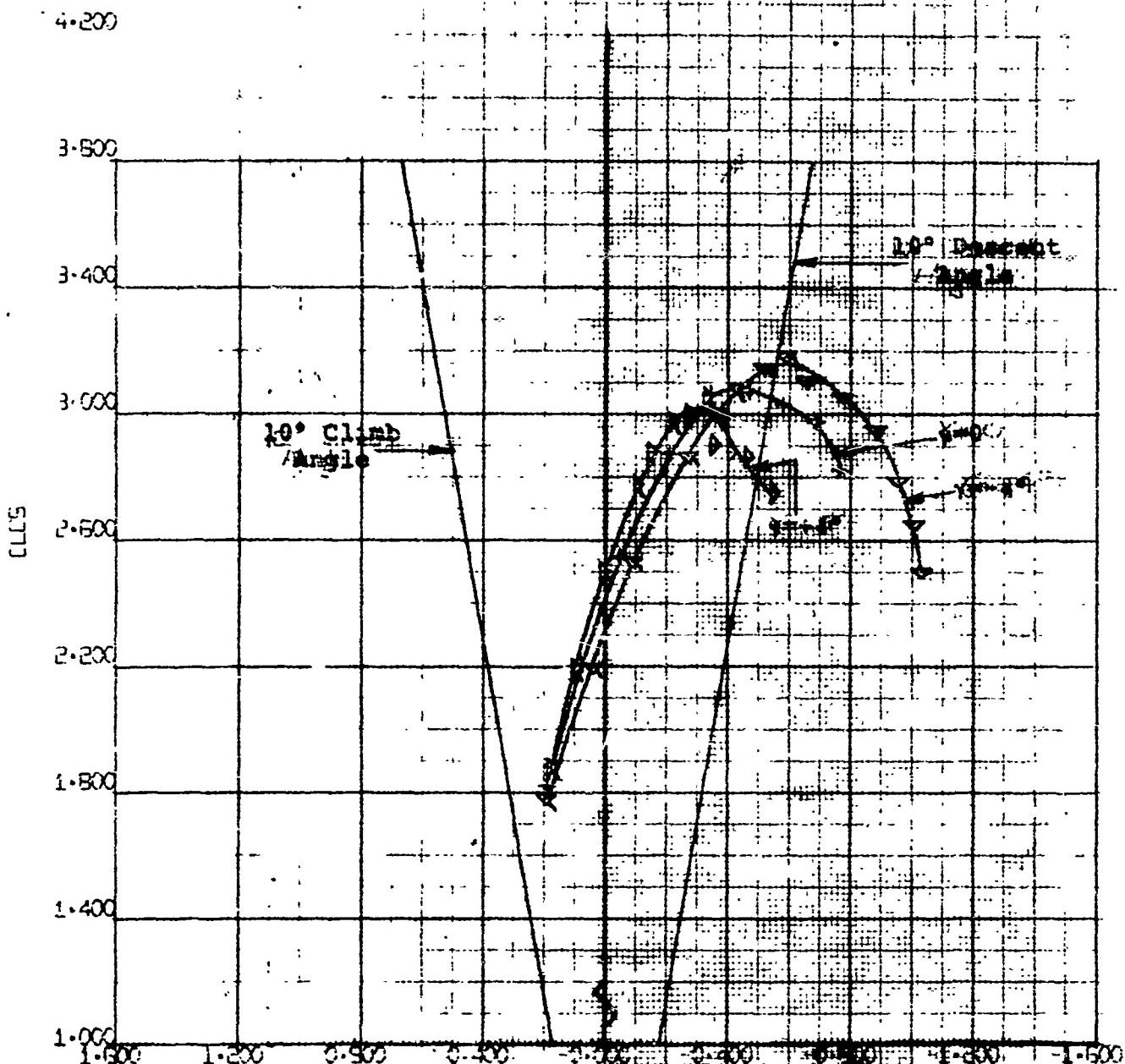
-143

RUN SYM $\frac{1}{4}$ $\frac{a}{8}$ γ
 59 + $+15^\circ$ 8.2 0°
 35&61 D&R \downarrow $+4^\circ$
 37&70 $\nabla \& \Delta$ \downarrow -4°

NUMBER D170-10099-1
REV. LIR.

Figure 54

CYCLOIC PITCH CONTROL/TAIL ON
 $\alpha = 30^\circ$, $\delta_p = 50^\circ$
FULL SPAN FLAPS
 NOM $C_T = .55$



DICS

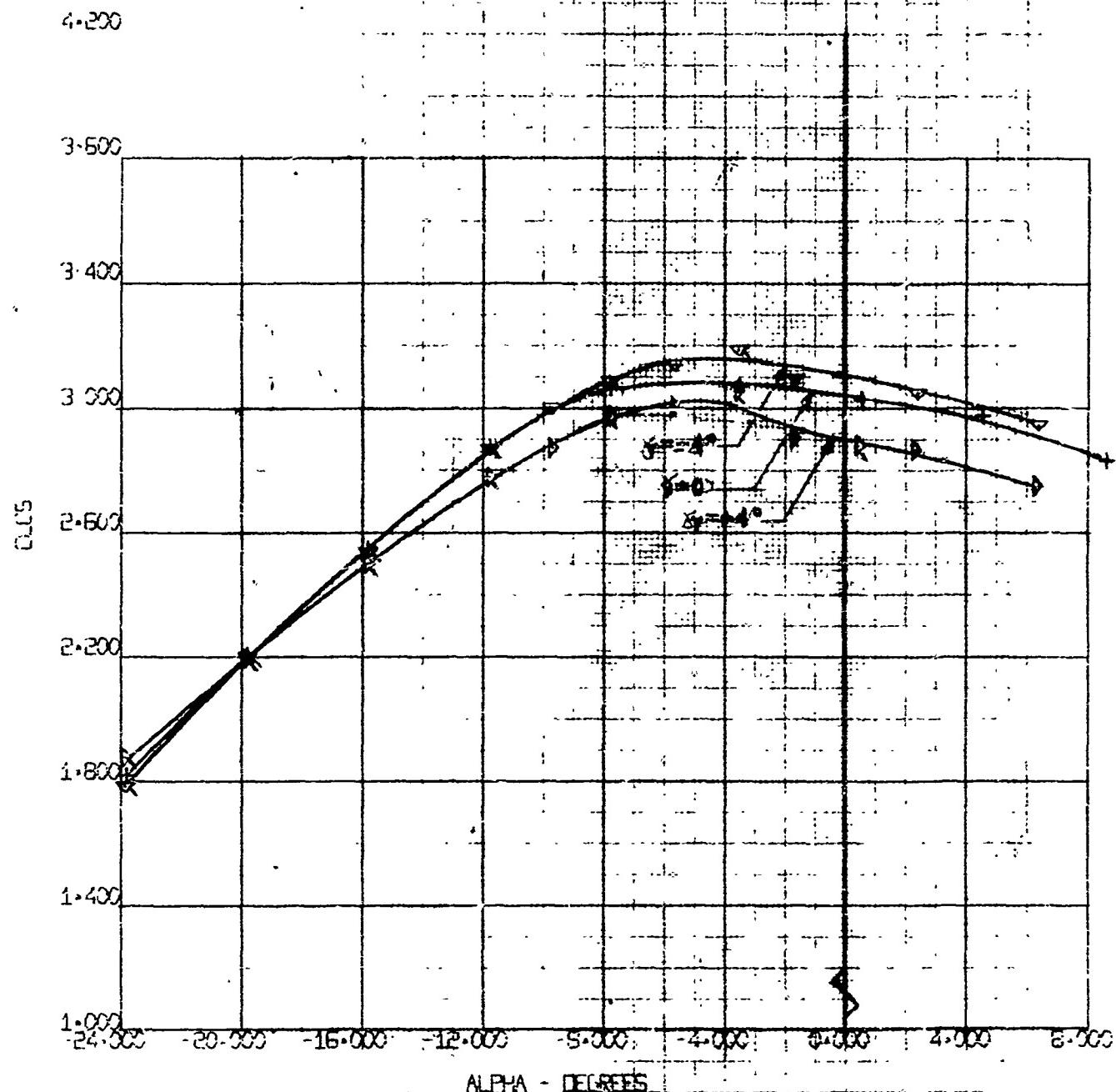
FOUR-PROF TILT WING	BWWT
MODEL V2000 (FULL SPAN)	67
FLDS VS. FMS	

12/10/70	
----------	--

RUN	SYM	α	a	y
50	+	+15°	8.2	0°
35&61	>&R			+4°
37&70	▽&X			-4°

Figure 55

CYCLOP PITCH CONTROL/TAIL ON
 $\delta_T = 30^\circ$, $\delta_E = 60^\circ$
 FULL SPAN FLAPS
 NOM C_T +.55



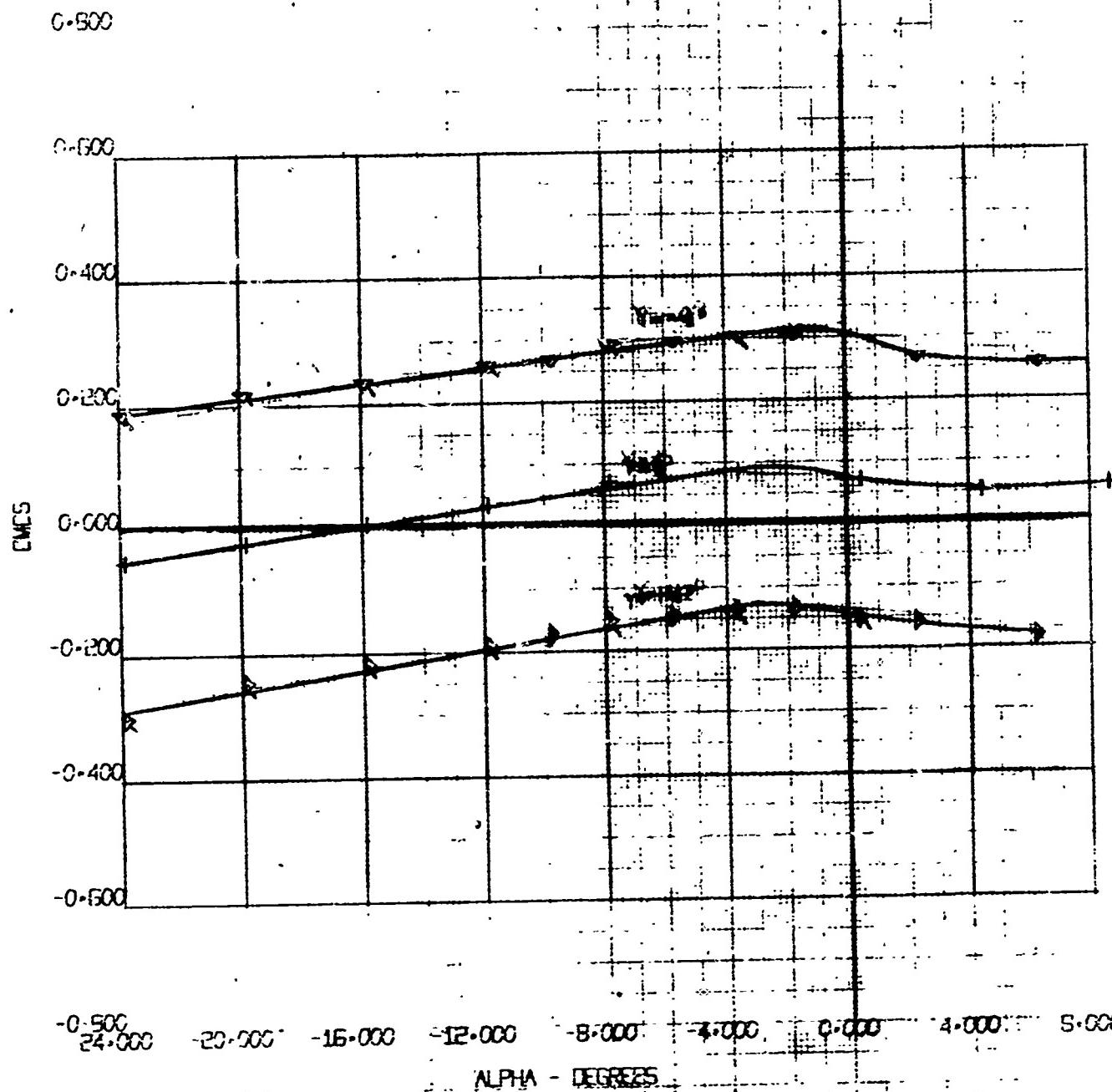
FOUR-PROP. TILT WING MODEL VROB6 (FULL SPAN) CL's VS. ALPHA	BWWT 67 12/10/70
---	------------------------

NOT REPRODUCIBLE

NUMBER D170-10039-1
REV. LTR. Figure 56

RUN	SYM	α	β	γ
51	+	+15°	5.3	0
34&60	△			+4°
36&69	▽			-4°
1.000				

CYCLOP PITCH CONTROL/TAIL ON
W = 30° T = 60°
FULL SPAN SLATS
NOM C_T = .79



FOUR-PROP TILT WING
MODEL YR06BQ (FULL SPAN)
CL vs. α

BWNT
67
12/10/70

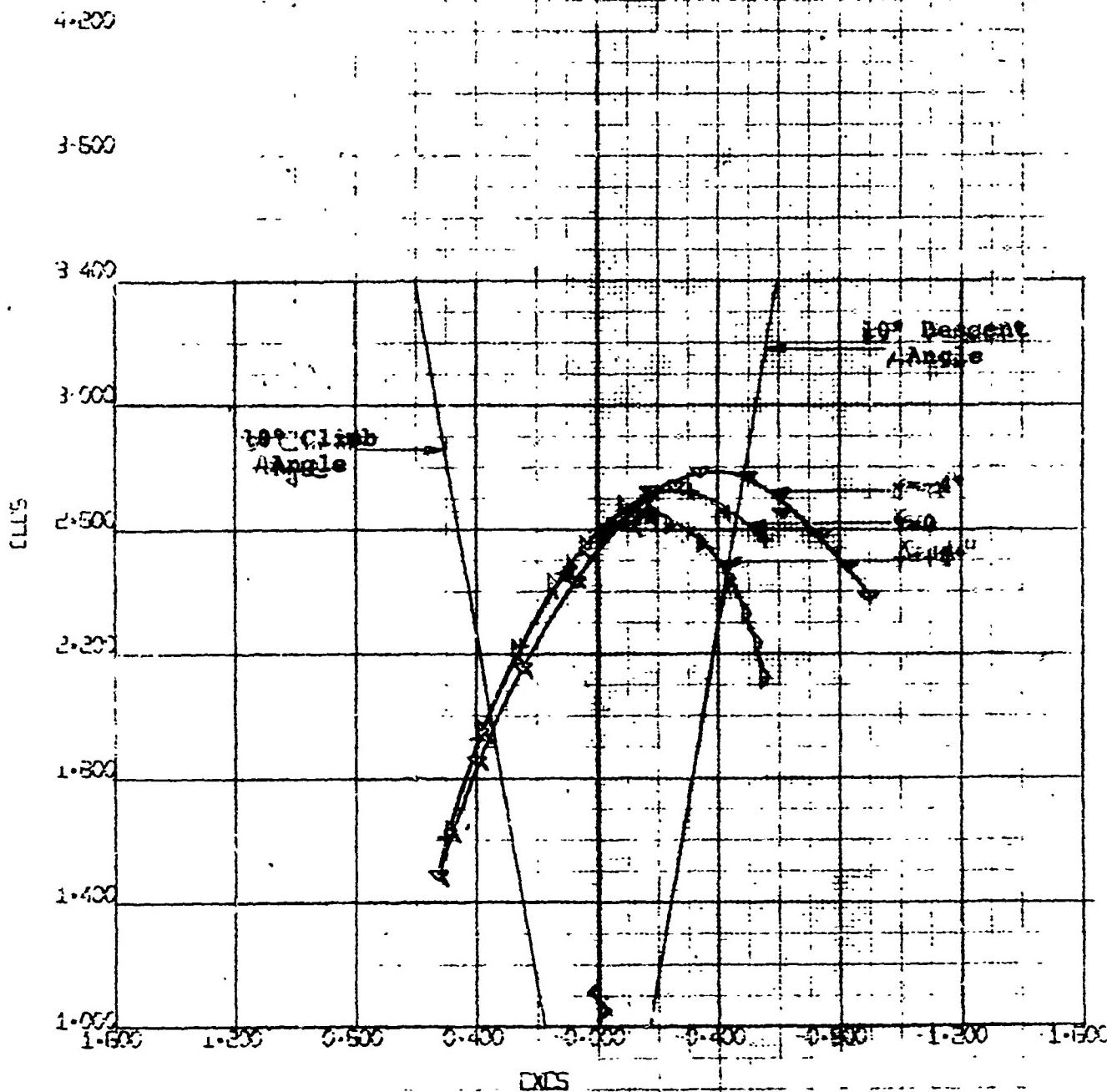
NUMBER D170-10039-1

REV. LTR.

Figure 57

RUN	SYM	α	β	γ
51	+	+15°	5.3	0
34860	▷ & R			+4°
36869	▽ & W			-4°

CYCLIC PITCH CONTROL/TAIL ON	
$i_W = 30^\circ$	$i_R = 63^\circ$
FULL SPAN SLATS	
NOM. $C_D = .70$	



FLUR-PROP TILT WING MODEL 100CB (FULL SPAN)	BWWT 67
CLS VS. CXCS	12/10/70

NOT REPRODUCIBLE

SHEET 115

NUMBER D170-19039-1

REV. LTR.

TYPE 58

RUN	SYM	δ	γ	χ
51	+	+15°	8.3	0
34&60	DGD			+4°
36&69	V&W			-4°

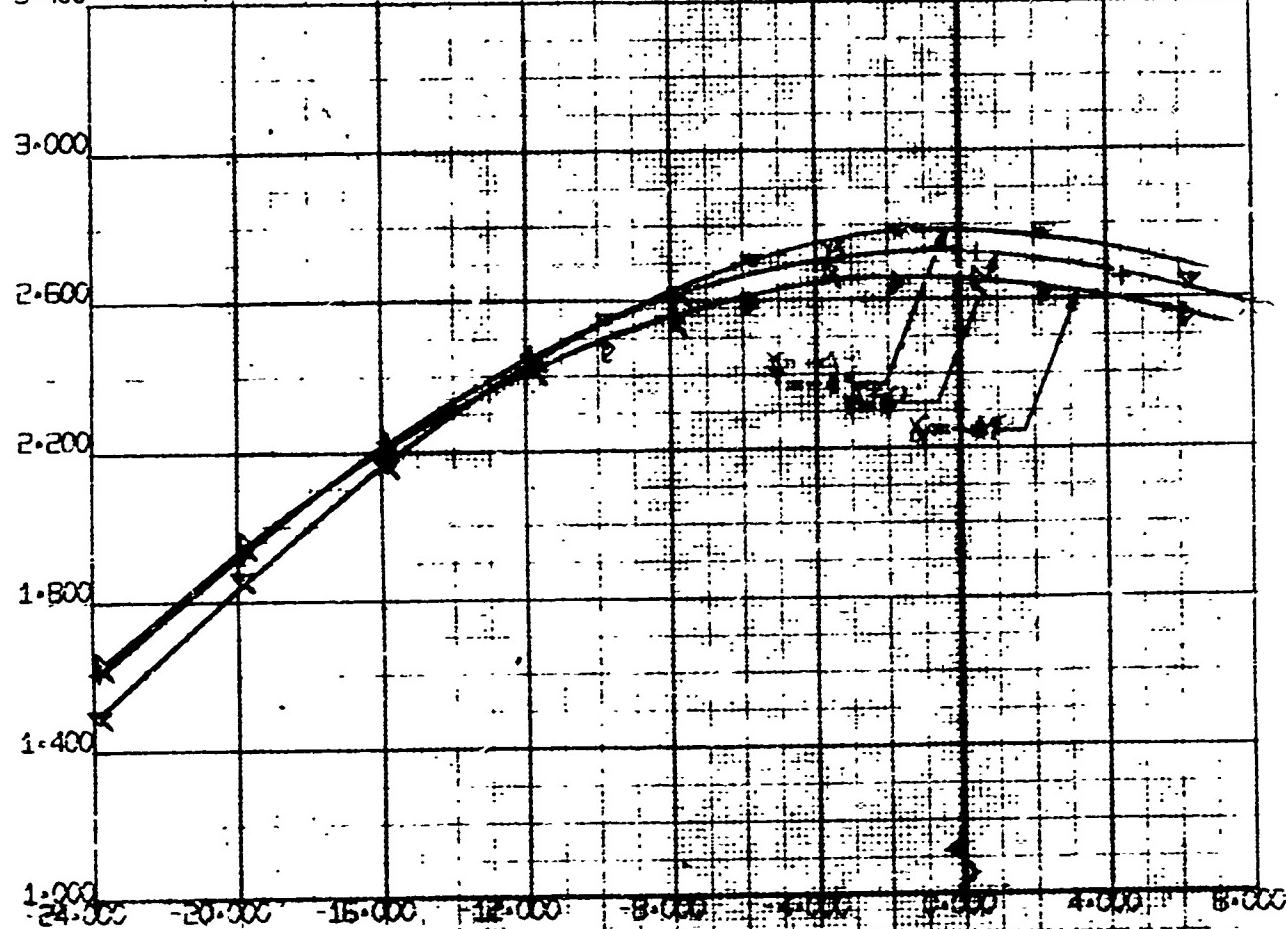
CYCLOIC PITCH CONTROL/TAILWING
1. M39, 5-60°
FULL SPAN SLATS
NOM Cx = .70

4.200

3.800

3.400

CL/D



ALPHA DEGREES

FOUR-PROP TILT WING
MIDSPAN WINGSPAN

EMNT
67

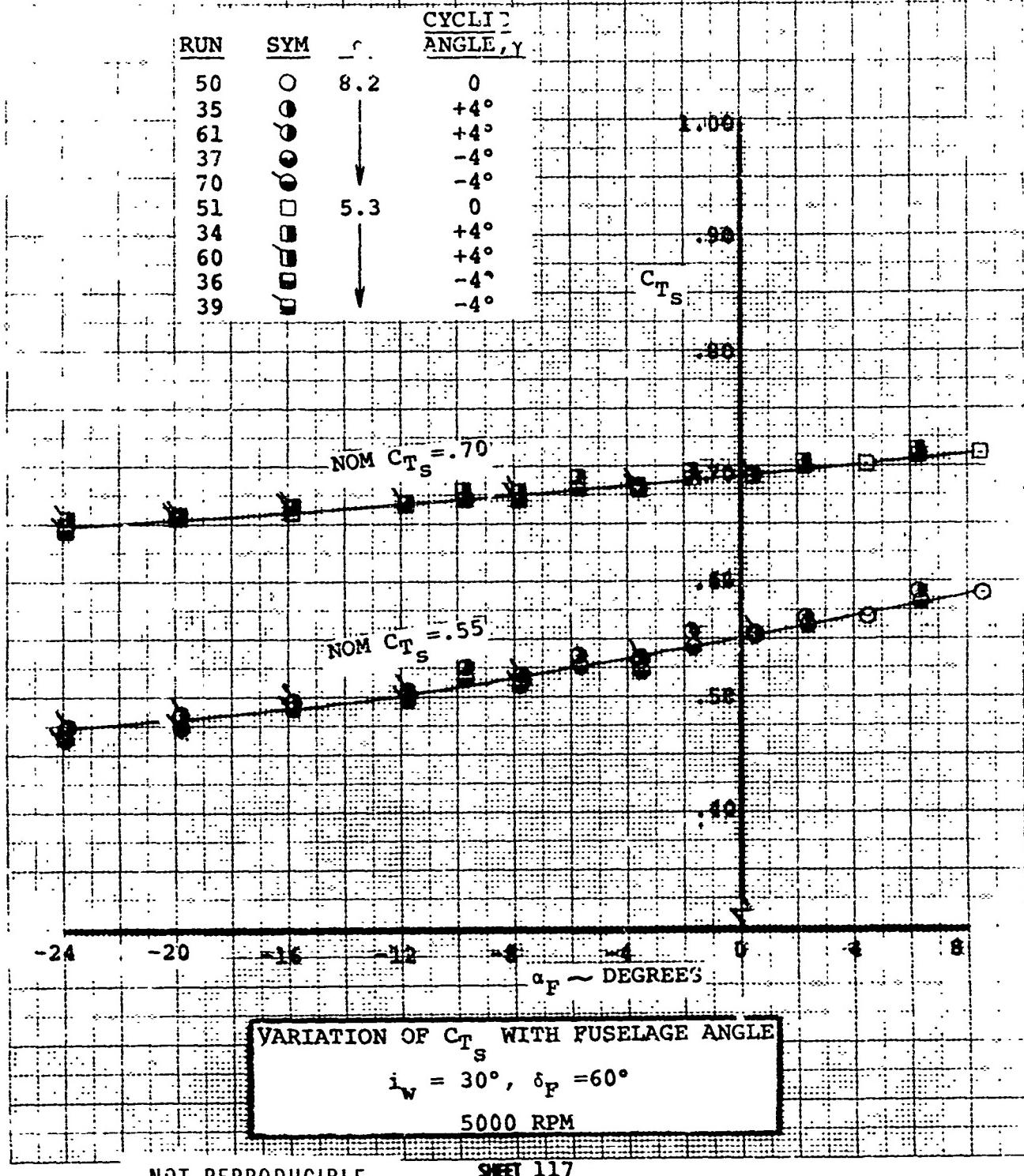
ELEVATOR ALRM

12/10/70

Figure 59

NOTES:

1. M.S.E. 144,641
2. Data from BVWT 067
3. Full Span Slats
4. Tail On ~ $\delta = +15^\circ$

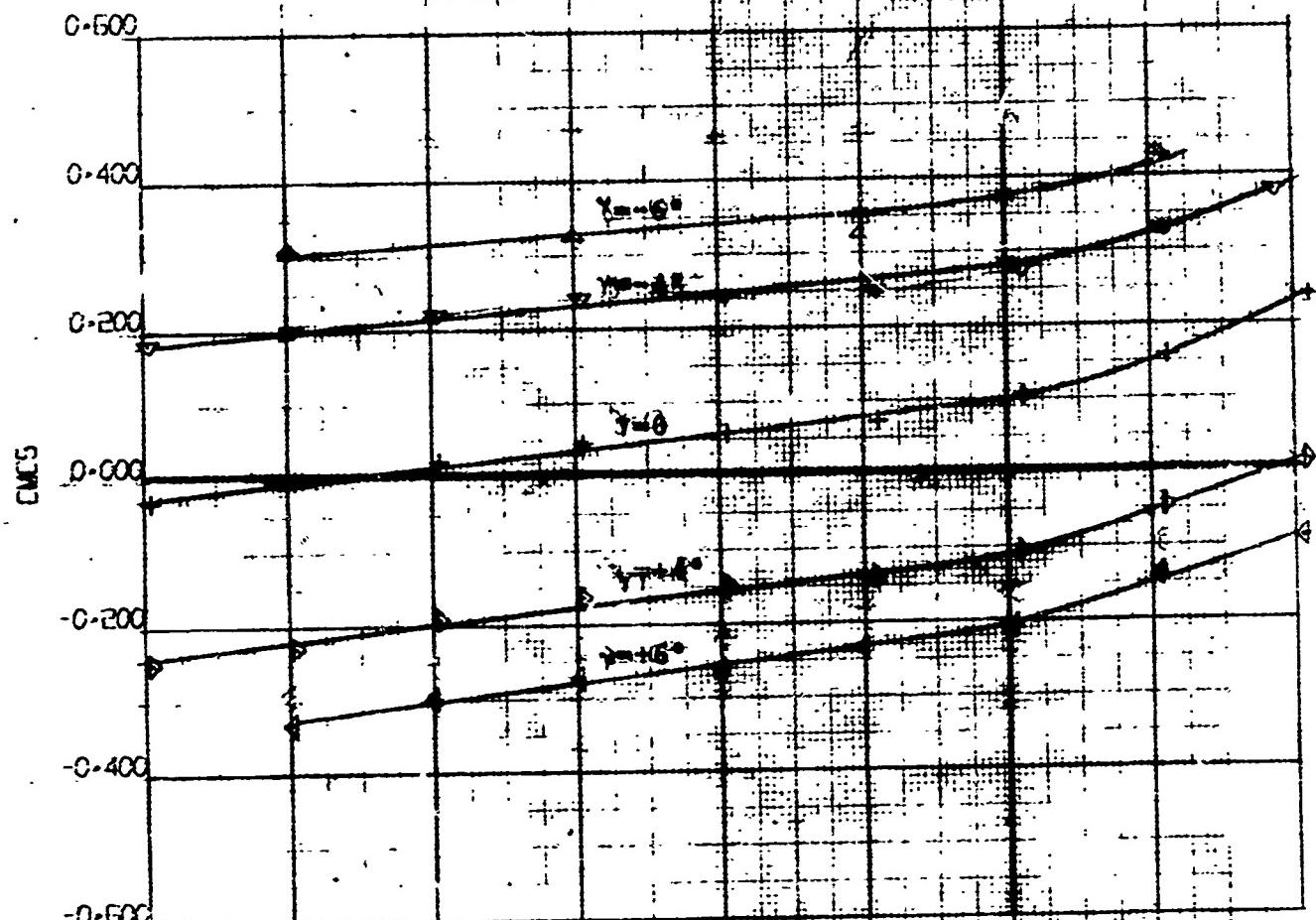


NUMBER D-70-10039-1
REV. LTR.

RUN	SYM	$\Delta\alpha$	σ	RPM	δ
52	+	+35°	3.33	5000	16°
54	>		3.33	5000	16°
171	<		2.70	4500	16°
65	<		3.33	5000	16°
169A	<		2.70	4500	16°

FIGURE 60

CYCLIC PITCH CONTROL TAIL ON
S-355, 6F-60°
WHILE SPAN STRESSES
 $\sigma_{max} = .01$



-0.500 -0.400 -0.300 -0.200 -0.100 0.000 0.100 0.200 0.300 0.400 0.500

ALPHA - DEGREES

FOUR-PROP LIFTING
MODEL VR355(FL) SPAN
CMCS VS. ALPHAS

BWWT
67

12/10/70

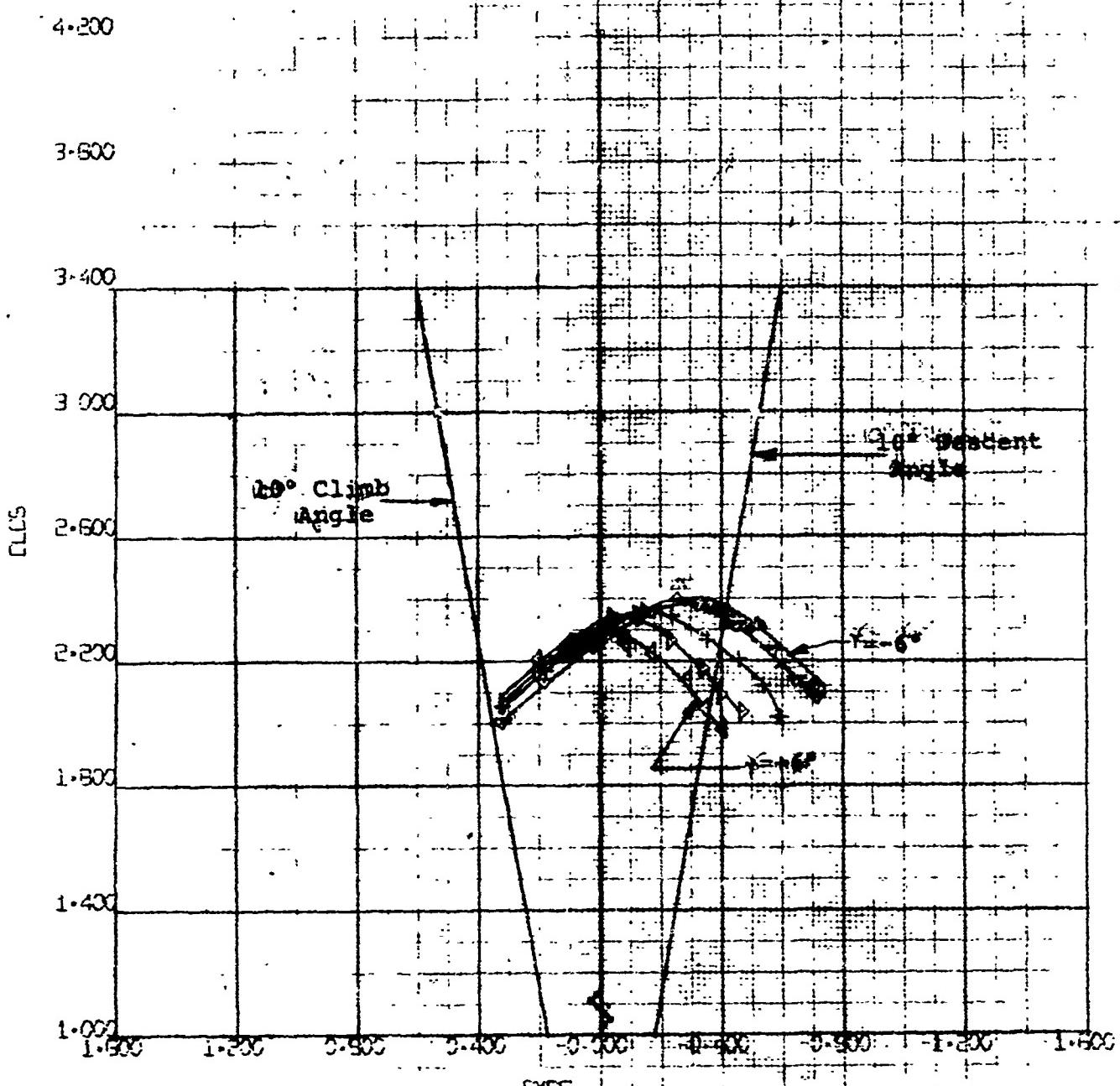
NUMBER D170-10039-1

REV. LTR.

Figure 61

RUN	SYM	α	q	RPM	δ
52	+	+35°	3.33	5000	0°
54	>		3.33	5000	+4°
171	△		2.70	4500	+6°
65	▽		3.33	5000	-4°
169A	△		2.70	4500	-6°

CYCLIC PITCH CONTROL, TAIL ON
 $\delta_{tail} = 15^\circ$, $\delta_p = 50^\circ$
 PORT SPAN SLATS
 WDM Cg = .81



EXCS

FOUR-PIECE WING	BWNT
MODEL VPROF (ALL SPAN)	67
EXCS VS. EXS	12/10/70

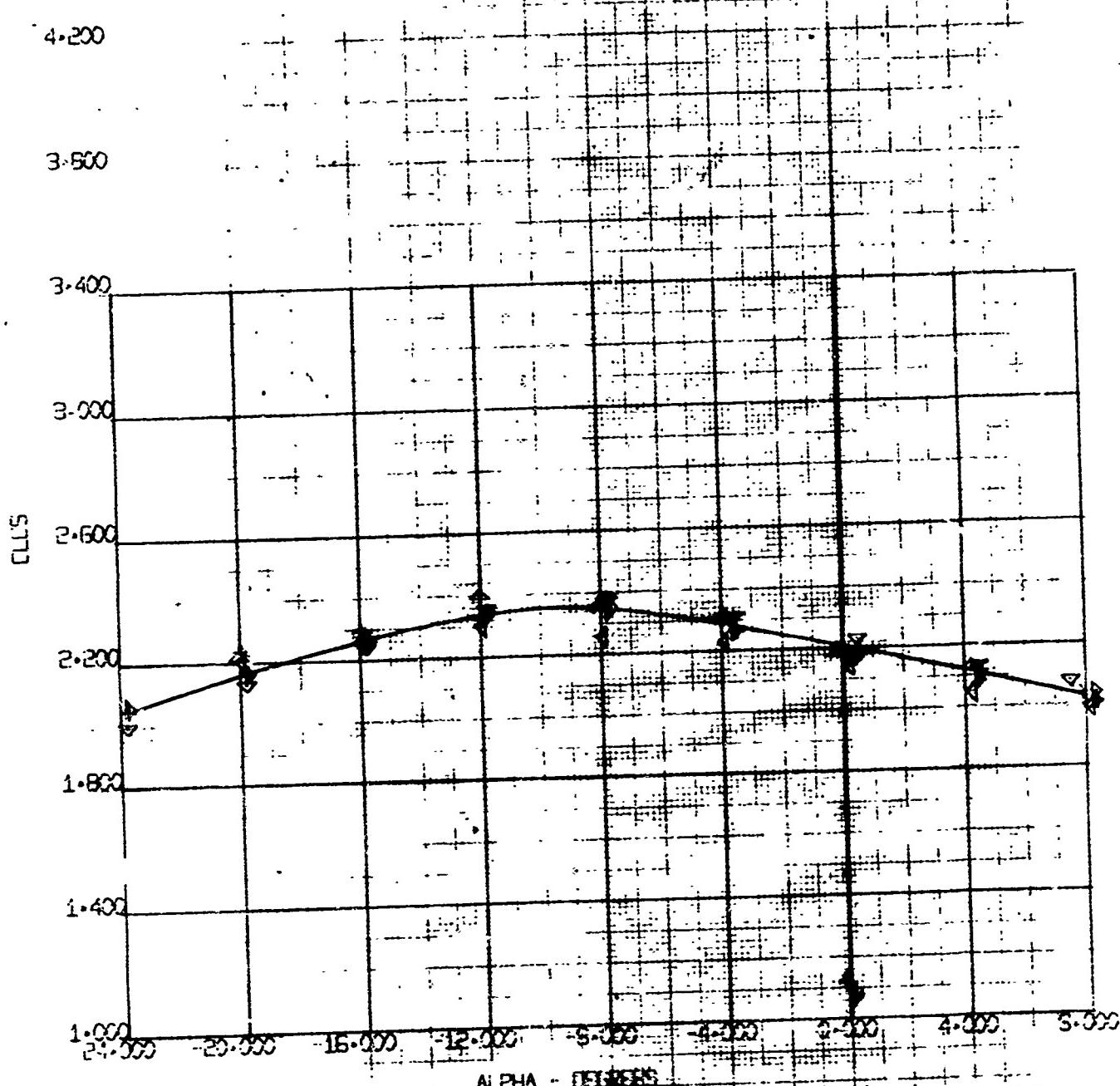
NOT REPRODUCIBLE SHEET 119

NUMBER D170-10039-1
REV. LTR.

Figure 62

RUN	SYM	α	q	RPM	λ
52	+	+35°	3.33	5000	0
54	△		3.33	5000	+4°
171	△		2.70	4500	+6°
65	△		3.33	5000	-4°
169A	△		2.70	4500	-6°

CYCLOIC PATCH CONTROL/TAIL ON
 $\alpha = 45^\circ$, $q = 60^\circ$
 FULL SPAN SlatS
 NEW CT = .81



FOUR-PROP TILT WING MODEL PROPS(FULL SPAN) CL(s) VS. ALPHA	BWWT 67
	12/10/70

RUN	SYM	α	q	REM	γ
53	+	+35°	1.16	5000	0
35	D	+	1.16	5000	+4°
170	△	+	1.00	4500	+6°
566	▽	+	1.16	5000	-4°
169	△	+	1.00	4500	-6°

NUMBER D170-10039-1

REV. TR.

Figure 63

CYCLIC PITCH CONTROL/TAIL ON

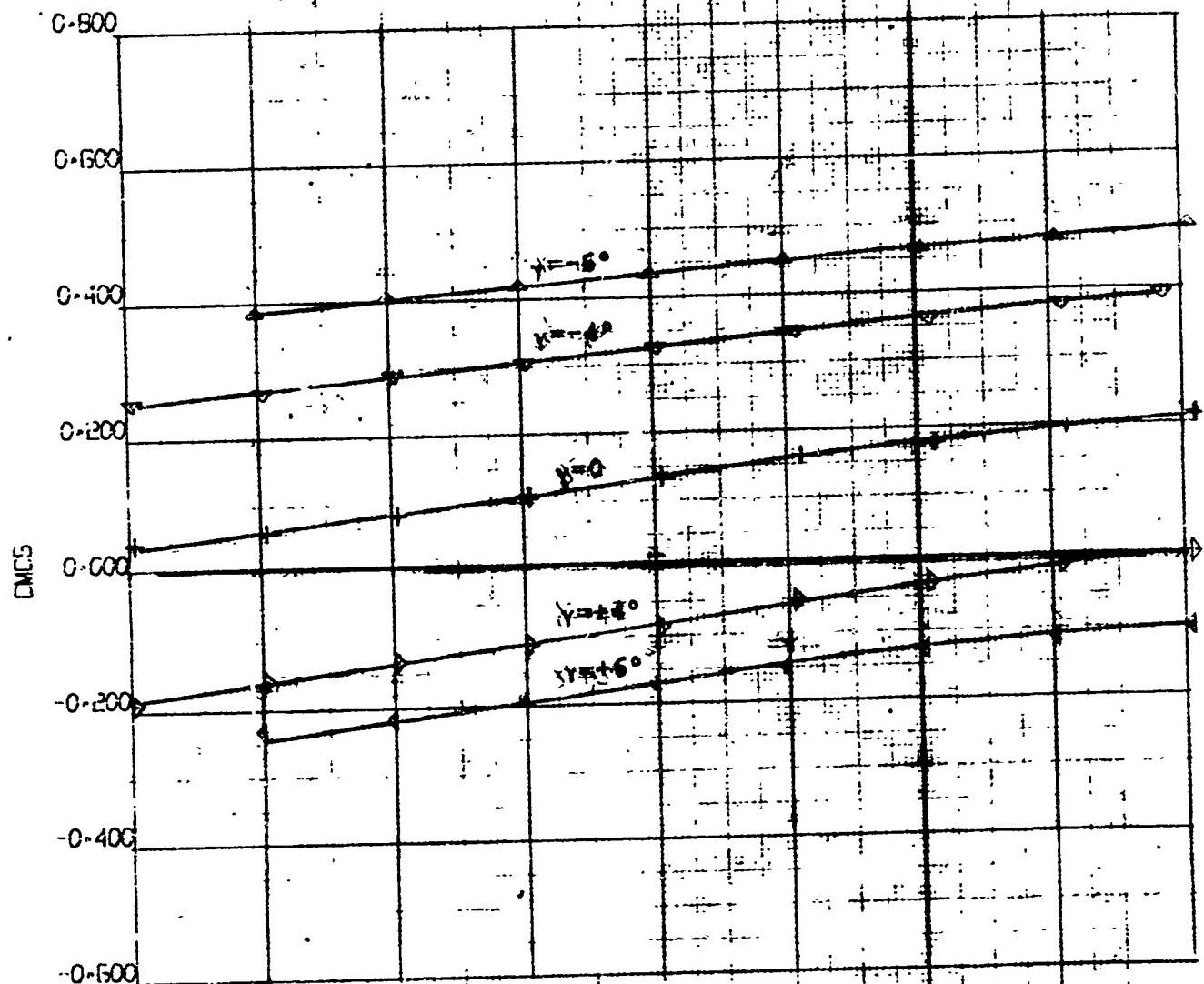
12.10.70

= 60°

FULL SPAN FLAPS

DOWN Cam = .93

B



-0.500 -2.000 -1.500 -1.000 -0.500 -4.000 0.000 4.000 + 6.000
 24.000 20.000 16.000 12.000 8.000 4.000 0.000 -4.000

ALPHA - DEGREES

FOUR-PROP TILT WING
 MODEL VRO680 (FULL SPAN)
 Cn(x) VS. ALPHA

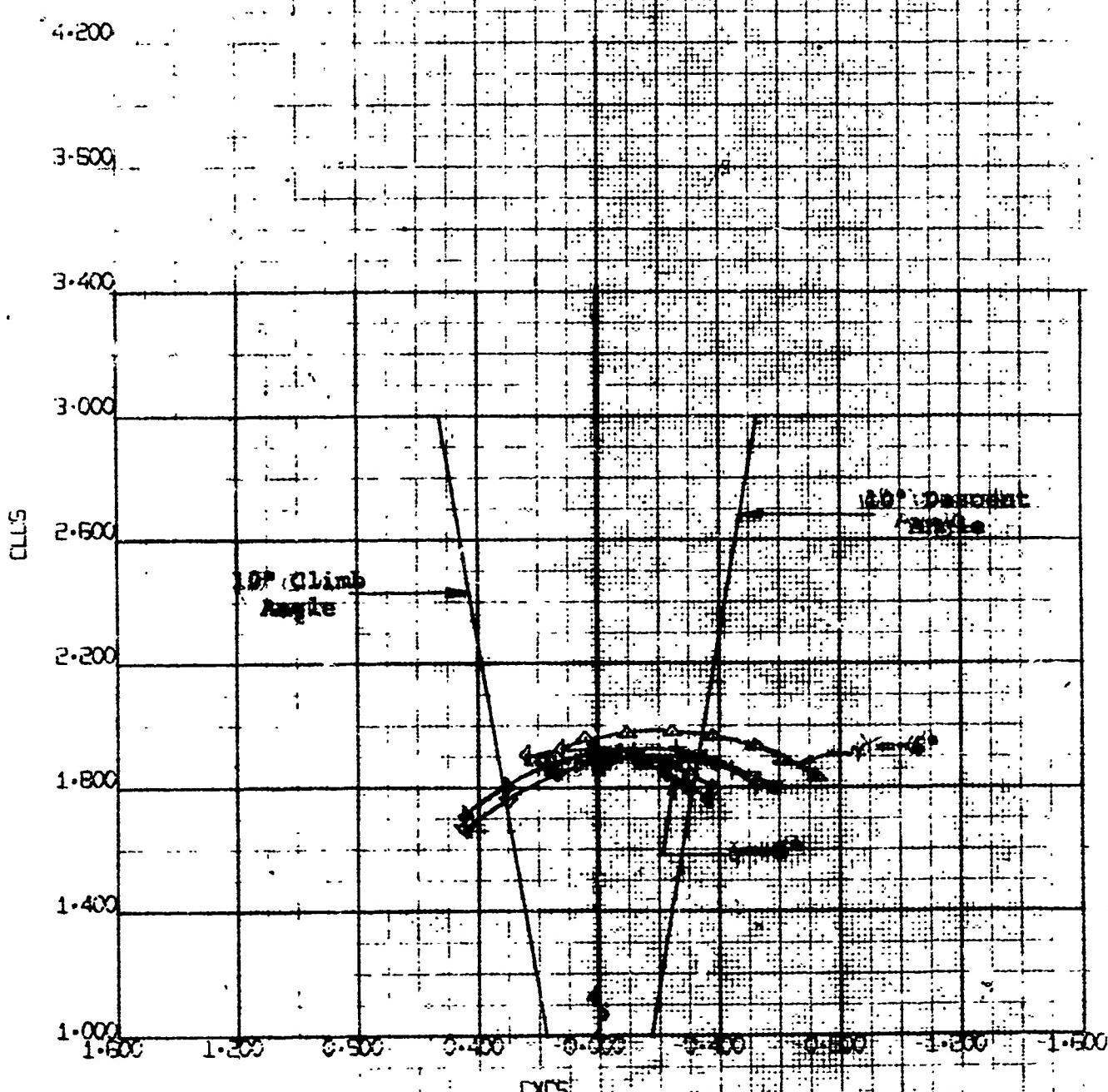
BVWT
67

12/10/70

SHEET 121

NOT REPRODUCIBLE

RUN	SYM	Δ	g	RPM	y	NUMBER	REV.	LTR.
53	+	+35°	1.16	5000	0	D179-10029-1		
55	▷		1.16	5000	11°			
170	△		1.00	4500	+5°			
66	▽		1.16	5000	+4°			
169	▲		1.00	4500	-6°			



FOUR-PROP TILT WING
MODEL VRCBEG (F1) SPAN
DIMS VS. EXIS

BVNT
67

12/10 '70

NUMBER 9118410039-1

REV. LTR.

Figure 65

RUN	SYM	α	q	RPM	γ
53	+	+35°	1.16	5000	0
55	>		1.16	5000	+4°
170	4		2.00	4500	+6°
66	▽		1.16	5000	-4°
169	△		1.00	4500	-6°

CYCLIC PITCH CONTROL/TAIL ON
 1. -55°, 67°-60°
 2. SPAN SLATS
 MAX CP = .93

-4.200

3.800

3.400

3.000

2.600

2.200

1.800

1.400

1.000

CL/CS

-24.000 -20.000 -16.000 -12.000 -8.000 -4.000 0.000 4.000 5.000

ALPHA = DEGREES

FOUR-PROPELLER WING
 MODEL VROSSEBOUL SPAN
 CL/CS VS. ALPHA

BVNT
67

12/10/70

NOT REPRODUCIBLE

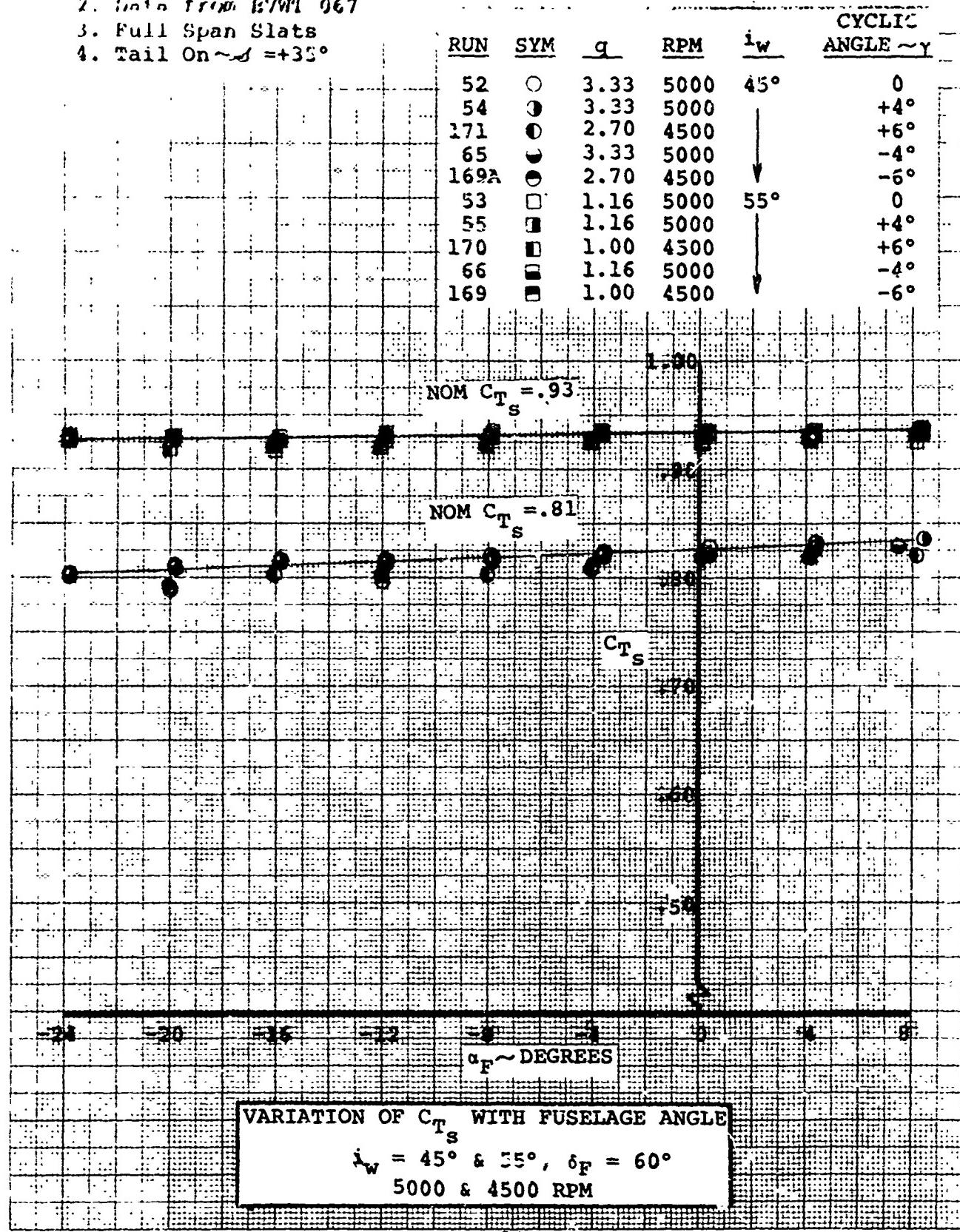
SHEET 123

Figure 66

NOTES:

1. Model VRO68Q
2. Data from E/WI 967
3. Full Span Slats
4. Tail On ~ $\delta_F = +35^\circ$

RUN	SYM	q	RPM	i_w	CYCLIC ANGLE ~ γ
52	○	3.33	5000	45°	0
54	●	3.33	5000		+4°
171	○	2.70	4500		+6°
65	●	3.33	5000		-4°
169A	○	2.70	4500	↓	-6°
53	□	1.16	5000	55°	0
55	■	1.16	5000		+4°
170	■	1.00	4500		+6°
66	■	1.16	5000	↓	-4°
169	■	1.00	4500		-6°

LUGENE D-EZEE FN 5.2
MARCHNO. J40R-MP DICTOEN GRAPH PAPER
MILLIMETER

RUN	SYM	Δ	α	y
42	▽	---	12.1	+4°
43	▷	---		+4°
47	+	---		0°

NUMBER D170-10039-1

REV. LTR.

Figure 67

CYCLIC PITCH CONTROL/TAIL OFF

WING TILT 0°
 FULL SPAN SLATS
 NO CH + .35

1.000

0.500

0.000

-0.200

-0.400

-0.600

-0.800

-1.000

CMCS

-0.500

-1.200

-1.500

ALPHA - DEGREES

8.000 10.000 12.000 14.000 16.000 18.000 20.000 22.000 24.000

SHEET 125

NOT REPRODUCIBLE

FOUR-PIPE TILT WING
 MODEL YR0680 (FULL SPAN)
 CMCS VS. ALPHA

BWNT
67

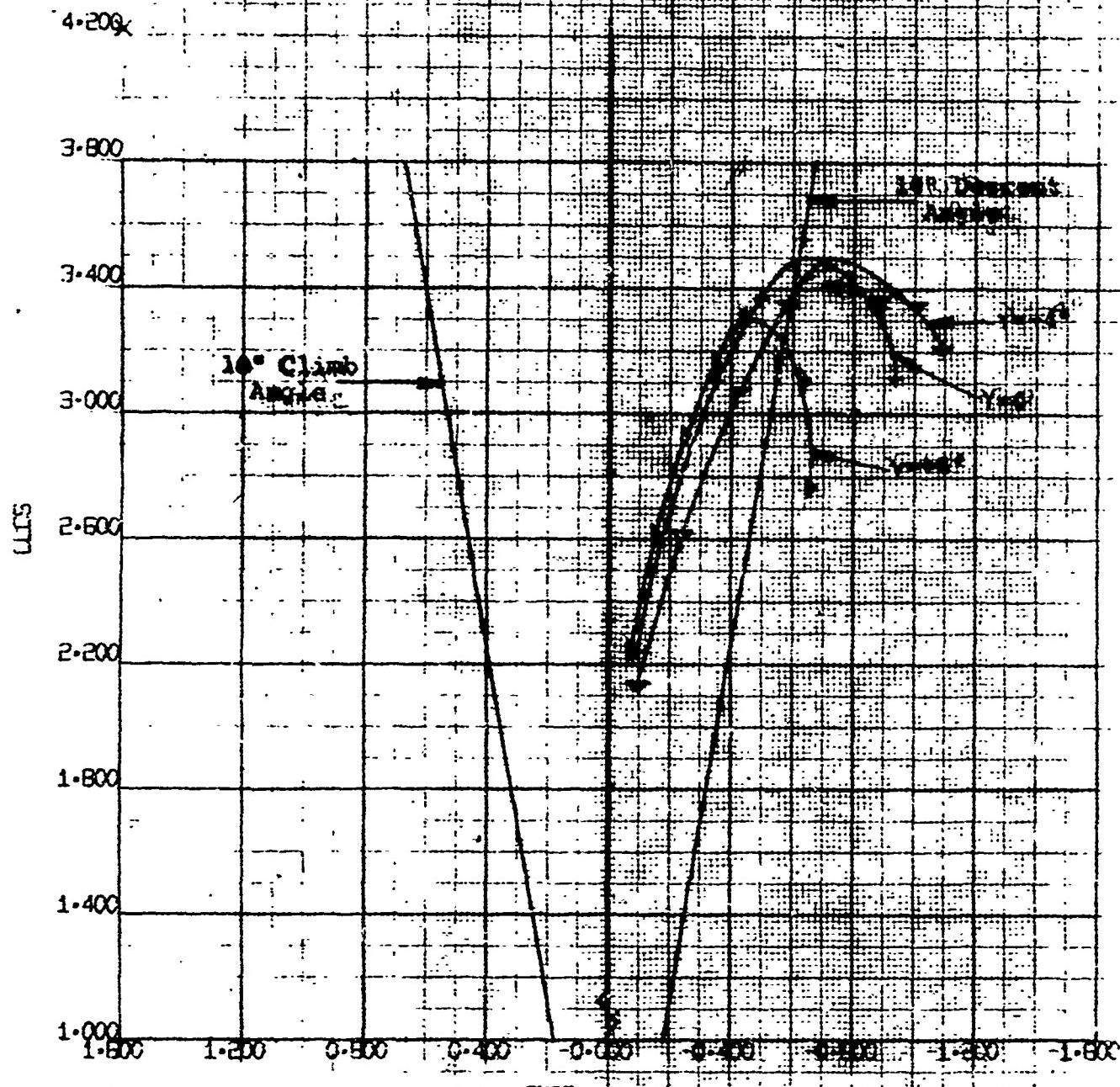
12/8/70

NUMBER D170-10039-1

RUN SYM

42 △
43 ◇
67 +

12.1

-4°
+4°
0°CROSS SECTION DRAWINGS
12.1 12.1 12.1
PULL SPAN PLATE
NEW CANTILEVER

CL vs.

FOUR-PROP TILT WING	BWNT
MODEL YR6000/FL1 SPAND	67
CL vs. α	12/ 8/70

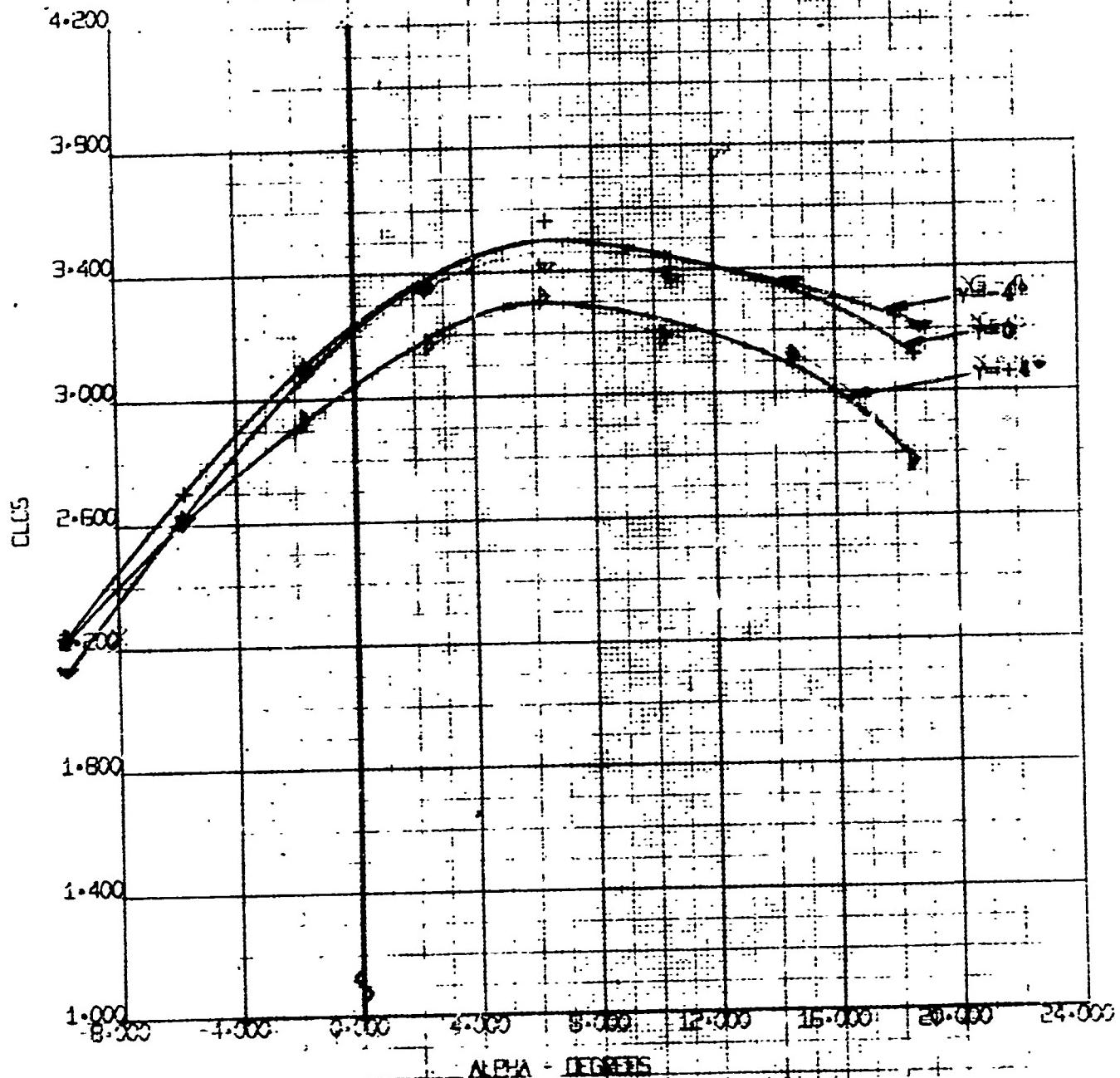
SHEET 126

NUMBER D170-10039-1

REV-LTR:

Figure 69

RUN	SYM
42	▽
43	△
47	+



FOUR-PROP TILT WING MODEL VROS90(FULL SPAN) CL _{FS} VS. ALPHA	BWNT 67
	12/8/70

NOT REPRODUCIBLE

SHEET 127

NOTES:

1. Model VRO68Q
2. Data from BVWT 067
3. Full Span Slats
4. Tail Off

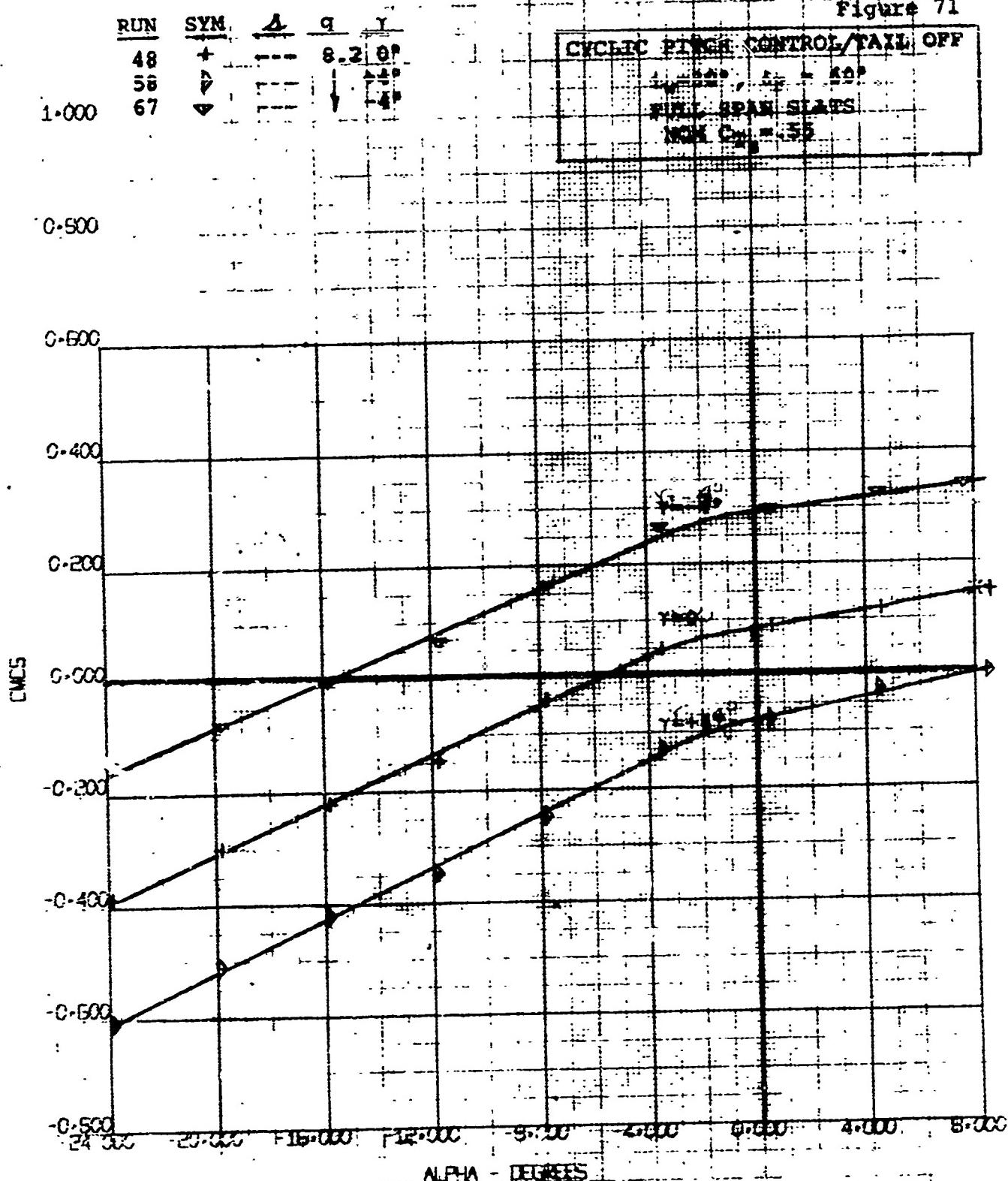
RUN	SYM	α	CYCLIC ANGLE, γ
47	○	12.1	0
43	●		+4°
42	○		-4°

 C_{T_s} NOM $C_{T_s} = .30$ $\alpha_F \sim$ DEGREESVARIATION OF C_{T_s} WITH FUSELAGE ANGLE $i_w = 15^\circ, \delta_p = 60^\circ$

5000 RPM

NUMBER D170-10039-1
REV. LTR.

Figure 71



FOUR-PROP TILT WING MODEL YR08B (FULL SPAN)	BWWT 67
CMCS VS. ALPHA	12/ 8'70

D170-10039-1

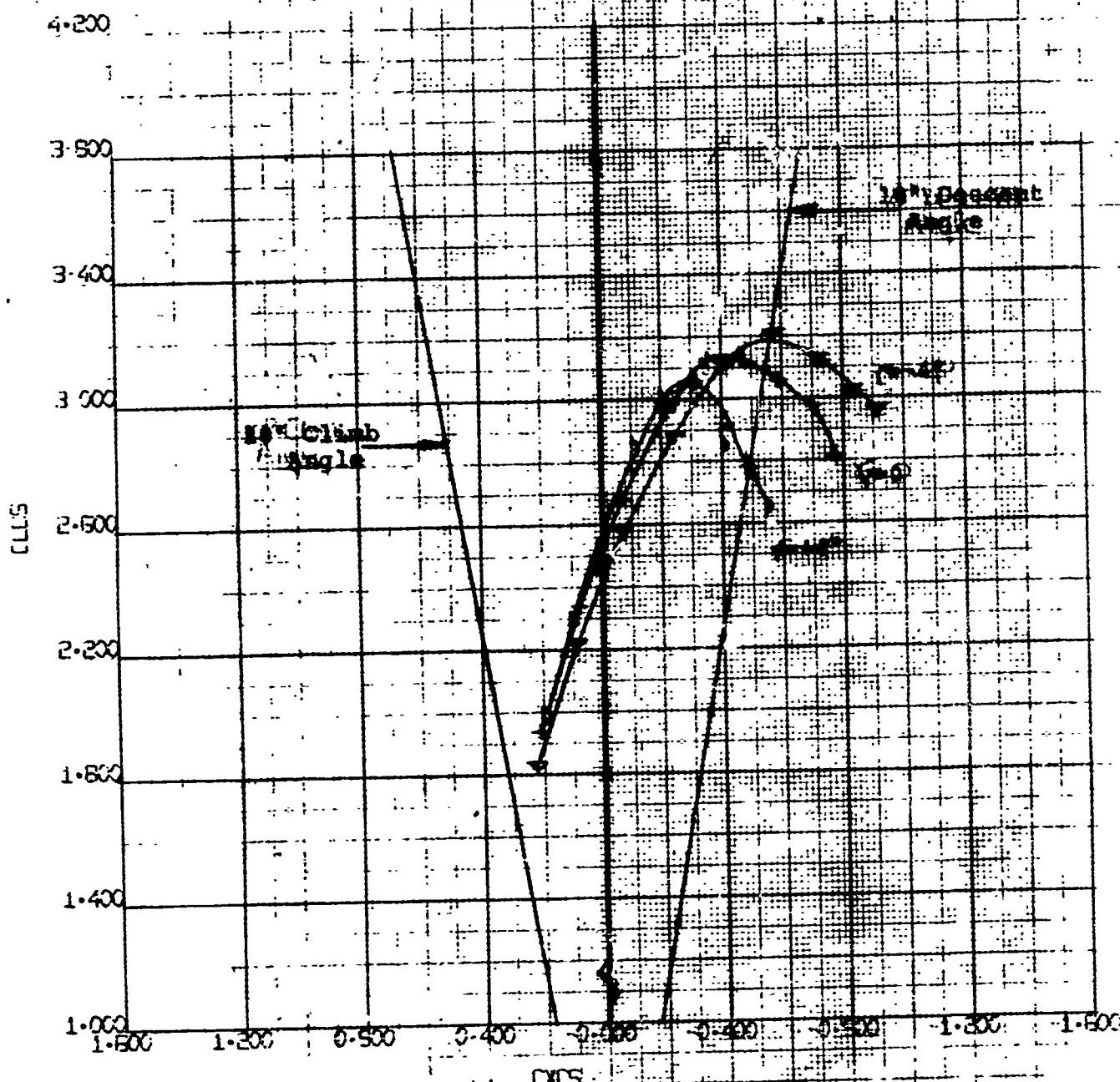
NUMBER

POW. LHR.

FIGURE 72

RUN	SYM	Δ	q	γ
48	+	---	8.2	0°
58	>	---		+4°
67	<	---		-4°

CYCLIC PITCH CONTROL/TAIL OFF
 $\Delta_W = 20^\circ$, $\Delta_T = 60^\circ$
 FULL REAM SLATS
 NEM C. = .55



FOUR-PIECE TEST SETTING
 MODEL VERBATIM FULL SPAN
 CLLS VS. DAS

BVNT
67

12/8/70

NOT REPRODUCIBLE

SHEET 130

NUMBER D170-10639-1

REV. LIR.

Figure 73

RUN SYM

48	+
58	-
67	▼

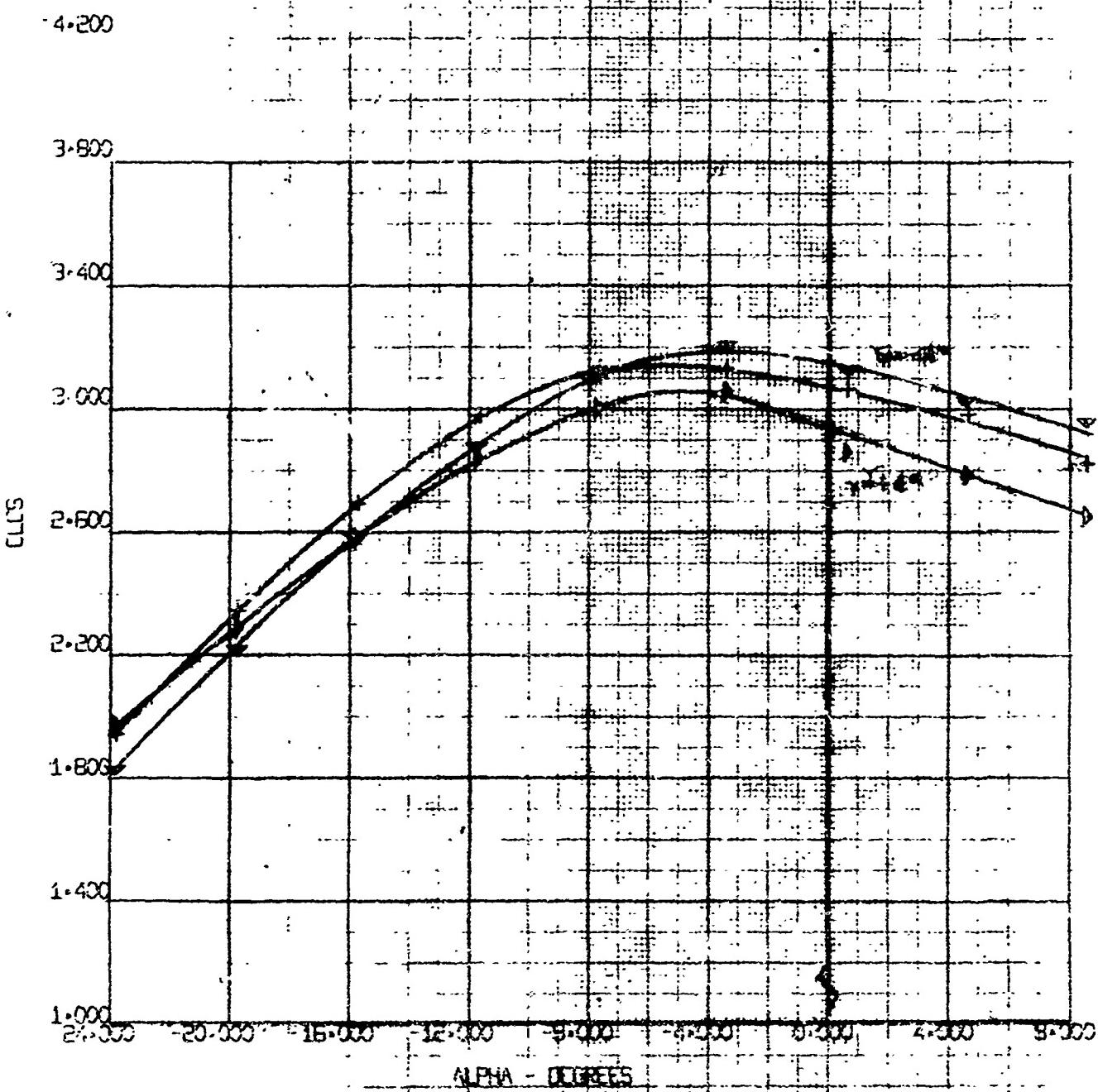
q
8.2

0°
+4°
-4°

CYCLIC PITCH CONTROL/TAIL OFF

L = 10°, S_P = 50°

FULL SPAN SLATS

NOM. C_L = 1.57

ALPHA - DEGREES

FOUR-PROP TILT WING
MODEL YROSS (FULL SPAN)
CL_L VS. ALPHA

BVNT
67

12/8/70

SHEET 131

NUMBER

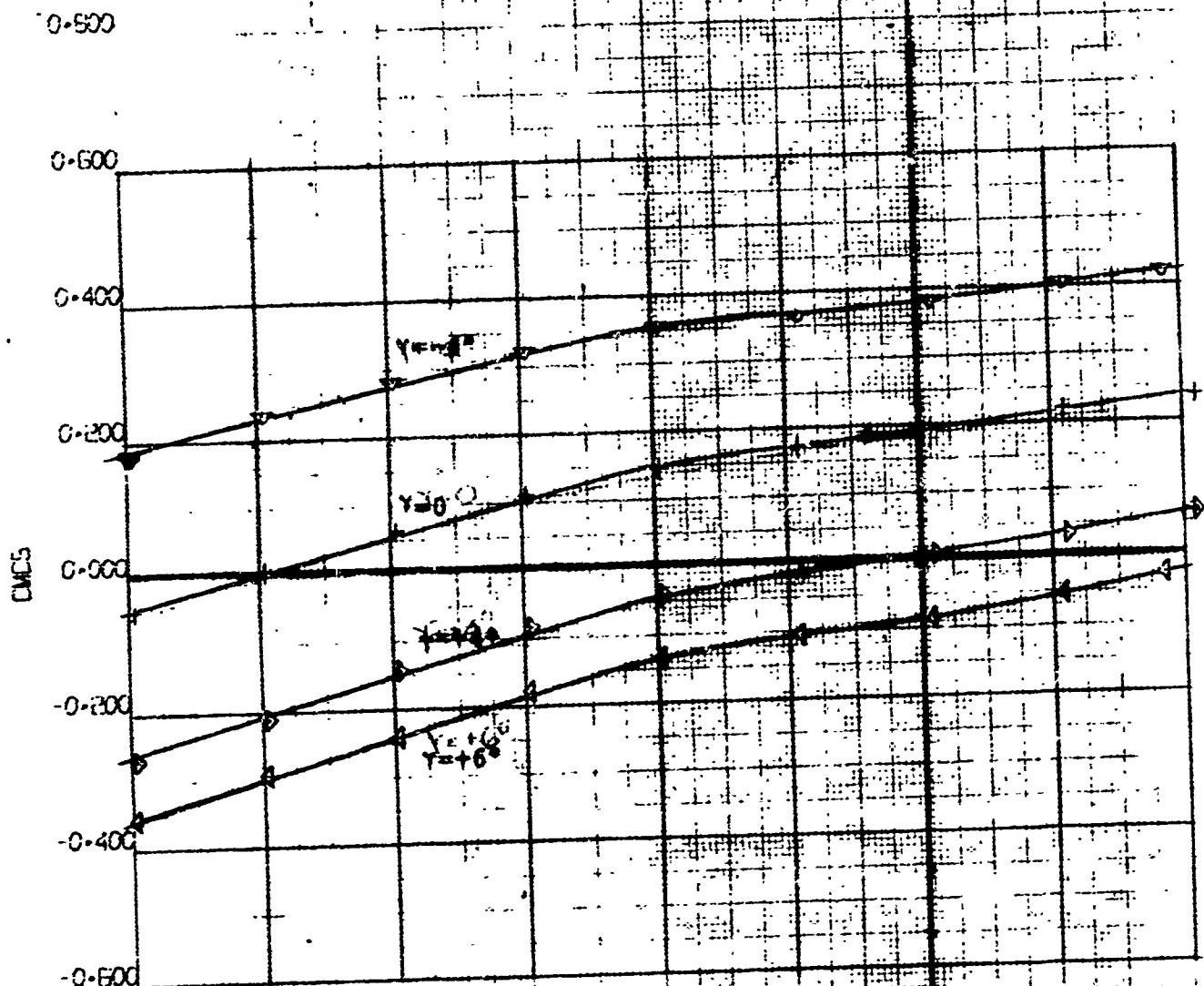
D170-10039-1

REV. L TR.

FIGURE 74

RUN	SYM	Δ	a	χ
49	+	---	3.33	0°
59	-	---		
68	-	---		-4°
1-000	71	SL		+6°

MODEL: PINTLE, EQUATORIAL/TAIL OFF
 $W = 45^{\circ}$, $A_p = 60^{\circ}$
 FULL SPAN SPAN
 NORM. $C_L = 0.1$



-0.500 -24.000 -20.000 -16.000 -12.000 -8.000 -4.000 0.000 4.000 5.000

FOUR PROP TILT WING
 MODEL: YROED/FULL SPAN
 DVS VS. ALPHA

EWWT
67

12/10/70

NOT REPRODUCIBLE

SHEET 132

NUMBER 1414-1074-8-2
REV-LIR- Figure 75

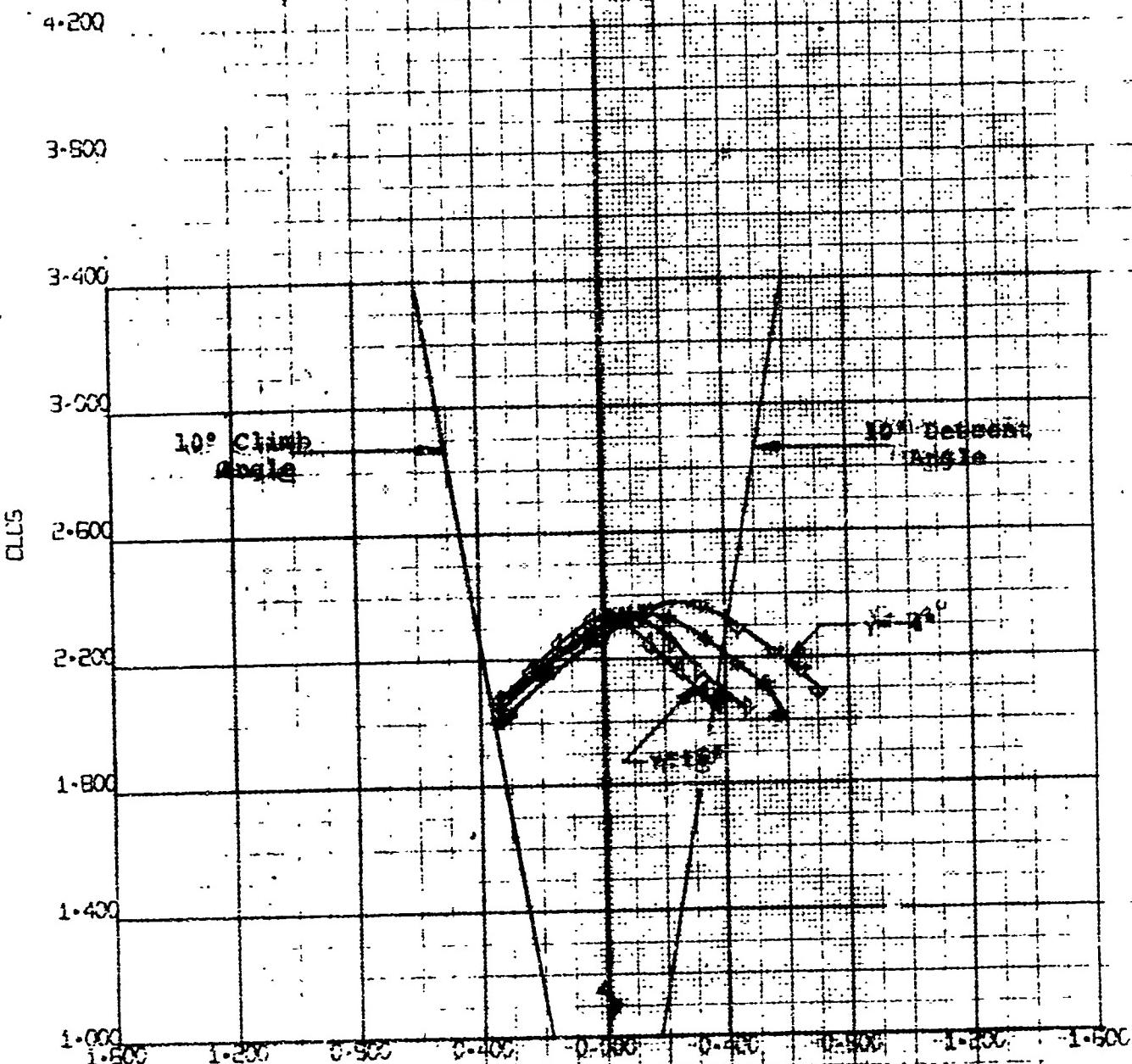
RUN	SYM	A	G	Y
49	+	---	3.33	0°
59	▷	---		+6°
68	▽	---		-4°
71	◐	---		+6°

CYCLOP PITCH CONTROL/TAIL OFF

W = 4000 Lb. 60°

FULL SPAN SLATS

NOM G = +81



FOUR-PROP TILT WING
MODEL 140000 FULL SPAN
CL vs. AOA

BWNT
67

12/10/70

NUMBER E170-10039-1

REV. LTR.

PAGE 76

RUN SYM

Δ a Y

49 +
59 ◆
68 ▽
71 ▲3.33 0°
+4°
+4°
+6°

CANTIC BRACH CONTROL TAIL OFF

SW = 4.00' HF = 60'

FLAPS SPAN SLEWS

NOTES

4.200

3.600

3.400

3.000

2.600

2.200

1.800

1.400

1.000

24.00

20.00

16.00

12.00

8.00

4.00

0.00

-4.00

-8.00

-12.00

-16.00

-20.00

-24.00

-28.00

ALPHA DEGREES

FOUR-PROP TILT WING
MODEL VR0606 (FLAP SPAN)
CLHS VS. ALPHABVNT
67

12/10/70

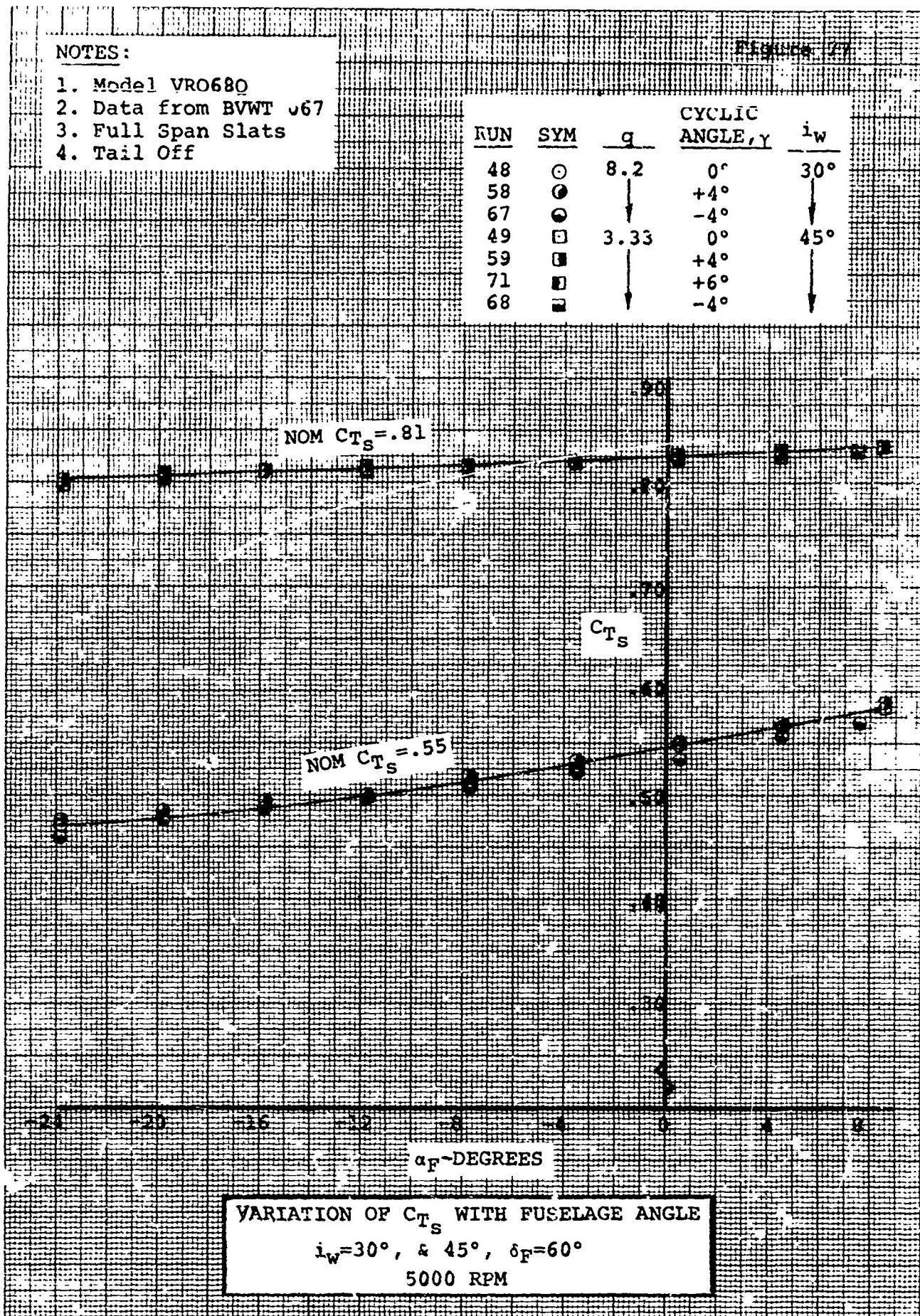
SHEET 134

NOT REPRODUCIBLE

NOTES:

1. Model VRO680
2. Data from BVWT J67
3. Full Span Slats
4. Tail Off

RUN	SYM	α	CYCLIC ANGLE, γ	i_w
48	○	8.2	0°	30°
58	●		+4°	
67	○		-4°	
49	□	3.33	0°	45°
59	■		+4°	
71	■		+6°	
68	■		-4°	

EUGENE DIETZGEN CO.
MADE IN U.S.A.NO. 34UR-MP DICTZOLL GRAPH PAPER
NO. 34UR-MP MILLIMETER

6.4.3 Horizontal Tail Effectiveness with Cyclic Pitch Inputs

Results of the investigation of horizontal tail effectiveness when longitudinal control is provided by coupled stabilizer and cyclic pitch control are presented in Figure 78. The test data in this figure is compared with the stabilizer effectiveness, in terms of $\Delta C_{M_s}/\Delta \alpha$ (increment of slipstream pitching moment per degree of stabilizer angle) obtained during the more extensive investigation with zero cyclic and 6800 propeller RPM. The reduction in propeller speed to 5000 RPM for cyclic pitch operation, which decreased the slipstream q by almost 50%, did not have a significant effect on the measured tail power in the linear range over which the data was interpreted.

Figure 78 shows that the application of cyclic pitch has only a small influence on the basic tail effectiveness in transition with the greatest effect occurring at $.27 C_{T_s}$ with 15° of wing tilt. Positive cyclic can be noted to increase the tail power. This result is reasonable, since positive cyclic effectively raises the thrustline and thus should increase the q acting on the tail. Tilting the wing to a higher angle will lower the slipstream wake with respect to the tail chord plane and should diminish the effect. It can be assumed that cyclic pitch would have a larger effect on stabilizer effectiveness if the horizontal tail was located in a lower position.

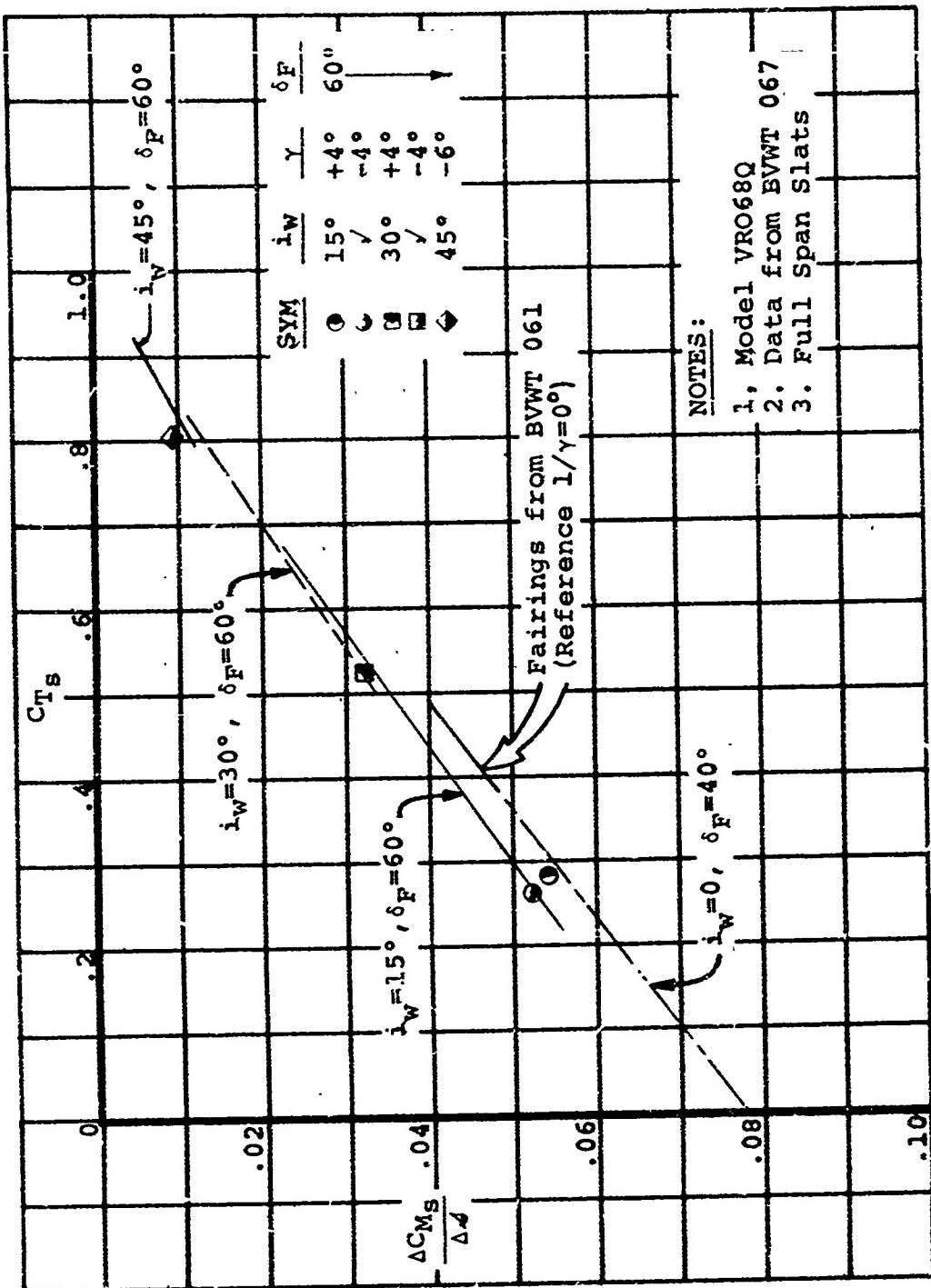
Figures 79 through 93 present the basic three component data in sets of three plots: pitching moment curve, force polar, and lift curve for a common wing tilt angle, nominal C_{T_s} , and cyclic angle input. See Page 101 for a definition of machine symbols. Each set presents a series of runs with different tail incidences relative to a fuselage waterline. The corresponding tail-off run has also been shown, when available.

In Figure 85, for example, the progressive reduction in tail-on pitching moment at more negative fuselage angles and the convergence of the various stabilizer angle curves to a constant incremental difference in pitching moment from the tail-off curve, reflects the normal stall of a horizontal tail and thus the maximum pitching moment capability from the tail. Since the tail is mounted high on the fin and is essentially outside the influence of the propeller slipstream at most wing tilt angles, the maximum trim capability of the stabilizer will vary almost linearly with C_{T_s} , the pattern established for the horizontal tail effectiveness ($\Delta C_{M_s}/\Delta \alpha$). See Page 116 of Reference 1. The low Reynolds number acting on the model tail should

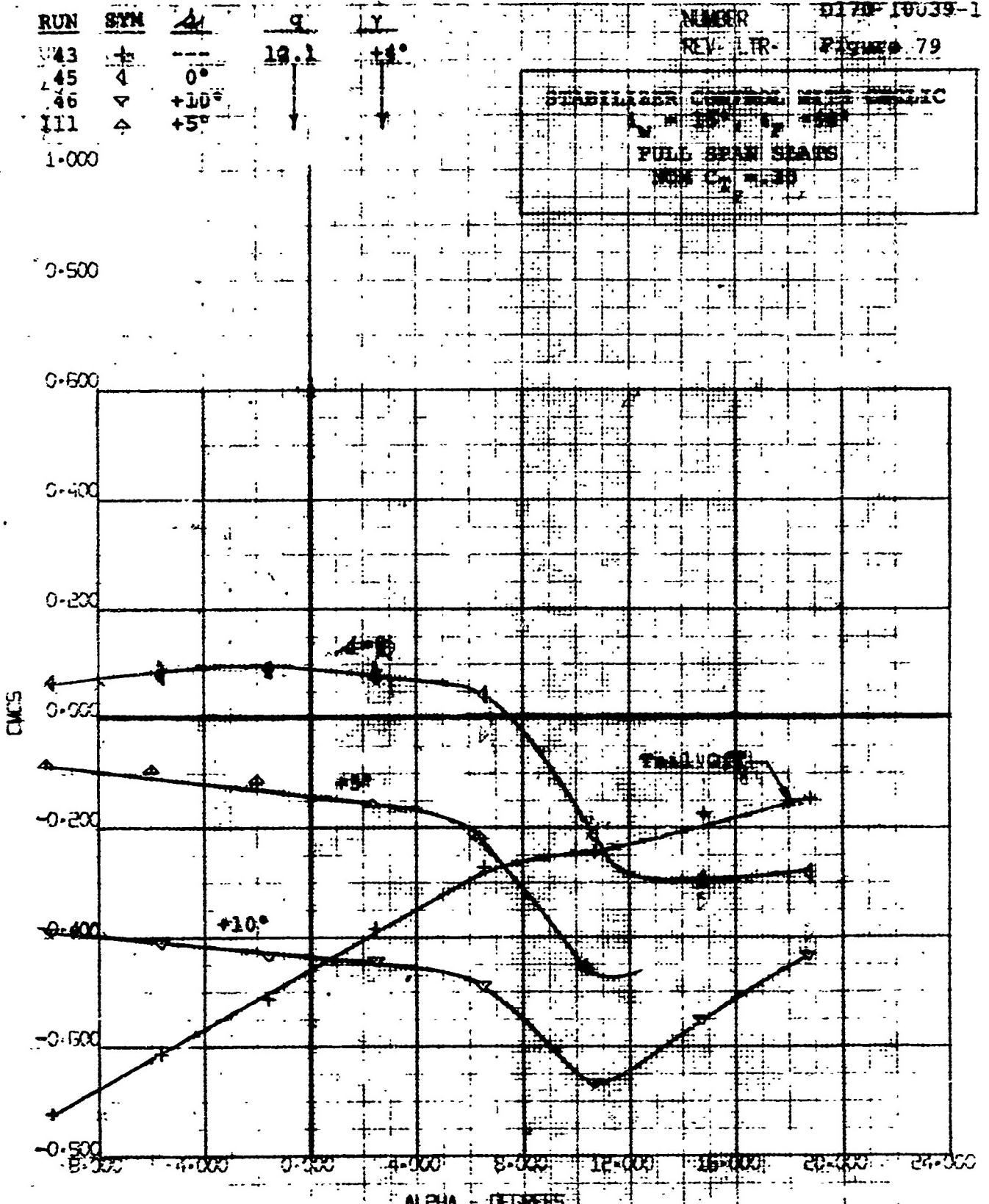
D170-10039-1

significantly decrease its maximum lift coefficient and resulting trim capability as compared to a full scale tail.

Figure 78



EFFECT OF CYCLIC PITCH ON
HORIZONTAL TAIL EFFECTIVENESS



FOUR-PROP TILT WING
MODEL WINGSPAN FULL SPAN
EFMCS VS. ALPHA

BWNT
67

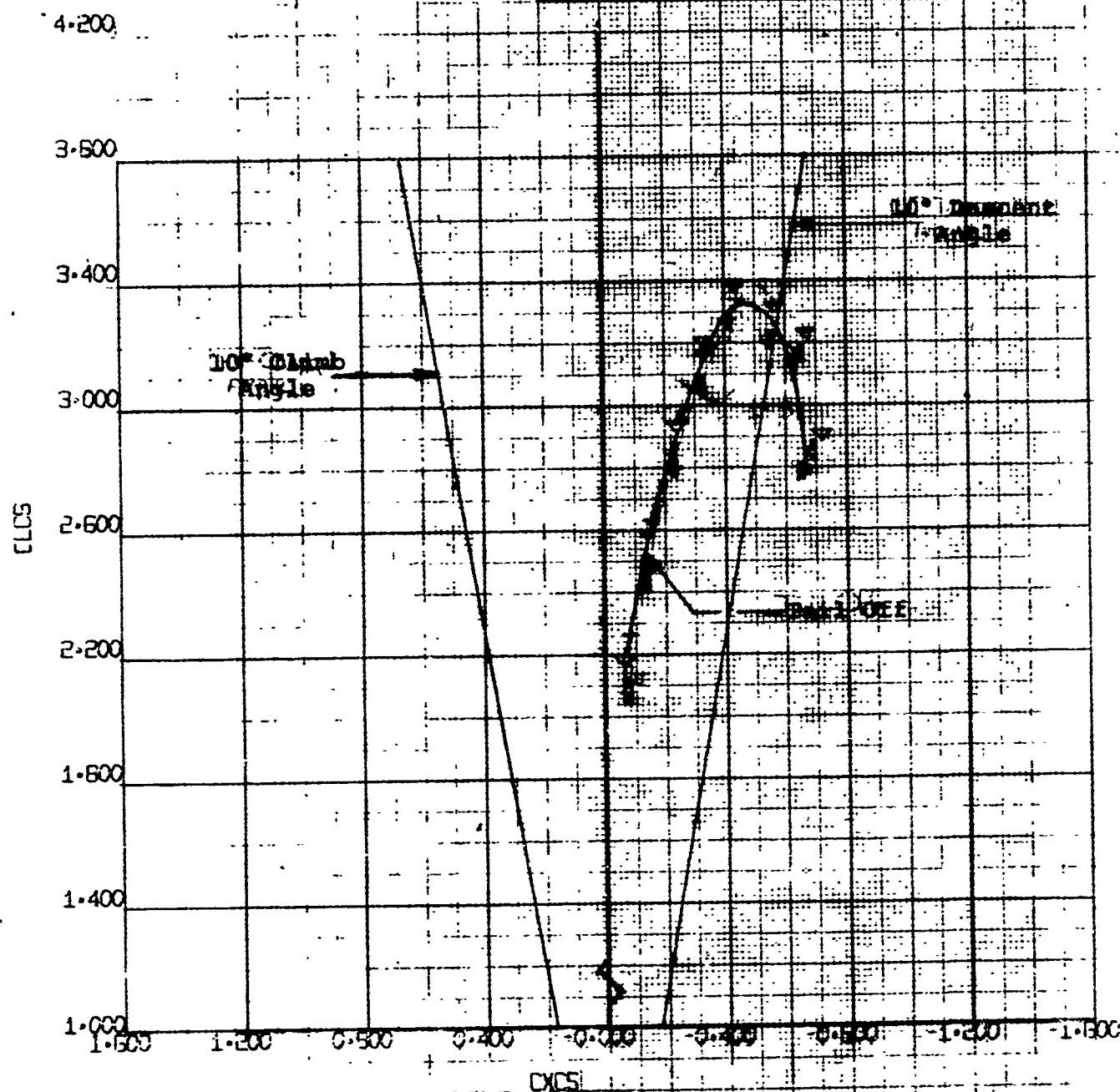
12/8/70

NOT REPRODUCIBLE

SHEET 139

RUN	SYM	q	γ
43	+	-	12.1
45	△	0°	
46	▽	+10°	

STABILIZER CONTROL WITH CYCLIC
 $\alpha_w = 15^\circ$, $\delta_p = 60^\circ$
 FULL SPAN STATE
 NOM C_L = 1.00



FOUR-PROP TILT WING
 MODEL VROSBC (FULL SPAN)
 CLDS VS. CXDS

BWWT
67

12/8/70

NUMBER P190-10835-1

REV-LTR. Figure 82

RUN SYM

43 +
45 0
46 -10°

12.1

CHARACTERISTICS OF WING WITH CANTILEVER

WINGSPAN = 60"

FUSELAGE SPAN = 28"

WINGSPAN = 28"

4.200

3.500

3.400

3.300

3.200

3.100

3.000

2.900

2.800

2.700

2.600

2.500

2.400

2.300

2.200

2.100

2.000

1.900

1.800

1.700

1.600

1.500

1.400

1.300

1.200

1.100

1.000

ALPHA - DEGREES

-8.000 -4.000 0.000 4.000 8.000 12.000 16.000 20.000 24.000

FOUR-PROP TILT WING

MODEL V4080(FULL SPAN)

CLLUS VS. ALPHA

BWWT

67

12/6'70

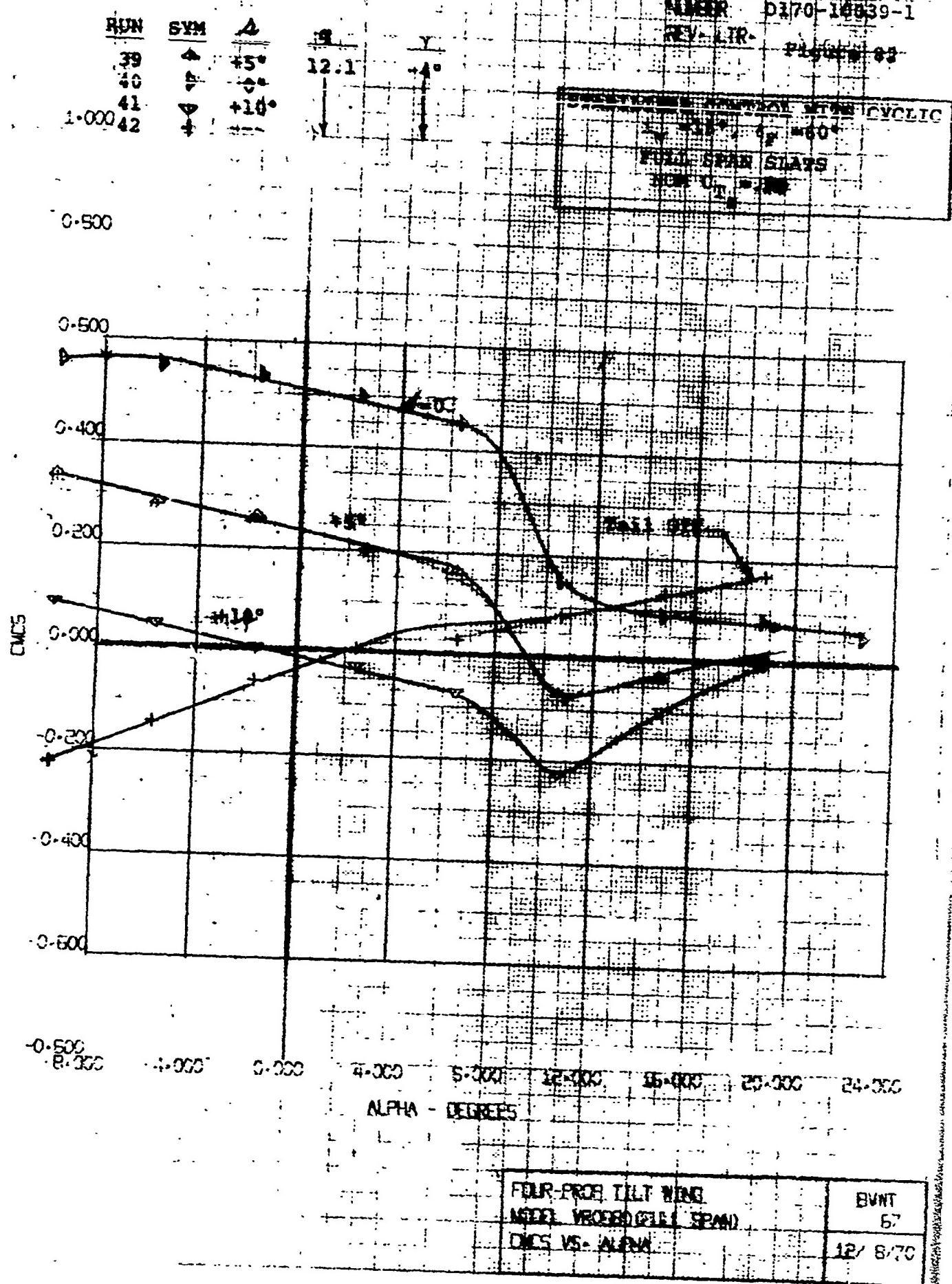
NOT REPRODUCIBLE

SHEET 141

NUMBER D370-14839-1

REV. LTR.

Page 82



SHEET 142

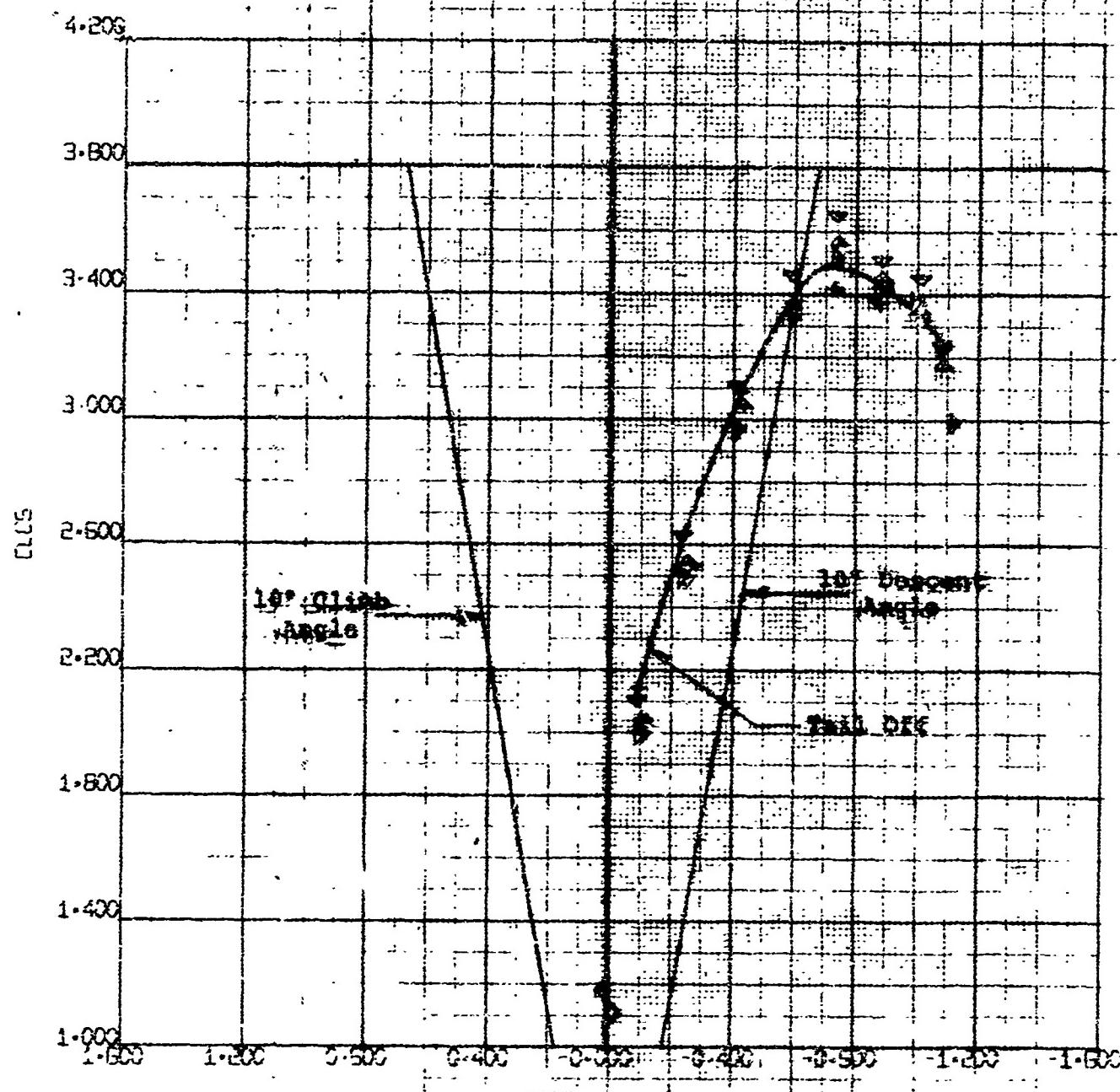
NUMBER 4170-10039-1

REV. 1D.

Flight 83-

ITEM	SVM	A	B	C
39	▲	+5°	12.1	-6°
40	▼	0°		
41	▼	+10°		
42	+	---		

FOUR-PROPELLER TILT WING WINGSPAN 100 FT. SPAN 40 FT.		
1.0	+15°	60°
FUEL TANK SLOTS		
DECK C. = 30°		



FOUR-PROP TILT WING	BWNT
MODEL VR0000 (FULL SPAN)	57
CHDS VS. CHDX	12/ 6/70

NOT REPRODUCIBLE

SHEET 143

NUMBER DIV0-10039-1

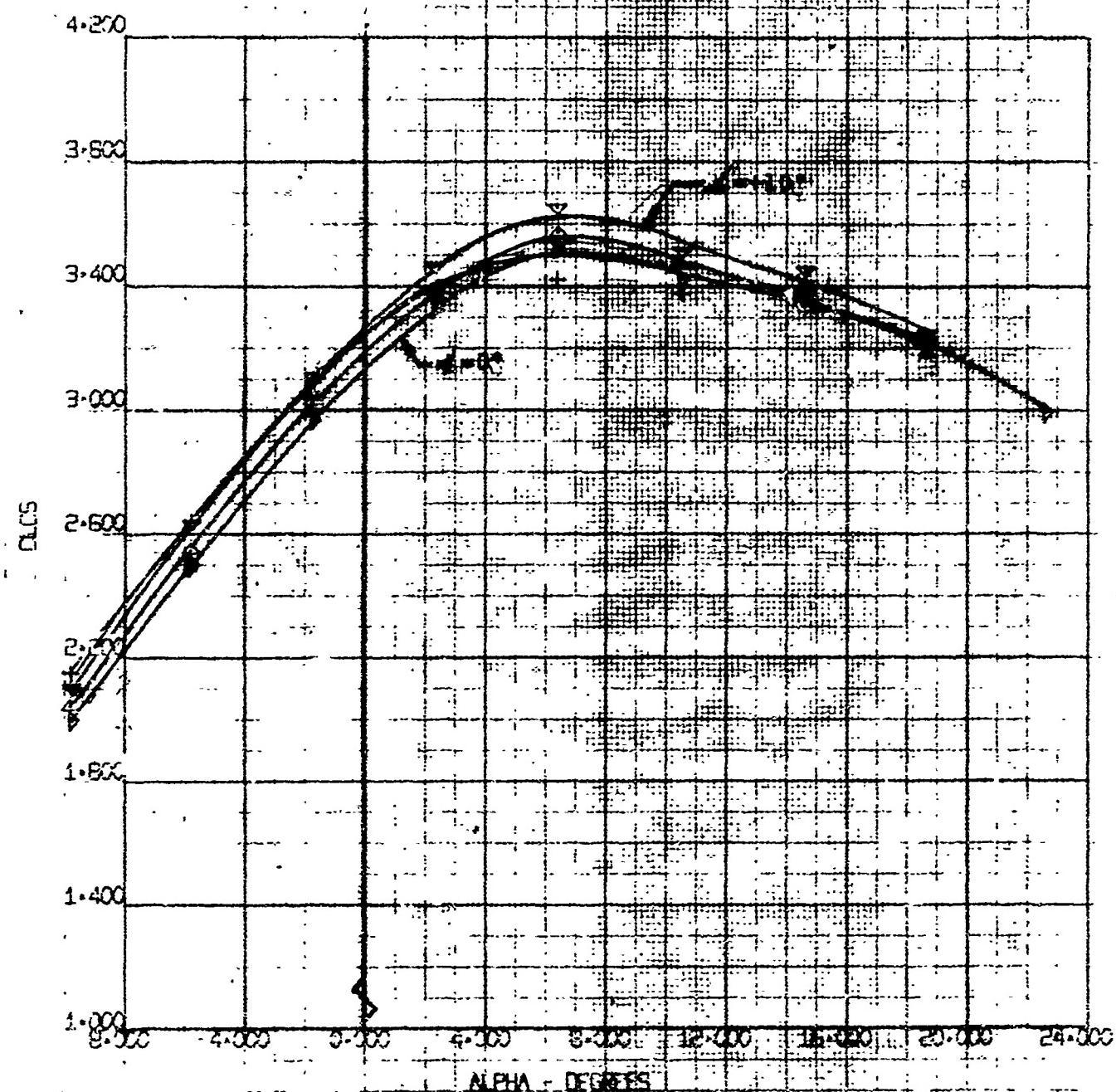
REV. LTR.

FIGURE 64+

RUN	SYM	Δ
39	\triangle	+5°
40	\triangleright	-6°
41	\triangledown	+10°
42	+	-11°

a
12.1 -14°

STABILIZER CONTROL WITH CYCLIC
 $\Delta_{stab} = 4^{\circ}$ $\Delta_{cyclic} = 60^{\circ}$
 FLAP TRIM SHATS
 $\Delta_{flap} = 10^{\circ}$ $\Delta_{shat} = 10^{\circ}$



FOUR-PROP TILT WING
 MODEL PROGRESSIVE SPAN
 CL_{CO} VS. ALPHA

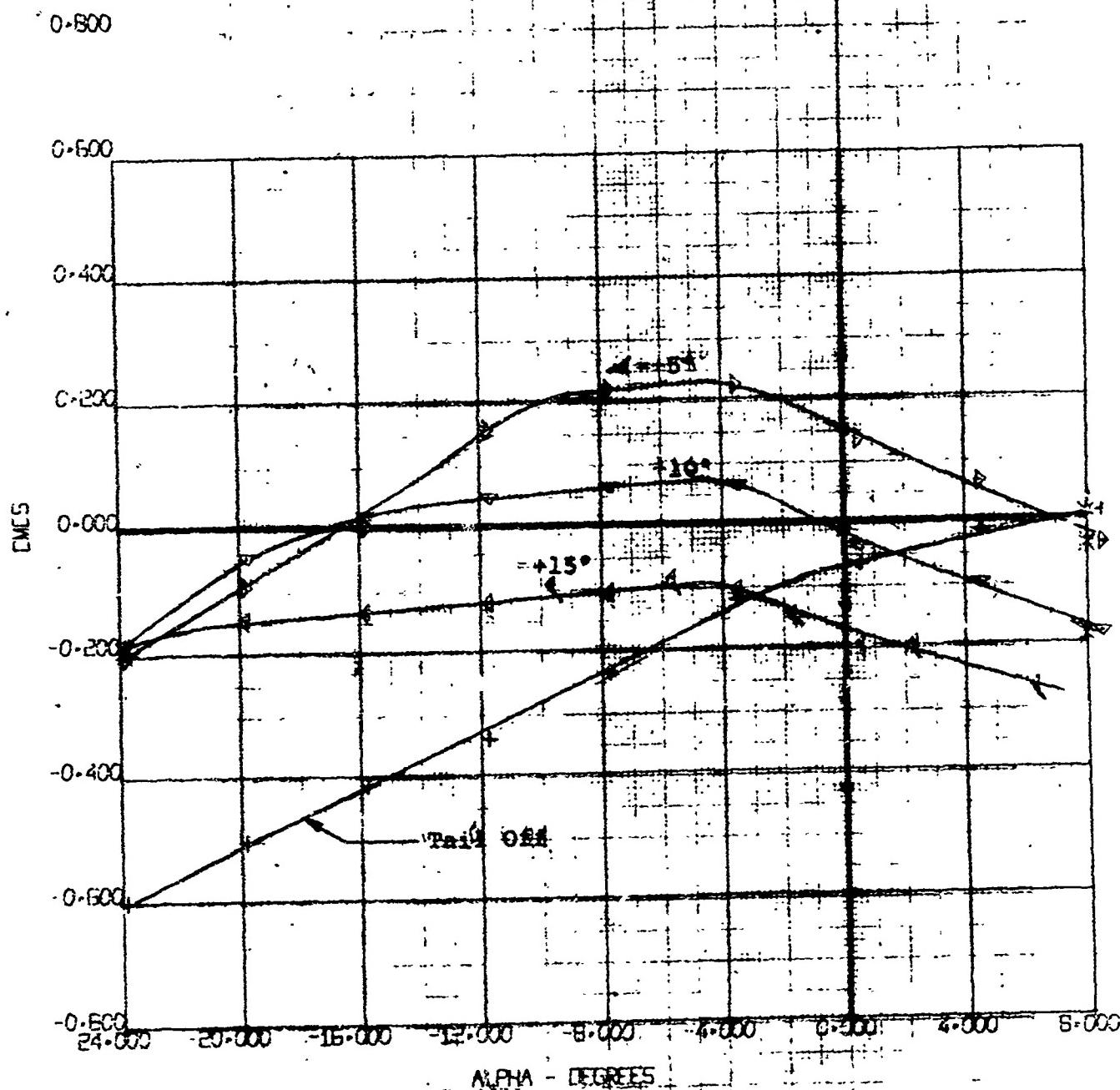
BWNT
67

12/8/70

NUMBER D170-10039-1
REV. LTR. Figure 85

RUN	SYM	$\Delta \alpha$
50	+	+10°
59	0	+5°
58	+	-5°
35861	<14	+15°
1-COO		

STABILIZER CONTROL WITH CYCLIC	
$\Delta \alpha = 360^\circ$	$\Delta \delta = 60^\circ$
FULL SPAN BLADES	
NOM $C_T = .55$	



FOUR-PROP TILT WING MODEL YR0B9 (FULL SPAN) CMGS VS. ALPHA	BWNT 67
	12/10/70

NOT REPRODUCIBLE

SHEET 145

RUN	SYM	δ
56	∇	+10°
57	\triangleright	+5°
58	+	-
35&61	$\Delta\Delta$	+15°

q y

8.2 +4°

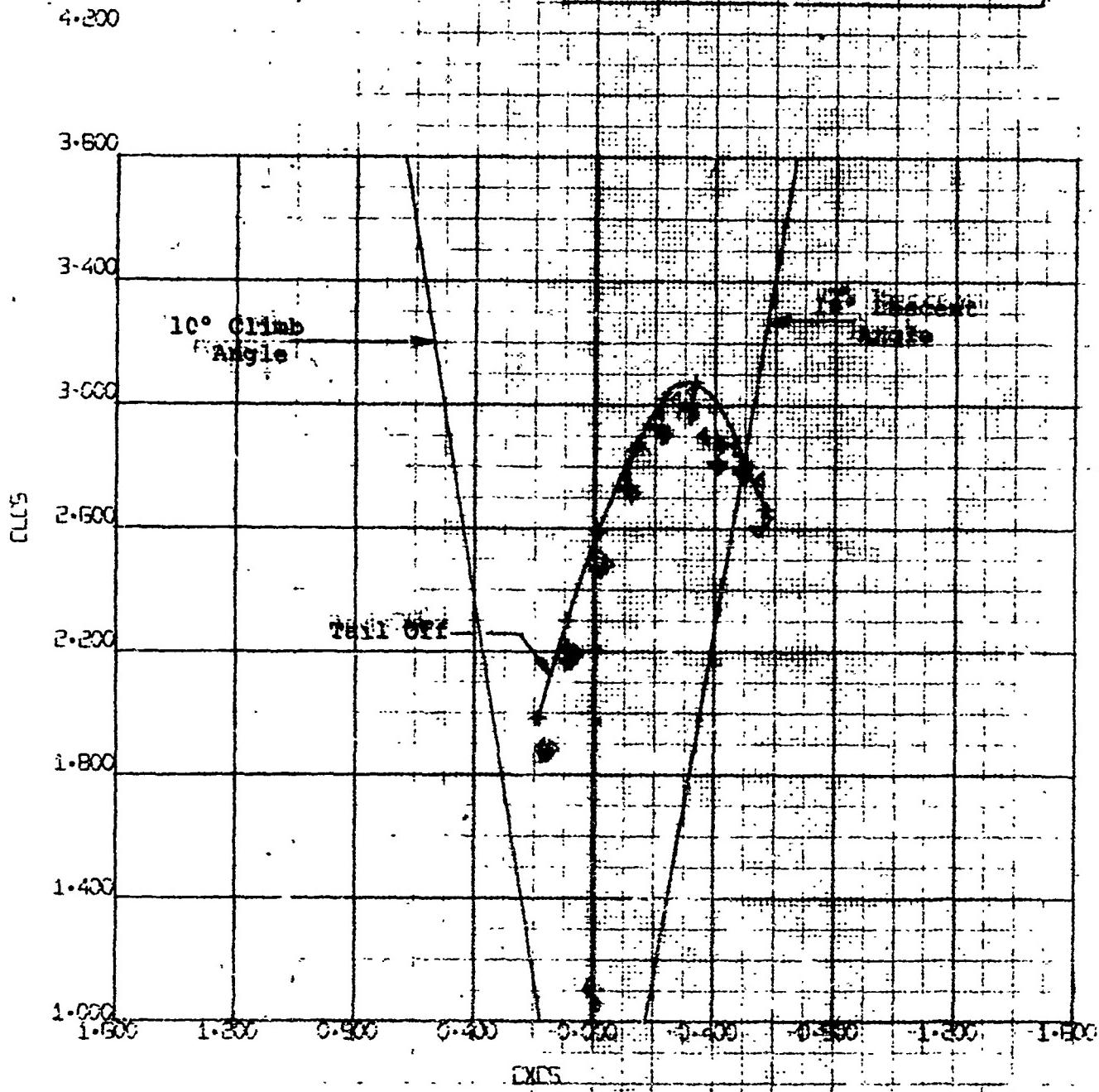
NUMBER D370-3003B-1
REV. LTR. Figure 86

STABILIZER CONTROL WITH CYCLIC

$W = 30^{\circ}$ $A_S = 60^{\circ}$

FULL SPAN FLAPS

MIN $C_L = .55$



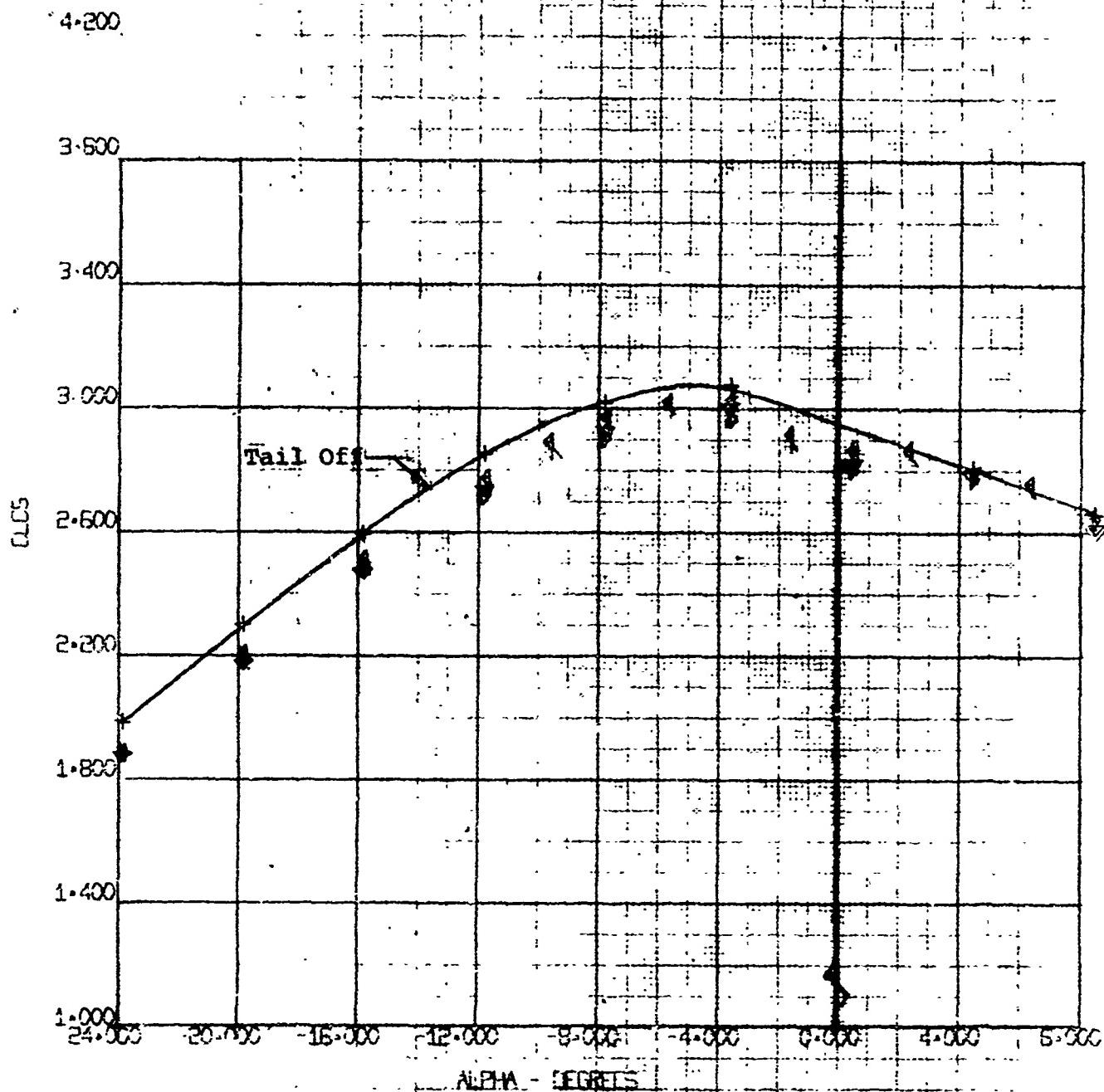
FOUR-PROP TILT WING	BVNT
MODEL YACED 0.11 SPAN	67
DPS VS. CLFS	12/10/70

RUN SYM Δ a
 56 ∇ $+10^\circ$ 8.2
 57 \triangleright $+5^\circ$
 58 $+$ -5°
 35&61 \triangle $+15^\circ$

NUMBER D101-1005A-1
 REV. TR.

Figure 17

STABILIZER CONTROL WITH CYCLIC
 $\Delta = 30^\circ$, $a = 8.2^\circ$
 FULL DOWN STAB
 NOM SPAN = .55



FOUR-PROP TILT WING
 MODEL VPROB (FULL SPAN)
 CLS VS. ALPHA

BWWT
67

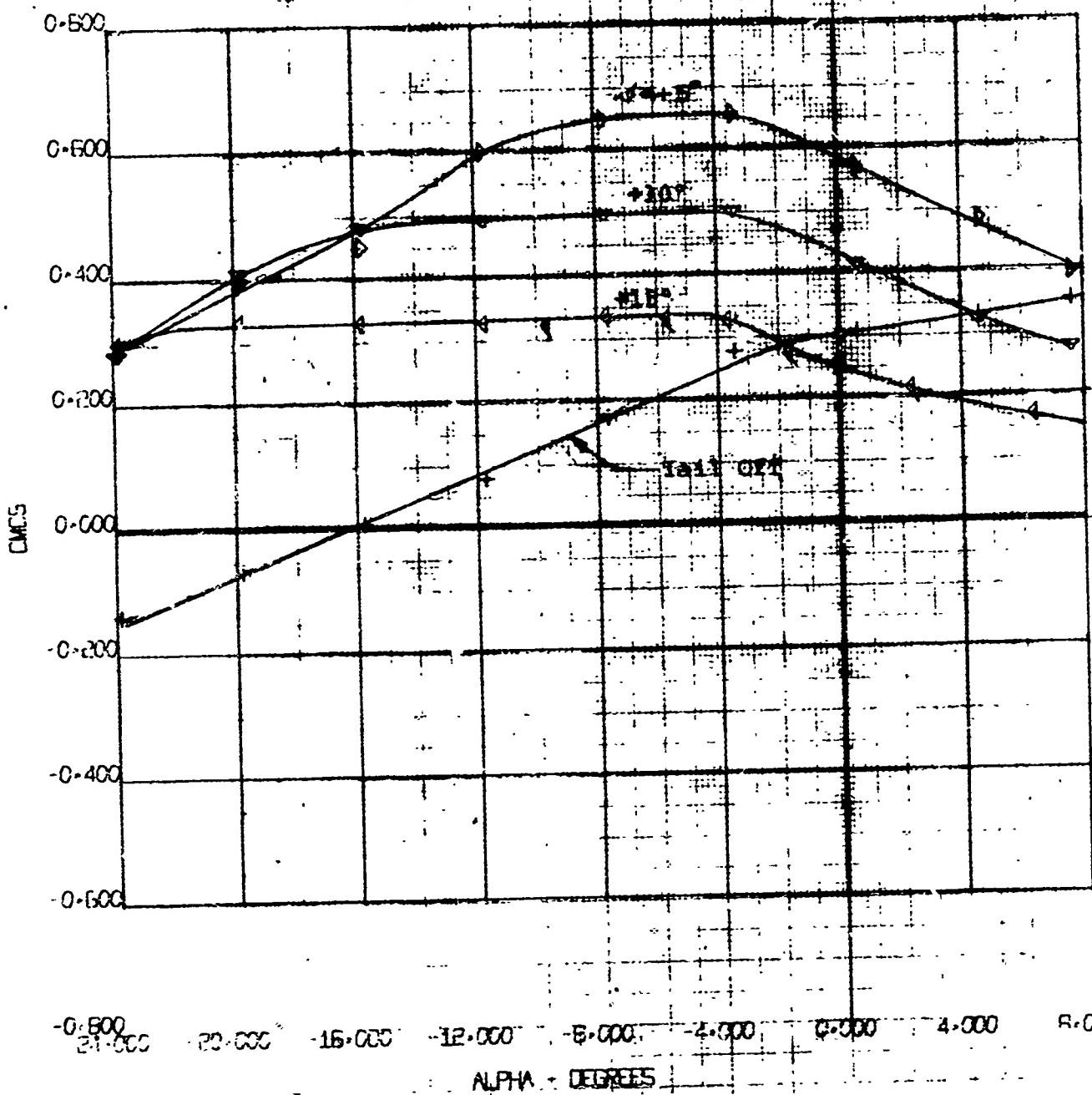
12/10/70

NUMBER D170-10039-1
REV. LTP.

Figure 88

RUN	SYM	Δ	α	γ
63	▽	+10°	8.2	-4°
64	△	+5°		
67	+			
1-000 37&70	△	+15°		

STABILIZER SPANWISE POSITION CYCLIC
 $i_w = 30^\circ$ $\delta_y = 60^\circ$
FULL SPAN SLATS
NONE OFT = 15



FOUR-PROP TILT WING MODEL YR66B(FULL SPAN) CL vs. α	BWNT 67
	12/10/70

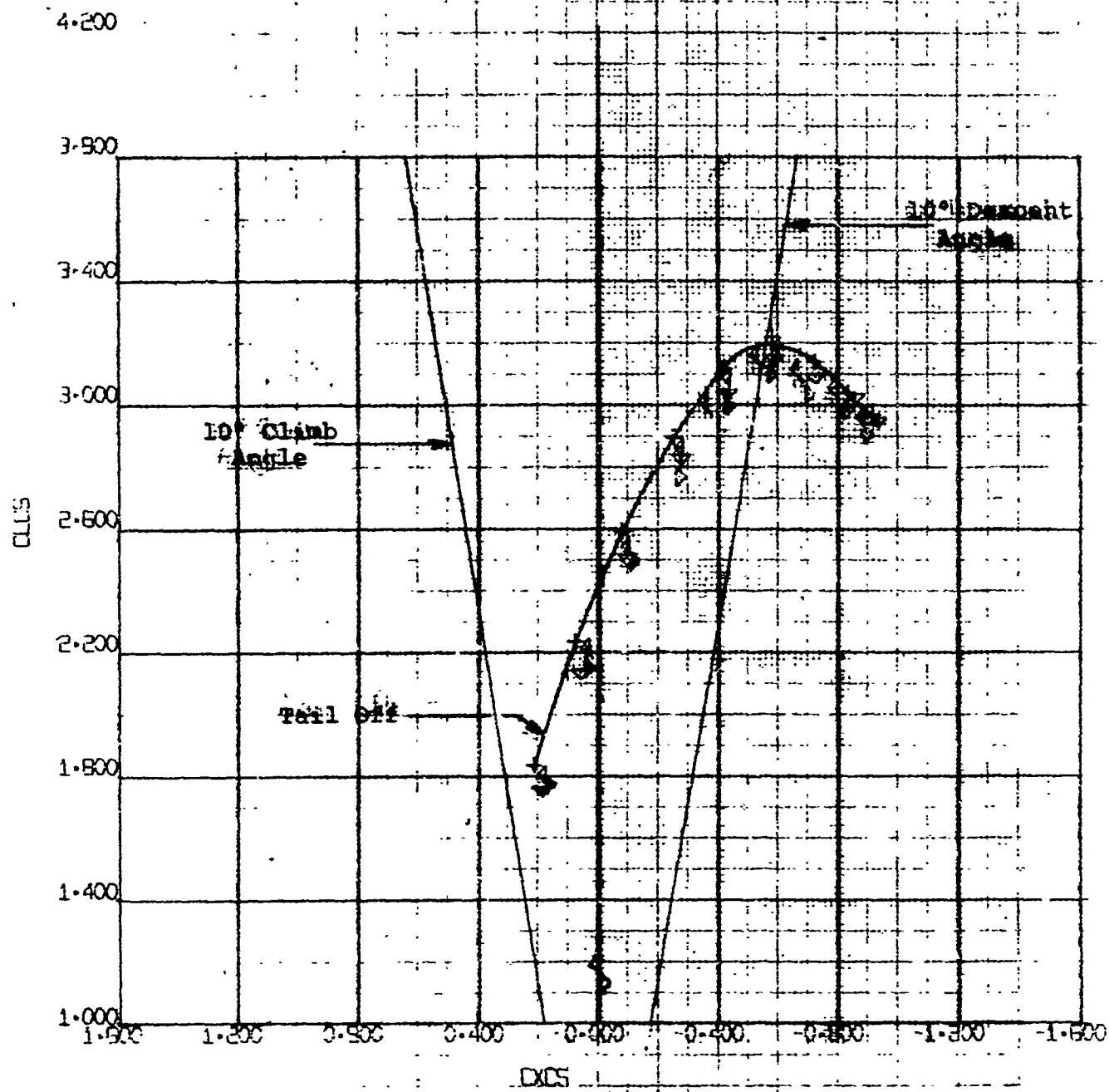
NUMBER D170-10039-1

REV. LTR.

Date 89

RUN	SYM	Δ	q	r
63	▽	+10°	8.2	-4°
64	▷	+5°		
67	+	---		
37&70	△△	+15°		

STABILIZER CONTROL WITH CYCLIC
 $\Delta = 30^\circ$, $\gamma = 50^\circ$
 FULL SPAN SLATS
 $\text{NOM } C_T = .55$



FOUR-PROP TILT WING	BVNT 67
MODEL VRO680 (FULL SPAN)	
DCL/D VS. DCL/S	12/10/70

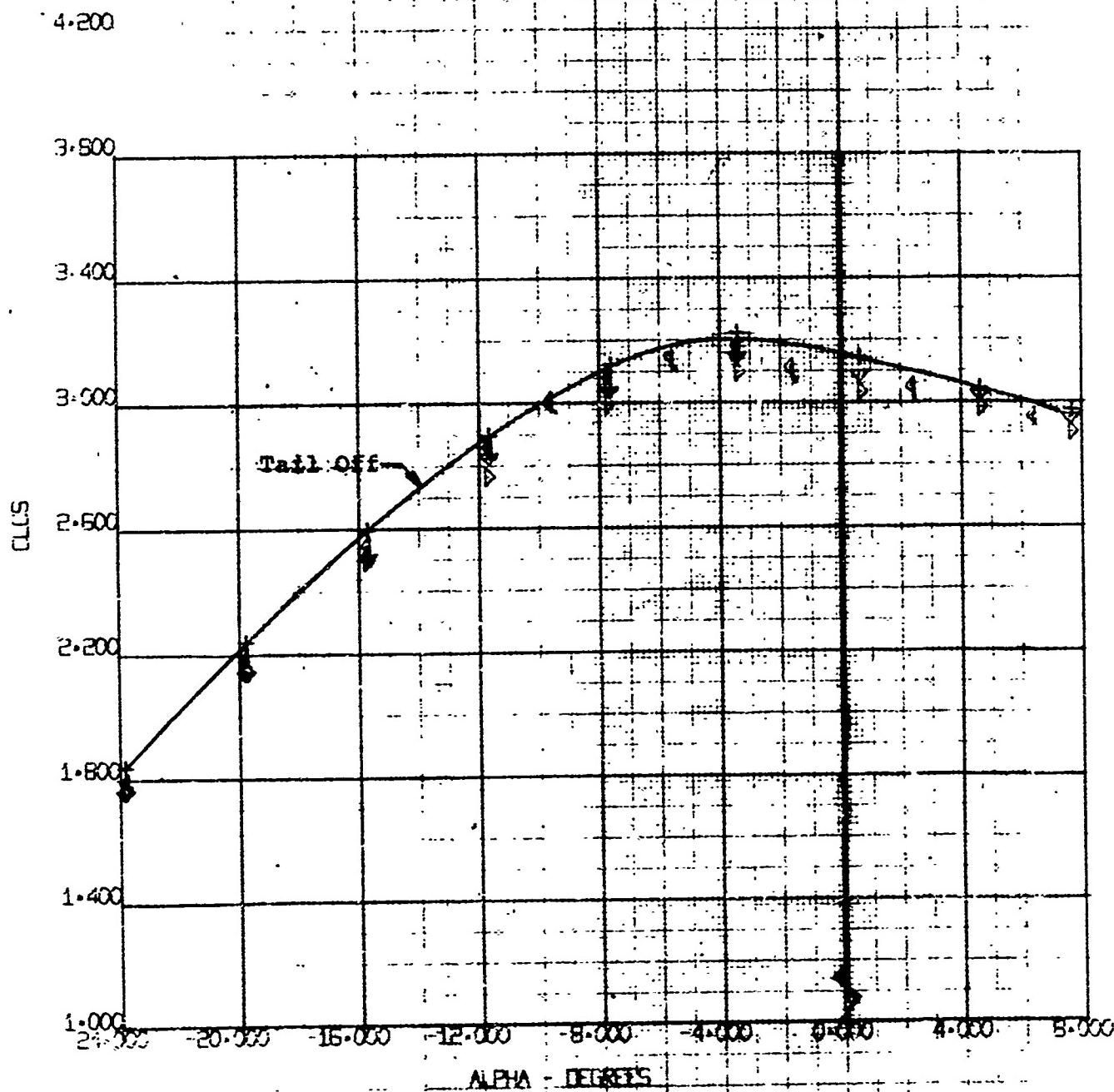
NOT REPRODUCIBLE

SHEET 149

NUMBER D170-10039-1
REV. LIR. Figure 90

RUN	S/M	Δ	q	y
63	▼	+10°	8.2	-4°
64	▼	+5°		
67	+			
87 & 70	▲ & ▲	+15°		

SPANNING ELEMENT WITH CYCLIC
L = 10°, q = 60°
FULL SPAN SLETS
WIND C.G. + .05



FOUR-PROP. LIFTING WING
MODEL YR660 (FULL SPAN)
CL(s) VS. ALPHA

BWWT
67

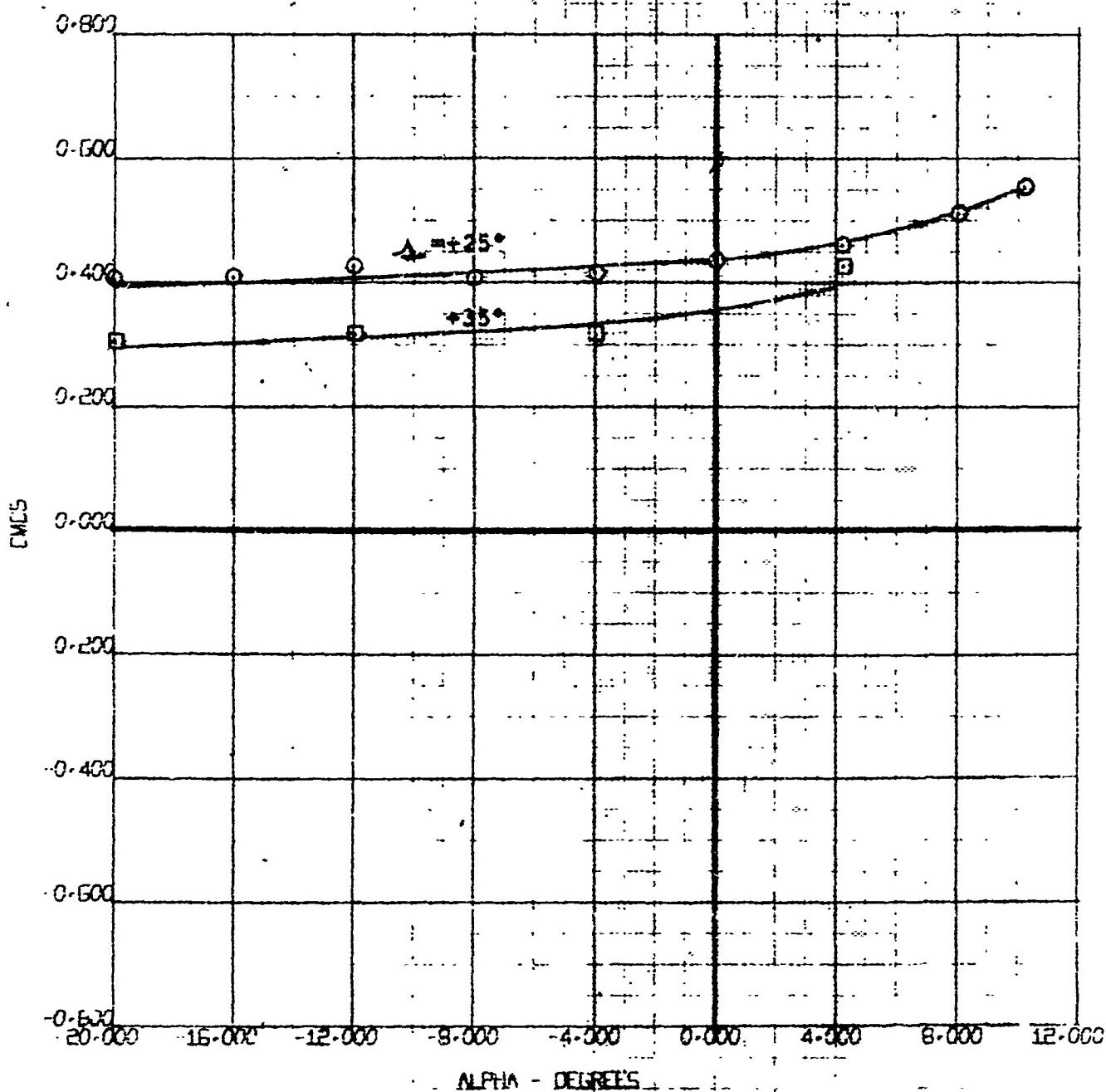
12/10/70

NUMBER D170-10039-1

R.V. JR. Figure 91.

RUN	SYM	Δ	q	γ
168	○	+25	2.64	-6.0
169	□	+35	↓	↓

STABILIZER CONTROL WITH CYCLIC
 $\Delta = 25^\circ$ $\Delta = 35^\circ$ $\gamma = 60^\circ$
 FULL SPAN SLATE
 NORM GR. = .81



FOUR-PROP TILT WING MODEL VR0688(FULL SPAN) CL vs. α	EWNT 67
	1/4/71

NOT REPRODUCIBLE
SHEET 151

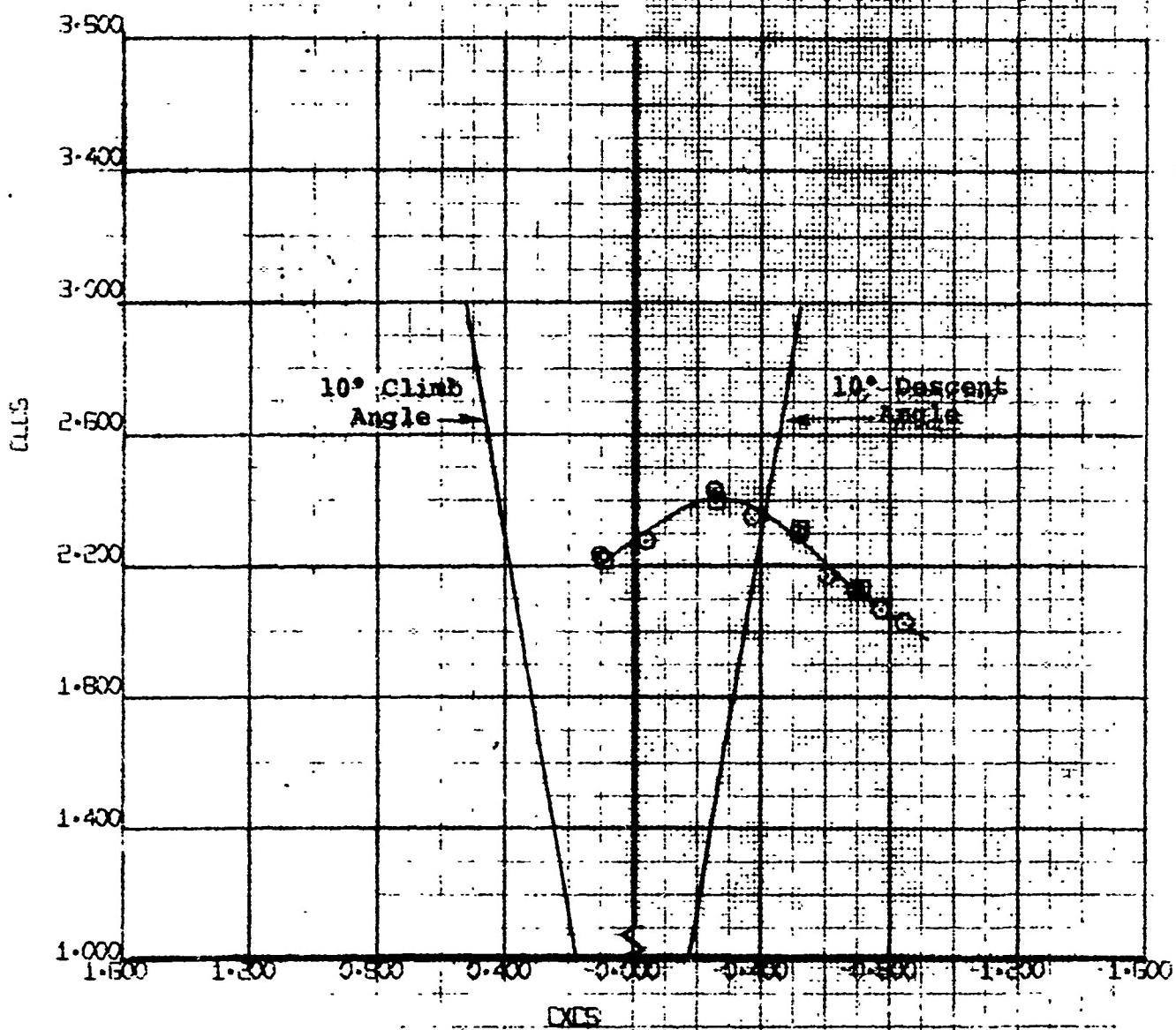
NUMBER F170-10039-1

REV. LTR. Figure 32

STARTUP CONTROL WITH CYCLIC

RUN	SYM	δ	q	γ
168	○	+25	2.64	-6.0
169	□	+35	↓	↓

SWING	δ	γ
FLAT SPAN STATE	0°	0°
NOSE DOWN	21°	21°



FOUR-PROP TILT WING MODEL VROBAGLI SPAN	BWWT 67
CLDS VS. CXDS	1/ 4/71

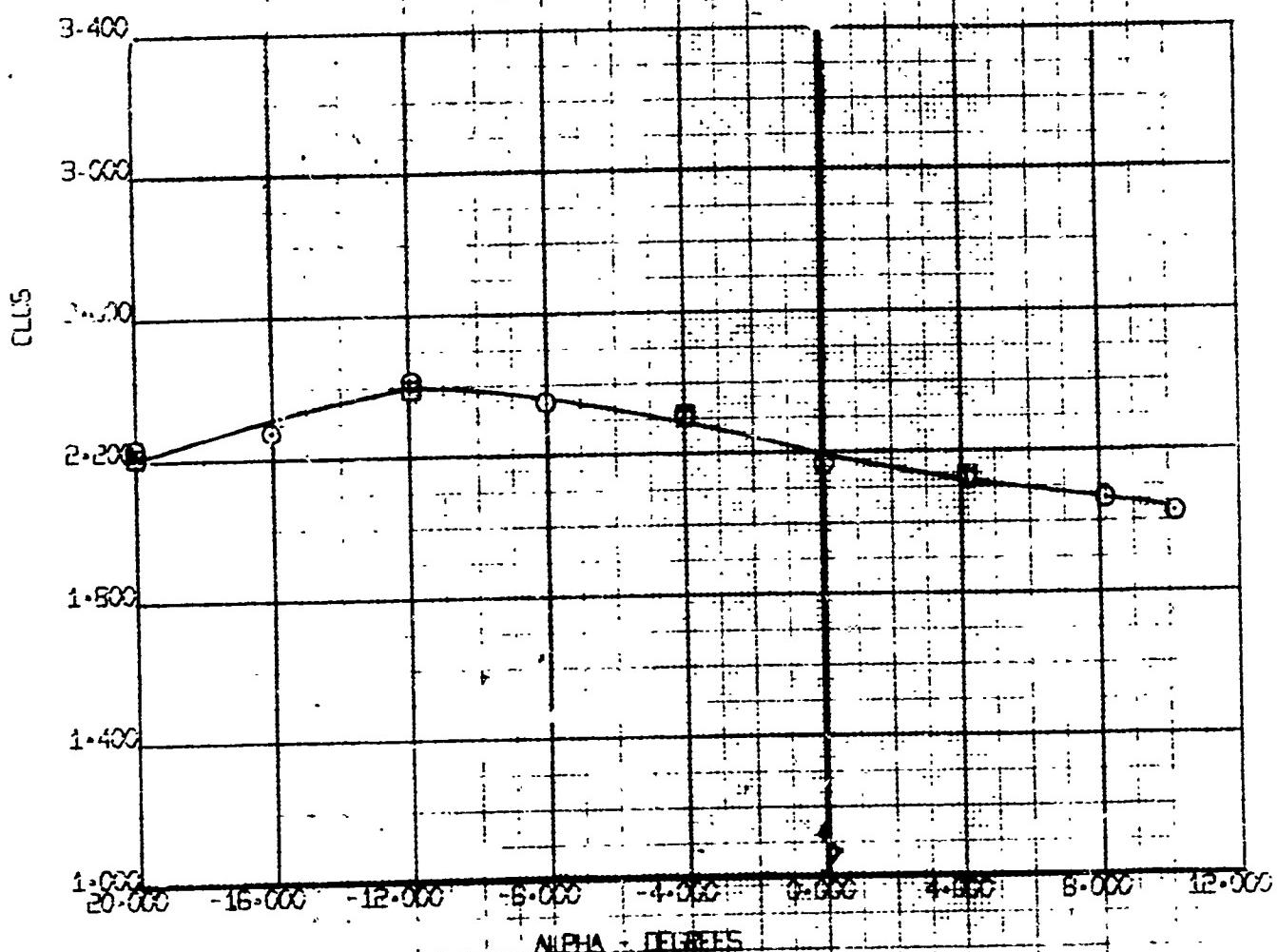
NUMBER D170+10039-1

REV. LTR.

Figure 93

STABILIZER CONTROL WITH CYCLIC
 $\alpha = 15^\circ$, $\delta_F = 60^\circ$
 FULL SPAN SLATS
 $M_{0.9} C_L = .81$

RUN	SYM	α	q	γ
168	○	+25	2.64	-6.0
169	□	+35	↓	↓



EGUR-PROF TILT WING
 MODEL VROSBOHEM SPAND
 CHCs VS. ALPHAS

BVNT
67

1/471

NOT REPRODUCIBLE

SHEET 153

6.5 LATERAL/DIRECTIONAL STABILITY IN TRANSITION

In this test, the lateral/directional stability characteristics of the four prop, tilt wing model VR068Q were investigated through the transition flight regime both with and without the vertical tail depicted in Figure 17. The positioning of the tail on the fuselage, which resulted in a tail volume of .083, is shown in Figure 15. This investigation was conducted with the horizontal tail mounted on the fin in its high position and with the stabilizer set at an angle representative for the wing tilt position. A check was made with the horizontal tail removed at low C_{Ts} values and the wing down to establish its contribution to the vertical tail effectiveness. The possible influence of cyclic pitch inputs on lateral/directional stability was also evaluated.

The yaw runs of this investigation were performed at a constant propeller RPM with selected combinations of wing tilt angle and flap angle that corresponded to typical combinations required through transition. All yaw data was acquired with zero fuselage angle, an angle that is representative of the normal body attitude in transitional flight. The off-setting of the model from the vertical centerline of the tunnel test section as shown in Figure 19, provided a yaw angular range of 8° (nose right) to -24° (nose left). This value, the maximum nose left yaw angle of -24° , was a limitation imposed by the allowable bending of the braided steel air hose inside the yaw adapter.

All moments obtained during the lateral/directional runs were transferred to the same wing down mid center of gravity location and movement with wing tilt angle as used for the longitudinal stability and control analysis. The body axis system was used for the data presentations.

6.5.1 Empennage Off Lateral/Directional Stability

The empennage off lateral/directional stability characteristics as measured from the basic three component yaw data are summarized in Figure 94. This plot presents the slipstream yawing moment, rolling moment, and side force derivatives (with respect to the sideslip angle, β), as a function of the slipstream thrust coefficient. All slopes plotted in Figure 94 were read over a yaw angle range that did not exceed $\pm 8^\circ$ and the C_{Ts} values were those prevailing at zero yaw angle.

It is apparent from an examination of the directional stability plot shown in Figure 94, that over the thrust coefficient range from zero C_{Ts} to 0.8 C_{Ts} which encompassed wing configurations from wing down and retracted flaps to 30° of wing tilt and 60° flaps, $C_{n_{S\beta}}$ generally varies linearly as a function of $(1-C_{Ts})$

or freestream q . This variation indicates that the major contributor to the tail-off directional stability is the fuselage, a component that is acted upon primarily by freestream q . The reduction in yaw instability at $0.55 C_{Ts}$ with 30° of wing tilt is a special case in that wing stall was present.

A change from an unstable yaw condition to a stable condition that occurred at $0.82 C_{Ts}$ when the wing was tilted up from 30° to 45° , probably resulted to a large measure from a redistribution of the longitudinal pressures on the fuselage. The corresponding side force picture, wherein no change in side force was recorded when the wing was raised is consistent with this reasoning as is the observed change via tuft studies in the character of the flow aft of the wing at combinations of a high C_{Ts} value and wing tilt angles in the order of 45° . In this case, the increase in the destabilizing propeller side force and propeller yawing moment is largely offset by the respective shortening of the moment arm between the propeller hub and c.g., and the lessening of the propeller yawing moment acting about the aircraft yaw axis.

A positive dihedral effect (negative sign on $C_{x\beta}$) was exhibited by the model with the wing down, flaps up, and slats extended in the low C_{Ts} range evaluated. Deflecting the flaps to 40° increased the dihedral effect. It is surmised that the major portion of this increase was caused by a modification in the wing/body interference effects.

A large change in the $C_{x_{S\beta}}$ from a negative value to a positive value, occurred at $0.2 C_{Ts}$ when the flap deflection was increased by 20° and the wing was tilted to 15° . A combination

of two factors could have produced this effect: the large constant percent chord flaps have a swept forward hinge line and the slipstream lift coefficient was increased by an increment of 2.15 as shown in Figure 95. The subsequent change in dihedral effect with increasing C_{T_s} follows the decrease in C_{L_s} illustrated in Figure 95.

Tilting the wing from 30° to 45° at $0.82 C_{T_s}$ increased the dihedral effect. It is a reasonable assumption that this increase primarily resulted from the change in spanwise lift distributions on the inboard portion of the upwind and downwind wings along with the increase in propeller forces and moments acting about the aircraft roll axis. Wing tilt increases the propeller forces and moments, plus vertically raises the vectors reacting about the aircraft rolling axis.

6.5.2 Empennage On Lateral/Directional Stability

Figure 96, presenting the empennage on lateral/directional stability characteristics, was developed from the basic three component yaw data in a similar manner to that used in generating Figure 94. Additional yaw data, over that obtained for the tail-off case, was acquired with a flap deflection of 40° in combination with the 30° of wing tilt. Likewise, data was also acquired with 55° of wing tilt at $0.93 C_{T_s}$.

The first item of interest in Figure 96 is the unstable directional characteristics measured with the wing down and retracted flaps. This situation has been identified with a low vertical tail effectiveness caused by the interaction of the flow emanating from the wing/body juncture on the root section of the vertical tail. Lowering the flaps to 40° , produced a stable aircraft directionally by improving the vertical tail effectiveness. Apparently, lowering the flaps increased the vertical tail effectiveness by deflecting the adverse wing/body juncture flow below the base of the fin. A redesign of the wing/body intersection and vertical tail/fuselage junction could probably rectify the deficiency.

At $0.2 C_{T_s}$, the increase in directional stability accompanying the 15° of wing tilt and additional 20° of flap deflection, largely reflects a further increase in vertical tail effectiveness. The subsequent decrease in directional stability with increasing thrust coefficient generally follows the linear reduction in freestream q or dynamic pressure acting on the vertical fin.

With a wing tilt angle of 30°, a reduction in flap deflection from 60° to 40° produced some increase in yaw stability and dihedral effect. These increases should have primarily resulted from the change in lift coefficient accompanying the flap angle change; however, the relatively large increase in dihedral effect does not appear to be consistent with the increment of lift coefficient illustrated in Figure 95.

The improvement in yaw stability at 0.93 C_{Ts} when the wing was tilted up to 55° from a 45° angle, is attributed to the redistribution of longitudinal pressures along the fuselage as mentioned previously in Section 6.5.1. At this thrust coefficient the vertical tail is essentially ineffective due to the low freestream q .

6.5.3 Vertical Tail Effectiveness

Vertical tail effectiveness through transition is presented in Figure 97 as an increment of yawing moment derivative in the slipstream coefficient format. The fin's contribution to the rolling moment and side force derivatives are also shown. These increments were directly obtained by subtracting the tail-off values noted in Figure 94 from the respective tail-on values plotted in Figure 96.

Figure 97 shows the large increase in tail effectiveness at low C_{Ts} values, discussed in Section 6.5.1, that occurred when the flaps were extended to the 40° position with the wing down. A further increase in fin effectiveness was produced when the wing was tilted up to the 15° setting. Section 6.5.1 pointed out that the wing/body juncture of the model was probably the prime factor in this problem.

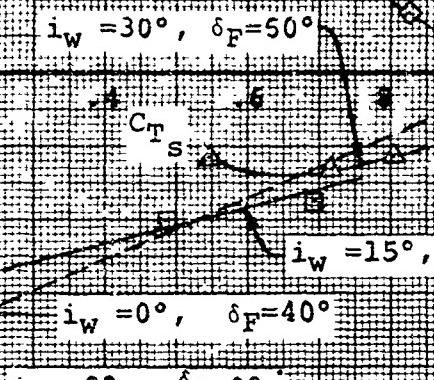
With 15° of wing tilt, the decrease in tail effectiveness with increasing thrust coefficient is linear and generally follows a $(1-C_{Ts})$ variation. The effectiveness is thus a direct function of the freestream q , acting on the tail. Except for the special case of 0.55 C_{Ts} where wing stall plus center section stall and fin "blanketing" were present, the tail effectiveness with 30° of wing tilt angle showed no significant departure from the $(1-C_{Ts})$ variation. Some "blanketing" at the base of the fin occurred at 0.8 C_{Ts} when the wing was tilted up to 45°.

Figures 98 through 127 present the basic data from which the plots of lateral/directional stability and vertical tail effectiveness characteristics were derived. Data in slipstream notation is presented in sets of three plots, C_{ns} vs β (yawing moment vs. sideslip angle), C_{ls} vs. β (rolling moment), and C_{ys} vs. β (side force), in the order of increasing wing tilt angle and flap angle. Each set of plots contains series of runs, empennage on and/or off, conducted at a constant propeller RPM (except the zero C_{Ts} runs) with a selected wing tilt/flap angle configuration. The three component data obtained for the wing down and retracted flap case at low values of slipstream thrust coefficient is plotted in Figures 98 through 100. As the wing was tilted up with the flaps extended, data was acquired over a range of thrust coefficients representative for the portion of the transition regime that was commensurate with the particular aircraft configuration. Figures 125 through 127 present data for the highest wing tilt angle evaluated (55°). This data was obtained at a thrust coefficient of 0.93 C_{Ts} .

In the following graphs, CYMCS, CYCS, and CRMCS, which represent body axis data, should be read as C_{ns} (positive-nose right), C_{ls} (positive - right wing down), and C_{ys} (positive-to the right), respectively. A positive sideslip angle is nose to the left.

BASIC LATERAL/DIRECTIONAL STABILITY
EMPENNAGE OFF

1961 YAWING MOMENT

 $C_{n_s \beta}$ $i_w = 30^\circ, \delta_F = 50^\circ$ C_{T_s}  $i_w = 45^\circ, \delta_F = 60^\circ$ $(1-C_{T_s})$
Variation

SYM	i'_w	δ_F
●	0	0
●	0	40°
□	15°	60°
△	30°	50°
◇	45°	60°

1962 ROLLING MOMENT

 $C_{l_s \beta}$ C_{T_s}

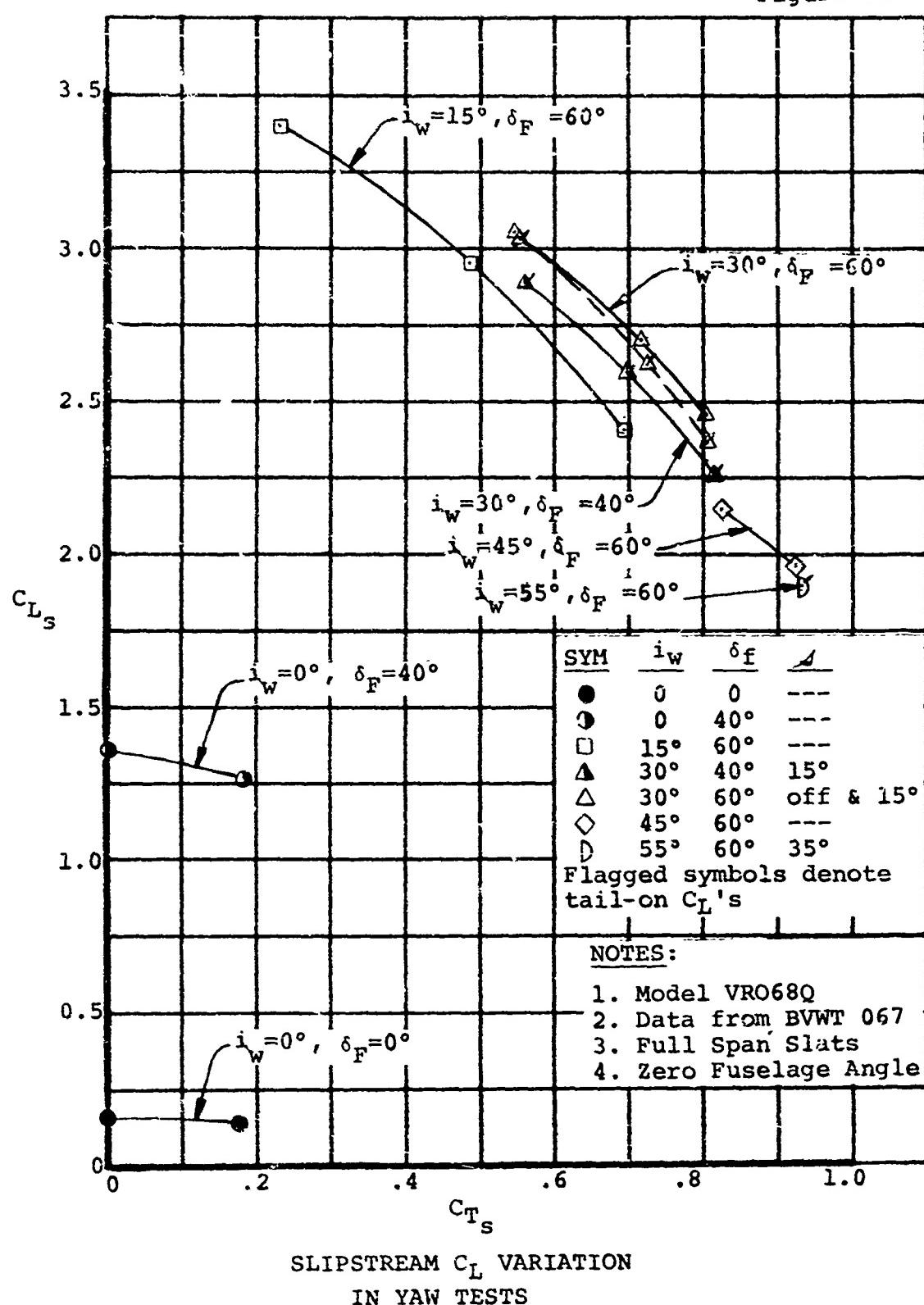
1963 SIDE FORCE

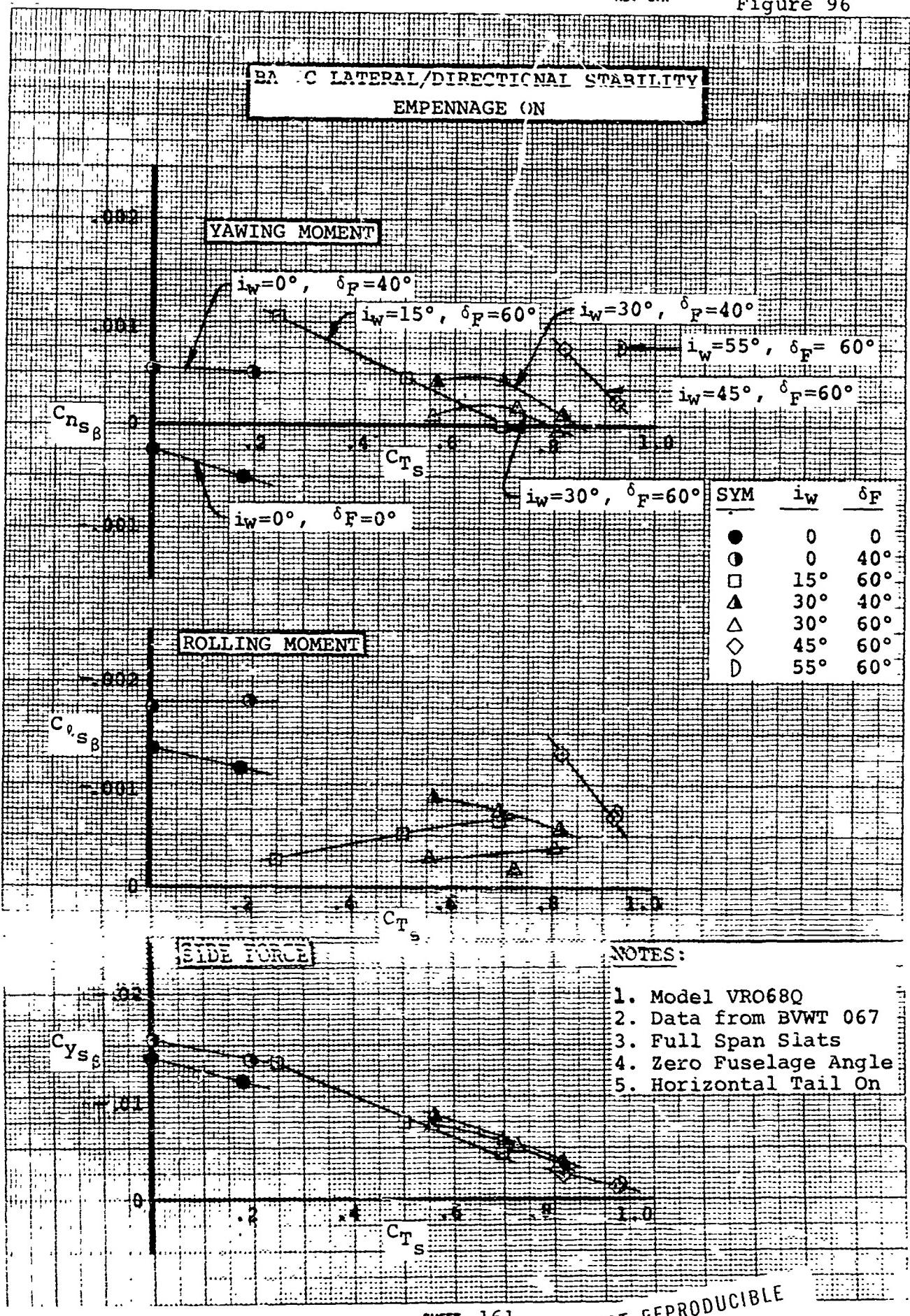
 $C_{y_s \beta}$ C_{T_s}

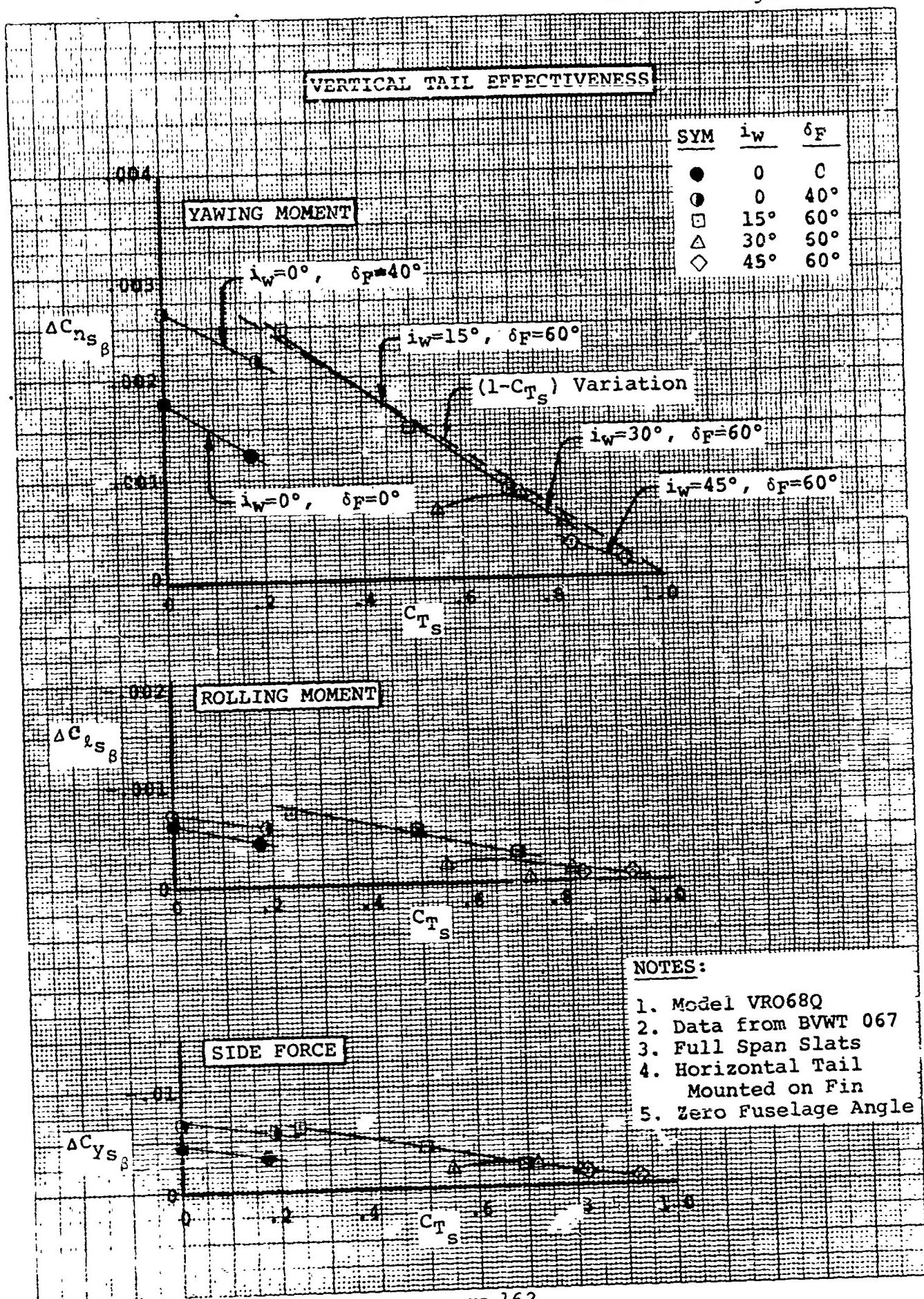
NOTES:

1. Model VRC68Q
2. Data from EVWT 067
3. Full Span Slats
4. Zero Fuselage Angle

Figure 95



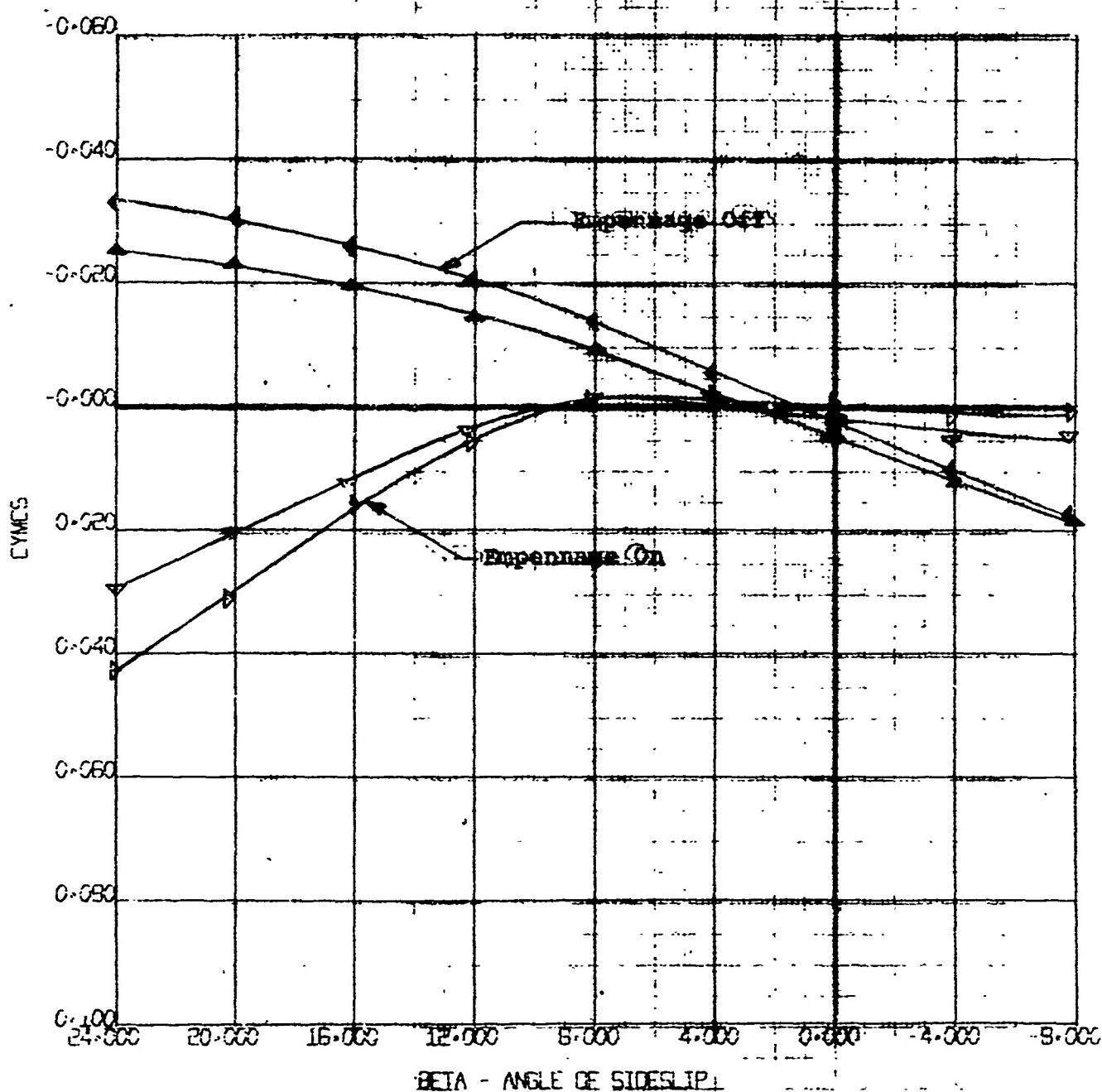




RUN	SYM	α	NOM CCTS
92	▷	0°	17.3 0
93	▽	0°	13.3 .20
94	◀	---	17.3 0
95	▶	---	13.3 .20
96	◆	---	13.3 .20

NUMBER D170-10039-1
REV. LTR. Figure 98

LATERAL/DIRECTIONAL STABILITY
WINGSPAN = 0°
FULL SPAN STRESSES



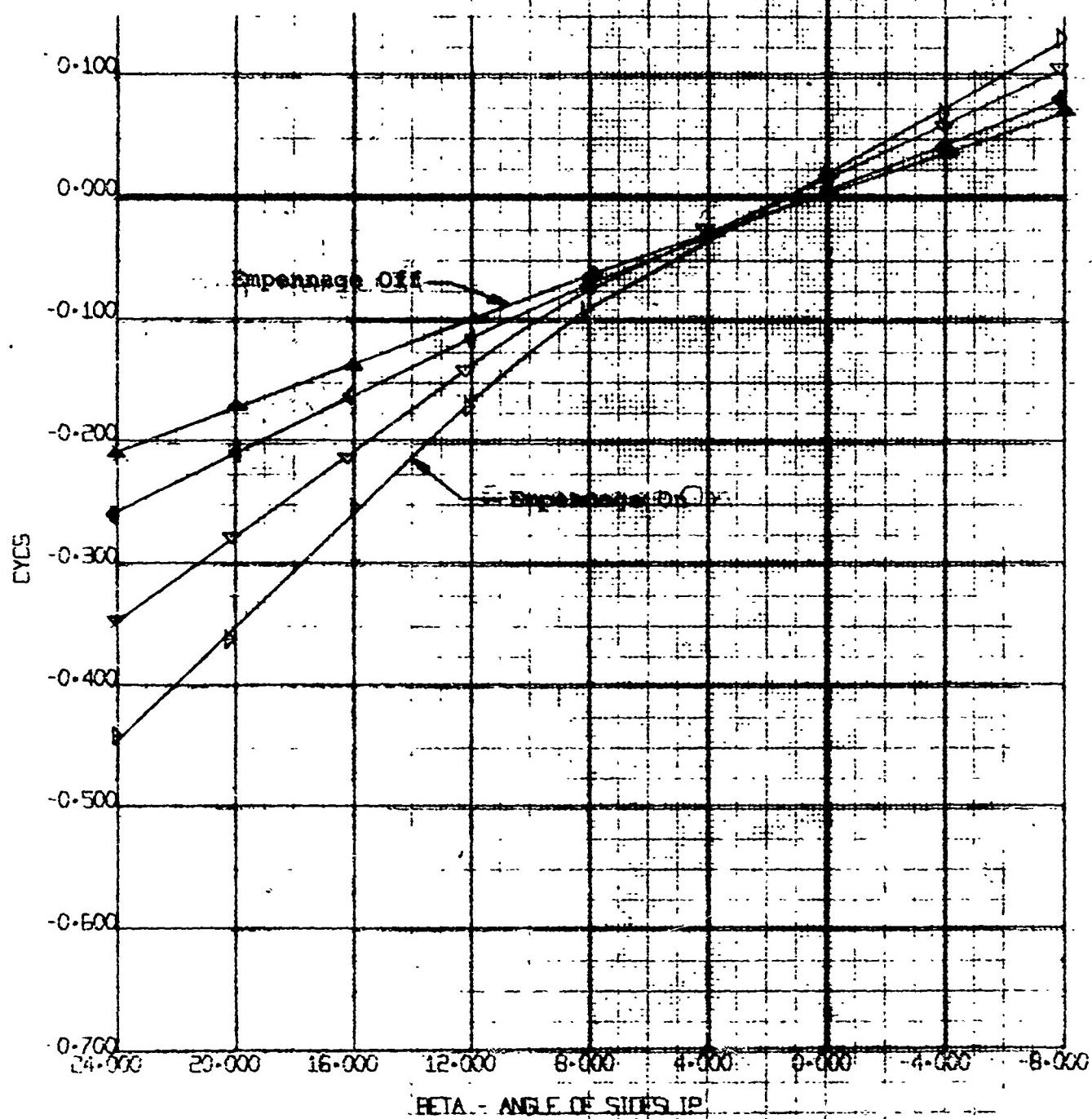
FOUR-PROP TILT WING MODEL VR06B0(FULL SPAN) SYNCS VS. BETA	BWNT 67 12/15/70
--	------------------------

NOT REPRODUCIBLE

SHEET 163

RUN	SYM	α	q	NOM CT _S	NUMBER	DI70-10039-1
92	▷	0°	17.3	0	REV. LTR. FIGURE 99	LATERAL/DIRECTIONAL STABILITY
93	▽	0°	13.3	.20		
94	◀	---	17.3	0		
95	▲	---	13.3	.20		FULL SPAN SLATS

0-200



FOUR-PROP. T-TAIL WING	BWNT
MODEL VROS89(FULL SPAN)	67
CYCS VS. BETA	12/15/70

RUN	SYM	A	a	NOM C_{Ta}
92	▷	0°	17.3	0
93	▽	0°	13.3	.20
94	◀	-	17.3	0
95	▲	-	13.3	.20

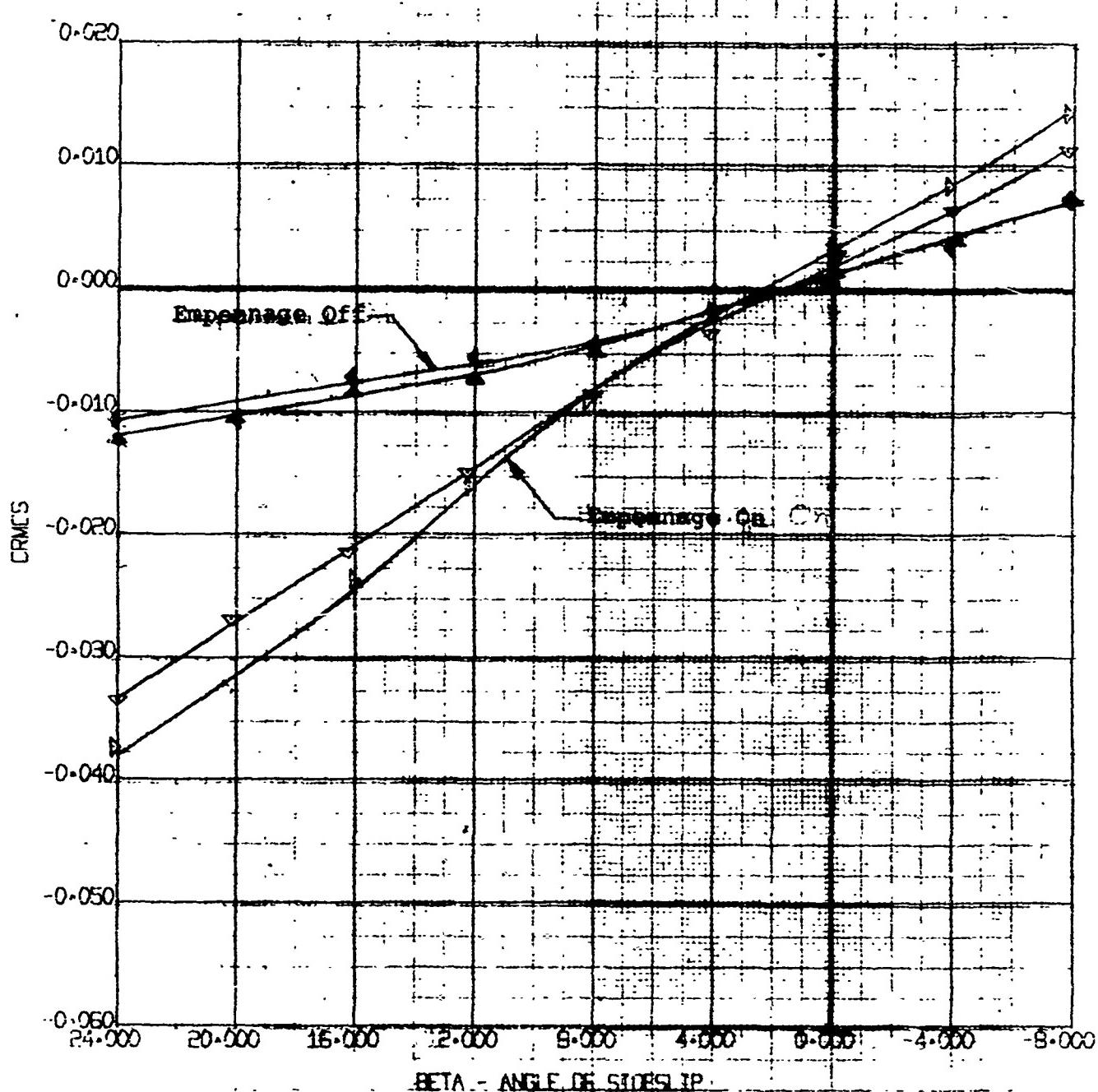
NUMBER D170-10039-1

REV. LTR. FIGURE 100

LATERAL/DIRECTIONAL STABILITY

 $\delta_w = 0^\circ$, $\delta_F = 0^\circ$

FULL SPAN SEATS



NOT REPRODUCIBLE

FOUR-PROP TILT WING
MODEL VRO681 (FULL SPAN)
CRIMES VS. BETA

EWNT
67

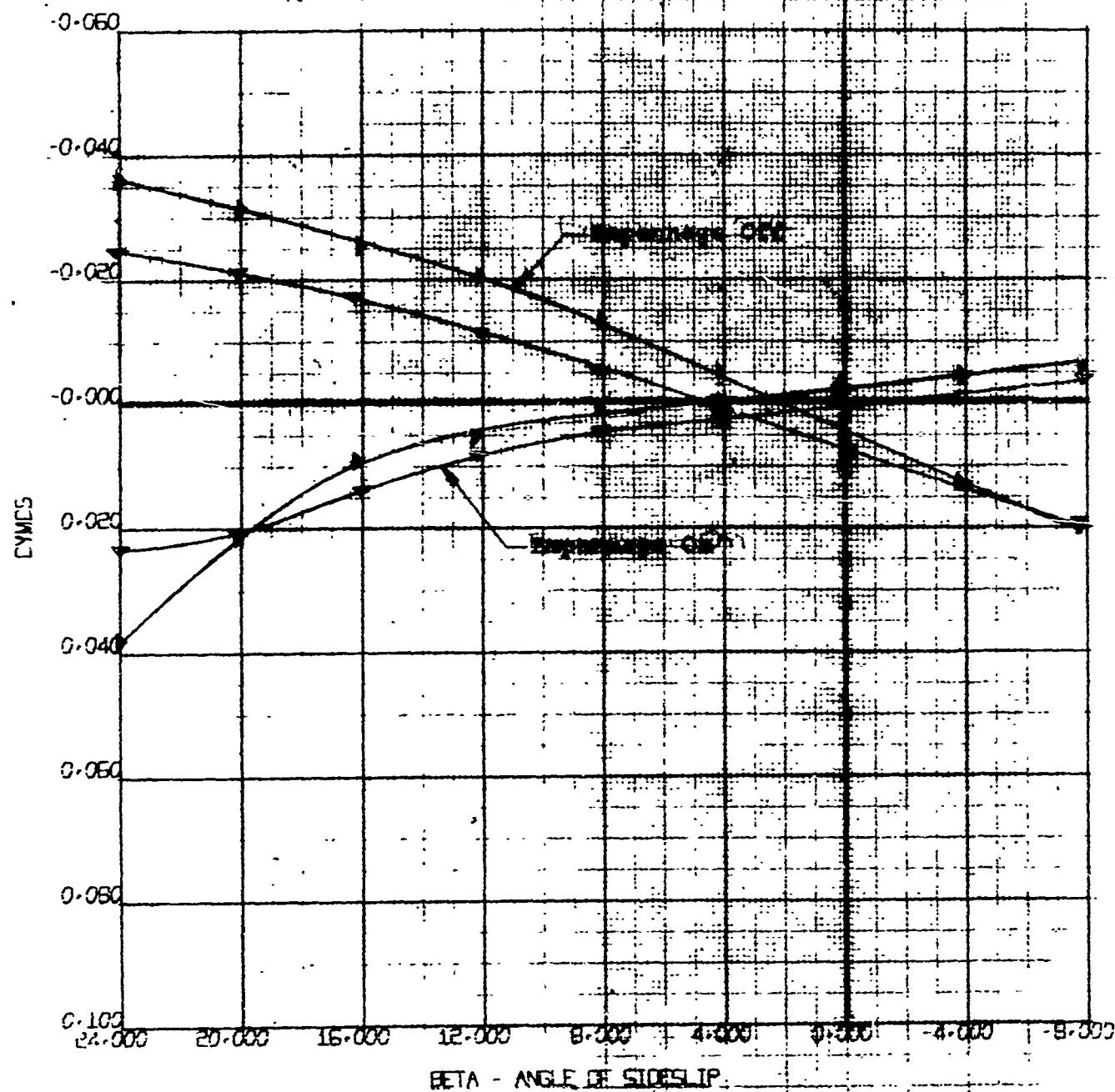
12/15/70

RUN	SYM	$\frac{A}{L}$	NOM	
			C_{T_0}	C_{T_S}
85	▷	09	17.3	0
86	▽	0*	13.3	.20
86	▶	---	17.3	0
87	▼	---	13.3	.20

-0.060

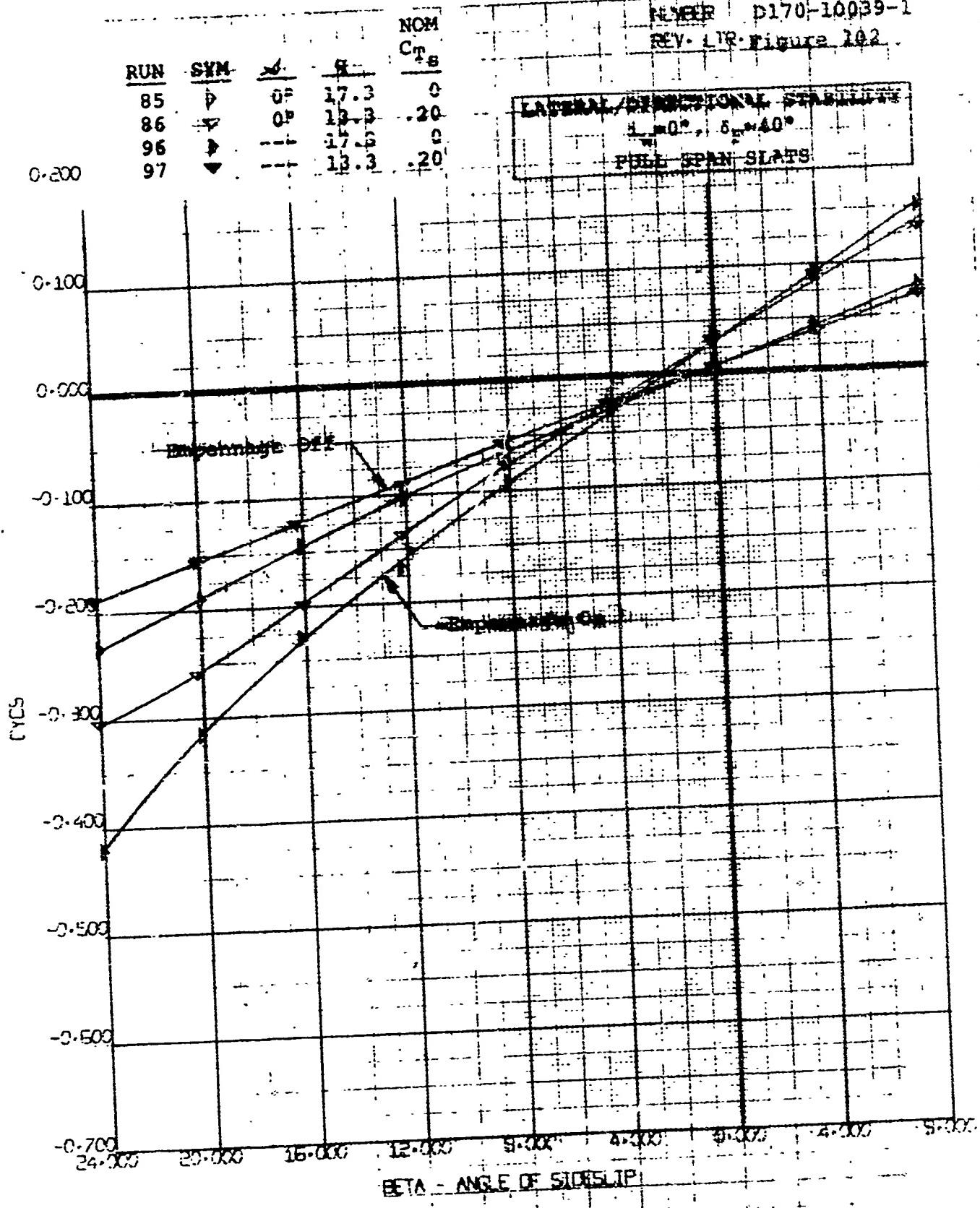
NUMBER B170-10039-1
REV. LR. Edition 1011

TEST CONDITIONS		WINGSPAN	WINGSPAN	WINGSPAN
WINGSPAN	WINGSPAN	WINGSPAN	WINGSPAN	WINGSPAN
WINGSPAN	WINGSPAN	WINGSPAN	WINGSPAN	WINGSPAN



BETA - ANGLE OF SIDESLIP.

FOUR-PROP TILT WING	BWWT
MODEL VROBQ (FULL SPAN)	67
CLADIS VS. BETA	1/4/71



NOT REPRODUCIBLE

SHEET 167

FOUR-PROP TILT WING
MODEL VROG0 (FULL SPAN)
CYCS VS. BETA

BWHT
67

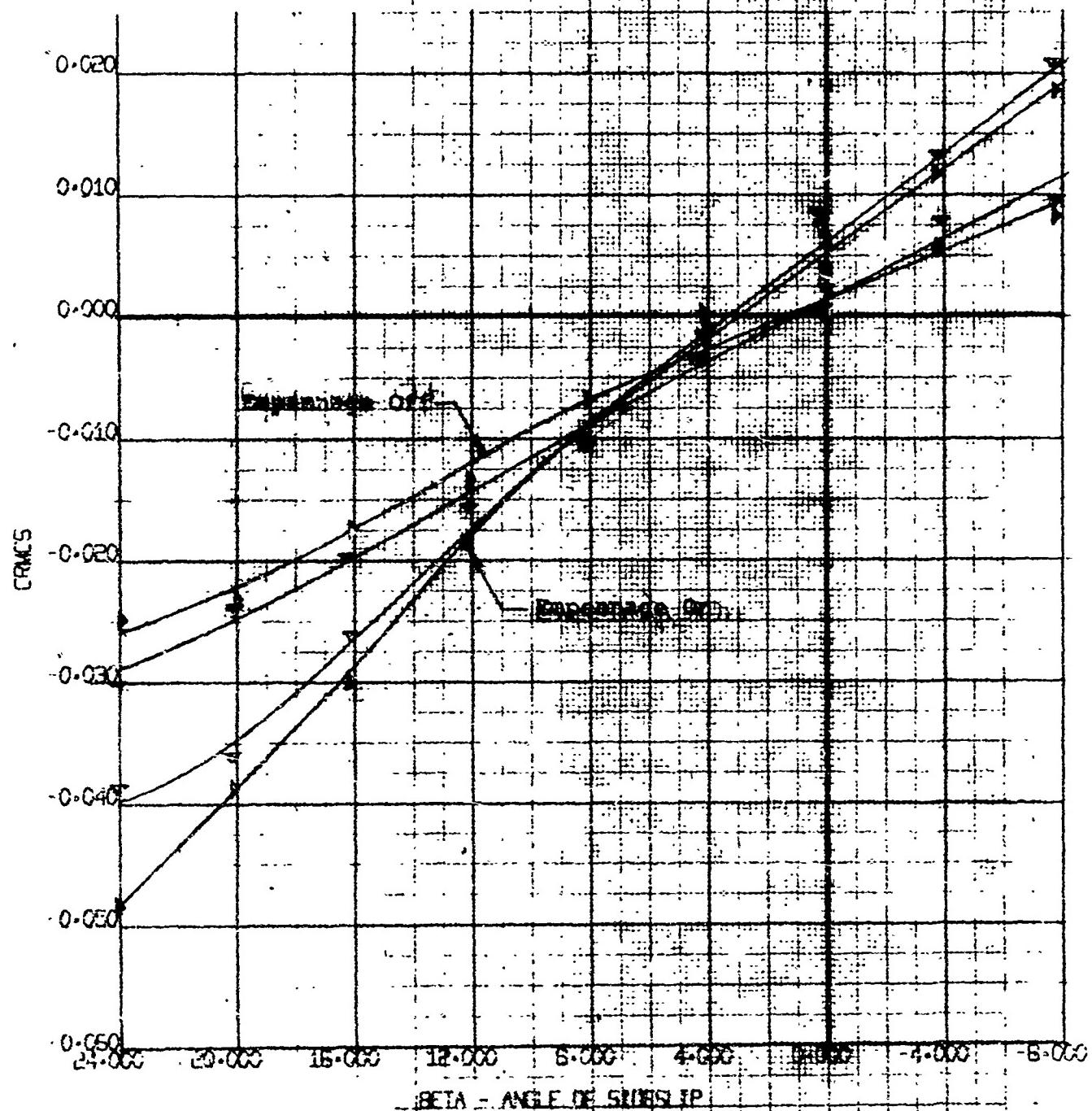
1/4/71

NUMBER D170-10039-1

REV. LIR. FIGURE 103.

RUN	SYM	α	NOM CTS
85	▷	0°	17.3 0
86	▽	0°	13.8 .20
96	▷	1°	17.3 0
97	▽	1°	13.3 .20

LATERAL DIRECTIONAL STABILITY
 CAP. 5° = 10°
 FULL SPAN SLATS

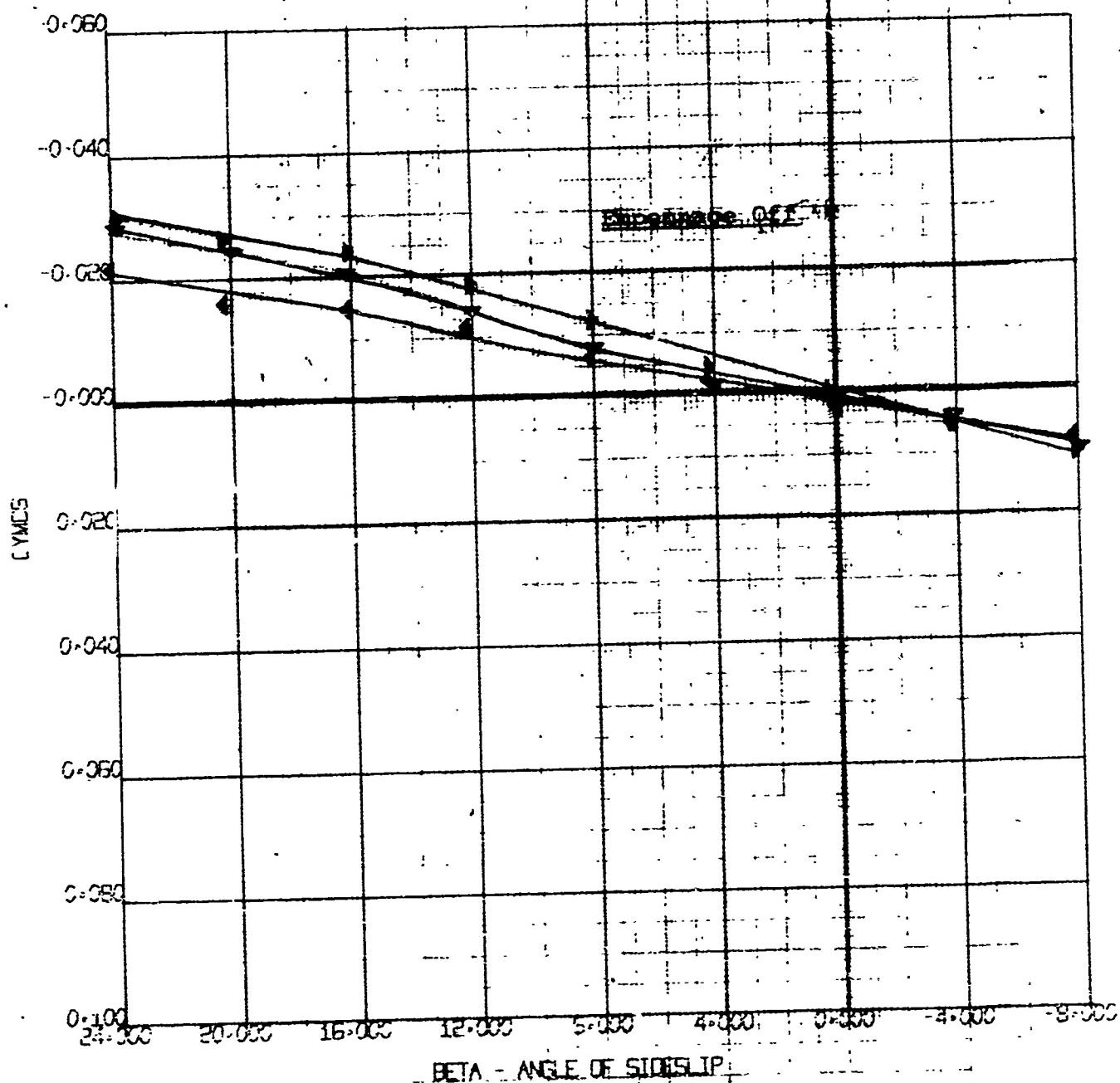


FOUR-PROPELLING TILT WING
 MODEL VROS60(FULL SPAN)
 BY CTS RS-BETA

BWWT
 67
 1/471

RUN	SYM	α	NOM C_{Ta}
98	+	13.5	.25
99	-	8.2	.50
100	0	4.7	.70

LATERAL/DIRECTIONAL STABILITY
 $\alpha = 15^\circ, \delta_F = 60^\circ$
FULL SPAN SLATS



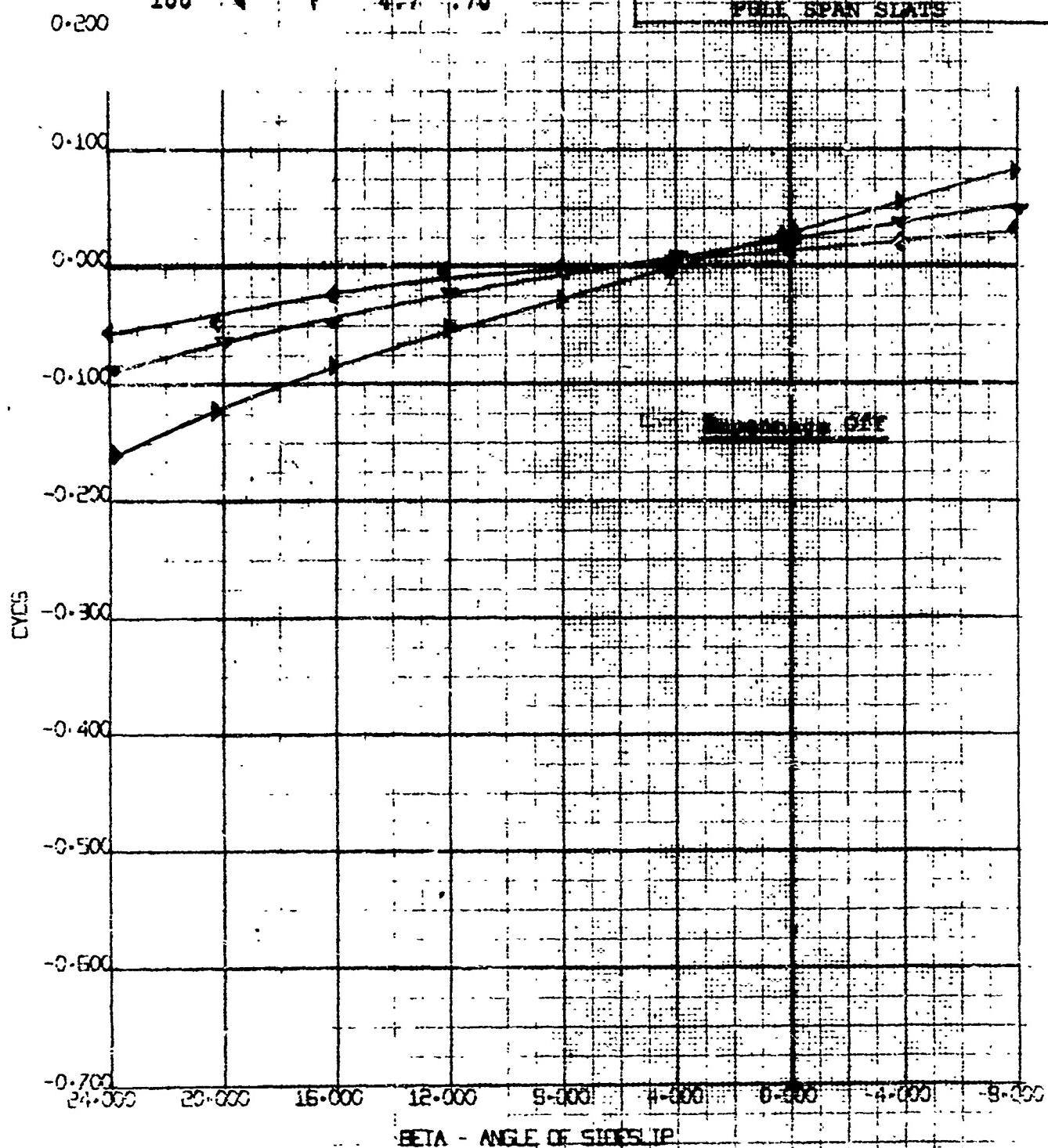
BETA - ANGLE OF SIDESLIP

FOUR-PROP TILT WING MODEL YR06BQ(FULL SPAN) CYDES VS. BETA	EWNT 67
	12/15/70

RUN	SYM	α	NOM	C_{T_s}
98	►	---	13.3	.25
99	▼	---	8.2	.50
100	↔	↓	4.7	.70

NUMBER D170-10039-1
REV. 1.DR. FIGURE 103

LATERAL/DIRIGEONAL STABILITY
LWING, $\delta_e = 30^\circ$
FULL SPAN SLATS



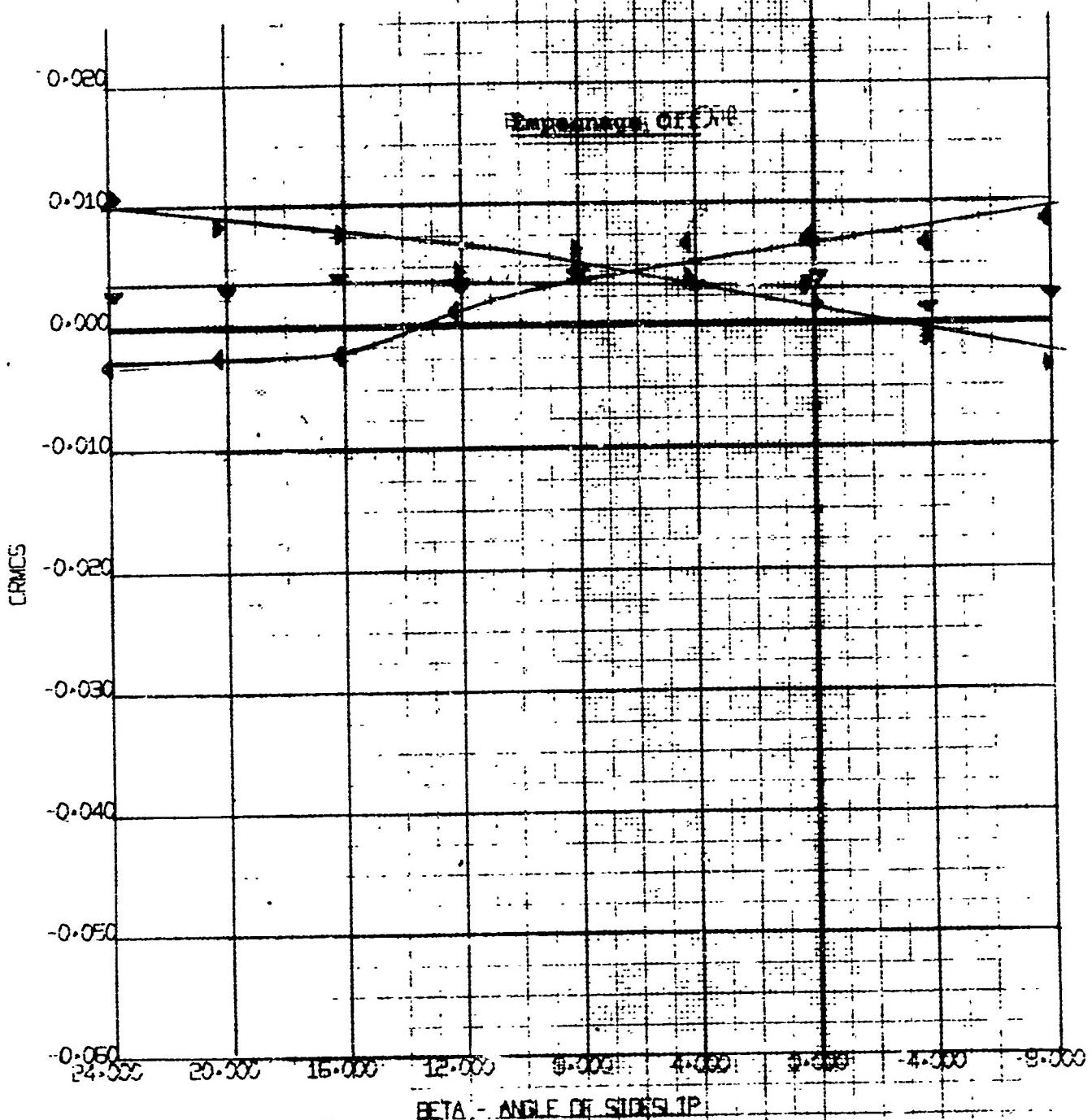
FOUR-PROP. TILT WING	EWNT
MODEL 140680 (FULL SPAN)	67
CYCS VS. BETA	12/15/70

RUN	SYM	a	NOM C _{Ts}
98	►	---	13.3 .25
99	▼	---	8.2 .50
100	◀	↓	4.7 .70

0.030

NUMBER D170+10039-1
REV. LIR. Figure 106

LATERAL/DIRECTIONAL STABILITY
 $\bar{L}_W = 15^\circ$, $\bar{\beta} = 60^\circ$
FULL SPAN PLATE

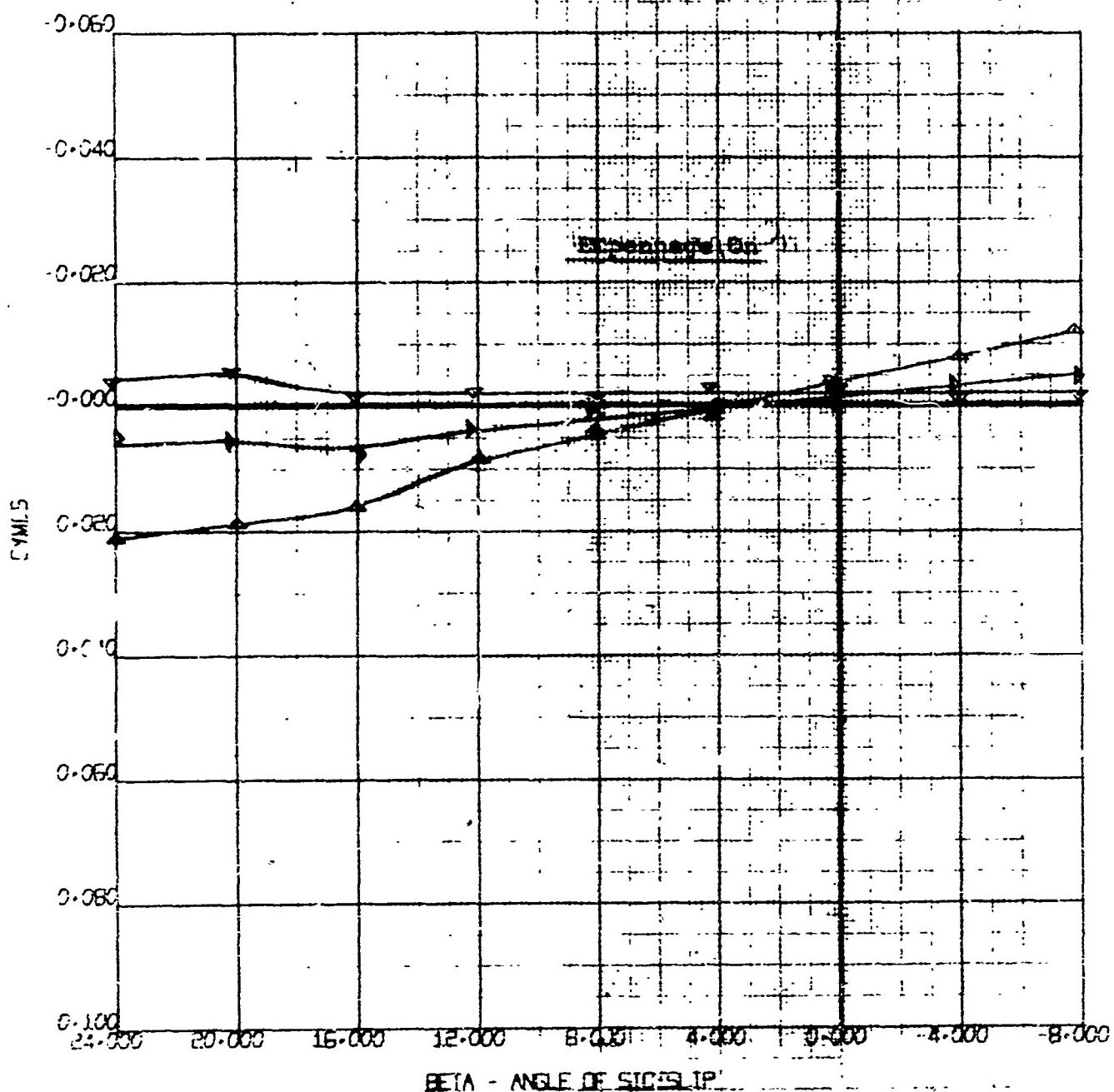


FLUR-PROP TILT WING MODEL YR06B0 (FULL SPAN)	BWWT 67
CRMCS VS. BETA	12/15/70

RUN	SYM	α	G	NON C _{T_S}
76	△	+10°	13.3	.25
77	▷		8.2	.50
78	▽		4.7	.70
C 080				

NUMBER D170-10039-1
REV. LUR. Figure 107

LATERAL/DIRECTIONAL STABILITY
 $i = 15^\circ$, $\delta_p = 60^\circ$
FULL SPAN SEATS

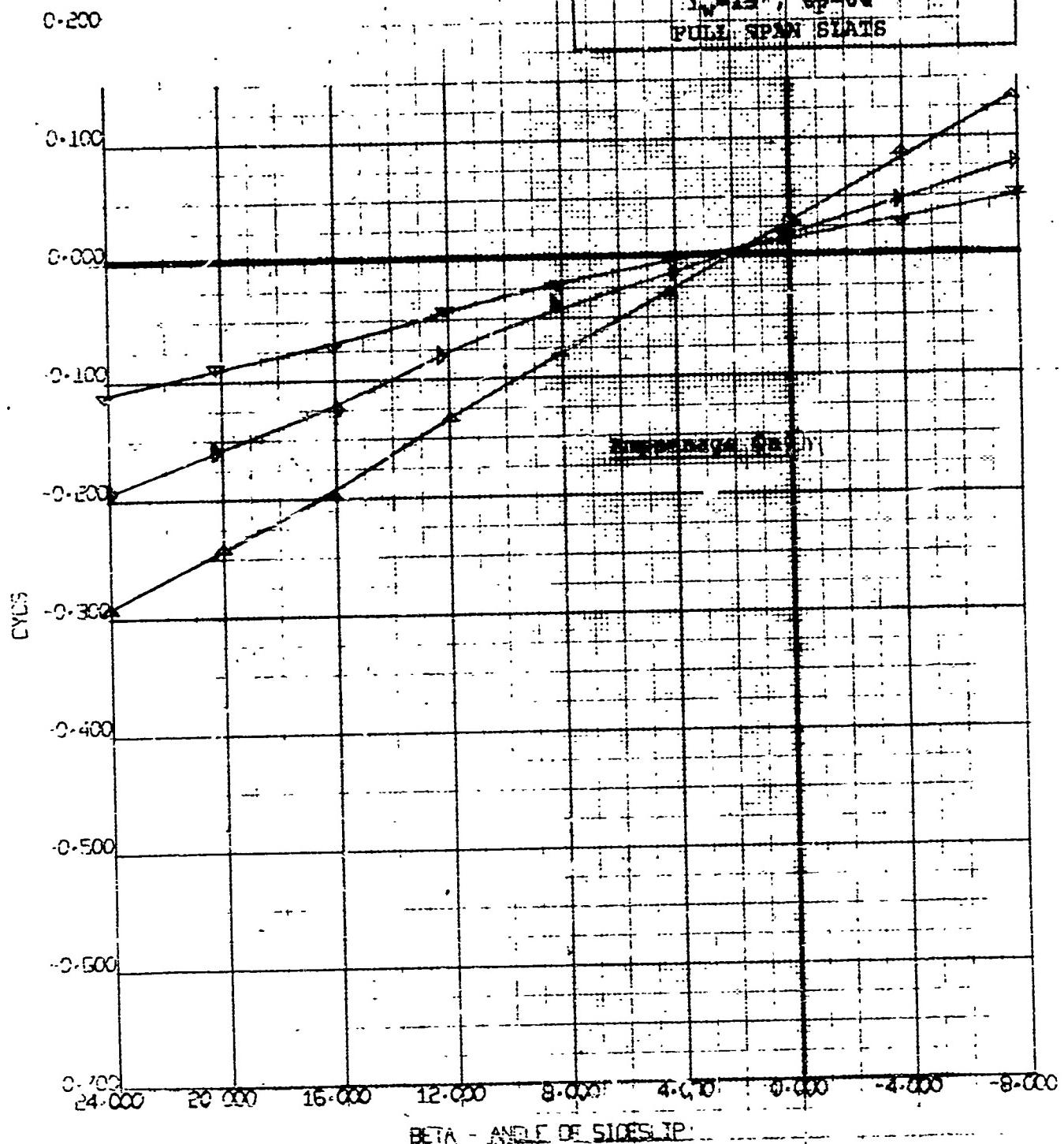


FOUR-PROP TILT WING MODEL YR080 (FULL SPAN) CYMCS VS. BETA	BWNT 67
	1/4/71

RUN	SYM	Δ	α	NOM C _{Ts}
76	△	+10°	13.3	.25
77	▷	-	18.2	.50
78	▽	-	4.7	.70

NUMBER D170-10839-1
REV. LTR. Figure 108

LATERAL/DERECTIONAL STABILITY
 $\alpha = 15^\circ$, $\delta_F = 60^\circ$
FULL SPAN SEATS

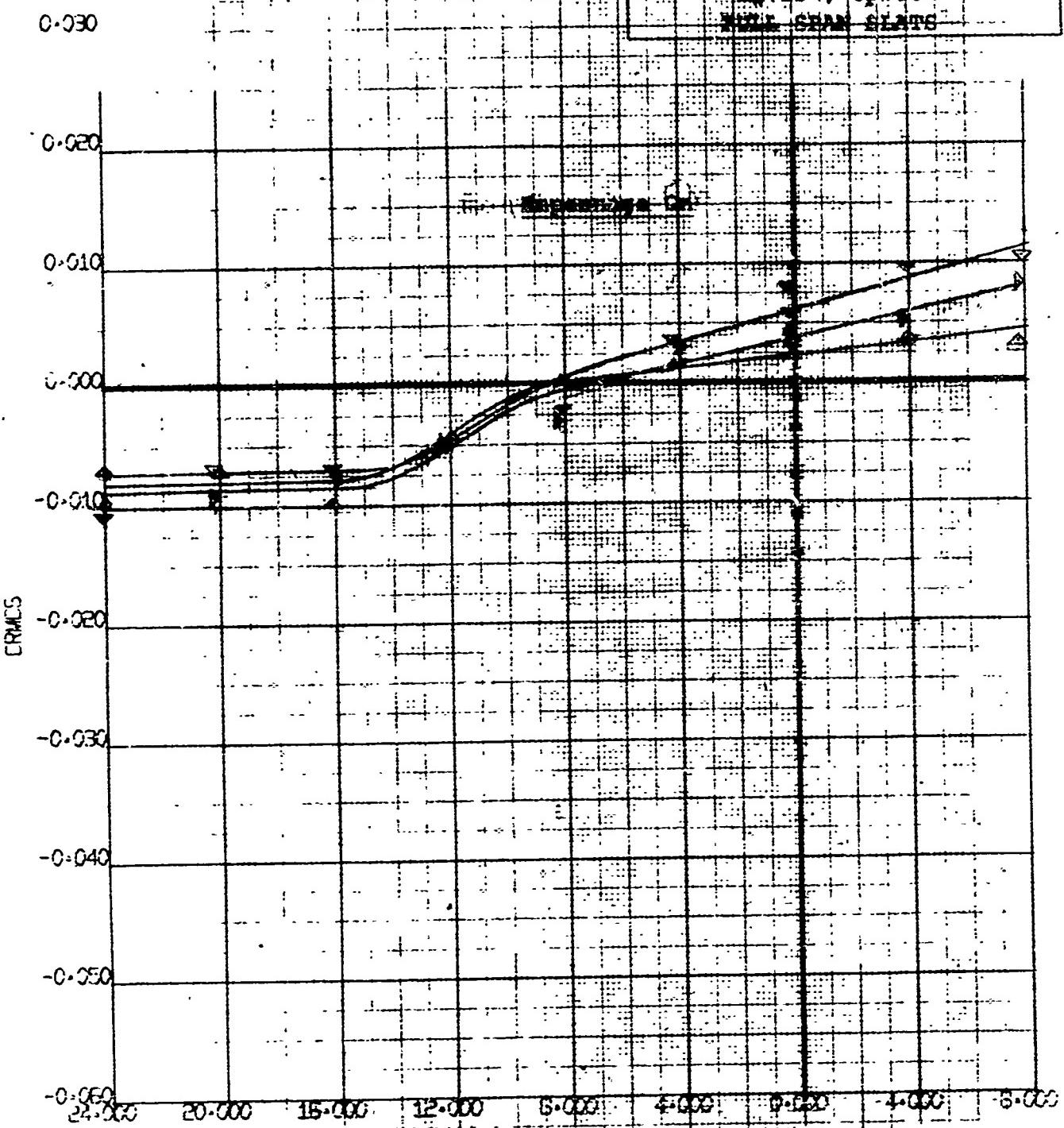


NOT REPRODUCIBLE

FOUR-PROP TILT WING
MODEL W/SEATS (FULL SPAN)
CYCLIC VS. BETA

BWHT 67
1/4/71

RUN	SYM	α	NOM C _{rs}	NUMBER	D170-10039-1
76	△	-1.0°	13.3	425	REV. LTR. Figure 109
77	□	-	8.42	.50	
78	▽	-	4.7	.70	



FOUR-PROP TILT WING	BWNT
MILIT VRC600(FULL SPAN)	67
CRMS VS. BETA	1/4/71

RUN	SYM	Δ	q	NOM C_{T_B}
87	►	15°	9.2	.55
88	▼		5.2	.70
89	↔		9.3	.81

NUMBER D170-10039-1
REV. LTR. Figure 110

0.050

-0.050

-0.040

-0.020

-0.000

0.020

0.040

0.060

0.080

LINES

LATERAL/DIRECTIONAL STABILITY

$\beta = 30^\circ$, $\delta_p = 40^\circ$

PULL SPAN SLATS

~~Experiments On~~

24.000 20.000 16.000 12.000 8.000 4.000 0.000 -4.000 -8.000

BET. - ANGLE OF SIDESLIP

FOUR-PROP TILT WING	
MODEL VR0660 (FULL SPAN)	
CYCLIC VS. BETA	

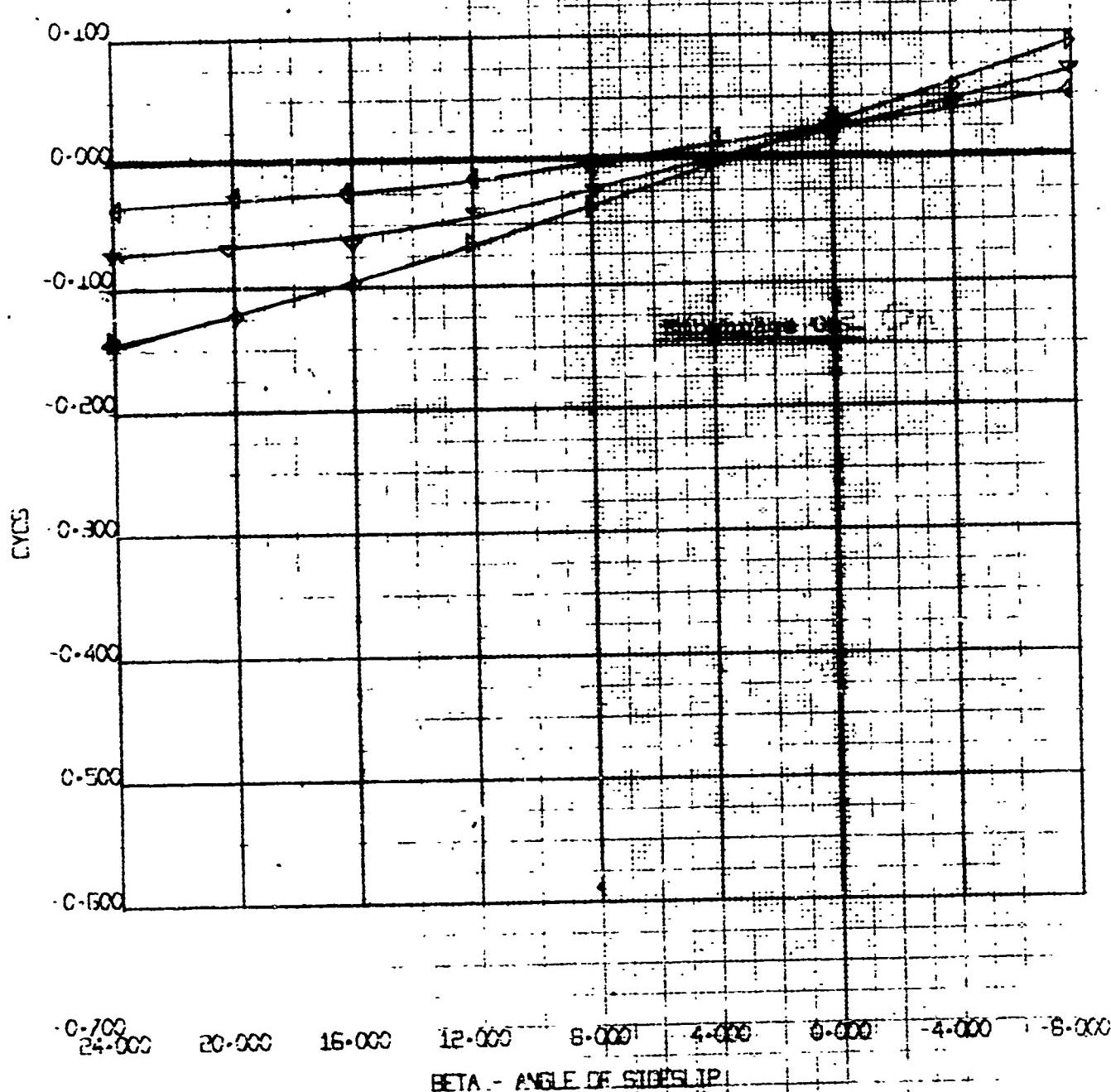
BWWT
67

12/15/70

NUMBER D1744-10039-1
REV. LTR. Figure 111

RUN	SYM	Δ	q	C_d^*	C_s
87	▲	15°	8.2	.55	
88	▼		5.2	.70	
0-200	89	◆	3.3	.81	

LATERAL/DIRECTIONAL STABILITY
 $\alpha = 30^\circ$, $\delta_E = 40^\circ$
FULL SPAN SLATS



NOT REPRODUCIBLE

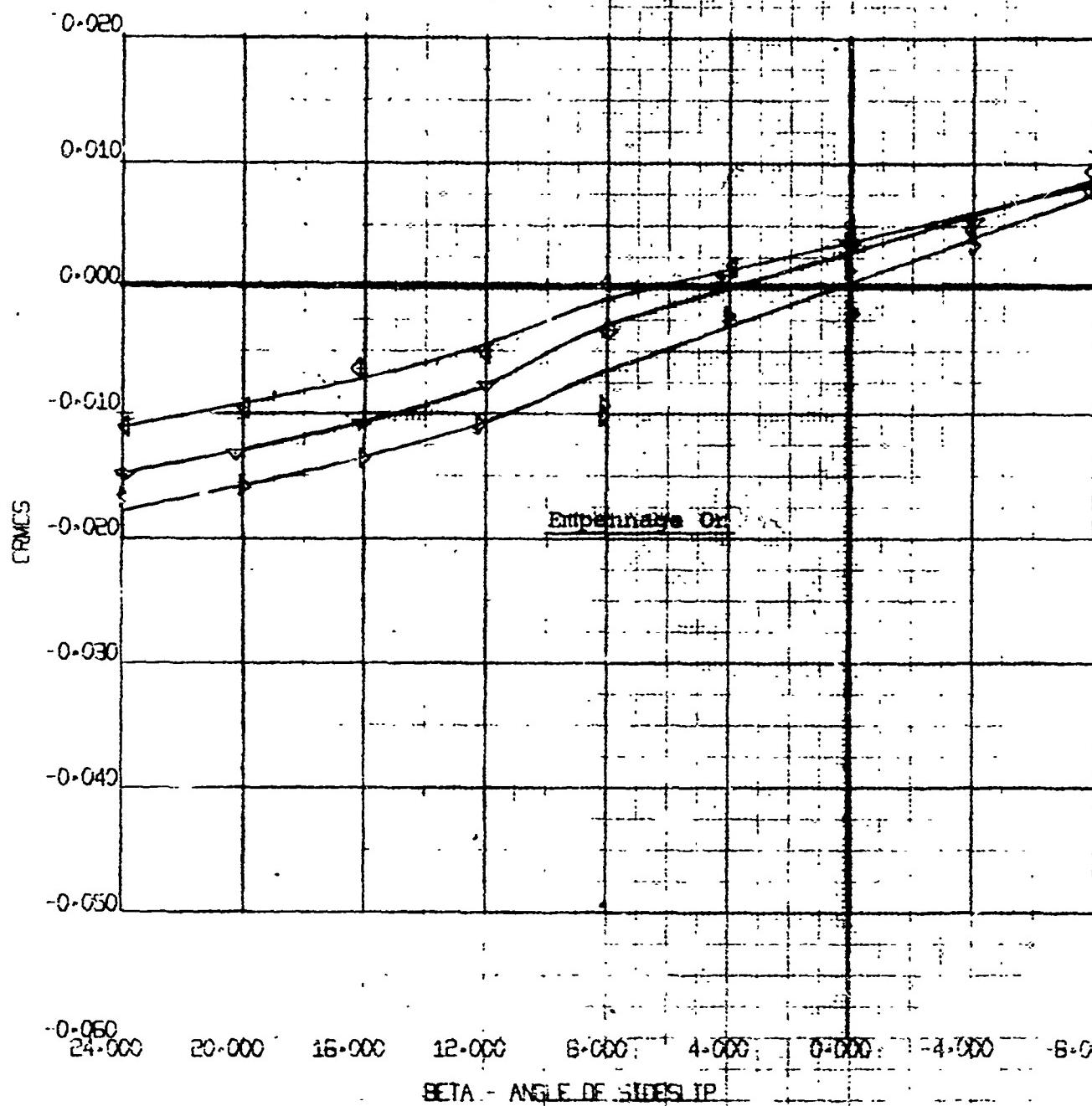
FOUR-PROP TILT WING	BVNT
MODEL VROEGEFULL SPAN	67
DVS VS. BETA	12/15/70

RUN	S:W	α	NOM	C _{TB}
87	►	15°	8.2	.55
88	▼	5.2	5.2	.70
89	▲	3.3	3.3	.81

0.030

NUMBER D170-10039-1
REV. LTR. Figure 112

LATERAL/DIRECTIONAL STABILITY
 $i_w = 30^\circ$, $\delta_p = 40^\circ$
FULL SPAN SLATS



FOUR-PROP. LIFTING WING	BVWT 67
MODEL VRO580(FULL SPAN)	
CMES VS. BETA	12/15/70

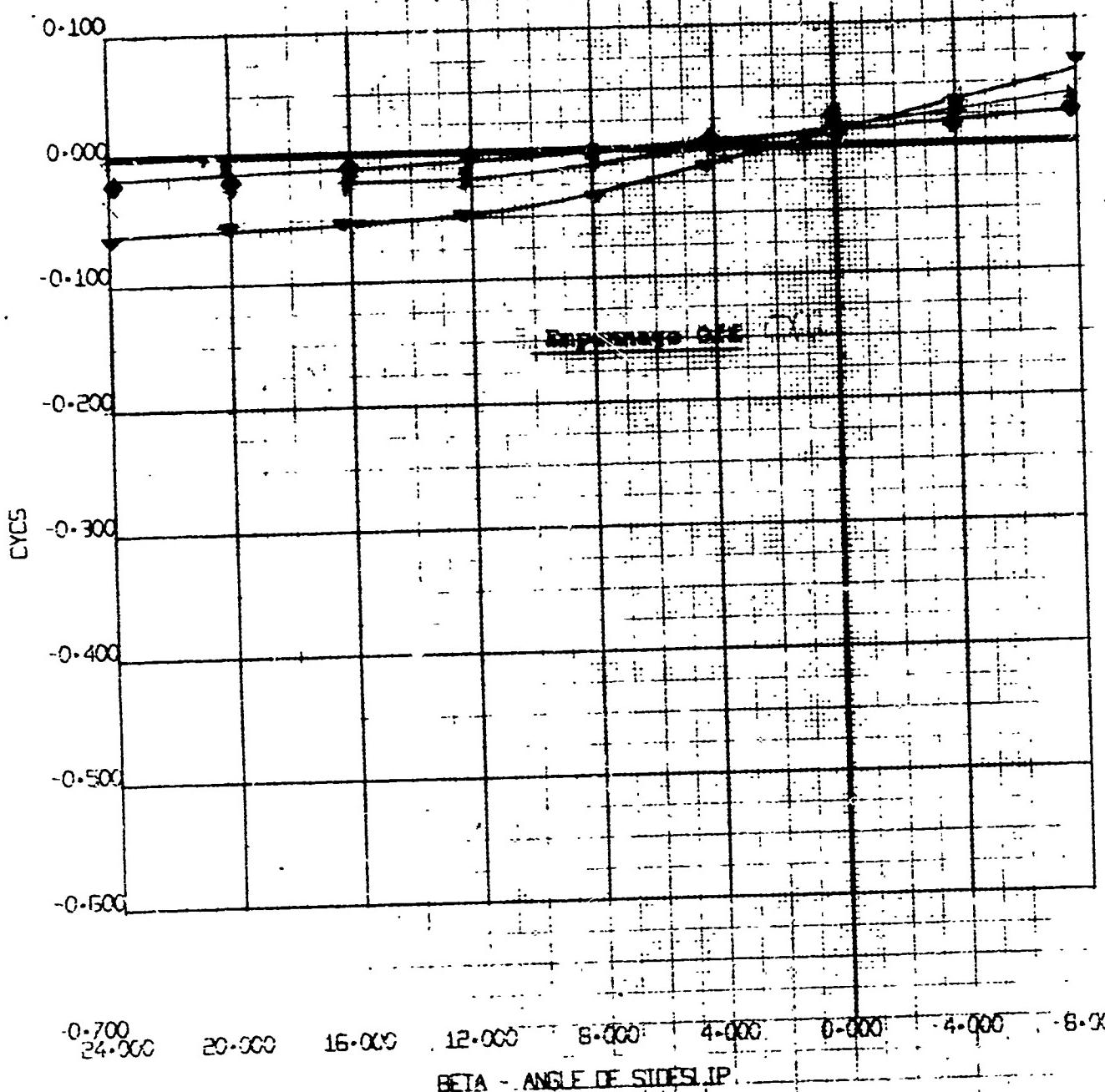
**THIS
PAGE
IS
MISSING
IN
ORIGINAL
DOCUMENT**

NUMBER D170-16099-1
REV. LTR. Figure 114

RUN	SYM	$\frac{q}{C_{T_0}}$	NOM
101	▼	8.2	.55
102	►	4.7	.70
103	◆	3.3	.81

0.200

LATERAL WIND TORSION TEST DATA
INCLINE, $\delta_T = 60^\circ$
FIELD SPAN SLATE



NOT REPRODUCIBLE

EQU-PROP TILT WING
MODEL VRO680(FULL SPAN)
CYCS VS. BETA

BWWT
67
12/14/70

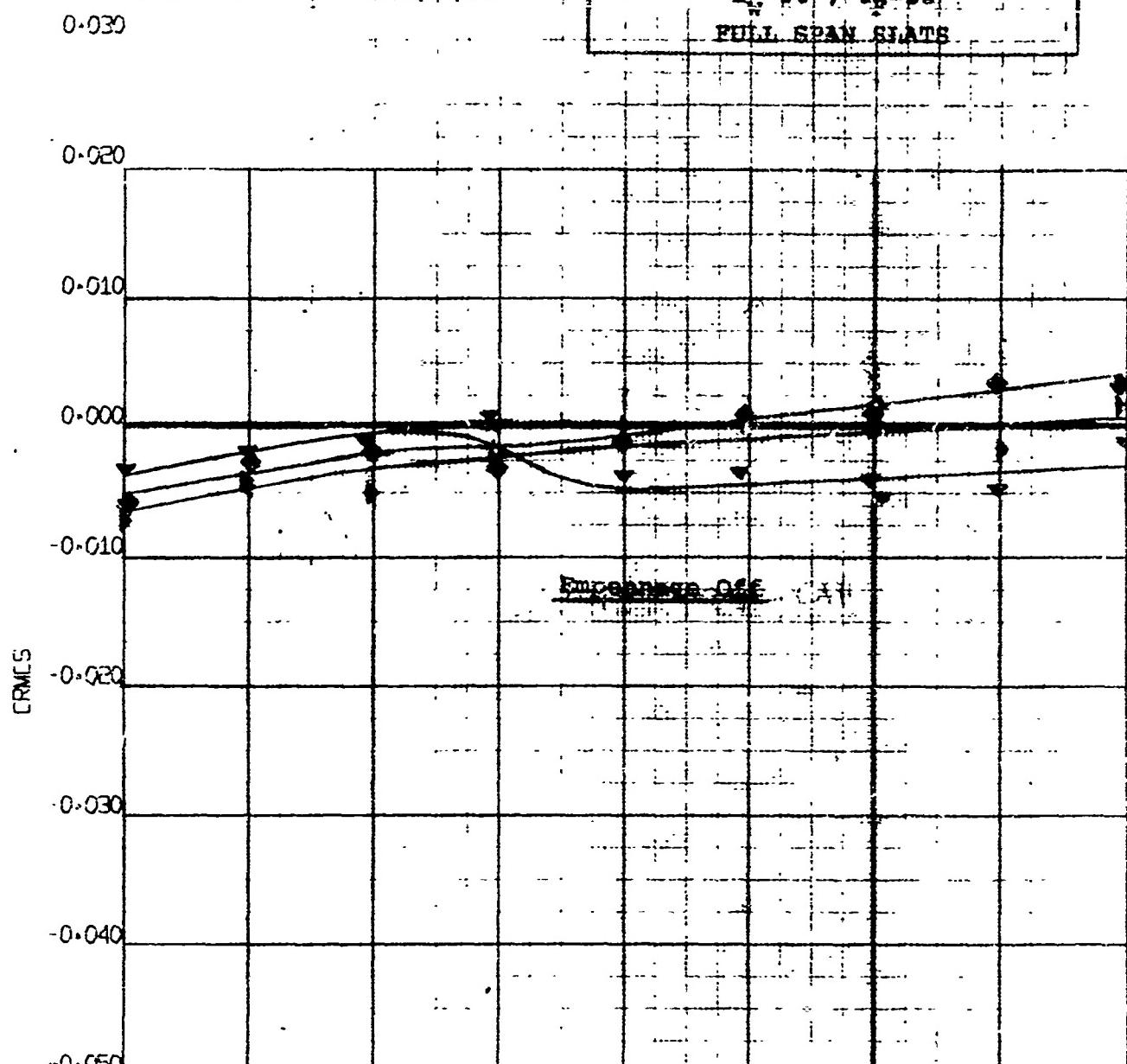
RUN	SYM	α	q	NOM CTS
101	▼	---	8.2	.55
102	►	↓	4.7	.70
103	◆	↓	8.3	.81

NUMBER D170-10039-1
REV. LR. Figure 115.

LATERAL/DIRECTIONAL STABILITY

$\alpha = 30^\circ$, $\delta_p = 0^\circ$

FULL SPAN SLATS



0.060
24.000 20.000 16.000 12.000 8.000 4.000 0.000 -4.000 -8.000

BETA - ANGLE DE SIDESLIP

FOUR-PROP TILT WING	
MODEL YROS8G(FULL SPAN)	
CRMCS VS. BETA	

BWNT	67
12/14/70	

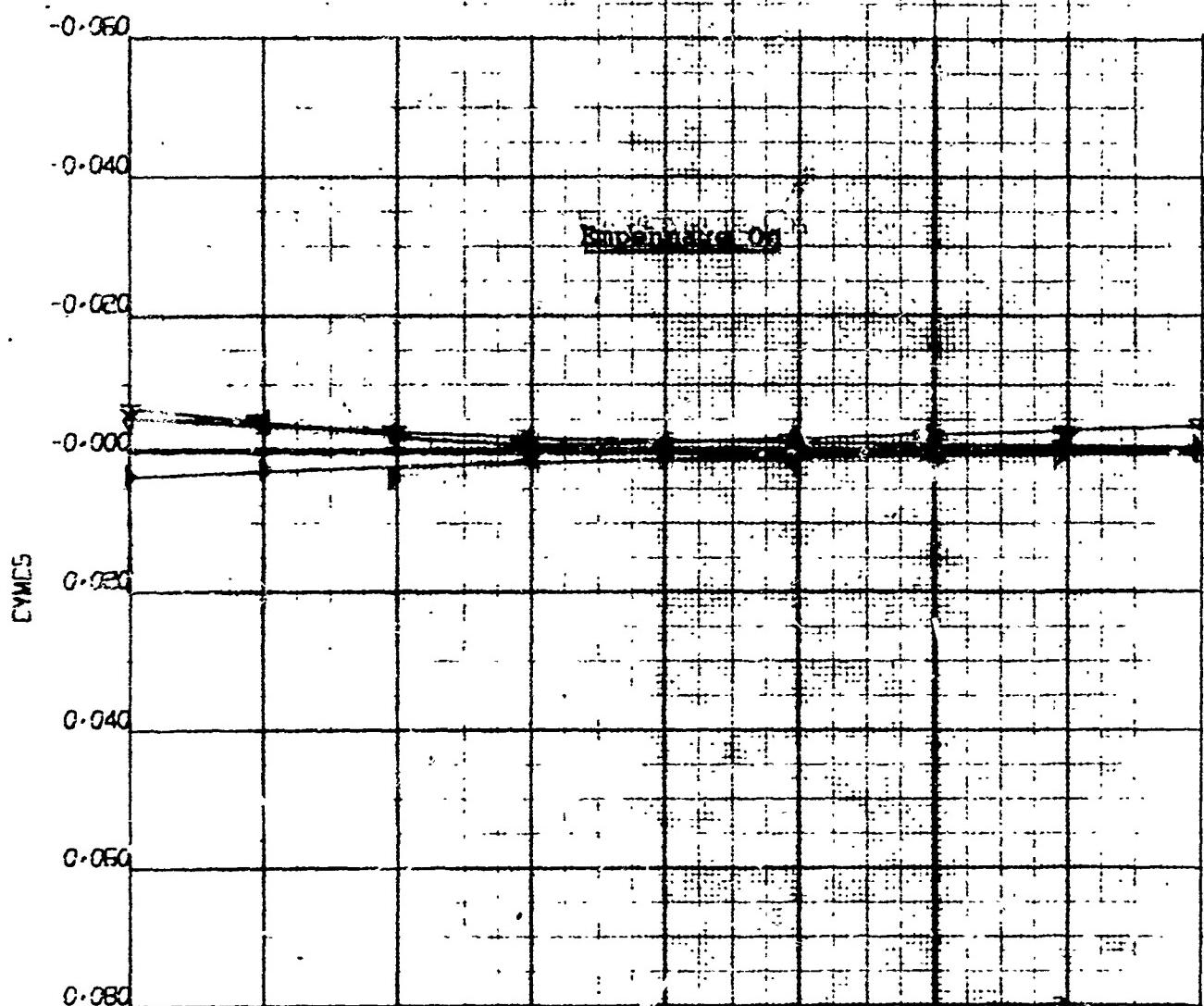
NUMBER D170-10039-1

Figure 116

RUN	SYM	Δ	15°	C_L	NOM
79	+			8.2	.55
80	-			4.7	.70
81	-			3.3	.81

0.060

LATERAL/DIRCTIONAL STABILITY
 $\alpha = 30^\circ$, $\delta_{P,W} = 0^\circ$
 FULL SPAN-SLATs



0.100
 24.000 20.000 16.000 12.000 8.000 4.000 0.000 -4.000 -8.000

BETA - ANGLE OF SIDE SLP

FOUR-PROP TILT WING	BWWT
MODEL YR06B0 (FULL SPAN)	67
CYMCS VS. BETA	1/ 4/71

RUN	SYM	δ	a	NOM C _m /s
79	▷	15°	3.2	.55
80	▽		4.7	.70
81	△		3.3	.81

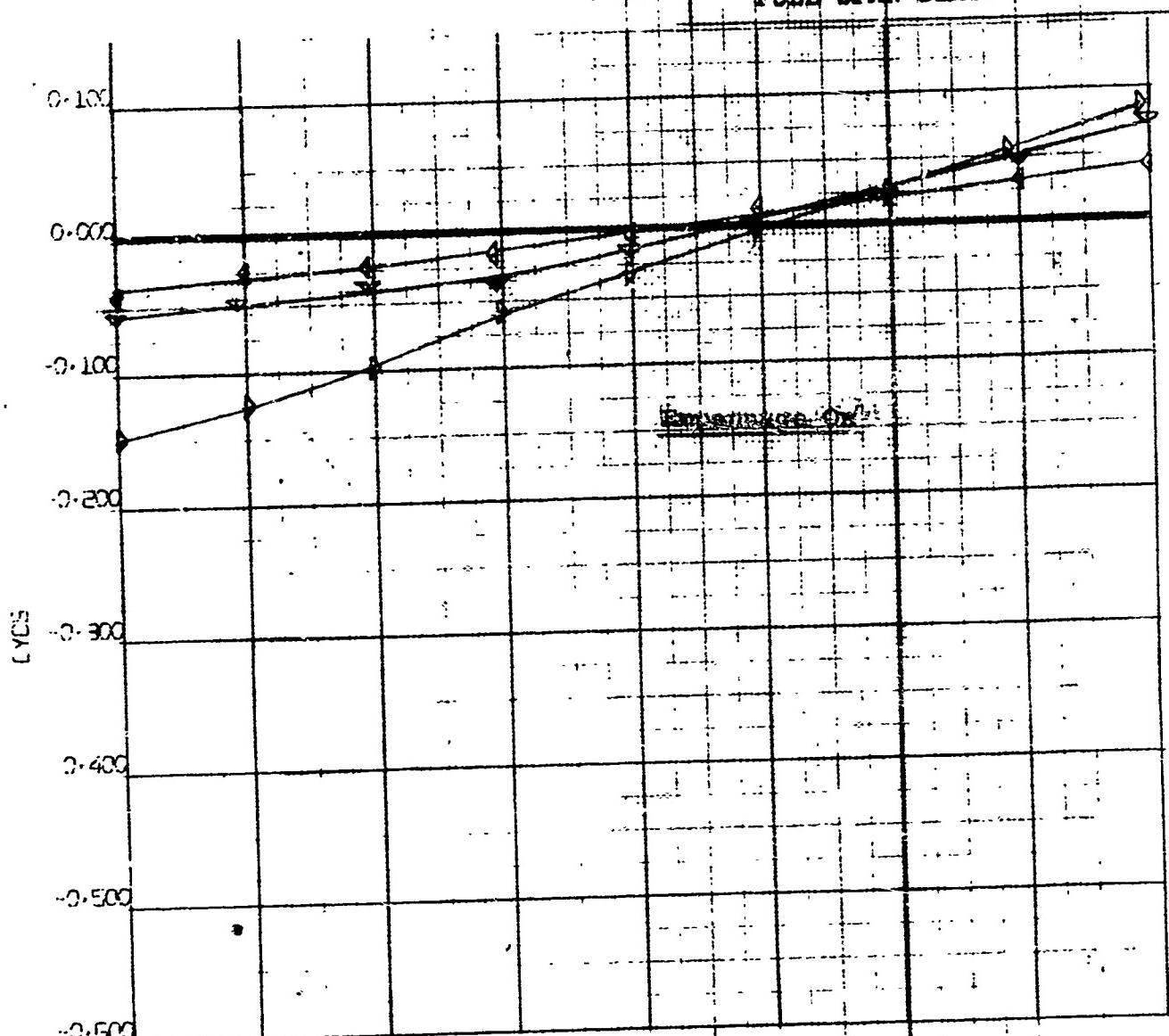
NUMBER D170-10039-1
REV. LTR. Figure 117.

0-200

LATERAL DIRECTIONAL STABILITY

$i_0 = 30^\circ$, $\delta_F = 60^\circ$

FULL SPAN SEATS



0.700 20.000 15.000 12.000 5.000 4.000 3.000 -4.000 -9.000
24.000 23.000 16.000 11.000 6.000 5.000 4.000 -5.000 -10.000

BETA - ANGLE OF SIDESLIP

NOT REPRODUCIBLE

FOUR-PROP TILT WING MODEL VRO680 (FULL SPAN) CYCS VS. BETA	BNNT 57 1/4,71
--	----------------------

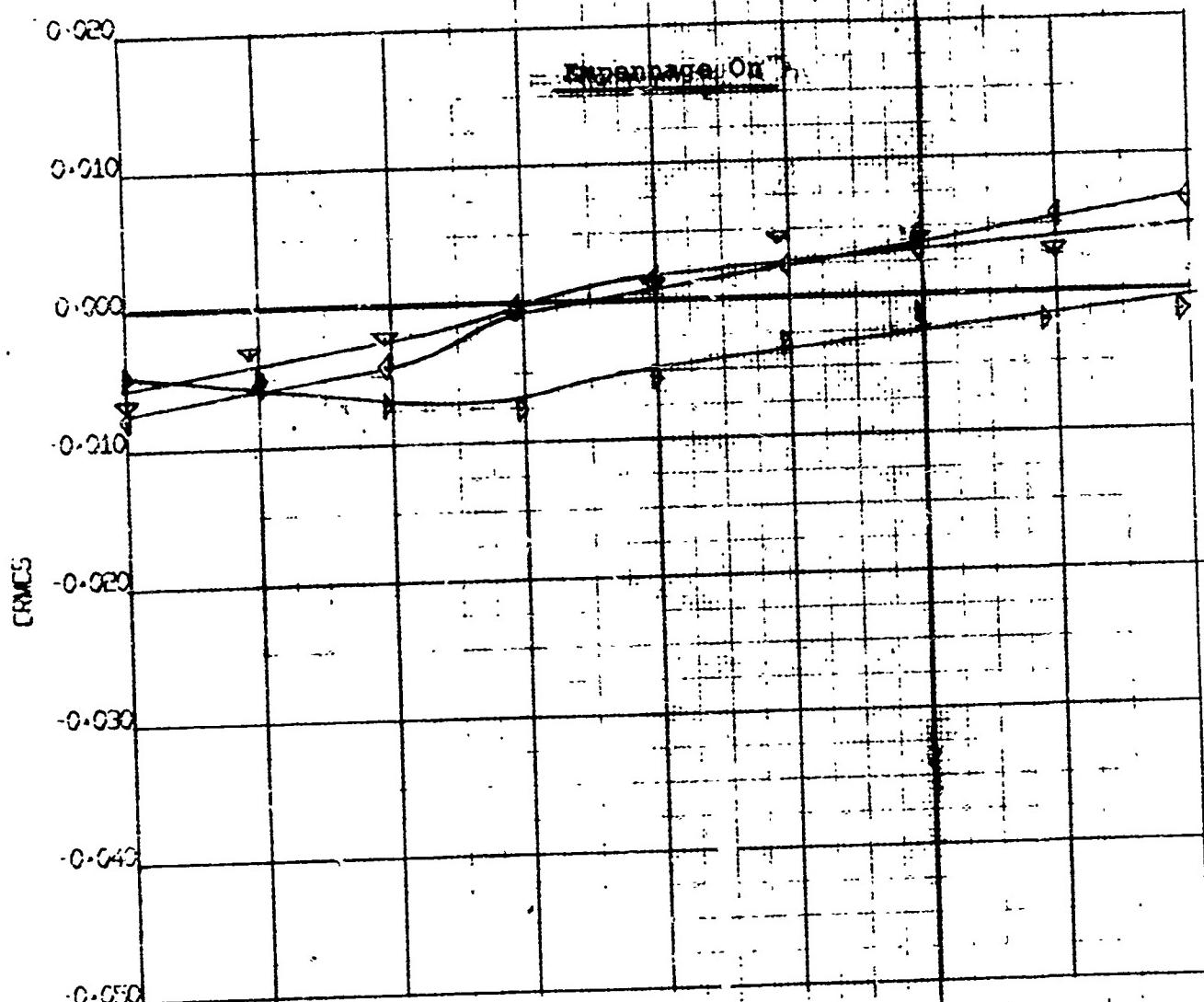
NAAER D170-10039-1

REV. LTR. Figure 118

RUN	SYM	Δ	α	NOM C_{T_B}
79	▲	15°	8.2	.55
80	▼		4.7	.70
81	△		3.3	.81

LATERAL/DIRECTIONAL STABILITY
 $\delta_w = 30^\circ$, $\delta_p = 50^\circ$
 FULL SPAN SLATS

C-330



-0.060 -0.050 -0.040 -0.030 -0.020 -0.010 0.000 0.010 0.020

BETA = ANGLE DE SIDRE IP

FOUR-PROP IIT WING
 MODEL VRC680 (FULL SPAN)
 CRMCS VS. BETA

BWWT
67
1/471

RUN	SYM	Δ	q	NOM C_{Ts}
104	▼	25°	3.3	.81
105	◆	↓	1.3	.92

NUMBER D170-10039-1
REV. LTR. Figure 119

LATERAL/DIRECTIONAL STABILITY
 $\alpha = 45^\circ$, $\delta_f = 60^\circ$
FULL SPAN SLATS

-0.050

-0.050

-0.040

CYMC5

Empennage Off

-0.020

-0.000

-0.020

0.000

0.020

0.040

0.060

0.080

0.100

24.000 20.000 16.000 12.000 8.000 4.000 0.000 4.000 8.000

BETA - ANGLE DE SIDESLIP

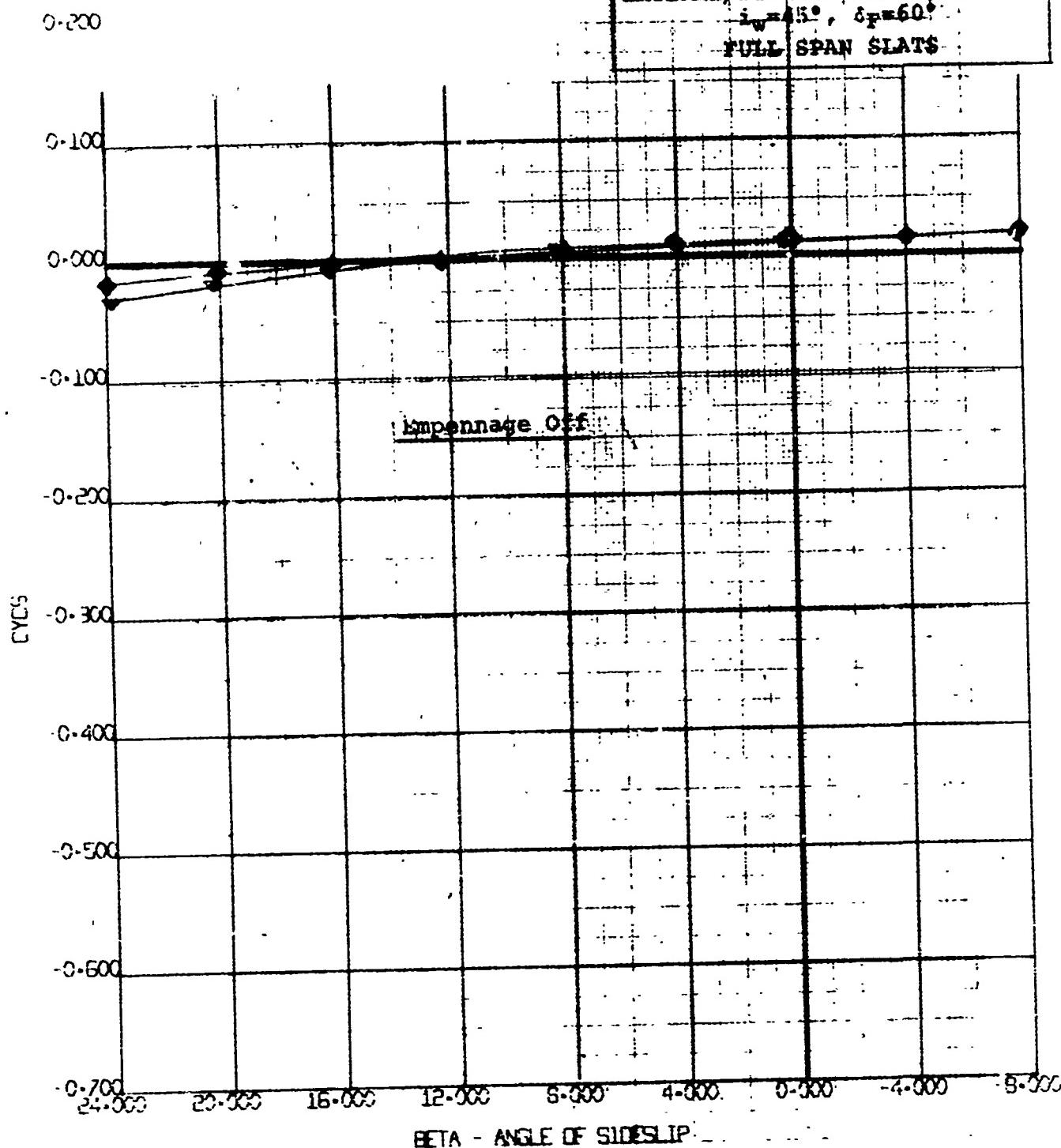
FOUR-PROP TILT WING MODEL VROGBQ(FULL SPAN) CYMC5 VS. BETA	BNWT 6° 12/15/70
--	------------------------

SHEET 184

RUN	SVM	Δ	α	NOM C_{Ts}
104	▼	25°	3.3	.81
105	◆	↓	1.3	.92

NUMBER D170-10039-1
REV. LTR. Figure 120

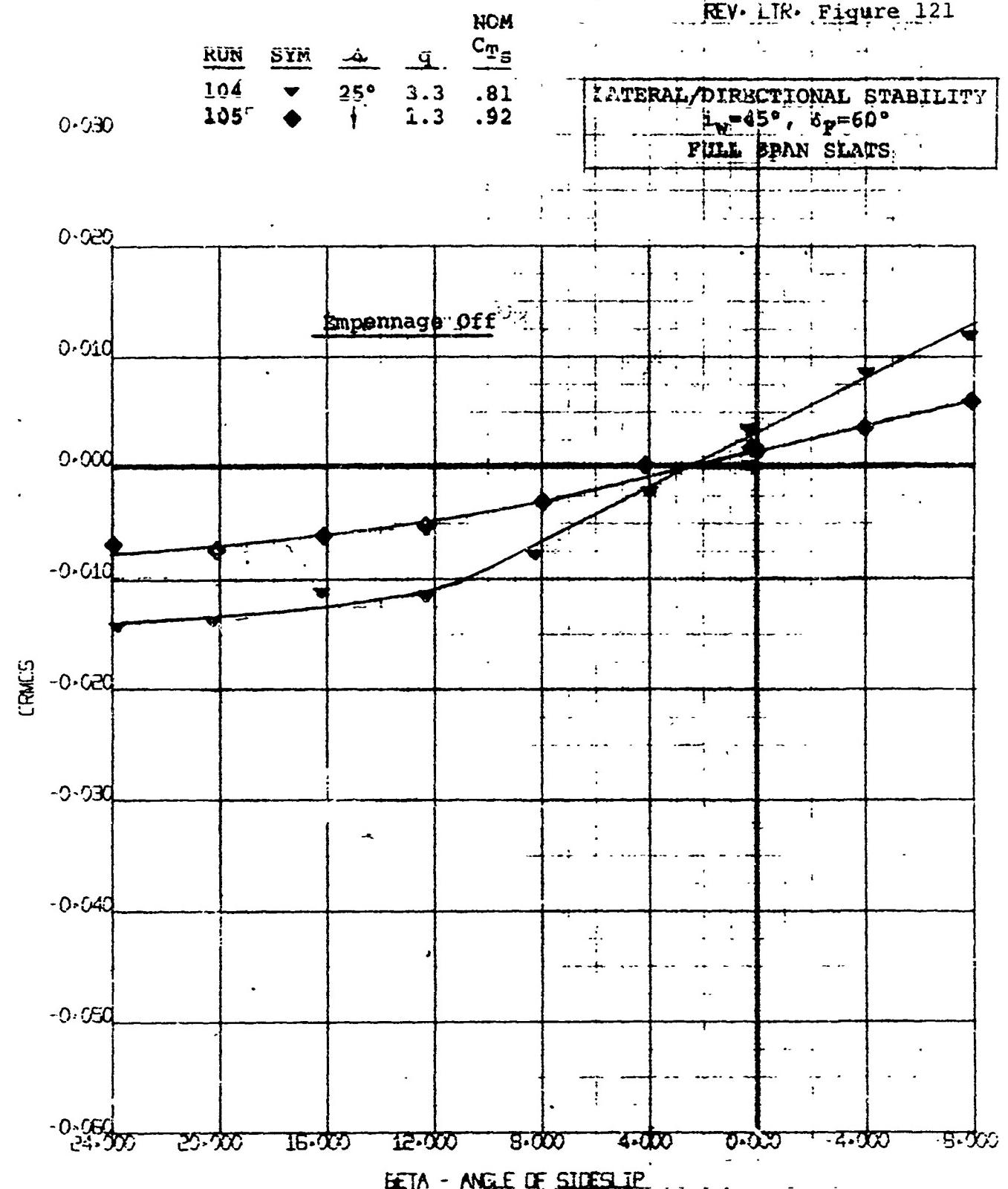
LATERAL/DIRECTIONAL STABILITY
 $i_w = 45^\circ$, $\delta_F = 60^\circ$
 FULL SPAN SLATS



NOT REPRODUCIBLE

FOUR-PROP TILT WING MODEL VRO680 (FULL SPAN) CYCS VS. BETA	BWWT 67
--	------------

12/15/70



FOUR-PROP TILT WING	BVWT 67
MODEL YR080(FULL SPAN)	
DRAGS VS. BETA	12/15/70

RUN	SYM	Δ	a	NOM C_{T_s}
82	▷	25°	3.3	.81
83	▽	↓	1.3	.93

NUMBER

REV. LTR.

D170-10039-1

Figure 122

LATERAL/DIRECTIONAL STABILITY

 $i = 45^\circ$, $s_f = 64^\circ$

FULL SPAN SLATS

-0.050

-0.060

-0.040

0.020

-0.000

0.020

0.040

0.060

0.080

Empennage On

CYMCS

C.100 20.000 16.000 12.000 8.000 4.000 0.000 -4.000 -8.000

BETA - ANGLE OF SIDESLIP

NOT REPRODUCIBLE

FOUR-PIR PIVOT TILT WING
MODEL VRCB9 (FULL SPAN)
CYMCS VS. BETA

BVHT

6"

12/14/70

RUN	SYM	δ	q	NOM C_{r_s}
82	▷	25°	3.3	.81
83	▽	↓	1.3	.92

NUMBER D170-10039-1
REV. LTR. Figure 123

LATERAL/DIRECTIONAL STABILITY
LW=45°, DF=60°
FULL SPAN SLATS

0.200

0.100

0.000

-0.100

-0.200

-0.300

-0.400

-0.500

-0.600

-0.700

24.000

20.000

16.000

12.000

8.000

4.000

0.000

-4.000

-8.000

BETA - ANGLE OF SIDESLIP.

SHEET 188

FOUR-PROP TILT WING MODEL VROGBO(FULL SPAN) CYCS. VS. BETA	BVNT 67 12/14/70
--	------------------------

RUN	SYM	Δ	q	NOM C_{Tg}
82	▼	25°	3.3	.81
83	▼	†	1.3	.92

NUMBER DL70-10039-1
REV. LTR-Figure 124

LATERAL/DIRCTIONAL STABILITY
 $\alpha_w = 15^\circ$, $\delta_F = 60^\circ$
 FULL SPAN SLATS

0.030

0.020

0.010

0.000

-0.010

-0.020

-0.030

-0.040

-0.050

Empennage On

CRMCS

-0.050 -24.000 -20.000 -16.000 -12.000 -8.000 -4.000 0.000 4.000 8.000

BETA - ANGLE DE SIDESLIP

NOT REPRODUCIBLE

PAIR-PROP TILT WING	BVNT 67
MODEL VROSBOUEILLE SPAN	
CRMCS VS. BETA	12/14/70

RUN SYM α q NOM
 84 D 35° 1.16 CTs

NUMBER D170-10039-1
 REV. LTR. Figure 125

LATERAL/DIRECTIONAL STABILITY
 $i_w = 55^\circ$, $\delta_p = 60^\circ$
FULL SPAN SLATS

0.050

-0.050

0.040

CYCLES

Empennage On

-0.020

0.000

0.020

0.040

0.060

0.080

0.100

22.000

20.000

18.000

16.000

14.000

12.000

10.000

8.000

6.000

BETA - ANGLE OF SIDESLIP

FOUR-PROP TILT WING
 MODEL VROS80 (FULL SPAN)
 CYCLES VS. BETA

BWK
 5°
 12/11/70

NOM
 RUN SYM Δ q C_{Ts}
 64 D 35° 1.16 .93

NUMBER D170-10039-1
 REV. LTR. Figure 126

DIRECTIONAL STABILITY
 $\alpha_v = 55^\circ, \delta_f = 60^\circ$
 FULL SPAN SLATS

0.200

0.100

0.000

-0.100

-0.200

-0.300

-0.400

-0.500

-0.600

-0.700

24.000

20.000

16.000

12.000

8.000

4.000

0.000

-4.000

-8.000

BETA - ANGLE DE SIDESLIP

NOT REPRODUCIBLE

FOUR-PROP TILT WING	BVNT 67
MODEL VRO6804111 SPAN	
CYCS VS. BETA	12/14/70

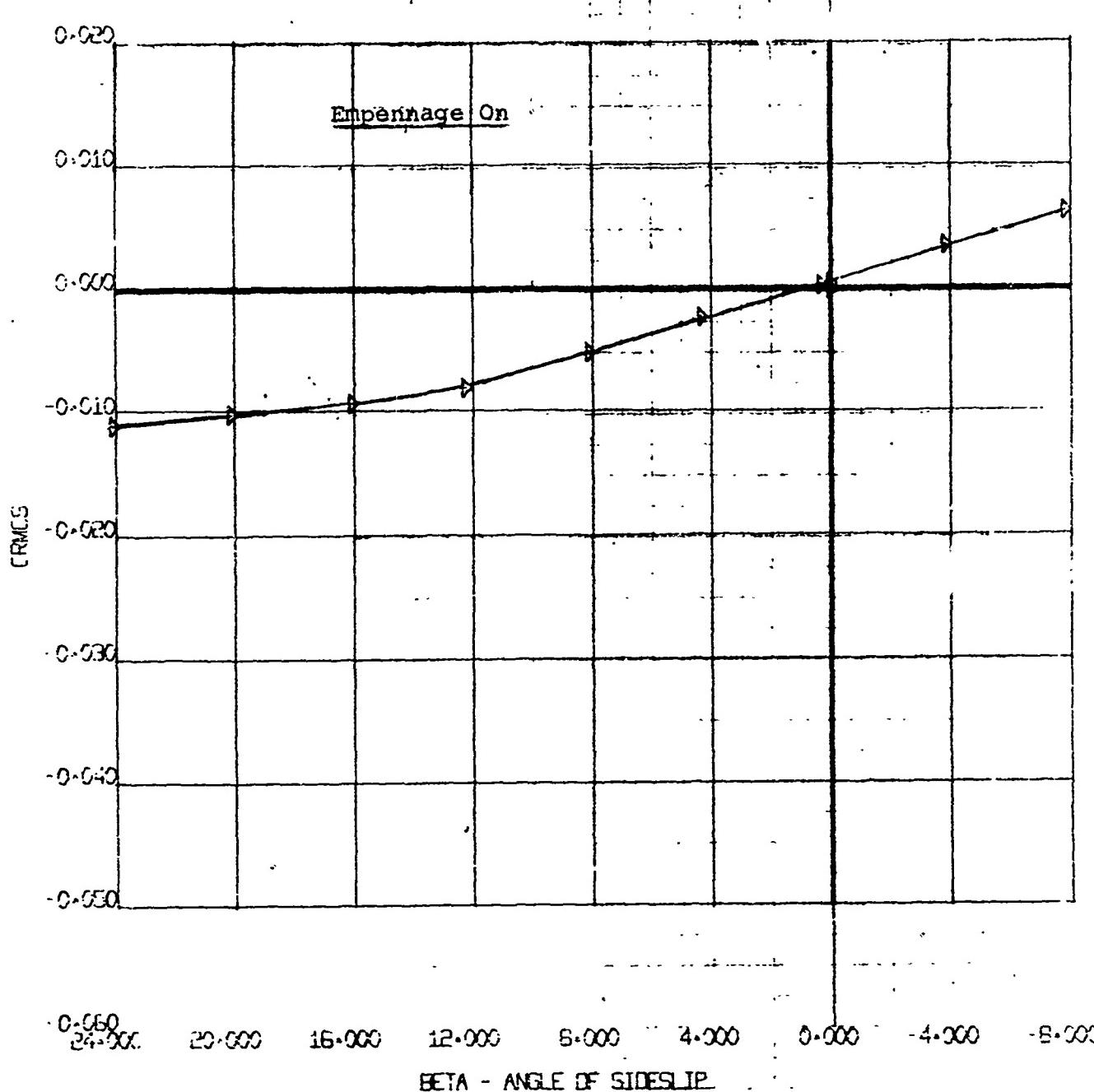
SHEET 191

RUN SYM α q NOM
84 D 35° 1.16 C_{T-S}

NUMBER D170-10039-1
REV. LTR. Figure 127

LATERAL/DIRECTIONAL STABILITY

$i_w = 55^\circ$, $\delta_F = 60^\circ$
FULL SPAN SLATS



FOUR-PROP TILT WING
MODEL VROB6Q(FULL SPAN)
CRMCS VS. BETA

BWNT 67
12/14/70

6.5.4 Effect of Horizontal Tail on Vertical Tail Effectiveness

The horizontal tail was mounted on top of the fin, as sketched in Figure 15, during the empennage-on lateral/directional stability testing. Stabilizer angles compatible with each wing tilt angle were selected, i.e., the stabilizer angle was manually set to a higher positive angle as the wing tilt angle was increased. Since this tail configuration should have added a substantial increment to the fin effectiveness, a check was made to ascertain the magnitude.

Figure 128 presents the results of this investigation. Compared in this figure are the lateral/directional stability characteristics of the model for the wing down and 40° of flap deflection case as measured with the horizontal on and off. This data shows that mounting the stabilizer on top of the vertical tail did provide some modest improvement in the yaw stabilizing capability of the fin at the low thrust coefficients where the vertical tail effectiveness should be a maximum. The magnitude of improvement is much less than the 25% anticipated, leading to the supposition that the fin's effectiveness was low for the runs with the horizontal tail off. This assumption is in agreement with Figure 97 and the comments made in Sections 6.5.2 and 6.5.3 pertaining to adverse flow conditions at the base of the fin emanating from the wing/body juncture. It would be expected with this type of flow problem which reduces the fin's effectiveness, that the span loading on the fin would be significantly altered over a major portion of the span. In this situation, endplating the fin with the horizontal tail should not produce the results that would normally occur.

The basic three component yaw data used in developing Figure 128 is presented in Figures 129 through 131. In these plots, the solid lines/open symbols represent the base runs with the horizontal tail installed and the dashed lines/solid symbols represent the runs with the horizontal tail removed.

NUMBER
REV LTR

D170-10039-1
Figure 128

BASIC LATERAL/DIRECTIONAL STABILITY
HORIZONTAL TAIL ON & OFF
 $i_w = 0$, $\delta_F = 40^\circ$

YAWING MOMENT

SYM

C 0°

Horizontal Tail On

$C_{n_s \beta}$

C_{T_s}

ROLLING MOMENT

$C_{l_s \beta}$

C_{T_s}

SIDE FORCE

$C_{Y_s \beta}$

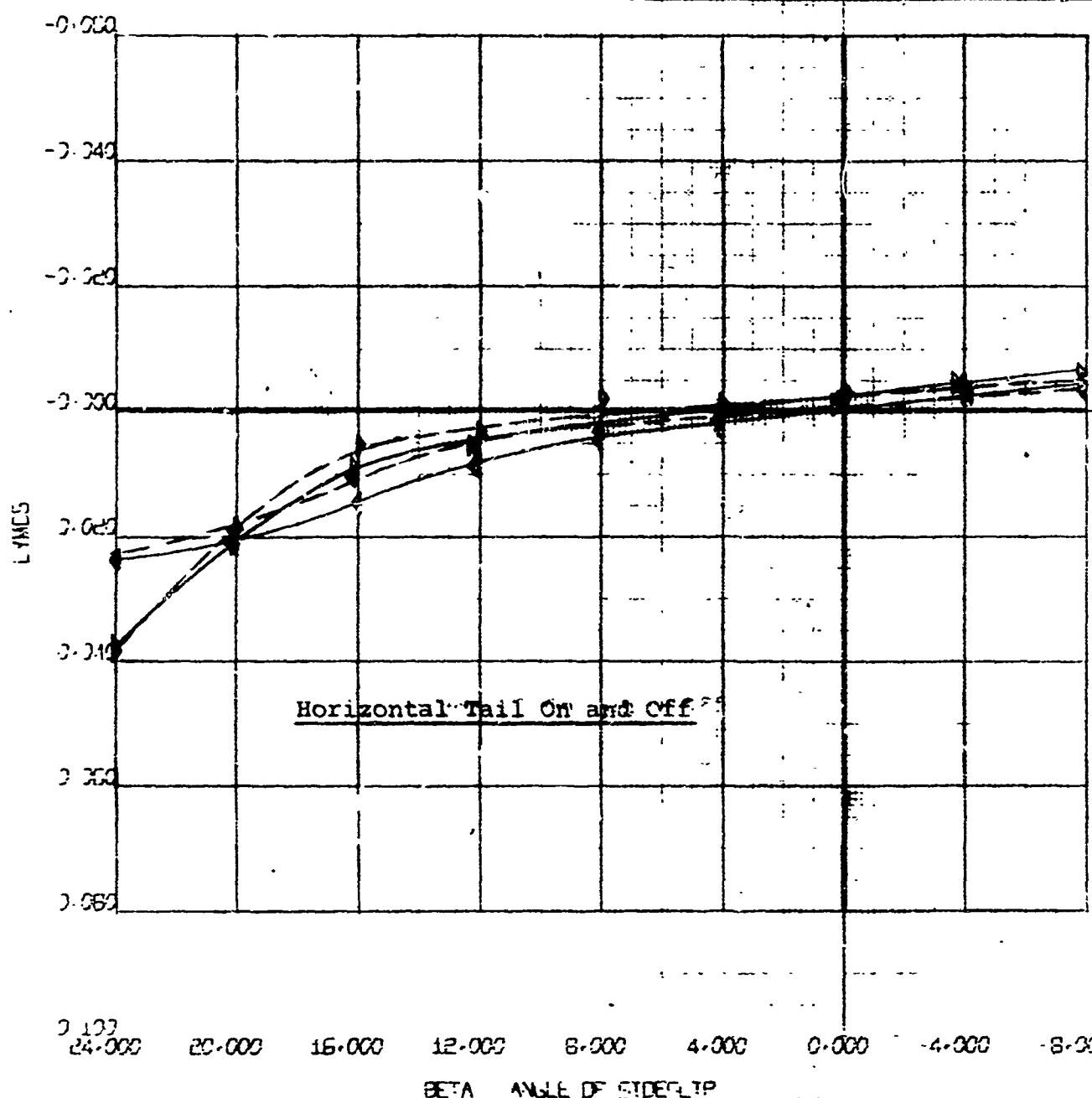
C_{T_s}

NOTES:

1. Model VRC68Q
2. Data from BVWT 067
3. Full Span Slats
4. Zero Fuselage Angle

RUN	SYM	q	C_{T_s}	Δ
85	▷	17.3	0	0°
86	△	13.3	.23	↓
90	◆	17.3	0	---
91	◆	13.3	.26	---

LATERAL/DIRECTIONAL STABILITY
 $i_w = 0^\circ$, $\delta_F = 40^\circ$
FULL-SPAN SLATS



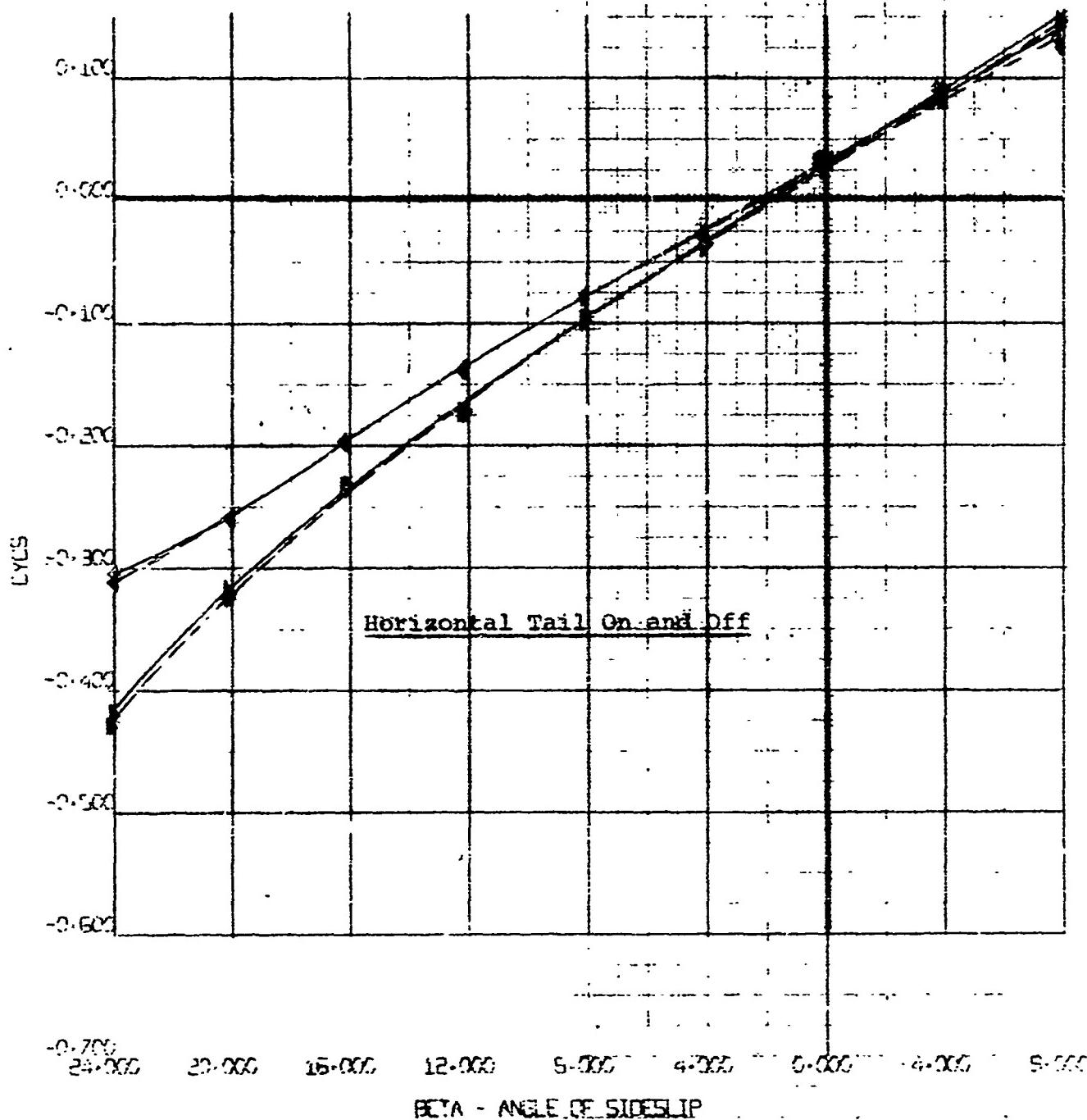
FOUR-PROP TILT WING
MODEL VR660 (FULL SPAN)
LYNCS VS. BETA

BWWT	67
1/17/1	

NUMBER D170-10039-1
REV. LTR. Figure 130

RUN	SYM	q	C_{Ts}	α
85	▷	17.3	0	0°
86	△	13.3	.20	1
90	●	17.3	0	---
91	◆	13.3	.20	---

LATERAL/DECELERATIONAL STABILITY
 $i_w = 0^\circ$, $\delta_F = 40^\circ$
—+— FULL SPAN SLATS



NOT REPRODUCIBLE

FOUR-PROF TILT WING
MODEL VROGIC (FULL SPAN)
CYCS VS. BETA

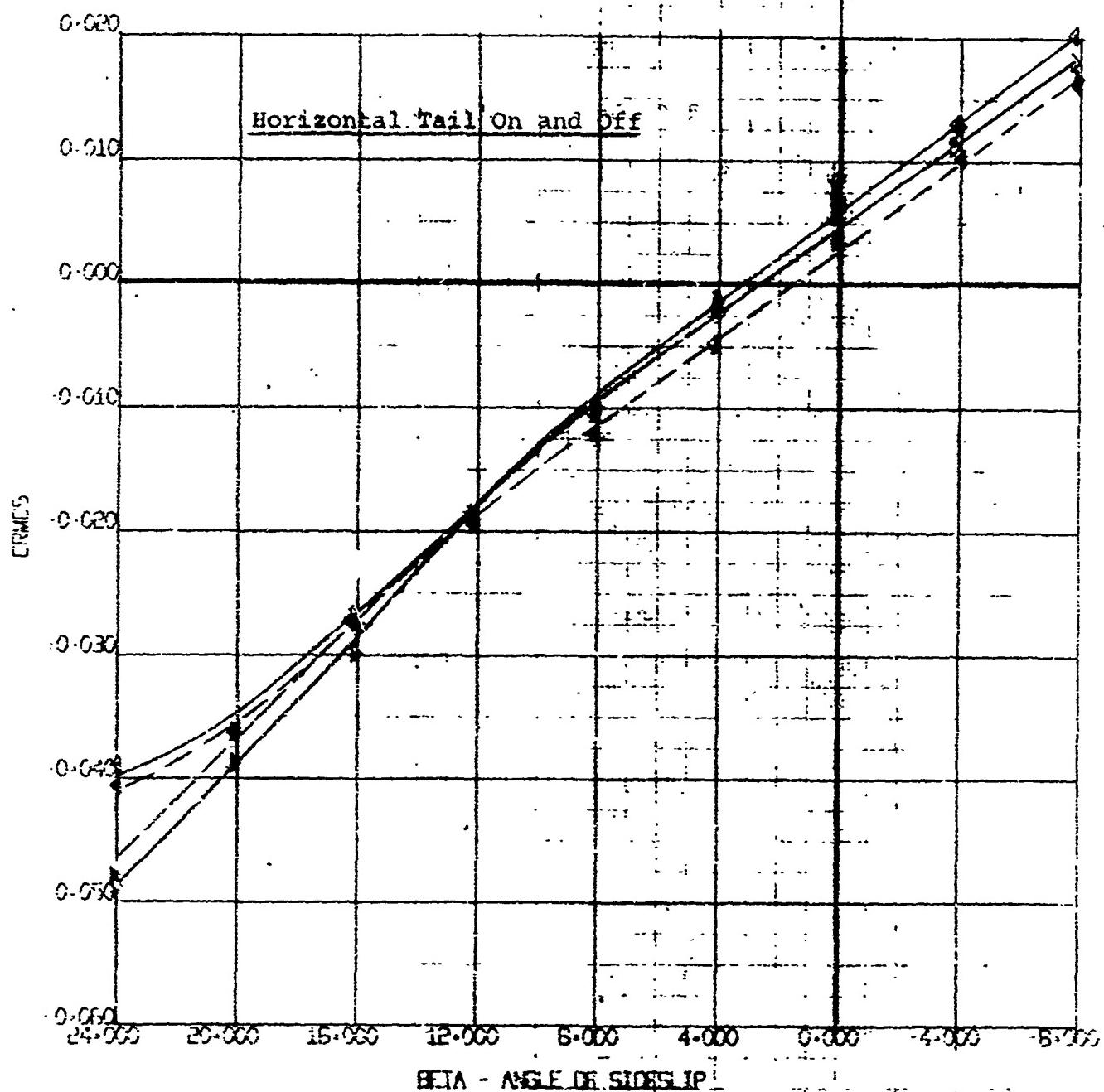
EWNT
5°
1/4/71

NUMBER D170-10039-1
REV. LTR. Figure 131

RUN	SVM	α	C_T	s	A
85	0	17.3	0	0°	
86	0	13.3	.20	↑	
90	0	17.3	0	---	
91	0	13.3	.20	---	

0.030

LATERAL/DIRECTIONAL STABILITY
 $i_w = 9^\circ$, $\delta_p = 40^\circ$
FULL SPAN SLATS



FOUR-PROP T-TAIL WING
MODEL VROS8Q(FULL SPAN)
C_Delta VS. BETA

BWNT
67

1/4/71

6.5.5 Effect of Cyclic Pitch on Lateral/Directional Stability

Following the investigation of basic lateral/directional stability characteristics, the effect of cyclic pitch on lateral/directional stability was examined at selected points in transition with 15°, 30° and 45° of wing tilt plus 60° of flap deflection. In Figure 132, the data acquired with the empennage on and at zero fuselage angle is presented in the slipstream derivative format. The zero cyclic fairings shown in Figure 132 are those previously shown in Figure 96.

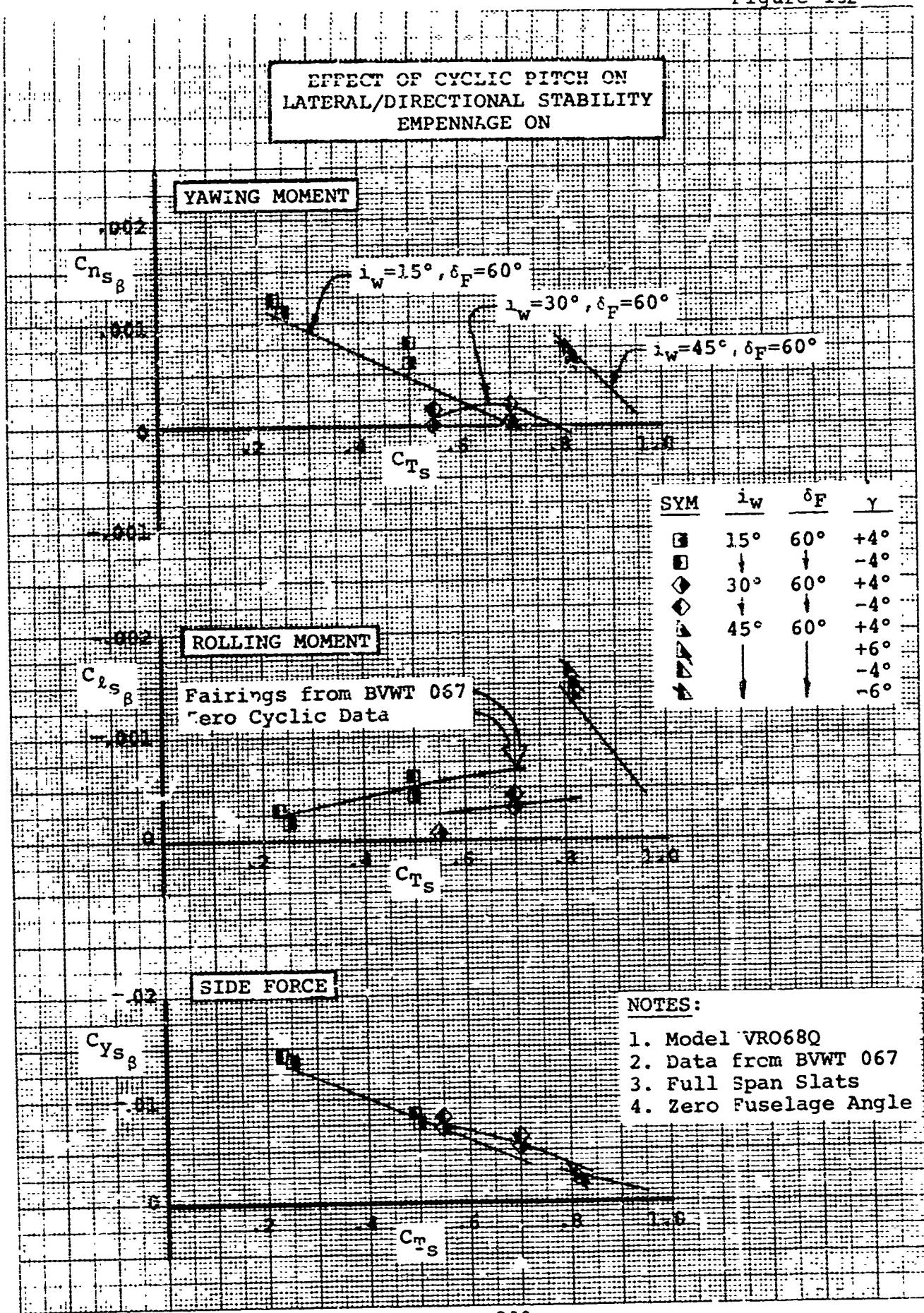
Both positive and negative cyclic pitch angles are seen to have only a minor effect on the directional stability (C_{nSg}) and dihedral effect (C_{lSg}) at all conditions tested with positive cyclic angles tending to decrease both the yaw stability and dihedral effect and negative angles tending to increase them. Thus, the cyclic pitch effects are in the same direction as established for the longitudinal mode, indicating again the influence of cyclic pitch on the propeller forces and moments.

Some data scatter is present in Figure 132, for example, the yaw stability measured with 15° of wing tilt and zero cyclic does not line up exactly with the comparable yaw stability data acquired with both positive and negative cyclic pitch inputs. This situation is understandable when it is realized that in powered model testing, back-to-back runs for accuracy purposes is not always feasible, because the length of a test series can extend over a couple of days.

Figures 133 through 141 present the basic three component yaw data from which the slopes shown in Figure 132 as data points, were measured. The various sets of plots, arranged in order of increasing wing tilt angle, use solid lines/open symbols to represent positive cyclic angles and dashed lines/solid symbols to represent negative cyclic angles. Slipstream thrust coefficients selected for each wing tilt angle correspond to typical points in transition; low thrust coefficients were selected for evaluation of cyclic pitch effects with 15° of wing tilt and a high thrust coefficient was selected with the 45° wing tilt angle.

One of the data accuracy problems associated with four-propeller powered model testing is the residual yawing moment encountered at zero yaw angle. As the wing is tilted up, this residual moment will be partially translated into a residual rolling moment. This data acquisition problem results from a combination of the inherent inaccuracy in individually setting the four propeller RPM's at each data point, the accuracy of each thrust calibration and the quality of thrust balancing achieved via the individual collective settings. An additional factor when air motors are used as in Model VR068Q is the jet thrust developed by each motor which can vary from motor to motor. The net result will be a displacement of the yawing moment curves and rolling moment curves about the zero yaw axis during the lateral/directional testing. This problem is particularly sensitive during the yaw testing due to the large moment arms involved. Zero shifts in the three component yaw data were minimized by incorporating subroutines into the data reduction program to subtract from the recorded yaw and roll moment, the contribution produced by the four individual jet thrusts and any unbalance in the individually measured propeller thrusts.

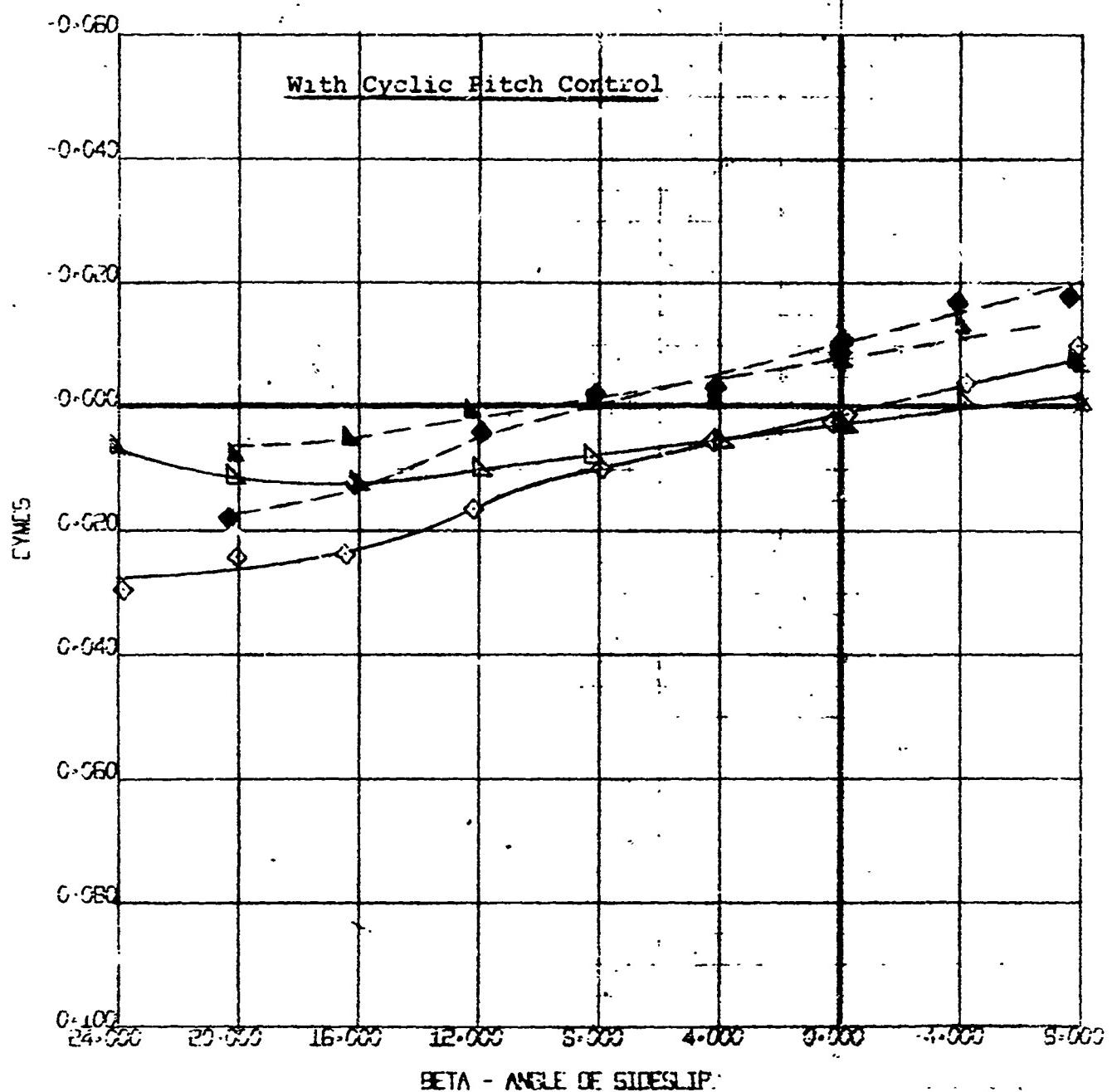
An examination of the three component yaw data plotted in Figures 98 through 127 and Figures 133 through 141 will reveal that this procedure was successful in most instances; however, in some data runs the tolerances must have buildup. Note that the scale used in plotting the rolling moment coefficient is twice that used for the yawing moment coefficient, which produced in some cases a larger apparent zero shift in the rolling moment data.



NUMBER D170-10039-1
REV. LTR. Figure 133

RUN	SYN	Δ	q	C_{Ts}	γ
106	◇	+10°	10.6	.25	+4°
107	△		6.3	.50	
117	◆		10.6	.25	+4°
118	▲		6.3	.50	
-0.060		Empennage Cn			

LATERAL/DERECTIONAL STABILITY
 $i_w = 15^\circ$, $\delta_F = 60^\circ$
FULL SPAN SLATS



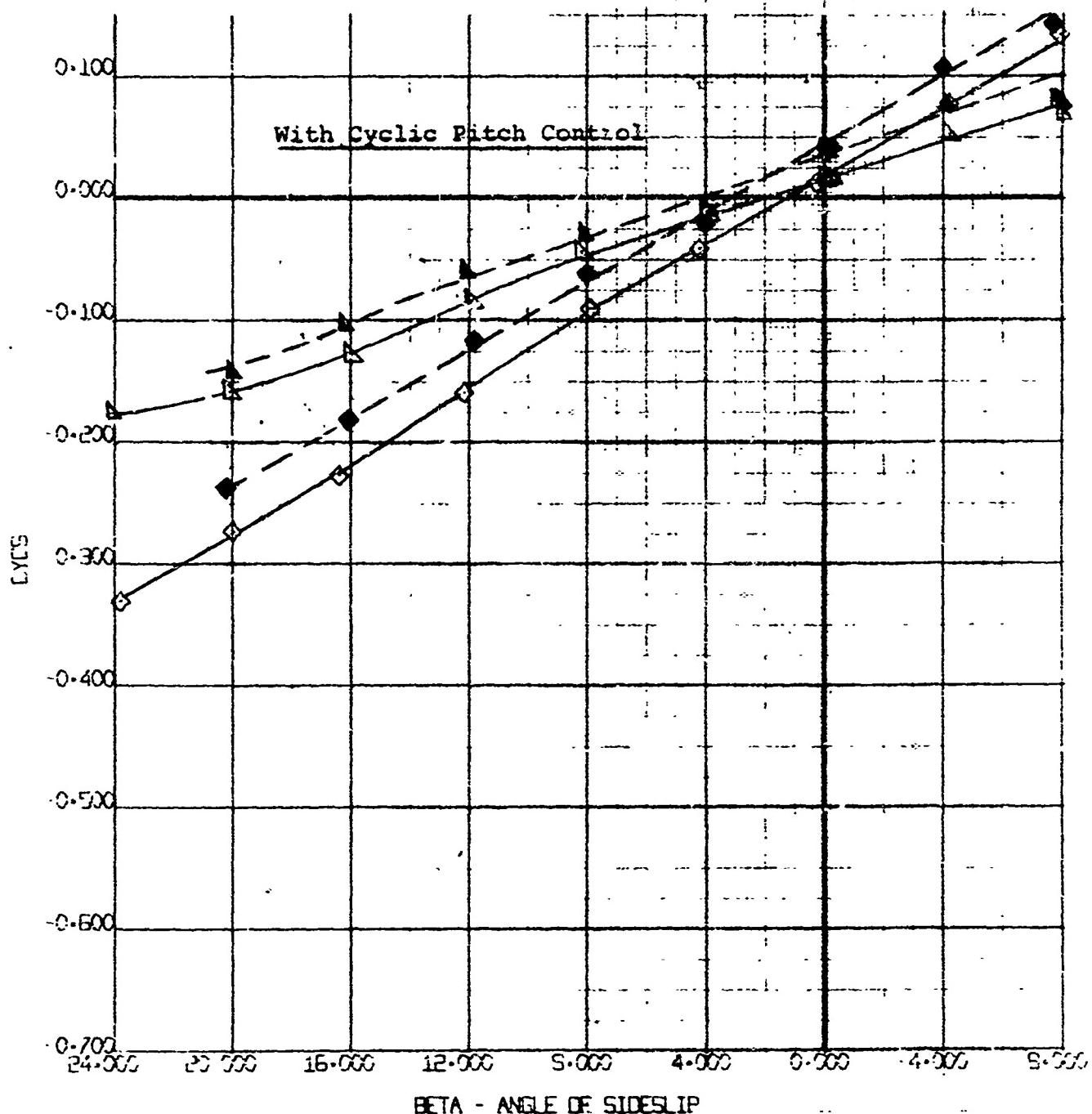
FOUR-PROP TILT WING MODEL VROB90 (FULL SPAN) CYMCS VS. BETA	BW1 67 12/15/70
---	-----------------------

RUN	SYM	α	a	C_{T_S}	γ
106	◇	+10°	10.6	.25	+4°
107	▽		6.3	.50	↑
117	◆		10.6	.25	-4°
0-200	118	▲	6.3	.50	↓

NUMBER D170-10039-1
REV. LIR. Figure 134

LATERAL/DIRECTIONAL STABILITY
 $\alpha_w = 15^\circ$, $\delta_F = 60^\circ$
FULL SPAN SLATS

Empennage On



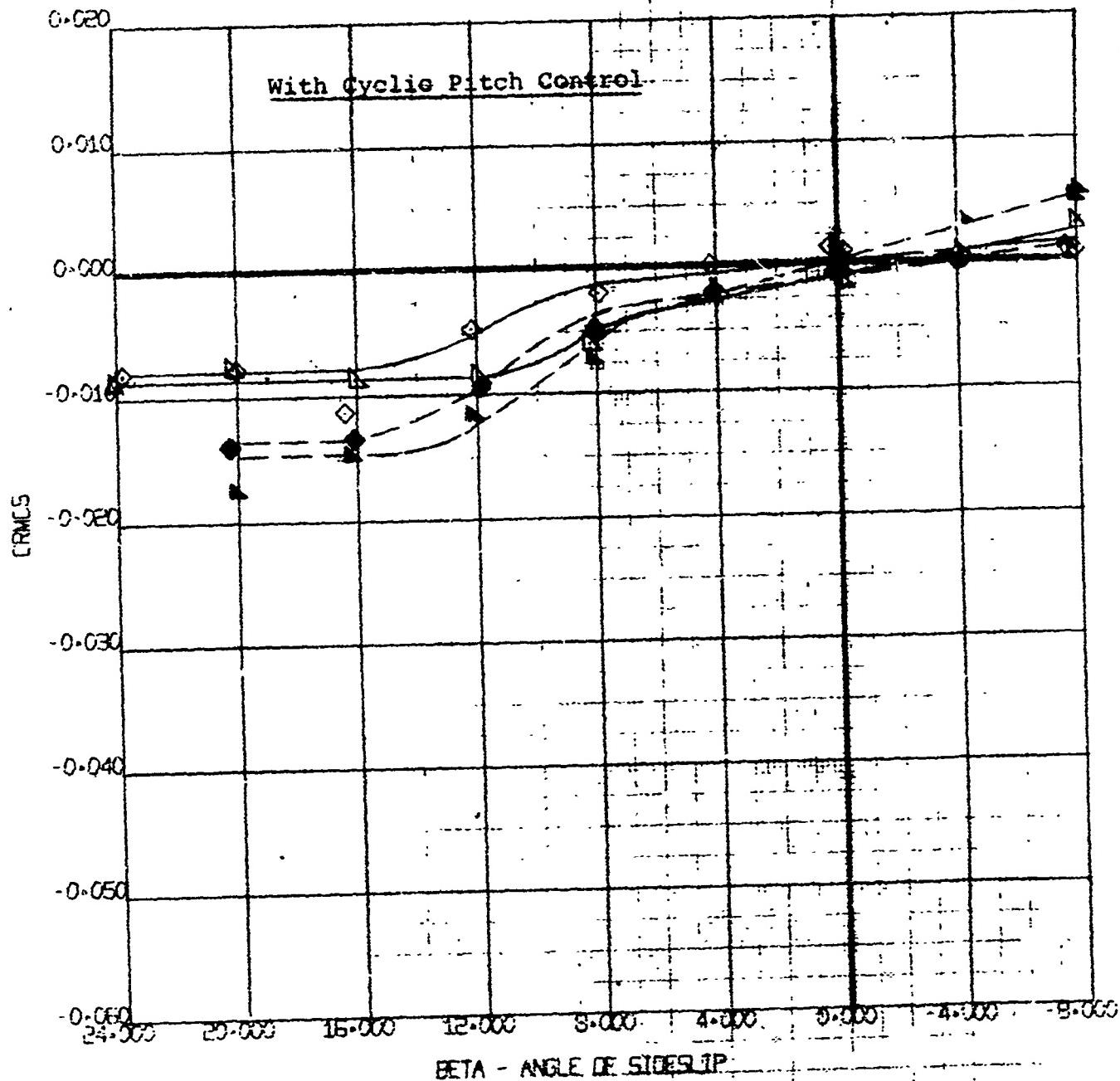
FOUR-PROP TILT WING MODEL VR0600 (FULL SPAN) CYCS VS. BETA	BWWT 6°
--	------------

12/15/70

NUMBER D170-10039-1
REV. LTR. Figure 135

RUN	SYM	α	q	C_{T_S}	γ
106	◇	+10°	10.6	.25	+4°
107	▽		6.3	.50	-
117	◆		10.6	.25	-4°
0-030	▲		6.3	.50	-
118	▼				
Empannage On					

LATERAL/DIRECTIONAL STABILITY
 $\delta_w = 15^\circ$, $\delta_r = 60^\circ$
FULL SPAN SLATS



NOT REPRODUCIBLE

FOUR-PROP TILT WING
MODEL VROB0(FULL SPAN)
DRAGS VS. BETA

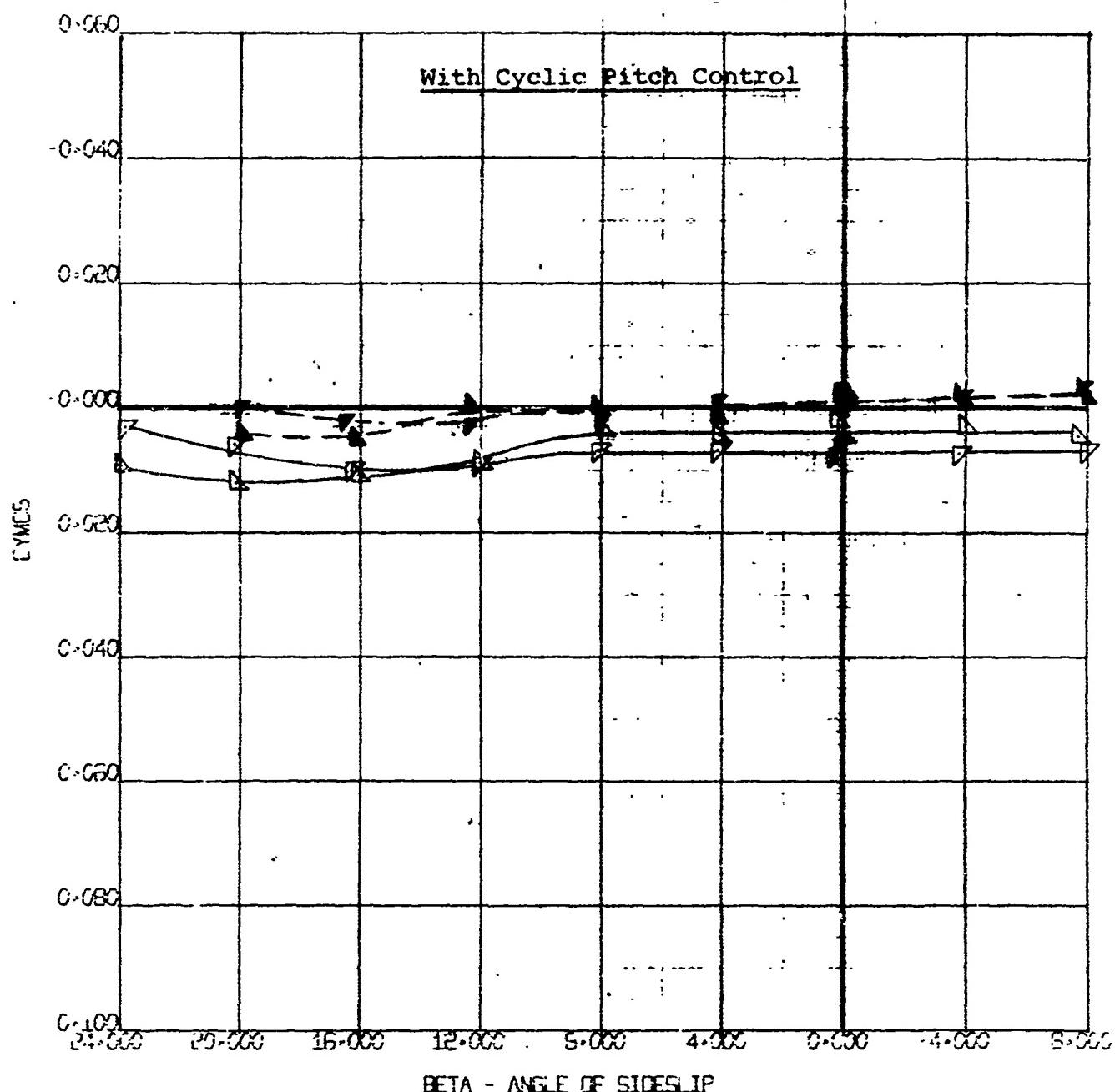
BWNT
67
12/15/70

NUMBER D170-10039-1
REV. LTR. Figure 136

RUN	SYM	Δ	q	NOM C_{Ts}	γ
108	▲	+15°	6.5	.55	+4°
109	▼		4.0	.70	-
119	■		6.5	.55	-4°
120	◆		4.0	.70	+

0.060 Empennage On

LATERAL/DIRECTIONAL STABILITY	
$i_w = 30^\circ$	$\delta_F = 60^\circ$
FULL SPAN SLATS	



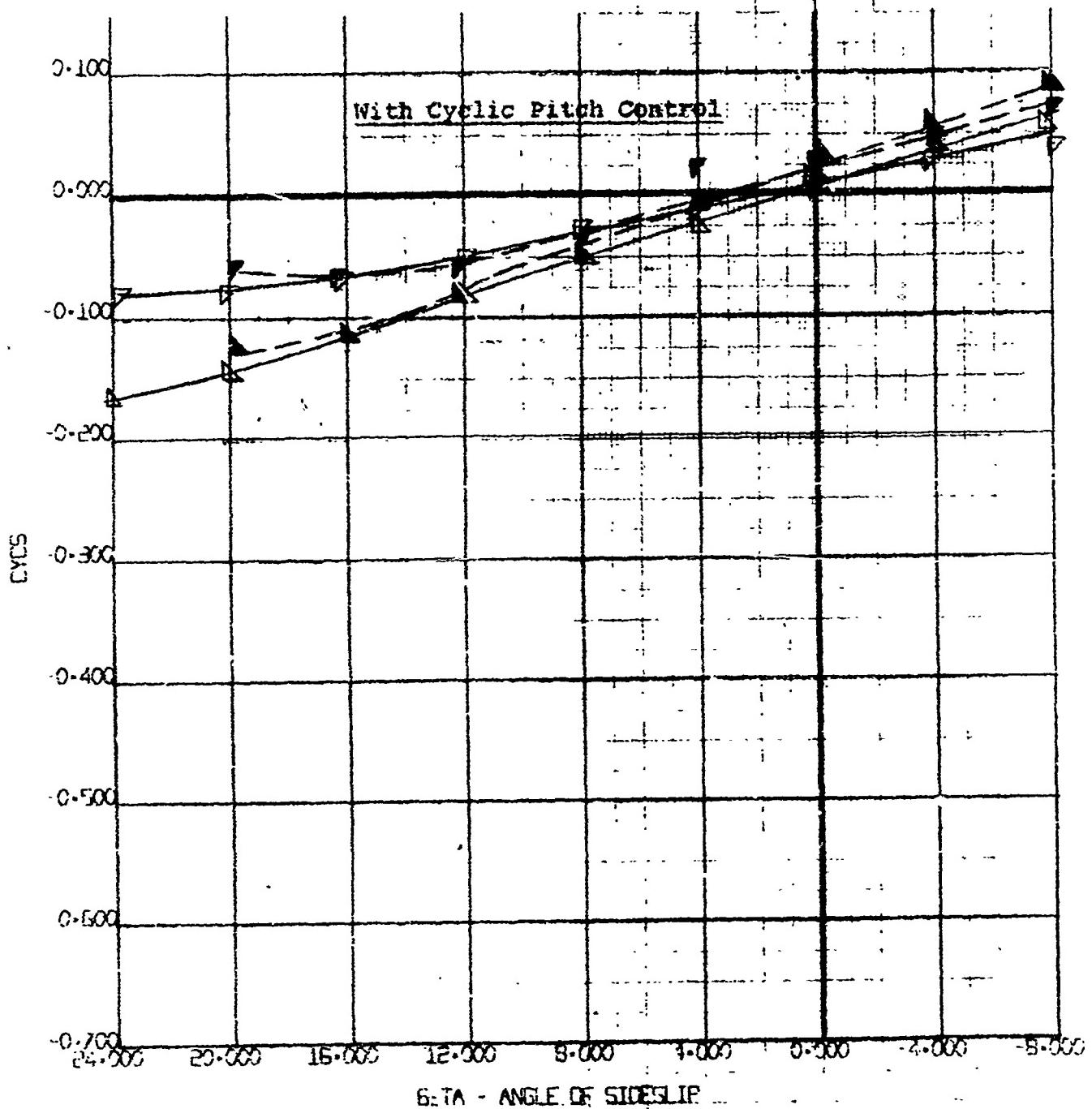
FOUR-PROP TILT WING MODEL VRC65G (FULL SPAN) CYMCS VS. BETA	EWHT 67 12/15/70
---	------------------------

RUN	SYM	Δ	a	NOM CT _S	γ
108	△	+15°	6.5	.55	+4°
109	▽		4.0	.70	
119	▲		6.5	.55	-4°
120	▼		4.0	.70	

0-200 Empennage On

NUMBER D170-49639-1
REV. CTR. Figure 137

LATERAL/STABILITY, STABILITY
 $\alpha_w = 30^\circ$, $\delta_g = 60^\circ$
FULL SPAN SLATS



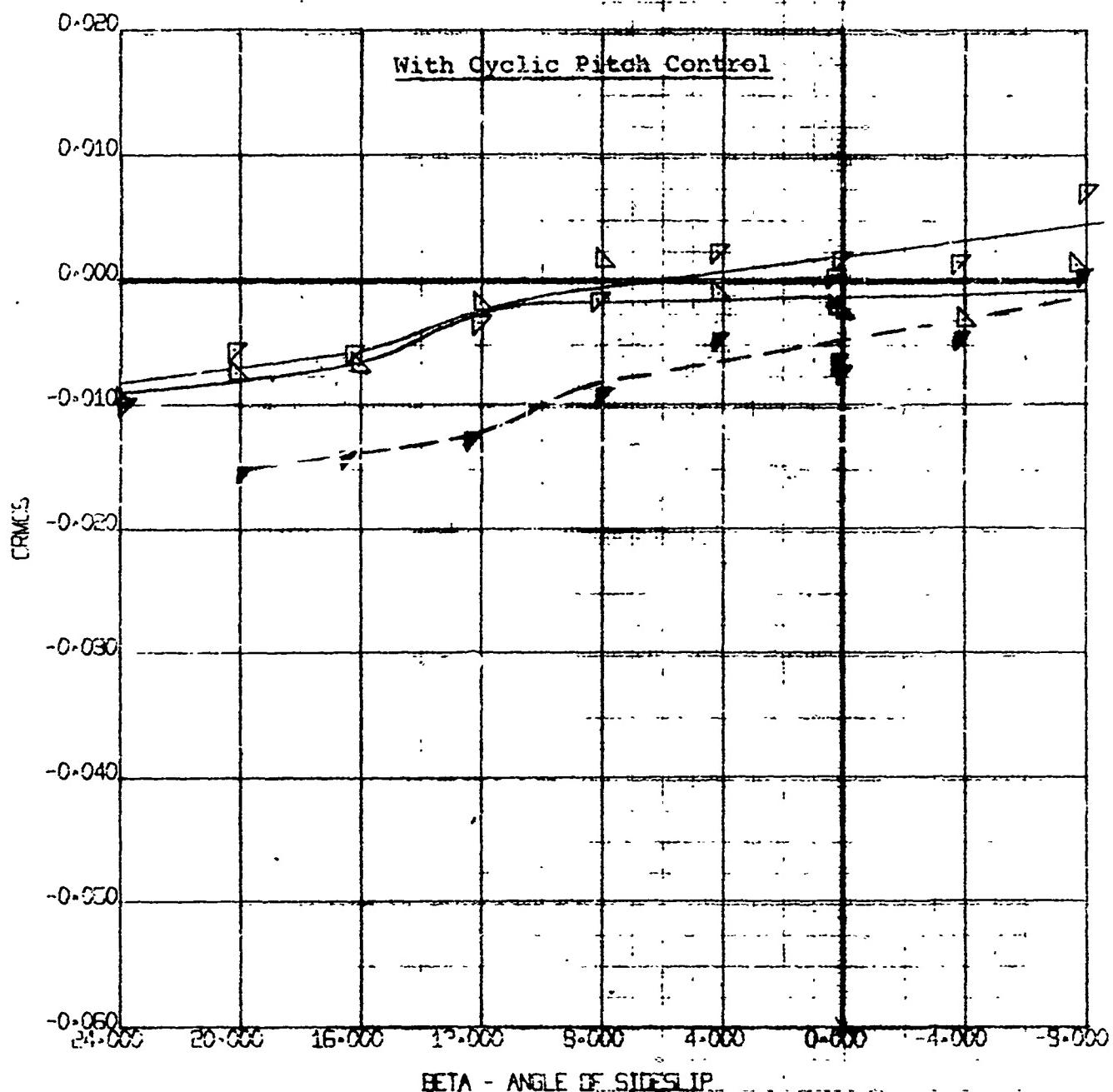
FOUR-PROP TILT WING MODEL VRO620 (FULL SPAN) CYCS VS. BETA	BWWT 67 12/15/70
--	------------------------

NUMBER D170-10039-1
REV. LTR. Figure 138

RUN	SYM	Δ	a	NOM $C_{T_{S1}}$	γ
108	B	+15°	6.5	.55	+4°
109	F		4.0	.70	
119	■		6.5	.55	
120	■		4.0	.70	

LATERAL/DIRECTIONAL STABILITY
 $\alpha_w = 34^\circ$; $\delta_F = 50^\circ$
FULL SPAN SLATS

Empennage On



FOUR-PROP TILT WING
MODEL VR068 (FULL SPAN)
CRMS VS. BETA

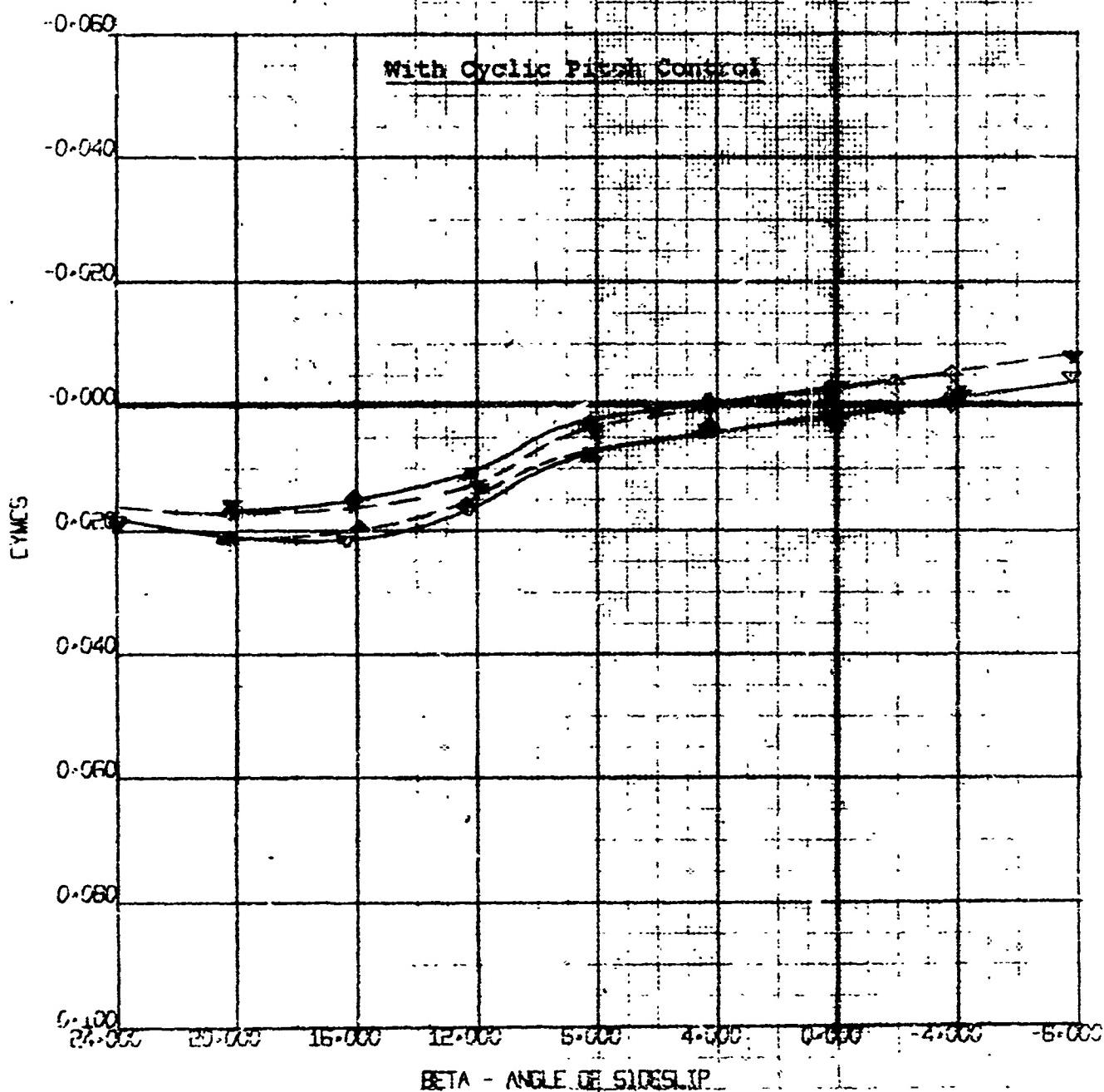
BWWT
67
12/15/70

RUN	SYM	Δ	α	T_s	γ
110	▽	+25°	2.7	.81	+4°
116	▼				-4°
172	▲	+35°			+6°
167	△	+25°			-6°

0.980
Empernage On

NUMBER D170-10039-1
REV. LR. Figure 1-9

LATERAL/DIRCTIONAL STABILITY
LW=45°, S2=60°
WING SPAN STABE



FOUR-PROP. TILT WING MODEL VR0580 (FULL SPAN) CYMCS VS. BETA	BWWT 67 12/15/70
--	------------------------

RUN	SYM	Δ	q	NOM	C_{T_E}	γ
120	▽	+25°	2.7		.91	+4°
126	▼					-4°
172	△	+35°				+5°
167	▲	+25°				-5°

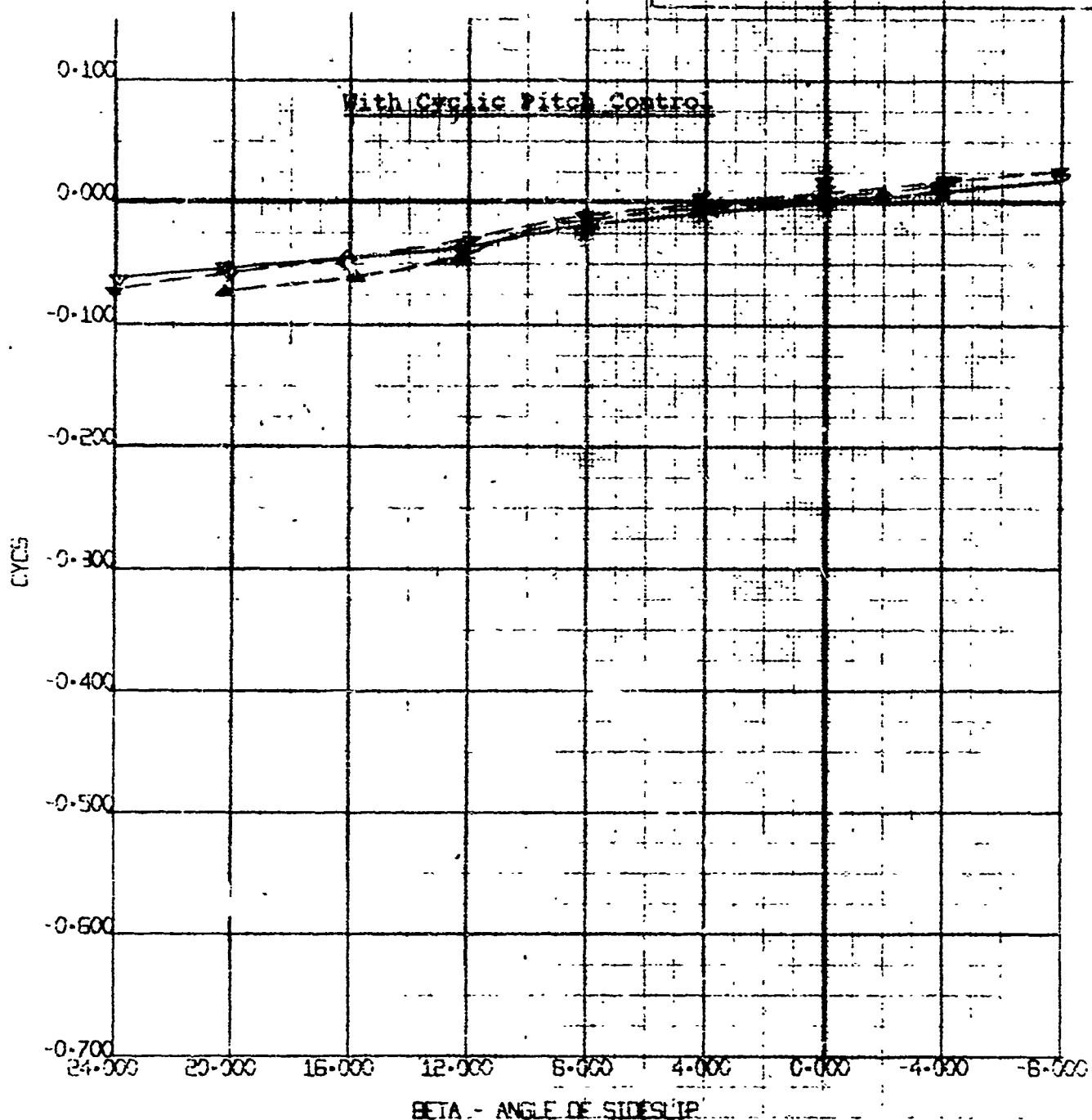
Empennage On

NUMBER D170-10039-1
REV. LIR. Figure 140

LATERAL/DIRIGEONAL STABILITY

$\alpha = 45^\circ$, $\delta_s = 60^\circ$

FULL SPAN STATS



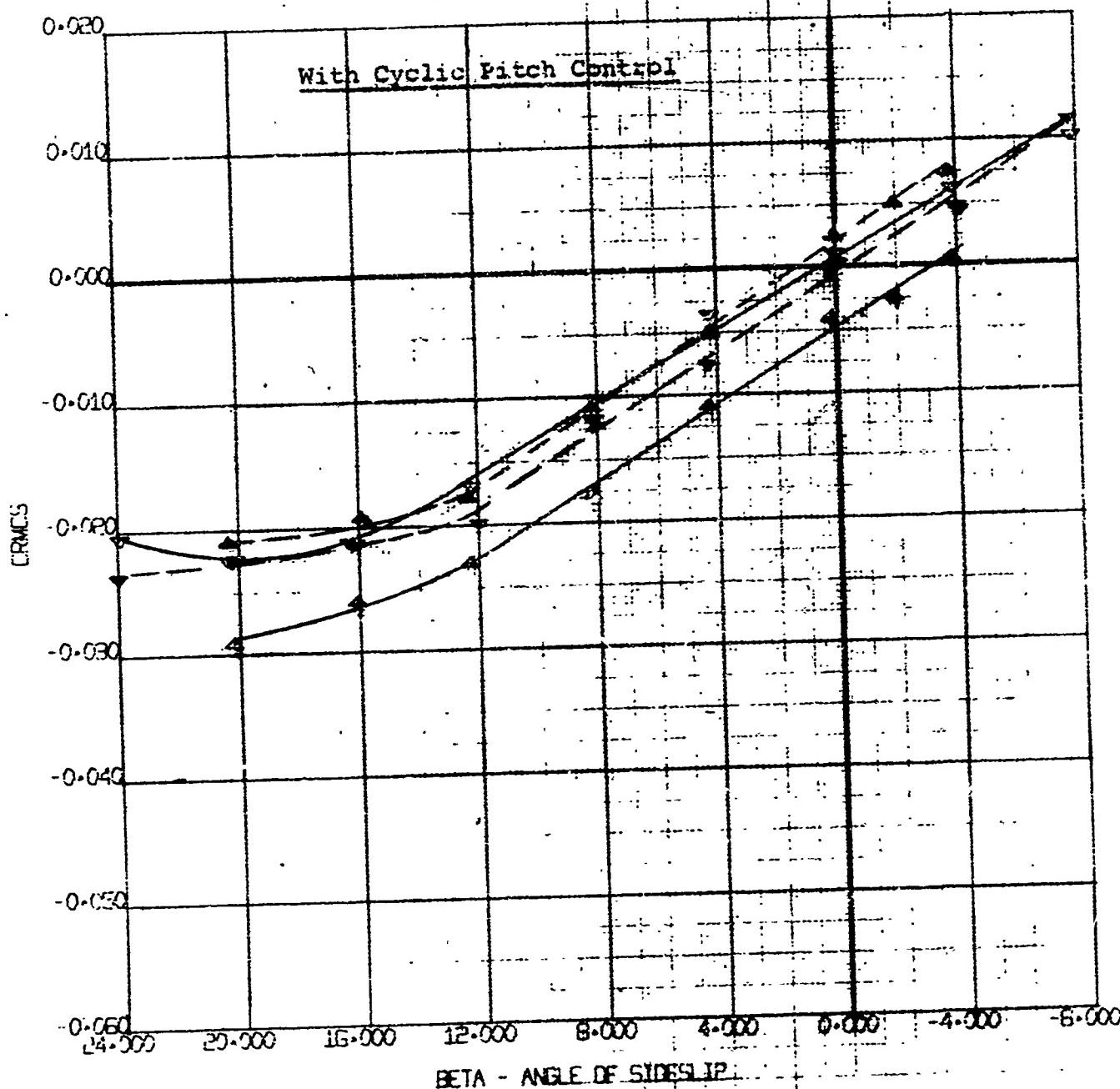
FOUR-PROP TILT WING MODEL VR068C (FULL SPAN) CYCS VS. BETA	BWNT 67
	12/15/70

NUMBER D170-10039-1
REV. LTR. Figure 141.

RUN	SYM	Δ	a	C_{Ls}	NOM
110	▽	+25°	2.7	.81	+4°
116	▼	-	-	-	-4°
172	△	+35°	-	-	+6°
167	▲	+25°	-	-	-6°

Empennage On

FOUR-PROP TILT WING STABILITY
 $L_0 = 45^\circ$, $\delta F = 60^\circ$
FULL SPAN STATS



FOUR-PROP TILT WING MODEL VROSBO (FULL SPAN) DRMS VS. BETA	BWWT 67
	12/15/70

6.6 CROSS-COUPING OF CYCLIC PITCH WITH ROLL/YAW SURFACE CONTROLS

Wing surface controls, used as a yaw control in hover with the wing tilted about 90°, become a combined roll and yaw control in transition where tilt angles can vary from about 45° at 0.81 C_{T_s} to 15° at 0.25 C_{T_s} . Roll and yaw control available from a control configuration consisting of 20° differential flaps and 40° spoilers was evaluated in fuselage pitch sweeps at three selective wing tilt/thrust coefficient combinations with a nominal 60° of flaps. The body axis data plotted in Figure 142 in slipstream form shows the buildup in roll control and phasing out of the yaw control as the wing is tilted down. This is illustrated in the figure by the dashed line representing a constant propeller shaft angle. The variation of rolling moment with fuselage angle is similar to the variation of slipstream lift coefficient with fuselage angle.

Figure 143 which shows the changes associated with cross-coupling cyclic pitch control and roll/yaw control includes the data previously presented in Figure 142, but referenced to the stability axis system instead of the body axis system. Both positive and negative pitch inputs of 4° magnitude are noted to have only a small percentage effect on the control effectiveness.

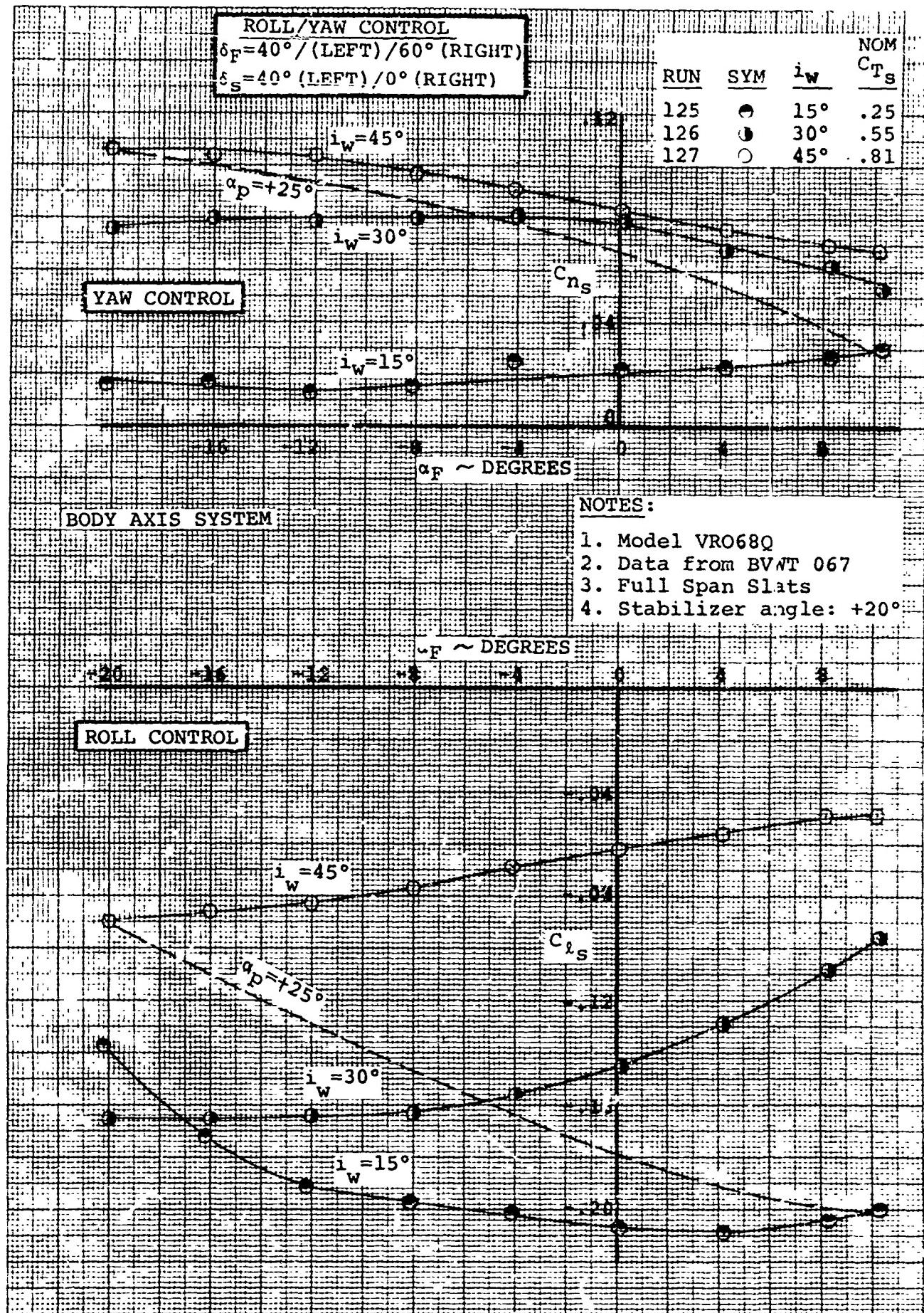
Whereas Figure 143 illustrates the effect of cyclic pitch inputs on the roll/yaw control in transition, Figure 144 presents the opposing effect of the aircraft surface controls on the cyclic pitch effectiveness. Cyclic pitch effectiveness with a coupled roll/yaw control configuration of 20° of differential flaps and 40° of spoilers is shown in Figure 144 as an increment in slipstream pitching moment per degree of cyclic. Two typical conditions in transition are compared with corresponding tail-on data obtained during the cyclic pitch effectiveness runs with a full 60° of flap deflection. The decrease in incremental cyclic pitching moment capability with fuselage angle of attack was mentioned earlier in the report as being largely a ramification of the constant RPM method of testing, wherein slipstream q is increased as the model was pitched.

Figure 144 indicates that at the 45° wing tilt/0.81 C_{T_s} condition, coupled roll/yaw control produced a change in cyclic pitch effectiveness that varied from -2% to +10%. At the 30° wing tilt/0.55 C_{T_s} condition the change varied between -3% and -7%. This total variation, though moderate in magni-

tude, does not appear to be consistent in its change in sign from a negative to a positive effect. A logical explanation would be that the overall effect of the application of roll/yaw controls on cyclic pitching capability is small and that the results shown in Figure 144 merely reflect a normal amount of data scatter that occurs when tests extend over a period of several weeks and back-to-back run comparisons are not always possible. Such items as the accuracy of cyclic angular settings and changing ambient conditions in the test section are involved.

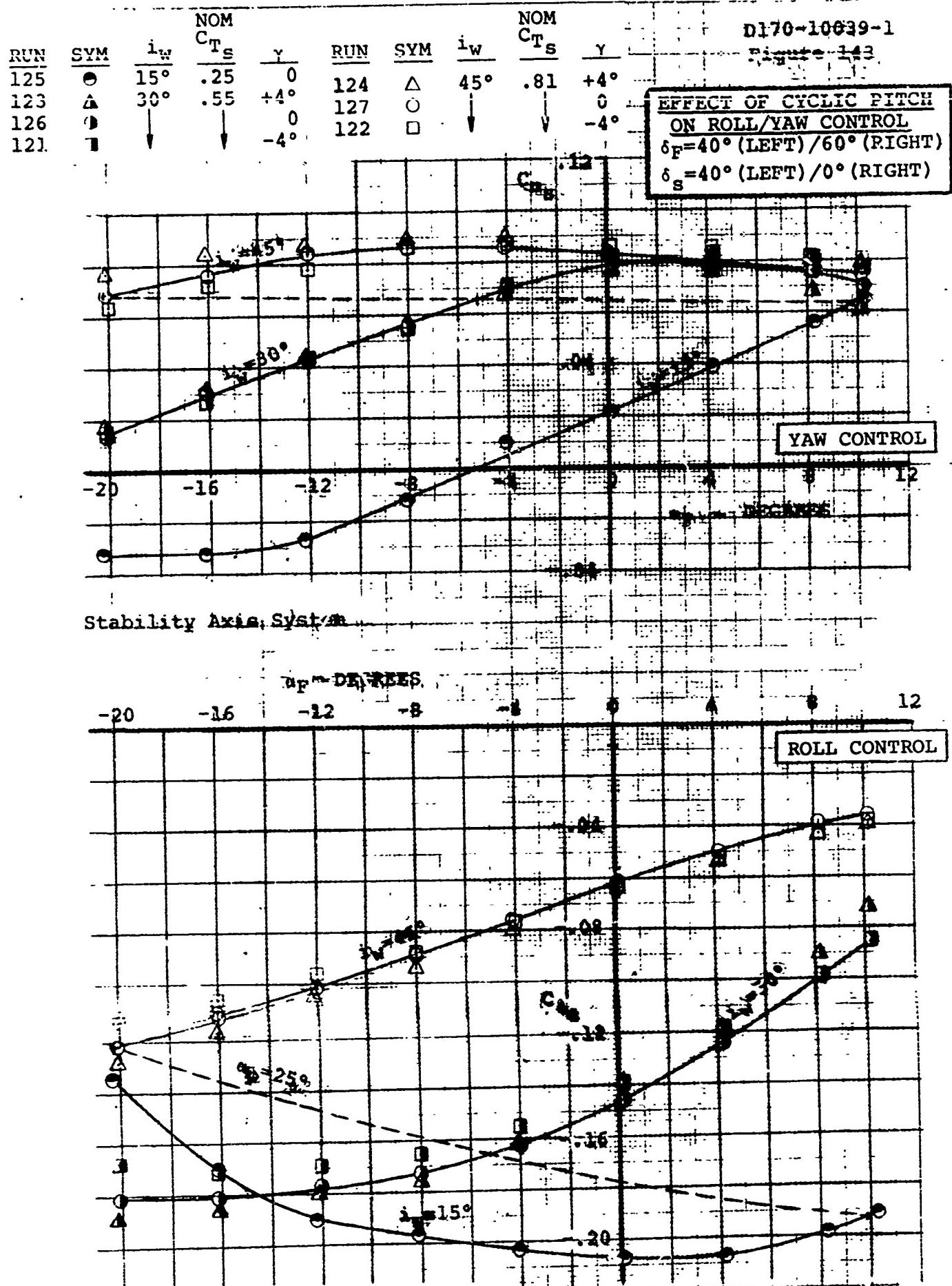
The basic pitching moment data used to develop the roll/yaw control coupled cyclic pitch effectiveness curves shown in Figure 144, is presented in Figures 145 and 146. This data is plotted as a slipstream pitching moment vs. fuselage angle of attack, with the moment being transferred about the previously described mid c.g. position. Figure 147 presents the corresponding variation of slipstream thrust coefficient for the constant RPM pitch runs.

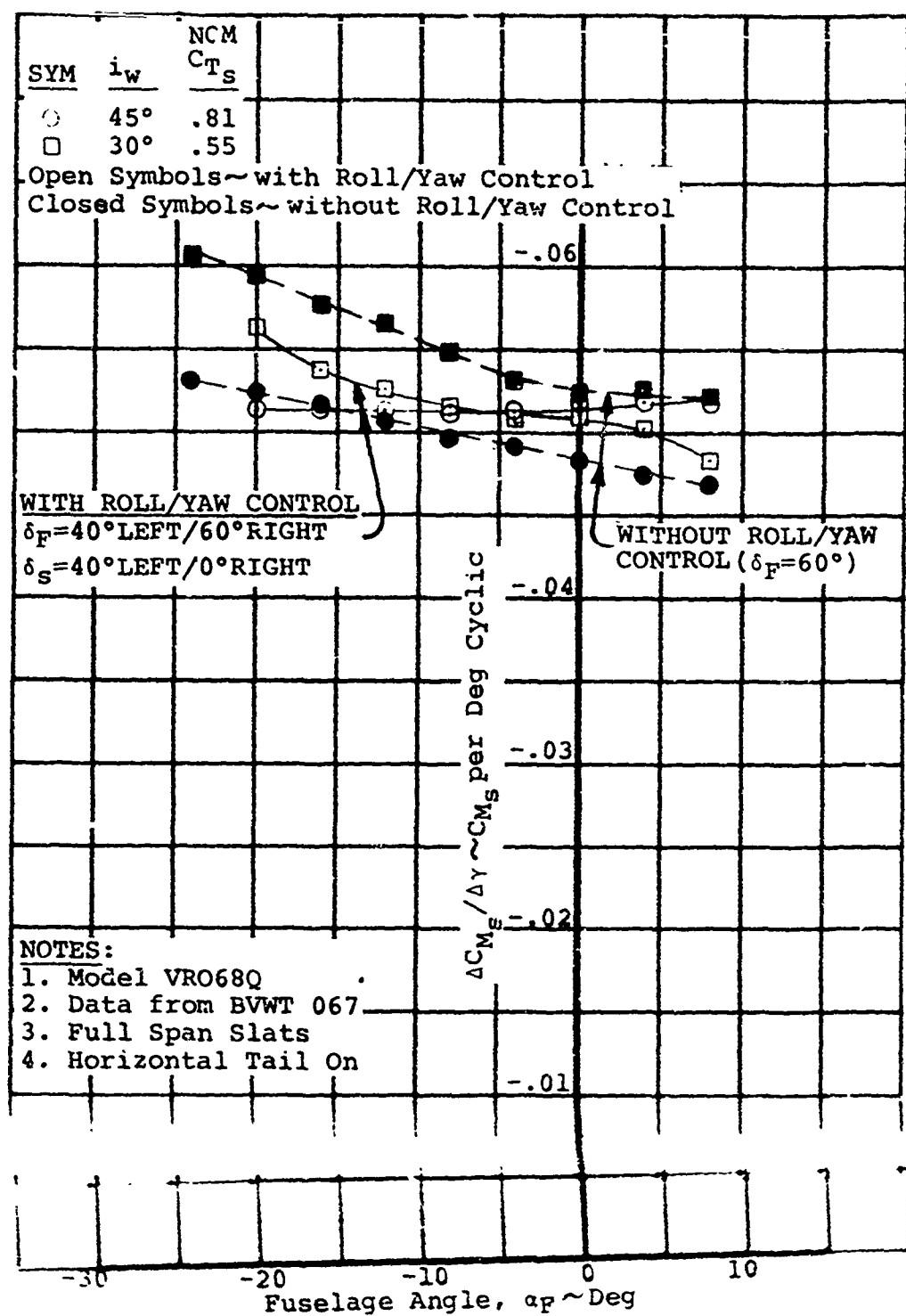
The basic tail-on data without coupled roll/yaw control used to calculate the comparative cyclic pitch effectiveness curves shown in Figure 144 were presented earlier in the report in Figures 53 and 60.



DI70-10039-1

Figure 143



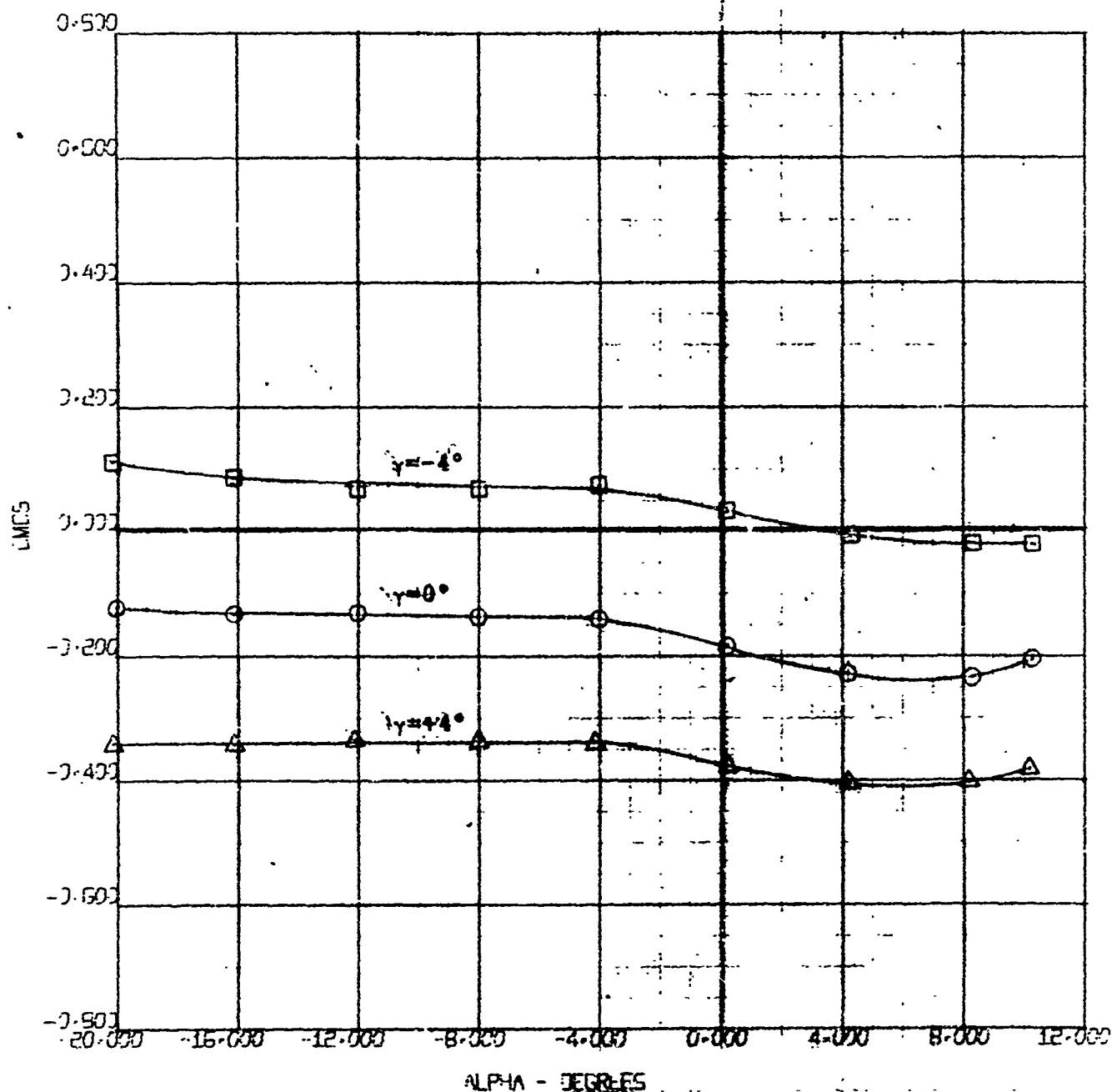


EFFECT OF ROLL/YAW CONTROL
ON CYCLIC PITCH EFFECTIVENESS

RUN SYM Δ 20° C_s $+4^\circ$
 123 Δ 20° 6.5 $+4^\circ$
 126 O 0 0
 121 \square -4°

NUMBER D170-10039-1
 REV. LTR. Figure 145

CYCLOIC PITCH WITH ROLL/YAW CONTROL
 $i_w = 30^\circ$, $\delta_p = 40^\circ$, LEFT/60° RIGHT
 $\delta_g = 40^\circ$, LEFT/0° RIGHT
 FULL SPAN SLATS
 NOM $C_{T_s} = .55$

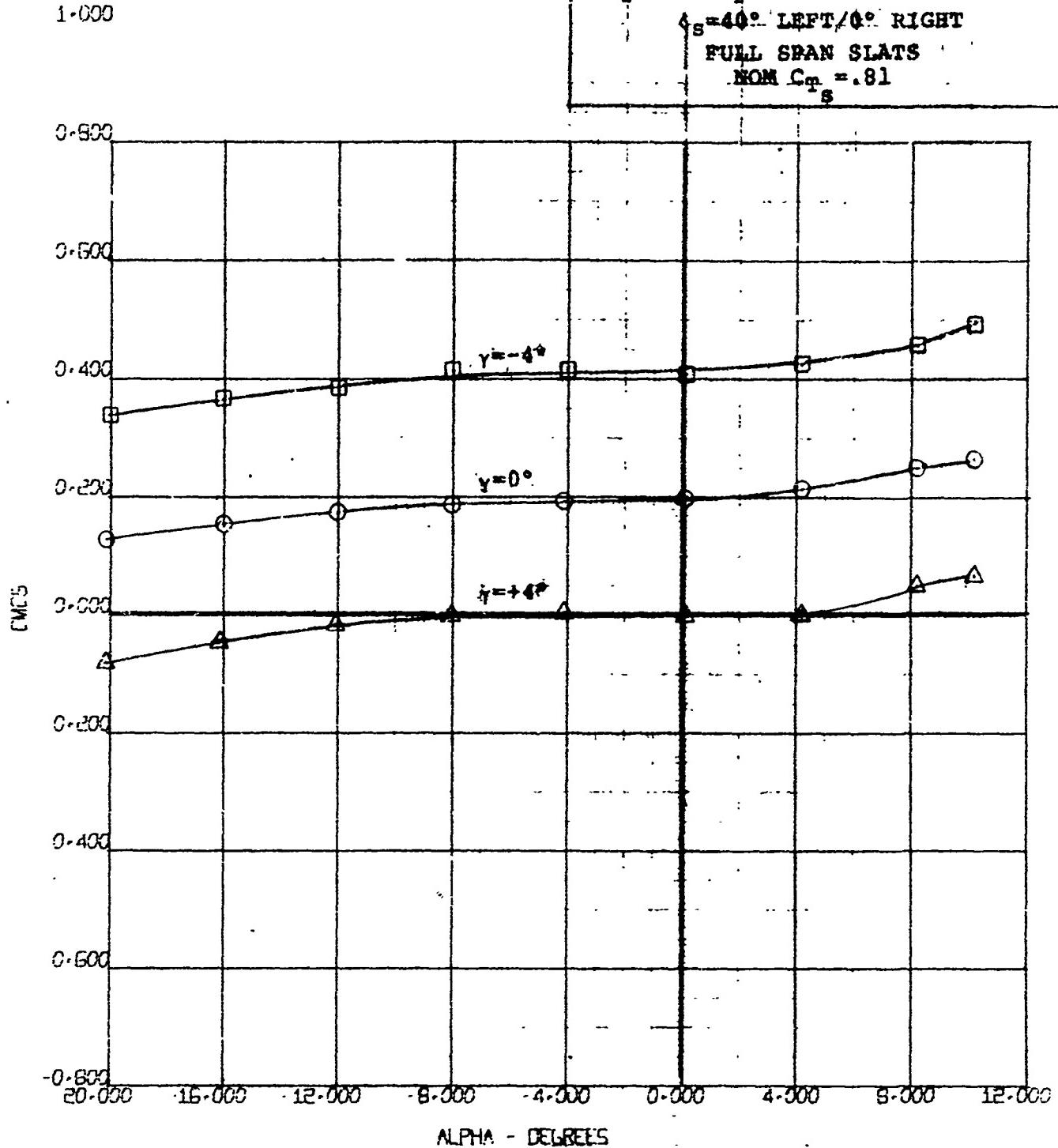


FOUR-PROP TILT WING MODEL VROS2 (FULL SPAN) CMCS VS. ALPHA	BWWT 67
	1/ 4/71

RUN SYM $\frac{q}{q_0}$ $\frac{y}{y_0}$
 124 Δ 20° 2.7 +4°
 127 \circ 1 0
 122 \square 1 -4°

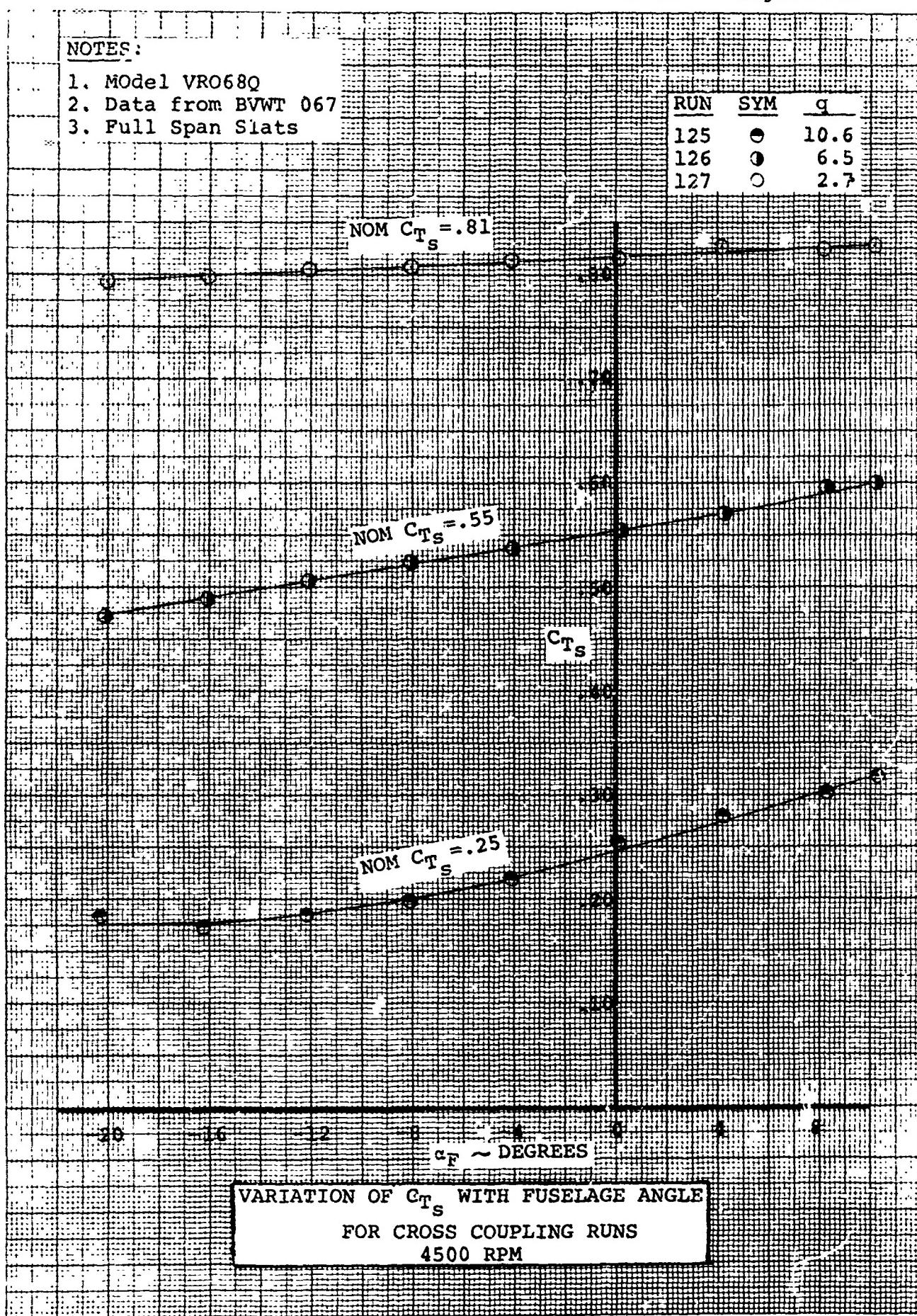
NUMBER D170-10039-1
 REV. A JR. Figure 146

CYCLOIC PITCH WITH ROLL/YAW CONTROL
 $\alpha_p = 45^\circ$, $\delta_B = 40^\circ$, LEFT/60° RIGHT
 $\delta_s = 40^\circ$ LEFT/0° RIGHT
 FULL SPAN SLATS
 NOM $C_{T_s} = .81$



FOUR-PROP TILT WING
 MODEL VR0680 (FULL SPAN)
 CL vs. ALPHA

BWHT
 67
 1/4/71



6.7 LONGITUDINAL CHARACTERISTICS IN GROUND EFFECT

An investigation of the basic longitudinal characteristics in ground effect and an evaluation of cyclic pitch effects on the longitudinal characteristics were performed with the full-span model utilizing the Boeing-Vertol moving ground plane. This investigation was conducted with the aircraft level and a scaled ground height of 1.25 h/D representing the aircraft with the wheels 3 feet off the ground. Slats were extended and the flaps were deflected both 40° and 60° for the longitudinal runs. The 40° flap setting corresponds to a compromise between a lower deflection for takeoff with a wing tilt angle in the order of 20° and a higher deflection for landing approach.

The desire to obtain in-ground effect information at a low wheel height precluded performing the longitudinal mode runs with the standard fuselage angle pitch sweeps and constant wing tilt angles as a result of the clearance problem between the long straight sting and the moving ground plane. Wing tilt sweeps, with a level fuselage and tail removed, that were made in place of the fuselage sweeps do not allow a direct data comparison to show the influence of ground effect on the aircraft longitudinal stability. The level fuselage corresponds to a normal fuselage attitude for a tilt wing aircraft operating in close proximity to the ground.

6.7.1 Influence of Ground on Out-of-Ground Effect Longitudinal Characteristics

Longitudinal characteristics were investigated in ground effect with both 40° and 60° of flap deflection over a range of thrust coefficients from 0.25 to 0.81 C_{T_s} (nominal values) using a propeller operating speed of 4500 RPM. Figures 148 and 149 provide a direct comparison of the lift and force polars, respectively, for the two flap settings.

Figure 148 compares the slipstream lift coefficient developed as a function of the slipstream thrust coefficient at wing incidence angles of 0° and 10°. A maximum C_{L_s} comparison is also shown. This figure, which illustrates the typical decrease in slipstream lift coefficient with an increase in slipstream thrust coefficient, shows that at zero wing incidence an additional 20° of flap deflection beyond the 40° setting produces a substantial increment in lift. The 0.82 C_{L_s} increment at

0.18 C_{T_S} agrees favorably with the 0.81 C_{L_S} increment previously obtained for the same configuration change during out-of-ground effect testing at zero C_{T_S} . (See Figure 68 of Reference 1.)

The increment in lift, from the change in flap angle, decreases with increasing wing incidence angle such that at maximum lift, the increment is reduced to 0.08 C_{L_S} , a value that is one-third the value obtained out-of-ground effect at zero C_{T_S} . As usual with flaps, the angle of attack at maximum lift was less with 60° of flap than with 40° of flap. This situation can sometimes completely cancel any incremental lift improvement resulting from an increase in flap angle even though full span slats are employed.

An additional point of interest in Figure 148 is the sharp drop in maximum lift that occurs at 0.8 C_{T_S} with the 60° flap setting. This condition is identified later in the report with ground recirculation.

Figure 149 provides a direct comparison of the force polars obtained in-ground effect with 40° and 60° of flaps. Except for the decrease in lift occurring as a result of ground recirculation at 0.81 C_{T_S} and 30° of wing tilt angle with the 60° flap angle, the force polars exhibit the normal trend usually associated with a flap change to a larger angle: higher drag or less propulsive force at a low wing angle of attack and more lift at the high wing angles. The propulsive force change at low wing incidence angles is produced by a combination of increased flow turning and higher drag with the larger flap angle.

Figures 150 and 151 were developed to illustrate the influence of ground proximity on the lift curves and force polars with 60° of flap deflection. In these figures, the in-ground effect data is plotted as acquired during the Phase II testing. The out-of-ground data as presented, is the result of cross-plotting the data previously presented in Figures 62 and 63 of Reference 1, but in another coefficient form. Reference 1 data in the slipstream format, that was acquired during similar wing tilt sweeps with a comparable model configuration of flaps/slats, cyclic hubs and 4750 RPM, was cross-plotted to provide data for a direct comparison at the same slipstream thrust coefficients.

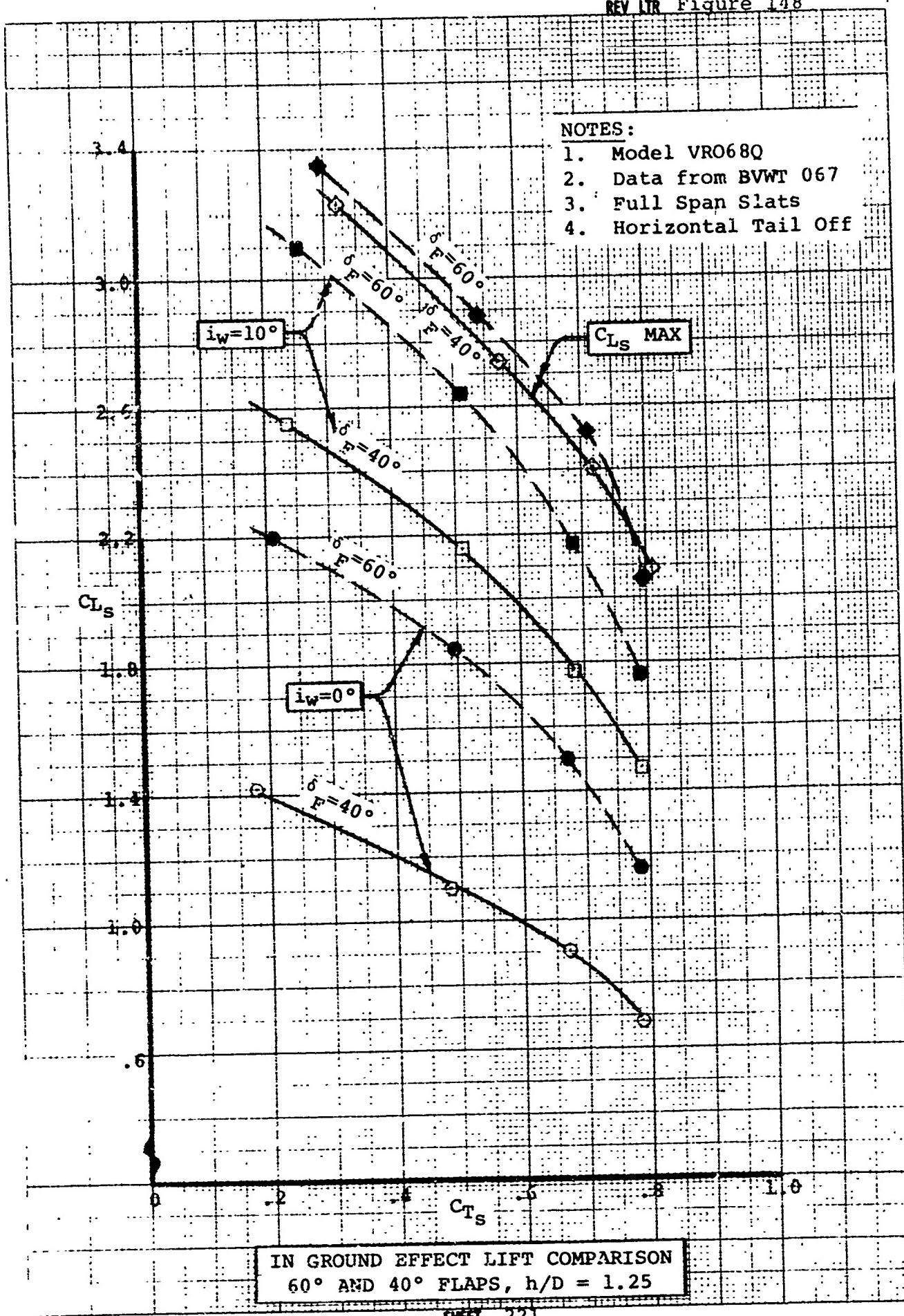
The lift curve comparison presented in Figure 150 shows an increase in lift at the three foot wheel height with the wing down. This lift increase due to ground effect was a maximum at the lowest thrust coefficient evaluated. Maximum lift in-ground effect was less than for the out-of-ground case; a condition primarily induced by the lower wing incidence angles involved. An examination of the curves will reveal that except for the ground recirculation incident at 0.81 C_{T_s} , the loss in maximum lift due to ground effect is essentially a constant increment over the C_{T_s} range tested.

Again, except for the 0.81 C_{T_s} ground recirculation condition, ground proximity has an effect on the O.G.E. force polars which can be considered typical. At the lower wing incidence angles, the effect of the ground plane is to reduce the drag by an increment of drag that varies inversely with the slipstream thrust coefficient.

Basic three component in-ground effect data with the two different flap deflections is presented in Figures 152 through 154 and Figures 155 through 157 for the 40° and 60° flap settings, respectively. The force polars, lift curves, and pitching moment curves are shown in the slipstream coefficient system used throughout the report. As with the other wing tilt runs, the pitching moments have been referred to the wing pivot located 42.6% MAC aft of the wing leading edge and 11.7% MAC below the wing chord plane. Figure 158 illustrates the variation in slipstream thrust coefficient with wing tilt angle that occurred during the constant RPM runs.

NOTES :

1. Model VRO68Q
 2. Data from BVWT 067
 3. Full Span Slats
 4. Horizontal Tail Off

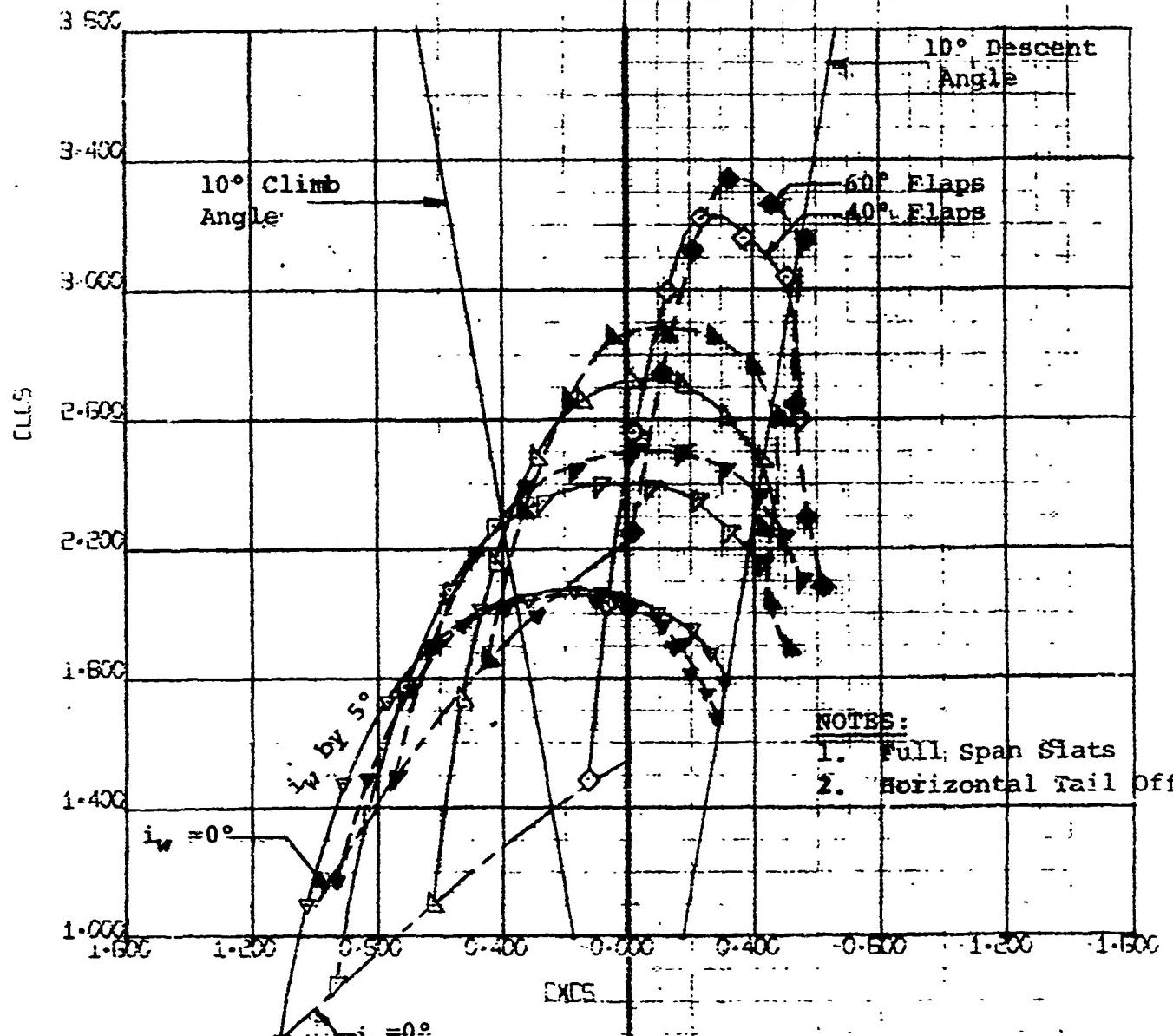


SYM NOM C_{T_S}

- $\nabla \blacktriangledown$.61
- $\nabla \blacktriangleright$.70
- $\triangle \blacktriangle$.55
- $\diamond \blacklozenge$.25

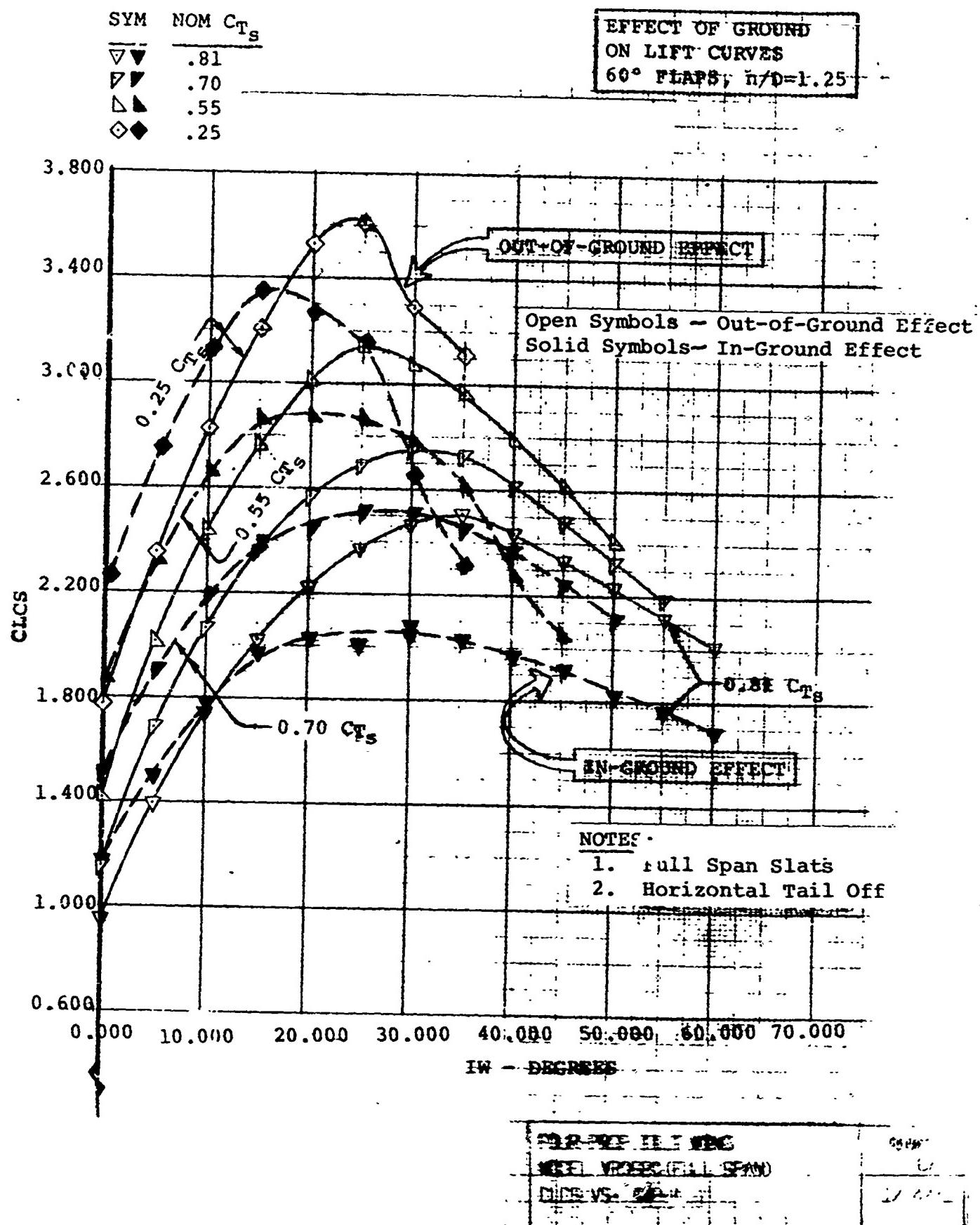
Open Symbols - 40° Flaps
Solid Symbols - 60° Flaps

IN GROUND EFFECT
FORCE POLAR COMPARISON
 60° & 40° FLAPS; $h/D = 1.25$



FOUR-PROP TILT WING
MODEL VR0000 (FULL SPAN)
CLs VS. CD

BWNT
67
1/4/71



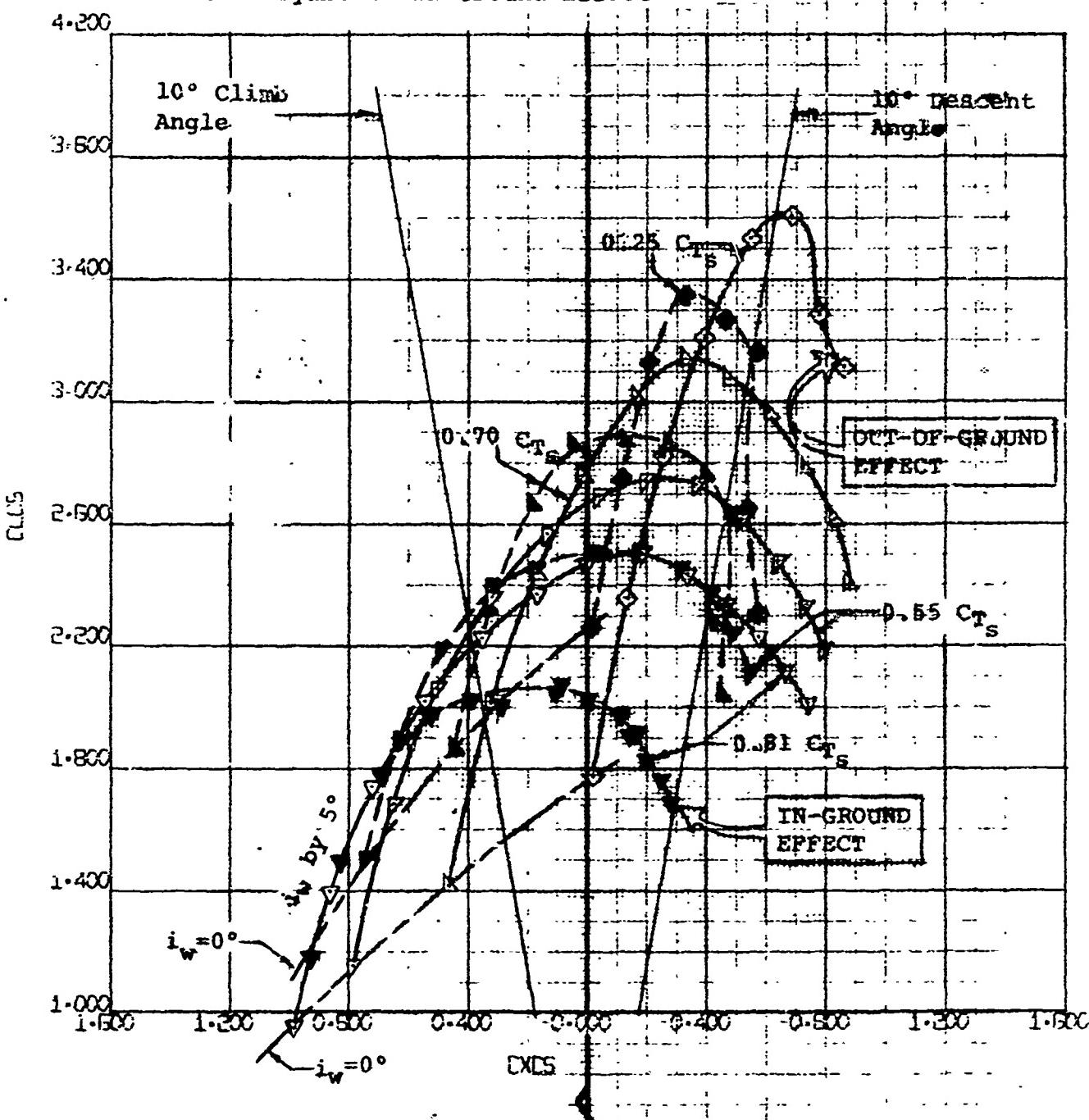
SYM. NOM C_{TS}

- $\nabla \nabla$.81
- $\nabla \blacktriangle$.70
- $\blacktriangle \blacktriangle$.55
- $\diamond \diamond$.25

EFFECT OF GROUND
ON FORCE POLARS
60° FLAPS, $h/D=1.25$

Open Symbols - Out-of-Ground Effect

Solid Symbols - In-Ground Effect



NOTES:

1. Full Span Slats
2. Horizontal Tail Off

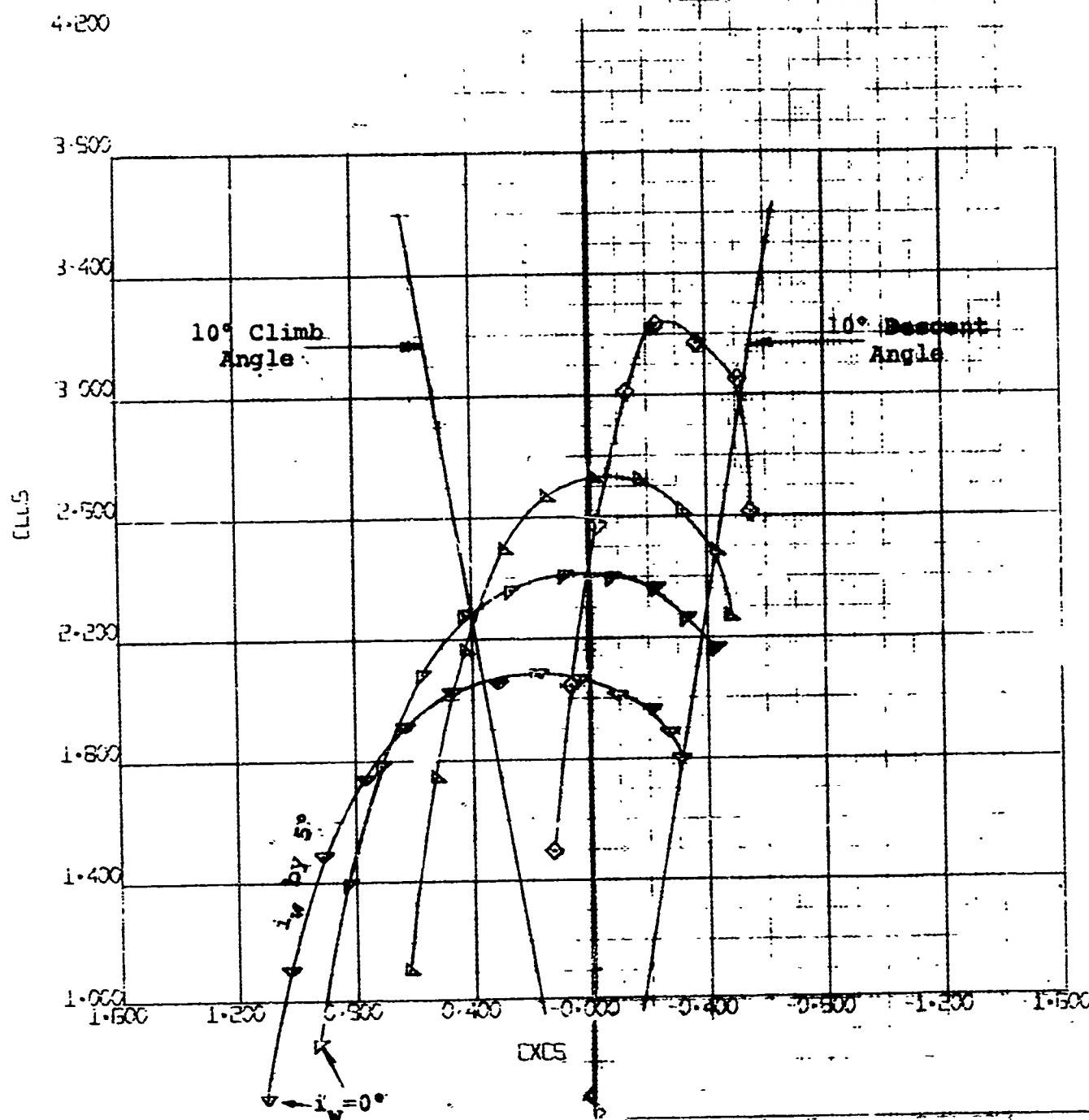
FOUR-PROP TILT WING MODEL VROBBQ(FULL SPAN) CLDS VS. CXDS	BWNT 6"
---	------------

1/ 4/71

RUN	SYM	Δ	S_e	NOM C_{T_s}	γ
140	▽	---	2.7	.81	0°
141	▽	---	4.5	.70	
142	▽	---	6.3	.55	
143	◇	---	10.6	.25	

NUMBER D170-10039-1
REV. C.F. Figure 152

LONGITUDINAL CHARACTERISTICS
IN GROUND EFFECT
 $\alpha_F = 0^\circ$, $\delta_F = -40^\circ$, $h/D = 1.25$
FULL SPAN SLATS



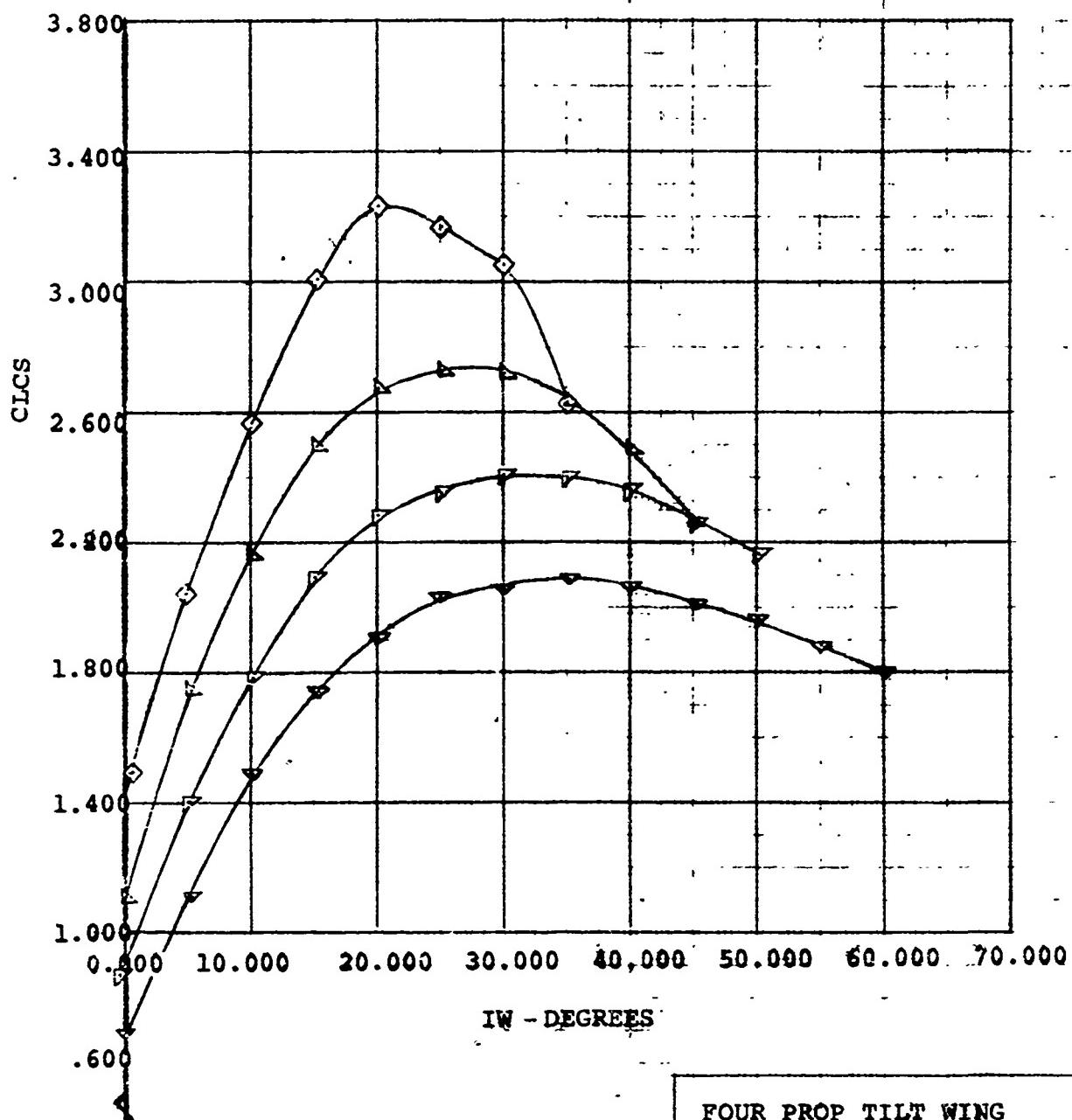
FOR 10° TILT WING	BWNT
ANGLE : 10° (FLW STAND)	67
CLLS VS. CXDS	17 471

RUN	SYM	s	q	NOM C_{T_s}	γ
140	▽	---	2.7	.81	0°
141	▽	---	4.0	.70	
142	△	---	6.3	.55	
143	◇	---	10.6	.25	

D170-10039-1

Figure 153

LONGITUDINAL CHARACTERISTICS
NO GROUND EFFECT
 $\alpha_F = 0^\circ$, $\delta_F = 40^\circ$, $h/B = 1.25$
FULL SPAN SLATS



FOUR PROP TILT WING MODEL VR068Q (FULL SPAN) CLCS VS IW DEGREES	BVWT 67 1/4/71
---	----------------------

RUN	SYM	Δ	q
140	▽	---	2.7
141	▽	---	4.0
142	▽	---	6.3
143	◇	---	10.6

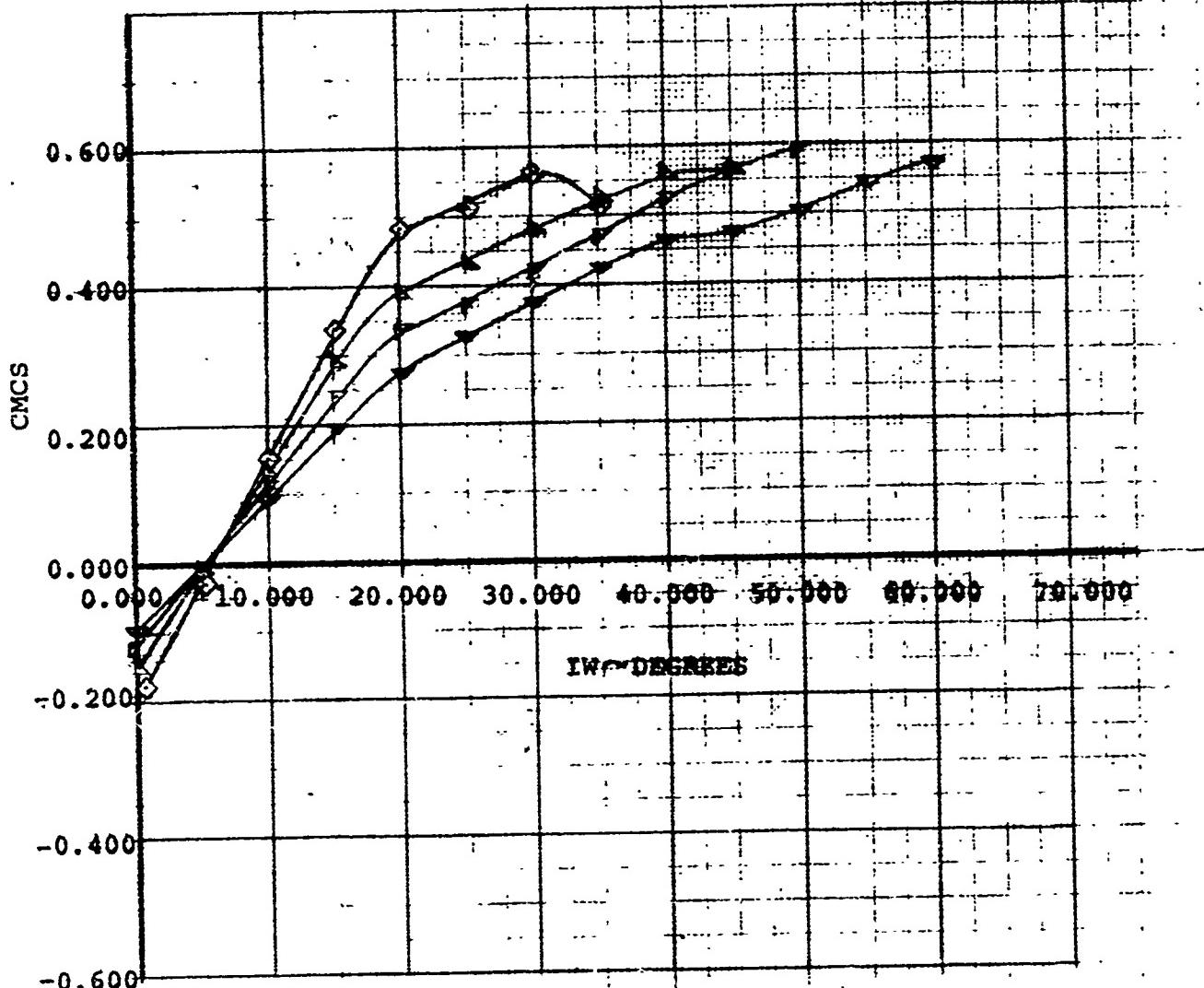
NOM C_{T_0}

Y

D170-10039-1

Figure 1454

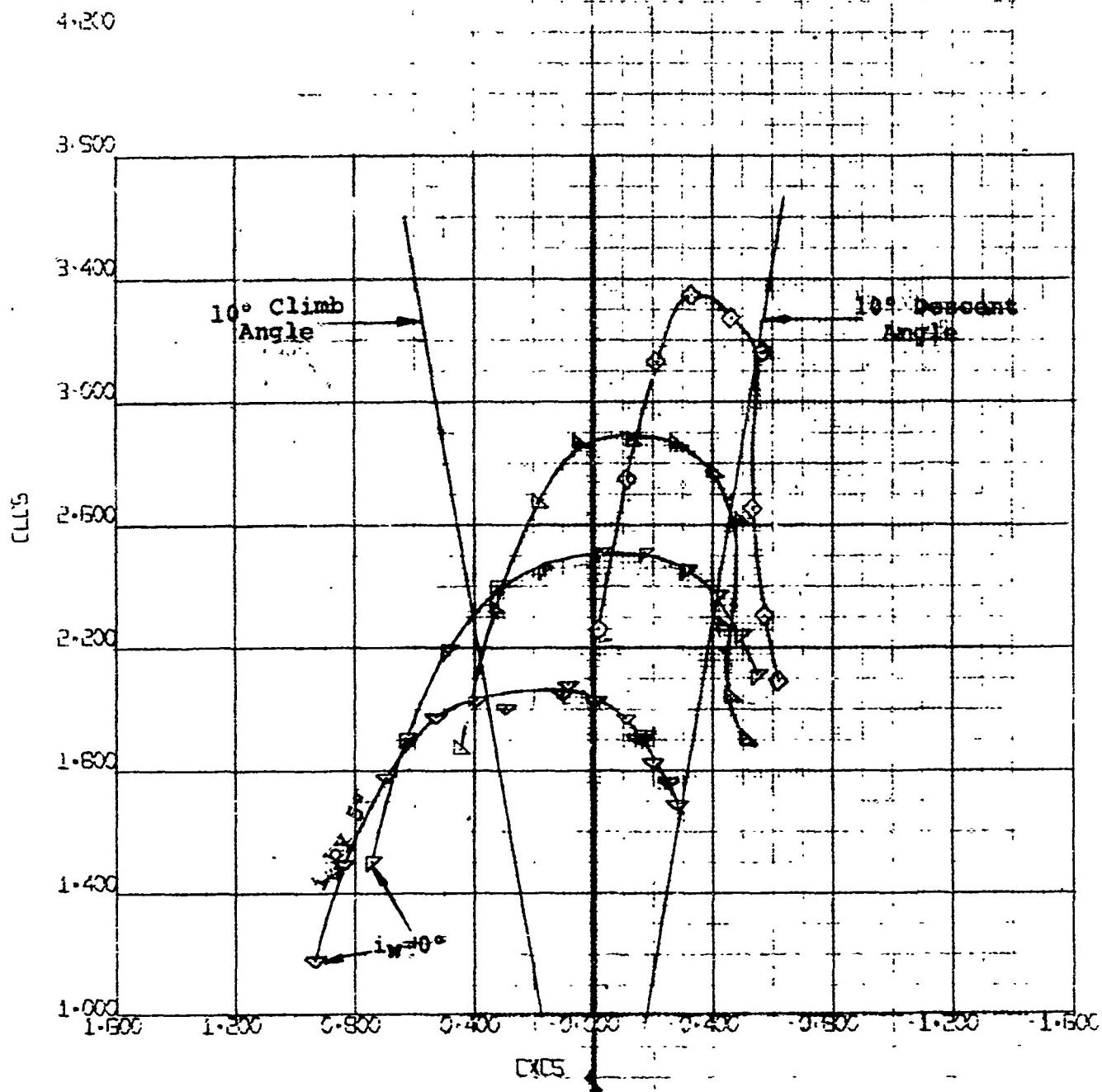
LONGITUDINAL CHARACTERISTICS
IN GROUND EFFECT
 $a_p = 0^\circ$, $a_g = 40^\circ$, $h/D_m = 2.5$
FULL SPAN SLATS



FOUR PROP TILT WING . BVWT
MODEL VRQ68Q (FULL SPAN) 67
CMCS VS IW DEGREES 1/4/71

RUN	SYM	Δ	q	NOM CT _s	γ
128	▽	---	2.7	.81	0°
129	▽	---	4.0	.70	
130	▽	---	6.3	.55	
131	◇	---	10.6	.25	

LONGITUDINAL CHARACTERISTICS
IN GROUND EFFECT
 $a_F = 0.6$, $\alpha_F = 60^\circ$, $h/D = 1.25$
FULL SPAN SLATS



FOUR-PROP TILT WING
MODEL VR08BG (FULL SPAN)
CLCS VS. CXCS

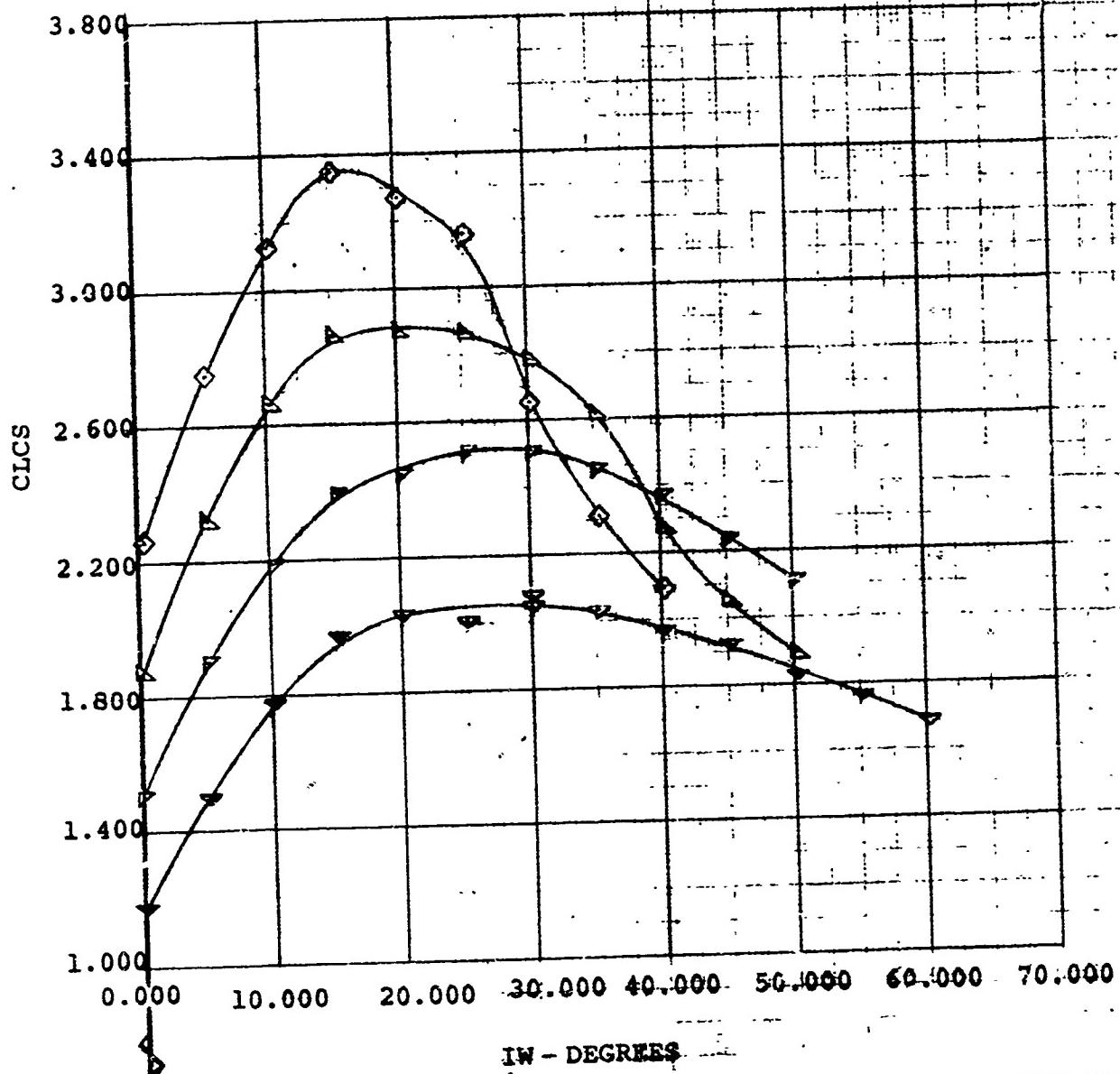
BWWT
67
11-4-71

D170-10039-1

Figure 156

RUN	SYM	Δ	q	NOM CT _S	γ
128	▼	---	2.7	.81	0°
129	▽	---	4.0	.70	
130	△	---	6.3	.55	
131	◇	---	10.6	.25	

LONGITUDINAL CHARACTERISTICS
IN GROUND EFFECT
 $\alpha_F = 9^\circ$, $\delta_F = 60^\circ$, $R/D = 1.25$
FULL SPAN SLATS



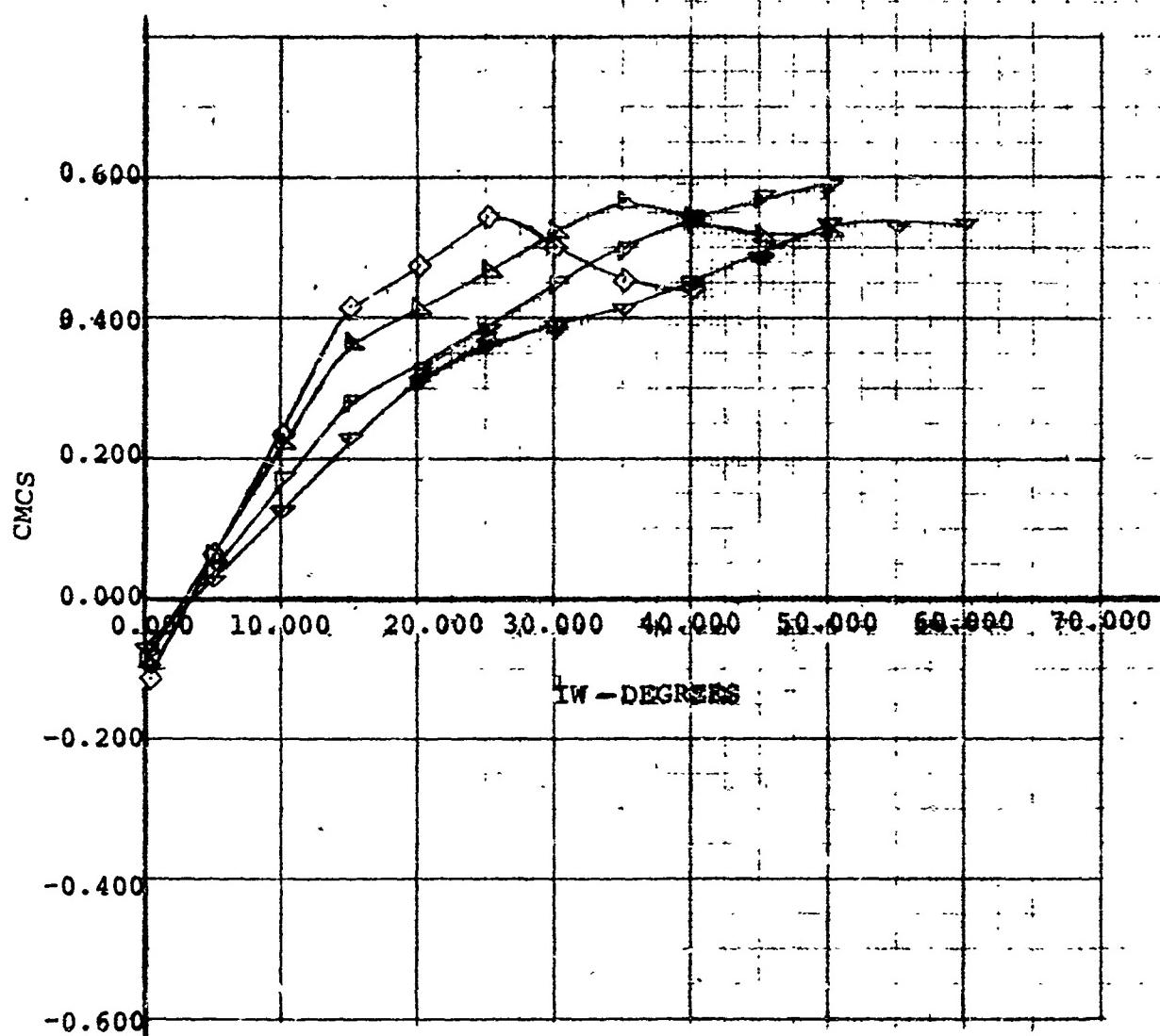
FOUR PROP TILT WING MODEL VR068Q(FULL SPAN) CLCS VS IW DEGREES	BVWT 67 12/17/70
--	------------------------

RUN	SYM	Δ	q	NOM	C_{T_s}	γ
128	▼	---	2.7	.81		
129	▽	---	4.0	.70		
130	△	---	6.3	.55		
131	◇	---	10.6	.25		

D170-10038-1

Figure 157

LONGITUDINAL CHARACTERISTICS
IN GROUND EFFECT
 $a_E = 0$, $\delta_E = 60^\circ$, $h/D = 1.25$
FULL SPAN SLATS

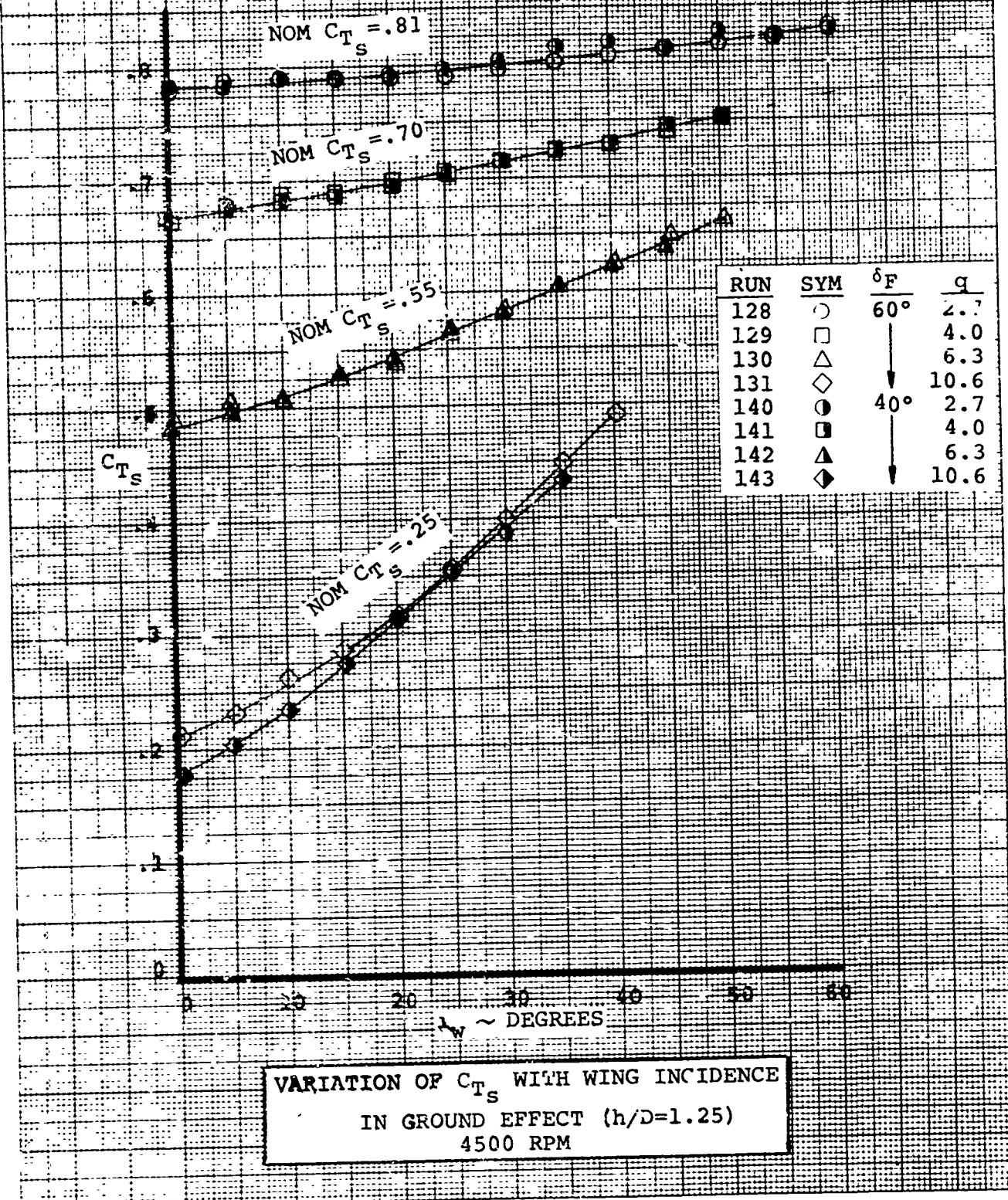


FOUR PROP TILT WING
MODEL VR068Q (FULL SPAN)
CMCS VS TW / DEGREES

BVWT	67
12/17/71	

NOTES:

1. Model VRO68
2. Data from BVWT 067
3. Full Span Slats
4. Horizontal Tail Off
5. Zero Fuselage Angle
6. Zero Cyclic Angle



A check of the stabilizer effectiveness in the influence of the ground was desired as a part of the longitudinal investigation. This check was made at nominal slipstream thrust coefficient of 0.55, which corresponds to a full scale speed in the order of 60 knots. At this selected transition speed, the horizontal tail is still an important element of the low speed longitudinal control system.

Figures 159 through 161 present the three component results of the investigation. As in the previous I.G.E. longitudinal runs, the testing was performed via wing tilt sweeps with a level fuselage. The data, shown in slipstream coefficient form, was acquired with a 40° flap deflection and a cyclic hub operating speed of 4500 RPM.

A wing tilt angle of 11° was chosen for determining the horizontal tail pitching moment effectiveness from the results of the stabilizer angle runs presented in Figure 159. This tilt angle matches the condition selected for establishing the comparable O.G.E. horizontal tail effectiveness with 15° of wing tilt. The O.G.E. tail effectiveness data presented in Figure 71 of Reference 1 was obtained with 60° of flap and the collective set of hubs operating at 6800 RPM, settings different than those used during the in-ground effect testing. These differences, however, should have only a minor influence on the comparison.

Figure 159 shows a $\Delta C_{M_S}/\Delta A$ of .0345 for the in-ground effect condition, which compares to an out-of-ground effect value of .0338 at 0.52 C_{T_S} (Figure 71 of Reference 1). It would be expected that the horizontal tail effectiveness in-ground effect would increase to some extent by the combined influence of a larger q acting at the tail due to the ground plane suppressing the downward deflection of the wake, plus the increase in effective aspect ratio of the tail due to ground proximity.

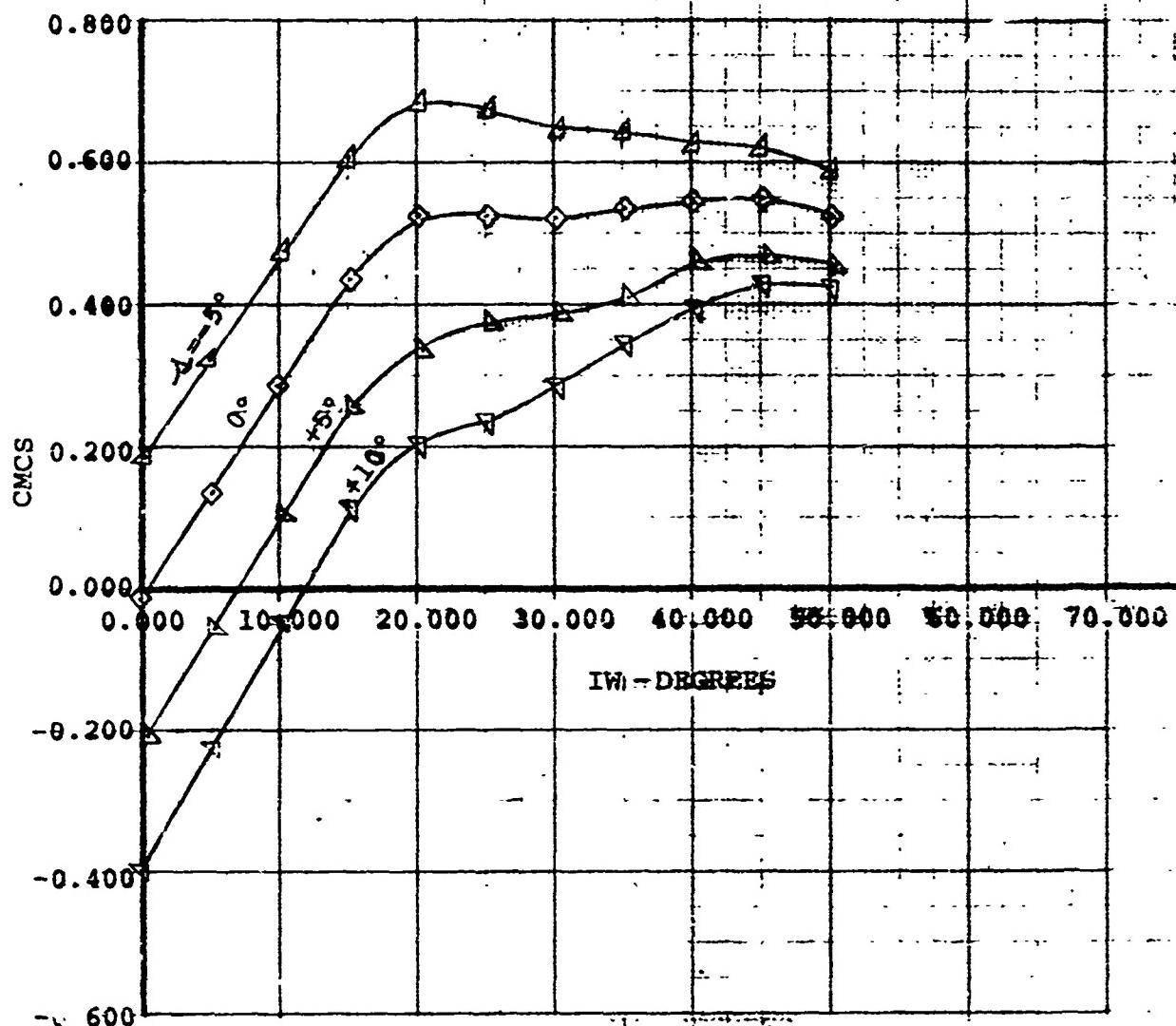
D170-10039-1

Figure 159

RUN	SYM	α	q	NOM C_{T_s}	γ
144	A	+5°	6.3	.55	0°
146	B	-5°			
147	C	+10°			
148	D	0°			

LONGITUDINAL CHARACTERISTICS
IN GROUND EFFECT
 $\alpha_F = 0$, $\delta_F = 40^\circ$, $b/D = 1.25$
FULL SPAN SLATS

HORIZONTAL TAIL ON
MOMENTS ABOUT WING PIVOT

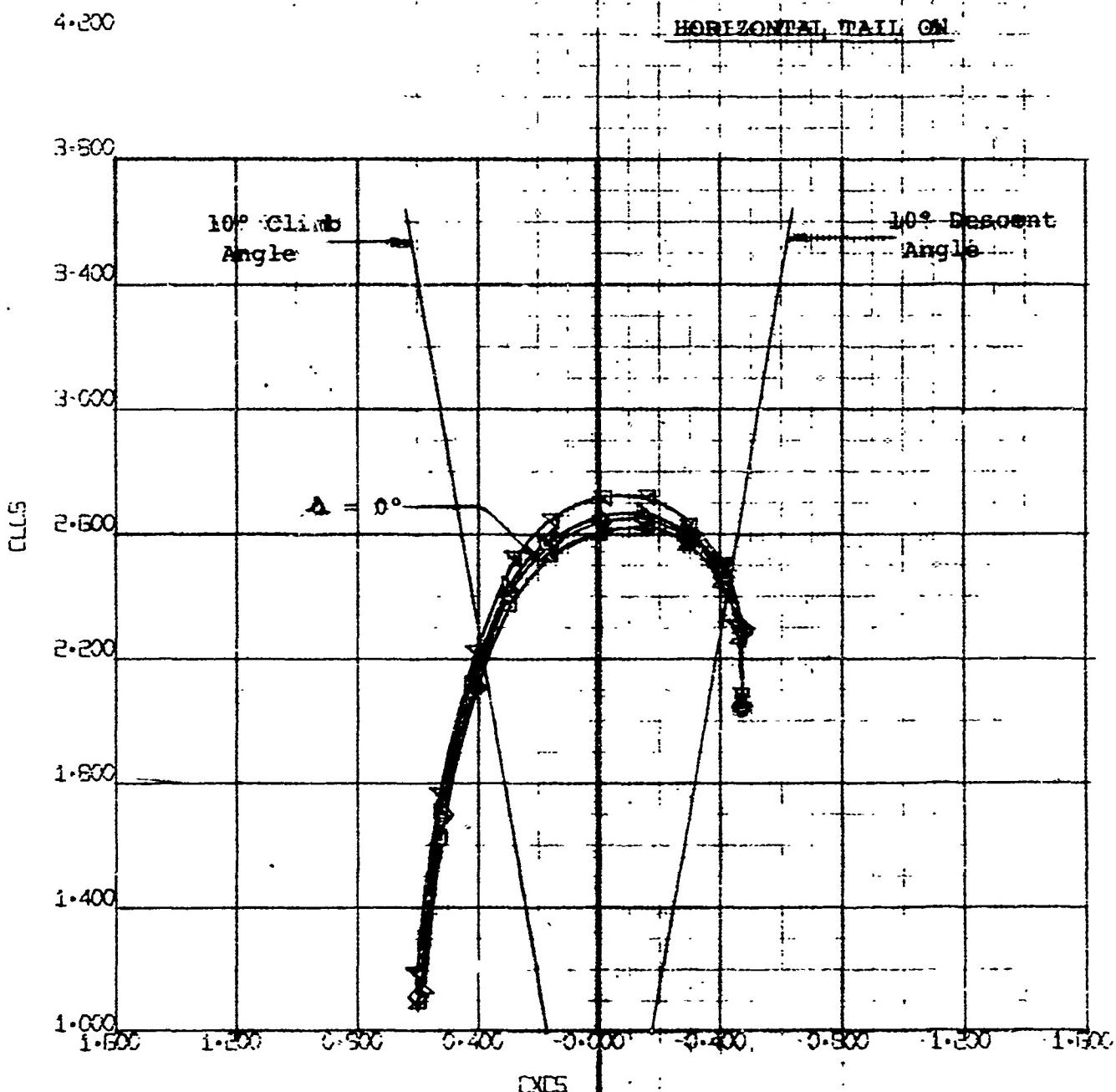


FOUR PROP TILT WING
MODEL VR068Q (FULL SPAN
CNCS VS IWI DEGREES)

BVWT
67
1/4/71

RUN	SYM	Δ	a	NOM CT _s
144	□	+5°	6.3	.58
146	△	+5°		
147	▽	+10°		
148	◊	0°		

LONGITUDINAL CHARACTERISTICS
IN GROUND EFFECT
 $\delta F = 0$, $\delta F = 40^\circ$, $h/D = 1.25$
FULL SPAN SLATS



FOUR-PROP TILT WING
MODEL VR06B0 (FULL SPAN)
CLDS VS. EXCS

BWWT
67
17 4/71

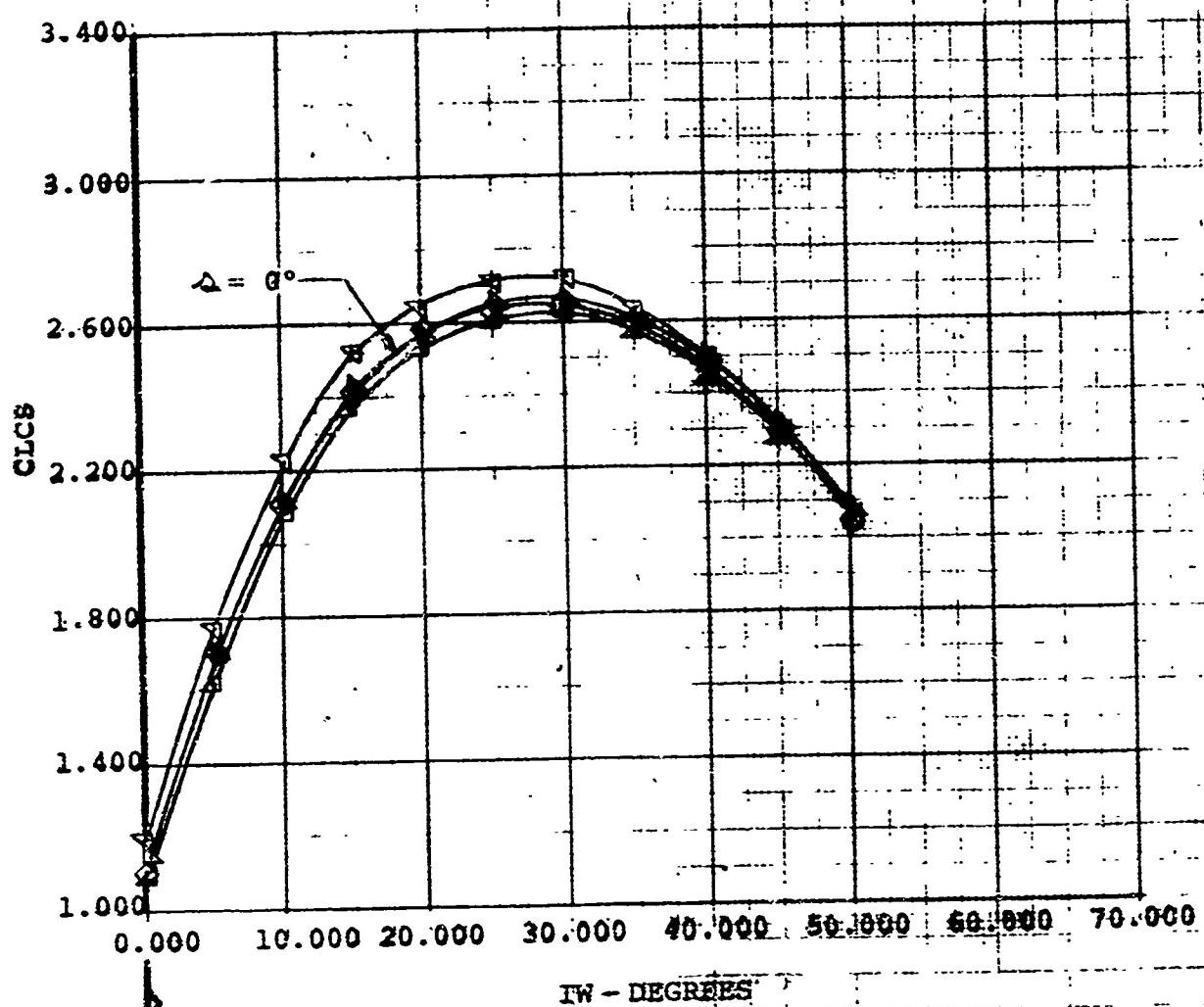
D170-10039-1

Figure 161

RUN	SYM	Δ	q	NOM C_{T_8}
144	▽	+5°	6.3	.58
146	△	-5°		
147	▽	+10°		
148	◇	0°		

LONGITUDINAL CHARACTERISTICS
IN GROUND EFFECT
 $S = 1.00, R = 40\%, h/D = 1.25$
FULL SPAN SLATS

HORIZONTAL TAIL ON



FOUR PROP TILT WING
MODEL VRO68Q (FULL SPAN)
CLCS VS IW DEGREES

BVWT
67
1/4/71

6.7.2 Cyclic Pitch Control Effectiveness in Ground Effect

This section presents the 40° flap data acquired on cyclic pitch control effectiveness in-ground effect during wing tilt sweeps with the tail off. Cyclic pitch angles of +4° and -4° were evaluated at the same slipstream thrust coefficients used for the non-cyclic portion of the in-ground effect longitudinal investigation.

Figure 162 compares the cyclic control pitch capability in terms of slipstream pitching moment per degree of cyclic, as measured in-ground effect from the data included in this report section, with that measured out-of-ground effect.

The O.G.E. data shown in Figure 162 was previously presented in Figure 41. Even though the flap angles are different for the two sets of data, 40° flaps for the I.G.E. data and 60° flaps for the O.G.E. data, this configuration change should not be of a magnitude that would materially alter the comparison. The variation of cyclic pitch effectiveness in-ground effect, namely, the small increase with C_{T_s} at a constant shaft angle (α_p) and the small decrease as the shaft angle is increased, are the same trends exhibited by the 1/12th scale isolated propeller data presented in Figure 41. Figure 162 shows that moving from an out-of-ground effect flight condition to a flight condition with the wheels 3 ft. off the ground results in some reduction in the cyclic pitch effectiveness, but only by an average of 6%.

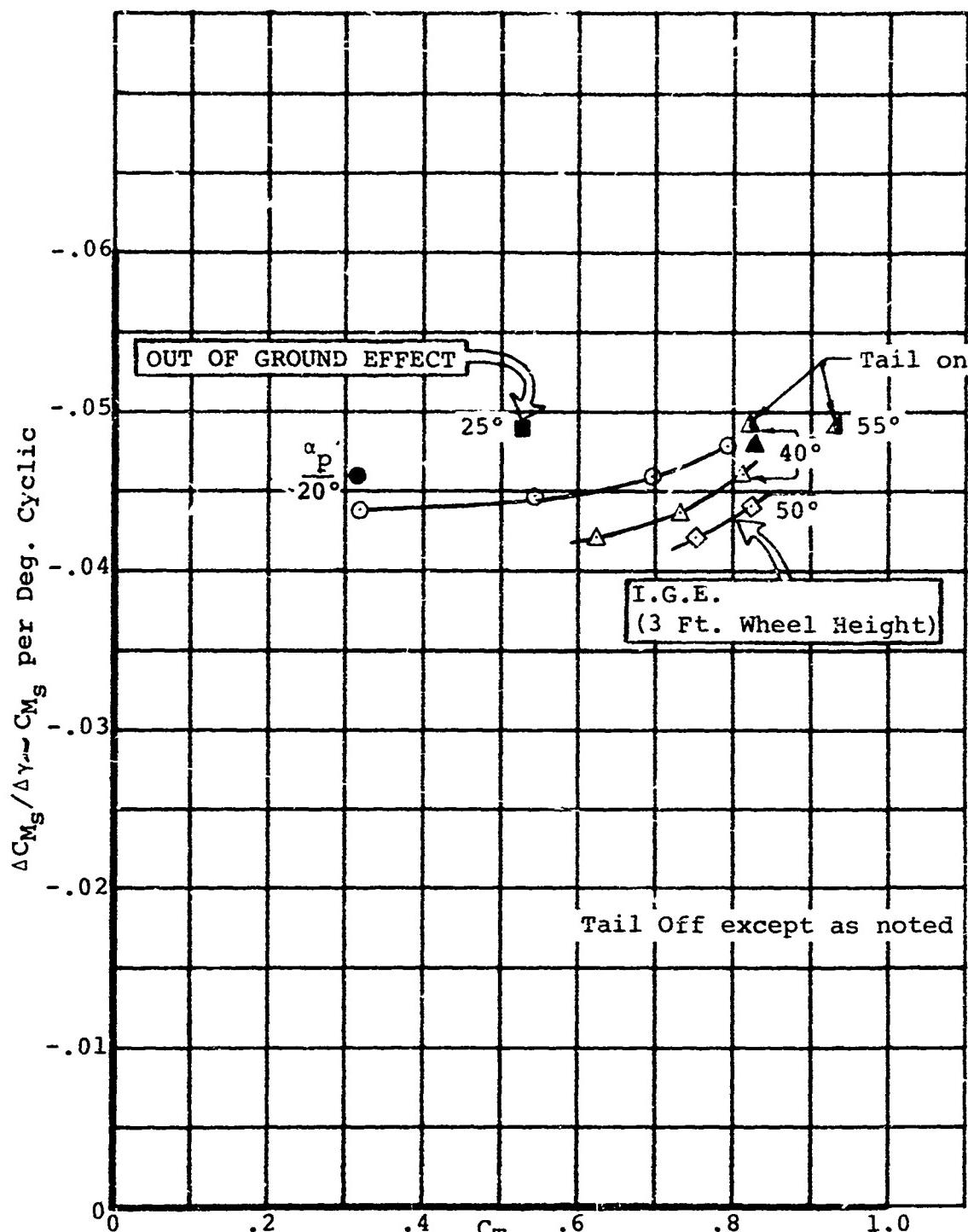
Three component data included in Figures 163 through 174 show a direct comparison of the influence of positive and negative cyclic on the pitching moment about the wing pivot, force polars and lift curves. The slipstream format data is presented in sets of three plots in the order of increasing slipstream thrust coefficient. Data of the first set was obtained at a nominal C_{T_s} of 0.25 and the last of the four sets was obtained at a nominal C_{T_s} of 0.81.

Wing tilt sweeps with a level fuselage, that were performed in lieu of the more conventional fuselage sweeps due to the low ground height involved, do not allow a direct data comparison to show the influence of ground effect on the aircraft longitudinal stability. An examination of the in-ground effect longitudinal pitching moment data does show, however, that the effect of cyclic pitch inputs on the variation of pitching moment with wing tilt angle to be small. A positive

cyclic pitch angle of +4° increases the tail-off pitching moment slope by a small percentage (about 6%) and a negative cyclic angle of -4° decreases it by a small percentage over the C_{T_s} range evaluated with representative wing tilt angles. This indication of the effect of cyclic pitch on longitudinal stability is in the same direction with respect to angularity of cyclic inputs and is of the same small magnitude as shown in Figure 45 for the out-of-ground effect tail-off case. Thus, it can be inferred that cyclic pitch control action in-ground effect has the same influence on longitudinal stability as recorded out-of-ground effect.

The in-ground effect lift curves interspersed in Figures 163 through 174 show the same trend observed out-of-ground effect, in that positive cyclic increases the lift curve slope and negative cyclic decreases it. Another item of interest is the larger incremental loss in maximum lift with positive cyclic at the lower thrust coefficients than was noted out-of-ground effect.

Figures 175 through 180 include the same three component data with cyclic pitch control applied, that was shown in Figures 163 through 174, but in a comparison of longitudinal characteristics for a constant cyclic pitch angle. Figures 175 through 177 present the +4° cyclic data and Figures 178 through 180 present the -4° cyclic data.



INFLUENCE OF GROUND EFFECT ON
CYCLIC PITCH EFFECTIVENESS

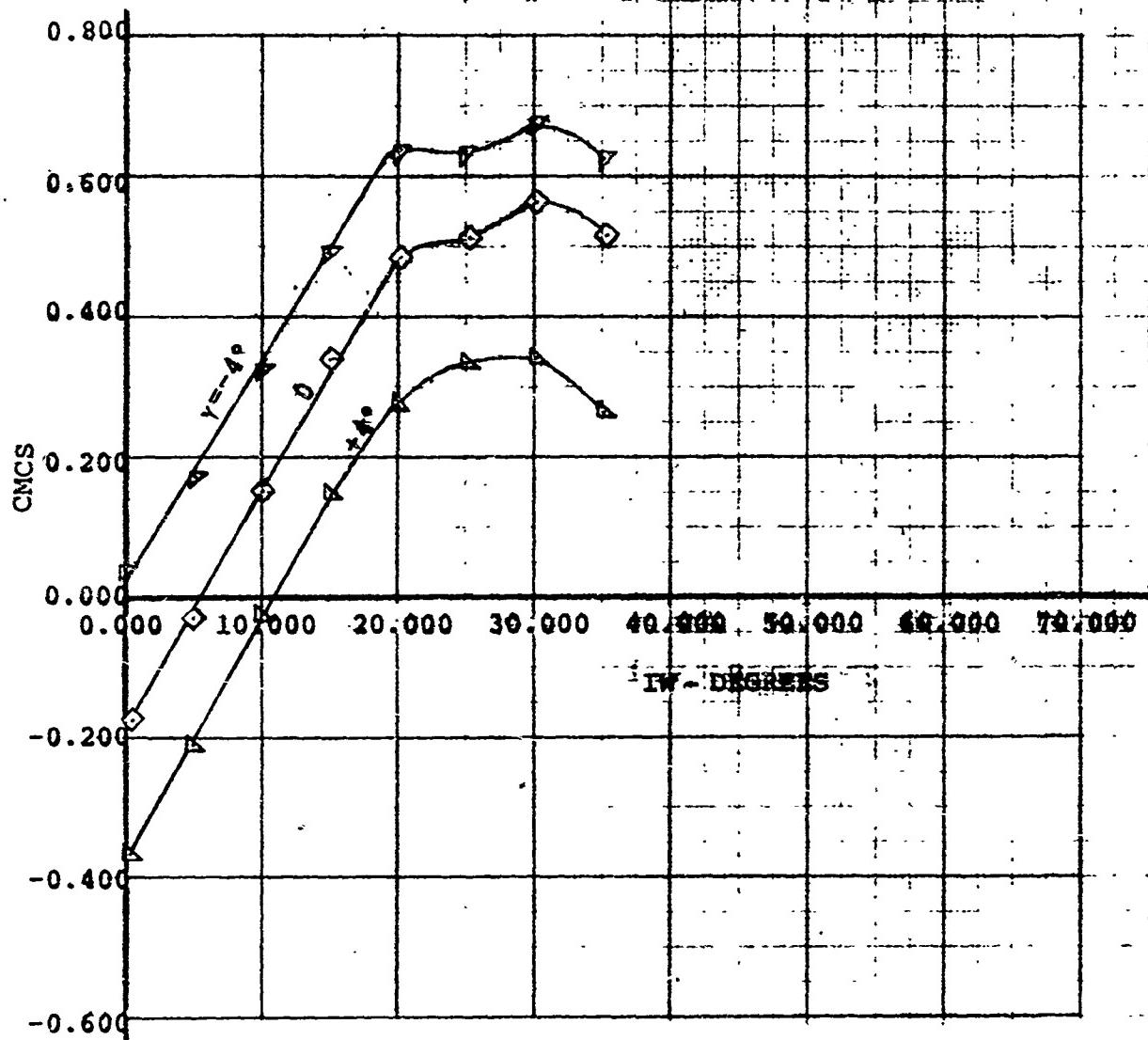
RUN	SYM	Δ	q	NOM C_{T_S}	γ
143	◇	---	10.6	.25	0
152	▽	---			+4°
156	▼	---			-4°

D170-1G039-1

Figure 153

LONGITUDINAL CHARACTERISTICS
IN GROUND EFFECT
 $c_F = 0^\circ$, $\delta_E = 40^\circ$, $h/D = 1.25$
FULL SPAN SLATS

With Cyclic Pitch Control



FOUR PROP TILT WING
MODEL VROSSQ (FULL SPAN)
CMCS VS IW - DEGREES

BVWT

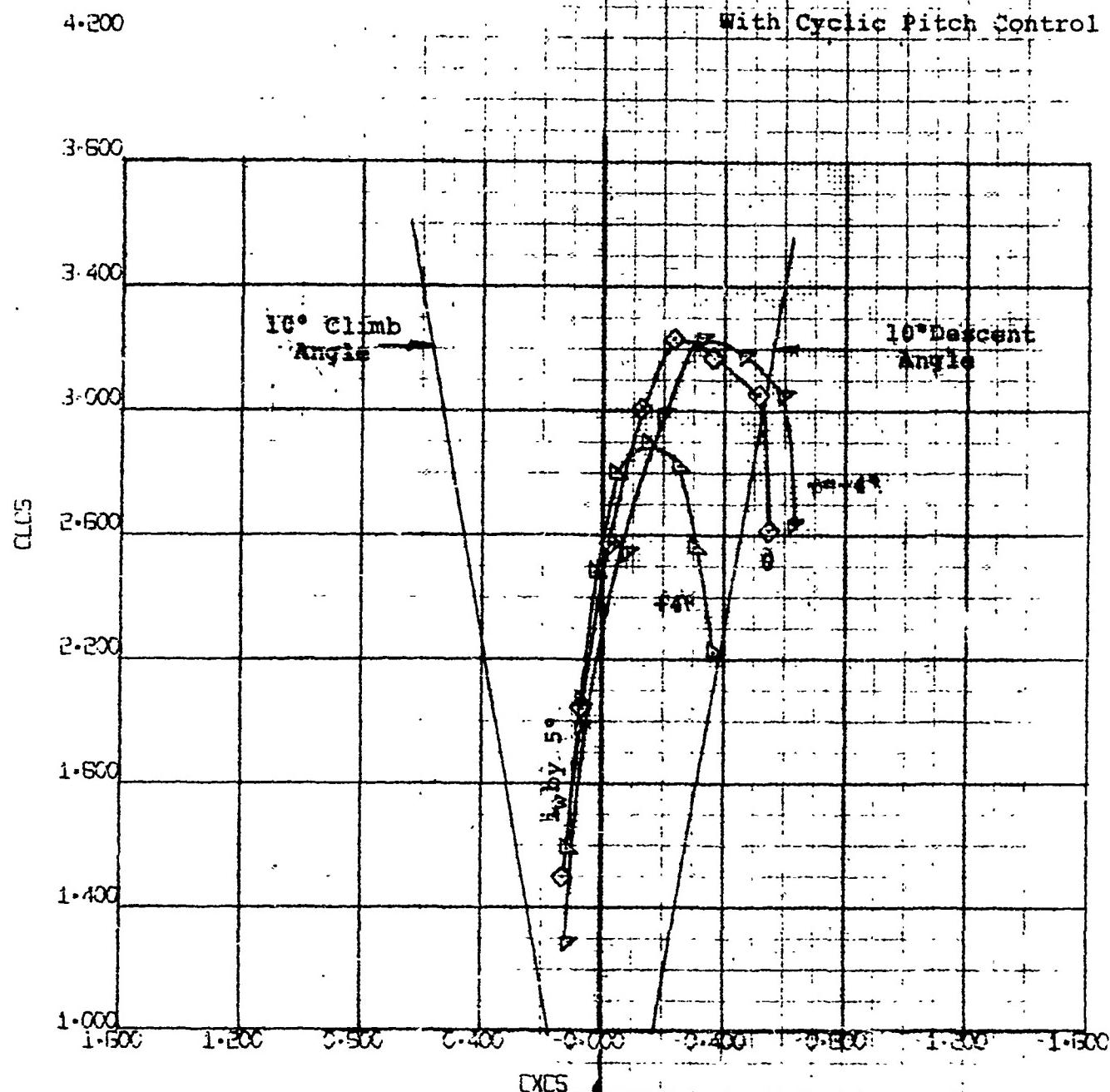
67

1/4/71

RUN	SYM	Δ	q	NOM C_{T_B}	y
143	◇	---	10.6	.25	0
152	△	---			+4°
156	▼	↓			-4°

NUMBER D170-10039-1
REV. LTR. Figure 164

LONGITUDINAL CHARACTERISTICS
IN GROUND EFFECT
 $\mu_F = 0^\circ$, $\delta_F = 10^\circ$, $n/D = 1.25$
FULL SPAN SLATS

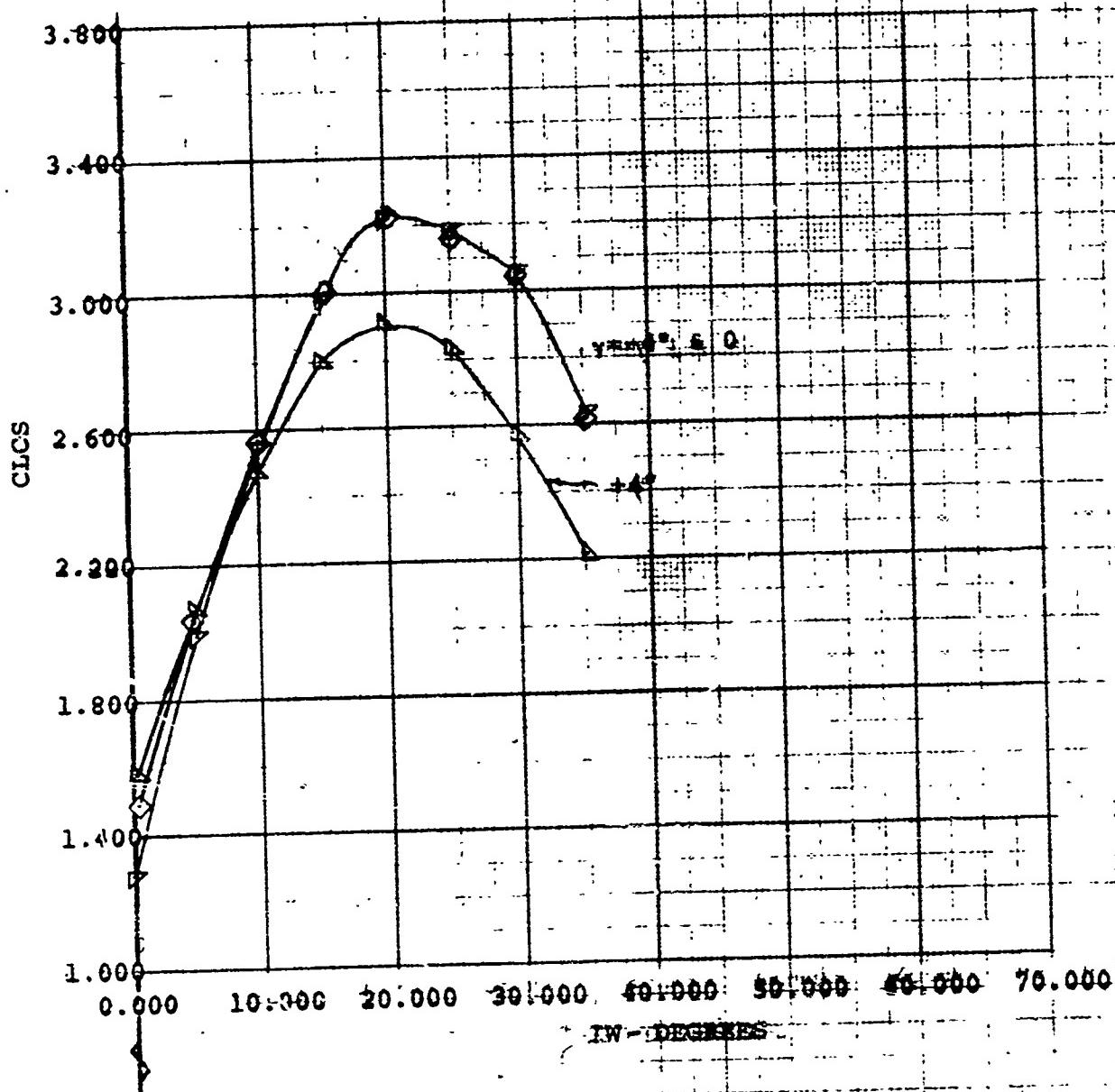


FOUR-PROP TILT WING MODEL YR058C (FULL SPAN) CLCS VS. CXCS	BWNT 67 1/4/71
--	----------------------

RUN	SYM	Δ	q	NOM CT _s	γ
143	○	---	10.6	.75	0
152	△	---			+4°
156	□	---			-4°

ZONALITUDINAL CHARACTERISTICS
IN GROUND EFFECT
 $a_s = 0^\circ$, $\alpha = 10^\circ$, $b/D = 1.25$
FULL SPAN SLATS

With Cyclic Pitch Control



FOUR PROP TILT WING BVWT
MODEL VR068Q (FULL SPAN) 67
CLCS VS TW - DEGREES 1/4/71

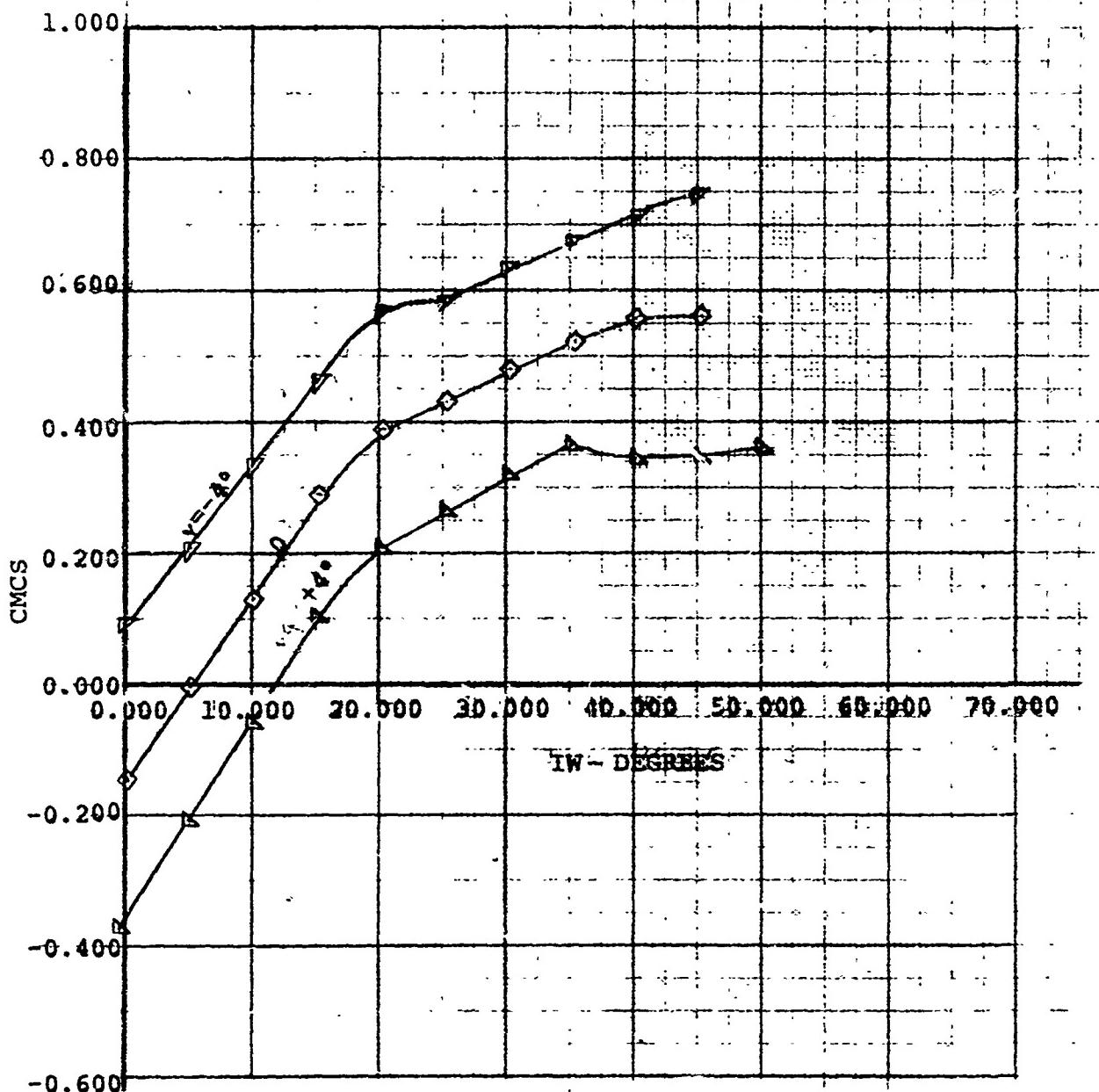
RUN	SYM	δ	q	NOM C_{Ts}	γ
142	◇	---	6.3	.59	0°
151	△	---	↓	↓	+4°
155	▽	---	↓	↓	-4°

B170-19839-1

Figure 166

LONGITUDINAL CHARACTERISTICS
IN GROUND EFFECT
 $\alpha_T = 0^\circ$, $\delta_T = 40^\circ$, $b/D = 1.25$
FULL SPAN SLATS

With Cyclic Pitch Control



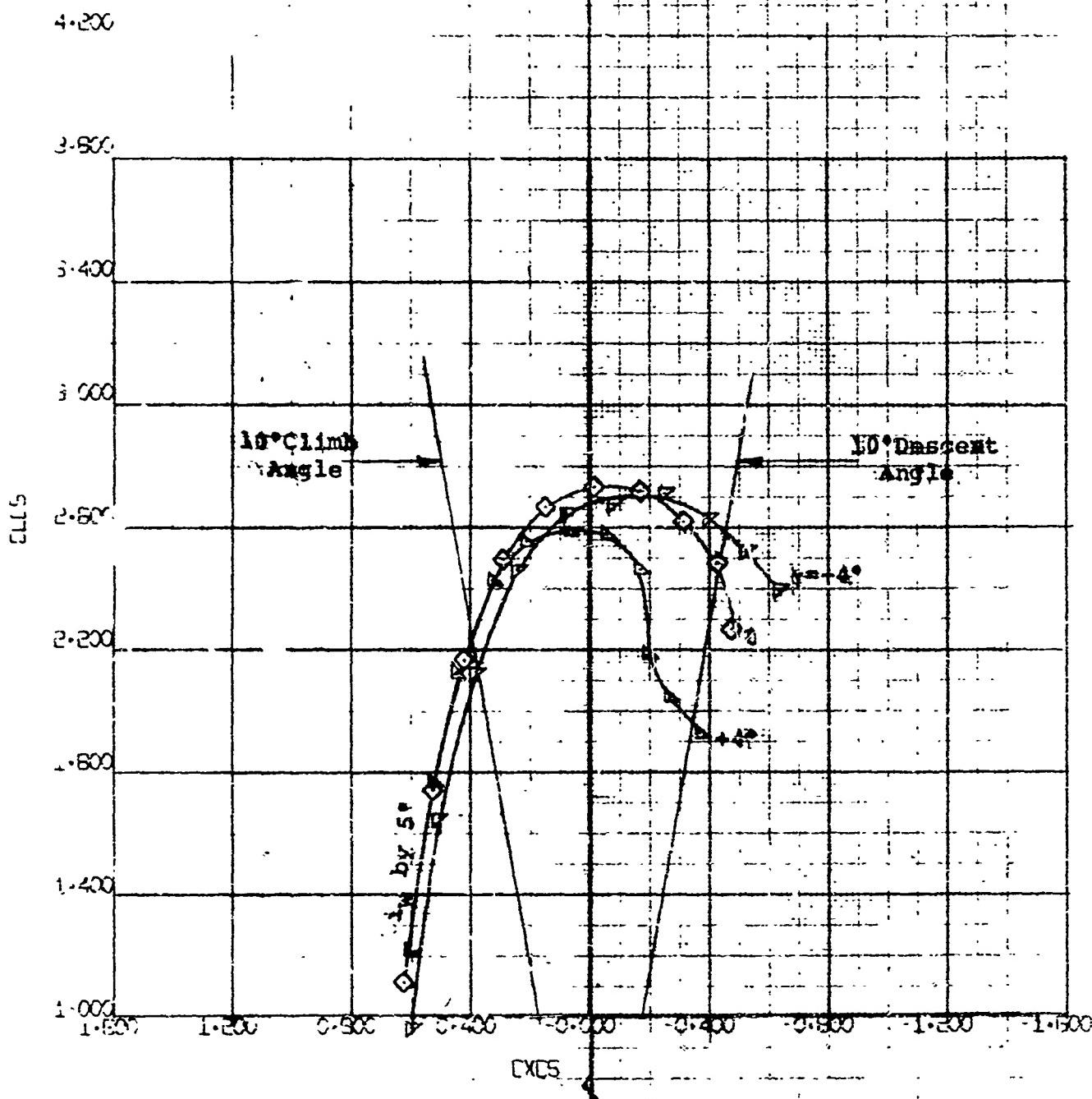
FOUR PROP TILT WING MODEL VRO68Q (FULL SPAN)	BVWT 67
CMCS VS IW - DEGREES	1/4/71

RUN	SYM	Δ	q	NOM C_{T_S}	γ
142	◊	---	6.3	.56	0°
151	■	---			+4°
155	□	---			-4°

NUMBER D170-10039-1
REV. LTR. Figure 167

LONGITUDINAL CHARACTERISTICS
IN GROUND EFFECT
 $a_F = 0^\circ$, $b_F = 40^\circ$, $R/D = 1.25$
FULL SPAN SLATS

With Cyclic Pitch Control



FOUR-PROP TILT WING
MODEL VR-200 (FULL SPAN)
CL(s) VS. EXCS

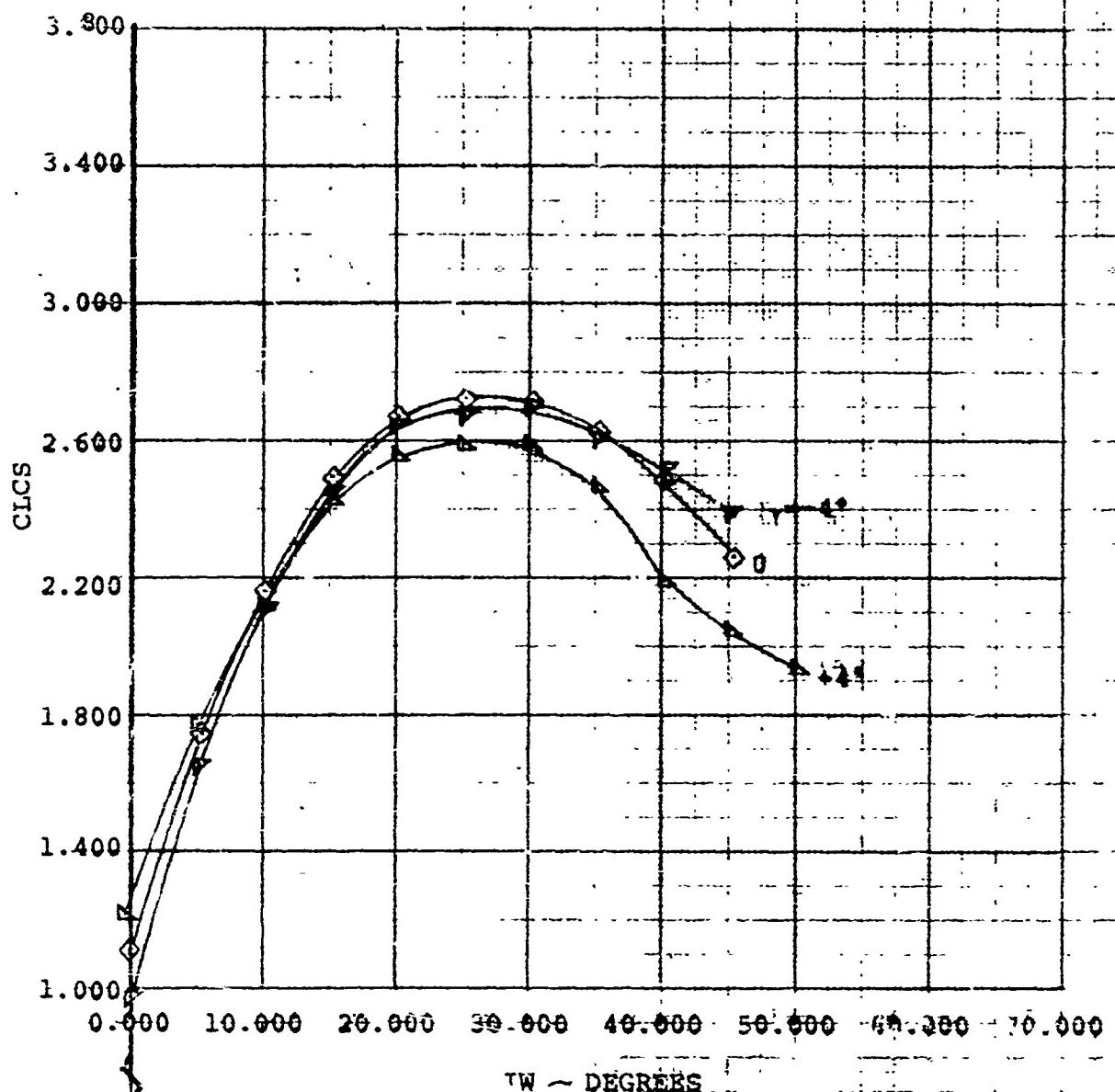
BWNT
67
1/4/71

RUN	SYM	Δ	a	NOM C_{T_0}	γ
142	◊	---	6.3	.58	0°
151	△	---	+		+4°
155	▽	---	-		-4°

D170-10039-1
Figure 168

LONGITUDINAL CHARACTERISTICS
IN GROUND EFFECT
 $\alpha_p = 9^\circ, \delta_F = 40^\circ, h/D = 1.25$
FULL SPAN SLATS

With Cyclic Pitch Control



FOUR PROP TILT WING MODEL VR068Q (FULL SPAN) CLCS VS TW - DEGREES	BVWT 67 1/4/71
---	----------------------

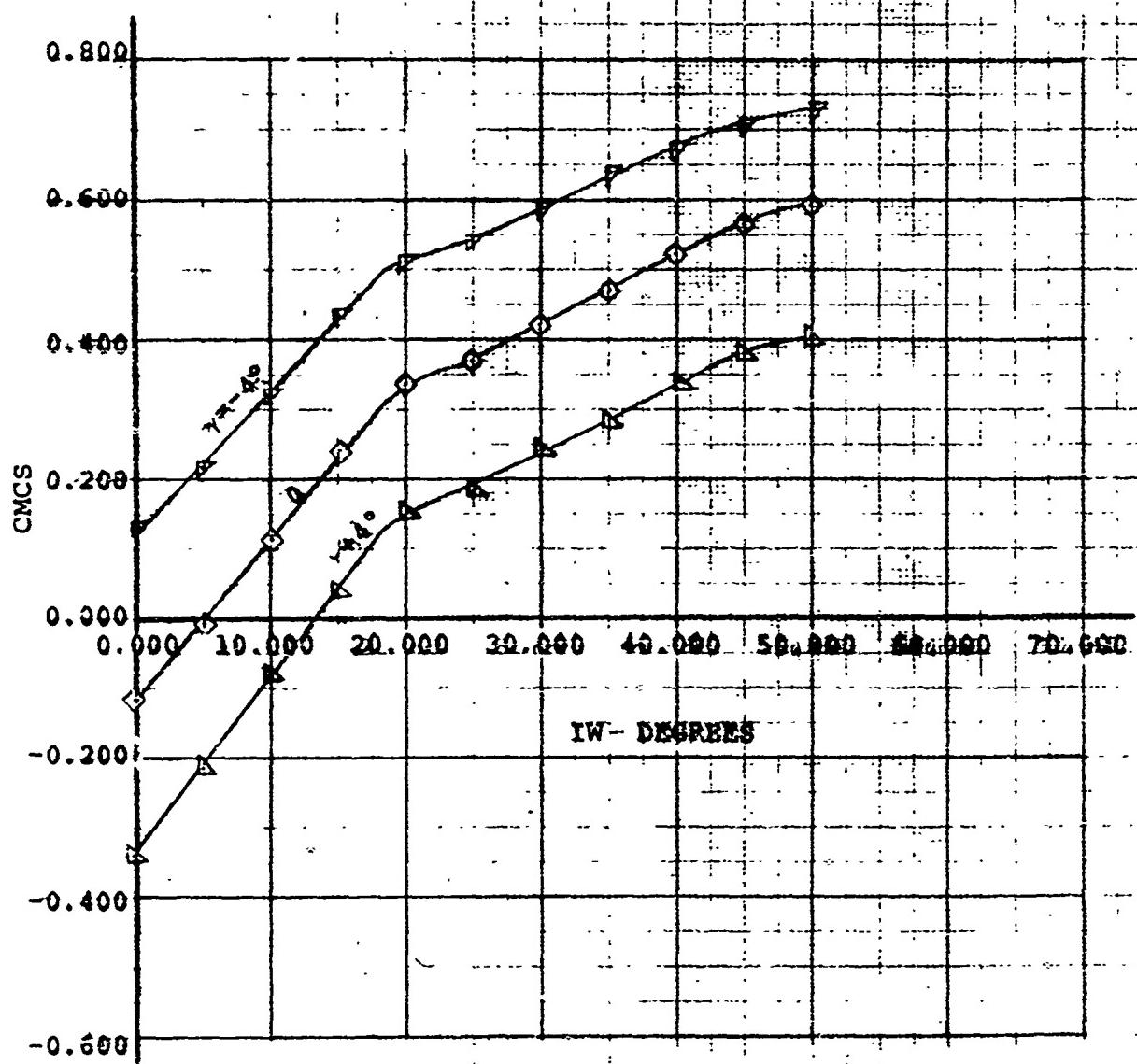
D170-10039-1

Figure 169

RUN	SYM	α	q	NOM C_T	γ
141	◊	---	4.0	.70	0°
150	▽	---			+4°
154	□	---			-4°

LONGITUDINAL CHARACTERISTICS
IN GROUND EFFECT
 $\delta F = 0^\circ$, $\delta p = 60^\circ$, $h/D = 1.25$
FULL SPAN SLATS

With Cyclic Pitch Control



IW - DEGREES

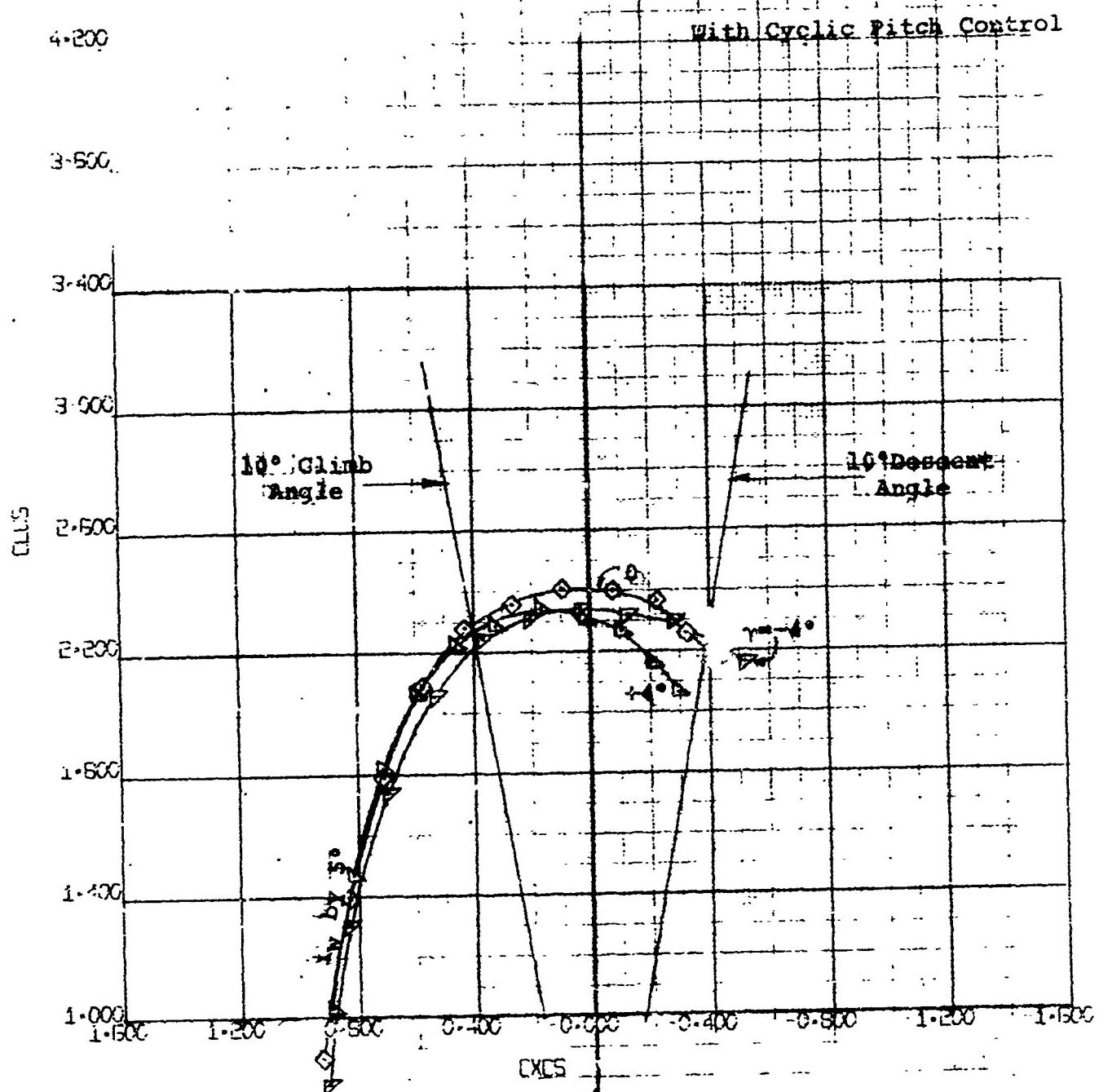
FOUR PROP TILT WING MODEL VRO68Q (FULL SPAN) CMCS VS IW DEGREES	BVWT 67
---	------------

1/4/71

NUMBER DL70-10039-1
REV. LTR. Figure 170

RUN	SYM	Δ	α	NOM C_{T_s}	γ
141	◊	---	4.0	.70	0°
150	△	---			+4°
154	▽	---			-4°

NONDIMENSIONAL CHARACTERISTICS
IN GROUND EFFECT
 $\alpha_F = 0^\circ$, $\delta_F = 40^\circ$, $B/D = 1.25$
FULL SPAN SLATS



FOUR-PROP TILT WING MODEL VROS60 (FULL SPAN) CL/CL _s VS. CX/Cs	BWHT 67
	1/4 71

D170-10039-1

Figure 47a

RUN	SYM	Δ	q	NOM-GTS	γ
141	◇	---	4.0	.70	0°
150	△	---			+4°
154	▽	---			-4°

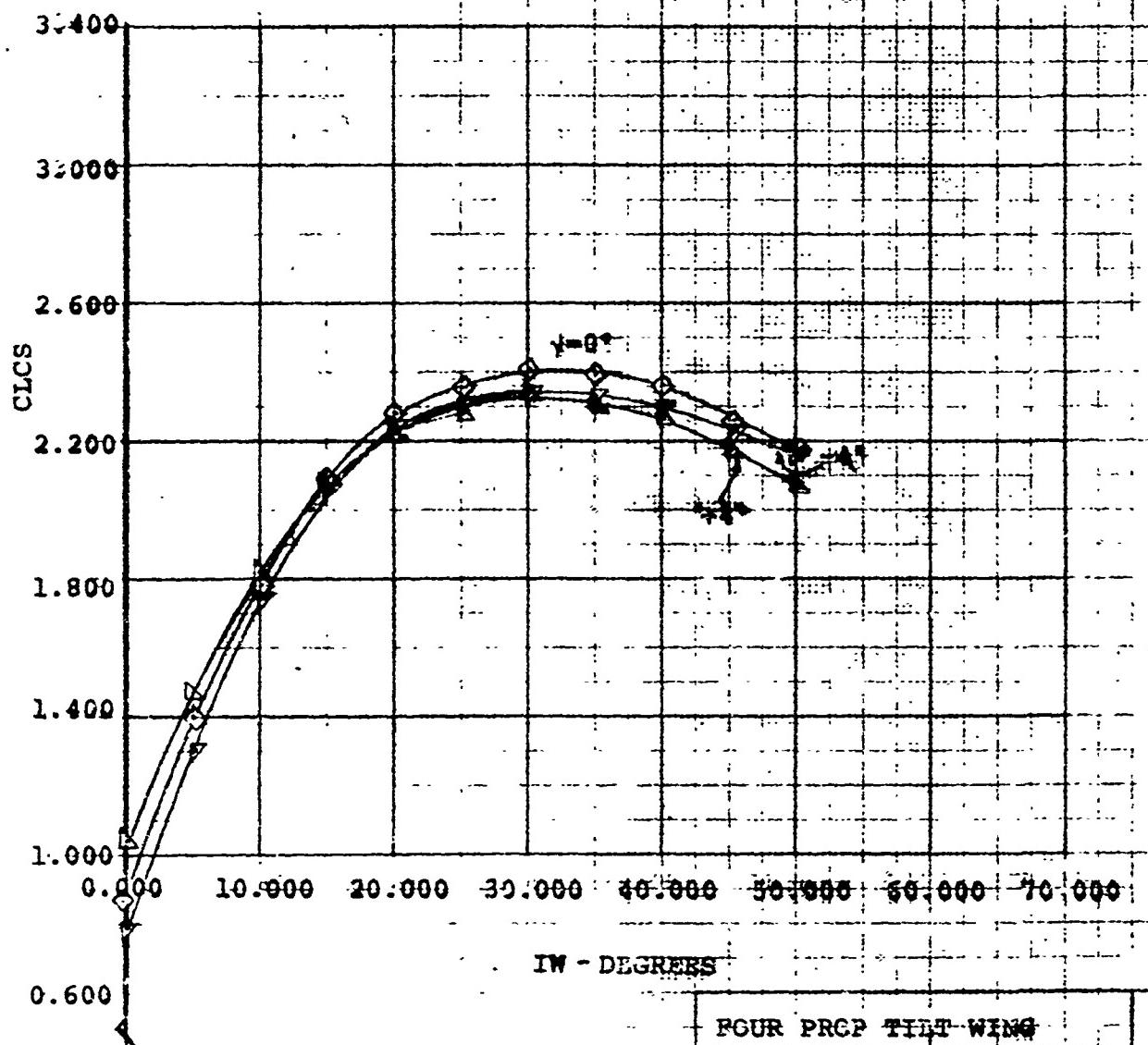
LONGITUDINAL CHARACTERISTICS

IN GROUND EFFECT

 $\beta_F = 0^\circ, \delta_F = 40^\circ, h/D = 1.25$

FULL SPAN SLATS

With Cyclic Pitch Control



FOUR PROP TILT WING MODEL VR068Q (FULL SPAN)	BVWT 67
---	------------

CLCS VS IW - DEGREES

1/4/71

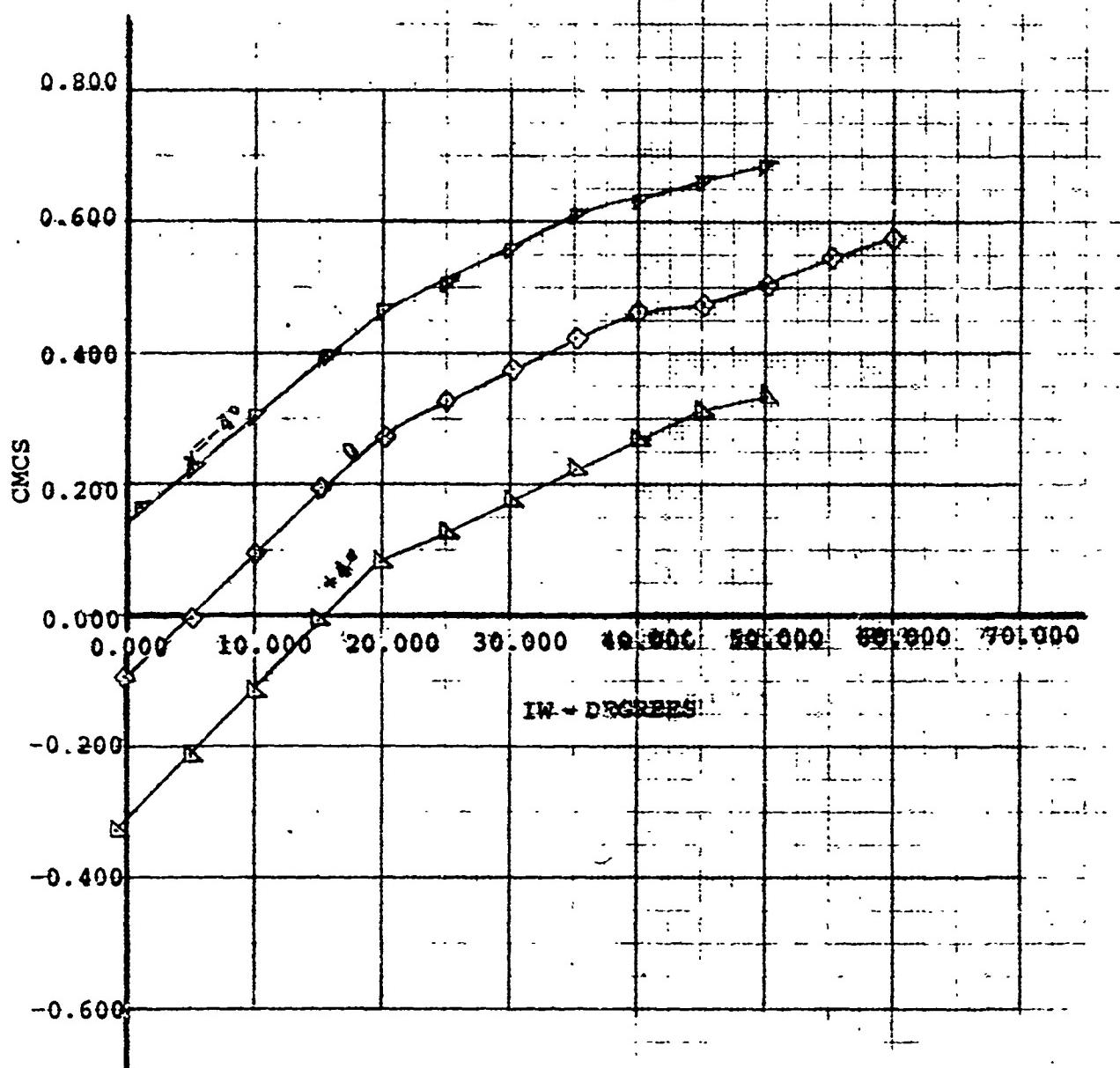
D170-10039-1

Figure 172.

RUN	SYM	Δ	q	NOM C_{T_8}	γ
140	◊	---	2.7	.81	0
149	▽	---			+4°
153	▼	---			-4°

LONGITUDINAL CHARACTERISTICS
IN GROUND EFFECT
 $\alpha_p = 0^\circ$, $\delta_g = 40^\circ$, $h/D = 1.25$
FULL SPAN SLATS

With Cyclic Pitch Control



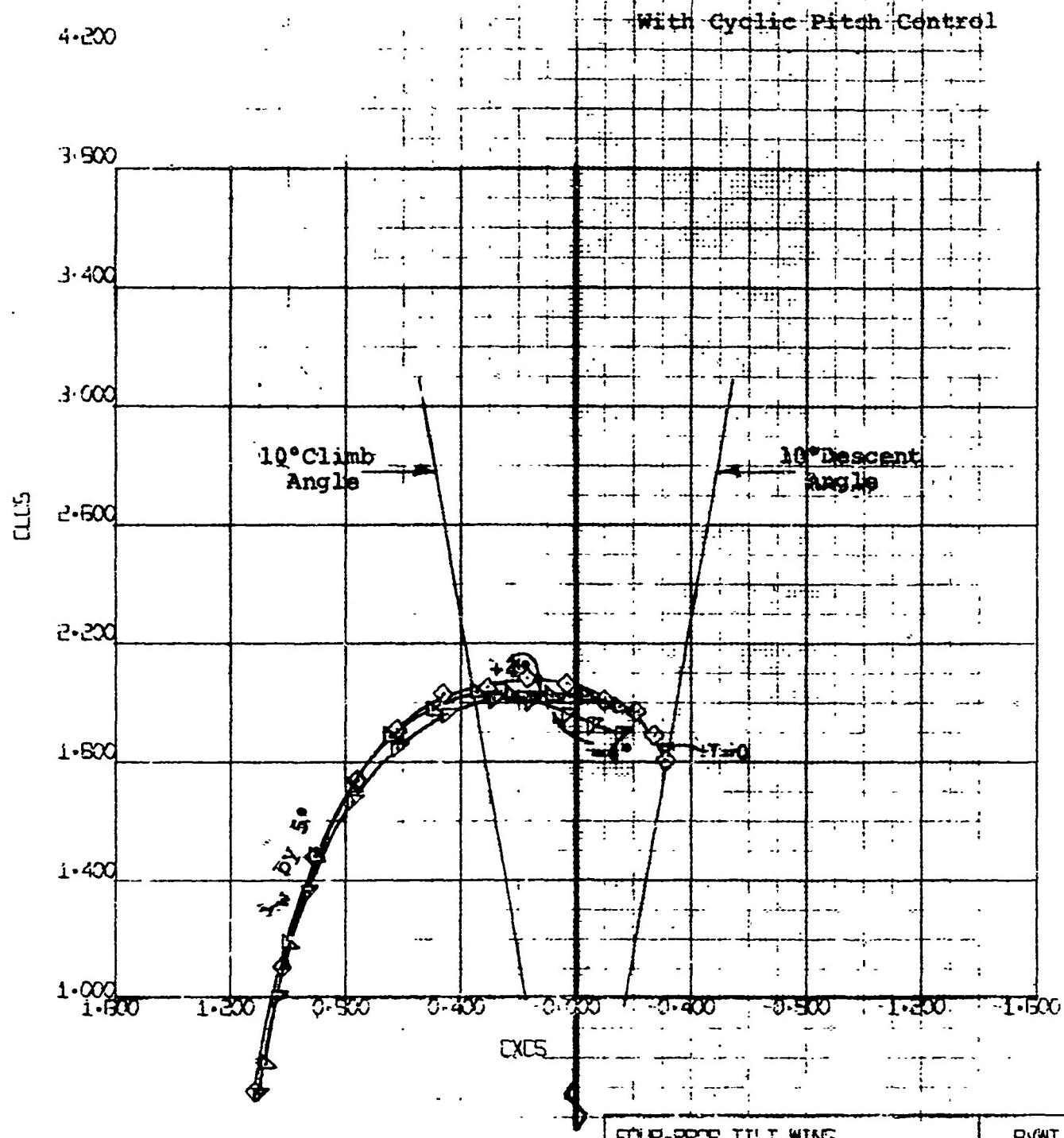
FOUR PROP TILT WING
MODEL VRO68Q (FULL-SPAN)
CMCS VS IW-DEGREES

BVWT	67
1/4/71	

RUN	SYM	Δ	q	NOM C_{T_8}	γ
140	◇	---	2.7	.81	0
149	△	---			+4°
153	▽	---			-4°

NUMBER D170-10039-1
REV. LTR. Figure 173

LONGITUDINAL CHARACTERISTICS
IN GROUND EFFECT
 $\alpha_F = 0^\circ$, $\delta_F = 40^\circ$, $H/D = 1.25$
FULL SPAN SLATS



FOUR-PROP TILT WING MODEL VR0820 (FULL SPAN) CLDS VS. EXCS	BWNT 67
	1/ 4/71

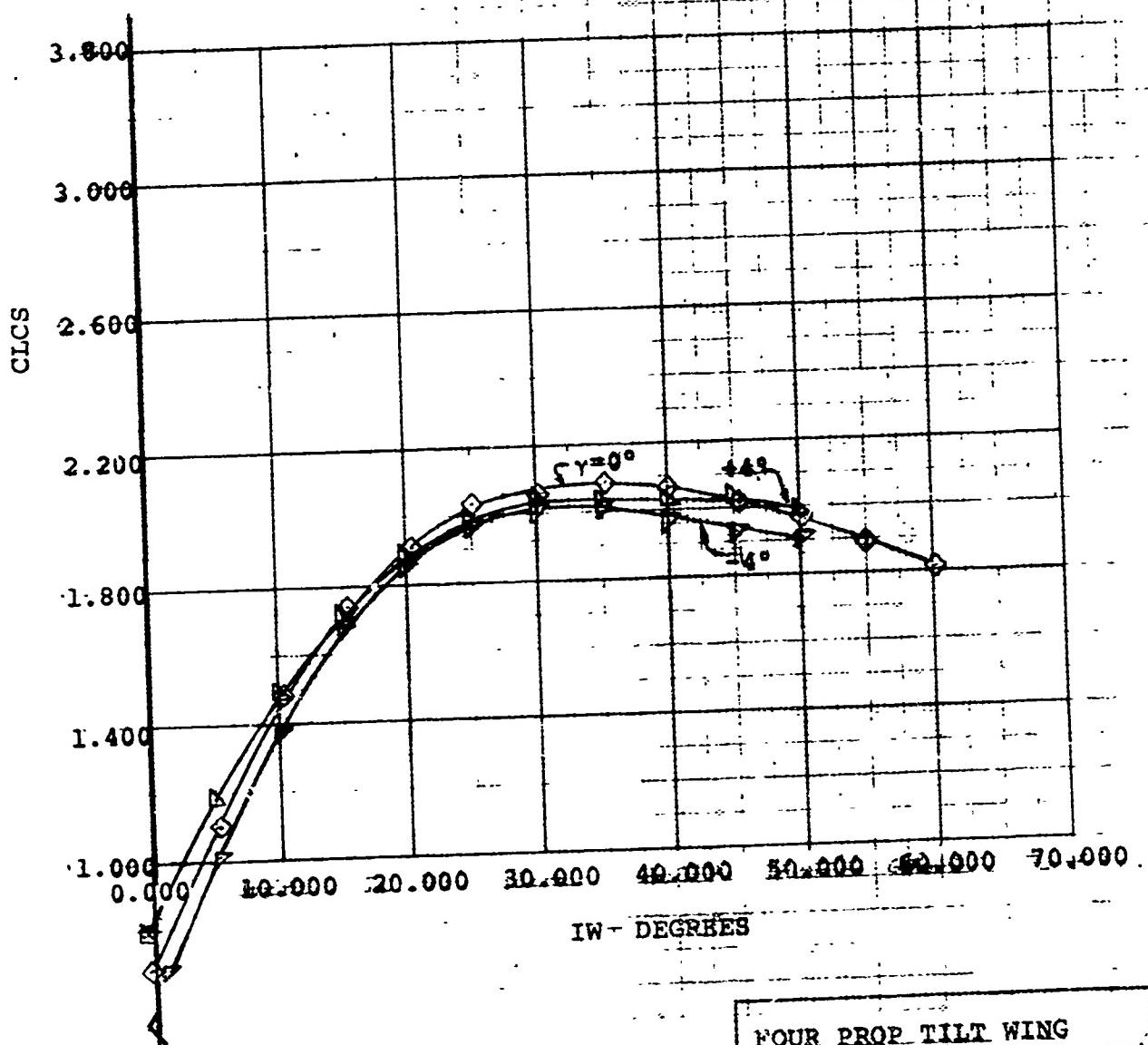
D170410039-1

Figure 174

RUN	SYM	Δ	q	NOM CT _S	γ
140	◇	---	2.7	.81	0
142	△	---			+4°
153	▽	---			-4°

LONGITUDINAL CHARACTERISTICS
IN GROUND EFFECT
 $a_p = 0^\circ$, $\beta = 40^\circ$, $b/D = 1.25$
FULL SPAN SLATS

with cyclic pitch control



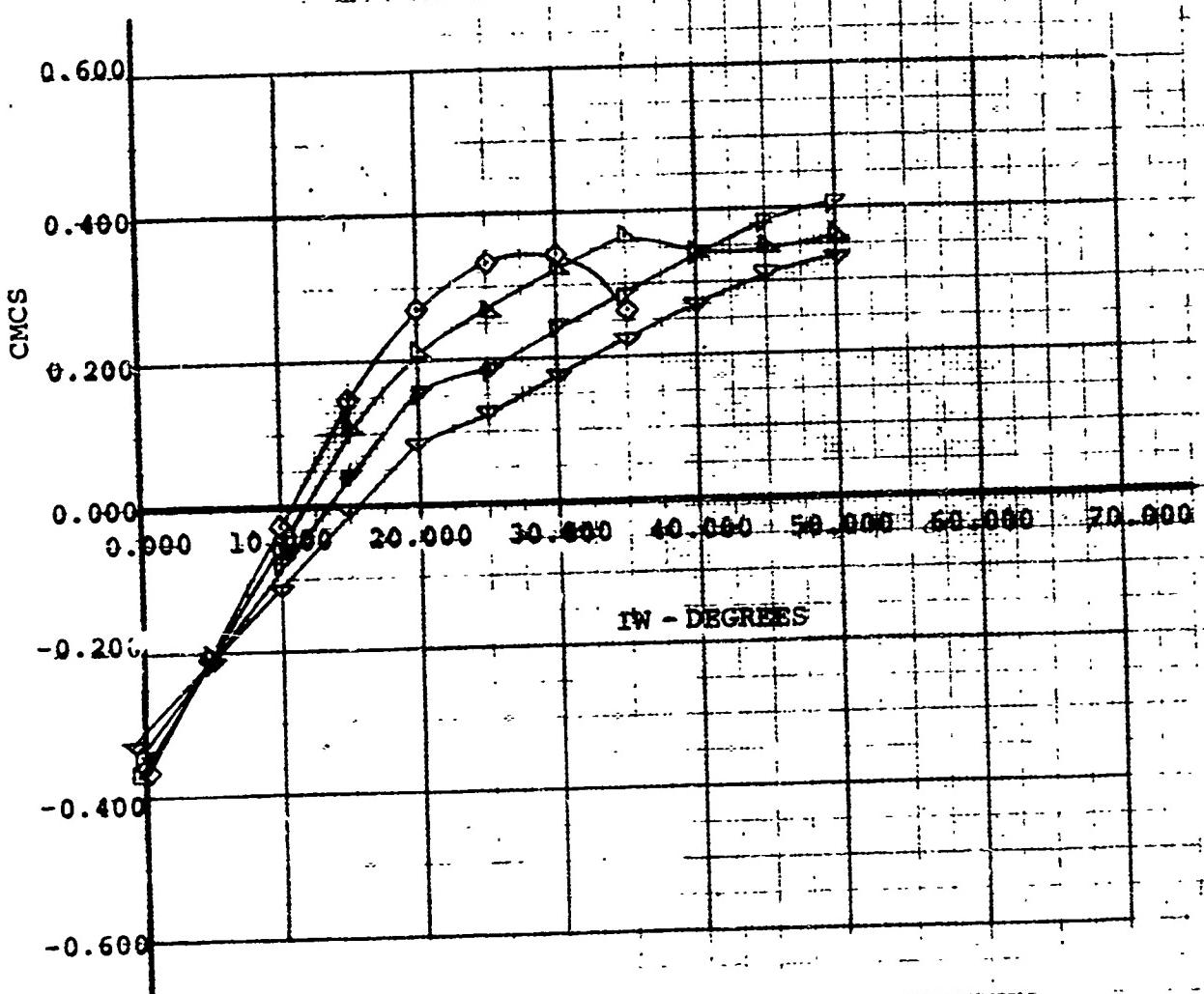
FOUR PROP TILT WING
MODEL VRO68Q (FULL SPAN)
CLCS VS IW DEGREES

BVWT
67

1/4/7

RUN	SYM.	Δ	S	NOM CT	γ
149	▽	---	2.7	.81	+4°
150	▼	---	4.0	.70	
151	▲	---	6.3	.55	
152	◇	---	10.6	.25	

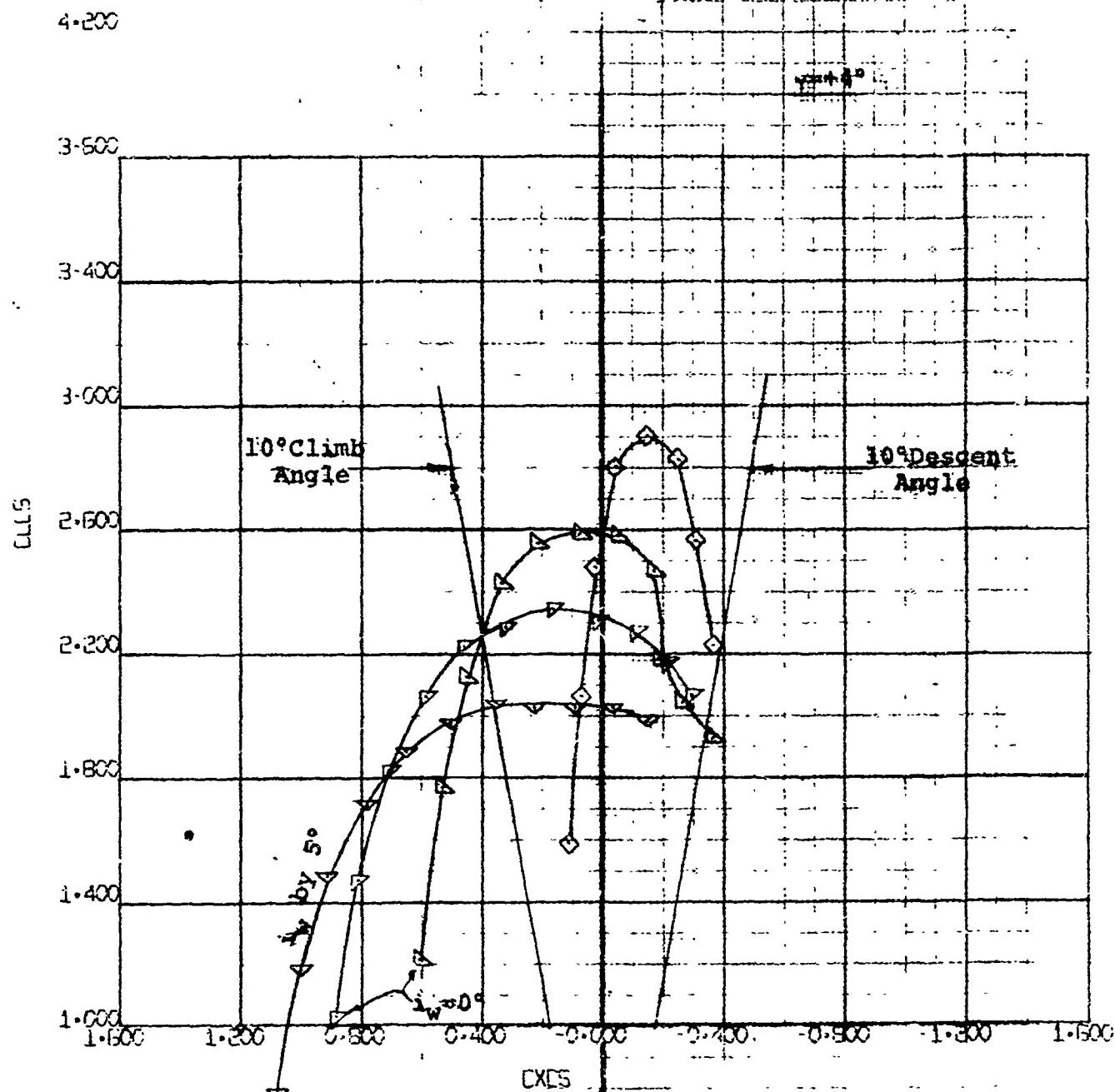
LONGITUDINAL CHARACTERISTICS
IN GROUND EFFECT
 $\alpha_p = 0^\circ$, $\delta_p = 40^\circ$, $h/D = 1.25$
FULL SPAN SLATS



POOR PROP TILT WING MODEL VROGING (FULL SPAN) CMCS VS IW DEGREES	BVWT 67 1/4/71
--	----------------------

RUN	SYM	Δ	q	NOM CT _s	γ
149	▽	---	2.7	.81	+4°
150	▽	---	4.0	.70	
151	▽	---	6.3	.58	
152	◊	---	10.6	.25	

LONGITUDINAL CHARACTERISTICS
IN GROUND EFFECT
 $\alpha_F=0^\circ$, $\delta_F=40^\circ$, $L/D=1.25$
FULL SPAN SLATS



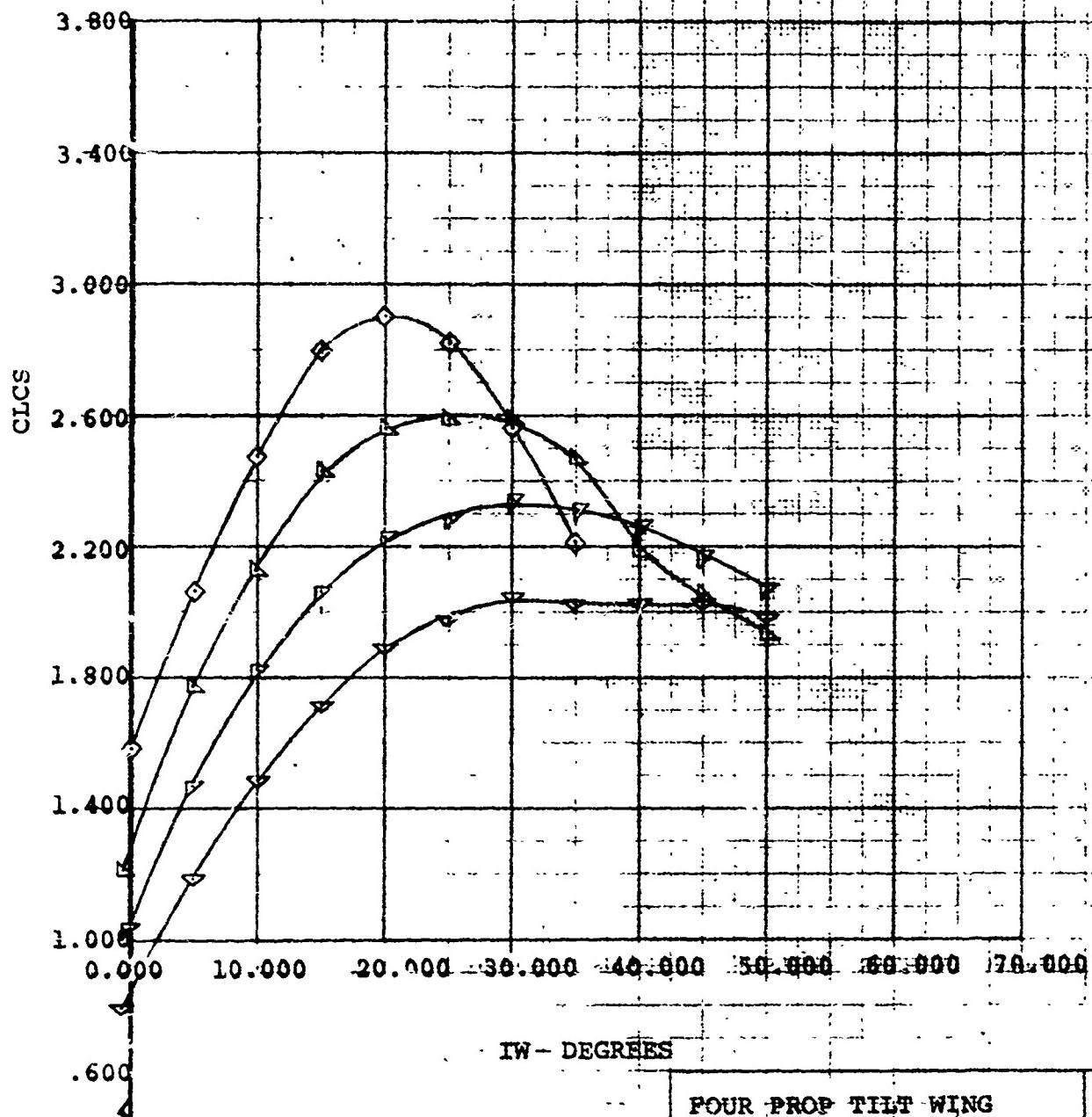
FOUR-PROP TILT WING MODEL VR0680 (FULL SPAN) CL(s) VS. CX(s)	BWWT 67 1/47.
--	---------------------

D170-10639-1

FIGURE 1.77

RUN	SYM	Δ	S	NOM CTS.	γ
149	■	---	2.7	.81	+4°
150	▽	---	4.0	.70	
151	△	---	6.3	.58	
152	◇	---	10.6	.25	

LONGITUDINAL CHARACTERISTICS
IN GROUND EFFECT
 $\alpha_F = 0^\circ$, $\alpha_T = 40^\circ$, $b/2 = 1.25$
FULL SPAN SLATS

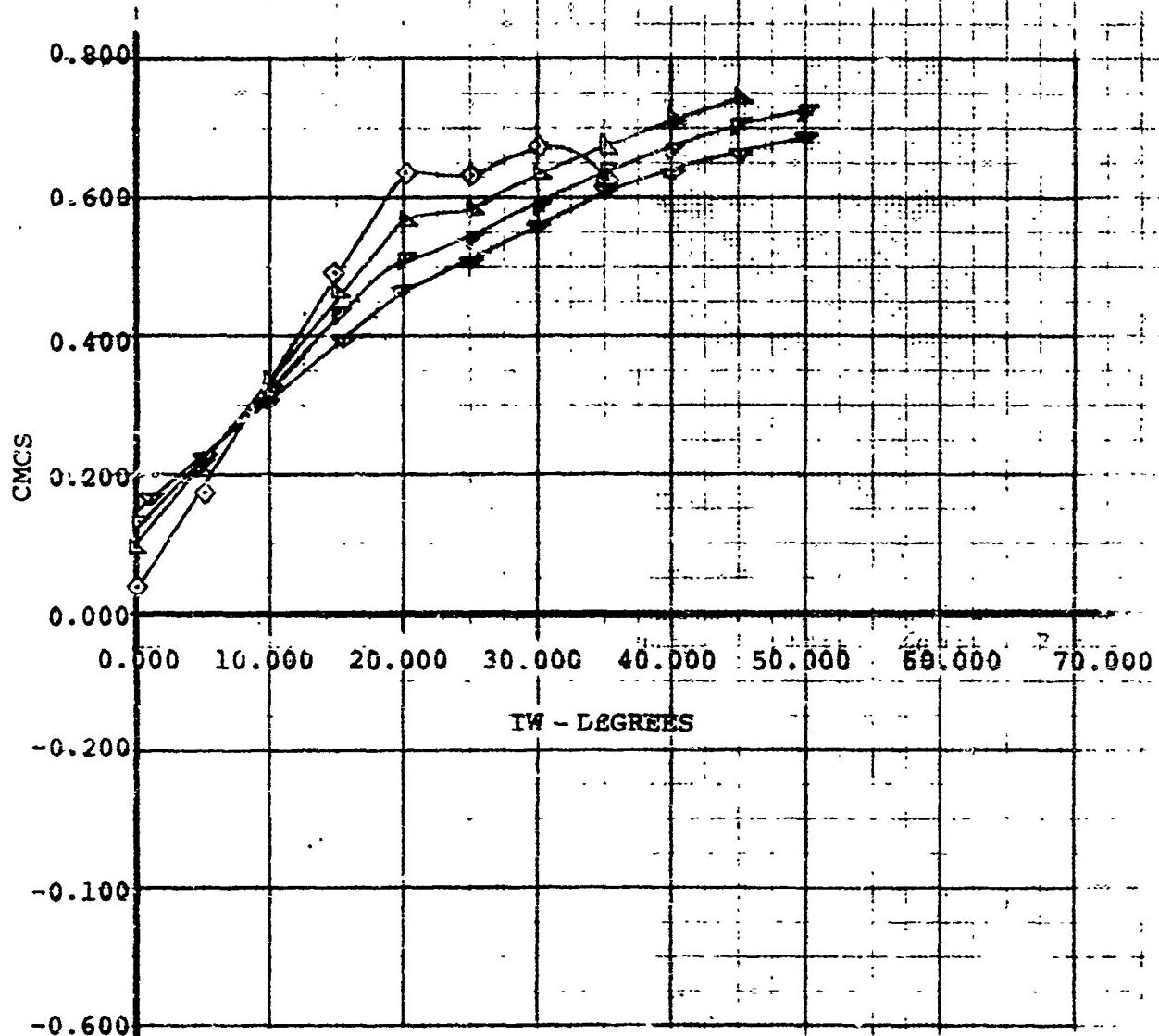


D170-10039-1

Figure 178.

RUN	SYM	Δ	q	NOM CT _E	γ
153	▽	---	2.7	.81	-4
154	△	---	4.0	.70	
155	▲	---	6.3	.55	
156	◊	---	10.6	.25	

LONGITUDINAL CHARACTERISTICS
IN GROUND EFFECT
 $\alpha_F = 0^\circ$, $\delta_F = 40^\circ$, $h/D = 1.25$
FULL SPAN SLATS

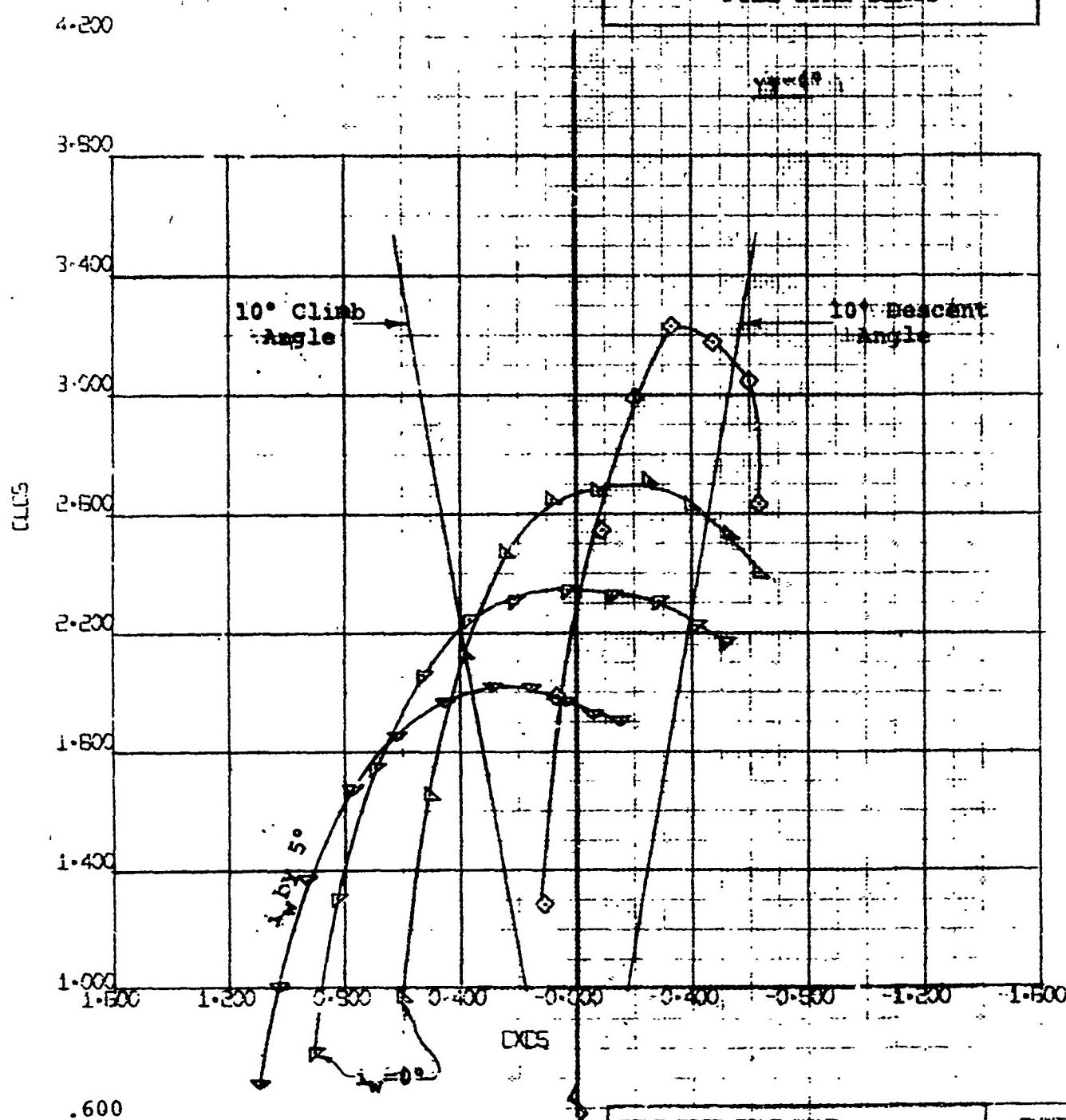


FOUR PROP TILT WING
MODEL VRO680 (FULL SPAN)
CMGS VS IW - DEGREES

BVWF
67
1/4/71

RUN	SYM	Δ	a	NOM C_{T_0}	-4
153	▽	---	2.7	.81	
154	△	---	4.0	.70	
155	▽	---	6.3	.56	
156	◇	---	10.6	.25	

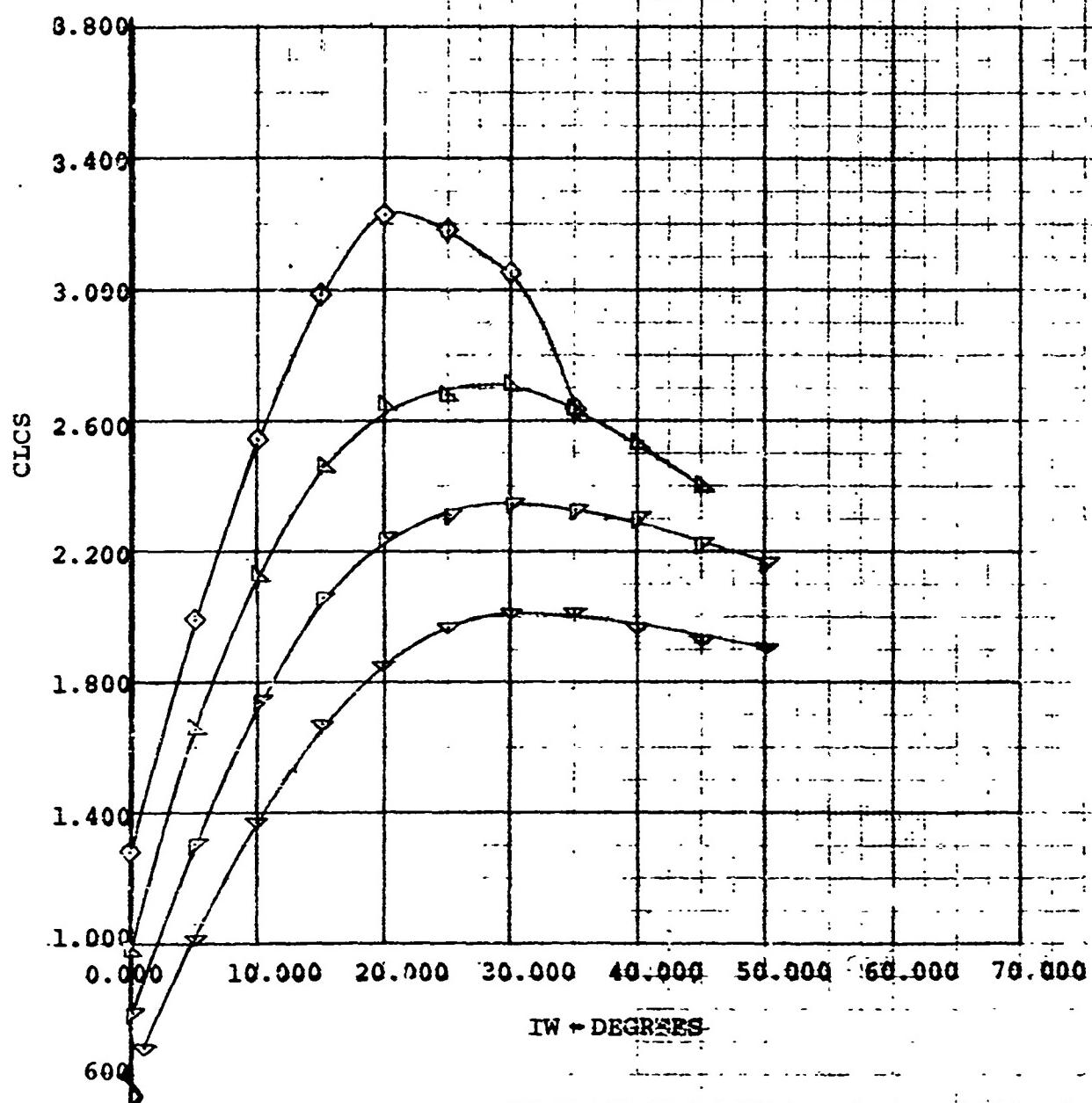
LONGITUDINAL CHARACTERISTICS
IN CLIMBING EFFECT
 $\alpha_F = 0^\circ$, $\delta_F = 40^\circ$, $h/D = 1.25$
FULL SPAN SLATS



FOUR-PROP TILT WING MODEL VRO680 (FULL SPAN) CLDS VS. DCDS	BVNT 67 1/ 4/71
--	-----------------------

RUN	SYM	Δ	q	NOM C_{T_B}	γ
153	▽	---	2.7	.91	-4
154	▷	---	4.0	.70	
155	△	---	6.3	.55	
156	◊	---	10.6	.25	

LONGITUDINAL CHARACTERISTICS
IN GROUND EFFECT
 $\alpha_F = 0^\circ$, $\delta_E = 40^\circ$, $b/D = 1.25$
FULL SPAN SLATS



FOUR PROP TILT WING
MODEL VRQ68Q (FULL SPAN).
CLCS VS IW - DEGREES

EWWT	67
1/14/71	

6.8 LATERAL/DIRECTIONAL STABILITY IN GROUND EFFECT INCLUDING CYCLIC PITCH EFFECTS

The same test configuration utilized for longitudinal in-ground effect testing was also used for the in-ground effect lateral/directional testing, namely, the Boeing-Vertol moving ground plane and a level fuselage with a scaled ground height of 1.25 h/D representing the aircraft with the wheels 3 ft. from the ground. Flaps were extended and the flaps were deflected to the 60° setting.

Empennage-on yaw sweeps were performed with and without cyclic pitch inputs at typical combinations of wing tilt angle and slipstream thrust coefficient, through transition, that were previously evaluated during the out-of-ground effect phase of the lateral/directional testing. All of these yaw runs were conducted with the horizontal tail mounted high on the fin per Figure 15 and with a constant propeller speed of 4500 RPM. As in the out-of-ground effect testing, the model was off-set from the vertical centerline of the test section so that a yaw angular range of 8° (nose right) and -24° (nose left) could be achieved.

All moments obtained during the in-ground effect lateral/directional runs were transferred to the same wing down mid center of gravity location and movement with wing tilt angle as used for the O.G.E. data analysis. Again, the body axis system was used for the data presentations.

The results of the in-ground effect lateral/directional stability investigation with empennage on are included in Figure 181 as slipstream stability derivatives. This plot presents the slipstream yawing moment, rolling moment, and side force derivatives (with respect to the sideslip angle, β) as a function of the slipstream thrust coefficient. As in the analysis of the lateral/directional data obtained out-of-ground effect, all slopes plotted in Figure 181 were read over a yaw angle range that did not exceed $\pm 8^\circ$ and the C_{Ts} values were those prevailing at zero yaw angle. Also shown in this figure is the comparable cut-of-ground data (dashed lines) obtained with zero cyclic angles. This empennage on O.G.E. data was originally presented in Figure 96.

With 15° of wing tilt and zero cyclic the primary influence of ground effect was to incrementally reduce the directional stability over the .29 to .69 C_{Ts} range evaluated. It is not discernible whether the decrease in directional stability is primarily caused by an increase in the basic tail-off instability or a loss in vertical tail effectiveness since only tail-on data was acquired. Increasing the wing tilt angle to 30° exhibited the same trend up to a C_{Ts} of 0.76, which corresponds to a full-scale speed of approximately 45 knots.

A possible source of a portion of the reduction in I.G.E. directional stability with 15° of wing tilt is the associated increase in slipstream lift coefficient over that developed O.G.E with the same empennage-on model configuration. This is shown in Figure 182 which compares the slipstream lift coefficients produced at zero yaw angle during the I.G.E. lateral/directional testing, with the lift coefficients produced during the comparable O.G.E lateral/directional testing.

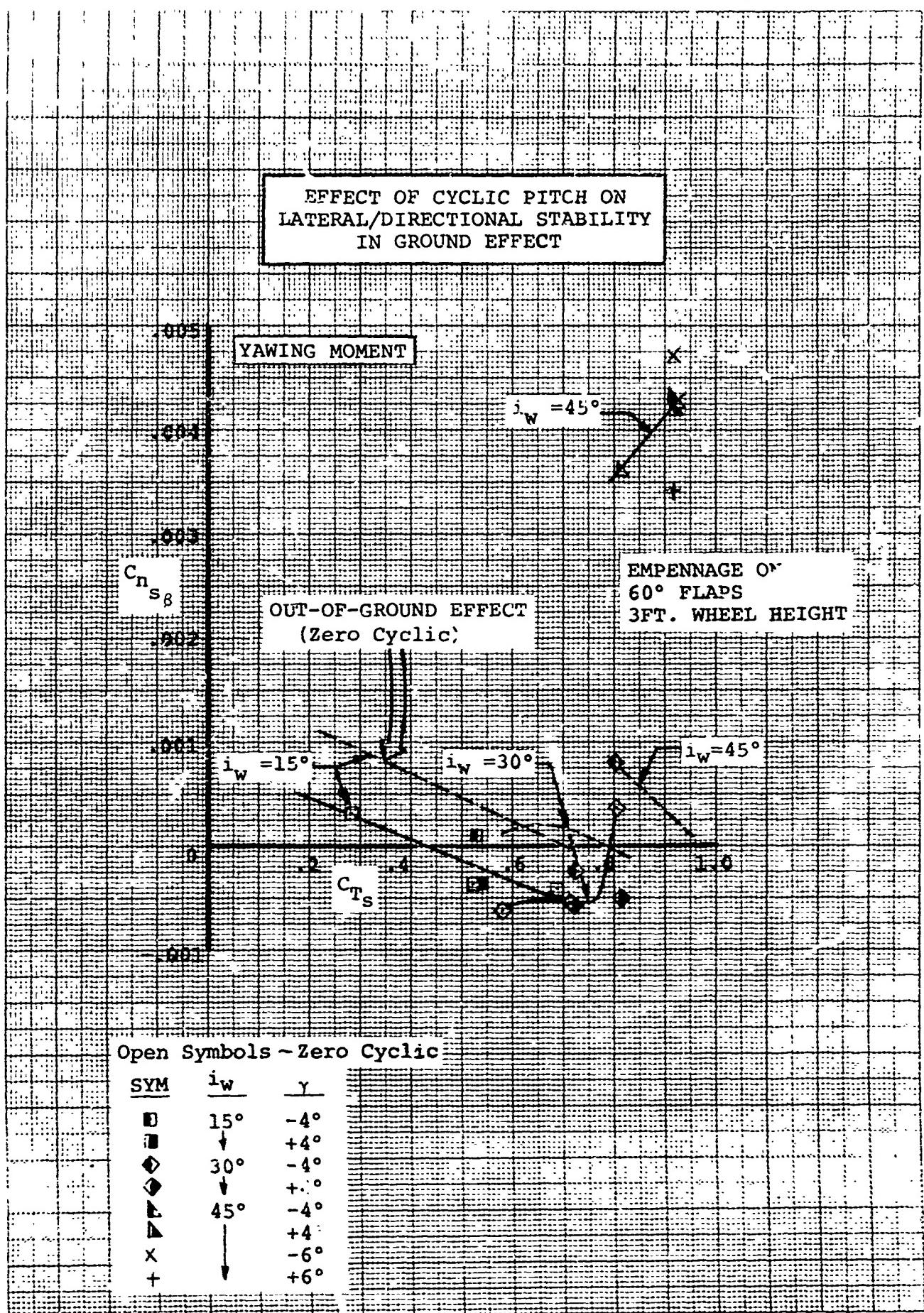
It can be noted in Figure 181 that in the C_{Ts} range up to 0.76 the effect of a positive cyclic input is similar to the result recorded out-of-ground effect in that the changes in lateral/directional stability are small. Negative cyclic has a more pronounced influence in-ground effect, increasing both the directional stability and dihedral effect by larger increments than for the out-of-ground effect case.

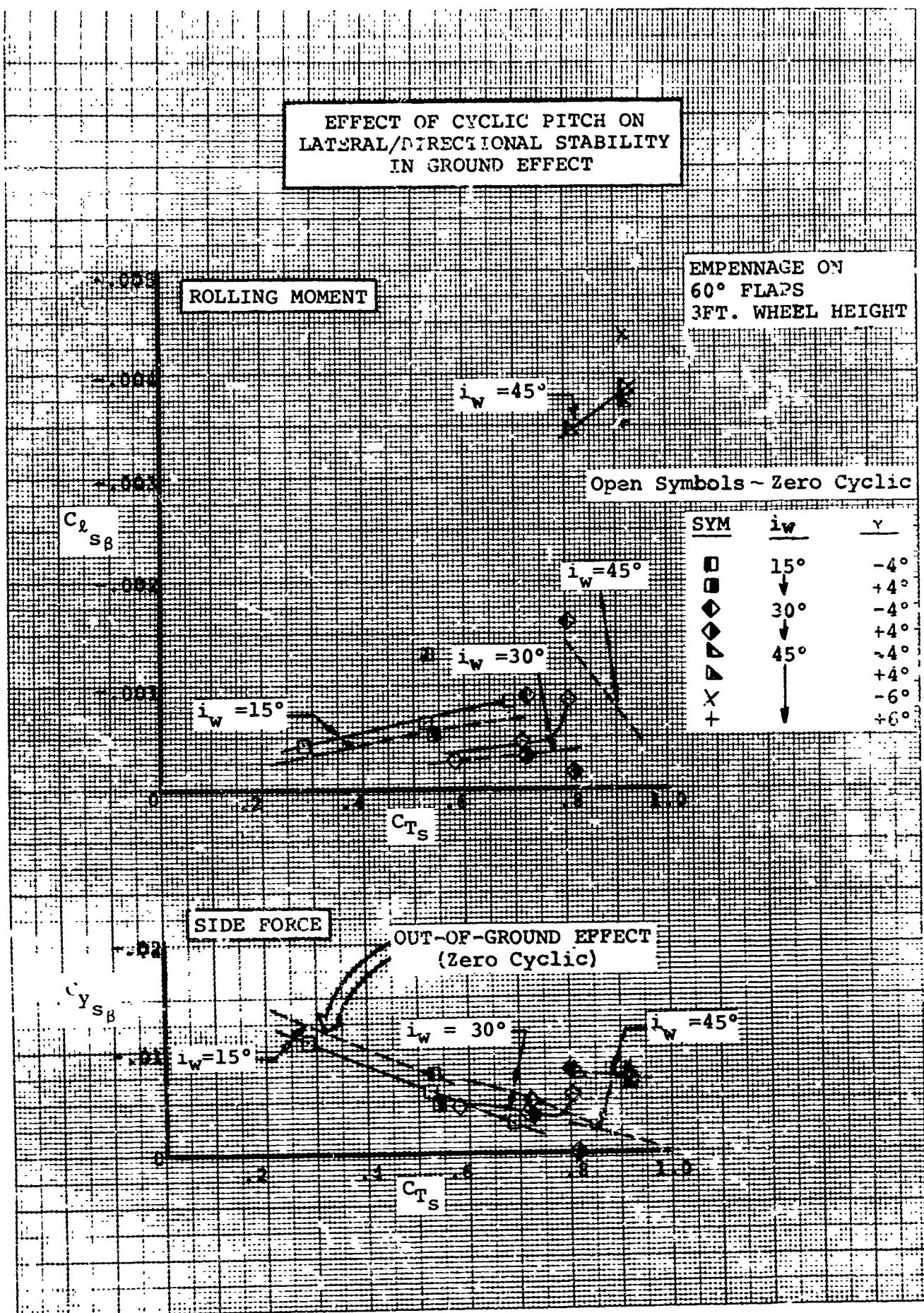
A condition was encountered at 0.8 C_{Ts} that is identified as ground recirculation. At this test point an increase in directional stability, dihedral effect, and side force were measured with zero cyclic pitch. The change to these derivatives that occurred with cyclic pitch inputs, a negative angle further increasing the derivatives and a positive angle reducing the derivatives to a level consistent with the lower C_{Ts} data, leads to the conclusion that at this condition ground recirculation was in the initial stages of formation. The application of negative cyclic, which effectively increases the propeller shaft angle and thus the angle of attack of the total lifting system, induced a stronger case of ground recirculation. Positive cyclic lowered the effective angle of attack sufficiently to completely relieve the model from ground recirculation. A lower flap angle would produce the same result. A question exists as to whether the low tunnel ζ prevailing at this test point ($2.7 \text{ lb}/\text{ft}^2$) was a factor in precipitating ground recirculation in this particular condition.

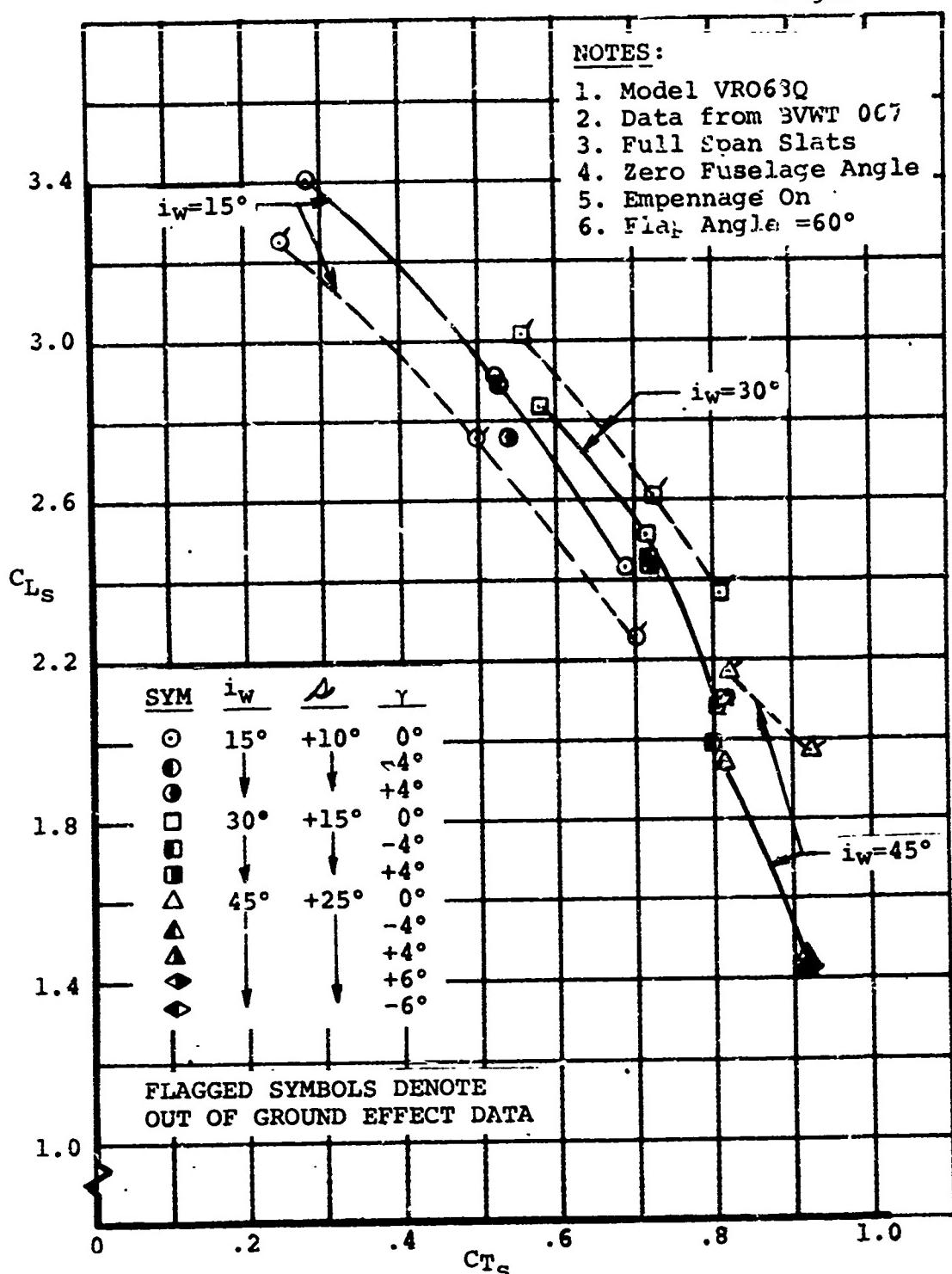
At the high C_{Ts} values of .81 to .92 investigated with 45° of wing tilt, ground recirculation was well developed as evidenced by a large increase in directional stability and dihedral effect over that recorded out-of-ground effect. The magnitude of these stability changes was probably influenced by the wing configuration; a tapered wing with straight leading edge and swept forward flap hingeline. It would appear from the direction of these forces and moments, nose-right yawing moment, right wing-up rolling moment and left side force that the up-wind wing and fuselage side tended to "funnel" the air into the wing/body junctio.. and the air on the down-wind wing side was partially diverted spanwise and around the wing tip.

Figures 183 through 191 include the basic three component yaw data with zero cyclic pitch that was acquired during the in-ground effect testing. The data, presented in sets of yawing moment, rolling moment and side force plots, is arranged in order of increasing wing tilt angle from 15° to 30° to 45°. Each set of plots depicts the data for the series of slip-stream thrust coefficients examined at a particular wing tilt angle.

The three component data obtained during the I G.E. lateral/directional testing with cyclic pitch inputs is presented in Figures 192 through 203. This data is arranged in a manner similar to that used in presenting the zero cyclic data, with each set of three plots depicting the data obtained from the various cyclic pitch runs performed with a particular wing tilt angle.





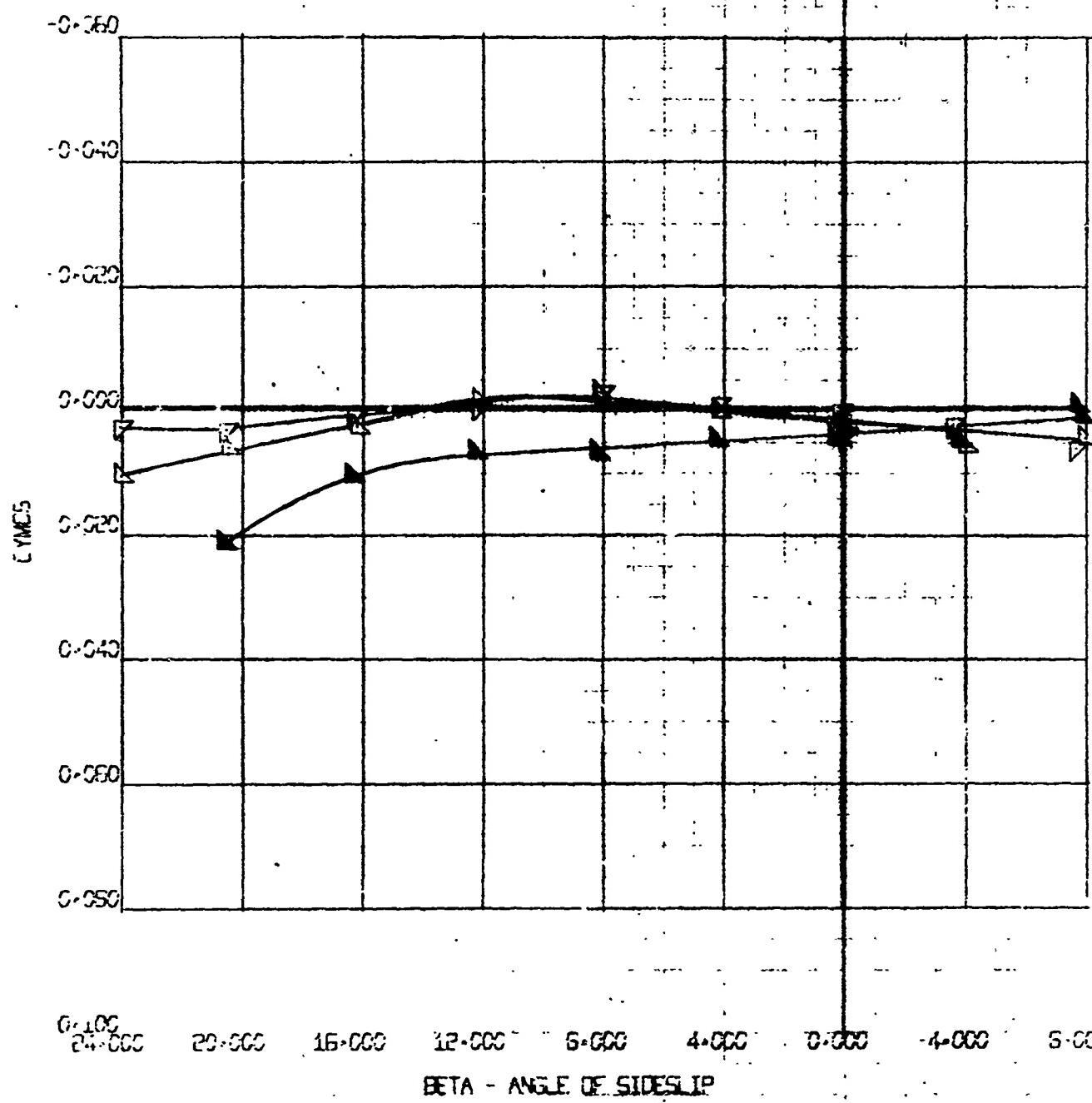


SLIPSTREAM C_L VARIATION DURING YAW TESTS
IN GROUND EFFECT, $h/D = 1.25$

RUN	SYM	α	q	NOM C_{T_s}	γ
132	▼	+10°	4.0	.70	0°
133	△		6.3	.50	
134	►		10.6	.25	
-0.050 Empennage On					

NUMBER D170-10039-1
REV. LTR. Figure 183

LATERAL/DIRECTIONAL STABILITY
IN GROUND EFFECT
 $i_w = 15^\circ$, $\delta_f = 60^\circ$, $b/D = 1.25$
FULL SPAN SLATS

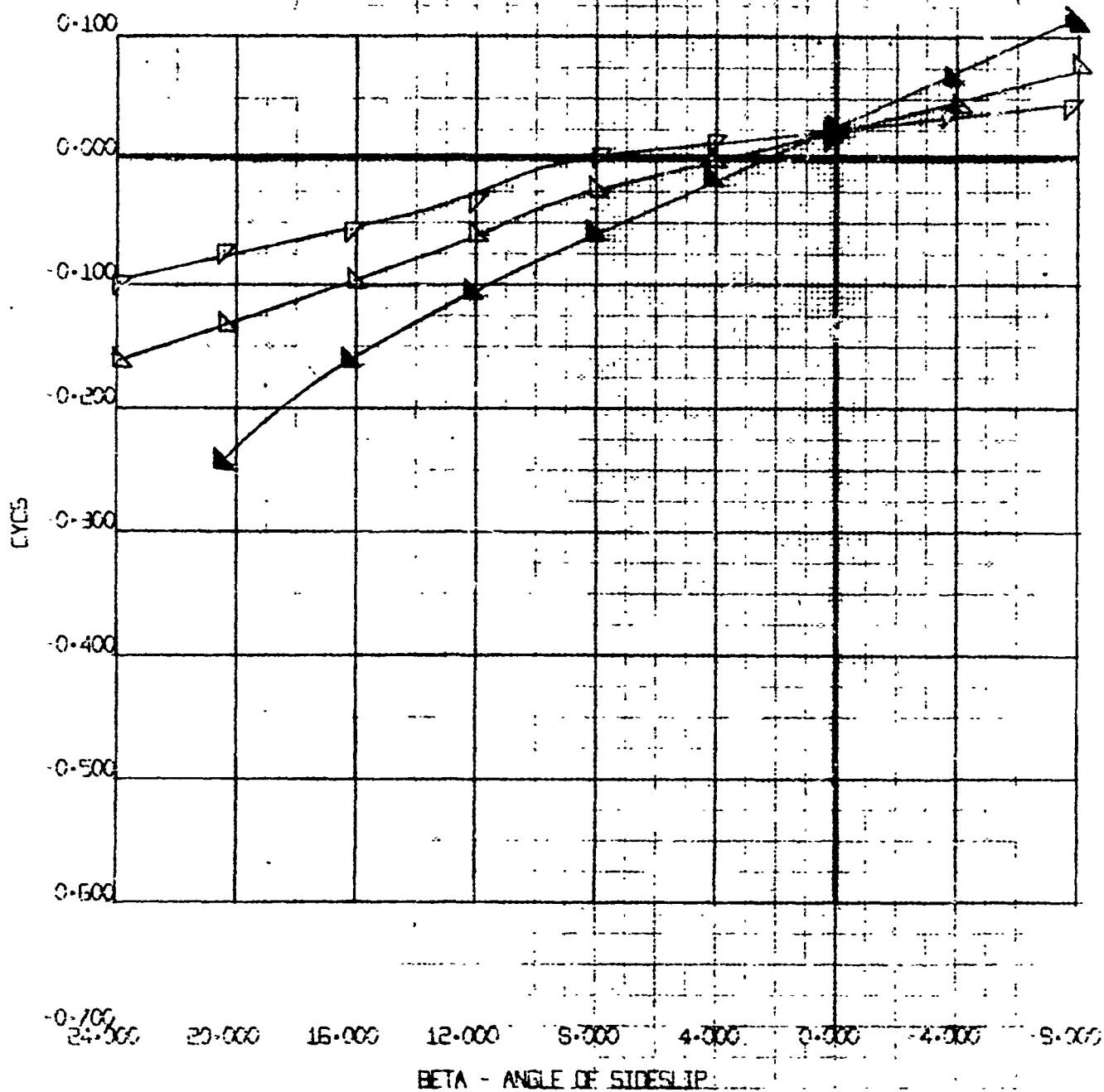


FOUR-PROP TILT WING MODEL VROB8 (FULL SPAN) C _l MACS VS. BETA	BWNT 67
	12/17/70

RUN	SYM	α	q	NOM C_{T_s}	γ
132	▽	+10°	4.0	.70	0°
133	△		6.3	.50	↓
134	■		10.6	.25	↓
0-200	Empennage On				

NUMBER D170-16039-1
REV. LTR. Figure 184.

LATERAL DIRIGORIAL STABILITY
IN TERRAIN EFFECT
 $i_w = 15^\circ$, $S = 600^\circ$, $h/D = 1.25$
FULL SPAN SLATS

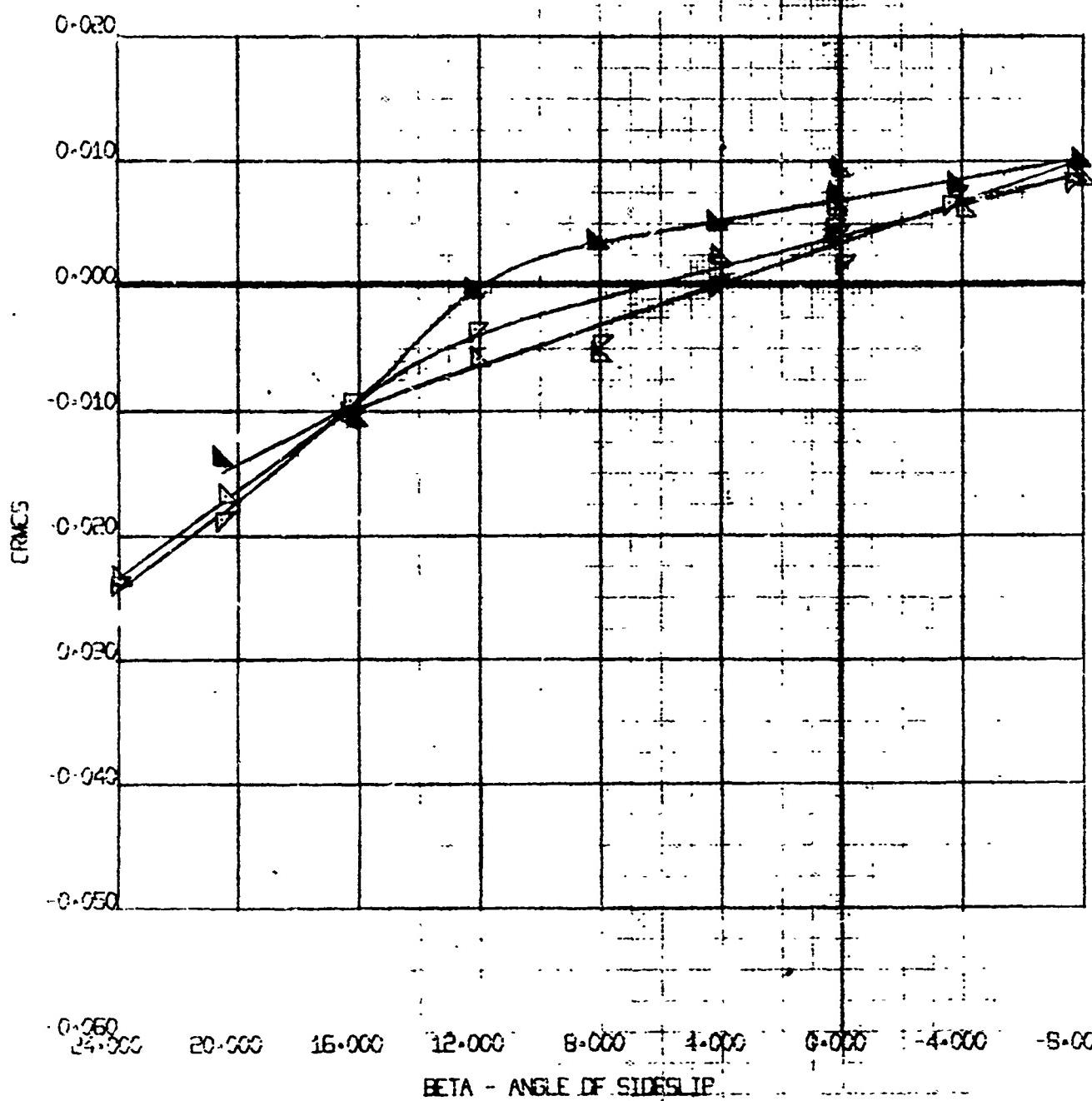


FOUR-PROP TILT WING MODEL VROS8G (FULL SPAN) CYCLES VS. BETA	BWNT 67 12/17/70
--	------------------------

NUMBER D170-10039-1
REV. LTR. Figure 185

RUN	SYM	Δ	q	NOM C_{TS}	γ
132	▼	+10°	4.0	.70	0°
133	△		6.3	.50	
134	▲		10.6	.25	
0-030	Empennage On				

LATERAL/DIRECTIONAL STABILITY
IN GROUND EFFECT
 $X_w = 1.0^{\circ}, \alpha = 10^{\circ}, V = 125$
FULL SPAN SLATS



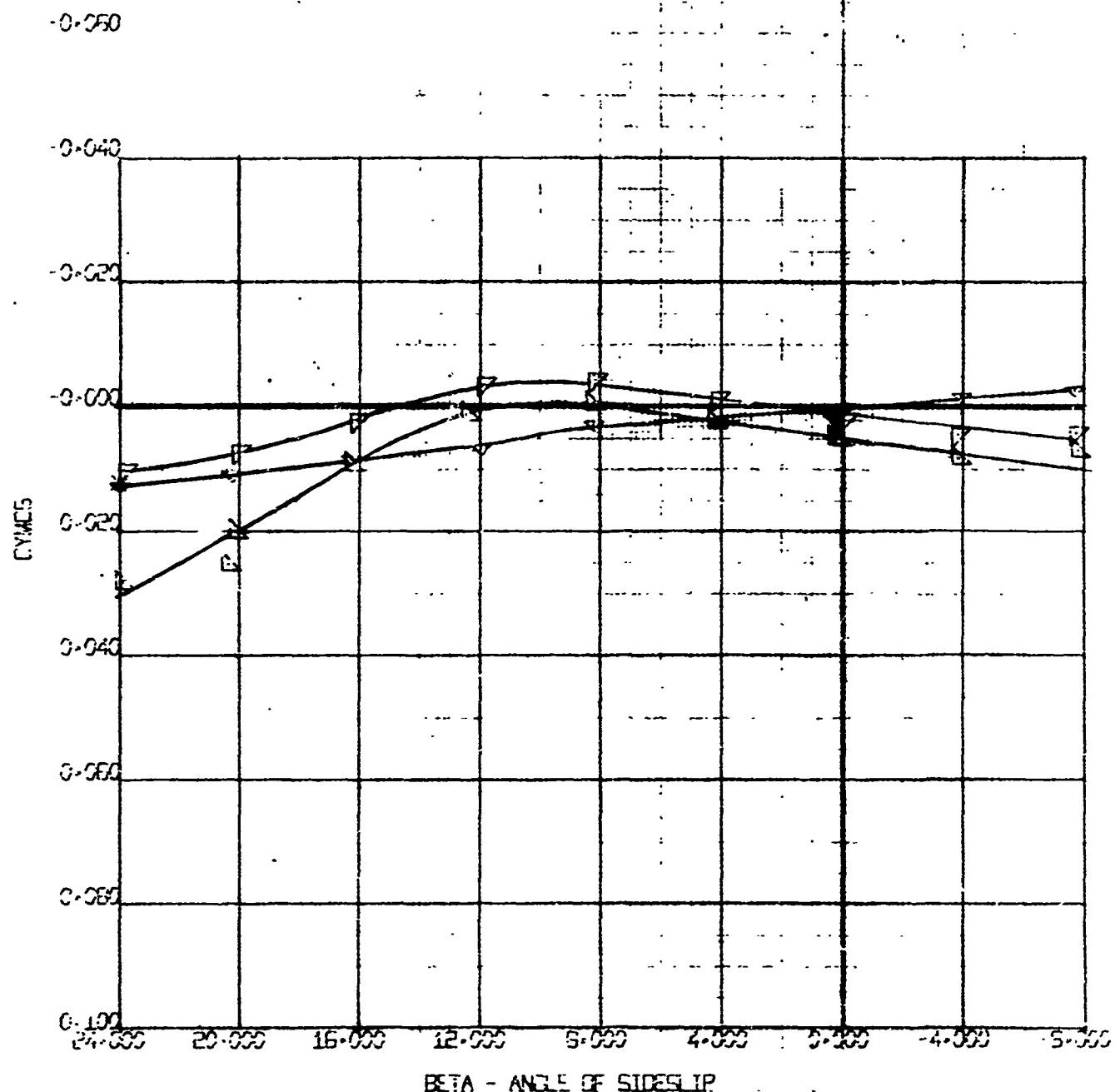
FOUR-PROP TILT WING MODEL VR0580(FULL SPAN) CRMS VS. BETA	BWNT 67
	12/17/70

RUN	SYM	Δ	G	NOM C_{T_0}	γ
135	▽	+15°	2.7	.81	0°
136	▽	1	4.0	.70	
137	△	1	6.5	.55	

Empennage On

NUMBER D170-10039-1
REV. LTR. Figure 186

LATERAL/DIRECTIONAL STABILITY
IN GROUND EFFECT.
 $i_w = 34^\circ$, $i_s = 60^\circ$, $\alpha_{BD} = 1.25$
FULL SPAN SLATS



FOUR-PROP TILT WING MODEL W/RODS(FULL SPAN) CYADS VS. BETA	BWWT 67
	12/17/70

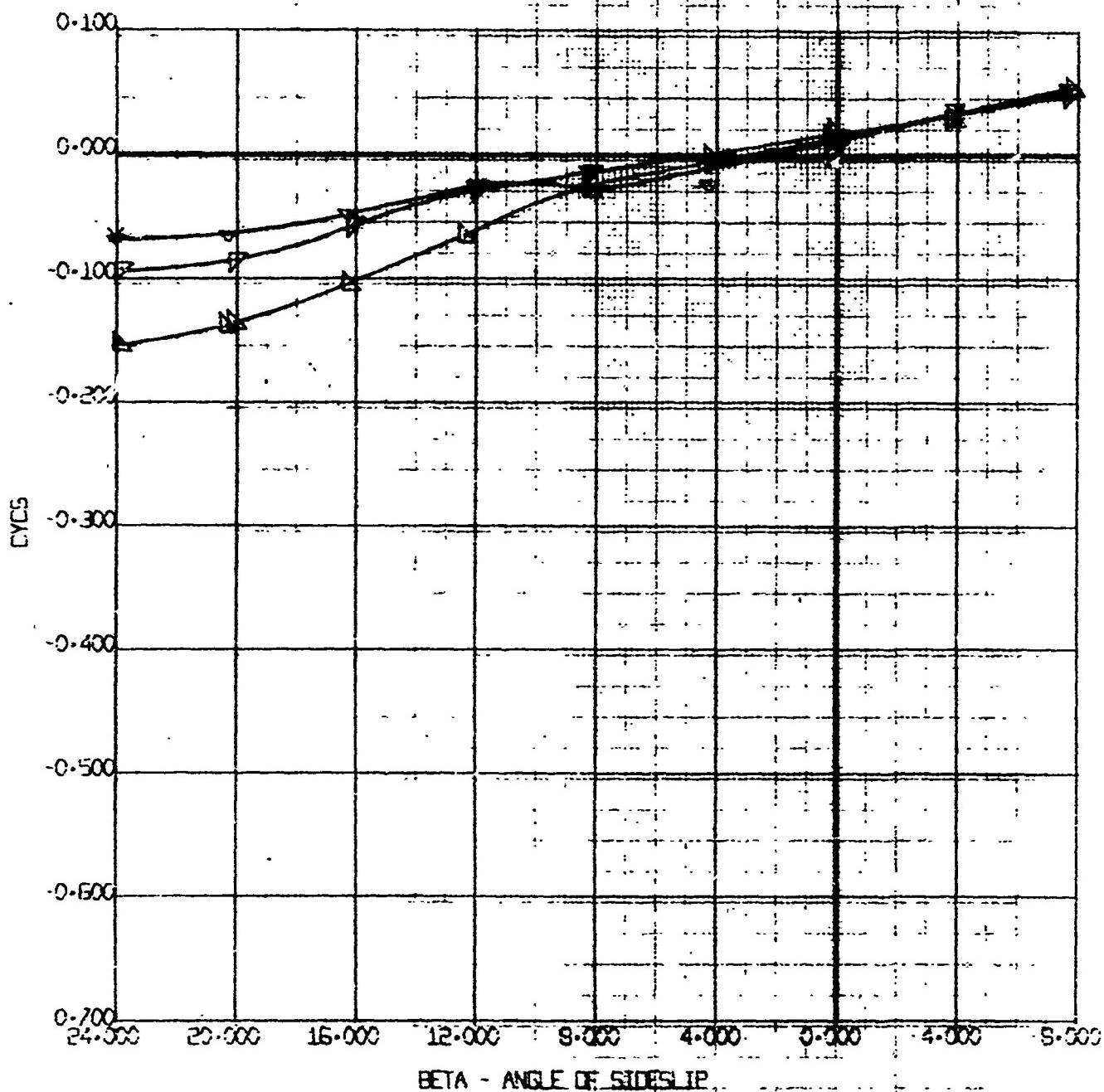
RUN	SYM	Δ	G	NOM C_{T_w}
135	▽	+15°	2.7	.81
136	▽	↓	4.0	.70
137	△	↓	6.5	.85

Empennage On

Y
0°

NUMBER D170-10039-1
REV. LIR. Figure 187

LATERAL/DIRECTIONAL STABILITY
IN WINDUP EFFECT
 $l_w = 30^\circ$, $l_d = 60^\circ$, $b/D = 1.25$
FULL SPAN SLATE



FOUR-PROP TILT-WING
MODEL WRO60 (FULL SPAN)
CYCS VS. BETA

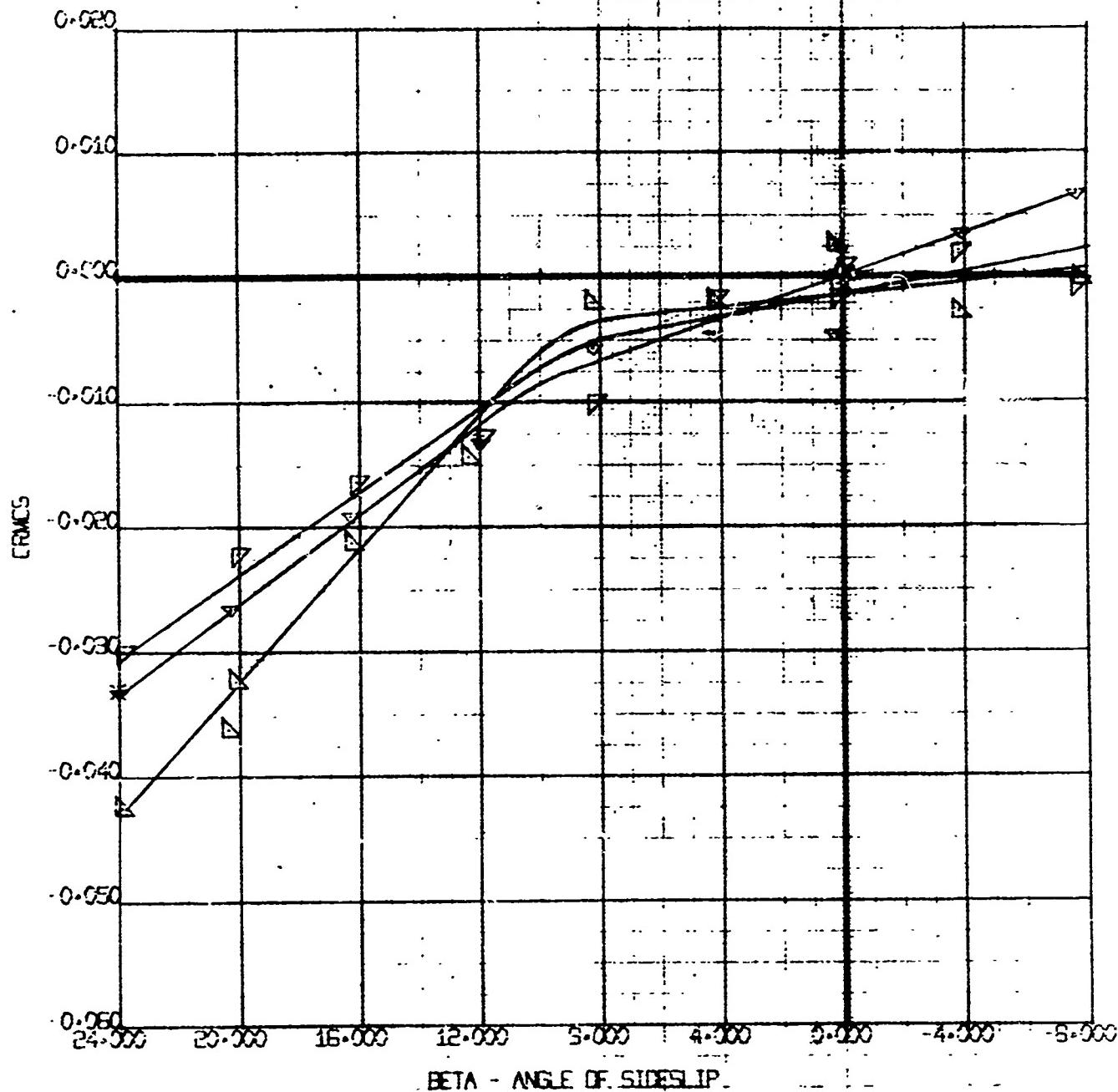
BWHT
67

12/17/70

NOM
 RUN SYM Δ S C_T Y
 135 ▵ +15° 2.7 .81 0°
 136 ▽ -15° 4.0 .76 ↓
 137 △ 0° 6.5 .53 ↓
 Empennage On

NUMBER D170-10039-1
 REV. LTR. Figure 188

LATERAL DIRECTIONAL STABILITY
 IN GROUND EFFECT
 $A_0 = 30^\circ$, $A_p = 60^\circ$, $h/D = 1.25$
 FULL SPAN SLATS

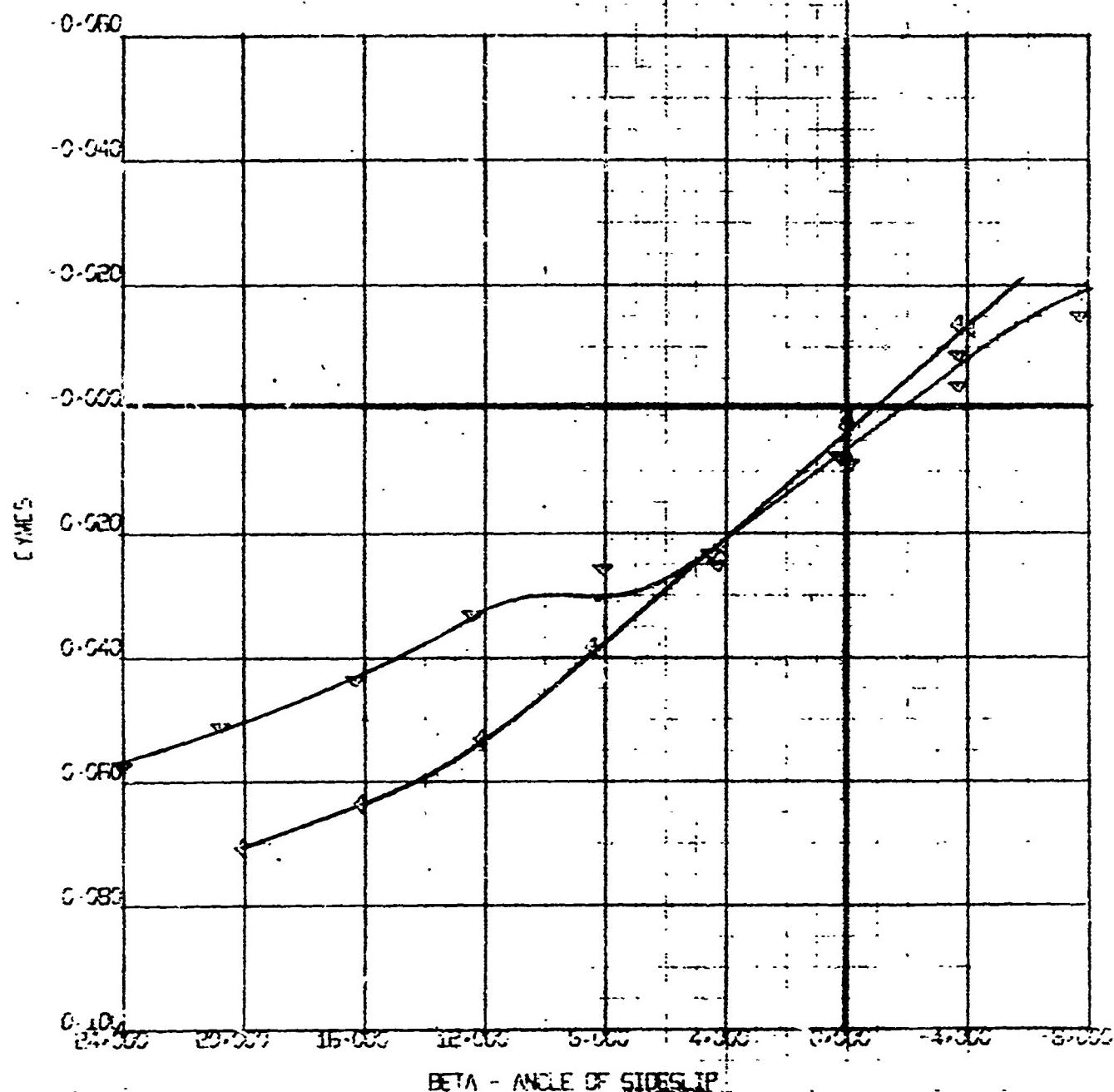


FOUR-PROP TILT WING MODEL VROGGS (FULL SPAN) CLMOS VS. BETA	BYWT 67 12/17/70
---	------------------------

NUMBER D170-10039-1
REV. LTR. Figure 189

RUN	SYM	Δ	q	NOM C_{Ts}	γ
138	∇	+25°	2.7	.81	0°
139	Δ	↓	1.0	.92	↓
Empennage On					

LATERAL/DIRECTIONAL STABILITY
IN GROUND EFFECT
 $i_w = 45^\circ$, $\phi_F = 60^\circ$, $h/D = 1.25$
FULL SPAN SLATS

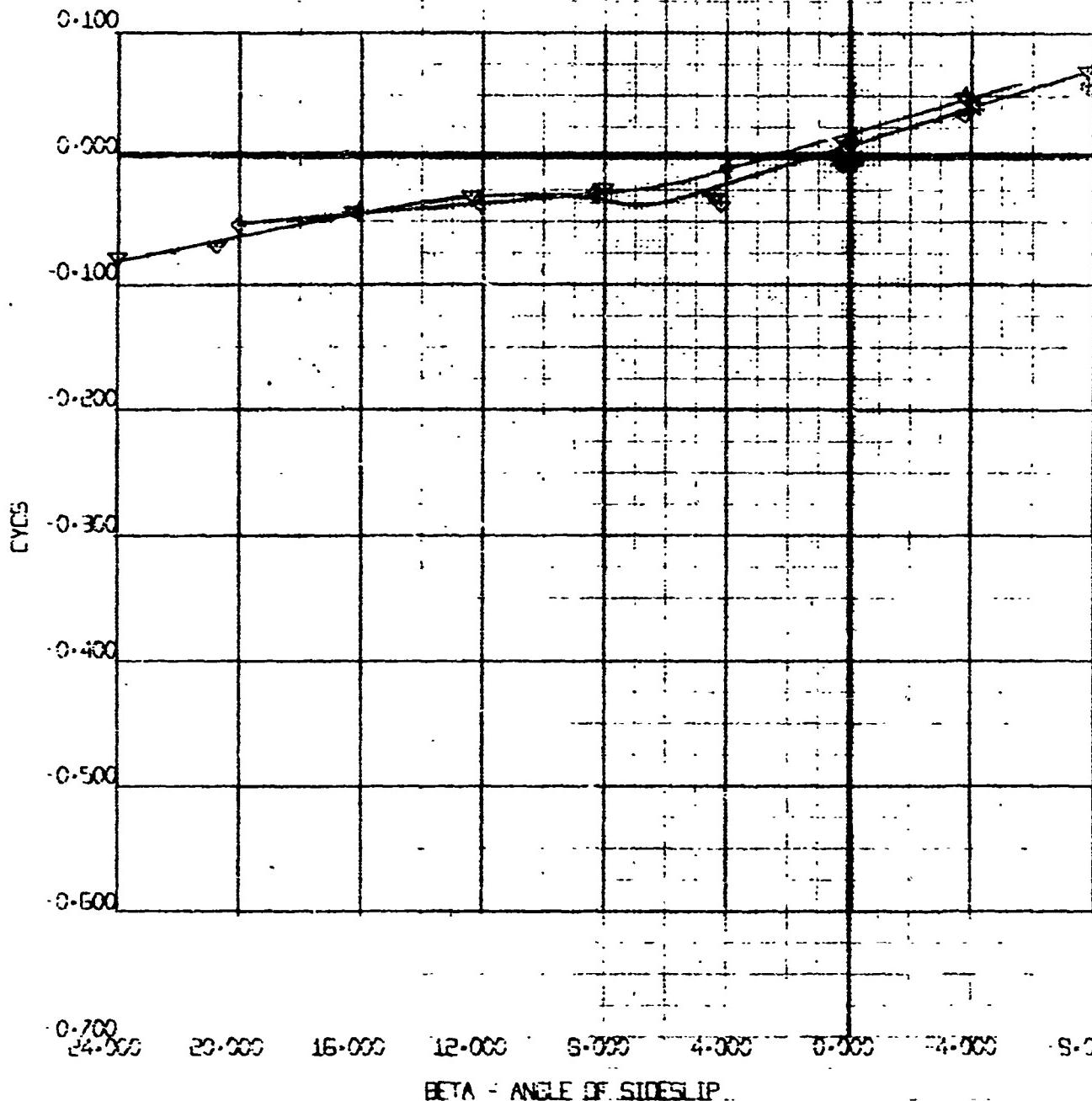


FOUR-PROF TILT WING MODEL VROBEC (FULL SPAN) CLINES VS. BETA	BWWT 67
	12/17/70

NUMBER D170-10039-1
REV. LTR. Figure 190

RUN	SYM	Δ	α	NOM C_{Ts}	γ	
138	◇	+2°	2.7	.81	0°	
139	◆	+	1.0	.92	1°	
0-200	Empennage On.					

LATERAL/DIRECTIONAL STABILITY
IN GROUND EFFECT
 $i = 45^\circ$, $s_p = 60^\circ$, $b/D = 1.25$
FULL SPAN SLATS



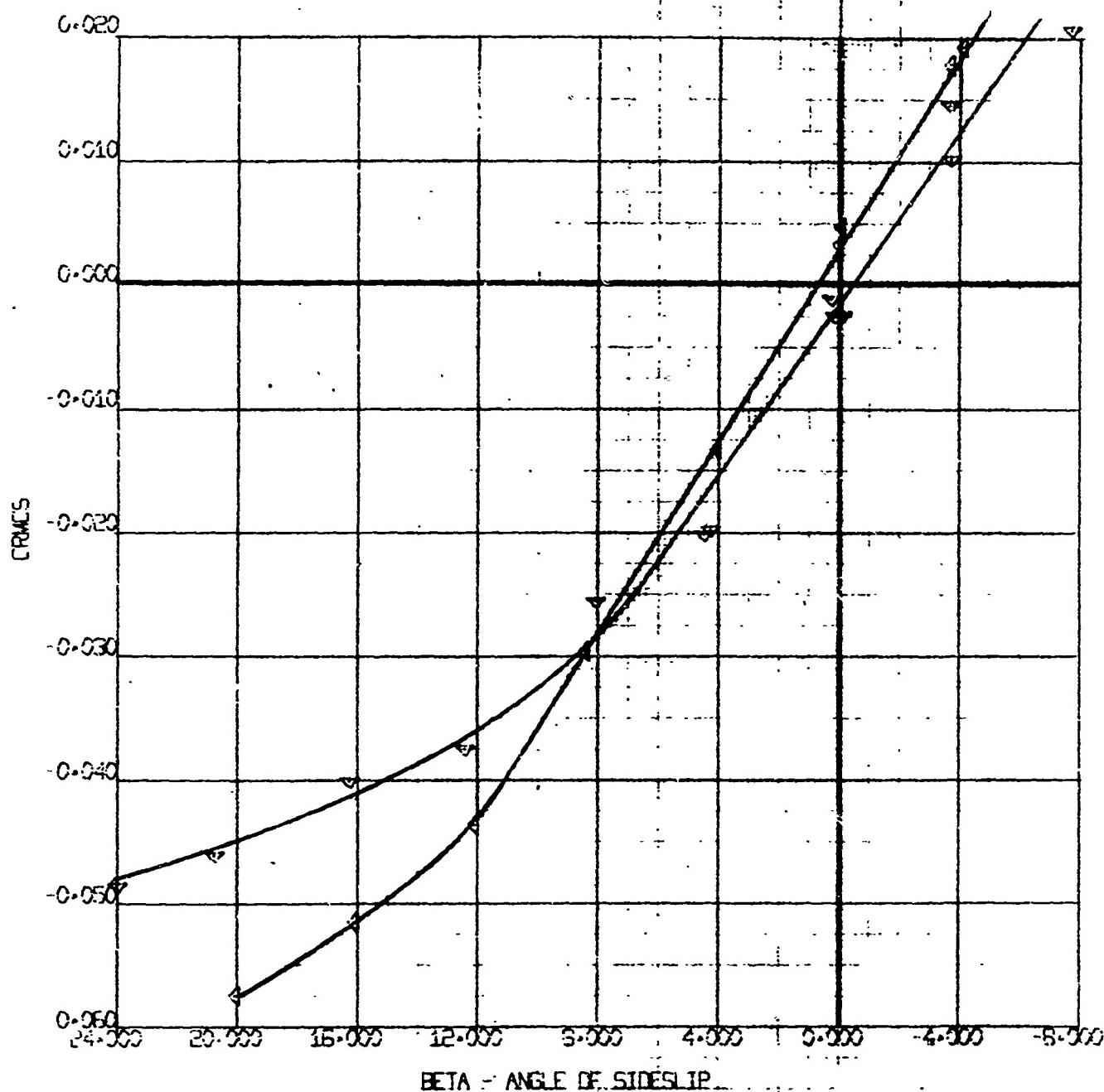
FOUR-PROP TILT WING
MODEL VR068S (FULL SPAN)
CYCS VS. BETA

BWNT
67
12/17 '70

NUMBER D170-10039-1
REV. LTR. Figure 191

RUN	SYM	Δ	q	NOM C _T	γ
138	▽	+25°	2.7	.81	0°
139	◊	↓	1.0	.92	↓
Empennage On					

LATERAL/DIRECTIONAL STABILITY
IN GROUND EFFECT
 $\beta_w = 45^\circ$, $\beta_p = 60^\circ$, $D/D = 1.25$
FULL SPAN SLATS

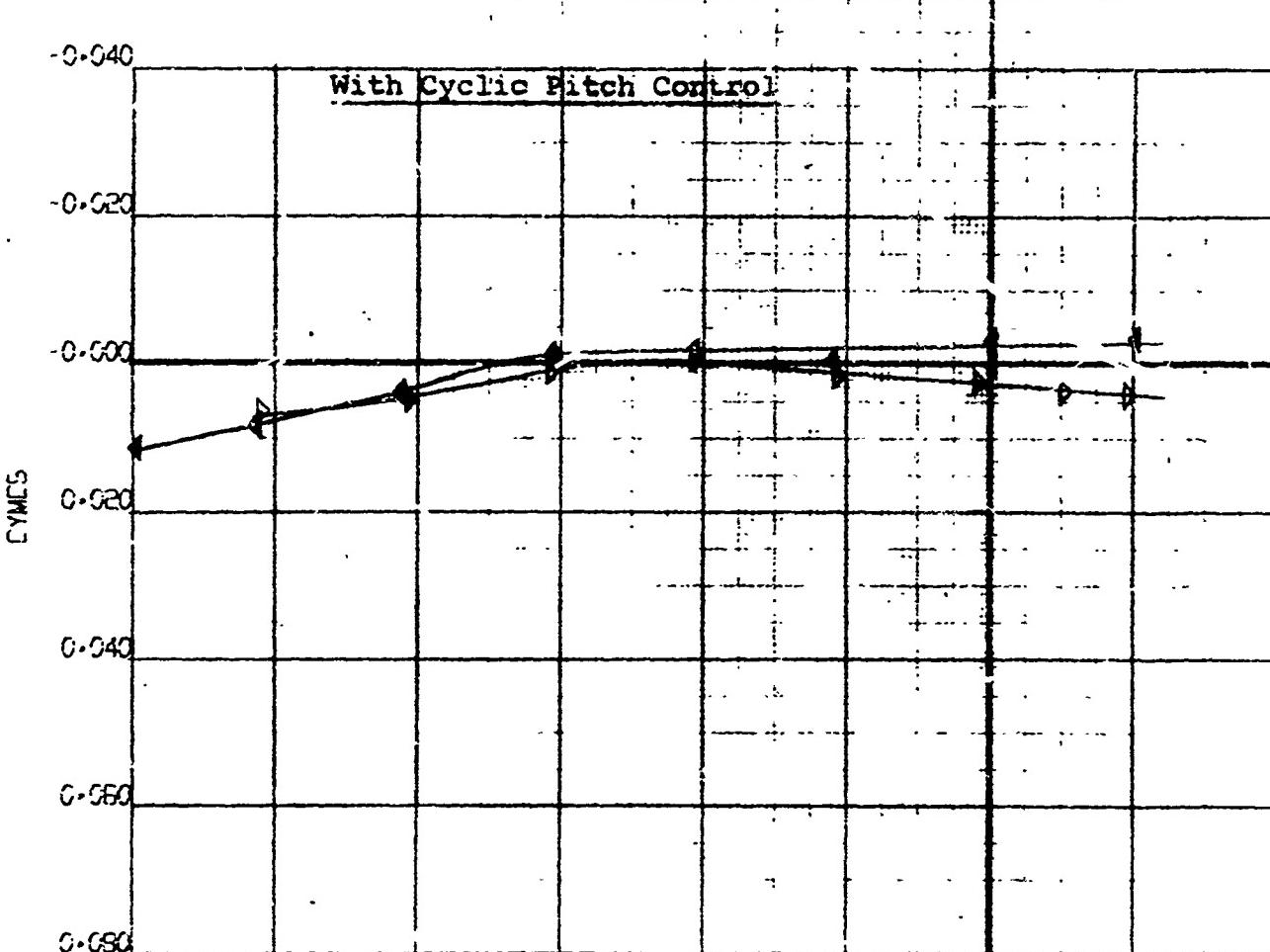


FOUR-PROP TILT WING MODEL VROSBD(FULL SPAN) DRMS VS. BETA	BWWT 67 12/17/70
---	------------------------

KINGER D170-10039-1
REV. LTR. Figure 192

RUN	SYM	Δ	q	NOM C_{TS}	γ
158	♀	+10°	6.3	.50	-4°
163	♂	↓	↓	↓	+4°
Empennage On					
-0.050					

LATERAL/DIRECTIONAL STABILITY
IN GROUND EFFECT
 $i_w = 35^\circ$, $\delta_p = 60^\circ$, $b/B = 1.25$
FULL F2AN SLATS



0.100
24.000 20.000 16.000 12.000 8.000 4.000 0.000 -4.000 -8.000

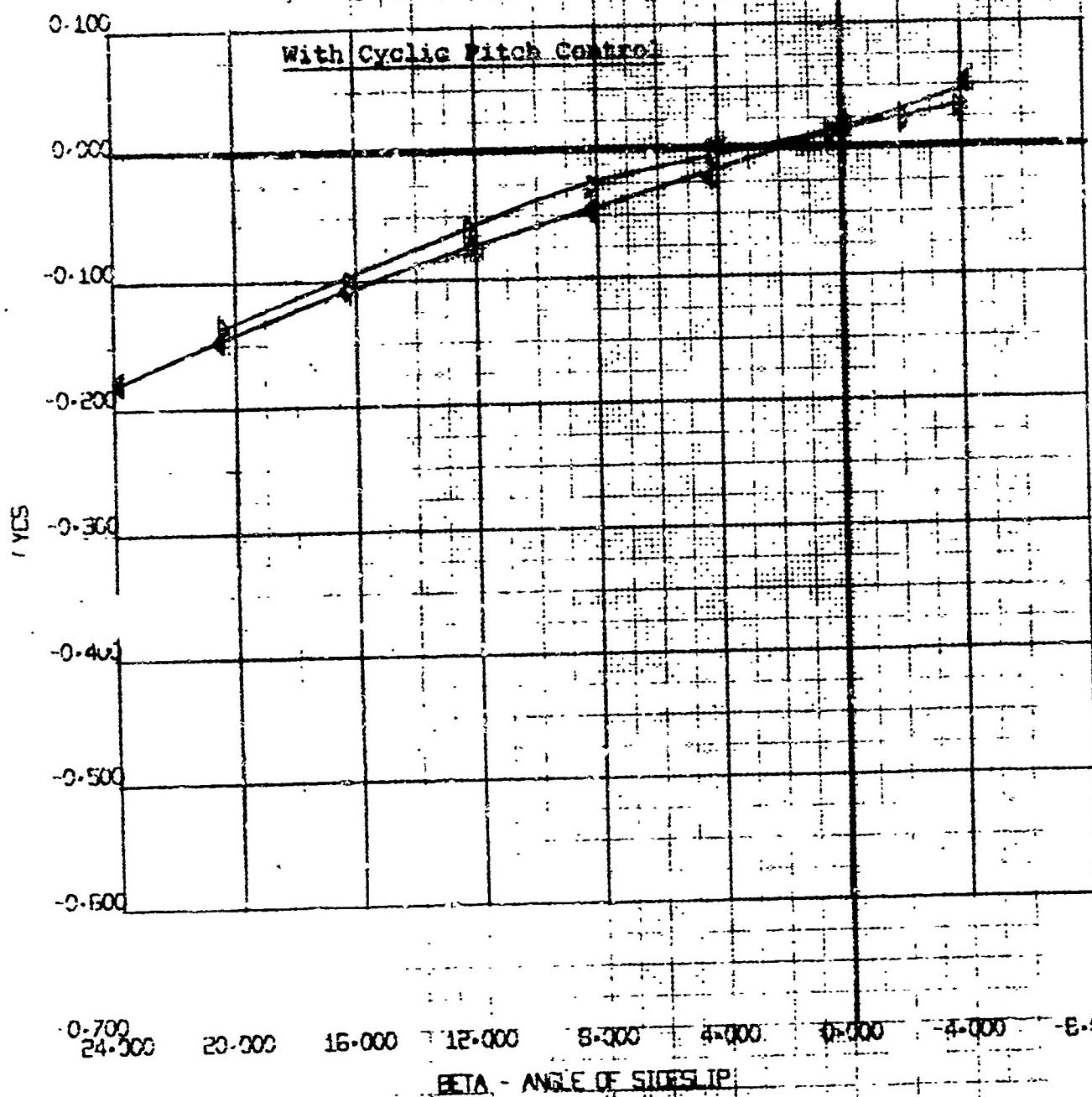
BETA - ANGLE DE SIDESLIP

FOUR-PROP TILT WING MODEL VR0680 (FULL SPAN) CYMCS VS. BETA	BWWT 67 1/25/71
---	-----------------------

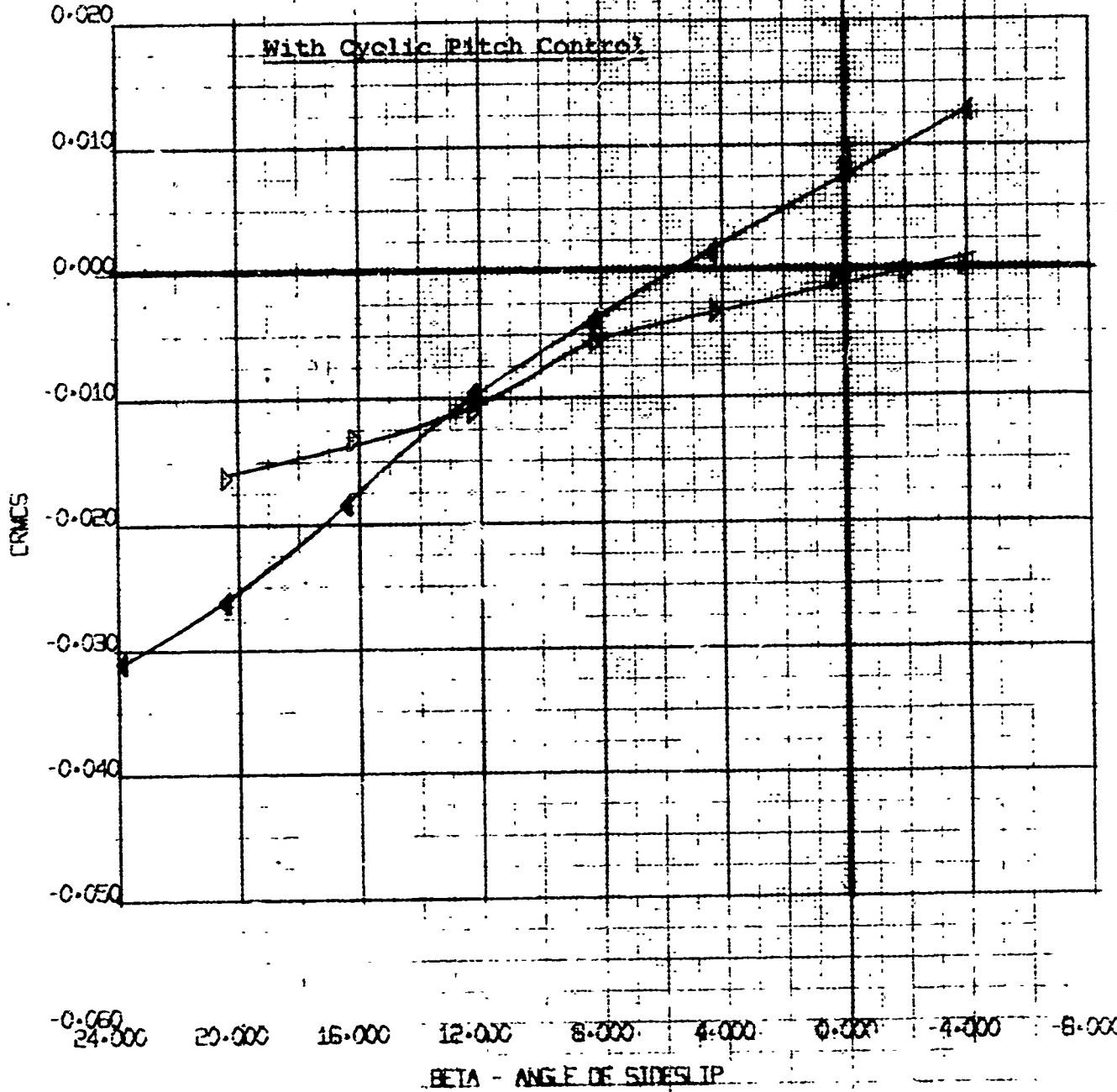
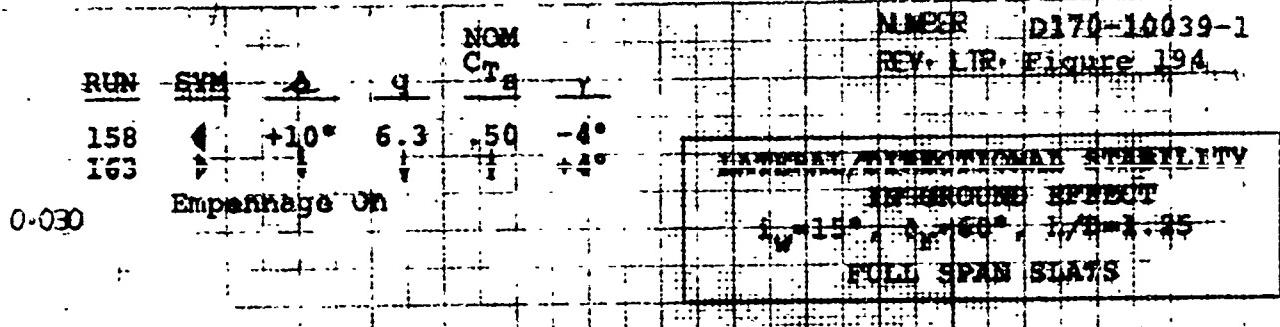
NAGER
REV. LTR.DI70-10039-1
Figure 193

RUN	SYM	Δ	q	NOM C_{Ts}	γ
158	9	+10°	6.3	1.50	-4°
163	8	+10°	6.3	1.50	+4°
Empanelage On					
0.200					

LATERAL/DIRECTIONAL STABILITY
IN GROUND EFFECT
4-PROPS, A=60°, 5/25/71-25
FULL SPAN SHARS



FOUR-PROP TILT WING MODEL YR250(FULL SPAN) LVS VS. BETA	BWWT 67
	1/25/71



FOUR-PROP TILT WING MODEL VROBQ(FULL SPAN) CRMS VS. BETA	BWWT 67 1/25/71
--	-----------------------

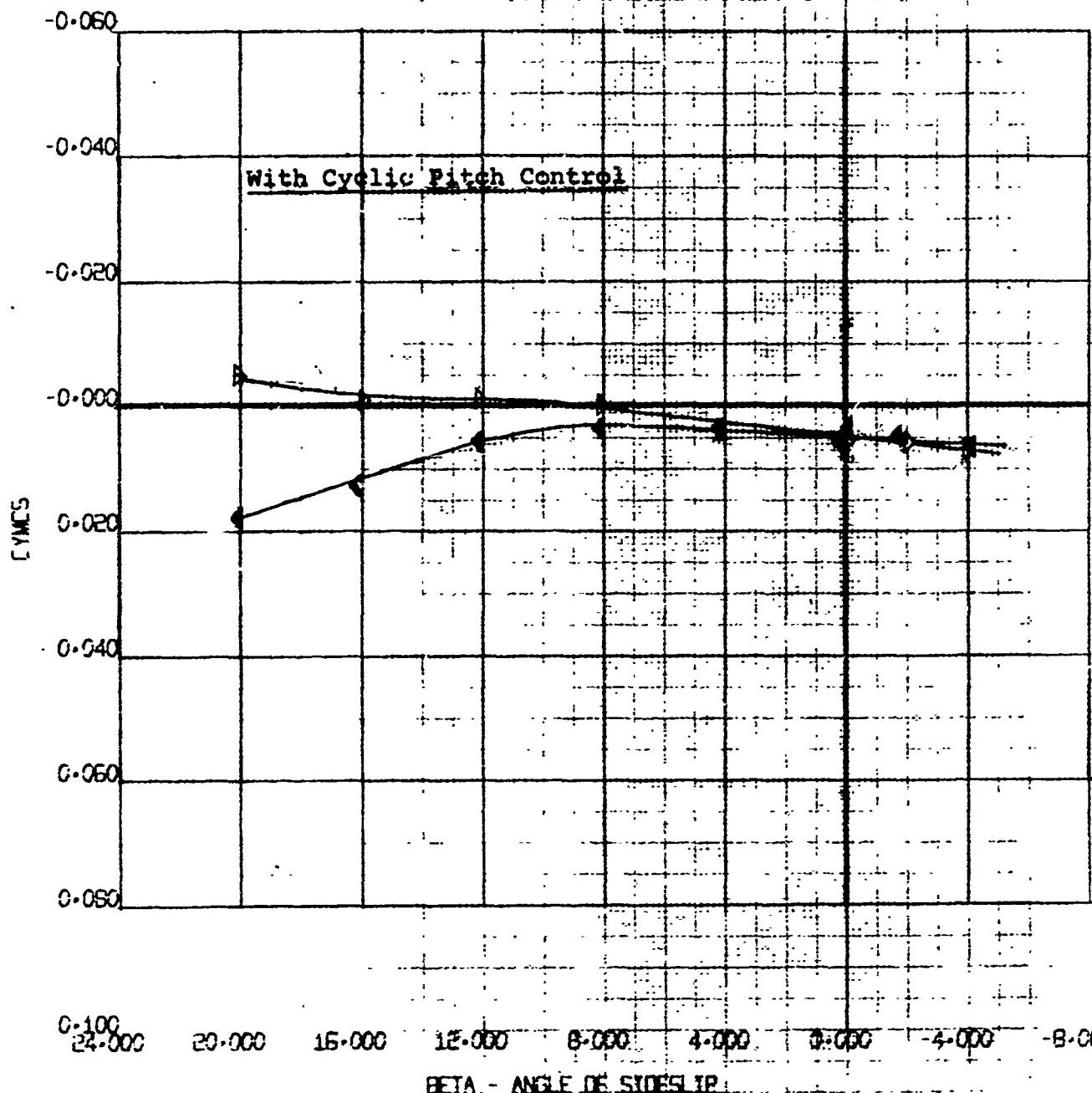
NOT REPRODUCIBLE
SHEET 274

NUMBER D170-10039-1

REV. LTR. Figure 195

RUN	SIM	Δ	α	NOM CT ₂	γ
160	◀	15°	4.0	-70	-4°
162	▶	↓	↓	↓	+4°
Empennage On					
-0.080					

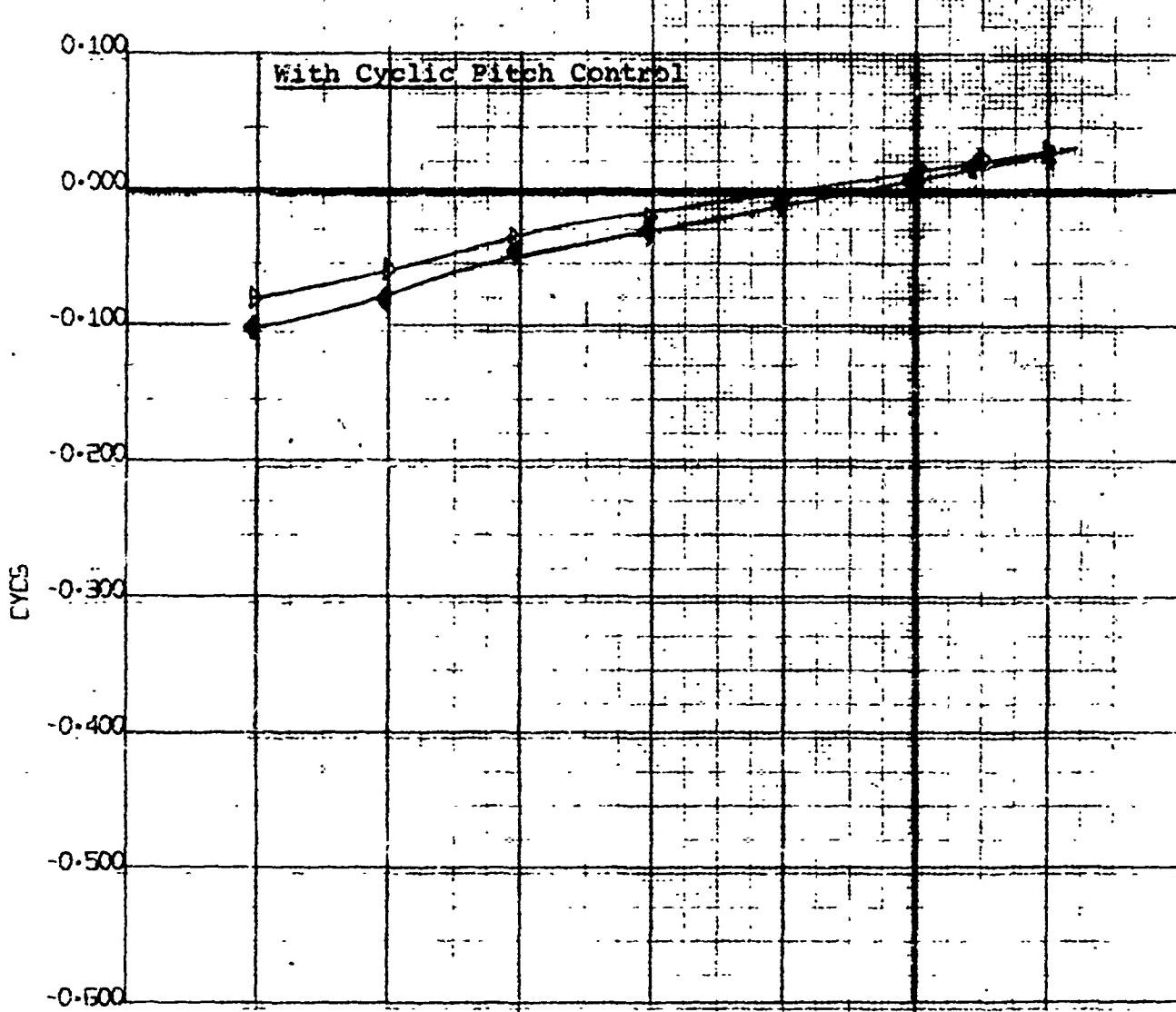
LATERAL/DIRECTIONAL STABILITY
IN GROUND EFFECT
 $\alpha = 15^\circ$, $\delta_F = 60^\circ$, $b/D = 1.25$
ELW: SPAN SLATS.



FOUR-PROP TILT WING MODEL VROSBO (FULL SPAN) CYMCS VS. BETA	EWWT 67
	1/25/71

NUMBER D170-10039-1
REV. LTR. Figure 196

RUN	SYM.	Δ	q	NOM. C_{Ts}	T_s
160	+	15°	4.0	.70	-6°
162	+	15°	4.0	.70	+4°
Empennage On					



24.000 20.000 16.000 12.000 8.000 4.000 0.000 -4.000 -8.000

BETA - ANGLE OF SIDESLIP

FOUR-PROP TILT WING	BVMT 67
MODEL YR060 (FULL SPAN)	
CYCS VS. BETA	1/25/71

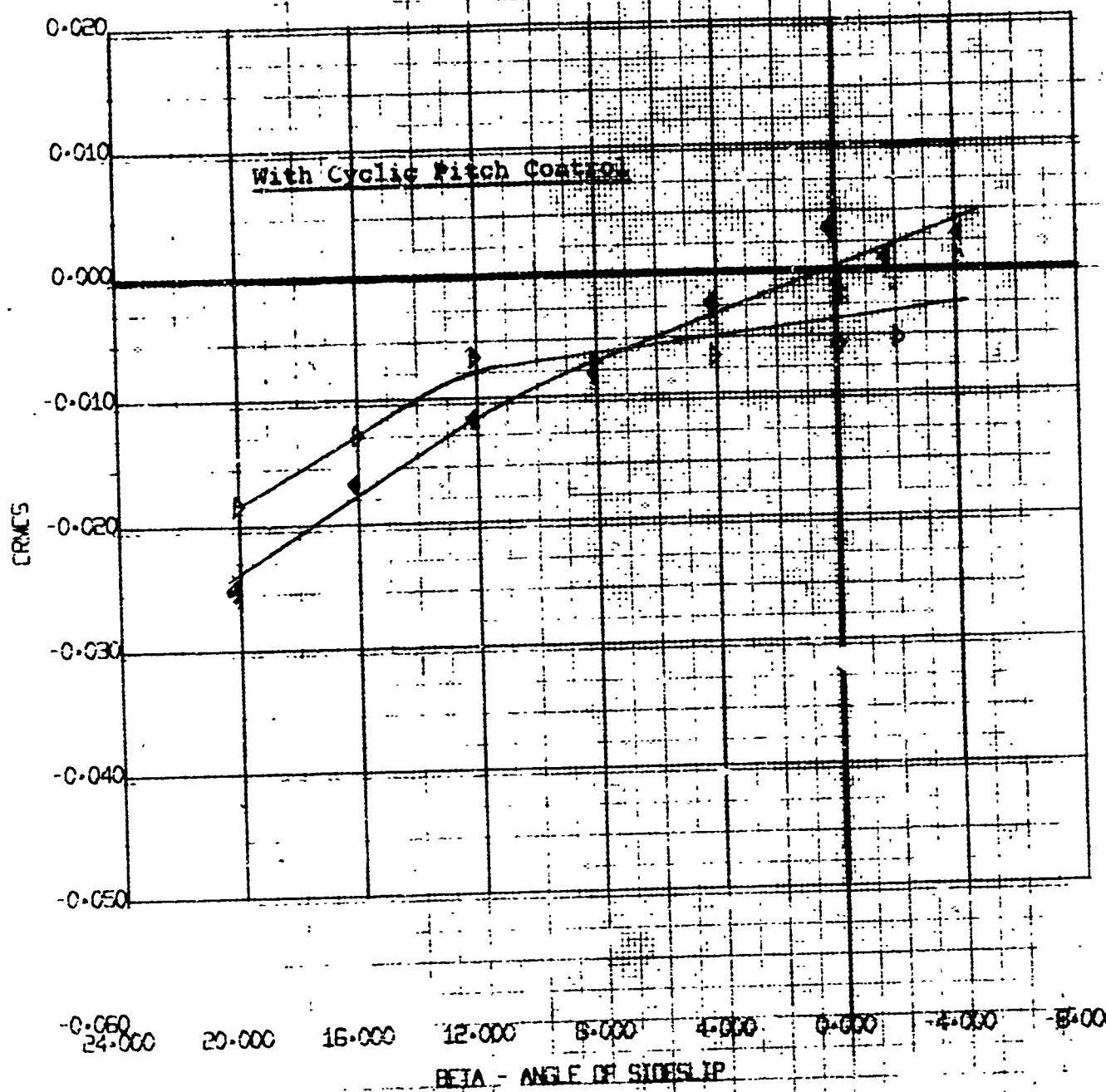
SHEET 276

NOT REPRODUCIBLE

NUMBER D170-10039-1
REV. LTR. Figure 197.

RUN	SYM.	α	q	NOM C _D	C _D	γ
160	6	15°	4.0	.70	-4°	
162	8				+4°	
0-030	Empennage On					

LATERAL/DIRECTIONAL STABILITY
IN GROUND EFFECT
 $\alpha = -30^\circ$, $\delta_e = 60^\circ$, R/D = 1.25
FULL SPAN SLATS



FOUR-PROP TLT WING MODEL VROS30(FULL SPAN) CRMCS VS. BETA	BWWT 67
---	------------

1/25/71

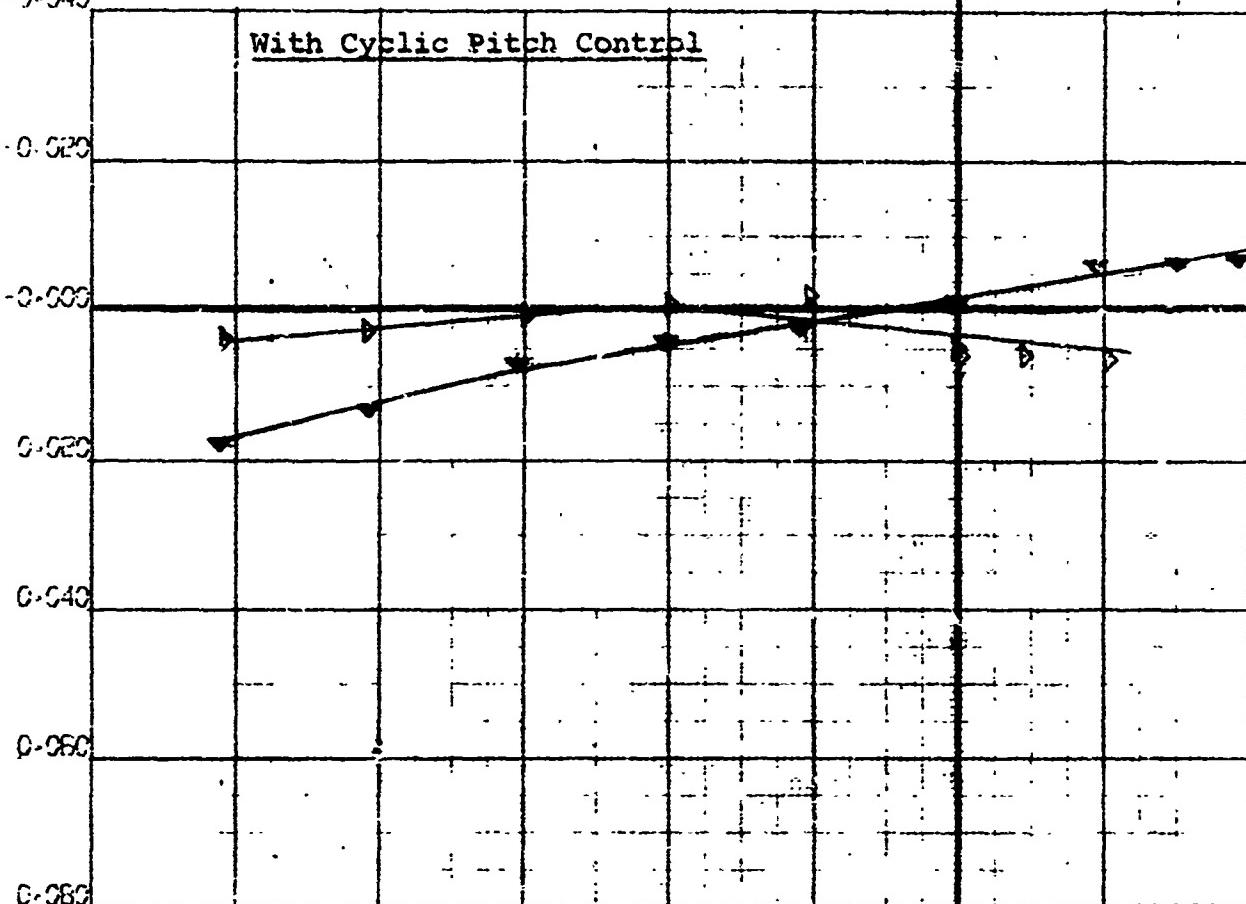
RUN	SYM	α	q	NOM CTS	γ
159	▼	+15°	2.7	.81	-4°
161	▷				+4°
-0.080	Empennage On				

LATERAL/DIRECTIONAL STABILITY
IN GROUND EFFECT
 $i_w = 30^\circ$, $\delta_p = 60^\circ$, $h/D = 1.25$
FULL SPAN SLATS

-0.050

-0.040

WIND



0.400 0.200 0.000 -0.200 -0.400 -0.600 -0.800 -1.000

BETA - ANGLE OF SIDESLIP

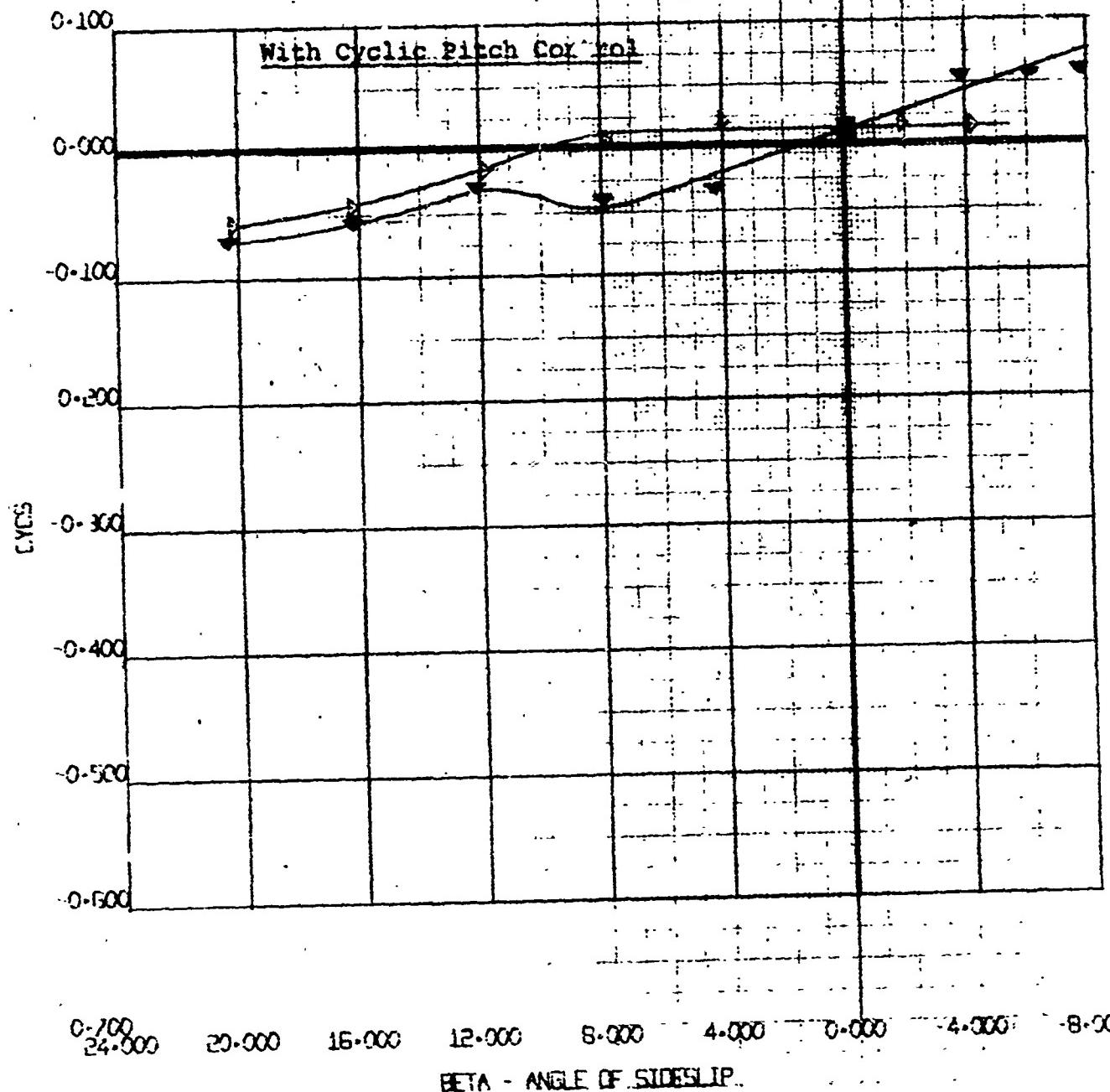
FOUR-PROP. TILT WING	BVWT 67
MODEL VR0680 (FULL SPAN)	
CWMS VS. BETA	12/21/70

NUMBER D170-10039-1
REV. LTR. Figure 199

RUN	SVM	α	γ	NOM C_{Te}	γ
159	▼	+15°	2.7	.81	-4°
161	►				+4°

0-200 Empennage On

LATERAL/DIRECTIONAL STABILITY
IN GROUND EFFECT
 $\alpha_w = 30^\circ$, $\alpha_p = 50^\circ$, $H/D = 1.25$
FULL SPAN SLATS



FOUR-PROP TILT WING
MODEL VROG60 (FULL SPAN)
CYC VS. BETA

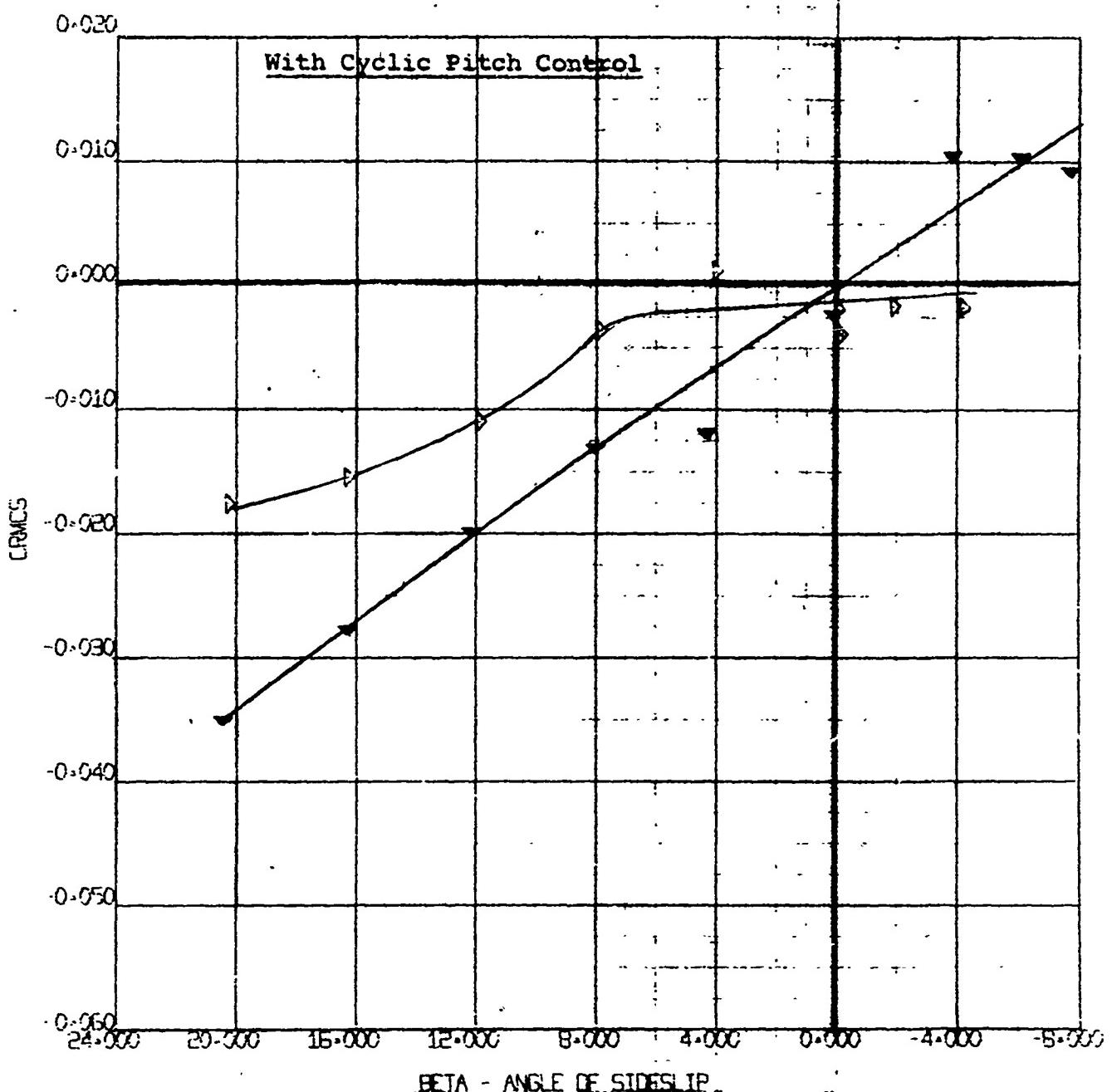
BART
67
12/21/70

RUN	SYM	Δ	α	NOM C_{Ts}	γ
159	▼	+15°	2.7	.81	-4°
161	►				+4°

0.030 Empennage On

NUMBER D170-10039-1
REV. LTR. Figure 200

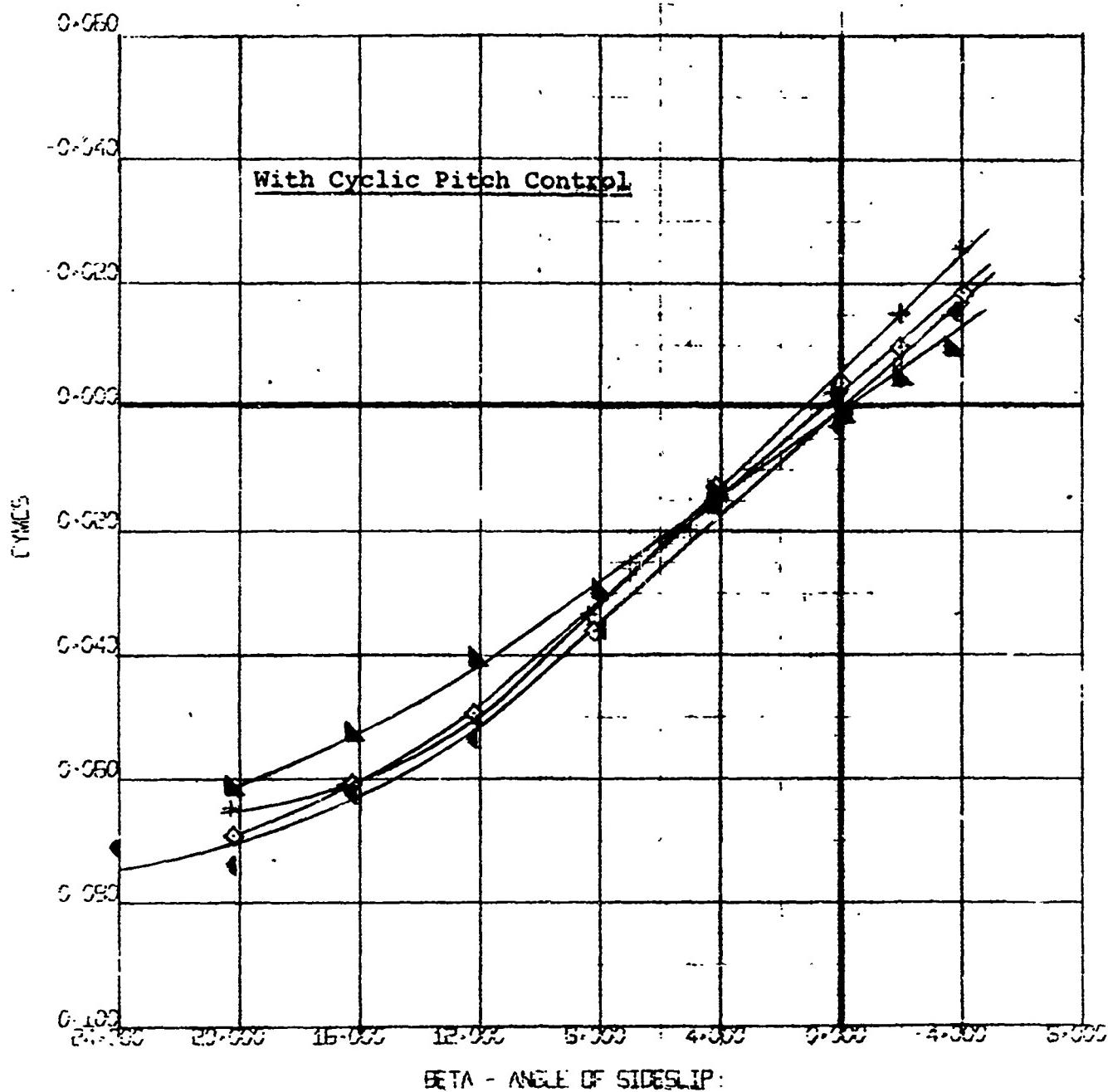
LATERAL/DIRECTIONAL STABILITY
IN GROUND EFFECT
 $\lambda_w = 30^\circ$, $\delta_F = 60^\circ$, $h/D = 1.25$
FULL SPAN SLATS



FOUR-PROP TILT WING MODEL VR020 (FULL SPAN) CRMCS VS. BETA	BWWT 67 12/21/70
--	------------------------

RUN	SYM	Δ	q	NOM	C_{TS}	γ
157	◆	+25	1.0		.92	-4°
164	◇					+4°
165	+					+8°
156	▼					-6°
						Empennage On

LATERAL/DIRECTIONAL STABILITY
IN GROUND EFFECT
 $i_w = 45^\circ$, $\delta_p = 60^\circ$, $h/D = 1.25$
FULL SPAN SLATS



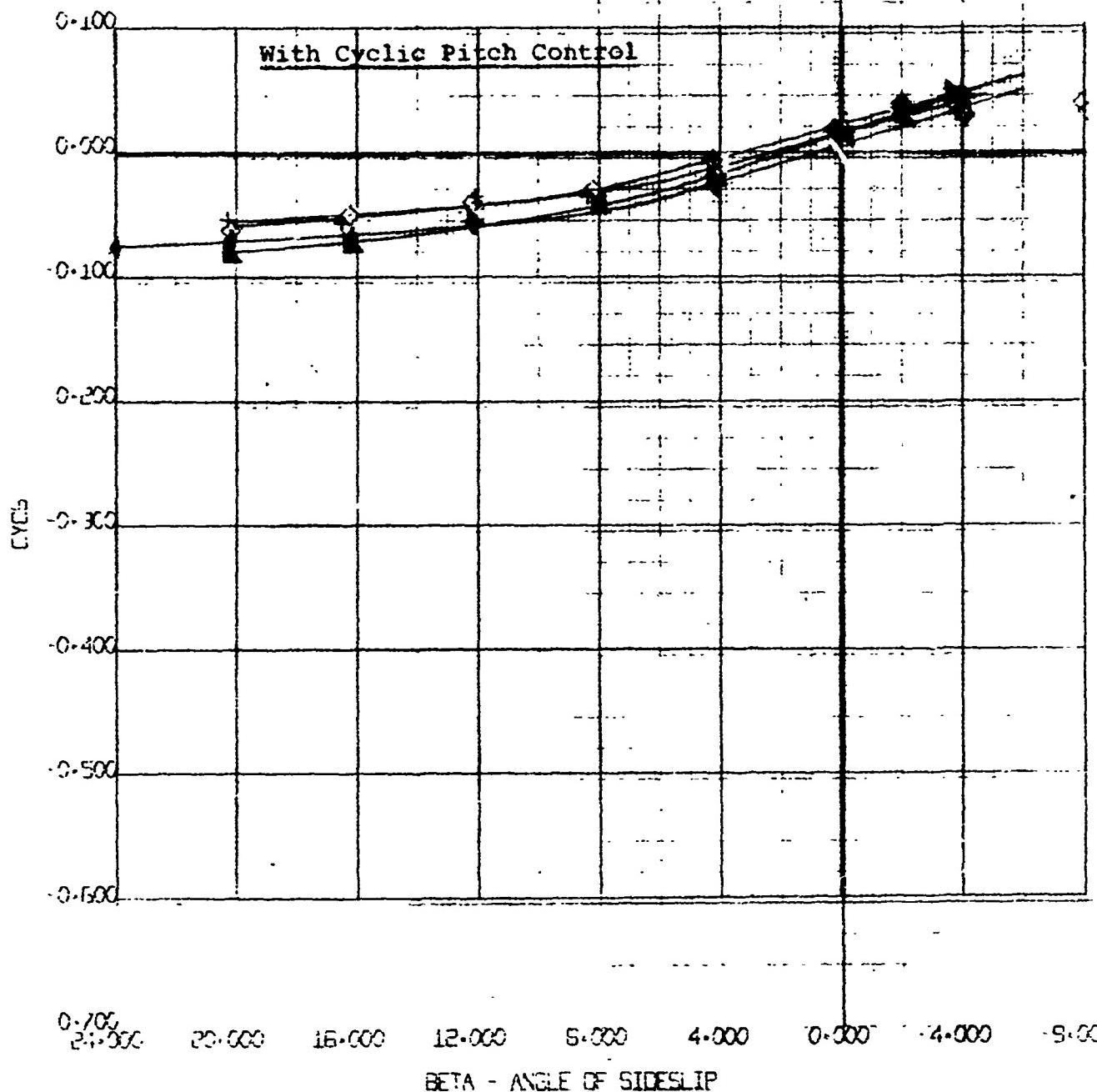
FOUR-PROFILE TILT WING MODEL VR060 (FULL SPAN) CYMCS VS. BETA	REV. 6/
	12/21/70

NUMBER D170-10039-1
REV. LTR. Figure 20.2

RUN	SYM	δ	q	NOM C_{Ts}	γ
157	◀	+25	1.0	.92	-4°
164	◇				+4°
165	+				+6°
166	▶				-6°

Empennage On

LATERAL/DIRECTIONAL STABILITY
IN GROUND EFFECT
 $i_w = 45^\circ$, $i_F = 60^\circ$, $h/D = 1.25$
FULL SPAN SIATS



FOUR-PROP TILT WING
MODEL VROBBO (FULL SPAN)
CYDS VS. BETA

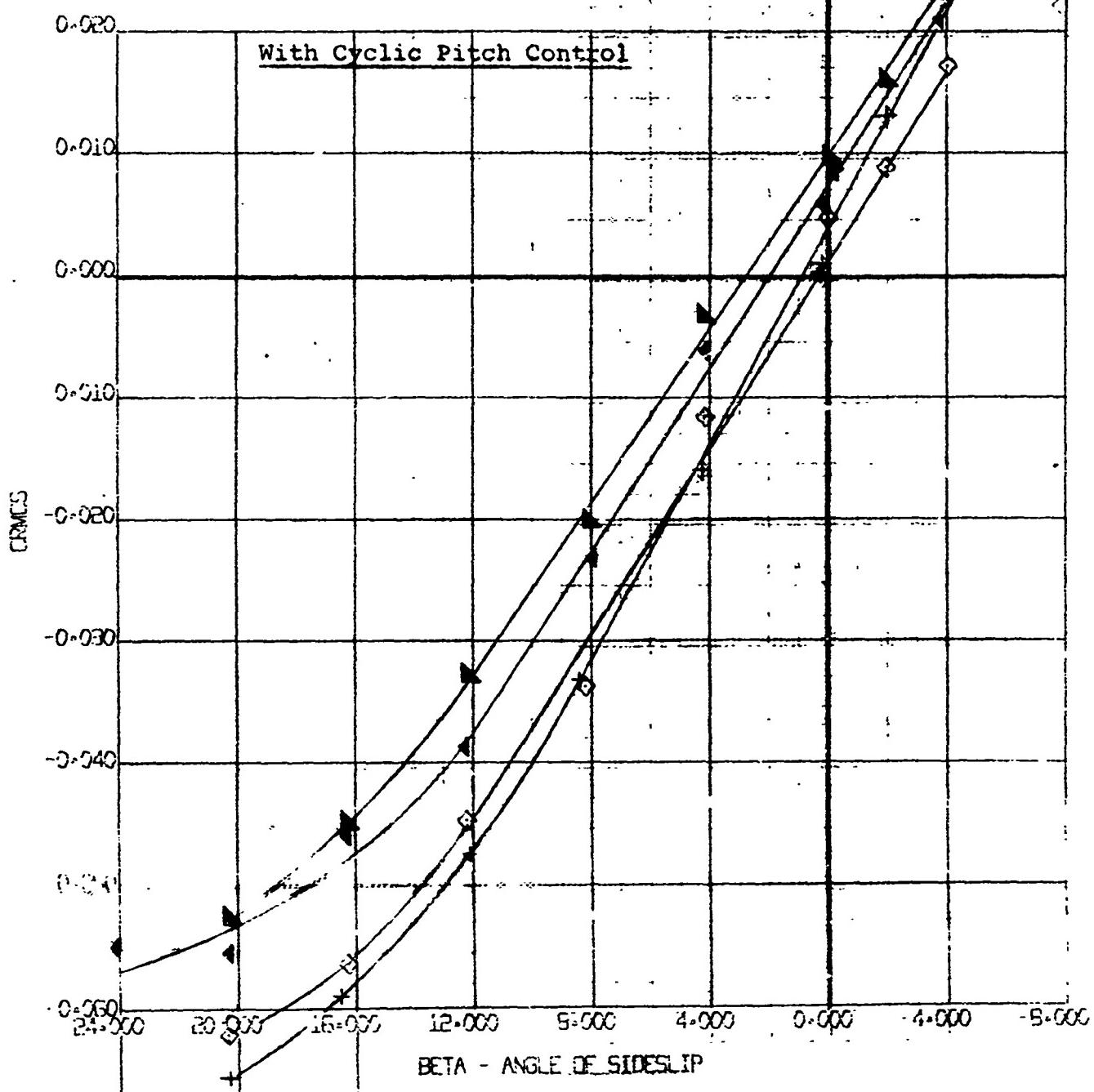
BVNT
67
12/21/73

NUMBER D170-10039-1
REV. LTR. figure 203

RUN	SYM.	δ	q	NOM G_m^*S	γ
157	◆	+25	1.0	.92	-4°
164	◇				+4°
165	+				+6°
166	▼				-6°

Empennage On

LATERAL/DIRECTIONAL STABILITY
IN GROUND EFFECT
 $i_w = 45^\circ$; $\delta_F = 60^\circ$, $h/D = 1.25$
FULL SPAN SLATS



FOUR-PROP TILT WING
MODEL YR0680 (FULL SPAN)
CHWS VS. BETA

BWWT
67
12/21/70

NOT REPRODUCIBLE

7.0 CONCLUSIONS

The primary conclusions that can be derived from this Phase II test of the full span tilt wing model in hover and through the transitional flight regime are as follows:

- a. Hub pitching moments due to cyclic pitch were the same in the presence of a highly flapped wing as for the isolated propeller. Total airplane pitching moments due to cyclic were greater than the sum of the hub moments, as a result of the favorable propeller normal forces generated by cyclic pitch action.
- b. Pitching moments per degree of cyclic were essentially unaffected by wing tilt, forward speed or ground effect. Cyclic effectiveness was maintained up to and beyond wing stall.
- c. Application of positive (nose down) cyclic reduced rate of descent capability by about 100 ft/min per degree of cyclic at 62 knots full scale speed and by about 50 ft/min per degree of cyclic at 38 knots.
- d. Cyclic pitch action had only a small effect in the transition regime on the stabilizer control capability and on the roll/yaw control power from the wing surface controls, flaps and spoilers. Cyclic pitch did alter the hover yaw control power from the flaps and spoilers with a positive cyclic angle of 6° increasing the surface control power by 15% and a negative cyclic angle of 6° decreasing it by 17%.
- e. Cross-coupling effects of the stabilizer and roll/yaw wing surface controls on the cyclic pitch control effectiveness were not significant.
- f. The use of cyclic pitch had no marked effect on either longitudinal stability or lateral/directional stability through transitional flight or in-ground effect at a 3 foot wheel height with the exception of the increase in directional stability and dihedral effect recorded in-ground effect with negative cyclic.

- g. A hover yaw control configuration of 60° down flaps on one wing and 60° up spoilers on the opposite wing appears to be the most favorable yaw control configuration of the various combined control configurations evaluated. This assertion considers both the out-of-ground effect control capability and the reduction that occurs in-ground effect (29% for the noted configuration at a 2 ft. wheel height).
- h. The necessary value of the non-dimensional yawing moment parameter ($Y.M./\delta T$) is 0.29 for a representative tilt-wing transport type aircraft hovering at its design "V" gross weight of 87,000 lbs. and meeting a 0.5 radian/sec² yaw angular acceleration level. The hover yaw control configuration of combined down flaps and up spoilers produces a moment that is within 14% of the goal. This percentage difference takes into account the 6.5% increase in out-of-ground control capability that was observed when the disc loading was increased from 16.7 lb/ft² to 33.4 lb/ft²
- i. Hover downwash due to application of yaw control increased approximately linearly with yawing moment, reaching a level of 14% of thrust with 60° flaps on one side and 60° spoilers on the other.
- j. At the high speed end of transition (low slipstream thrust coefficients) with the wing in the down position, the effectiveness of the vertical tail in terms of developing yawing moment was low. This problem has been identified as a flow problem and could be corrected by redesigning the wing/body juncture and the intersection between the base of the fin and the top of the fuselage.
- k. In the low speed part of the transition (high slipstream thrust coefficients) with the wing tilted up to angles in the order of 45° and 55°, the aircraft was directionally stable. This situation is attributed to the observed change in the character of the flow about the fuselage at high wing tilt angles and the subsequent redistribution of longitudinal pressures on the fuselage.

1. A ground recirculation condition was encountered during the in-ground effect testing with the model set at an equivalent full scale wheel height of 3 ft. With the wing tilted to 30° and the flaps deflected to 60°, ground recirculation was in the initial stages of formation at 0.8 C_{Ts} . At higher C_{Ts} values with 45° of wing tilt, ground recirculation was well developed.
- m. The influence of the ground on the lift curves and force polars for the 60° flap deflection was typical except for the ground recirculation condition at high C_{Ts} values. At low wing incidences, an increase in the slipstream lift coefficient was recorded and a decrease in the slipstream drag coefficient was generally evident. Maximum slipstream lift coefficient was decreased by a constant increment of 0.25 C_{Ls} .
- n. A check of the stabilizer effectiveness in-ground effect at a C_{Ts} of 0.55 showed some increase in $\Delta C_{M_s}/\Delta \alpha$ over that recorded out-of-ground effect with comparable model conditions.
- o. The major influence of the ground on the lateral/directional stability characteristics in the C_{Ts} range from 0.28 to 0.71 was to decrease the directional stability.

REFERENCES

1. D170-10038-1, FOUR PROP TILT WING WITH CYCLIC PITCH PROPELLERS: RESULTS OF FULL SPAN WING TUNNEL TEST/ PHASE I, The Boeing Company, Vertol Division, Philadelphia, Pa.
2. D170-10037-1, ISOLATED CYCLIC PITCH PROPELLER: RESULTS OF WING TUNNEL TEST, The Boeing Company, Vertol Division, Philadelphia, Pa.